OCCURRENCE AND MOVEMENT OF GROUND WATER IN AUSTIN CHALK AND EAGLE FORD AND OZAN FORMATIONS AT THE SUPERCONDUCTING SUPER COLLIDER (SSC) SITE, ELLIS COUNTY, TEXAS

Topical Report

by

Alan R. Dutton, Edward W. Collins, Susan D. Hovorka, Robert E. Mace,
Bridget R. Scanlon, and Jiannan Xiang

assisted by

Carolyn E. Condon, Alan J. Cherepon, Karen Herrington, H. Seay Nance, Rainer K. Senger,
Erika Boghici, David Hill, Ian Jones, Sreevathsa Ramachandra,
and Ganesh Rao

Prepared for

Texas National Research Laboratory Commission
under Contract No. IAC(92-93)-0301

Bureau of Economic Geology
W. L. Fisher, Director
The University of Texas at Austin
University Station, Box X
Austin, Texas 78713-7508

May 1994

CONTENTS

APPENDICES

Figures

Tables

ABSTRACT

This report defines hydrologic properties and describes rates and modes of ground-water flow in weathered and unweathered Austin Chalk and Ozan ("lower Taylor Marl") and Eagle Ford Formations at the Superconducting Super Collider (SSC) site in Ellis County, Texas. Fractures probably are the primary conduit of ground-water flow in these formations because unfractured bedrock has low hydraulic conductivity. Distribution and fabric of detrital versus authigenic clays, rather than total clay content, influence the mechanical properties and log-response character of chalk and marl. The middle Austin Chalk typically has lower fracture intensity and abundance, greater ductility, lower porosity, and lower average hydraulic conductivity than the upper and lowermost Austin.

Precipitation over upland drainage divides percolates into the ground and moves downward through the soil zone and weathered bedrock to the water table. Water levels in both weathered and unweathered bedrock generally mimic topography, reflecting a dynamic balance between rate of recharge from precipitation and rates of discharge by evapotranspiration, flow to springs and seeps, and pumping of wells. Ground water percolates along vertical fractures and horizontal bedding-plane joints and through the more permeable sedimentary layers. Flow paths are generally eastward but bend toward discharge points in springs and seeps in the valley bottoms and stream banks. Vertical movement is retarded by unfractured, low-permeability beds. Only a small amount (<1 percent) of the ground water moving through the surficial weathered bedrock moves downward into unweathered, low-permeability bedrock. Vertical circulation of ground water in fractured zones locally is deep. At the eastern side of the SSC, ground water moves downward from the Ozan into the Austin beneath the upland drainage divides but upward from the Austin through the Ozan beneath stream valleys.

Hydraulic conductivity of the weathered Austin Chalk ranges from 0.0015 to 64.16 ft/d ($10^{-8.28}$ to $10^{-3.65}$ m/s) and decreases with depth. Transmissivity, ground-water flow rate, and potential for contaminant transport vary seasonally as the water table fluctuates within the weathered zone. Hydraulic conductivity of unweathered Austin Chalk ranges over 6 orders of magnitude from $10^{-6.0}$ to $10^{-0.07}$ ft/d ($10^{-11.5}$ to $10^{-5.5}$ m/s). Average hydraulic conductivity of fractured chalk statistically differs among the four subdivided units of the Austin Chalk.

Chemical composition and salinity of calcium-bicarbonate to sodium-chloride ground waters appear to be controlled by mineralogic reactions and incomplete flushing of ancient seawater by circulating recharge water during the time that the stratigraphic section has been in its present hydrological setting. Flushing of marine salts is most complete in the near-surface weathered zone and in unweathered bedrock where fractures are most abundant and interconnected. The ^{14}C and ^{3}H data suggest that ground water in fractured bedrock was recharged within the last 40 to 50 years. Ground water in bedrock with less well interconnected fractures was possibly recharged within the past 15,000 to 20,000 yr, and average ground-water age in unweathered, unfractured bedrock is 1 million years. The local geothermal gradient matches the regional gradient of 1.7°F/100 ft (30.3°C/km).

The estimated well density on and around the SSC footprint is 9.1 wells/mi^2 (3.5 wells/km^2). There are 419 wells on SSC land parcels and 40 wells within 150 ft (45.72 m) of the accelerator beam line. Most of the located wells are shallow dug wells less than 50 ft (15.24 m) deep and 15 percent are in the regional confined aquifers at depths in excess of 420 ft (128 m). Only about 13 percent of the shallow wells on the SSC footprint are being used. As many as 2,700 shallow wells might be unused or abandoned in the entire study area in Ellis County. Many are in poor repair and have been used for disposal of trash, creating a potential for contamination of the shallow aquifer.

Three numerical models of ground-water flow were constructed and used as tools to better understand the parameters that control ground-water flow paths and travel times at the SSC site: a "West Campus" model, an "Ellis County" model, and an "Interaction Hall" model. These models can be modified to locate optimum locations of ground-water monitoring wells and to predict travel time between specific SSC facilities and a monitoring well.

Analysis of ground-water flow at the interaction hall IR8 shows that (1) total inflow probably will be less than 2,000 gal/d ($10^{-4.06}$ m^3/s) and will decrease with time, (2) ground water will be captured from at least 115 ft (35 m) away in the Ozan and 492 ft (150 m) in the Austin, and (3) fluid pressure drawdown and capture-zone size would be cost-effectively increased with drainage holes limited to two rows on northern and southern walls, each with more columns of boreholes located at the middle and the bottom of the wall.

INTRODUCTION

The Superconducting Super Collider (SSC) is designed as a state-of-the-art particle accelerator to explore the basic structure of matter at energies 20 times higher than can be done with existing particle accelerators. The intent of the SSC is to accelerate two beams of protons each to an energy of 20 trillion electron volts (20 TeV), near the speed of light, and monitor the results of collisions between proton beams at energies of 40 TeV in controlled experiments. The U.S. Department of Energy (DOE), after a national competition in November 1988, identified the site in Ellis County, Texas (fig. 1), as the preferred location for the SSC Laboratory (SSCL). In August, 1993, the DOE terminated construction of the SSC.

The SSC collider ring would have been 54 mi (87 km) in circumference and located in a 14-ft-diameter (4.3-m) tunnel at an average depth of 150 ft (45.7 km) below ground surface in the Cretaceous-age Eagle Ford Formation, Austin Chalk, and Ozan Formation ("lower Taylor Marl") (fig. 2). The SSC facilities can be grouped into East Campus and West Campus areas, where laboratory and office buildings and experimental halls would have been located, and north and south arcs of the collider tunnel (fig. 2). The suitable geology of the site was among the most important criteria for selecting the Ellis County site. The bedrock is soft and easily mined, yet competent to stand unsupported in excavations, and has generally low permeability that limits potential for ground-water flow. On the basis of existing regional data, difficulties for construction were expected to be minimal and environmental impacts on surface and ground water were expected to be very low. Nonetheless, needs remained for additional information on the hydrogeology of the SSC site with which to address ground-water-related issues and to design a cost-effective ground-water monitoring program. In particular the following information was needed to supplement existing regional data:

- position and variability of the water table in each hydrologic unit,
- location of water wells on properties affected by the SSC,
- background or ambient water level and water quality in host formations and other hydrologic units potentially impacted by construction and operation of the SSC,

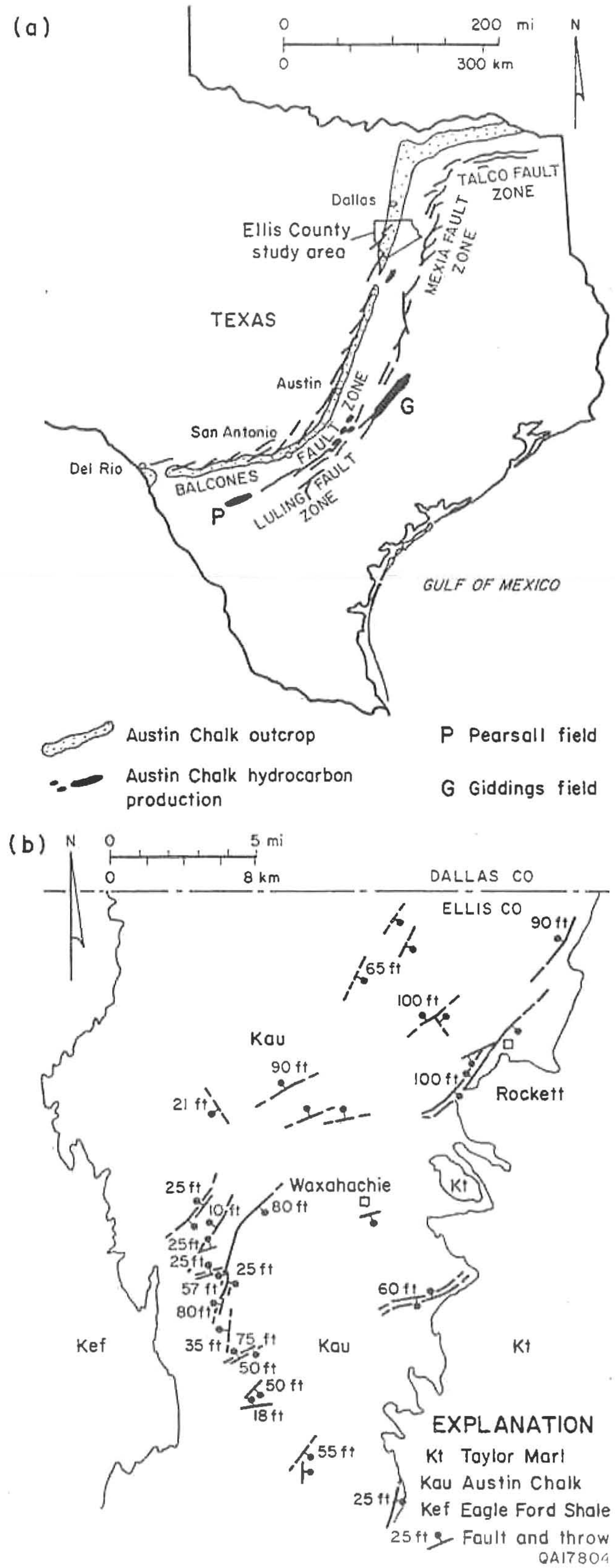

Figure 1. Locations of (a) the Ellis County study area in north Texas, the Balcones Fault Zone, and Austin Chalk outcrop and hydrocarbon production and (b) large faults within the outcrop of bedrock units at the SSC site. From Collins and others (1992).

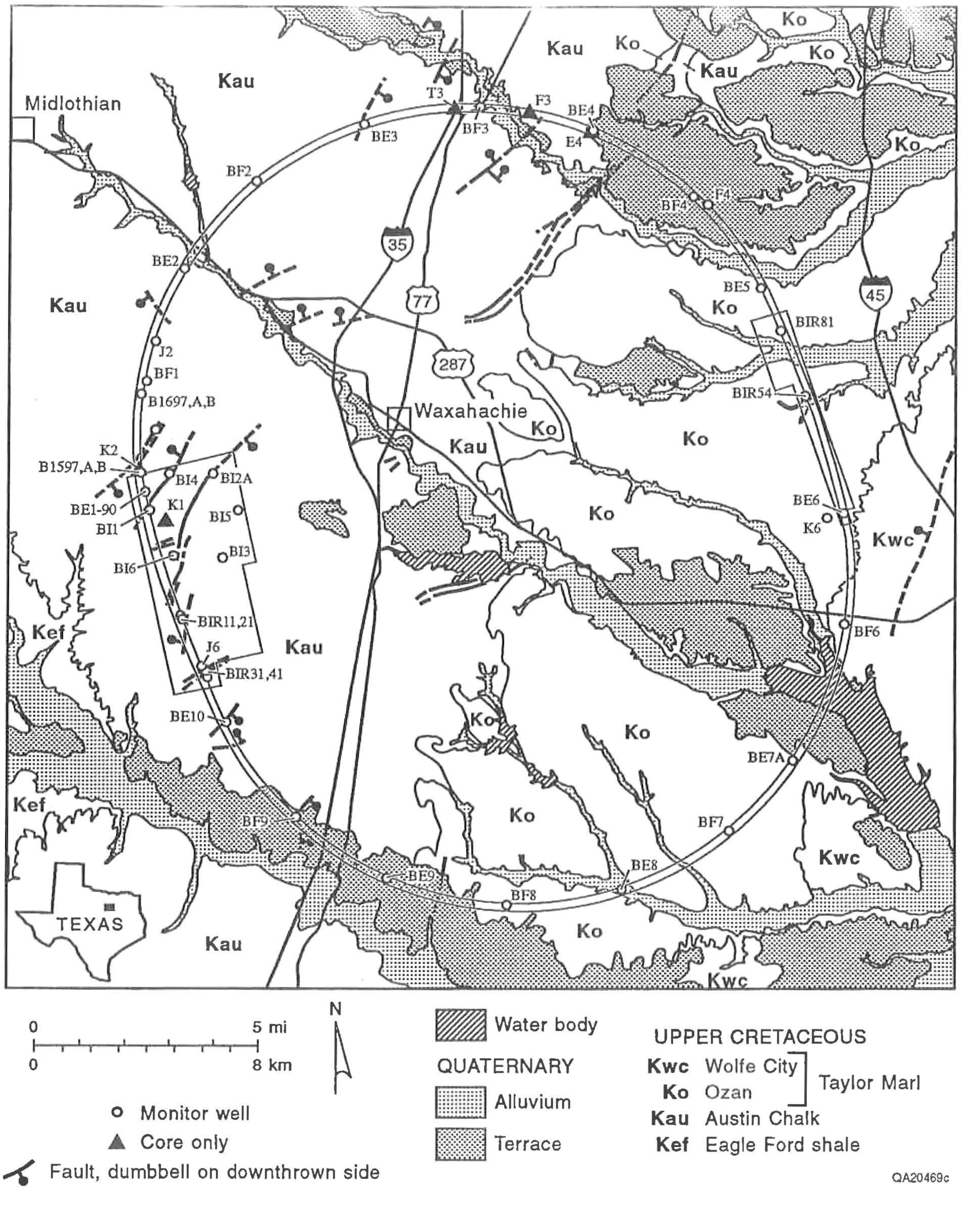

Figure 2. Generalized geologic map of part of Ellis County in north Texas, outline of SSC project area, and location of boreholes used for stratigraphic and hydrogeologic data.

- hydrogeologic controls on recharge, discharge, flow rates and flow paths,
- basic data on hydrogeologic properties, and
- potential for ground-water contamination.

This report presents results of a comprehensive hydrogeologic investigation designed to establish the hydrologic properties and conditions of the SSC site in sufficient detail to address these needs. Field hydrologic studies and hydrologic modeling were carried out to better define rates and modes of hydrologic processes at the SSC site. The work has been conducted in three phases. Phase I (April 1990 to September 1991) studied ground water in surficial alluvium that overlies bedrock along the northeastern side of the SSC ring (Wickham and Dutton, 1991). Phase II (November 1990 to August 1993) focused on ground water in the Austin Chalk and Ozan and Eagle Ford Formations that will host the subsurface SSC facilities but included additional measurements in surficial alluvium and weathered chalk and marl bedrock. Phase III (June 1992 to August 1994) involved an assessment of water resources and prediction of future water-level changes in the deep regional aquifers that underlie the SSC site.

Results of the Phase II investigation are the topic of this report. The scope of work included geologic studies to support the hydrologic investigations, a comprehensive inventory of water wells, monitoring water levels at more than 120 public, private, and SSC project wells, analyses of chemical composition of ground water, hydrologic testing, and use of numerical models as tools for interpreting ground-water flow.

The two sections of this report after this introduction outline the hydrogeologic setting of the SSC site and the methods used in this investigation.

The next two sections present a detailed description of the geologic characteristics of the Austin Chalk at the SSC site. Part of the purpose of this stratigraphic analysis was to better understand the controls on fracture intensity. Ellis County, where the SSC is being built, lies at the northern end of the Balcones Fault Zone (fig. 1). Fractures associated with small normal faults and open folds in the Austin Chalk and the Eagle Ford and Ozan Formations will be intersected by SSC tunnels. These fractures are the pathways for regional ground water flow as well as for movement of potentially radioactivated ground water in the vicinity of the SSC. Knowledge of site-specific fracture characteristics and ground-water flow velocity at the SSC remains limited because geologic and hydrologic data collected at ground surface during this study can be used to determine only general indications of subsurface conditions.

Results and discussion of hydrologic studies follow in the succeeding sections, including a summary of ground-water resources, an inventory of water wells that reflects past development of ground-water resources, and description of hydrogeologic properties and water chemical composition of the various hydrologic units. Interpretations are made of recharge and ground-water flow rates, sources of ground water and its age or water residence time, the role of springs and seeps in the local hydrological cycle, artesian conditions, influence of fractures on ground-water flow, and effects of SSC construction on ground-water flow. Numerical models of ground-water flow are constructed based on these hydrologic measurements and include a "West Campus" model, an "Ellis County" model, and an "Interaction Hall" model.

REGIONAL HYDROGEOLOGIC SETTING

Hydrologic Units

The main hydrologic units in the Ellis County area, in order of increasing depth, are (table 1):

- local surficial aquifers in Quaternary alluvium and weathered Cretaceous bedrock near land surface,
- a regional confining system in unweathered Upper Cretaceous bedrock of the Austin Chalk, and the Ozan ("lower Taylor Marl") and Eagle Ford Formations, and
- a regionally confined aquifer system with principal units in the Upper Cretaceous Woodbine and Lower Cretaceous Paluxy and Twin Mountains Formations. The Paluxy and Twin Mountains Formations together make up the Trinity Group aquifer (Nordstrom, 1982).

Table 1. Geologic units in the region.

<table>
<tr><th>Era</th><th>System</th><th>Series</th><th>Group</th><th colspan="2">Stratigraphic Unit</th></tr>
<tr><td rowspan="2">Cenozoic</td><td rowspan="2">Quaternary</td><td>Holocene</td><td></td><td colspan="2">Alluvium</td></tr>
<tr><td>Pleistocene</td><td></td><td colspan="2">Fluviatile terrace deposits</td></tr>
<tr><td rowspan="10">Mesozoic</td><td rowspan="10">Cretaceous</td><td rowspan="5">Gulf</td><td rowspan="2">Taylor</td><td colspan="2">Wolfe City Formation</td></tr>
<tr><td colspan="2">Ozan Formation
"lower Taylor Marl"</td></tr>
<tr><td>Austin</td><td colspan="2">Austin Chalk</td></tr>
<tr><td>Eagle Ford</td><td colspan="2">Eagle Ford Shale Formation</td></tr>
<tr><td>Woodbine</td><td colspan="2">undifferentiated</td></tr>
<tr><td rowspan="5">Comanche</td><td>Washita</td><td colspan="2">undifferentiated</td></tr>
<tr><td rowspan="2">Fredericksburg</td><td colspan="2">undifferentiated</td></tr>
<tr><td rowspan="3">Antlers Formation</td><td>Paluxy Formation</td></tr>
<tr><td rowspan="2">Trinity</td><td>Glen Rose Formation</td></tr>
<tr><td>Twin Mountains Formation</td></tr>
</table>

QA17455c

Surficial Aquifers

Unconfined and semi-unconfined aquifers of limited extent overlie the low-permeability chalk, marl, and shale bedrock in Ellis County. These surficial aquifers consist of alluvium and weathered Cretaceous bedrock. Discontinuous patches of Pleistocene and Holocene stream-valley alluvium that compose unconfined and semi-unconfined aquifers lie unconformably above the Cretaceous formations (Wickham and Dutton, 1991). The Pleistocene deposits are unconsolidated and typically contain a thin, basal-pebble conglomerate of fossil fragments, chert, and carbonate-rock fragments in a sandy, carbonate-rich matrix. Above the basal bed, sediment consists of stratified clay, sand, granules, and pebbles consisting mainly of carbonate-rock fragments, overlain by calcareous clay with a thick clayey soil containing numerous caliche nodules. The Phase I study focused on Pleistocene alluvial deposits that make up the surficial aquifer between Red Oak and Brushy Creeks along the northeastern portion of the SSC ring in the vicinity of Palmer and Rockett. Alluvial deposits also occur adjacent to the western end of Bardwell Lake and along the northern side of Chambers Creek. Deposits similar to ones at the SSC site occur along the Trinity River and its tributaries in Ellis County and parts of North-Central Texas (Taggart, 1953; Reaser, 1957; Brooks and others, 1964). The alluvial material is normally small in areal extent and typically less than 50 ft (15.2 m) thick. Erosion during the Holocene stripped most of the Pleistocene alluvium from the surface, and Modern streams locally have cut through to underlying bedrock, leaving isolated deposits of Pleistocene alluvium at elevations higher than those of the surrounding strata (Hall, 1990). These geomorphologic features are referred to as terraces. Holocene floodplain deposits of clay and silty clay form an alluvial veneer along rivers and streams in the region and range in thickness from a few feet to more than 30 ft (9.14 m).

Weathering and unloading have significantly increased porosity and permeability of the chalk and marl bedrock, allowing enhanced recharge, storage, and shallow circulation of ground water in otherwise tight rock strata. Thickness of the weathered zone is generally less than 12 to 35 ft (3.66 to 10.67 m). Open fractures are the primary means by which ground water is conducted in the bedrock formations because matrix permeability is low, although matrix porosity is higher in weathered than in unweathered bedrock. Fracture-controlled springs at ground surface also have been affected by weathering, unloading, and other surficial modifications to hydraulic conductivity.

Use of ground water from the surficial alluvium and weathered bedrock historically has been to supply the domestic water of landowners and tenant farmers or to provide water for cattle and horses. Large-scale cropland irrigation is uncommon in Ellis County.

Unweathered Chalk, Marl, and Shale Bedrock

The subsurface facilities of the SSC will be constructed mainly in low-permeability unweathered bedrock of the Upper Cretaceous Austin Chalk and Ozan ("lower Taylor Marl") and Eagle Ford Formations (table 1). This stratigraphic section composes a regional confining system, which means that the low permeability of the rock retards the vertical and lateral flow of ground water and separates underlying aquifers from surficial aquifers. The formations dip as much as 0.54° east-southeastward from their outcrop in Ellis and neighboring counties in North Texas (Thompson, 1967). Because the plane of the SSC ring dips less steeply (0.198°) than the formations, the ring crosses from the Eagle Ford Formation at its westernmost limit into the Austin Chalk and into the Ozan Formation at its easternmost limit. Approximately 60 percent of the collider ring is in the Austin Chalk, 30 percent in the Ozan Formation, and 10 percent in the Eagle Ford Formation (fig. 2).

Most of the effort of the Phase II hydrologic investigation was on the Austin Chalk and Ozan Formation. The Austin Chalk is made up of fine-grained chalk and marl deposited in a deep-water marine-shelf environment. The Ozan Formation is made up of fine-grained marl, calcareous mudstone, and shale and was deposited in a nearshore (neritic) marine-shelf environment. The Eagle Ford and Wolfe City Formations are exposed in the westernmost and easternmost vicinity of the SSC project, respectively (fig. 2). The Eagle Ford Formation is composed of a dark shale with very thin limestone beds and concretions and pyrite nodules (The Earth Technology Corporation, 1990a). The Wolfe City consists of thin beds of fine-grained calcareous sandstone interbedded with sandy marl (Thompson, 1967).

Water movement through fractured bedrock of the Autin Chalk and Ozan Formation is restricted by low hydraulic conductivities, previously measured between less than 1.8×10^{-6} and 0.55 ft/d (7×10^{-11} and 2.1×10^{-6} m/s) in field tests (The Earth Technology Corporation, 1990e) and less than 2.8×10^{-4} ft/d (1×10^{-9} m/s) in laboratory tests of core (Texas National Research Laboratory Commission, 1987, unpublished data). Additional measurements of hydraulic conductivity were made in this study. Fractures undoubtedly play a significant role in moving ground water in these rocks, as discussed later.

Regionally Confined Aquifers

Regional aquifers in the Woodbine, Paluxy, and Twin Mountains Formations at depth are confined in the Ellis County area by the Eagle Ford Formation, Austin Chalk, and Ozan Formation and by minor confining units, such as those occurring locally in the Washita and Fredericksburg Groups and the Glen Rose limestone (table 1). The 250- to 375-ft-thick (76.2- to 114.3-m) Woodbine is a medium- to coarse-grained iron-rich sandstone, with some clay and lignite seams. Depth to the top of the Woodbine ranges from 600 to 1,000 ft (182.9 to 304.8 m) beneath ground surface at the SSC facility. Most wells are completed in the lower part of the formation, which yields better quality ground water. Transmissivity values range from approximately 176 to 1,510 ft^2/d (1.9×10^{-4} to 1.6×10^{-3} m^2/s) and average about 668 ft^2/d (7.2×10^{-4} m^2/s). Nordstrom (1982) referred to the Paluxy and Twin Mountains Formations together as the Trinity Group aquifer. The Twin Mountains is as much as 550 to 850 ft (167.6 to 259.1 m) thick in the area and is composed principally of sandstone with a basal gravel and conglomerate section where most wells are completed. To the east and north of Ellis County, the Twin Mountains is laterally equivalent to the Travis Peak Formation. The top of the Twin Mountains Formation lies approximately 1,200 to 1,500 ft (365.8 to 457.2 m) below the base of the Woodbine at depths ranging from approximately 2,000 to 3,000 ft (609.6 to 914.4 m) beneath ground surface. Transmissivity values range from approximately 727 to 2,212 ft^2/d (7.8×10^{-4} to 2.4×10^{-3} m^2/s) and average about 1,203 ft^2/d (1.3×10^{-3} m^2/s).

Recharge occurs by precipitation on formation outcrops to the west and northwest of Ellis County, and discharge occurs by cross-formational flow in the subsurface and by pumping at water-supply wells. Comparison of water levels measured in 1976 (Nordstrom, 1982) suggests that the vertical flow component is directed downward between aquifers in the Woodbine and Twin Mountains Formations in the Ellis County area. Thompson (1967) suggested that average ground-water flow rate in the Woodbine is 10 to 40 ft/yr (3.05 to 12.19 m/yr). Average flow rate in the Twin Mountains is 1 to 4 ft/yr (0.31 to 1.22 m/yr). These velocity estimates suggest that the age of ground water in the regional aquifer system is between approximately 8,000 and 40,000 yr, from west to east across the SSC site in Ellis County.

Ground water use from the deep regional aquifers has gradually increased during the past 30 yr and more than doubled in Ellis County from 1974 to 1988, reaching almost 9,000 acre-ft/yr (11.1×10^6 m^3/yr). Predevelopment water levels in the confined aquifers were reportedly near or above land surface (Thompson, 1967), and direction of ground-water flow is inferred to have been to the southeast (Nordstrom, 1982). A major cone of depression in the potentiometric surface of the Trinity aquifers, owing to the ground-water withdrawals, is centered in the Dallas–Fort Worth area and extends toward the southwest across Ellis County (Nordstrom, 1982). The direction of ground-water flow in Trinity aquifers beneath the SSC ring actually is northwestward toward the Dallas–Fort Worth area under present conditions. During the 1980's the rate of increase in demand for ground-water supplies decreased regionally as new surface-water supplies became available. Waxahachie and Ennis have turned completely to surface-water sources. A few municipalities in the area, including Italy, Glenn Heights, and Midlothian, use ground water for as much as 60 percent of their water. The Texas Water Development Board projects a fairly constant municipal use of ground water from 1990 to 2020 (B. Moltz, unpublished data from Texas Water Plan, 1991). These projections are based on population-growth models. It is possible that water levels will continue to decline during the next 40 yr even if pumpage decreases, if ground-water withdrawals exceed inflow from recharge areas. The possible magnitude of future decline, considering projected demand, recharge at the distant outcrop, and regional ground-water flow, has not been adequately addressed.

Physiography, Climate, and Land Use

Ellis County lies in the Blackland Prairie physiographic province of the West Gulf Coastal Plain. The area lies in the Trinity River watershed. Drainage is largely dendritic, but in some areas stream positions in the Austin Chalk outcrop are controlled by fractures or faults. Regional topography consists of low floodplains, broad, flat upland terraces, and rolling hills. Topographic slope is generally toward the southeast at approximately 0.27°. Topography is remarkably flat across the surface of Pleistocene terraces. The outcrop of the lower Ozan Formation forms rolling hills with highly dissected slopes. Topography over the Austin Chalk outcrop consists of smooth, broad hills with crests of resistant limestone strata. The White Rock Escarpment marks the western limit of the Austin Chalk. The Eagle Ford Formation underlies the broad valley west of the White Rock Escarpment. Land-surface elevation across Ellis County ranges from about 300 ft (91 m) above mean sea level on the lower part of the Trinity River floodplain to about 800 ft (244 m) on the White Rock Escarpment.

Ellis County lies on the boundary between the subtropical humid and subtropical subhumid climatic zones (Larkin and Bomar, 1983). Major climatological factors are the onshore flow of tropical maritime air from the Gulf of Mexico and the southeastward movement of weather fronts across the continental interior. Average low temperature during January, the coldest month, is about 33°F (0.56°C), and average high temperature during July, the hottest month, is about 97°F (36.1°C). Winter and spring are the wettest months, whereas summer rainfall is low. Average annual precipitation is 34 inches (86 cm) in the western part of Ellis County and 38 inches (97 cm) in the eastern part (Thompson, 1967; Larkin and Bomar, 1983). Average annual gross lake-surface evaporation rate is approximately 64 inches (163 cm) in northeastern Ellis County (Larkin and Bomar, 1983).

The economy of the study area is dominated by agriculture, the principal crop being cotton, although sorghum, hay, corn, oats, wheat, barley, and soybeans are also grown. A variety of pesticides and herbicides are used on the crops throughout the area; the most commonly used agricultural chemicals in Ellis County are Atrazine, arsenic acid, Poast, Treflan, Fusilade, Roundup, Tilt, and Glean

(G. Moore, personal communication, 1990). Some livestock is raised. There are several quarries of varying size in the study area that yield limestone, sand, and gravel.

METHODS

Stratigraphy

Variations of petrology and composition within the Austin Chalk, uppermost Eagle Ford Formation, and lowermost Ozan Formation were analyzed in cores from the SSC site (fig. 2). This task was designed to evaluate the correlation of depositional facies and stratigraphy with fracture occurrence and fracture intensity. The Austin Chalk was subdivided into several mappable subsurface zones based on gamma-ray log patterns. A composite stratigraphic section of the entire Austin Chalk was developed on the basis of six slabbed cores, four additional unslabbed cores, and accompanying gamma-ray logs. Additional cores were examined to study lateral changes. Thickness of chalk and marl beds, sedimentary structures, grain size, relative clay content, and macrofauna in the Austin Chalk were logged. Rock color was described using the rock-color chart of the Geological Society of America. Petrologic examination of 109 samples included transmitted-light microscopy of thin sections. Hydrochloric acid-insoluble residues were made, and grain size, total organic carbon, and clay mineralogy of the insoluble component were determined. Composition and fabric of fractured and etched chalk chips were examined by scanning electron microscope (SEM). Stable isotope composition of $\delta^{13}C$ and $\delta^{18}O$ of calcite in the Austin Chalk was measured by mass spectrometry, and porosity and permeability were measured in 1-inch-diameter (2.54-cm) plugs taken from core at selected intervals.

Regional study of the Austin Chalk involved correlation of data from commercial wireline logs, cores, and thin sections. Data also were compared from the overlying Taylor Group and underlying Eagle Ford and Buda Formations but to a lesser extent. Gamma-ray logs were used, and log spacing was designed to examine regional facies changes. Most core and good-quality logs are from hydrocarbon-producing areas of South Texas (fig. 1).

Fracture Studies

Austin Chalk exposures that were studied included quarry walls, road cuts, and natural outcrops, mainly along stream courses. Photographic collages were used for base maps, and electronic distance-measuring devices were used for accurate spacing and length measurements. Fracture spacing was gauged in traverses as long as 1,660 ft (500 m), and fractures were mapped at scales of 1:25 to 1:40 adjacent to faults and in traverses perpendicular to the predominantly northeasterly fracture strike.

Subsurface information collected by The Earth Technology Corporation (1990a) in the vicinity of the SSC was reexamined. The information comprises core and geophysical logs from 86 vertical wells and 13 slant wells in the Austin Chalk and stratigraphically adjacent units. Core depths are shallow, ranging from near surface to 425 ft (130 m). Of a total of 12,765 ft (3,890 m) of 2-inch (5-cm) diameter core, about 11,880 ft (3,621 m) is from chalk not cut by large faults (greater than 15 ft [4.6 m]), providing an excellent perspective on the attributes of regional fracture patterns as seen in core. As discussed later, information on fracture characteristics and fracture distribution was compared to measurements of hydraulic conductivity and chemical composition of ground water.

Well Inventory

Results of a census by Universal Field Services (UFS) mailed to local property owners served as a starting point for a detailed inventory and mapping of water wells. The UFS census asked owners if they had wells on their property. Results were used to prioritize initial field mapping of wells on identified SSC land parcels. Owners or residents of remaining parcels who were not reached by the census were contacted by telephone to arrange a property inspection. Even if the owner indicated that there were no wells, the property was inspected from the road. Any well that had been filled, capped, or abandoned was also mapped and any possible measurements made. For areas off the SSC site, property inspection from roadways and owner interviews provided the necessary information for locating wells.

At each parcel visited, the well was located as accurately as possible on a blueline copy of 1:4,800-scale aerial photographs. Where these detailed aerial photographs were unavailable inside and outside the ring, wells were approximately located on 1:24,000-scale, 7.5-minute topographic maps. Thorough measurements of well depth, diameter, casing height above ground surface, and so forth were made at 362 of the shallow wells. Due to time constraints, each well not on the SSC site was not measured. Data concerning contact with the owner, owner response, and well measurements were recorded on standardized well inventory data forms. Forms were organized in numerical order by parcel number. Each well location was digitized from the aerial photographs or topographic sheets and assigned NAD83 state plane coordinates. Information from well inventory data forms also was transferred into a computerized data base.

Well data are presented in two appendices. Wells located on parcels near the SSC footprint and on the east and west campuses are included in appendix A. Wells located inside and outside the ring are included in appendix B.

Water-Level Monitoring

Water levels were measured to determine the magnitude, frequency, and seasonality of fluctuations. This information is useful for interpreting the nature and amount of recharge to unconfined aquifers and the degree of isolation of ground water in low-permeability rock. Water levels also were measured as part of hydrologic tests and to map the distribution of hydraulic head in the subsurface for estimating direction of ground-water flow. Water-level measurements in surficial alluvium and weathered bedrock were made monthly in 45 shallow wells and each quarter in an additional 50 wells (fig. 3). The wells were selected for monitoring on the basis of their distribution across the study area, depth, geology, well condition, and accessibility. Water levels also were monitored in the 37 wells constructed by The Earth Technology Corporation (TETC) (1990c, d) between May 1989 and September 1990. Measurements in the Superconducting Super Collider Laboratory (SSCL) monitoring wells made before December 1990 were by TETC, after which time the Texas Bureau of Economic Geology (BEG) monitored water levels. The screen interval of the SSCL monitoring wells was set at

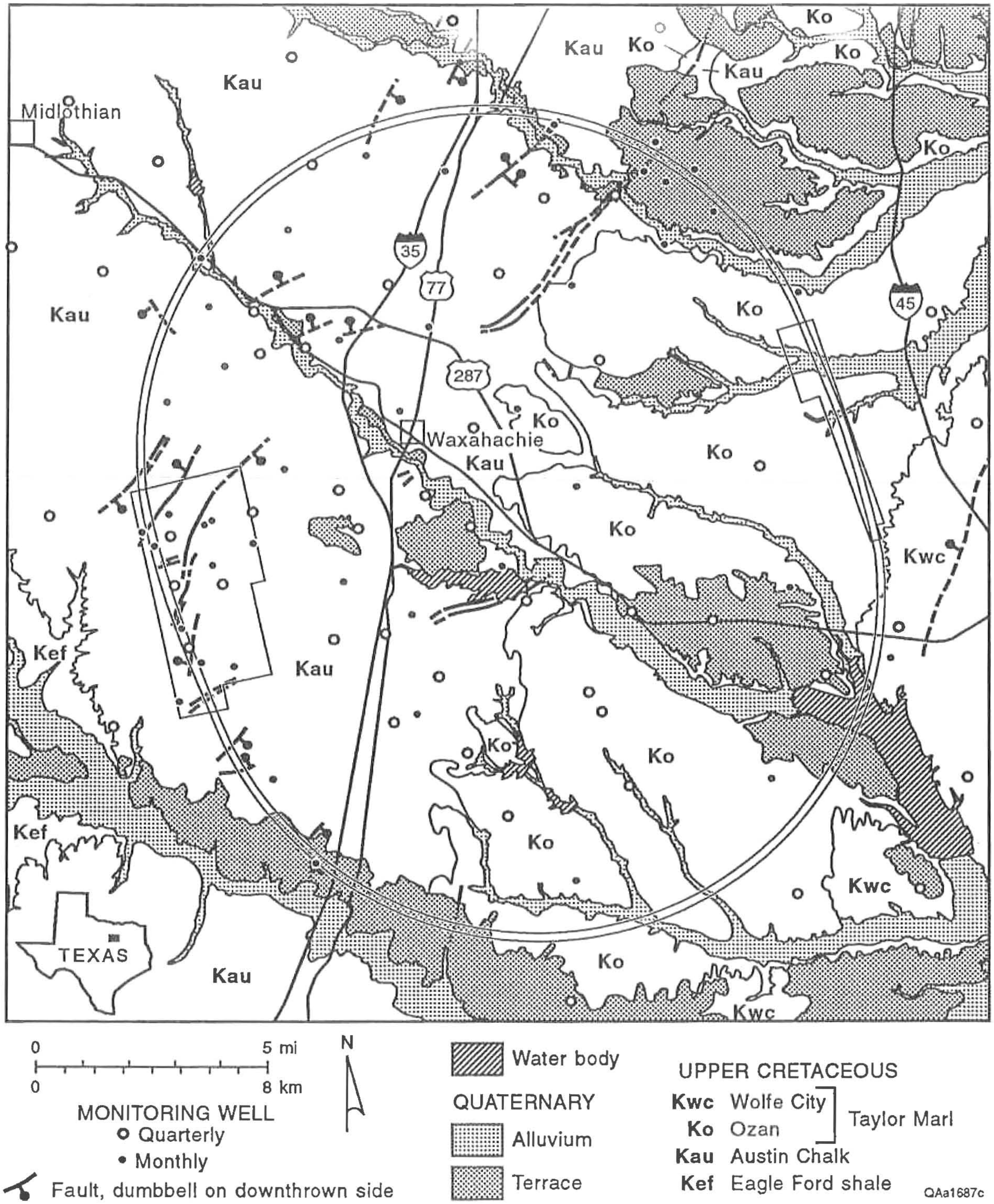

Figure 3. Locations of monitoring wells in weathered bedrock and alluvium used for monthly and quarterly water-level measurements.

the approximate depths where the SSCL subsurface facilities would be constructed. Subsequent design revisions decreased the dip of the plane of the collider ring, however, resulting in many of the monitoring wells on the eastern half of the collider being quite deeper than the final-design collider elevation (The Earth Technology Corporation, 1990c, d). Nonetheless, these monitoring wells in the low-permeability chalk and marl provide a valuable and unique basis for mapping hydraulic head, determining the nature and magnitude of short-term, seasonal, and long-term fluctuations in water levels, and interpreting geologic controls on the occurrence and movement of ground water in the region around the SSC ring.

Water levels were obtained with an electric probe, steel tape, or a pressure transducer. With either the electric probe or steel tape, depth to water was measured relative to the measuring point, usually the top of well casing. Transducers were hung at a given depth in the water column and connected to the data logger. The data logger converts strain across the pressure transducers measured by electrical current to pressure of the water column overlying the transducers and stores the reading in internal memory. Water-column measurements were programmed to be recorded at regular intervals, usually set to 0.5 or 1 hr, giving 24 to 48 readings per day. Stored pressure data were downloaded from the data logger each month and converted to water-level elevations. The various transducers differed in sensitivity; the precision of water-level reading, therefore, was not the same at each well. At three of the SSCL monitoring wells (BF3, BE6, and BIR54), water levels were often above ground surface. Water pressure at these wells was read with a pressure gauge attached to the well head. Pressure gauged in units of pounds per square inch (psi) was converted to hydraulic head in units of feet of water (assuming specific weight of water to be 0.433 psi/ft). Water-level elevation was determined by subtracting depth to water from measuring-point elevation or by adding pressure head to the measuring-point elevation.

Data were plotted as hydrographs to track aquifer response to rainfall events and also to study the magnitude, if any, of daily fluctuations that might be due to evapotranspiration or atmospheric-pressure changes. Monthly and quarterly measurements of water levels, plotted against time, indicated seasonal fluctuations related to recharge and discharge. Plan-view maps of the water table in surficial alluvium and weathered bedrock were constructed for winter (wet) and summer (dry) months.

Barometric Efficiency

Atmospheric-pressure fluctuations, associated with passing weather systems as well as the daily cycle induced by warming and cooling of the atmosphere during day and night, can cause water levels to fluctuate in wells penetrating confined aquifers. Water levels in an open observation well penetrating a confined aquifer fluctuate in response to atmospheric-pressure changes because aquifers are elastic. In response to this change in atmospheric pressure, pressure in the aquifer will respond to return to equilibrium with the atmosphere. Therefore, water will flow into or out of the well to attain this equilibrium. Water levels in wells in confined aquifers fall in response to increases in atmospheric pressure and rise in response to decreases in atmospheric pressure. Atmospheric-pressure changes also can affect water levels in unconfined aquifers. Peck (1960) showed that changes in atmospheric pressure change the volume of trapped air bubbles above the water table. For example, as atmospheric pressure increases, air bubbles compress and water levels decrease. Peck (1960) showed that this effect is greatest where the water table is near land surface. The difference between water-level fluctuations in confined and unconfined aquifers lies in the mechanism causing the fluctuation: compression of solids in a confined aquifer and compression of entrapped gas in an unconfined aquifer. However, water levels in even deep unconfined aquifers can respond to atmospheric-pressure fluctuations. Weeks (1979) showed that changes in atmospheric pressure almost instantaneously affect water levels in a well but that resistance to gas flow through the unsaturated zone retards the average effect on the water table.

Observing and comparing pressure fluctuations in the atmosphere and aquifer allows aquifer properties related to rock elasticity, compressibility of water, porosity, and hydraulic conductivity to be estimated. Thus, monitoring short-term fluctuations in water levels might be used to identify degree of confinement, to determine hydraulic conductivity, and possibly to estimate rock mechanical properties. Comparison between wells might yield insight into the spatial distribution of hydrogeologic properties that control the movement of ground water.

Theory

If the magnitudes of the atmospheric and water-level pressure fluctuations are known, barometric efficiency, B_e, can be calculated as

$$B_e = \frac{\Delta h}{\Delta P_a} \tag{1}$$

where

B_e = barometric efficiency (unitless),

Δh = amplitude of water level change,

ΔP_a = amplitude of barometric pressure change, and

Δh and ΔP_a are in equivalent units, for example, of pressure.

Barometric efficiency represents how efficiently the aquifer absorbs atmospheric-pressure fluctuation. A barometric efficiency of unity indicates that the aquifer is confined and responds fully to the atmospheric pressure. Barometric efficiency usually falls between 0.20 and 0.75 and can be used as an indication of the degree of aquifer confinement between fully unconfined, unconfined with delayed yield, semiunconfined, or fully confined (Kruseman and De Ridder, 1983).

Barometric efficiency is related to the elasticity of the aquifer material (Jacob, 1940):

$$B_e = \frac{n\,E_s}{n\,E_s + E_w} \tag{2}$$

where

n = porosity,

E_s = modulus of elasticity of aquifer material, and

E_w = bulk modulus of elasticity of water.

If E_w and n are known, E_s can be found. Barometric efficiency can also be related to the specific storage, S_s, of the aquifer (Jacob, 1940, p. 582–584):

$$S_s = \frac{npg}{E_w B_e} \tag{3}$$

where

ρ = fluid density

g = gravitational acceleration.

One important source of error is time lag in water-level fluctuations (Freeze and Cherry, 1979). Because aquifer material resists flow, it takes time for the aquifer to respond to the atmospheric-pressure change. Further slowing the response is the well bore storage. More time is needed to reach equilibrium in a large-diameter well than in a small well. These resistance and storage effects are expressed as a phase shift in the water levels (fig. 4). This error is especially important in formations of low permeability and/or wells of large diameter. Fortunately, time lags and phase shifts can be determined and the water levels corrected (Hvorslev, 1951). In the case of sinusoidal water-level fluctuations at steady state:

$$\frac{x_a}{x_a} = cos\left(2\pi\frac{t_s}{T_w}\right) = \frac{1}{\sqrt{1 + \left(2\pi T_o / T_w\right)^2}} \tag{4}$$

where

x_w = water-level amplitude in well,

x_a = pressure amplitude in formation,

t_s = phase shift,

T_w = wave period, and

T_o = time lag.

From equation 4 the phase shift and the fractional decrease in amplitude in the piezometer can be determined with knowledge of the time lag, T_o. Likewise, if the phase shift is known, time lag can be found. However, it is very difficult to accurately determine phase shift directly from water level plots. Therefore time lags are determined from a semilog plot of relative head response over time (Hvorslev, 1951) or determining the cross correlation between atmospheric-pressure and water-level fluctuations.

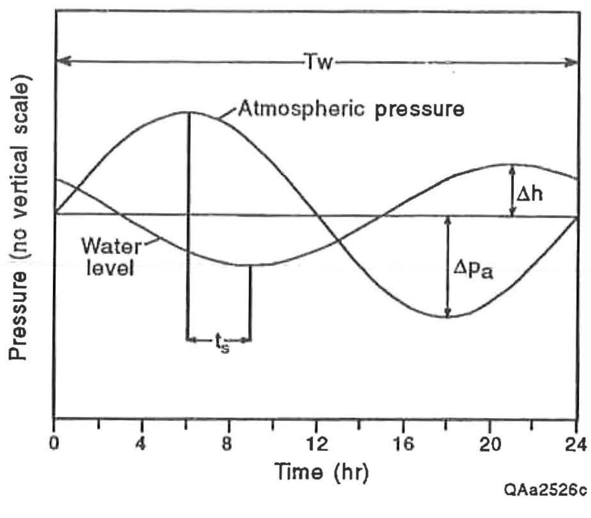

Figure 4. Idealized barometric and water-level fluctuations. *Tw* – wave period, Δh – amplitude of water-level change, Δp_a – amplitude of barometric pressure change, t_s – phase shift.

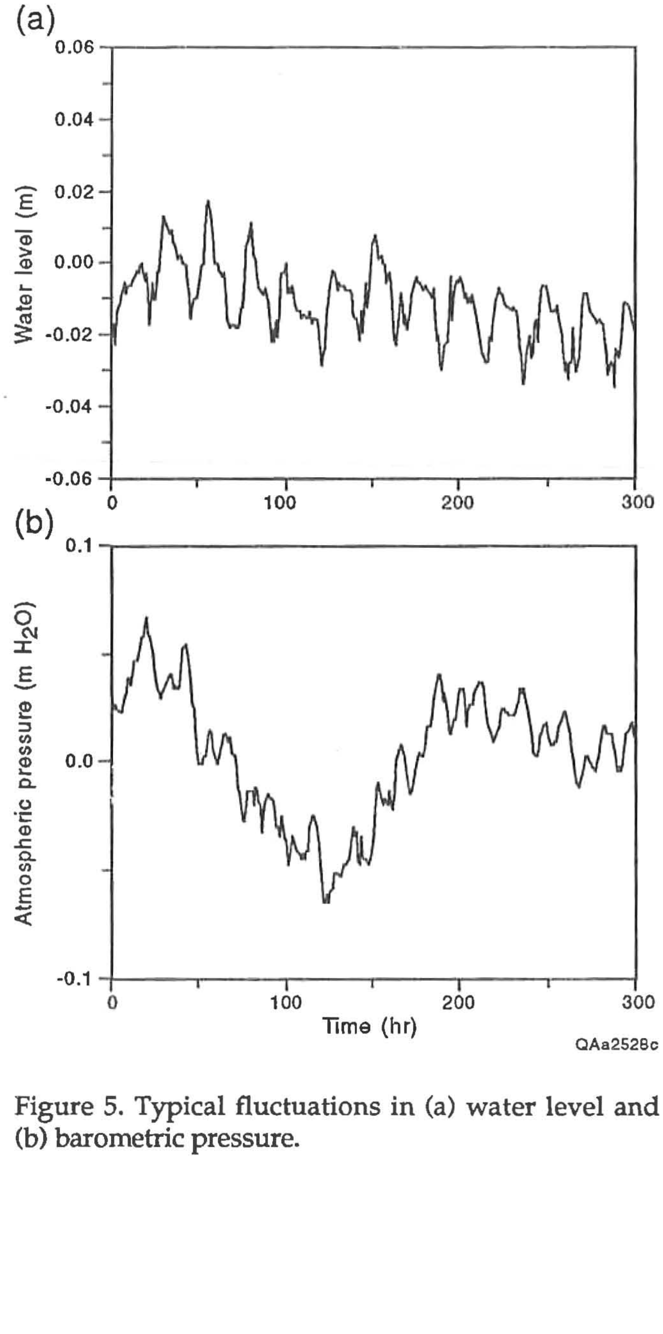

Figure 5. Typical fluctuations in (a) water level and (b) barometric pressure.

Because the time lag is related to how quickly water flows into and out of the formation, it can be used to find hydraulic conductivity (Hvorslev, 1951). Using time lag and well geometry, the hydraulic conductivity is found using an equation commonly used for analyzing piezometer tests:

$$K = \frac{r^2 \ln(L/R)}{2LT_0} \tag{5}$$

where

K = hydraulic conductivity,

r = well radius,

L = length of screen section, and

R = radius of screened casing.

An estimate of hydraulic conductivity obtained by this method is not likely to be very accurate owing to the small radius of the aquifer being tested. A more accurate hydraulic conductivity could be determined from a piezometer test in which a larger portion of the aquifer can be tested. However, this method allows an initial estimate of conductivity, which can be important for aquifer test design.

Analysis Technique

Water-level and barometric-pressure fluctuations are generally found by inspecting atmospheric and water-level pressure plots and recording the amplitudes. Daily water-level fluctuations were monitored at 37 SSC monitoring wells using pressure transducers and data loggers, as previously described. Water levels were recorded every 30 minutes for 2 to 4 weeks. Records were transferred to computer, pressure was converted to meters of water, and hydrographs were drawn (fig. 5). Hourly atmospheric pressure data measured at the DFW International Airport for the period from September 1991 to June 1992 were obtained from the National Weather Service in Fort Worth, Texas.

Because daily fluctuations are time series, harmonic or Fourier analyses are useful for finding mean amplitude of fluctuations for large data sets. Water-level fluctuations and atmospheric fluctuations over the same time periods were harmonically analyzed to determine mean fluctuation amplitudes for one and two cycles per day using algorithms described in Baher (1990). A program was written to use these algorithms and verified by using sinusoidal wave forms of known character. The program output consisted of a power spectrum in which the height of any given frequency represented the mean amplitude of that frequency (fig. 6). The statistics program SPSS (SPSS, 1990) was used to find cross correlations between atmospheric and water-level fluctuations. Any phase shift was identified from this plot (fig. 7). Barometric efficiency was used to calculate the modulus of elasticity and specific storage. The time lag was used to calculate hydraulic conductivity of the formation. This conductivity was then compared to more accurate results from piezometer tests conducted at the well.

Hydrologic Testing

Shallow Wells in the Weathered Zone

Numerous large-diameter wells provide many opportunities for measuring hydraulic conductivity of the weathered bedrock and surficial alluvium. Tests were made during the period between September 1991 and June 1992 at 43 shallow wells in the weathered Austin Chalk and Ozan Formation (fig. 8). The wells were chosen for testing using the well inventory as a guide.

Several analytical and numerical methods have been proposed for analyzing hydrologic test data from large-diameter wells. Papadopulos and Cooper (1967) developed type curves for analyzing drawdown data from large-diameter wells in confined aquifers. Sammel (1974) discussed various methods based on experience in India. Wikramaratna (1985) improved the type curves of Papadopulos and Cooper (1967). Fenske (1977a) extended the Theis equation to allow finite diameter and storage capacity in abstraction and observation wells. Other authors investigated the effects of leaky layers (Lai and Su, 1974), decreasing abstraction rates (Lai and others, 1973; Rushton and Singh, 1984), fractured aquifers (Kumaraswamy, 1973; Zdankus, 1974; Barker, 1985), well loss (Chachadi and Mishra, 1992), unconfined conditions (Boulton and Streltsova, 1976), and different well-face boundary conditions (Rajagopalan, 1983). In addition, a discrete kernel method (Patel and Mishra, 1983) and the Cooper-Jacob approximation (Chapatis, 1992) have been used to consider storagae effects.

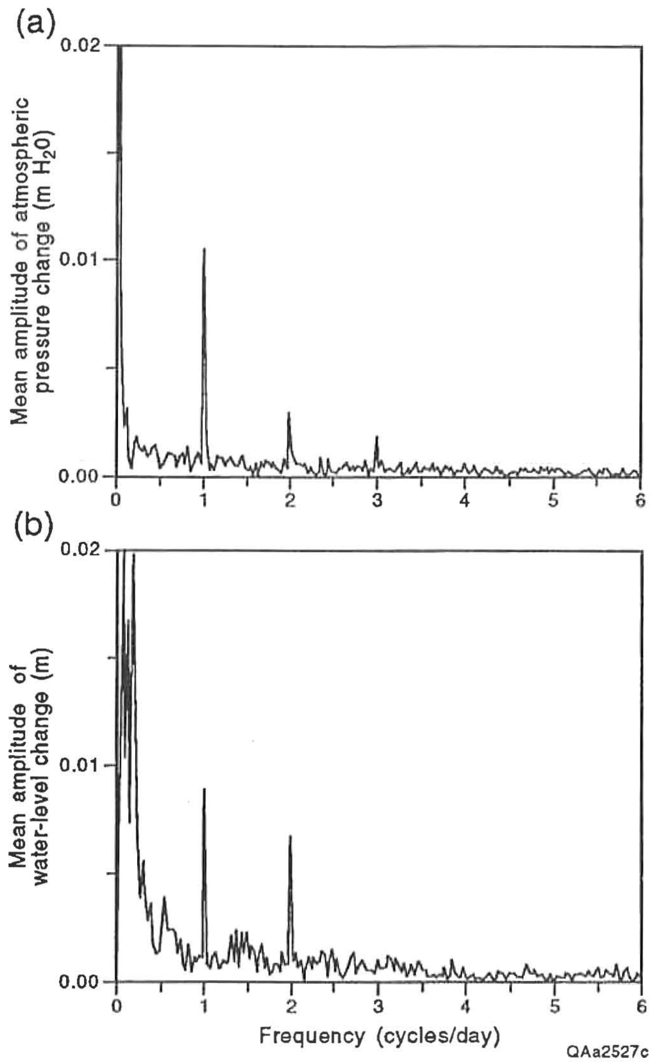

Figure 6. Harmonic analysis of typical fluctuations in (a) barometric pressure and (b) water level.

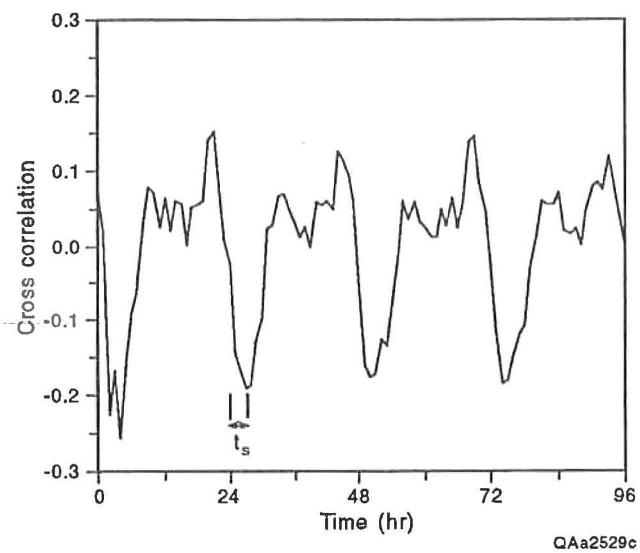

Figure 7. Example of cross correlation between water level and barometric pressure. t_s – phase shift.

(a)

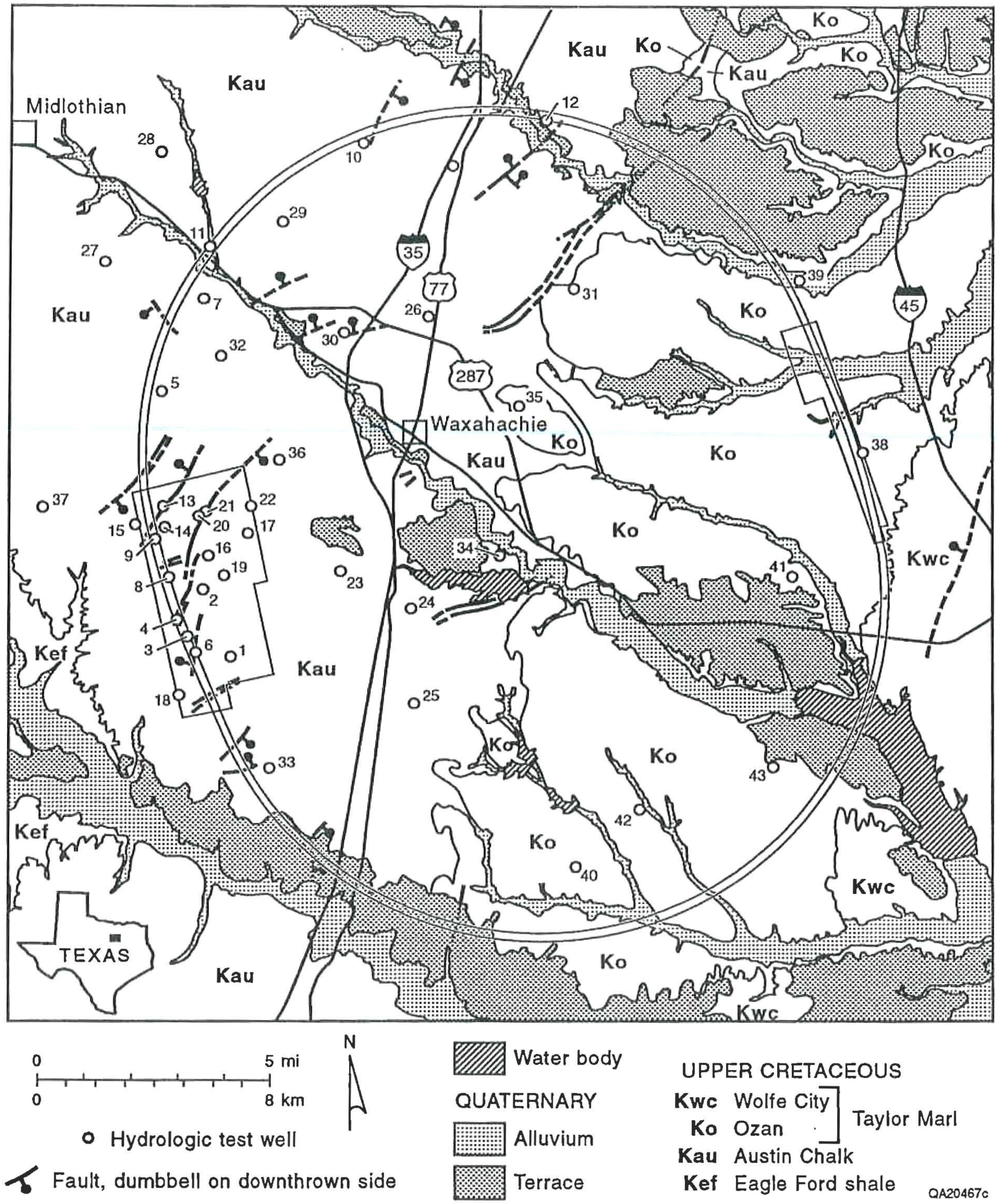

Figure 8. Locations of wells used for (a) measuring hydrologic properties and (b) collecting water samples for chemical analyses from the surficial aquifer and springs in fractured chalk.

(b)

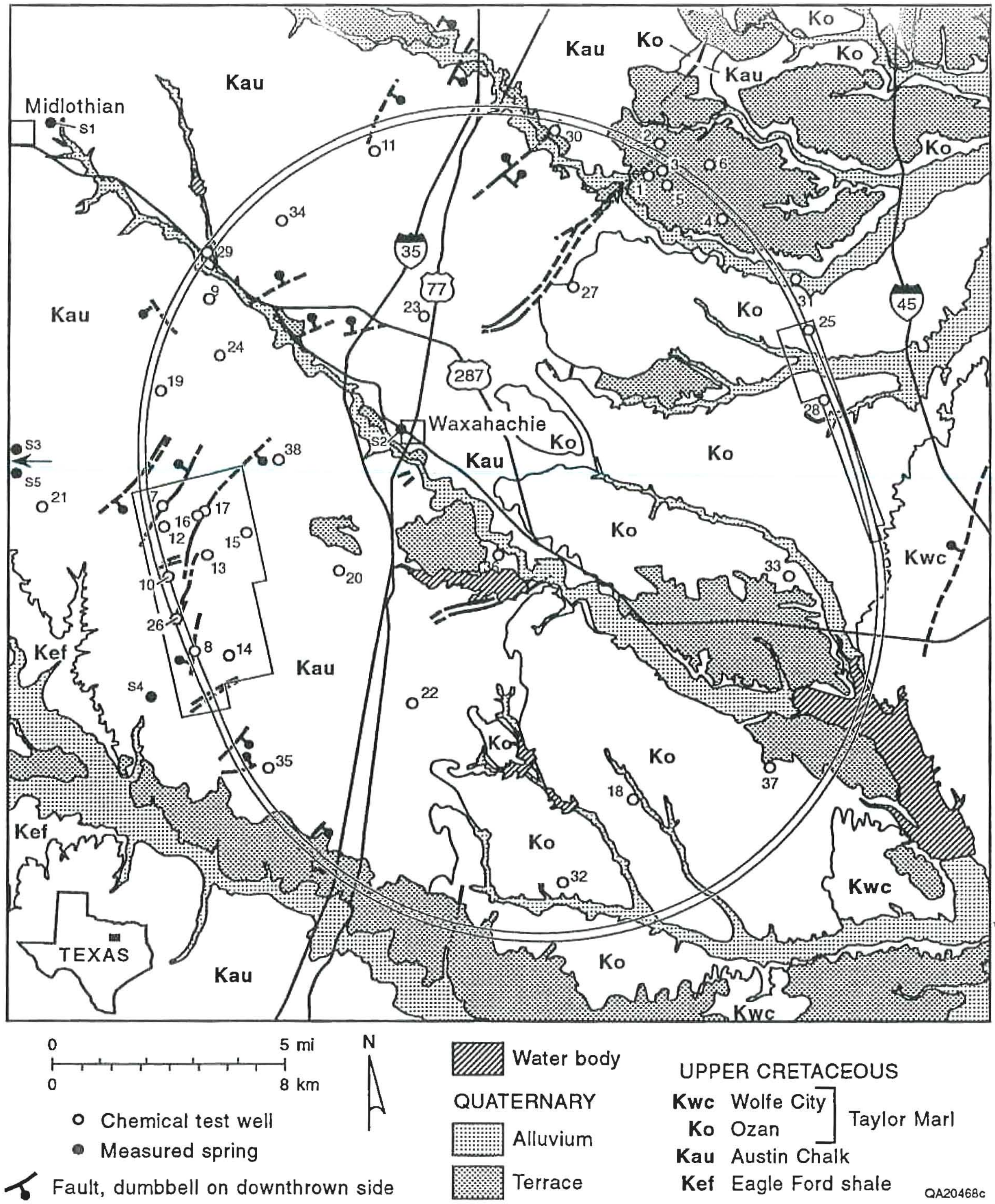

Figure 8 Cont.

Many of the above methods rely on water-level drawdown data to determine aquifer properties. Drawdown data might not be practical for analysis because large-diameter wells are commonly found in rocks of generally low storativity and transmissivity, such as limestone or crystalline rock. For instance, Papadopulos and Cooper (1967) state that ideal Theis behavior is not observed during pumping tests until

$$t > 250\frac{r_c^2}{T} \tag{6}$$

where

t = time since start of pumping,

r_c = radius of the well casing, and

T = transmissivity of the aquifer.

For a well-casing radius of 2 ft (0.6 m) and aquifer transmissivity of 5 ft^2/d (0.46 m^2/d), approximately 200 days of low-yield pumping are required before an accurate estimate of transmissivity can be obtained using Papadopulos and Cooper's (1967) curve-matching technique.

To circumvent this limitation, methods have been developed that use water-level recovery to estimate aquifer properties. Fenske (1977b) produced a set of type curves that account for well bore storage in water-level recovery. Herbert and Kitching (1981) used models to derive an empirical equation and a shape factor for recovery data. Mishra and Chachadi (1985) applied the discrete kernel method to water-level recovery in a large-diameter well. Several authors described numerical methods to simulate both drawdown and recovery (Rushton and Holt, 1981; Rajagopalan, 1983; Barker, 1989; Sakthivadivel and Rushton, 1989).

Apparently overlooked in the literature is the use of piezometer tests for analyzing water-level recovery data where well bore storage is significant. Piezometer tests, which include slug and bail tests, are commonly used to estimate hydrologic properties in relatively impermeable material (Hvorslev, 1951; Cooper and others, 1967; Bouwer and Rice, 1976; Bouwer, 1989). Type curves developed by Fenske (1977b) approach those of Cooper and others (1967) when recovery time is much greater than jumping time. The Cooper and others (1967) method, therefore, can be used for interpreting tests that meet this requirement. Barker and Herbert (1989) suggest using slug-test methods for very tight formations that are below the range of applicability for their method.

The design of the bail-type tests used in this study at large-diameter wells followed procedures of Herbert and Kitching (1981). No more than 10 percent of a well's water column was pumped out. A 1/3-hp submersible pump or a centripetal pump was used, and the 10-percent drawdown was made in approximately 1 hr. The falling and subsequently recovering water levels were recorded with a data logger and pressure transducer, as previously described. Drawdown also was measured manually using a water-level electrical probe. Discharge rate was measured using a stopwatch and a calibrated 5-gal bucket.

For interpreting the recovery data, this study evaluated eight methods (appendix C):

(1) 50- and 90-percent-recovery methods (Herbert and Kitching, 1981),

(2) nomogram method (Barker and Herbert, 1989),

(3) time-lag permeability test with shape factors (Dracher, 1936, as cited by Hvorslev, 1951; Schneebeli, 1966, as cited by Chapuis, 1989),

(4) slug-test method (Cooper and others, 1967; Bouwer and Rice, 1976),

(5) convolution method (Singh and Gupta, 1986),

(6) simulation and analysis programs (Barker, 1989), and

(7) finite-difference modeling (appendix D).

The first two methods are empirically derived from numerical solutions, methods three and four are piezometer tests, and methods five through seven are numerical solutions and models. The methods of Bouwer and Rice (1976), Barker (1989), Barker and Herbert (1989), and Hvorslev (1951), and the 50-percent-recovery method of Herbert and Kitching (1981) were found most applicable as non-numerical solutions. Only the values from the Herbert and Kitching 50-percent-recovery method were used in calculating mean hydraulic parameters. The other methods were used only for comparison. For the purpose of analysis, wells were considered fully penetrating.

SSCL Monitoring Wells in Unweathered Bedrock

The 37 SSCL monitoring wells provide the only opportunities for hydrologic testing and sampling of ground water in the unweathered bedrock of the Eagle Ford Formation, Austin Chalk, and Ozan Formation. The Earth Technology Corporation (1990e) conducted packer tests of hydraulic conductivity in uncased boreholes during construction of the monitoring wells and other special-purpose test wells. Their test results were reevaluated in terms of this study's data on fracture characteristics and fracture distribution. Most (42) of the 77 reported values were from the Austin Chalk. Tests also were conducted at the contact between the Austin Chalk and the Eagle Ford Formation (13), at the contact between the Austin Chalk and Ozan Formation (10), and within the Ozan (7) and Eagle Ford (5) Formations. Tests were done by packing off a test interval of varying lengths and injecting water at selected pressures while flow rate was measured with a cumulative flow meter. Pumping was continued until consecutive readings indicated stabilization of flow rate, and hydraulic conductivity was calculated using standard Bureau of Reclamation procedures. Locations of tested wells are shown in figure 8.

In two monitoring wells shown by packer tests to have the highest permeability, BI3 and BF9, hydraulic conductivity was tested during this Phase II study by pumping water from the well and measuring the relationship between discharge and drawdown and recovery. The pump used was either a reciprocating-piston, positive-displacement pump, powered by an air compressor, or a 2-inch-diameter (5-cm), submersible electric pump. A test at the BIR41 well, likewise selected on the basis of the earlier packer-test data, failed because pumping rate exceeded ground-water inflow rate. Water-level drawdown data were analyzed using standard techniques described by Theis (1935), Walton (1970), and Cooper and Jacob (1946). Recovery data from the pumping test were analyzed using the Theis recovery method (Kruseman and De Ridder, 1983).

Yield of water at the remaining wells was too small, owing to low hydraulic conductivity, to sustain pumping at even 0.5 gal per minute (gpm [0.032 L/s]). Hydrologic tests at these low-permeability intervals, therefore, were performed by bailing or pumping water from the well and monitoring water-level recovery. Estimates of hydraulic conductivity were made in 20 of the 37 SSCL monitoring wells on the basis of these piezometer (slug) tests. Recovery data were analyzed using various methods including (1) Bouwer and Rice (1976), assuming unconfined conditions, (2) Ferris and Knowles (1954), assuming an instantaneous line source for the water-level change in the well, and (3) Cooper and others (1967), accounting for the finite diameter of the well. The Cooper and others (1967) method is considered more realistic than the Bouwer and Rice (1976) or Ferris and Knowles (1954) methods. The Cooper and others (1967) method is an exact solution for water-level response to an instantaneous charge of water. The Bouwer and Rice (1976) method depends on early time data. The Ferris and Knowles (1954) solution assumes an instantaneous line source to account for water-level change and ignores well bore storage.

Water-level drawdown and recovery were recorded using a transducer and data logger, as previously described. A laptop computer connected to the data logger allowed direct monitoring of water-level changes during tests. Water-column measurements were programmed to be recorded at time intervals varying with rate of water-level change. Discharge rate during the pumping tests was measured with a stopwatch and 1-liter graduated cylinder.

Permeabilities of five core plugs, taken from the unfractured section of rock core from well BI3, corresponding in depth to the screened interval, were determined by Core Laboratories, Inc., using the standard Hassler Sleeve method.

Review of Construction Problems at Monitoring Wells

The typical SSCL monitoring well was constructed by placing a 2-inch (nominal)-diameter, schedule-40 PVC pipe with a 20-ft-long (6.1-m) screen in a 6.75-inch (nominal)-diameter bore hole drilled with mud-rotary method (The Earth Technology Corporation, 1990b, d). The annulus between the pipe and formation was backfilled with sand to a height of 2 to 6 ft (0.61 to 1.83 m) above the top of the screen, topped with a 2 to 6 ft (0.61 to 1.83 m) layer of 1/4-inch bentonite pellets and followed by cement grout to land surface. The grout was pumped into the annulus. The wells were bailed to varying degrees for well development after completion.

Water samples were collected for chemical analyses from all 37 SSCL monitoring wells. About 40 percent of the sampled wells yielded water having an anomalous chemical composition with pH generally greater than 11, a neutral-pH titration-equivalence point, and very low to negligible dissolved magnesium (Mg^{2+}) content. The SSC Laboratory and the U.S. Army Corps of Engineers ran a televiewer survey in 31 of the 37 SSCL wells in June 1992 to identify well-construction problems that might explain the anomalous composition of water samples (U.S. Army Corps of Engineers, 1992). About 48 percent of the logged wells showed some wellbore problem such as broken or unscrewed casing joints and evidence of inflow of cement (table 2). Wells with some construction problems were found to account for 12 of the 15 water samples (80 percent) with anomalous chemical compositions; two wells that yielded samples with anomalous chemical compositions were not logged. Wells that were found in good condition account for 15 of the 22 water samples (68 percent) with a chemical composition normal for limestone and marl; 4 wells that yielded samples with normal chemical compositions were not logged (table 2). This correspondence clearly shows that the anomalous chemical composition is related to well-construction problems. The most likely source of the anomalous chemical composition is calcium-hydroxide (CaOH) from cement grout (Lin-Hua and Atkinson, 1991). It seems most likely that this CaOH water entered the well either through gaps in casing or through the screened section where the sand pack and bentonite seal were not effective. It is possible that the contamination continues, with the high pH, CaOH water reentering wells that are purged and that temporarily yield a normal ground water (Lin-Hua and Atkinson, 1991).

Table 2. Comparison of normal and anomalous chemical compositions of water samples in terms of observed well construction problems.

	Well condition			
Water composition	Good	Problem	Not logged	Total
Normal	15	3	4	22
Anomalous	1	12	2	15
Not analyzed	0	0	0	0
Total	16	15	6	37

For comparison with reported depth, total well depth was remeasured using a 200-ft-long (60.1-m) fiberglass tape with a plumb weight. The discrepency between reported design depth and plumbed depth generally was less than ± 3.5 ft (± 1.1 m), which could be partly due to stretch in the fiberglass tape and to error in taking up slack when the plumb weight reached total depth. Where plumbed depth was much less than design depth, as at wells BE4, BI6, BI2A, B1597, and B1697B, an obstruction in the well or plugging of the bottom of the well by cement is suggested. Cement plugging was confirmed at B1597 by a bailed sample and at the other wells by video photographs (U.S. Army Corps of Engineers, 1992).

Results of chemical analyses of samples from these "problem" wells cannot be used to infer chemical composition of naturally occurring ground water. It is uncertain whether a prolonged effort in well development and purging of water from the well will remove all contamination and yield a natural ground water. The well-construction problems also cast some doubt on the validity of results of hydrologic testing and of measurements of water-level fluctuations at these wells.

Chemical Sampling and Analyses

Where yield of water at SSCL monitoring wells was small, water samples for chemical analyses were collected using a PVC bailer. Where yield of water at SSCL monitoring wells was high enough to sustain pumping, either a reciprocating-piston, positive-displacement pump or a small-diameter, submersible electric pump was used for water sampling. Where sustained pumping was possible, samples were collected after several wellbore volumes had been pumped from the well. Pumped samples are expected to best reflect water contained within the subsurface formation and to be least affected by residence time within the wellbore.

Figure 8 shows the locations of samples collected for chemical analyses from springs and from shallow wells in the weathered zone. Water samples from the weathered zone were taken at 20 wells at which hydrologic tests had been conducted. At well R875-4 (no. 32, fig. 8a), several wellbore volumes were pumped before samples were collected from the discharge line. At other shallow wells, it was infeasible to pump several wellbore volumes because of their large storage capacity and low aquifer discharge. Water was purged from these wells, therefore, and samples were taken after water level recovered enough to allow efficient bailing. Samples from springs were collected by using the hydraulic head of the spring discharge to drive water through tubing into a sample filtering chamber.

Water sampling followed standard techniques (Feltz and Hanshaw, 1963; Gleason and others, 1969; Brown and others, 1970; Wood, 1976; Hassan, 1982). Temperature, pH, and Eh were measured in a flow cell connected to the water-discharge line from the sample pump. Temperature of spring water was measured with a thermometer placed into the surficial fracture or fissure from which the spring is discharged. For bailed-well and spring-water samples, temperature and pH were measured in the sample container, but Eh was not measured. Pumped samples were filtered through an in-line disposable 0.45-µm filter connected to the discharge line. Bailed samples and spring samples were filtered by pressurizing a sample container with nitrogen (N_2) gas to drive water through the 0.45-µm filter. Alkalinity was measured by titration of unfiltered samples with a standard dilute (approximately 0.02 N) HCl solution at field sites or within several hours of collection; alkalinity measurements were repeated in the laboratory. Water samples for determination of cation concentrations were acidified in the field with 6N HCl or HNO_3. Dissolved carbon for ^{14}C and $\delta^{13}C$ analyses was precipitated from water samples at well sites using a pH-buffered $SrCl_2$ reagent. Sample bottles were sealed with tape and kept cool during storage and delivery to the laboratory. Most cations were analyzed using inductively-coupled plasma-optical emission spectrometry; silver was measured by flame atomic adsorption and mercury by cold-vapor atomic adsorption. Chloride, sulfate, fluoride, nitrate, and bromide were determined by ion chromatography. Carbon-14 and $\delta^{13}C$ were analyzed by scintillation counting at Beta Analytic, Inc. Tritium was determined by low-level proportional counting of water samples that had undergone electrolytic enrichment at the University of Miami Tritium Laboratory. Radioactive isotopes dissolved in ground water were analyzed to establish a baseline record of ambient concentrations. Samples were collected in 1-gal plastic containers and analyzed for

^{7}Be, ^{22}Na, ^{45}Ca, ^{54}Mn, ^{60}Co, ^{40}K, ^{137}Ca, total radium, and isotopic thorium. Total exchange capacity and exchangeable-ion composition in samples of chalk, organic-rich marl, marl, and bentonite cored from the Austin Chalk section were analyzed following standard methods for NH_4^+ displacement to constrain the simulations.

Geochemical Modeling

Mineral saturation, activity coefficients, ionic molalities, and rock-water reaction paths were calculated by geochemical modeling programs SOLMINEQ*88 (Kharaka and others, 1988), PHRQPITZ (Plummer and others, 1988), and PHREEQE (Parkhurst and others, 1980).

Bottom-Hole Temperature in SSCL Monitoring Wells

Bottom-hole temperature was measured with an Envirolab temperature probe. The calibration of the probe was checked; it spanned 32° F (0°C) in an ice bath to 212° F (100°C) in boiling water. The probe was lowered to total depth in the monitoring wells; that is, until the cable went slack. Reported well depth was accepted as the depth of the probe. Temperature readings were made for several minutes to check for drift owing to thermal equilibration, but no meaningful trend was observed in that timeframe.

Stream Flow Gauging

Discharge rate was gauged in streams fed by springs issuing from fractures in the Austin Chalk at several sites in Ellis County. The objectives of the stream gauging were to determine the amount of base flow added to the streams from springs and seeps along the stream courses and to monitor seasonal fluctuations in stream discharge.

Flow rate was measured using a mini-type current meter (Buchanan and Somers, 1969). Locations of the springs are shown in figure 8b. At each station, a straight stream reach with a relatively smooth channel bed was chosen. The same section of stream was repeatedly gauged at each station. Stream width was less than 5 ft (1.52 m) and depth of water was less than 0.5 ft (0.15 m). A folding wood ruler lain across the stream perpendicular to the direction of flow was used to divide the stream into uniform increments of 3 or 4 inches (7.62 or 10.16 cm). At the midpoint of each increment, the depth of water was measured and the bucket wheel of the current meter placed at 0.6 times the depth from water surface. The number of revolutions of the bucket wheel was counted over an interval of time and recorded. The manufacturer's calibration chart related revolutions to flow velocity. The velocity was then multiplied by the width and depth of the increment to arrive at a value of discharge for that increment. The sum of the incremental discharges gives the total discharge for that section of the stream.

Numerical Modeling of Ground-Water Flow

Numerical simulation of ground-water flow in chalk and marl was used as an interpretive tool to better understand ground-water circulation and travel times. These influence the fate of contaminants, including potentially radioactivated ground water. MODFLOW, a block-centered, finite-difference computer program (McDonald and Harbaugh, 1988), was used to simulate ground-water flow. The model's governing equation is the three-dimensional, partial differential equation describing ground-water flow:

$$\frac{\partial}{\partial x}\left(K_{xx}\frac{\partial h}{\partial x}\right) + \frac{\partial}{\partial y}\left(K_{yy}\frac{\partial h}{\partial y}\right) + \frac{\partial}{\partial z}\left(K_{zz}\frac{\partial h}{\partial z}\right) + W = S_s\frac{\partial h}{\partial t} \qquad (7)$$

where

x, y, and z are Cartesian coordinates of the system,

K_x, K_y, and K_z are hydraulic conductivities in the x, y, and z directions,

h is the hydraulic head,

W is a volumetric flux per unit volume representing sources and sinks,

S_s is the specific storage, and

t is time.

All simulations used the strongly implicit procedure (SIP). Convergence criteria for hydraulic head changes were set to 0.001 ft (0.0003 m).

A variety of models were constructed and simulated. In their Phase I study, Wickham and Dutton (1991) defined a two-dimensional horizontal (plan-view) model of flow in surficial alluvium at the SSC site. This Phase II study developed vertical, cross-sectional models. A cross-sectional model consists of more than one layer but only one horizontal dimension, for example, one row with numerous columns. By design, a profile model assumes that all flow is within the plane of the profile (Anderson and Woessner, 1992). Therefore, equation 7 is only required for two dimensions, x and z. For simulating steady-state flow of ground water, the right side of equation 1 becomes zero.

Three cross-sectional models were constructed (fig. 9): a NE-SW profile across the west campus (A–A′), a NW-SE profile across Ellis County (B–B′), and a NE-SW profile across the east Campus (C–C′).

The sections were oriented along predominant flow lines. Sections A–A′ and B–B′ were constructed to evaluate regional flow of ground water in the weathered and unweathered bedrock. Section C–C′ was constructed to evaluate effects of interaction-hall excavation on ground-water flow. Table 3 defines the dimensions of the models.

Boundaries of the cross-sectional models were chosen to coincide with natural hydrological boundaries, such as topographically low areas or surface-water divides. Model sides therefore could be treated as no-flow boundaries. The boundaries were located far enough from areas of interest to minimize unwanted boundary effects. The southwestern end of the West Campus model, for example, was placed at Chambers Creek, a topographic low, and the northeastern end at a topographic high. The northwestern boundary of the Ellis County model was placed at Lake Joe Pool, a topographic low, and the southeastern boundary was placed on Walker Creek east of the SSC ring. The base of sections A–A′ and B–B′ were placed in and at the bottom of the Eagle Ford to identify whether ground water circulated in the shale. The upper surface of these models used the general head boundary package in MODFLOW (McDonald and Harbaugh, 1988). The upper boundary represented the seasonal mean water level in the surficial aquifers, generalized at about 8 ft (2.44 m) below land surface. Model bottoms also were assumed to be no-flow boundaries.

Vertical/horizontal anisotropy ratio was adjusted by trial and error. Permeability values for weathered bedrock and unweathered chalk, marl, and shale were initially assigned based on field test results, then were adjusted by trial and error. Fracture zones were represented as equivalent porous media to assess the effect fracture-enhanced permeability would have on fluid circulation and particle travel times.

MODPATH (Pollock, 1989) was used to find ground-water pathlines and residence times. MODPATH uses hydraulic head and cell-by-cell flow output files from MODFLOW along with a porosity file to make calculations. A program was written to statistically analyze particle residence times and to calculate particle velocities. Using the flux inflow data from the general head boundary package, particles were proportionally placed in each active surface cell and allowed to travel until discharged from another cell. This indicated the movement of water from recharge to discharge points. Travel times were calculated for the entire model and for individual zones. Sensitivity of particle travel time, path, and velocity was evaluated by varying both vertical and horizontal hydraulic conductivities by a factor of 1,000.

Table 3. Dimensions of ground-water flow models.

Section	A–A′	B–B′	C–C′
Number of layers	52	58	22
Number of columns	142	170	120
Column width (ft)	303	1,000	variable
Layer thickness (ft)	10	30	variable
Section length (ft)	43,026	170,000	8,200
Section height (ft)	520	1,740	500
Active nodes	5,959	4,704	2,640

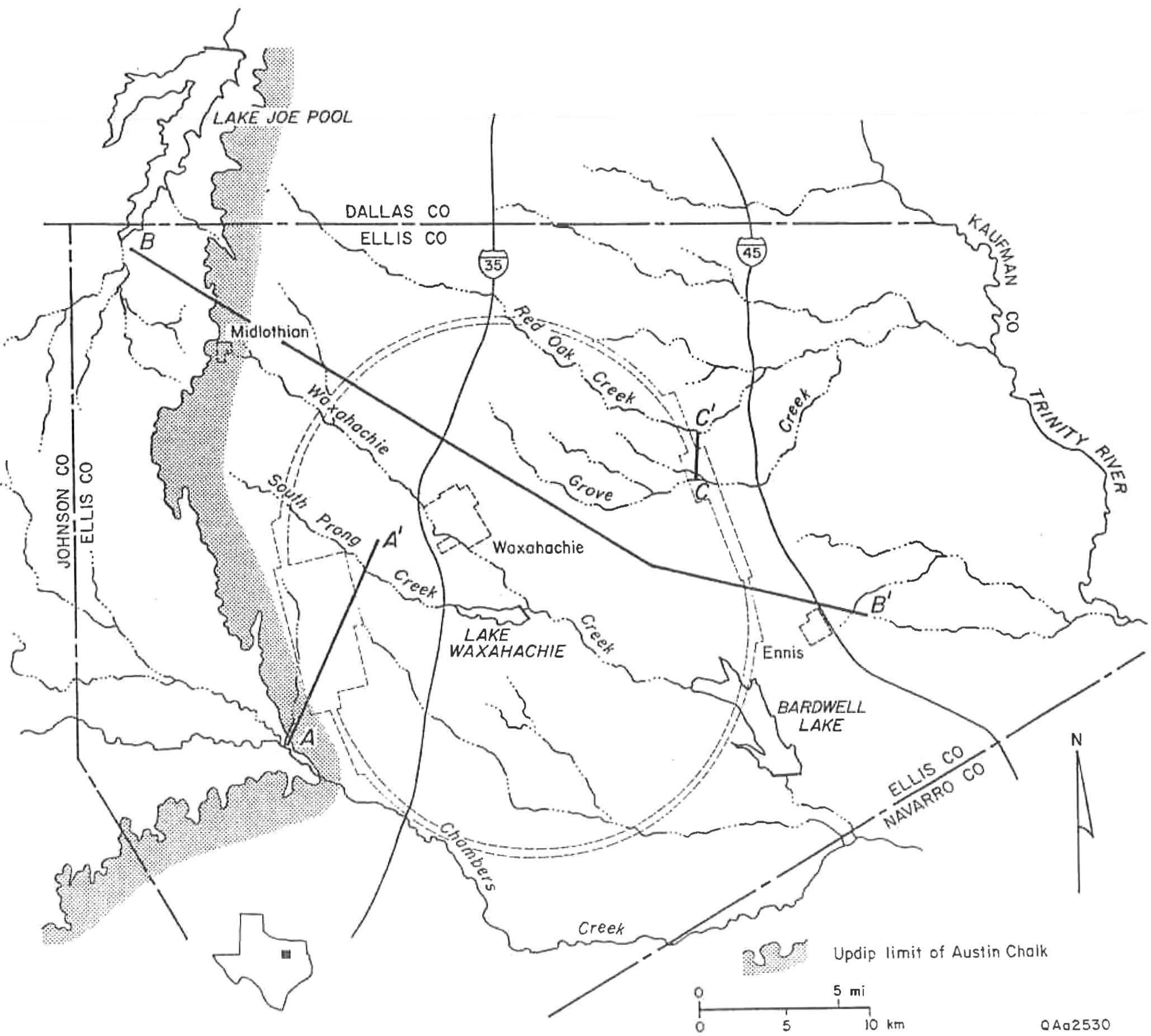

Figure 9. Projections of vertical profile models of ground-water flow. A–A′ is the West Campus model, B–B′ is the Ellis County model, and C–C′ is the Interaction Hall model. Also shown are major surface-water features.

PETROLOGY OF THE AUSTIN CHALK AT THE SSC SITE

Summary

Worldwide sea-level highstand during the upper Cretaceous (Coniacian–Santonian) resulted in displacement of siliciclastic and shallow-water carbonate environments and formation of planktonic oozes in moderately deep-water, high-productivity, flooded continental shelves. Rhythmically interbedded chalk and marl of the Austin Chalk were deposited over an extensive platform in Texas. Facies of the Austin Chalk are defined by variations in character of the cycles, including character of the chalk-marl contacts, biogenic contribution and amount of reworking of the carbonate fraction, and marl composition and presence of lamination. Variations in petrologic characteristics of chalks and marls reflecting evolution of the depositional environment have subtle effects on the mechanical behavior of the rock (for example, fracture spacing and weathering characteristics) and on the geochemistry of the rock and water in contact with the rock.

The middle Austin Chalk typically has lower porosity and permeability and greater ductility compared to the upper and lower Austin Chalk. These properties are controlled by clay distribution around and between individual coccoliths rather than clay content. The distribution of clay is interpreted to be a product of authigenic alteration of minor but frequent volcanic ash falls during chalk deposition. Volcanic materials sourced from Cretaceous volcanism along the Balcones fault trend and from more distant silicic volcanic provinces influence the clay distribution and therefore the mechanical properties of the chalk and marl.

Subtle vertical facies changes in the Austin Chalk in Ellis County reflect

- marine flooding (phosphate/glauconite/quartz-sand-rich condensed section);
- maximum relief (locally channeled, macrofauna-poor, strongly cyclic unit);
- deepest water (high organic/low detrital marls);
- shallowing (increased silicalstic detrital as well as volcanic material, and development of firmgrounds and oyster communities.

- continued shoaling (local winnowed carbonate accumulations); and
- resumption of detrital siliciclastic accumulation (Ozan Formation overlying the Austin Chalk).

Introduction

The Austin Chalk in central Ellis County at the SSC site is an approximately 400- to 500-ft-thick (121.9- to 152.4-m) sequence of chalk beds alternating with thinner marl beds. Matrix porosity and permeability are low, but the unit is fractured both along fault zones and by more widely spaced regional fracture systems, as discussed in the following section and by Collins and others (1992). Understanding the distribution of these fractures is key to understanding ground-water flow in the Austin Chalk in Ellis County as well as hydrocarbon production in South Texas.

Petrologic studies of the Austin Chalk, the upper part of the underlying Eagle Ford Formation, and the lower part of the overlying Ozan Formation ("lower Taylor Marl") were undertaken to support hydrologic studies at the SSC site in central Ellis County. The focus of this study is on petrologic characteristics that might influence rock-mechanical properties, especially fracture spacing, and genetic relationships between petrologic characteristics and depositional and diagenetic evolution of chalk and marls. The petrologic study is focused on a detailed study of facies, chalk-marl cyclicity, composition, and fabric of the Austin Chalk and adjacent units within Ellis County. Locations of cored wells used in this study are shown in figure 2.

Stratigraphic Setting

The widespread distribution and lithologic homogeneity of the Austin Chalk (fig. 1) reflect its deposition in a pelagic shelf environment with water depths of less than approximately 300 ft (91.4 m) (Dawson and Reaser, 1985) during worldwide sea-level highstand during the Coniacian and Santonian stages of the Late Cretaceous (fig. 10). Marls of the overlying Ozan Formation (lower Taylor Marl) and underlying Eagle Ford Formation indicate increased siliciclastic deposition in neritic environments

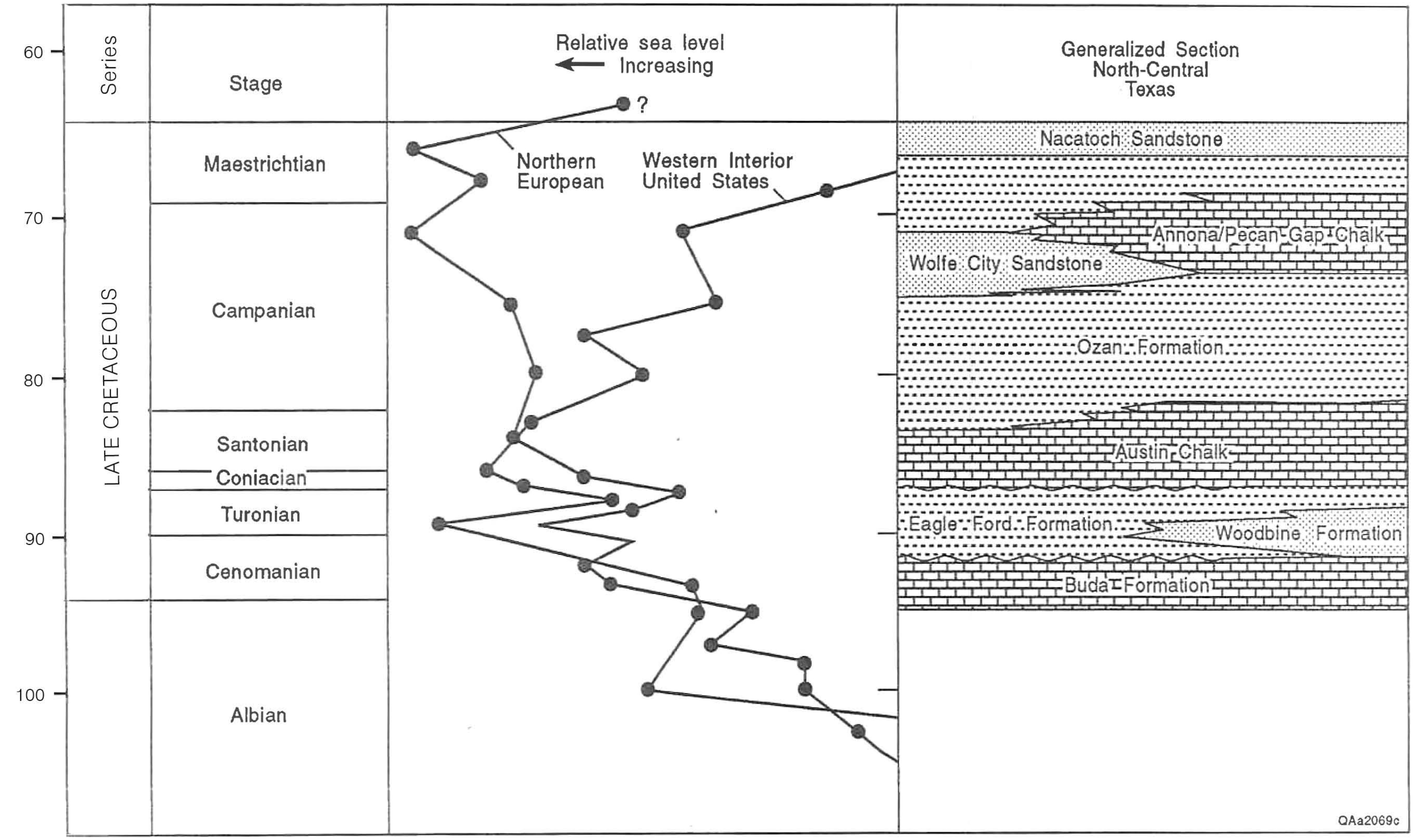

Figure 10. Sedimentation on the Texas shelf and its relationship to sea-level curves. Formations and ages from Pessagno (1969), Marks and Stam (1983), Thompson (1983), and Phillips (1987). Sea-level curves from Hancock and Kauffman (1979).

during lower sea-level stands (Beall, 1964; Charvat, 1985; Phillips, 1987). High productivity of calcareous nonnoplankton during chalk deposition produced soft bottom conditions that restricted bottom environments to specially adapted faunas such as inoceramids (Kennedy, 1975; Dawson and Reaser, 1985). Exceptions are where sediment erosion and long episodes of nondeposition allowed development of firmgrounds or hardgrounds suitable for growth of more diverse oyster and other mollusk communities. Multiple episodes of burrowing typically blur or eliminate sedimentary structures in chalk. Distant source areas for terrigenous clastics a... low-energy bottom environments limited detrital siliciclastic input. Contemporaneous basaltic volcanism along the trend of the Balcones Fault Zone in Central and South Texas (Ewing, 1986) and more distant Laramide volcanic centers are other potential sources of siliciclastics in the Austin Chalk.

Formal stratigraphy and biozonation of the Austin Chalk have been extensively discussed (table 4). The lower contact of the Austin Chalk with the Eagle Ford Formation in the Ellis County area is thought to be an erosional unconformity, with chalk deposition beginning near or below the Turonian–Coniacian boundary (McNulty, 1965; Pessagno, 1969; Reaser, 1989). Thickness changes within the Eagle Ford and the Austin Chalk are attributed to erosion of the Eagle Ford prior to chalk deposition (Beall, 1964; The Earth Technology Corporation, 1990a) as well as movement on faults (Beall, 1964). The upper contact of the Austin Chalk with the Ozan Formation is more controversial. Some investigators interpret the sharp lithologic change as a phosphatized lag, firmground, or an erosional unconformity with tens of meters relief (Smith, 1955; Durham, 1957; Hallgarth, 1959; Pessagno, 1969; Tucker and Henecy, 1987; Durham and Hall, 1991). Others (Fürsich and others, 1981; Marks and Stam, 1983; Young and Woodruff, 1985; Podell and others, 1993) consider the contact to be a time-transgressive facies change, locally marked by phosphatized hardgrounds with the amount of time missing so minor that it is faunally unresolvable. Structural influence on Ozan sedimentation has been described by Ewing and Caran (1982) and Surles (1983).

Lateral facies changes within the Austin Chalk include shoaling over the San Marcos Arch and deepening to the south and southwest toward the platform edge (Dravis, 1980; Thornhill, 1982; Young and Woodruff, 1985). The shallow-water facies of the Austin Chalk have been removed by erosion

Table 4. Literature on stratigraphy and biozonation of the Austin Chalk.

Topic	Author	Contribution
Austin Chalk facies/stratigraphy, regional	Durham and Hall, 1991	Correlation and facies analysis
	Miller, 1978	Outcrop–subsurface study
	Young and Woodruff, 1985	Regional facies relationships
Austin Chalk facies/stratigraphy, North-Central Texas	Baker, 1982	Subsurface isopachs
	Brown, 1981	Subsurface
	Champlin, 1976	Surface to subsurface cross section
	Dawson and Reaser, 1985	Depositional environments
	Dawson and others, 1980	Outcrop to subsurface correlations
	Koger, 1981	Surface to subsurface correlations
	McNulty, 1965	Eagle Ford–Austin Chalk relationships
	Reaser, 1989	Outcrop descriptions
	Seewald, 1959	Regional lithologic description
	Smith, 1955	Channels within the Austin Chalk, conformable Austin–Taylor contact
	Stehli and Creath, 1969	Biofacies maps
	Stehli and others, 1972	Depositional environments
	Surles, 1983	Subsurface isopachs
	The Earth Technology Corporation, 1990a	Stratigraphy at the SSC site
Austin Chalk facies/stratigraphy, Central Texas	Young and others, 1975	Shallow-water (McKown Fm.) around volcanic plug
	Young, 1986	Regional stratigraphy
	Young and others, 1985	Facies around volcanic plug
Austin Chalk facies/stratigraphy, south-central and south Texas	Dravis, 1991	Depositional environments
	Lock, 1984	Channel facies in outcrop
	Martinez, 1982	Subsurface sections, maps, South Texas
	Scholle, 1977a–c	Synthesis of chalk sedimentology
	Thornhill, 1982	Subsurface correlations

Table 4 (cont.)

Topic	Author	Contribution
Austin Chalk biozonation, regional	Barrier, 1980	Based on coccoliths
	Marks and Stam, 1983	Austin–Taylor contact is time transgressive
	Pessagno, 1967	Correlation and foraminiferal biozonation
	Smith, 1981	Calcareous nannoplankton
Austin Chalk biozonation, North-Central Texas	Bottjer and Bryant, 1980	Nature of Austin–Taylor contact
	Fürsich and others, 1981	Minimal time missing at Austin–Taylor unconformity
Austin Chalk biozonation, Central Texas	Hallgarth, 1959	Local unconformities related to volcanic plug
	Young, 1963	Ammonite zonation

along most of its outcrop. Longoria (1991) has proposed that the younger Anacacho Formation in Bexar County resembles the shallower-water facies and fauna of the Austin Chalk. Shallow-water facies developed around volcanoes that built to wave-base during chalk deposition (Young and others, 1975).

Diagenetic modification of the Austin Chalk, like that of most chalks, has been simple relative to shallow-water limestones. Pressure solution and porosity loss with depth are the dominant diagenetic processes (Cloud, 1975; Dravis, 1980; Scholle and others, 1983). The Austin Chalk in Ellis County has not been deeply buried and therefore has had minimal diagenetic modification. Other aspects of burial alteration discussed in the literature are vein formation (Corbett and others, 1991a), hydrocarbon generation (Grabowski, 1984; Hunt and McNichol, 1984), and the extent to which the Austin Chalk is an isotopically open (sufficient fluids introduced from outside the chalk after burial to modify its stable isotope chemistry) or closed system (Scholle and Cloud, 1977; Czerniakowski and others, 1984).

Results

Depositional Environments of the Austin Chalk

The Austin Chalk was deposited in a moderately deep-water shelf setting that resulted from marine flooding of the craton during sea-level highstand. Lithologic changes therefore reflect variations in percentages of the components of chalk. These components are

- nannoplankton tests (dominantly coccoliths),
- sand-sized plankton (dominantly foraminifers),
- macrofauna (dominantly inoceramids, oysters, and *Gryphaea*),
- glauconite,
- phosphatic bones, scales, and teeth and reprecipitated phosphatic nodules,
- macerated organic carbon, and
- fine siliciclastic/volcaniclastic clay with lesser amounts of silt and sand.

The dominant end-member lithologies recognized in core and thin section in this study are shown in table 5. Variation in the percentages of these materials defines beds less than 3 ft (<1 m) thick. Recognition of patterns in the interbedding between different lithologies defines cycles. In this study, facies definition focused on cycle patterns. Seven facies are identified in cores (table 6). The depositional environments of each facies with respect to depth and current and wave energy are interpreted in table 6.

Stratigraphy of the SSC Site

Thirteen subsurface units (fig. 11) are delineated on the basis of gamma-ray patterns (table 6). Units T, A, B, C, and D are approximately correlative with the lower Austin Chalk defined by a moderate response on commercial spontaneous potential (SP) logs (fig. 12). Units E through I are approximately equivalent to the low-SP middle Austin Chalk, and units J, K, and L to the slightly higher and variable SP upper Austin Chalk. The units delineated based on log character were then

Table 5. Dominant lithologies within the Austin Chalk.

Lithology	Composition
Chalk	>67% nannoplankton, lesser amounts of sand-sized plankton, broken and intact macrofauna, and siliciclastics
Marl	>33% siliciclastics; the remainder is nannoplankton, sand-sized plankton, and broken and intact macrofauna
Organic marl	Organic material abundant enough to give the bed a dark color, >10% siliciclastics, also nannoplankton, sand-sized plankton, and broken and intact macrofauna
Skeletal packstone	33% broken and intact macrofauna; the remainder is nannoplankton, sand-sized plankton, and siliciclastics
Globigerinid/inoceramid packstone	33% sand-sized plankton and/or broken macrofauna in a matrix of nannoplankton and siliciclastics
Bentonite (altered volcanic ash)	Macroscopically recognizable bed or blebs of white montmorillonite and associated silt-sized biotite, quartz, and feldspar admixed with other lithologies by burrowing organisms

Table 6. Summary of characteristics of Austin Chalk facies.

Lithology	Cycle type	Log character	Energy/depth
Skeletal packstone, nannoplankton chalk, ± glauconite, ±VRF's	Thick, upward-fining, irregular thicknesses, bounded by hardgrounds and firmgrounds	Low to high GR (glauconite), low to high SP (cementation)	Shoal, winnowed environment
Nannoplankton chalk with inoceramids, marl	Meter-thick cycles	Low GR, high SP	Low energy, outer shelf
Nannoplankton chalk with oysters, marly chalk, marl	Poorly defined meter thick cycles	Low GR, low SP	Shoaling, shelf marginal to most distal neritic
Nannoplankton chalk, dark, laminated marls with inoceramids	Meter-thick, well-defined cycles	High GR marls, moderate SP	Deep, stratified outer shelf
Globigerinid/ inocermid prism packstone, nannoplankton packstone	Meter-thick discontinuous beds	Low GR, moderate SP	Channel fill in outer shelf fan
Nannoplankton chalk, organic marls	Decimeter cycles, laminated marls, stylolite bounded	Moderate GR, low SP	Outermost shelf/slope
Dark nannoplankton chalk, organic marls	Decimeter cycles, millimeter lamination locally	Moderate to high GR, low SP	Outermost shelf/slope

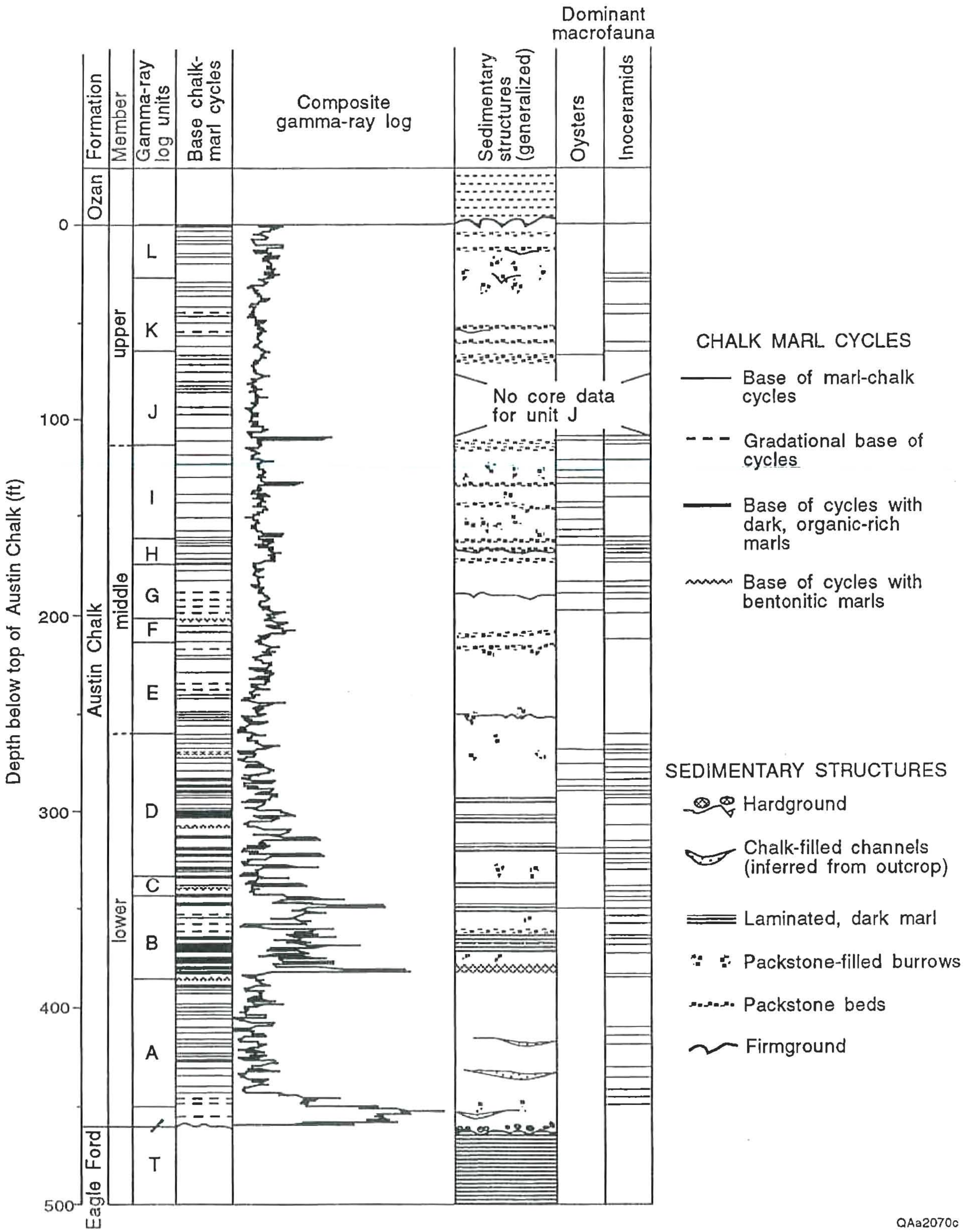

Figure 11. Composite section of Austin Chalk. Conventional (upper, middle, and lower) stratigraphic subdivision of the Austin Chalk is based on SP log correlations of Champlin (1976, shown in Dawson and others [1983]). The approximate relationship between the wireline stratigraphic units of Werner and others (1990) developed for the SSC and those developed for this study are shown. Informal units and bed numbers assigned in this study on the basis of gamma-ray character are difficult to trace outside of Ellis County.

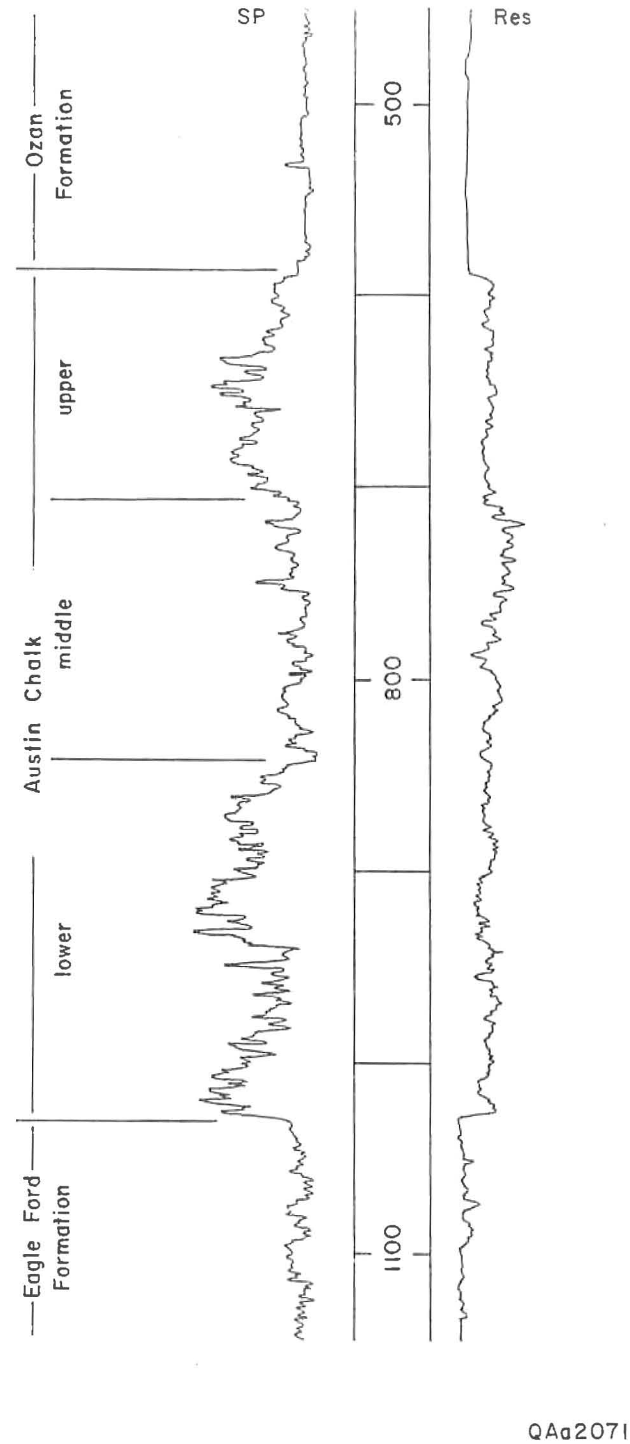

Figure 12. Commercial wireline log showing typical SP log character of the Austin Chalk in Ellis County. SP logs from the SSC wells have an atypical character because the boreholes were drilled with water rather than with drilling mud and therefore were not used for this study.

examined in core. Individual gamma-ray peaks were matched to marl beds and assigned unique letter-number references (fig. 11). Subtle changes in petrologic features and fauna characteristic of subsurface units can be recognized in outcrop, although the discontinuous nature of most outcrops rarely allows identification of individual beds or unit boundaries. Projection of subsurface units to the surface were used to produce a geologic map and structural cross sections. The distribution of gamma-ray defined subsurface units identified in the field and projected from the subsurface corresponds to the general outcrop divisions of the lower, middle, and upper Austin Chalk in Ellis County (Dawson and others, 1983).

The 13 informal subsurface units defined for this study generally agree well with the wireline units prepared by Werner and others (1990) (fig. 11). Two major differences are that there is some offset in stratigraphic boundaries and that part of the upper Austin Chalk is missing from the stratigraphic section described by Werner and others (1990). Stratigraphic boundaries in this study were consistently set at the base of marls in order to facilitate cycle-based analysis, resulting in minor differences with the results of Werner and others (1990). The composite stratigraphic section of Werner and others (1990) is based on early borehole and core data; the "missing" upper Austin Chalk interval was not cored or logged during this initial drilling phase. This "missing section" was identified by recorrelating newer geophysical logs (for example, BE5). Adding this interval to the cross section, however, has little impact on the interpretation of the structure or stratigraphy at tunnel depth, the major effect being to slightly increase dips along the eastern part of the ring.

The stratigraphy and structural variability of the Austin Chalk were examined around the SSC ring and used to construct a three-dimensional stratigraphic model. This, in turn, was used to construct structural cross sections, which were then used for hydrologic modeling (fig. 9). Thicknesses of the informal units were mapped around the ring; most exhibited little systematic thickness variation, except as noted in the following discussions. Although a large number of logs and cores are available from the SSC ring, the data set is inadequate for characterizing stratigraphic variability in detail because

- boreholes were drilled only to tunnel depth, so that the stratigraphic overlap is minimal in different parts of the ring;
- most core has been preserved whole for engineering purposes; therefore, it is unsuitable for stratigraphic study, which requires slabbed core in order to observe sedimentological features; and
- thickness of units has been slightly modified by fracture or dip changes, obscuring subtle changes in the thickness of units.

The typical lithologies, cycle character, and petrology of each informal unit are described next.

Eagle Ford Formation

The Eagle Ford Formation underlying the Austin Chalk in Ellis County is approximately 300- to 425-ft-thick (91.4- to 129.5-m) dark-gray (rock color N3 [Geological Society of America, 1979]) calcareous shale. It is laminated and somewhat fissile. Flattened small burrows are locally recognizable. Pyrite and limonite nodules and burrow casts are present. In outcrops just west of Midlothian, large calcite and siderite septarian nodules (Dawson and others, 1983) are found in two layers about 33 and 43 ft (10.1 and 13.1 m) beneath the Austin Chalk contact. The septarian nodules are localized in slightly siltier layers near the top of the Eagle Ford that are regionally identified on logs by increased SP and resistivity response.

Lower Austin Chalk

The lowermost subsurface Austin Chalk unit "T" (6.9- to 14.1-ft [2.1- to 4.3-m] thick) includes the gradational transition from the basal sandstone and conglomerate into typical chalk lithologies with an upward-decreasing gamma-ray response. The basal sandstone and conglomerate is 0.3 to 2.3 ft (0.1 to 0.7 m) thick and is composed of quartz and glauconite in a clay matrix (fig. 13a). Phosphate nodules, phosphatic teeth, skeletal material, and carbonized wood are abundant. The top of the conglomerate is laminated and intraclastic (fig. 13b). The overlying 6.6 ft (2 m) is composed of admixtures of material

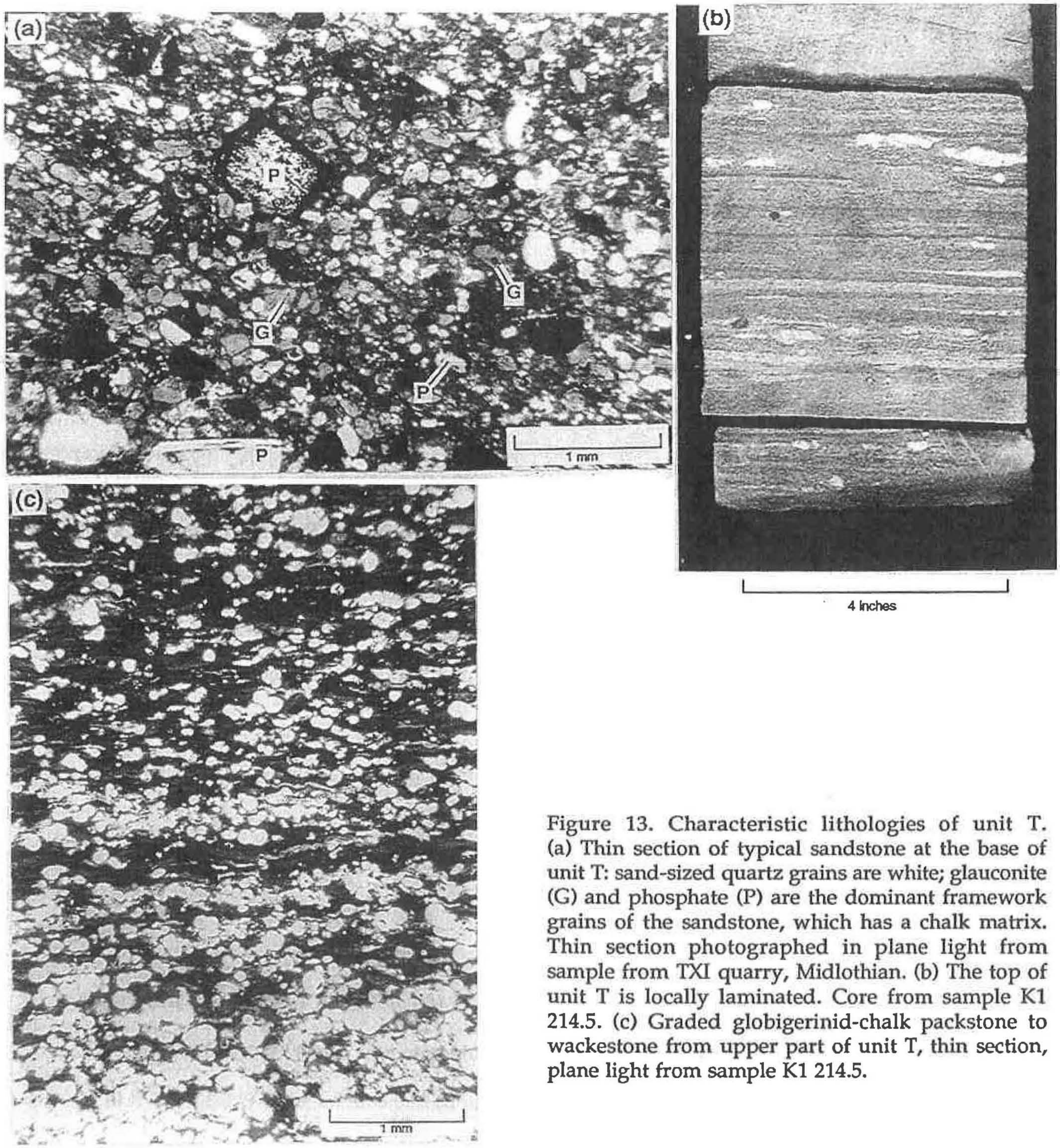

Figure 13. Characteristic lithologies of unit T. (a) Thin section of typical sandstone at the base of unit T: sand-sized quartz grains are white; glauconite (G) and phosphate (P) are the dominant framework grains of the sandstone, which has a chalk matrix. Thin section photographed in plane light from sample from TXI quarry, Midlothian. (b) The top of unit T is locally laminated. Core from sample K1 214.5. (c) Graded globigerinid-chalk packstone to wackestone from upper part of unit T, thin section, plane light from sample K1 214.5.

from the sandstone beds and chalk. Some graded beds are globigerinid packstones to wackestones (fig. 13c). In outcrop, unit T is dark gray (N3 [Geological Society of America, 1979]) and appears massive (fig. 14b).

Unit "A" (57.7 to 67.9 ft [17.6 to 20.7 m]) is cyclic Austin Chalk with low gamma-ray response in both the chalk and marl (fig. 15). Unit A thickens to the east in Ellis County. Macrofauna is less abundant in unit A than elsewhere in the Austin Chalk, with fragmented robust inoceramids the dominant grain (fig. 14a). In outcrop, unit A forms resistant cliffs along the White Rock Escarpment (western edge of the Austin Chalk outcrop) (fig. 14b). Channels are noted in unit A outcrops in TXI quarry, Midlothian. Channels are 0.7 to 6.6 ft (0.2 to 2 m) deep and as much as 82 ft (25 m) wide (fig. 14c, d). They cut through the marl and into the chalk of the underlying cycles. Channels are filled with one or more chalk and marl couplets that thin and merge toward the channel margins. One sample of channel fill is a well-sorted globigerinid and chalk-intraclast grainstone (fig. 14e). Channels are characteristically observed regionally in unit A, representative of this stratigraphic interval but possibly influenced by the preferential siting of large quarries in this interval. In the subsurface, marl beds throughout unit A have a low gamma-ray response. A prominent (2-ft- [0.6-m-] thick) bentonite bed marks the base of unit B.

Unit "B" (34.1 to 42.0 ft [10.4 to 12.8 m] thick) has the highest gamma-ray response in the Austin Chalk, 60 to 100 counts per second (cps), and is strongly cyclic (fig. 15). Marls are dark (N5 to N7 [Geological Society of America, 1979]) and some are conspicuously laminated. Thin-shelled inoceramids and sand-sized inoceramid prisms are concentrated (relative to chalk) in some marl beds (fig. 16a, b). Localized firmgrounds marked by packstone-filled vertical burrows are identified near the top of unit B. The contact between units B and C is defined by the sharp decrease in gamma-ray response (figs. 11 and 15).

Unit "C" is 13.8 to 20.0 ft (4.2 to 6.1 m) thick. Both chalk and marls have lower gamma-ray response than do units B and D. Two of the low-gamma marl beds within unit C contain white clay-rich patches interpreted as bentonite admixed with marl by burrowers. Intact and fragmented inoceramids are more abundant than in unit A.

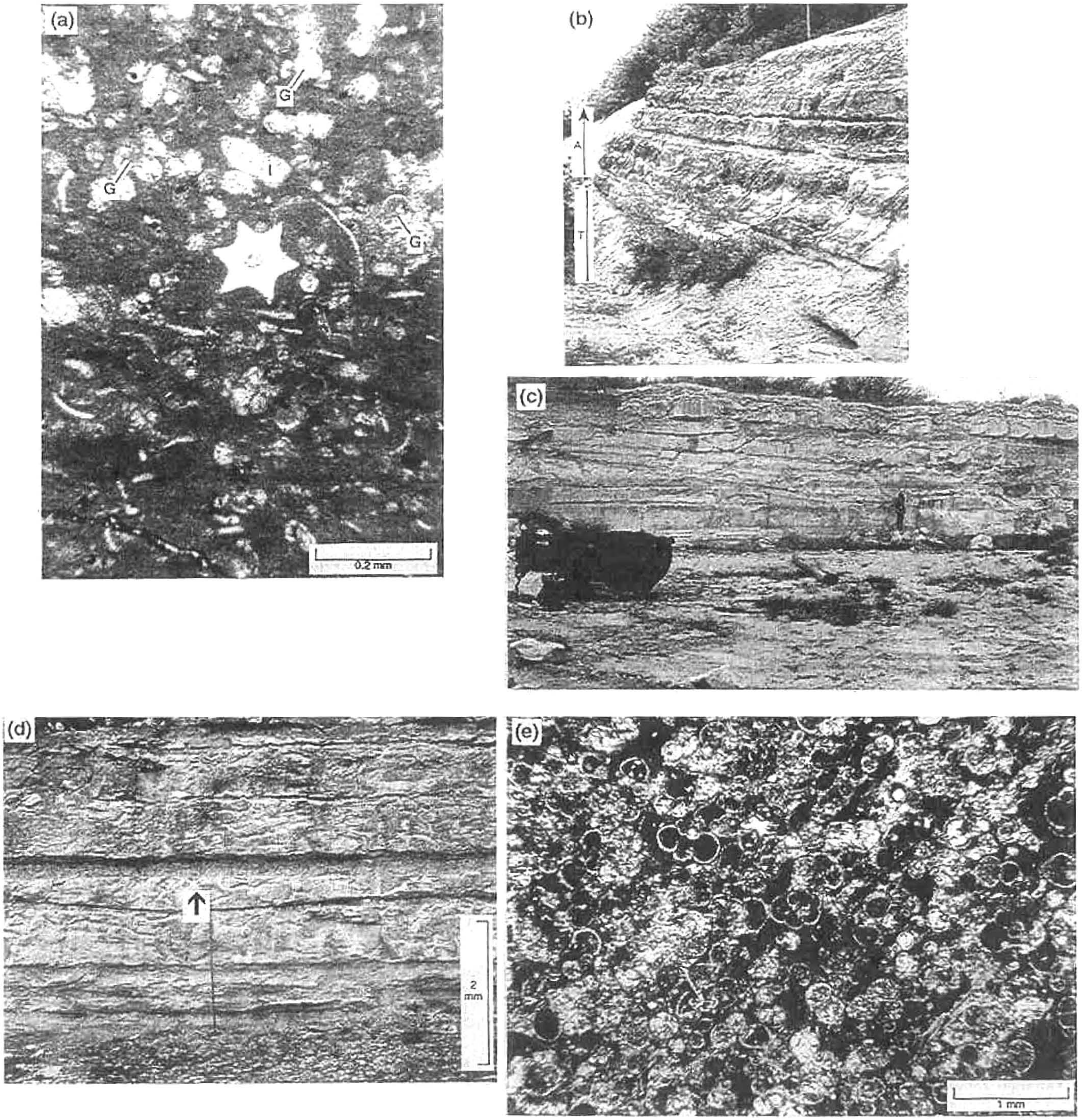

Figure 14. Characteristic lithologies of unit A. (a) Typical chalk in thin section. Inoceramid-globigerinid packstone, sample K1 178.0. Star-shaped grain is an echinoderm plate. (b) Resistant cliffs typical of unit A in outcrop, north side of Beltline Road, Cedar Hill, southern Dallas County. "T" indicates the generally massive upper part of unit T; the overlying highly cyclic beds are unit A. (c) Large chalk-filled channel cuts into the underlying cycles and contains several beds of fill, lower part of unit A, TXI Quarry, Midlothian. (d) Small channel cuts into only underlying marl bed, Clark Street, High Pointe subdivision, southern Dallas County. (e) Photomicrograph of globigerinid intraclast grainstone from a small channel-fill deposit from the TXI Quarry, Midlothian. Photographed in plane light.

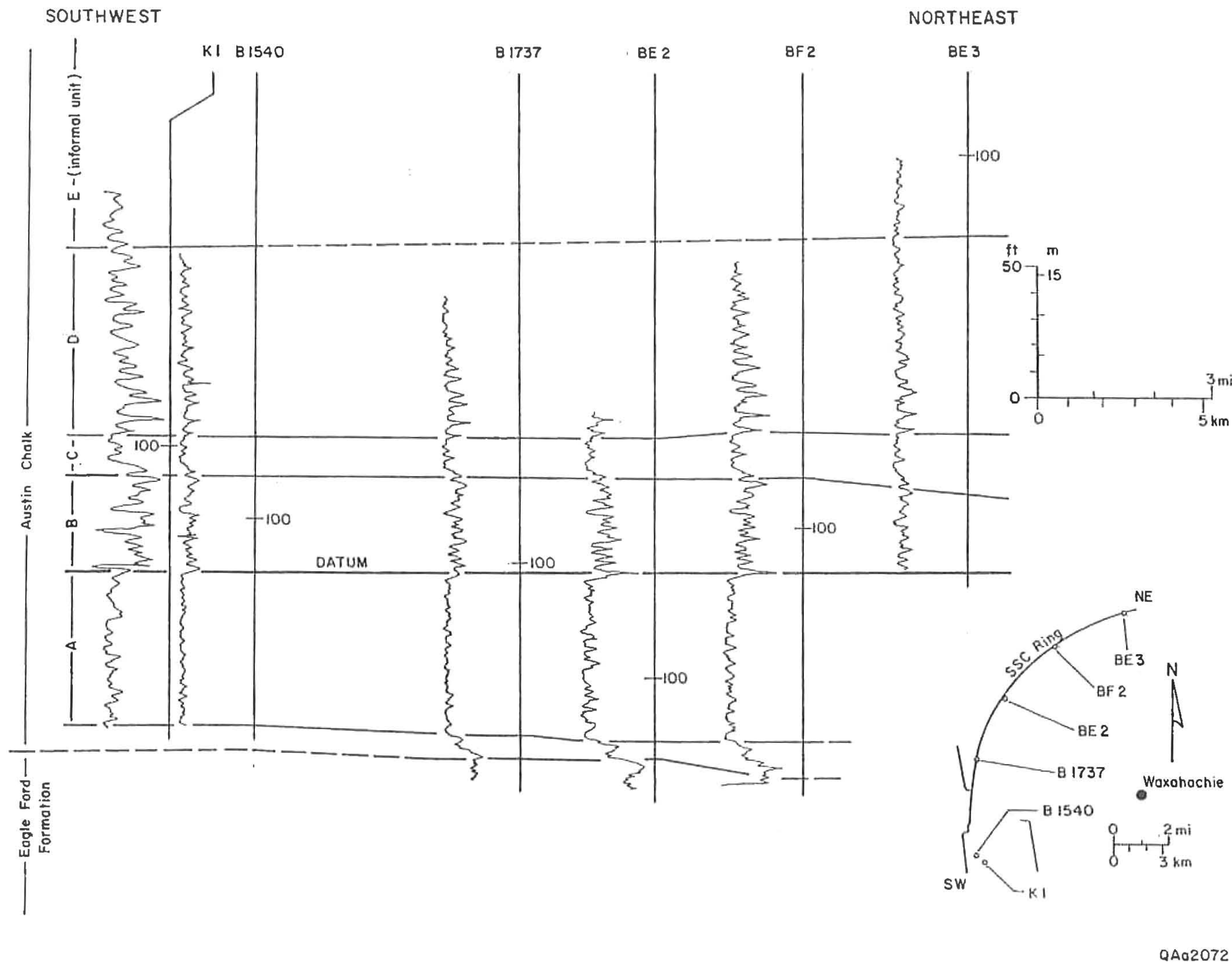

Figure 15. Representative log correlations of units A, B, C, and D along strike, northwest part of the SSC ring, show substantial continuity of units and a repetitive pattern of individual gamma peaks marking the base of cycles. 100-ft depths are labeled.

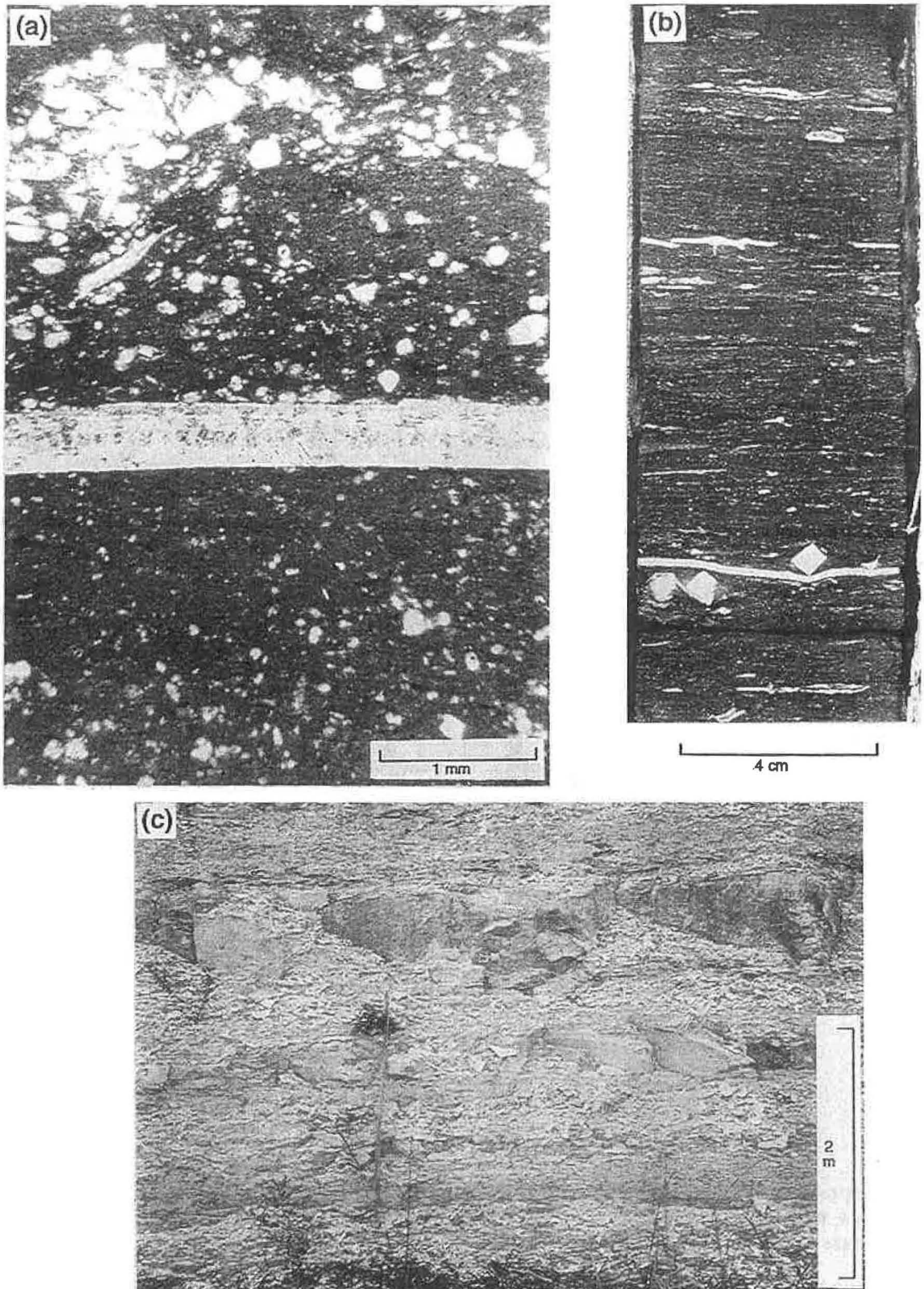

Figure 16. Characteristic lithologies of units B and D. (a) In thin section, chalk with fine, randomly oriented allochems grades upward into marl with wispy dark organic concentrations, small pyrite crystals (black), and sorted and concentrated inoceramids and inoceramid prisms. Photomicrograph of K1 90.6, base unit D marl, plane light. (b) Typical dark, organic-rich, weakly laminated marl with abundant thin-walled, flat-lying inoceramids, from sample BE3 196, bed D-23. (c) Outcrop of unit D, Bell Branch, south of Chambers Creek, Ellis County. Weathered organic-rich marls are week and splintered.

Unit "D" is 68.9 to 75.1 ft (21.0 to 22.9m)thick. The lower part is similar to unit B, but gamma-ray response decreases upward (figs. 11 and 15). High gamma-ray response again corresponds to dark, locally laminated marls (fig. 16a). Oysters and *Gryphaea* are locally abundant in unit D. Marl bed D-18 (fig. 11) contains pods of bentonite that have been partly admixed with marl by burrowing. In outcrop, the dark laminated unit B and D marls weather to light brown or orange (10YR 6/2 [Geological Society of America, 1979]) and are weak and splintered, producing poor outcrops (fig. 16c). The top of unit D is selected at the top of an interval of decreasing gamma-ray response above a pair of distinctive peaks on gamma-ray logs.

Middle Austin Chalk

Units E through I have a generally low gamma-ray response and are subdivided into map units on the basis of higher gamma-ray response in units "F" and "H." Although the thin F and H markers can be traced 9.3 mi (15 km) to the eastern part of Ellis County, individual marl beds within any of the units are difficult to trace even over short distances laterally. Pyritized burrows and nodules are characteristic of all the middle Austin Chalk units. Unit E (38 to 52.8 ft [11.6 to 16.1 m] thick) has sparse inoceramids, but abundant small thin-shelled bivalves as well as oysters and *Gryphaea* are present (fig. 17a). A thin bentonitic bed is locally preserved at its base. Beds E-6 and E-4 are locally recognized as firmgrounds marked by packstone-filled burrows (fig. 17b). Unit F (6.9 to 14.1 ft [2.1 to 4.3 m] thick) appears to contain some chalk beds with slightly higher clay content than average, some dark (organic-rich) marls, and one thin bentonite in bed F-3. Inoceramids and oysters are locally abundant. Unit G (20 to 24.9 ft [6.1 to 7.6 m] thick) contains whole and fragmented inoceramids throughout. The base of bed G-3 is marked by a firmground in the BE-3 core and contains oysters and a skeletal sand lag in the F3 core. Unit H (10.8 to 15.1 ft [3.3 to 4.6 m] thick) contains abundant whole and fragmented inoceramids and several probable firmgrounds marked by packstone-filled burrows. Unit I (45.9 to 53.1 ft [14.0 to 16.2 m] thick) contains abundant skeletal grains, including inoceramids and inoceramid fragments and very abundant oysters and *Gryphaea*. Centimeter packstone beds and

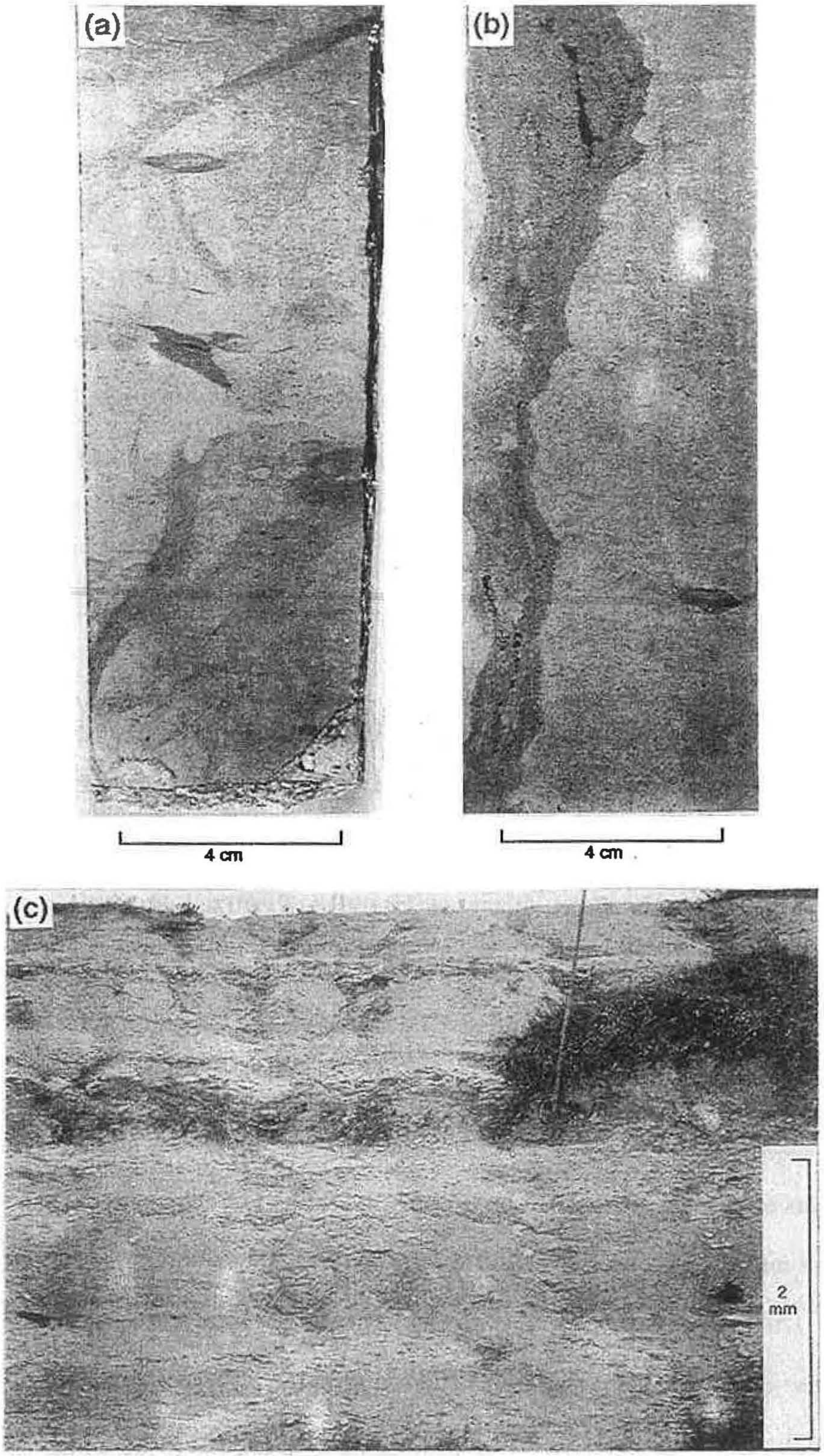

Figure 17. Characteristic lithologies of units E through I. (a) Typical chalk core from unit E sample BE3 104, bed E-4a. Core does not appear weak or clay rich. (b) Inoceramid prism packstone-filled burrows indicate episodes of sediment winnowing, although a firmground was not identified in core. Core BE3 115, bed E-6. (c) Typical weak-weathering profile of the middle Austin Chalk was previously interpreted as indicative of a high clay content in this unit (Koger, 1981). Railroad cut south of Business 287 west of Waxahachie, Ellis County.

packstone-filled burrows mark frequent episodes of winnowing and firmground development. Chondrites (small, branching burrows) are abundant in some of the darker fine-grained intervals. The subdivisions of the middle Austin Chalk defined by gamma-ray character were not identified in outcrop because of small and discontinuous exposures. Middle Austin Chalk outcrops weather weakly and recessively (fig. 17c) as if they have a high clay content and therefore are described as marly or chalk-marls (Dallas Geological Society, 1965, cited in Reaser and Collins, 1988; Dawson and others, 1983).

Upper Austin Chalk

Units J, K, and L have a low gamma-ray character and the units are subdivided by correlation of individual marl beds with high gamma-ray response. Cycles in these units are less rhythmic than the lower Austin Chalk, and chalks, marly chalks, and marls are more gradational into one another. Unit thicknesses are more variable than in other members of the Austin Chalk and there is some doubt that the marker beds defining the base of the units are exactly the same stratigraphic position in all wells. Unit J (30.8 to 32.8 ft [9.4 to 10.0 m] thick) has not been examined in core. Units K (46.9 to 51.8 ft [14.3 to 15.8 m] thick) and L (28.9 to 54.8 ft [8.8 to 16.7 m] thick) continue the pattern of abundant packstone lags and packstone-filled burrows (fig. 18a) seen in unit I. Fragmented inoceramids are the dominant microfossil in unit K and are less abundant in unit L. In outcrops at the Lake Waxahachie spillway, inoceramid prism packstone beds are ledge-formers (fig. 18b, c). Dawson and Reaser (1985) have interpreted an increase in infaunal burrowers upward through this section, based on interpretation of abundant burrows in the packstone as *Thallasinoides,* a burrow type with open branching passages analogous to modern shrimp that is formed only in firm substrates. Core F4 contains abundant 0.4- to 3.9-inch-thick (1- to 10-cm) packstone beds but no single thick packstone correlatable to the beds observed at the spillway. Lateral variability in thin cycles explains the variation in patterns of gamma-ray logs in this interval.

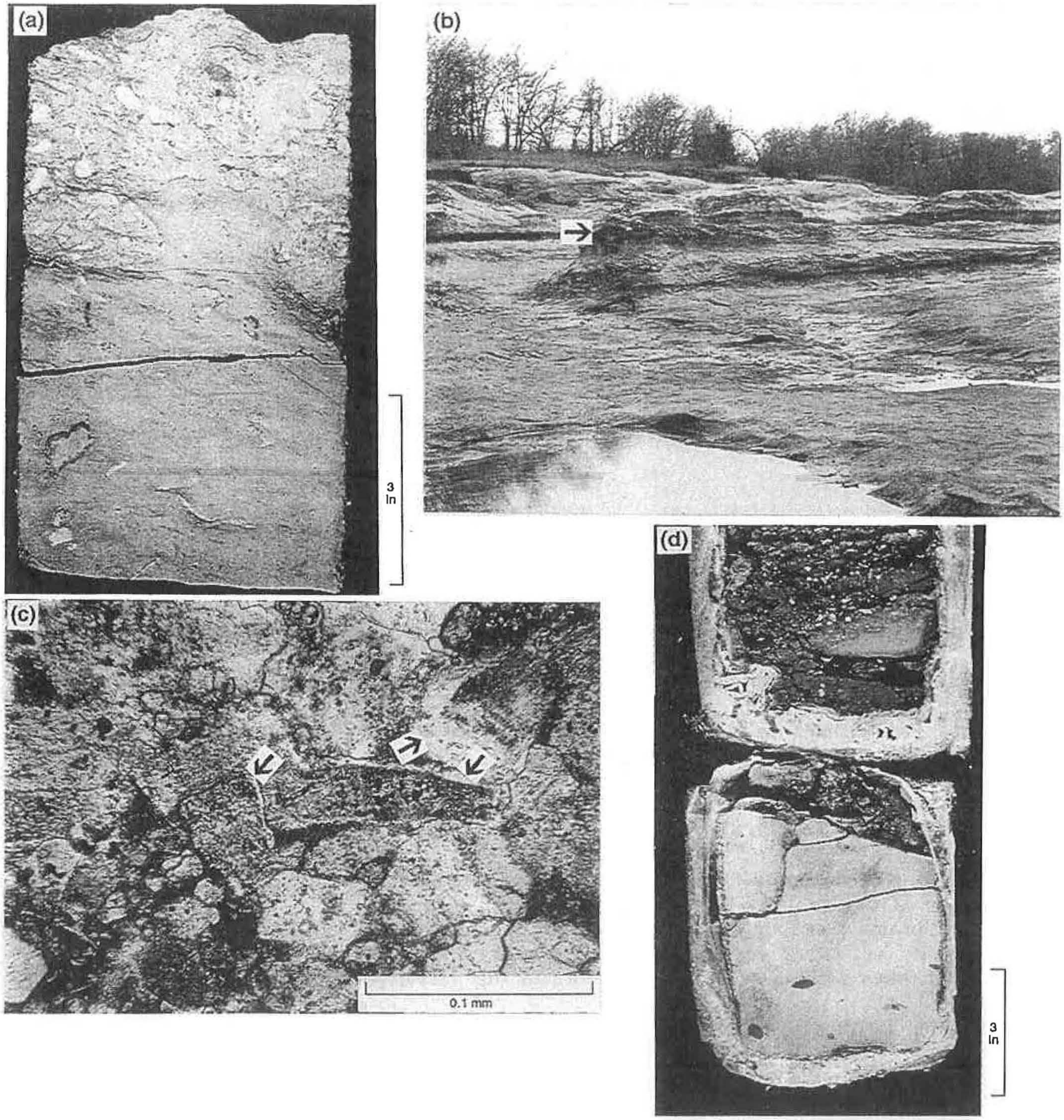

Figure 18. Characteristic lithologies of units K and L. (a) Disrupted packstone-bed and packstone-filled burrows, sample BE3 25. (b) Packstone ledges (arrow) in unit L at Lake Waxahachie spillway, Ellis County. Photograph by C. Kerans. (c) Photomicrograph of echinoderm/inoceramid chalk packstone-filling burrows, sample F4 114.3, photographed in plane light. Arrows indicate syntaxial calcite rims on echinoderm plates, "I" shows cross section of prisms in a typical inoceramid shell. (d) Top of the Austin Chalk and base of the Ozan Formation ("lower Taylor Marl"), sample F4 71. The Austin Chalk was lithified prior to Ozan marl-sediment accumulation. Borings in the chalk are filled with red shale and oxidized carbonate. A chalk clast is incorporated in the marl at the base of the Ozan Formation.

The top of the Austin Chalk in Ellis County is marked by a phosphatized reworked, and bored hardground (Fürsich and others, 1981). In the F4 core, an 8-inch-thick (20-cm) conglomerate above the bored surface is composed of clasts of oxidized red chalk, phosphatic, and fragmented inoceramid debris in a dark shale matrix (fig. 18d). The Austin Chalk–Ozan Formation contact in Ellis County is placed at the Santonian–Campanian boundary on the basis of planktonic foraminifers (Marks and Stam, 1983). This is a young age for the lithologic change relative to other locations along the Austin–Dallas outcrop belt.

Ozan Formation

The Ozan Formation (lower Taylor Marl) is a dark-gray calcareous shale. Its gamma-ray response and its appearance in core and outcrop are homogeneous. The Ozan Formation is overlain by the Wolfe City Sandstone east of the SSC ring where the Ozan Formation is approximately 300 to 500 ft (~91.4 to 152.4 m) thick.

Patterns of Chalk-Marl Cycles

Cycles in the Austin Chalk are defined by repetitive alternation of carbonate-dominated beds (chalk) and beds with a higher impurity content (marls). Marls are identified in core by darker gray to olive colors (N3 to N5, 5Y4/1) relative to light-gray chalks (N7, 5Y 8/1). In outcrop, marls weather recessively (fig. 19a). Chalk-marl contacts are typically gradational over 2 to 10 inches (1 to 25 cm) because of changes in insoluble content. Contacts that are gradational over less than 1 inch (2 cm) are described as sharp, those in which one sediment has been mixed into the other by discrete burrows are described as burrowed contacts (fig. 19b, c), and those in which the transition occurs over a long interval are described as gradational. Insoluble content and total organic carbon (TOC) were measured in representative chalk-marl cycles (fig. 20a, b). Cycles determined by inspection of core had a good match to the cyclic variation measured by acid-insoluble content as well as the cycles defined by gamma-ray log response. Marls in unit A are composed of as much as 40 percent insoluble material in

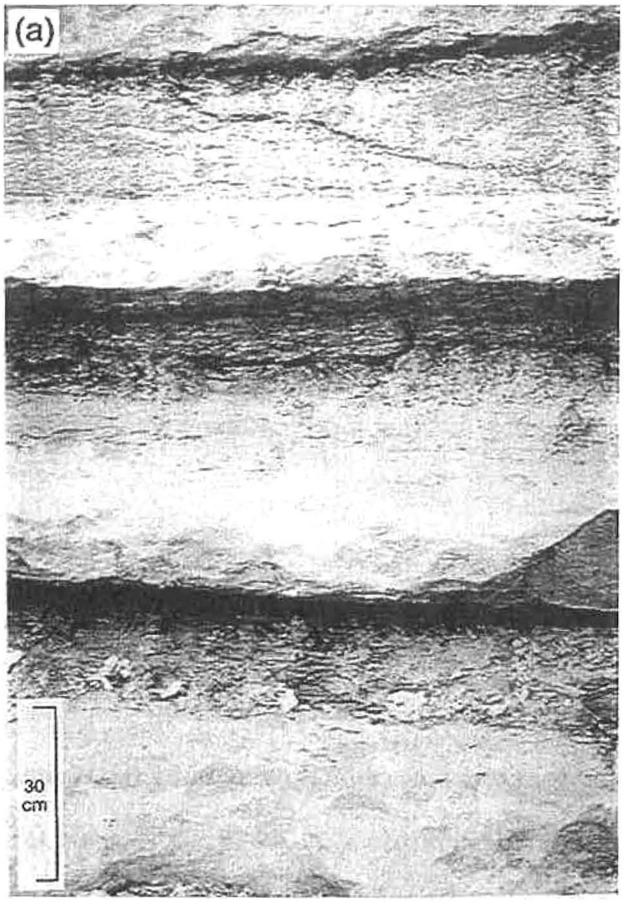

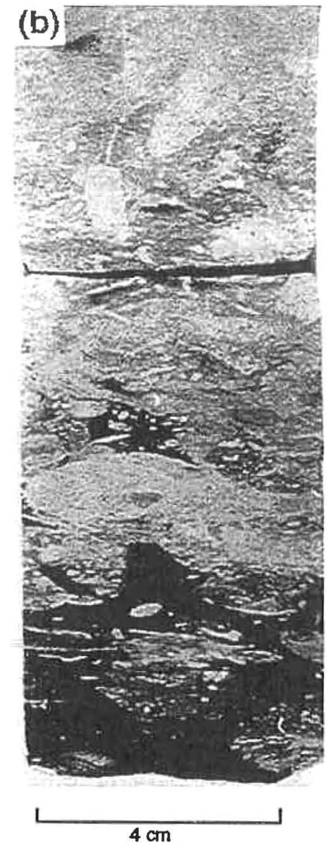

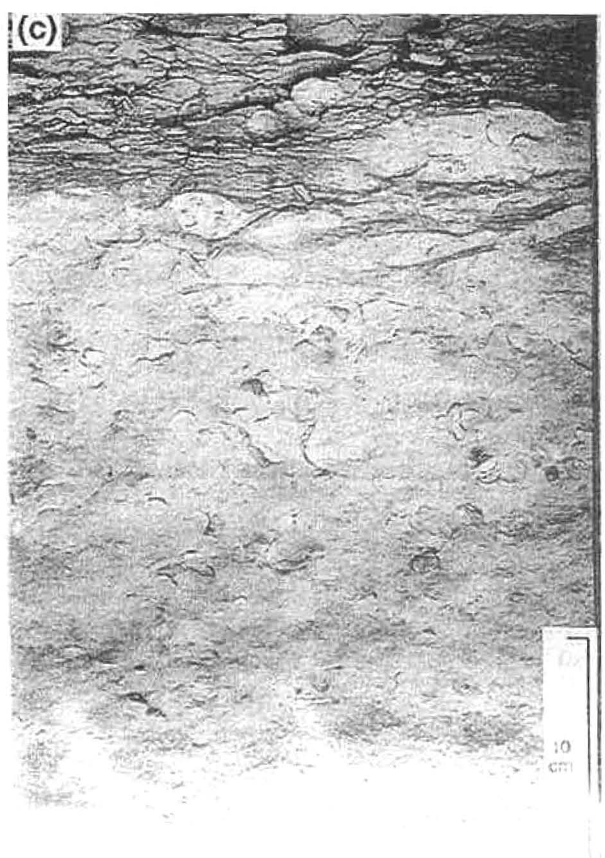

Figure 19. Characteristics of chalk-marl cycles observed in outcrop and core. (a) Typical unit A chalk-marl cycles in outcrop, Clark Street, High Pointe subdivision, southern Dallas County. These cycles have sharp contacts of chalks with underlying marl and gradation from chalk into overlying marl. (b) Burrowed, originally sharp (?) basal contact of chalk with dark marl, sample BE3 178. (c) Top of chalk bed, marl contact piped into chalk by burrowers. Abundant *Gryphaea* within chalk may indicate firmer substrate during chalk deposition. Lake Waxahachie spillway, unit K.

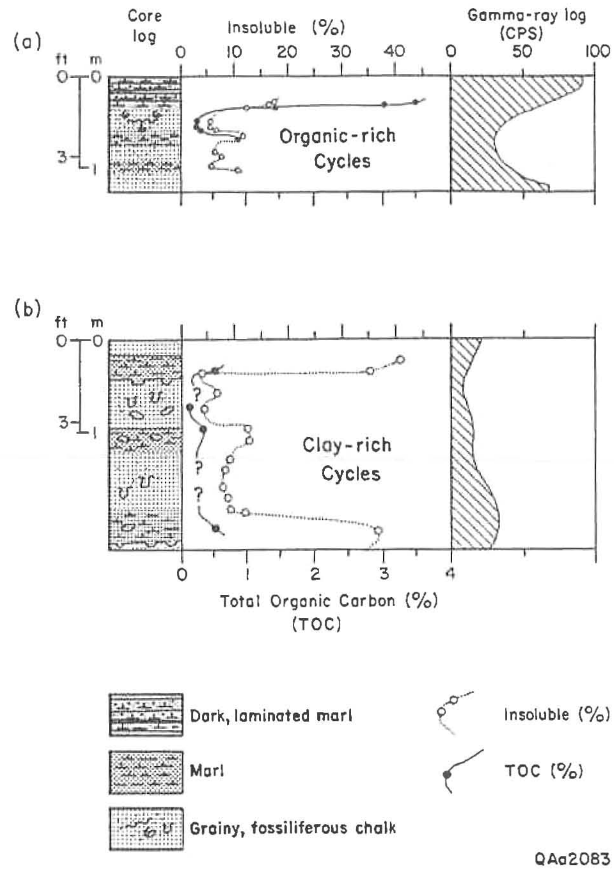

Figure 20. Cycle defined by insoluble residues and total organic carbon (TOC). (a) In a typical cycle in unit D, compositional variation between chalk and marl is defined mostly by variation in TOC. Note different scales for acid-insoluble residue and TOC. (b) In typical cycle in unit A, compositional variation is defined by variation in acid-insoluble residue (mostly argillaceous material).

contrast to much lower insoluble content of chalks. The unit A marl has slightly higher TOC concentrations than does the chalk. Dark-colored laminated organic marls in unit D contained high TOC but lower insoluble content than unit A marls.

Four marl beds contain segregated blebs or separate beds of white to iron-oxide-stained clay rich beds (fig. 11). This clay has the characteristic appearance and "soapy feel" of bentonite. Six other marl beds contain small clayey patches tentatively identified as reflecting a bentonitic contribution. Discrete bentonite was identified only within marl beds, not in chalk beds. The thickest bentonite is the prominent marker used as the base of unit B. In outcrops on the Clark Street, High Pointe subdivision road cut, in Cedar Hill 9.3 mi (15 km) northwest of the SSC ring, several marl beds below this marker are dark and laminated, appearing more similar to unit B marls. If the thick bentonite is assumed to be a correlatable time line, onset of organic marl-producing conditions was earlier north of Ellis County, toward the Dallas Basin, than on the northeast side of the SSC ring, where core was examined.

The depth of the base of each marl bed and the thickness of the marl bed (from the position of the most rapid color change) were measured to examine the effect of bed thickness on mechanical behavior of the chalk (appendix F). A good correlation is apparent between individual gamma-ray peaks on 1:120-scale logs and marl beds observed in core. Units A, B, and D exhibit patterns in the relative gamma-ray peak height traceable along the eastern edge of the SSC ring, indicating that the chalk-marl cyclicity pattern has minimal variability in this direction (fig. 15). Cycle thickness averages slightly less than approximately 3 ft (~1 m) (fig. 21). Cycles in unit A are thinnest, perhaps because chalk-marl contacts are sharp and regularly spaced, indicating that no cycles are obscured. Average marl thickness is slightly higher in units B and D. The middle and upper Austin Chalk have thicker cycles and slightly thicker marl beds than unit A. Unit T has the thickest cycles and the chalk-marl alternation is poorly defined because of the high average insoluble content of this unit.

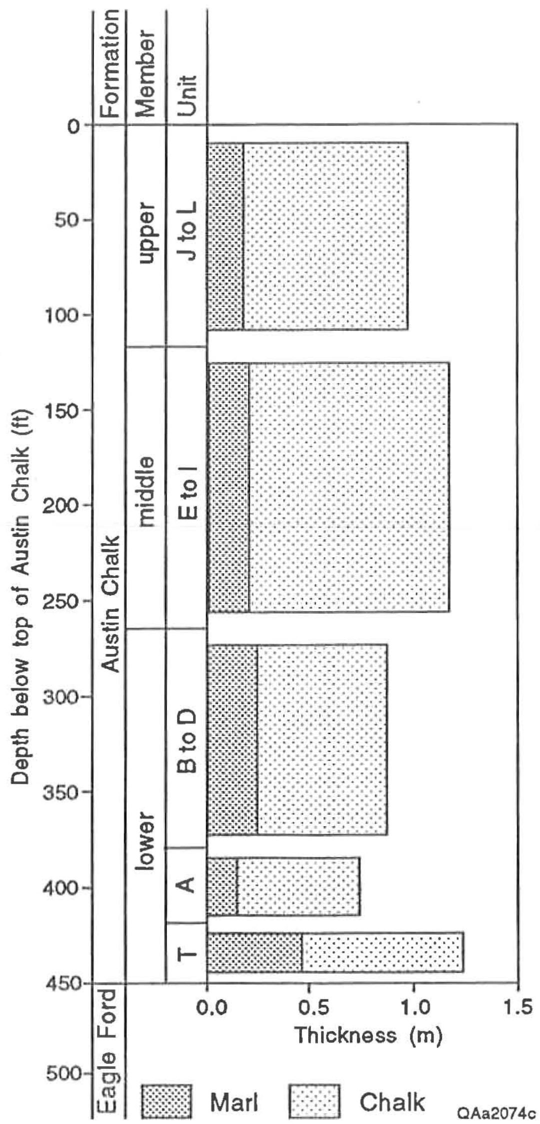

Figure 21. Average chalk and marl bed thickness for grouped informal subsurface units.

Petrographic Description

Chalk

Chalk, by definition (Scholle and others, 1983), is composed of plates and fragments of coccoliths and other nannoplankton (figs. 22 and 23). Nannoplankton in thin section (fig. 22a) appear as carbonate mud (micrite). Rare intact coccolithophores (less than 10 mm diameter) are identified in thin section by radial extinction. Sand-sized foraminifers (dominantly globigerinids with lesser amounts of more robust forms) and calcite prisms that are derived from fragmentation of the calcite layers of inoceramid shells (fig. 22b) make up 5 to 25 percent of most samples (fig. 22a). The macrofauna is dominated by inoceramids. Oysters and *Gryphaea* are locally abundant and can be identified in thin section by characteristic wall structures (fig. 22b).

The microfabric in SEM view of chalk is characterized by five components (figs. 22 through 26): (1) nannoplankton (coccolith plates and fragmented plates), (2) foraminifers, (3) intact and fragmented macrofauna (principally macerated inoceramid prisms), (4) calcite cement, and (5) clay. All chalk samples are similar in that these components are present, but relative abundance and distribution vary within samples, between samples, and between units (table 7). Nannoplankton preservation varies, reflecting calcite dissolution, calcite precipitation, and clay distribution. Nannoplankton preservation is typically excellent in units B, D, K, and L chalk samples (figs. 22 and 23). Preservation of some coccoliths in unit A is modified by slight dissolution around the margins and is locally obscured by calcite and clay precipitated on the grains (fig. 23a).

Most coccoliths are obscured by heavy clay coats in unit E, G, and I samples (fig. 24). Clay exhibits three microfabric variations: (1) discrete flakes, (2) coats on grains, and (3) rare intergranular clay cements. The amount of clay coat visible on nannoplankton tests is not linearly related to percent clay in chalk samples. Samples in units E, G, and I with low (<10 percent) clay content typically have much more visible clay in SEM view than do chalk samples from other units with higher clay content.

Calcite cements are pore filling and occur as well-formed rhombs with abundant minor faces expressed (fig. 23d) as well as overgrowth on foraminifers and skeletal grains. Large calcite rhombs

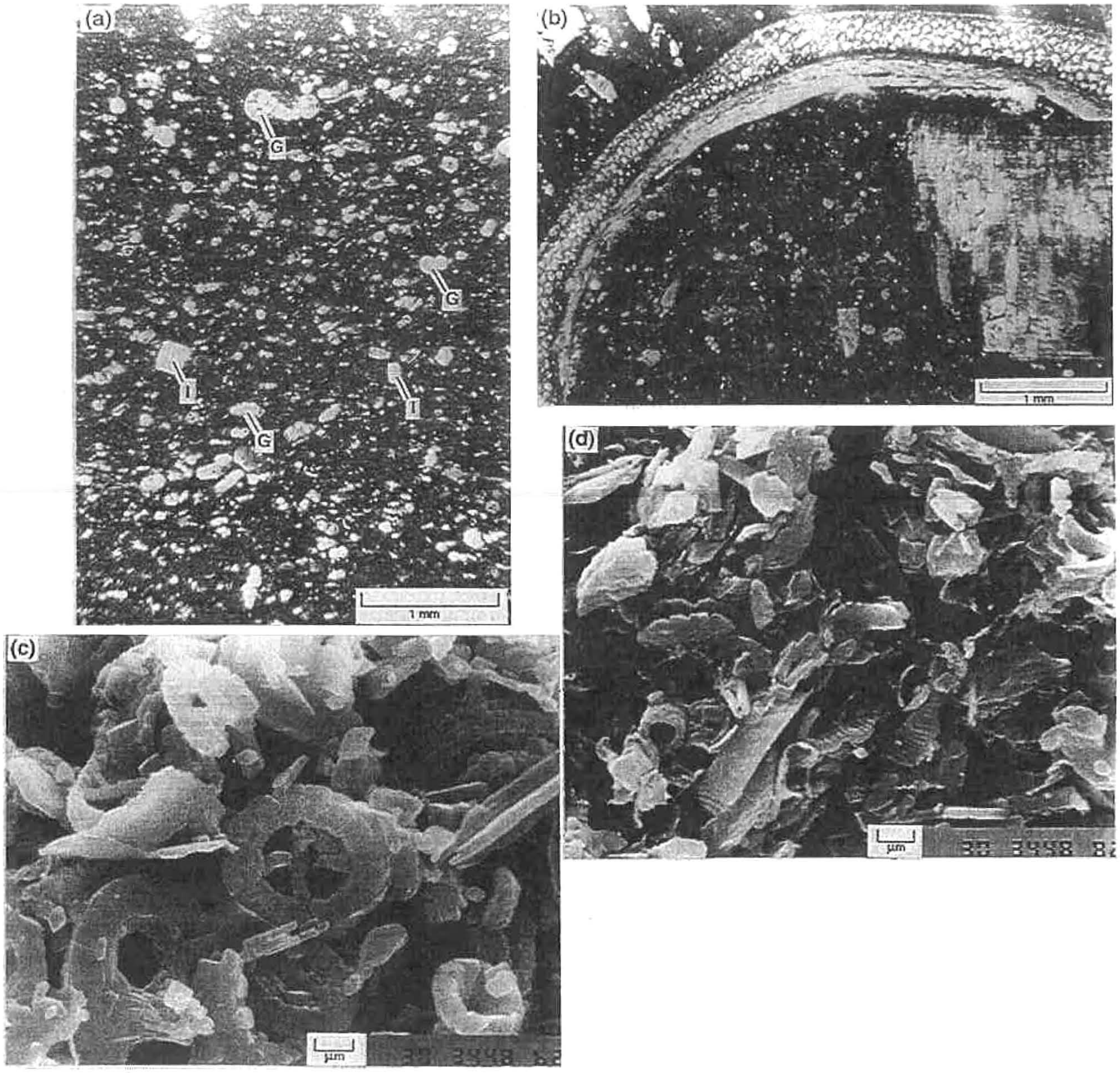

Figure 22. Petrography of typical chalk. (a) Globigerinid (G) and inoceramid fragments (I) are the major allochems in chalk wackestone, photographed in plane light, sample K1 92.1, unit C. (b) Fragments of typical macrofauna in thin section. The large shell with prominent cellular structure is *Gryphaea*, and the prismatic material is a vertical section through a piece of a robust *Inoceramus* shell. Thin-section sample F4 146, plane light. (c) Typical excellent preservation of coccoliths (resemble wheels), prismatic crystallites from macerated inoceramids, and euhedral coccolith crystallites. Sample J2 35, unit D, 34-percent porosity. (d) Whole and fragmented coccoliths are well preserved, typical of unit B. Sample is K2 89.3.

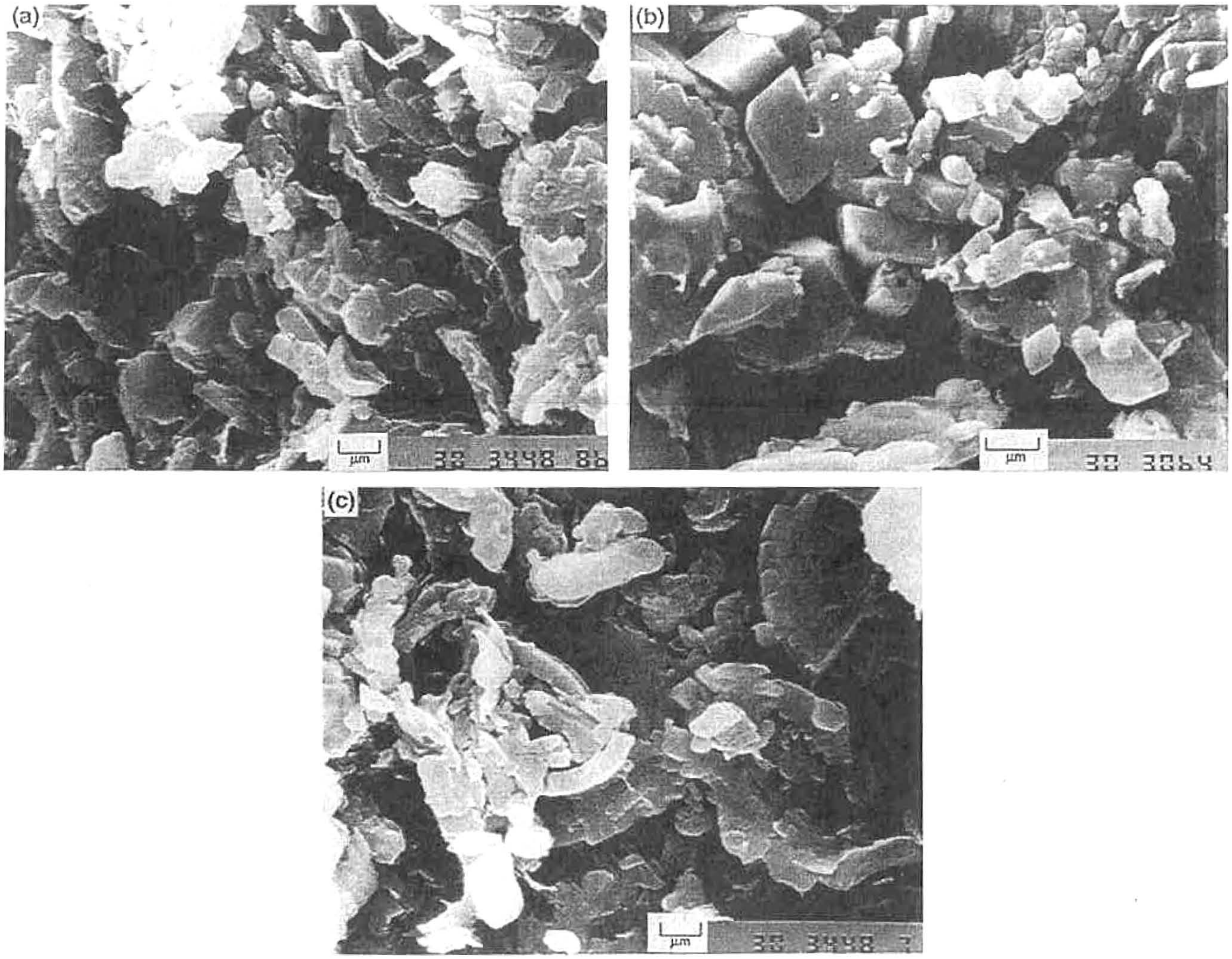

Figure 23. Typical SEM views of chalk. (a) Unit A chalk: fragmented coccoliths and other grains are slightly corroded. Sample K2 154, 7-percent insoluble residue. (b) Chalk from unit K has well-preserved coccoliths and euhedral calcite cement. Pristine appearance of nannoplankton indicates that the calcite was probably derived from aragonite dissolution rather than dissolution of coccoliths. Sample E4 64.8, 26-percent porosity. (c) Well-preserved nannoplankton typical of unit L. Sample from prominent packstone bed at Lake Waxahachie spillway.

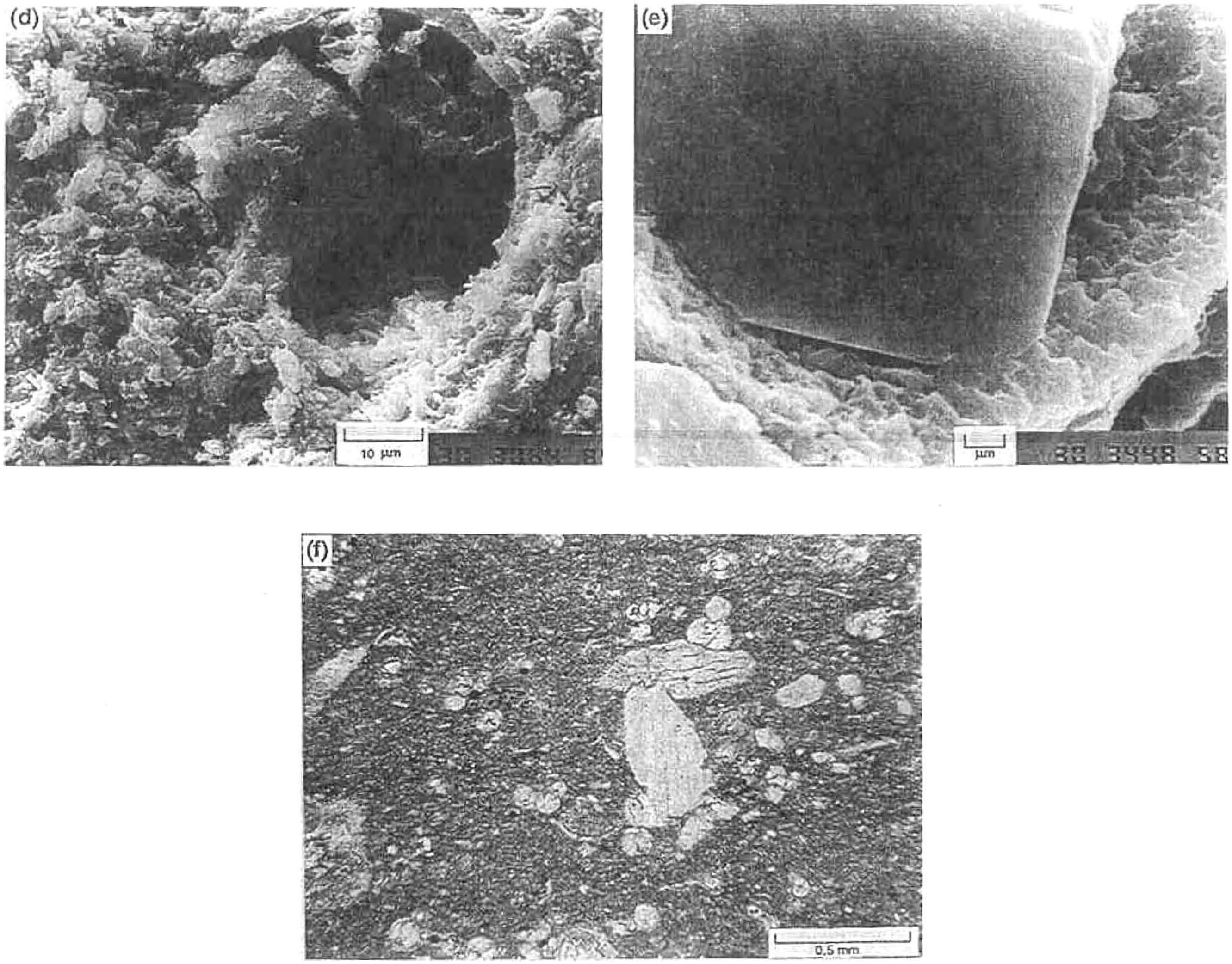

Figure 23 cont. (d) Foraminifer partly filled with calcite cement. Nannobacteria are commonly observed on calcite within foraminifer tests, but not on calcite cement in intergranular areas. Sample E4 64.8. (e) Detail of nannobacteria on calcite cement within a foraminifer. Sample J2 35, unit D, etched fractured surface. (f) Pressure solution has occurred where inoceramid prisms are in contact. Pressure solution is typically minor in Ellis County, as evidenced by excellent preservation of most nannoplankton tests. Photomicrograph is from sample F4 119, unit K.

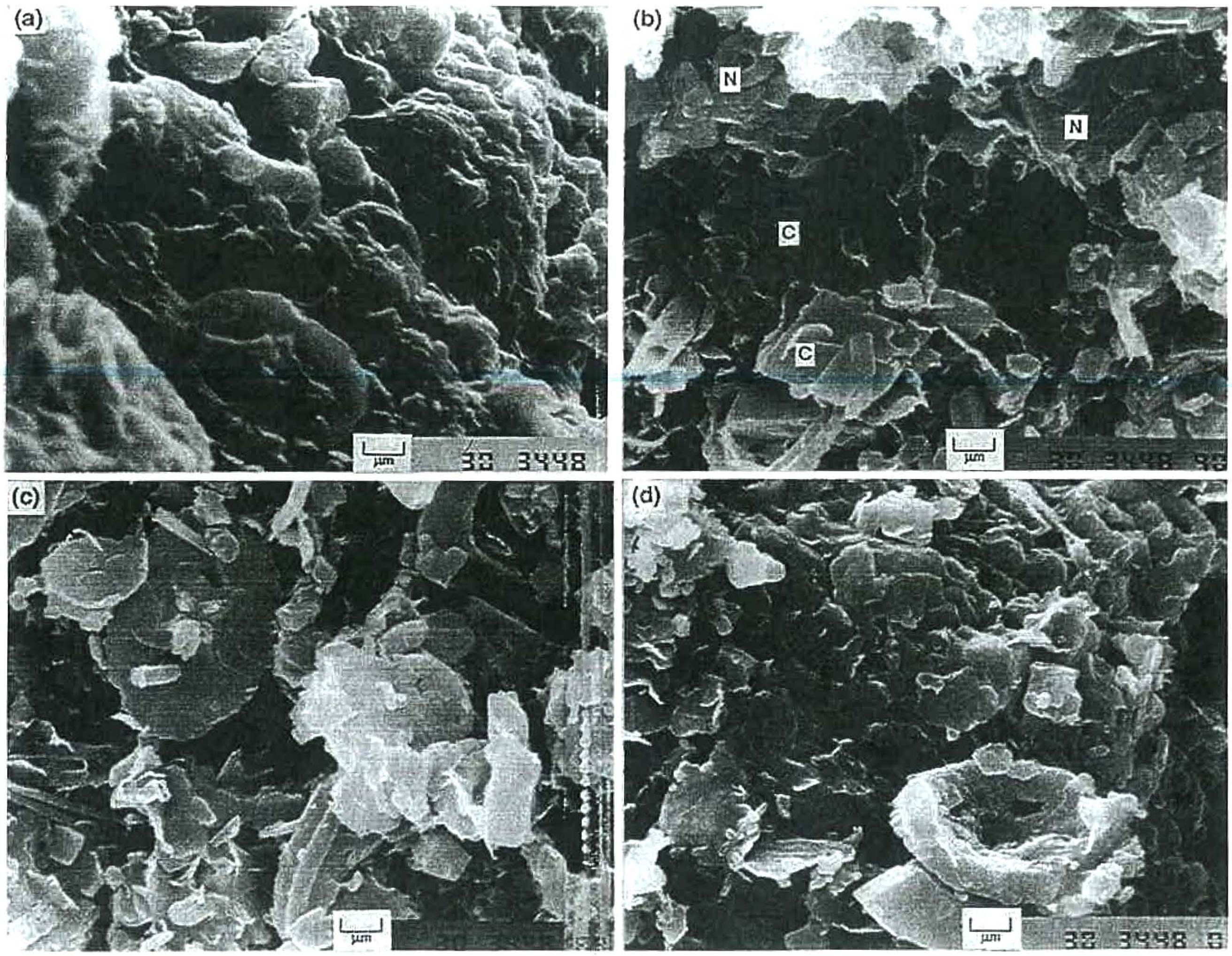

Figure 24. Clay coats obscure details of nannoplankton tests and fill pores in most chalk samples from the middle Austin Chalk. (a) Clay coats almost obscure coccolith fabrics on fractured surface of sample F3 64.7, unit I. EDS (energy dispersive system) analysis yields peaks for Ca, Al, and Si, indicating that calcite and clay are present. (b) Some calcite (c) and nannoplankton fragments (n) can be seen in areas not covered by thick clay coats. Sample is F3 94.1, unit G, with 7-percent insoluble material. (c) Clay obscures most grains in chalk from sample BI3 81, unit E. This sample, with 18-percent porosity, is from an unfractured core plug removed from a highly fractured zone with high transmissivity. Microfabrics are typical of the middle Austin Chalk and document no significant alteration of host rock in a fractured zone. (d) Clay coats and clay flakes are abundant in samples of the middle Austin Chalk with only 5-percent insoluble residue. Sample number F3 43.5, unit I.

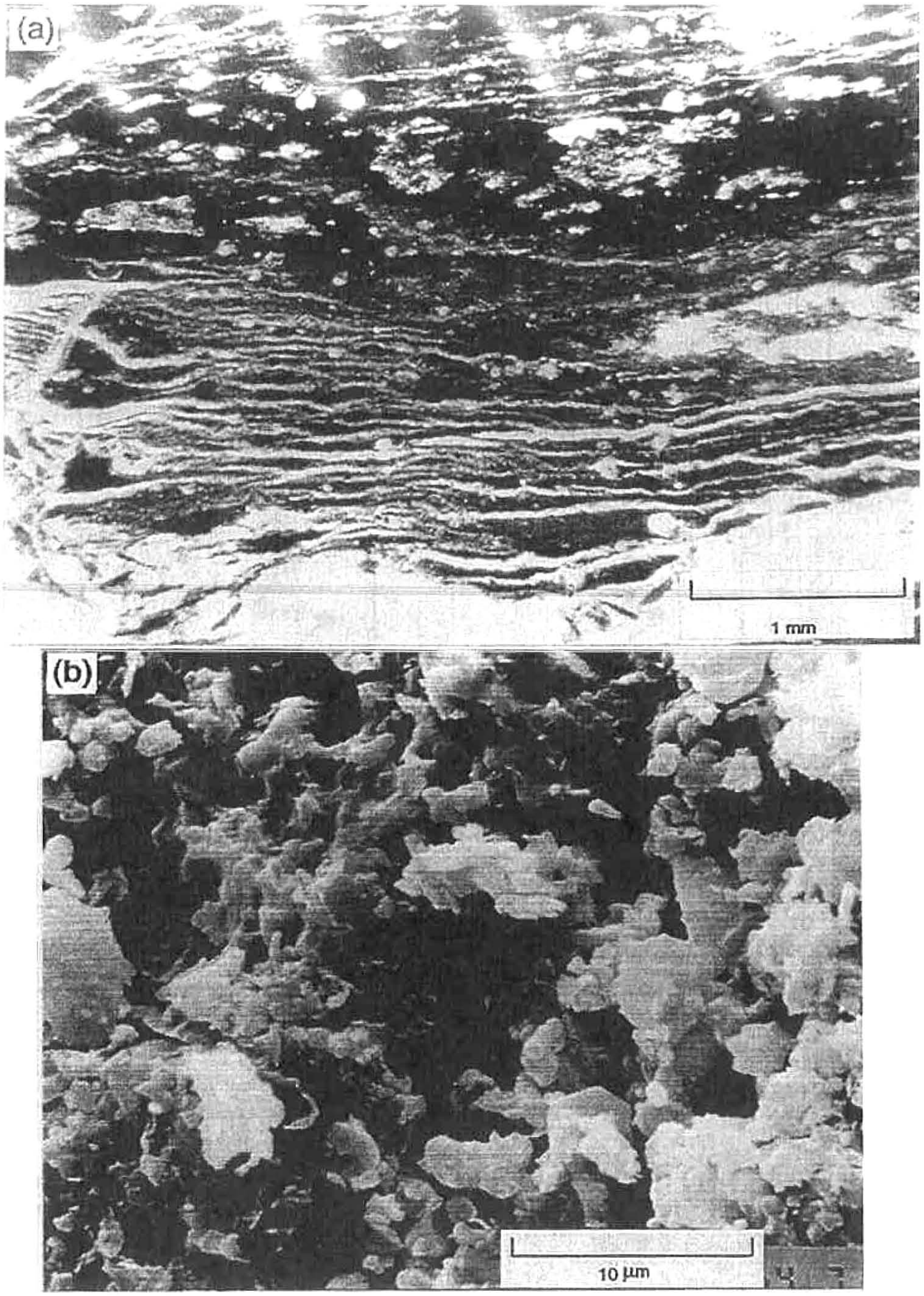

Figure 25. Petrography of typical marl. (a) The high clay content of marl produces fissility and plucking during thin section preparation. Sample from K1 91.25, unit D, photographed in plane light. (b) Clay coats everything in marl in SEM view. Arrows show detrital clay flakes and coccoliths. Sample K1 174.7, unit A, has 41-percent insoluble residue.

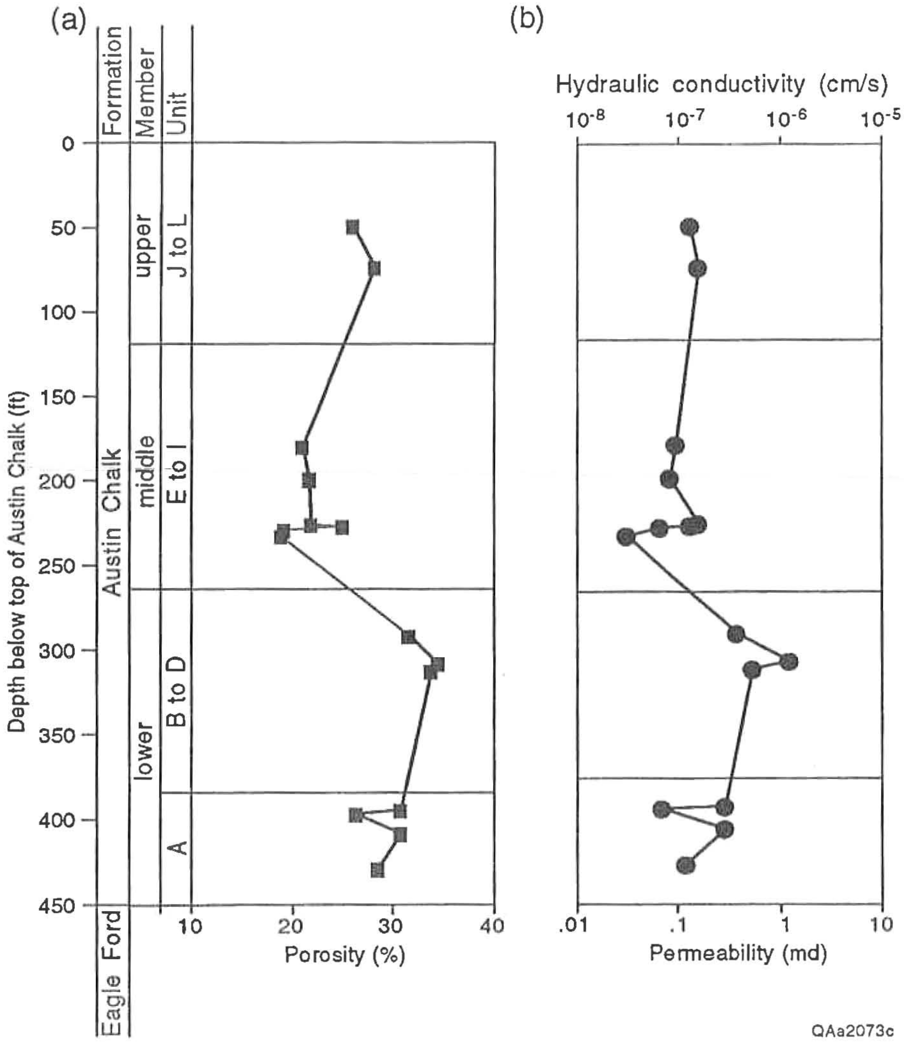

Figure 26. Trend with depth in (a) porosity and (b) permeability. Compare to the SP log in figure 12. SP log value is low in upper and lower Austin Chalk where porosity is high, and high in middle Austin Chalk where porosity is low.

Table 7. Petrologic characteristics of informal Austin Chalk units.

Unit	Thickness, type log (ft)	Log character	Cycle character	Burrow character	Dominant macrofossils
D	73	High, marls 140 cps, decreasing upward; chalks 20–30 cps	Strongly cyclic, dark, laminated marls	*Planolites*, *Chondrites* especially abundant in lower part	Abundant whole and fragmented thin-walled inoceramids, especially in marls, oysters in D-10, D-12
C	27	Low, 20–70 cps	Cyclic, one bentonite, marls laminated	*Planolites* abundant, *Chondrites* especially in marls	Inoceramids abundant in chalks and marls
B	35	High, 40–120 cps	Thick, dark marls, well bedded	*Planolites* abundant, *Chondrites* present	Inoceramids abundant especially in marls
A	64	Low, 20–50 cps	Well-defined chalk-marl cycles	*Planolites* abundant, *Chondrites* increase upward through some cycles	Sparse
T	10	High (200 cps) deceasing upward	Not well defined	*Planolites* abundant	Inoceramids and oysters, phosphate bones and teeth at base
Eagle Ford		High	Not cyclic	Compressed burrows	Sparse
Ozan (Lower Taylor Marl)		Characterless high gamma-ray response	Not cyclic	Strongly compressed	Sparse
L	30	Moderate, variable 20–40 cps	Poorly cyclic, chalk gradational into marl, firmgrounds, grainy beds, grainy burrow fills	*Planolites* abundant, *Chondrites* abundant locally limonitized, possible *Thalassinoides*	Sparse oysters
K	51	Low (20 cps) with sharp peaks (40 cps) that correlate to thin marls	Typical meter-thick cycles, firmgrounds, grainy beds, grainy burrow fills	*Planolites* abundant, *Chondrites* present, especially in marls and darker layers	Inoceramids and inoceramid fragments in both chalks and marls, oysters present in bed K8
J	33	Low (20 cps) with sharp peaks (40 cps) that correlate to thin marls	Not seen in core	Not seen in core	
I	50	Low (20 cps) with sharp peaks (40 cps)	Typical chalk–marl cycles	*Planolites* and *Chondrites*	Inoceramus and inoceramid fragments abundant in chalk and marls, abundant oysters
H	12	30–40 cps, more sharp peaks, slightly higher overall	Well-defined cycles, sharp base of marls	*Planolites* and *Chondrites*	*Inoceramus* and inoceramid fragments
G	26	Generally low, 20–40 cps	Weakly cyclic, local firmgrounds	*Planolites* dominant, large pyrite nodules	Sparse
F	12	Slightly higher, 20–50 cps, more peaks	Typical chalk–marl cycles	*Planolites* dominant, large pyrite nodules	Sparse
E	46	Low, 20–40 cps	Typical chalk–marl cycles, local firmgrounds, grainy beds	*Planolites* and *Chondrites*, large pyrite nodules	Sparse, thin-walled mollusks

partly filling foraminifers (fig. 23d, e) have abundant 0.2-mm spherical or rod-shaped objects on the surface, interpreted by R. L. Folk (personal communication, 1992) as calcified nannobacteria. Calcite is most abundant in unit K and L samples, moderately abundant in units A and E, and sparse in unit D. Evidence of minor amounts of pressure solution has been seen in a few chalk and marl samples (fig. 23f) but is minor compared to chalks from the deeper subsurface where all chalk-marl contacts are enhanced by wispy lamination and porosity has been reduced (Scholle, 1977a, c; Dravis, 1980).

Very low (<0.1 percent) amounts of dolomite rhombs and pyrite framboids were identified in a few samples examined with the SEM and only where chalk had been lightly etched in weak hydrochloric acid to concentrate the less soluble component at the surface of the sample.

Marl

Marl is the term customarily applied to mixtures of chalk and argillaceous material (Scholle and others, 1983). Marl samples contain a disseminated, optically recognizable, low-birefringence clay component, yielding darker colors in transmitted light and poor mechanical strength, evident in fractures and plucking within the thin section (fig. 25a), as well as a tendency for samples to fracture during handling. Segregated clay seams or discrete organic grains are rare in marl thin sections. Compositional differences are minimal in marl so that lamination is rarely seen in thin section. Foraminifers and inoceramid prisms, as well as intact inoceramids, are present in most marls in concentrations equal to or greater than those in chalk. In SEM view, most marls are uninformative because clay coats both fractured and etched surfaces (fig. 25b). The thick bentonite at the base of unit B contains macroscopically visible black biotite concentrated at its base.

Porosity and Permeability

Matrix porosity of the Austin Chalk measured in 15 samples ranges between 19 and 34 percent (table 8). These high porosities are typical of chalk that has not been deeply buried (Schlanger and Douglas, 1974; Scholle and Cloud, 1977; Travis, 1980; Scholle and others, 1983; Pollastro and Martinez,

Table 8. Porosity and permeability data from analysis of core plugs.

Sample no.	Depth (ft)	Depth below TAC (ft)	Unit	Lithology	Permeability (md)	Porosity (%)	Density (g/cm^3)	Comment
E4 64.8	64.8	49	K	chalk	0.138	26	2.69	
E4 94.95	94.95	74	K	chalk	0.164	28.1	2.7	
T3 48.3	48.3	180	G	chalk	0.1	21	2.7	
T3 65.55	65.55	200	G	chalk	0.088	21.7	2.7	
B13 78.1	78.1	227	E	chalk	0.167	21.9	2.69	Fracture zone
B13 79.3	79.3	228	E	chalk	0.137	25	2.71	Fracture zone
B13 81.4	81.4	230	E	chalk	0.07	19.1	2.67	Fracture zone
BI3 84.1	84.1	234	E	chalk	0.033	18.8	2.68	Fracture zone
B13 94.9	94.9	292.9	D	chalk	0.394	31.6	2.72	Below fault
J2 35.1	35.1	309	D	marl (org.)	1.27	34.5	2.71	
J2 40.3	40.3	314	D	chalk	0.558	33.9	2.61	
J2 123.2	123.2	396	A	chalk	0.3	30.9	2.7	
J2 125.8	125.8	398	A	marl	0.072	26.4	2.7	
J2 140.8	140.8	410	A	chalk	0.299	30.8	2.71	
J2 160.05	160.05	431	A	marl	0.123	28.5	2.7	

1985). The lower Austin Chalk (units A and D sampled) consistently has the highest porosities. The lowest porosities were all measured in the middle Austin Chalk in units E and G, and upper Austin Chalk porosities are intermediate (fig. 26a). Permeability is low (0.03 to 1.27 md) (table 8). Low permeability is the result of the fine grain size of coccoliths and correspondingly small pore throats in the chalk. Nevertheless, the vertical permeability trends (fig. 26b) parallel the porosity trends. One set of samples collected from unfractured intervals within a faulted zone (R. K. Senger, personal communication, 1992) has porosity and permeabilities as well as microfabrics indistinguishable from those collected from unfractured zones, indicating that fracturing is not responsible for altering matrix properties. Permeability is linearly related to porosity (fig. 27). The samples from the middle Austin Chalk plot along a slightly different trend than do those from the rest of the formation.

Insoluble Residue

The insoluble content of 93 representative chalk and marl samples through the Austin Chalk section was separated by dissolution of crushed samples in dilute hydrochloric acid. The grain size distribution was measured in 52 of these samples by sieving and settling tube analysis. Clay mineralogy and TOC were measured on end-member and representative samples. Table 9 shows the results of these analyses.

Insoluble content varies from 86 percent for the bentonite in marl bed B-12 to as little as 3 percent in chalk (fig. 28). The average insoluble content in chalk varies between units (fig. 29). Units B, C, and D have low average insoluble and also low silt content, so that a higher percentage of the acid-insoluble material is clay size. Marls have consistently higher insoluble content than do adjacent chalks, with average chalks having clay contents of 8 to 15 percent and marls having clay content of 18 to 26 percent (fig. 21). Bentonitic marls contain fairly abundant sand- and silt-sized material. Optical examination of this material (discussed below) demonstrates that much of the sand- and silt-sized material is quartz and feldspar phenocrysts that were part of the volcanic ash

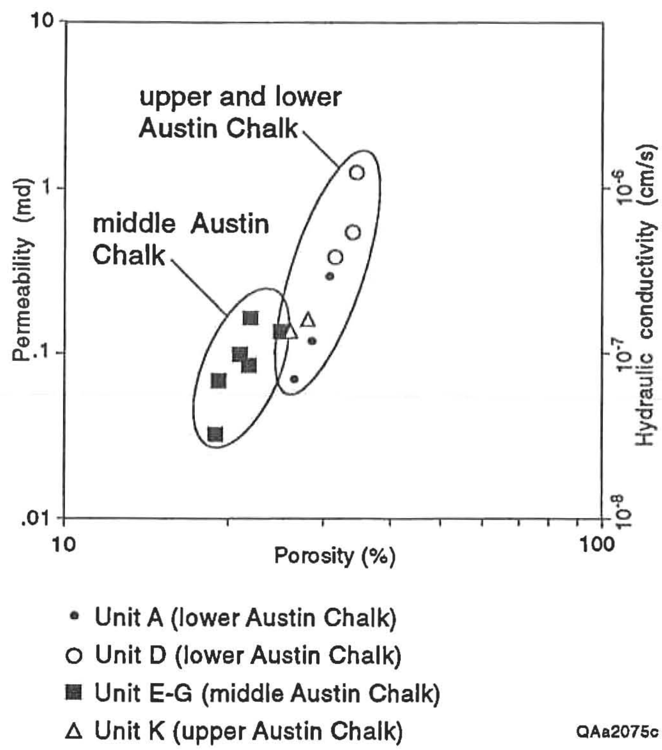

Figure 27. Relationship between porosity and permeability. Samples from the middle Austin Chalk, units E to G, plot along a different trend than the rest of the samples.

Table 9. Grain size and compositional analysis of insoluble residue (IR) from acid dissolution of chalk (C) and marl (M).

Sample location				Grain size and analysis						Mineralogy of the sand-sized fraction (100 × % of whole rock)						
Well	Sample no.	Depth below TAC	Bed no.	Composition	% IR	% TOC	% Sand	% Silt	% Clay	% Pyrite	% Hematite	% Limonite	% Quartz + feldspar	% Biotite	% Glauc.	% Phos.
F4	63.3	-8.7	TM	M	80.66	–	1.60	41.13	37.93	0.160	0.160	0.000	0.000	0.160	0.000	0.000
F4	64	-8	TM	M	80.32	–	0.09	43.19	37.04	0.465	0.093	0.465	0.000	0.093	0.000	0.000
F4	67	-5	TM	M	82.72	–	1.35	22.57	58.80	6.760	0.000	0.000	6.760	0.135	0.135	0.135
F4	71.4	-0.6	TM	M	81.00	–	0.58	22.81	57.61	23.100	0.058	11.550	0.577	0.058	0.058	0.058
F4	71.6	-0.4	TM	M	63.55	–	0.05	20.70	42.80	0.094	0.235	0.469	0.938	0.141	0.005	0.000
F4	80.6	8.6	L1	C	21.24	–	0.05	3.18	18.01	0.099	0.000	0.247	0.990	0.000	0.000	0.000
F4	85	13	L1	C	17.38	0.23	–	–	–	–	–	–	–	–	–	–
F4	88.7	16.7	L1	M	33.19	–	0.02	12.81	20.36	0.023	0.000	0.115	0.000	0.000	0.002	0.000
F4	92.5	20.5	L1	M	52.61	0.23	0.07	8.97	43.57	0.138	0.007	0.000	2.765	0.069	0.000	0.007
F4	97.2	25.2	L2	C	16.13	–	–	–	–	–	–	–	–	–	–	–
F4	104	32	L3	M	53.73	–	31.51	9.45	12.76	–	3.151	0.000	3.151	3.151	0.000	0.000
F4	105.5	33.5	L4	M	20.18	–	–	–	–	–	–	–	–	–	–	–
F4	114.3	42.3	K1	M	14.71	–	–	–	–	–	–	–	–	–	–	–
F4	119	47	K2	M	17.25	–	–	–	–	–	–	–	–	–	–	–
F4	124	52	K4	C	8.75	–	–	–	–	–	–	–	–	–	–	–
F4	126	54	K4	M	12.69	–	0.00	2.91	9.78	–	–	–	–	–	–	–
F4	131	59	K4	C	14.68	–	0.03	2.38	12.27	0.063	0.003	0.127	0.000	0.003	0.003	0.000
F4	135.4	63.4	K5	M	22.48	–	0.19	2.17	20.12	0.019	0.000	0.019	10.248	0.190	0.000	0.019
F4	141.4	72.4	K8	M	17.29	–	0.01	3.23	14.04	0.000	0.001	0.001	0.316	0.210	0.000	0.000
F4	143.8	74.8	K9	M	37.53	–	–	–	–	–	–	–	–	–	–	–
F4	146.1	77.1	K	C	8.03	–	–	–	–	–	–	–	–	–	–	–
F3	32.2	118.2	I1	C	16.99	–	–	–	–	–	–	–	–	–	–	–
F3	33.1	119.1	I1	M	33.75	–	0.03	5.80	27.92	0.000	0.000	0.061	0.306	0.919	0.000	0.031
F3	43.5	129.5	I2	C	5.30	0.15	0.00	0.56	4.74	0.000	0.000	0.002	0.000	0.000	0.000	0.000
F3	49.8	135.8	I2	C	31.63	–	–	–	–	–	–	–	–	–	–	–
F3	64.7	150.7	I4	M	44.85	0.34	0.10	16.83	27.92	0.199	0.000	0.199	3.980	0.199	0.000	0.000
F3	65.8	151.8	I5	M	18.35	–	0.00	3.84	14.50	0.017	0.000	0.087	0.070	0.000	0.000	0.000
F3	90.9	176.9	H3	C	14.03	–	–	–	–	–	–	–	–	–	–	–
F3	93.2	179.2	H3	M	75.59	–	0.42	25.70	49.89	0.000	0.000	0.000	24.529	0.416	0.042	0.000
F3	94.1	180.1	G1	C	7.39	–	–	–	–	–	–	–	–	–	–	–
F3	113.2	199.2	F1	C	32.70	–	0.03	10.14	22.53	0.000	0.000	0.003	0.851	0.387	0.000	0.052
F3	137	223	E3	M	19.90	–	0.39	6.27	13.24	0.783	0.039	0.039	6.653	0.783	0.000	0.000
F3	151.3	237.3	E5	M	22.74	–	–	–	–	–	–	–	–	–	–	–
F3	158.1	244.1	E6	M	26.96	–	0.04	6.78	20.14	0.588	0.039	0.039	0.078	0.039	0.004	0.000
K2	16.8	268.8	D3	M	19.82	–	0.06	4.13	15.63	0.059	0.118	0.059	0.000	0.006	0.000	0.000
K2	20.6	272.6	D4	M	20.08	–	0.02	4.07	15.99	0.091	0.002	0.000	0.729	0.018	0.000	0.000
K2	25	277	D6	C	6.65	–	0.02	0.52	6.11	0.673	0.067	0.000	0.084	0.000	0.000	0.000
K2	33.6	285.6	D8	M	27.86	–	0.16	5.61	22.09	0.163	0.163	0.000	0.000	0.016	0.000	0.016
K2	39.4	291.4	D10	M	48.73	–	0.06	1.18	47.49	2.929	0.006	0.000	1.172	0.000	0.006	0.006
K2	41.7	293.7	D12	C	3.11	–	–	–	–	–	–	–	–	–	–	–
K2	55.9	307.9	D18	M	49.55	–	–	–	–	–	–	–	–	–	–	–
K2	65.3	317.3	D20	M	13.51	–	0.01	1.86	11.63	0.001	0.000	0.000	0.497	0.001	0.000	0.124

Table 9 (cont.)

Sample location				Grain size and analysis						Mineralogy of the sand-sized fraction (100 × % of whole rock)						
K1	89.4	327.4	D23	M	20.63	2.60	–	–	–	–	–	–	–	–	–	–
K2	75.7	327.7	D23	M	18.05	–	0.01	4.66	13.38	0.060	0.001	0.121	0.121	0.001	0.000	0.000
K1	89.9	327.9	D23	M	18.11	3.50	0.02	3.29	14.80	0.002	0.000	0.002	0.020	0.002	0.000	0.000
K1	90	328	D23	M	17.77	3.05	–	–	–	–	–	–	–	–	–	–
K1	90.1	328.1	D23	M	12.90	1.43	–	–	–	–	–	–	–	–	–	–
K1	90.6	328.6	D24	C	6.00	0.26	–	–	–	–	–	–	–	–	–	–
K1	90.8	328.8	D24	C	5.81	0.24	–	–	–	–	–	–	–	–	–	–
K1	90.9	328.9	D24	C	7.21	0.29	0.00	0.80	6.41	0.146	0.000	0.098	0.049	0.024	0.000	0.000
K1	91.1	329.1	D24	M	12.05	–	–	–	–	–	–	–	–	–	–	–
K1	91.2	329.2	D24	M	37.44	0.86	–	–	–	–	–	–	–	–	–	–
K1	91.7	329.7	D25	C	6.47	–	–	–	–	–	–	–	–	–	–	–
K1	91.8	329.8	D25	C	7.97	–	–	–	–	–	–	–	–	–	–	–
K1	92.1	330.1	D25	C	5.62	–	–	–	–	–	–	–	–	–	–	–
K1	92.2	330.2	D25	M	10.62	–	–	–	–	–	–	–	–	–	–	–
K2	82	334	C1	M	11.75	–	0.04	1.64	10.08	2.501	0.004	0.004	0.385	0.000	0.000	0.192
K2	85.7	337.7	C2	M	61.70	0.53	0.00	7.40	54.30							
K2	88.3	340.3	C3	M	12.37	–	0.00	4.88	7.48	0.201	0.000	0.000	0.150	0.000	0.000	0.000
K2	89.3	341.3	C4	C	5.96	–	0.04	0.72	5.20	1.897	0.000	0.004	0.190	0.000	0.004	0.000
K2	98.2	350.2	B1	M	15.95	2.05	0.01	6.25	9.69	0.053	0.000	0.000	0.107	0.000	0.000	0.000
K2	100	352	B2	C	14.23	–	0.03	6.59	7.61	0.151	0.000	0.003	0.000	0.000	0.000	0.000
K2	103.2	355.2	B2	M	19.01	–	0.12	7.08	11.81	0.120	0.000	0.000	0.598	0.012	0.000	0.000
K2	104.3	356.3	B2	M	50.66	–	–	–	–	–	–	–	–	–	–	–
K2	109.6	361.6	B4	C	9.16	–	–	–	–	–	–	–	–	–	–	–
K2	113.6	365.6	B5	M	22.60	2.96	0.03	4.33	18.24	–	–	–	–	–	–	–
K2	119.9	371.9	B8	M	17.95	–	0.16	8.03	9.76	0.160	0.000	0.000	0.800	0.016	0.000	0.000
K2	132.4	384.4	B12	M	85.58	–	0.69	46.21	38.51	3.466	0.000	0.000	31.194	13.864	0.000	0.000
K2	140.3	392.3	A4	M	18.34	–	–	–	–	–	–	–	–	–	–	–
K2	142.5	394.5	A5	C	15.05	–	0.00	13.35	1.70	0.002	0.000	0.000	0.048	0.000	0.000	0.000
K2	150.5	402.5	A9	M	21.37	–	0.04	5.27	16.07	0.037	0.000	0.000	0.371	0.000	0.000	0.000
K2	154.6	406.6	A	C	7.40	–	0.01	1.15	6.23	0.065	0.000	0.840	0.000	0.000	0.000	0.000
K1	174.7	412.7	A12	M	40.85	–	–	–	–	–	–	–	–	–	–	–
K1	175.15	413.1	A12	C	3.87	–	–	–	–	–	–	–	–	–	–	–
K1	175.1	413.1	A12	M	35.18	0.54	0.12	7.34	27.72	1.154	0.000	4.038	1.730	1.730	0.000	0.000
K1	175.8	413.8	A12	C	7.11	–	–	–	–	–	–	–	–	–	–	–
K1	176.3	414.3	A12	C	4.03	0.11	–	–	–	–	–	–	–	–	–	–
K1	177	415	A13	M	12.79	0.33	0.06	1.96	10.77	3.478	0.000	1.897	0.000	0.000	0.000	0.000
K1	177.4	415.4	A13	M	12.79	–	–	–	–	–	–	–	–	–	–	–
K1	178	416	A13	C	9.28	–	–	–	–	–	–	–	–	–	–	–
K1	178.4	416.4	A13	C	8.36	–	–	–	–	–	–	–	–	–	–	–
K1	178.9	416.9	A13	C	7.84	–	–	–	–	–	–	–	–	–	–	–
K1	179.3	417.3	A13	C	8.99	–	–	–	–	–	–	–	–	–	–	–
K1	179.7	417.7	A13	C	9.45	–	–	–	–	–	–	–	–	–	–	–
K1	179.8	417.8	A13	M	12.27	–	–	–	–	–	–	–	–	–	–	–
K1	180.3	418.3	A13	M	36.59	0.52	0.27	9.31	27.00	–	0.000	5.477	1.369	0.274	0.000	0.000
K2	170.2	422.2	A15	M	26.46	–	0.03	3.90	22.53	0.131	0.000	0.131	0.000	0.000	0.000	0.000

Table 9 (cont.)

Sample location				Grain size and analysis						Mineralogy of the sand-sized fraction (100 × % of whole rock)						
K2	177.7	429.7	A18	M	24.25	–	0.01	9.61	14.63	0.105	0.000	0.132	0.330	0.001	0.001	0.000
K2	186.6	438.6	A20	M	17.83	–	0.02	6.42	11.38	0.223	0.002	0.223	0.223	0.112	0.002	0.000
K1	213.6	451.6	T	C	11.36	1.32	0.08	2.78	8.49	0.008	0.008	0.000	1.687	0.169	0.844	0.675
K1	214.5	452.5	T	C	10.85	–	–	–	–	–	–	–	–	–	–	–
K1	215	453	T	M	31.10	–	3.64	12.76	14.70	–	0.000	0.000	72.813	7.281	36.406	72.813
K1	218.6	456.6	EF	MR	81.92	0.71	0.03	39.39	42.50	0.057	0.003	0.003	0.571	0.000	0.228	0.000

– = No data

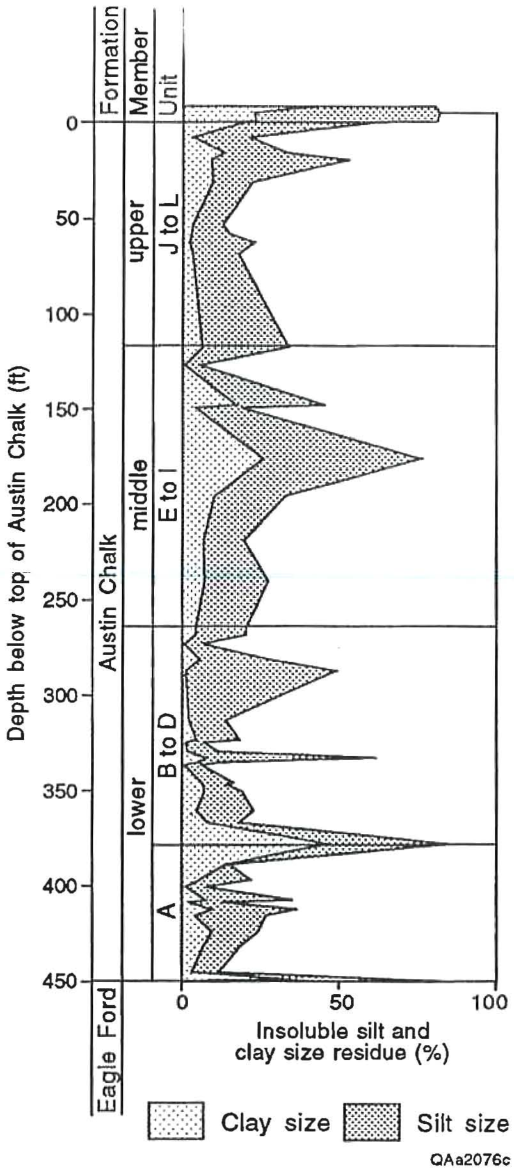

Figure 28. Vertical distribution of acid-insoluble material in chalk and marl.

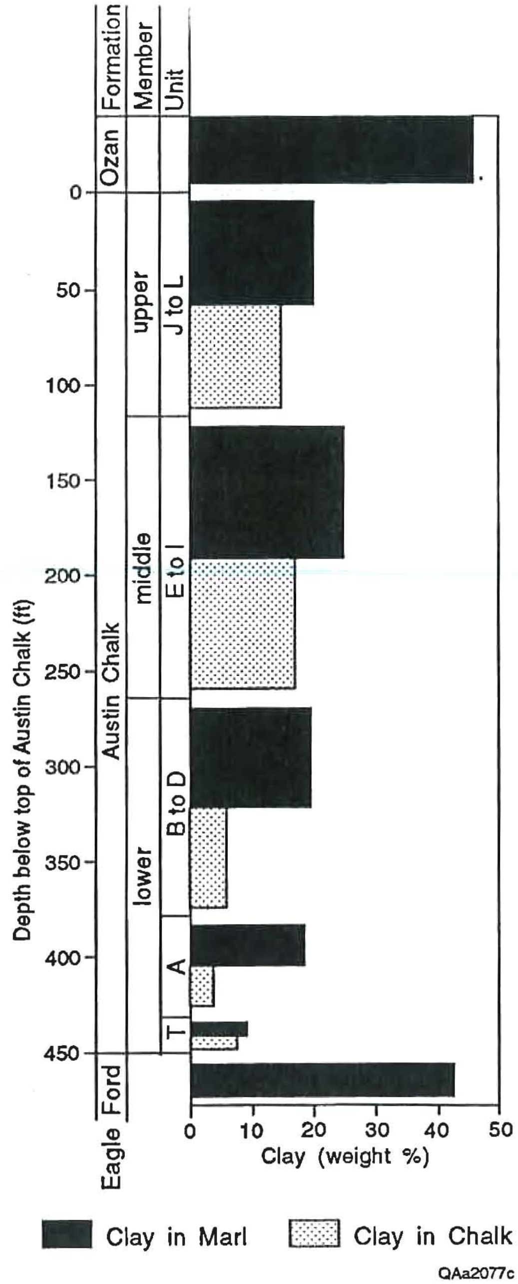

Figure 29. Average percent clay in acid-insoluble residue in chalk and marl.

Clay Composition

Clay minerals typical of chalks and marls include montmorillonite, some possibly mixed-layer montmorillonite, with lesser amounts of kaolinite and illite. Samples from the top of the Eagle Ford and base of the Ozan Formation contained similar clay minerals. A sample from the B-12 bentonite contained only montmorillonite in the clay-sized fraction. Other beds with blebs of bentonite contained a more diverse suite of clays.

Sand-Sized Material

Quartz, feldspar, biotite, pyrite, hematite, limonite, glauconite, black organic grains, and phosphate are the components of the sand-sized fractions of insoluble residues (fig. 30, table 9). Clay aggregates and gypsum present in insoluble residues are interpreted as artifacts of sample handling and preparation and were eliminated from further calculation. Sand-sized material makes up a very minor component of chalk and marl (<0.01 to 0.4 weight percent) but provides information about the provenance of argillaceous material. Examination of more abundant silt-sized material with the binocular microscope confirmed the general compositional similarity between sand and silt.

Quartz is the most abundant material in the sand-sized fraction of most samples. Three petrographically separable types of quartz were identified: clear quartz, inclusion-rich quartz, and chert. Inclusion-rich quartz and chert indicate influx of terrigenous detrital material reworked from older sediments. Although they are present in most chalk and marl samples (fig. 30a), they are especially abundant in the condensed section at the base and top of the Austin Chalk. Clear quartz is locally euhedral and is abundant in the B-12 bentonite, demonstrating a probable volcanic origin. Much of the clear quartz is conchoidally fractured. The cause of this fracturing is not understood. If it is not an artifact, the extreme angularity of this quartz supports an airborne origin. Quartz is abundant in most samples from the middle Austin Chalk (units E–I, fig. 30a) and is present in lesser quantities throughout the Austin Chalk(table 9). In most samples, clear and cloudy quartz are mixed.

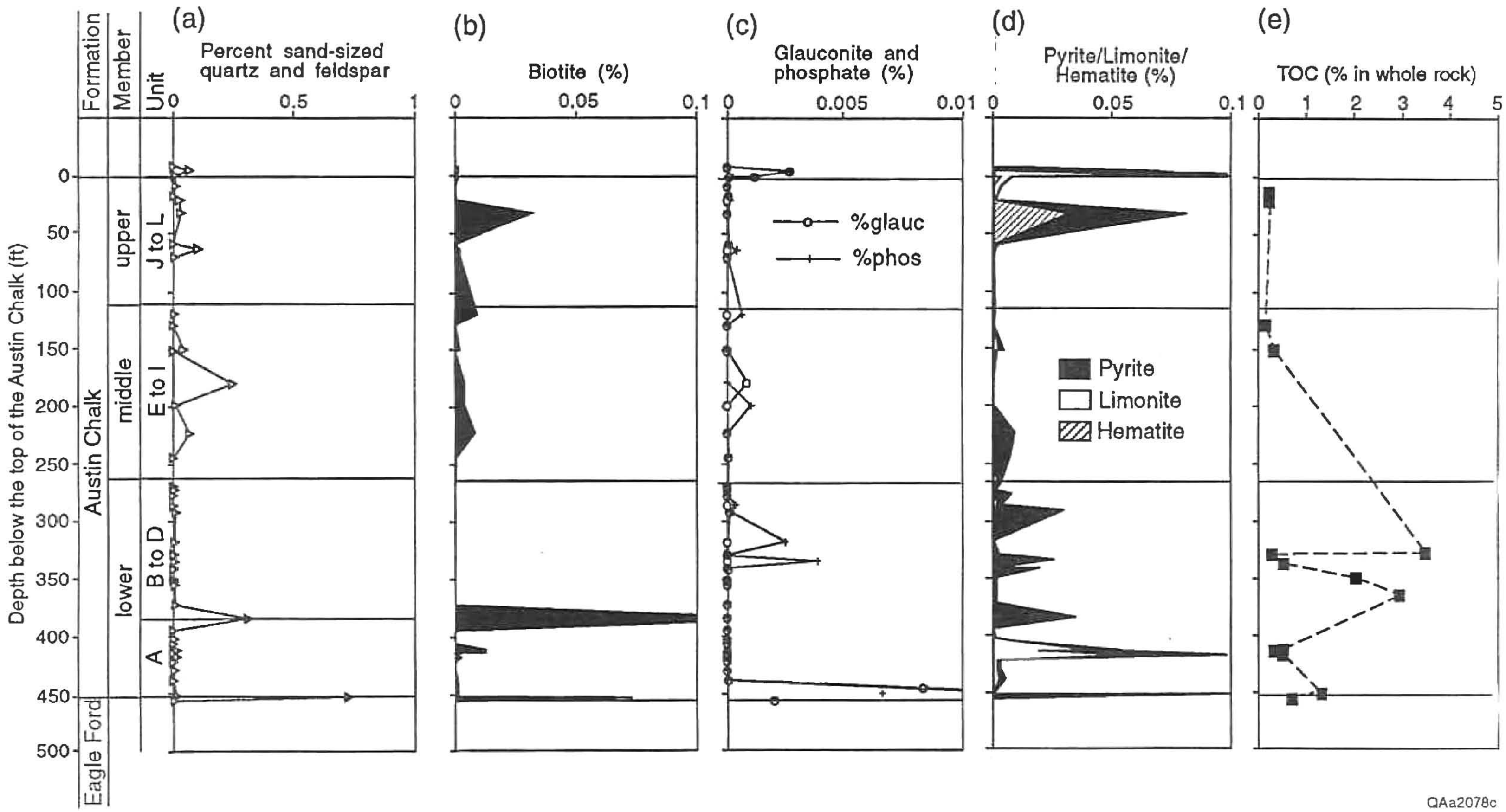

Figure 30. Vertical distribution of percent of sand-sized materials from acid-insoluble residue. (a) quartz and feldspar, (b) biotite, (c) glauconite and phosphate, (d) pyrite, limonite, and hematite, and (e) total organic carbon (TOC).

Feldspar is present and associated with quartz and biotite. Feldspar was not quantitatively separated from quartz because of the small sample size and therefore is not shown in table 9. X-ray diffraction analysis of the B-12 bentonite shows quartz, feldspars, biotite, and pyrite. Energy dispersive spectrum (EDS) analysis of feldspars suggests that Ca plagioclases are more abundant than Na plagioclases. Ca plagioclase has been vacuolized and cleaved; Na plagioclase has been corroded and rounded.

Biotite is unweathered and some is clearly euhedral. It makes up as much as 33 percent of the sand-sized fraction. Biotite is macroscopically identifiable in the B-12 bentonite. Other high concentrations (fig. 30b, table 9) indicate an important bentonitic contribution to other marl beds and confirm that many of the blebs of white clay are bentonites (altered volcanic ash). Biotite is abundant in the base of chalk-condensed section. Lesser concentrations of biotite are present in all of the samples from the middle Austin Chalk. This distribution matches the interval of increased abundance of clear quartz and feldspar discussed above.

Glauconite and phosphate occur as rounded sand-sized grains (fig. 13a). Both glauconite and phosphate were concentrated in the condensed section at the base and top of the Austin Chalk. Either glauconite or phosphate is slightly concentrated in a few beds within the chalk, notably within two samples in units C and D (fig. 30c).

Pyrite is more abundant than quartz in some acid-insoluble residue samples of chalk and marl. Scattered macroscopic pyrite nodules are observed in outcrop and core in chalk and marl, especially in the middle Austin Chalk. A few insoluble residue samples that intersected a pyrite nodule were eliminated from further quantitative analysis because they are not representative of the average rock composition. Discounting the samples with high pyrite concentrations, disseminated pyrite is consistently abundant in units B and D (fig. 30d). Pyrite occurs as cubes, irregular aggregates, pyritohedrons, and framboids. Various degrees of oxidation of pyrite to hematite and limonite are observed, and casts of these minerals after pyrite are common, especially in the upper parts of cores within 32.8 ft (10 m) of the top of bedrock.

Total Organic Carbon

Total organic carbon (TOC) was measured in 21 samples of chalk and marl selected to represent typical ranges for each unit (fig. 22e, table 9). The highest TOC values (1.4 to 3.5 weight percent) were measured in marls from units B and D and correspond to dark color and to preserved lamination. Chalk has a consistently low TOC, 0.1 to 0.3 weight percent in all units sampled.

Stable Isotopes

Representative chalk and marl samples from the Austin Chalk were sampled for $\delta^{13}C$ and $\delta^{18}O$ (table 10). $\delta^{18}O$ ranges from –2.62 to –3.49‰ (measured versus the PDB standard), and $\delta^{13}C$ ranges from 1.81 to 1.35‰ PDB. No clear trend in $\delta^{13}C$ or $\delta^{18}O$ is evident by unit or with depth in the Austin Chalk (fig. 31), and selected samples across one cycle showed no pattern to the fluctuation of $\delta^{13}C$ and $\delta^{18}O$ within one cycle (fig. 31). A possible trend of increasing $\delta^{13}C$ with increasing $\delta^{18}O$ may be defined by plotting $\delta^{13}C$ versus $\delta^{18}O$ (fig. 32), although anomalously heavy carbon was measured in two samples from chalk, one in unit D and one in unit K.

Discussion

Stratigraphic Variation in Microfabrics

SEM examination of representative samples of chalks showed systematic variability in clay distribution. As seen on a freshly fractured surface of chalk from the middle Austin Chalk, clay coats almost all of the nannoplankton, so that the coccoliths and calcite cement seen in the lower and upper Austin Chalk are obscured. Chalk samples from the middle Austin Chalk, however, do not have a much higher clay content than other samples (figs. 28 and 29). The difference, then, is in microdistribution of clay (fig. 33). In the middle Austin Chalk, a thin layer of clay coats all grains in comparison to other chalk beds in the Austin Chalk, where similar quantities of clay occur as 1-mm flakes and larger structureless masses. The microdistribution of clay varies from percent acid-insoluble

Table 10. Stable isotopes from representative chalk and marl in the Austin Chalk.

Sample no.	Depth below TAC (ft)	Unit	Lithology	$\delta^{13}C$	Stand. dev. $\delta^{13}C$	$\delta^{18}O$	Stand. dev. $\delta^{18}O$	Comment
E4 64.8	49	K	chalk	1.66	0.04	–2.62	0.03	
E4 94.95	74	K	chalk	1.55	0.04	–3.28	0.03	
T3 48.3	180	G	chalk	1.57	0.01	–3.16	0.03	
T3 65.55	200	G	chalk	1.73	0.03	–3.49	0.03	
BI3 81.4	230	E	chalk	1.62	0.07	–2.98	0.06	Fracture zone
BI3 84.1	234	E	chalk	1.53	0.03	–2.86	0.03	Fracture zone
	292.9	D	chalk					Below fault
J2 35.1	309	D	marl (org.)	1.35	0.05	–3.19	0.05	
J2 40.3	314	D	chalk	1.81	0.04	–3.84	0.05	
J2 40.3				1.78	0.04	–3.88	0.02	
K1 178.0	416	A	chalk	1.47	0.02	–3.30	0.04	
K1 178.9	416.9	A	chalk	1.23	0.01	–3.56	0.03	
K1 179.7	417.7	A	chalk	1.37	0.14	–3.32	0.11	
K1 180.3	418.3	A	marl	1.47	0.07	–3.49	0.01	

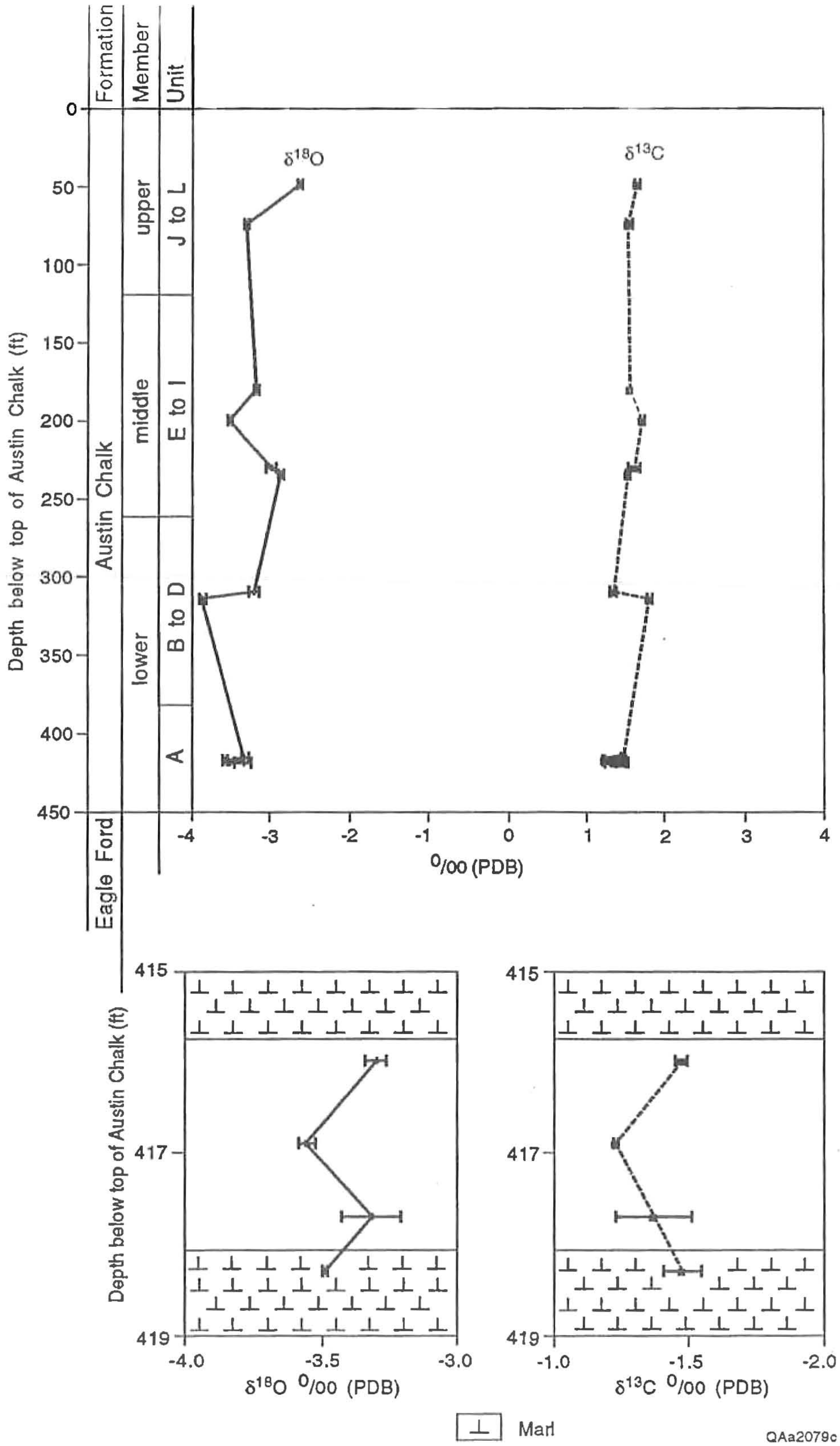

Figure 31. Vertical distribution of $\delta^{18}O$ and $\delta^{13}C$ in calcite through the Austin Chalk. Detail boxes show the distribution of stable-isotopic composition of four samples within a marl-chalk cycle.

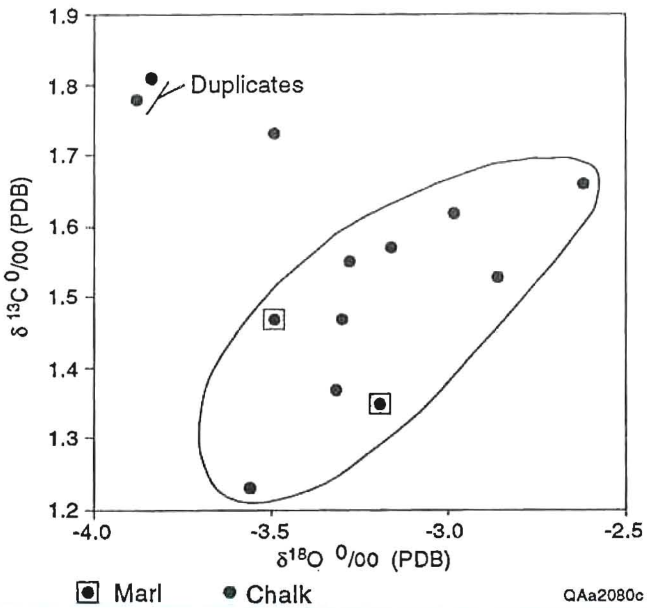

Figure 32. Relationship between $\delta^{13}C$ and $\delta^{18}O$ in chalk and marl samples.

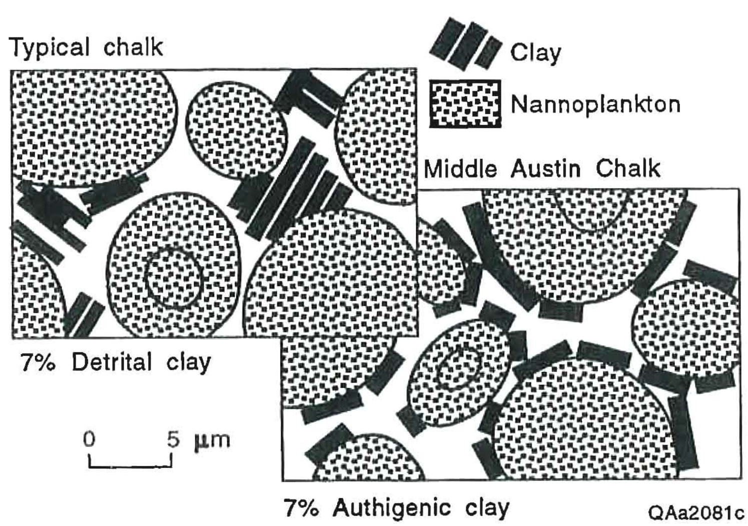

Figure 33. Microdistribution of clay, drawn on the basis of SEM examination of typical samples from various Austin Chalk units. SEM view is limited in that fractured faces go between, not through, the micron-scale particles that compose the chalk. In this view, the particles are shown as if they have been sliced to enhance the differences in clay distribution.

of percent clay-sized material, which is similar in the middle and upper Austin Chalk. A sample of the upper Austin Chalk with moderate-insoluble content (14 percent) lacks pervasive clay coatings, whereas low-insoluble content (7 percent) chalks in the middle Austin Chalk have clay coatings on most component grains. However, all marl samples with high-insoluble content have pervasive clay coating all surfaces.

The differences in the microdistribution of clay are interpreted as a contrast between clay coats, formed by authigenic precipitation of clay, and clay that was deposited as detrital material sourced from distant upland areas or reworked altered volcanic ash. This interpretation is based on the coincidence of clay-coated nannoplankton with persistent biotite, quartz, and feldspar phenocrysts in the middle Austin Chalk. The distinction between the middle Austin Chalk and the other units is that almost every sample in the middle Austin Chalk has some evidence of volcanic contribution, in comparison to higher but more sporadic discrete bentonites in other units. During middle Austin Chalk deposition, minor ash fall must have occurred frequently. Authigenic clay derived from devitrification of volcanic ash codeposited with the chalk efficiently coated most of the grains. The detrital clay was not as efficient at coating the nannoplankton grains, possibly because the detrital clay was flocculated in seawater or otherwise not dispersed. Grains are, however, obscured in all marls because of high concentrations of either detrital or volcanogenic clay.

The clay distribution is a factor influencing permeability and log character. The low SP response of the middle Austin Chalk is classically interpreted as a middle high-clay unit (e.g., the Bruceville chalk-marl of Durham, 1957; Dallas Geological Society, 1965, cited in Reaser and Collins, 1988). However, clay content in the middle Austin Chalk in Ellis County is not markedly higher than in other units (figs. 21 and 28). This holds true if the clay and insoluble material are averaged in chalk and marls through the interval, measured only in chalk, or measured as average marl bed thickness. However, the middle Austin Chalk in Ellis County exhibits low plug porosity and permeability as well as the low response on SP logs characteristic of this unit regionally. The porosity/permeability response is interpreted as an effect of the abundance of authigenic clay coats in this interval. The authigenic clay fills many intercoccolith areas, reducing porosity. The permeability of the middle

Austin Chalk is higher than an equally low porosity sample of upper or lower Austin Chalk would be, based on the porosity/permeability cross plot. This observation supports the picture of authigenic clay coats on grains shown in figure 33 because the clay preferentially coating grains impedes flow slightly less than a large amount of detrital clay in interpore areas.

The increased abundance of calcite cement in the upper Austin Chalk (units J, K, and L) is interpreted as a product of aragonite stabilization. Its stratigraphic distribution may reflect increased faunal diversity in units J, K, and L. The relationship between calcite cement and aragonitic fauna has been noted in the Austin Chalk of South Texas and interpreted as a cause of decreasing porosity crosscutting the typical depth- and dissolution-related trends (Dravis, 1991). Analogous calcite cements sourced by dissolution of the aragonitic nacreous layer of inoceramids and cephalopod shells have been documented in the Campanian Annona Formation of southwest Arkansas (Bottjer, 1985). The pressure solution of calcite common in the subsurface Austin Chalk (Scholle and Cloud, 1977; Czerniakowski and others, 1984) is minor in Ellis County, evidenced by good coccolith preservation and only very minor fabric evidence of compaction (few of the fractured grains or wispy laminations typical of subsurface Austin Chalk). Minimal pressure solution is typical of the Austin Chalk in outcrop where burial has been minimal. The moderate SP response and permeability in the upper Austin Chalk in Ellis County may reflect either fairly abundant fine calcite cement or a moderately high clay content in chalk.

Bentonite Beds

Bentonites (altered volcanic ash beds) have been recognized in the cores of the Eagle Ford Formation, Austin Chalk (Dallas Geological Society, 1965, cited in Reaser and Collins, 1988), and Taylor Group (Dawson and others, 1985). The Wolfe City Sandstone (Taylor Group) contains abundant volcanic rock fragments and Na-plagioclase as well as quartz and heavy minerals indicative of recycled older sediments with metamorphic source areas (Beall, 1964).

Volcanic contribution is evidenced in cores from the SSC ring by both discrete monimorillonite concentration within marl beds and in volcanic components disseminated through chalk and marl beds.

Bed B-12, the marker at the base of unit B, is a bentonite thick enough to have been preserved as a compositionally distinct unit even after burrowing. It has a coarse concentration of biotite, quartz, and feldspar at its base in a montmorillonite matrix. Feldspar, biotite, and clear, angular (conchoidally fractured or euhedral) quartz are interpreted as volcanic contributions because of their abundance in the B-12 bentonite and because of their typical association with volcanic ashes. Other volcanic quartz, biotite, and feldspar, as well as montmorillonite, are disseminated in both chalk and marl beds. Clear, angular quartz and biotite are present in every sample from the middle Austin Chalk, as well as in about half of the other samples. Presumably these disseminated components originated in small ash fall events but were mixed with the sediment by burrowing and reworking. Transportation of volcanic components as detrital material from distant emergent or more local winnowed shelf areas is also possible, as documented by the inclusion-rich quartz and chert in the sand-size fraction in many samples. In most samples more than half of the quartz is clear and angular, which gives a rough indication of the relative importance of volcanic and detrital contribution. Likewise, the montmorillonite-dominated clay suite in chalk and marls reflects a mixture of clay derived from (1) alteration of volcanic ash-fall glass deposited in the chalk and marl and (2) clay of either altered volcanic or other origins reworked from emergent or shelf areas. Illite and possibly kaolinite may be indicators of nonvolcanic contribution to the chalk.

Possible sources for ash are Balcones trend volcanism (Ewing and Caran, 1982; Ewing, 1986), volcanics from Arkansas, and western United States volcanic source areas. Balcones volcanism occurred during upper Austin Chalk and Ozan deposition (Ewing and Caran, 1982) and was dominantly mafic, so it is an unlikely source for the quartz-bearing bentonites through the entire Eagle Ford–Austin Chalk–Taylor Group section.

Chalk-Marl Cyclicity

Rhythmically bedded, meter-thick cycles may have formed in response to allochthonously driven variables (for example, climatic fluctuations caused by regularly occurring shifts in the Earth's orbit) or be related to regular but localized shifts in sedimentation patterns. Chalk-marl alternation falls in the production/dissolution style of cyclicity (Einsele, 1982; Research on Cretaceous Cycles [ROCC] Group, 1986). That is, the alternation between chalk and marl accumulation can reflect either (1) variation in nannoplankton productivity or (2) variation in argillite input. Preferential dissolution of calcite along clay–calcite grain boundaries in marl beds causing concentration of clay in marl beds (rhythmic unmixing) is important in many cyclic sediments (Einsele, 1982; Hallam, 1986). Preferential dissolution of calcite-creating microstylolites and concentration of insoluble materials at the edges of macrofaunal components is recognized but appears to have had minimal impact on bed thickness and clay content in the Austin Chalk in Ellis County. Firmgrounds characteristic of scour cycles (ROCC Group, 1986) are few, stratigraphically restricted, and may be of only local extent in the Austin Chalk in the Ellis County area. Firmgrounds in the Austin Chalk in Ellis County have not been lithified. The surface developed on the top of the Austin Chalk at its contact with the Ozan Formation is the exception because it is phosphatized, indicating a more prolonged episode of nondeposition.

Diagenesis

Fabrics observed during this study support the conclusion that has been reached for most shallowly buried chalks, namely, that diagenetic modification has been minimal because of the original mineralogical stability of chalk (Scholle and others, 1983). In the Austin Chalk, petrologic textures indicate that the original sediment has been modified by the following processes: (1) coccolith ooze dewatered, (2) volcanic ash devitrified sourcing authigenic clay, and (3) aragonitic fossils dissolved and the $CaCO_3$ reprecipitated as pore-filling calcite cement and overgrowths. Pressure solution along stylolites and large skeletal grains was minimal.

The Austin Chalk has been variously interpreted as an open or a closed geochemical system. This has implications in the SSC area for the chemical evolution of the chalk and enclosed fluids. Dravis (1980), Cloud (1977), and Scholle and Cloud (1977) documented changes in whole rock stable isotopes with depth, which they interpreted as evidence of pressure solution at higher temperature leading to isotopic fractionation. Dravis (1980) also interpreted calcite cements as evidence of freshwater invasion of shallow-water Austin Chalk facies on the San Marcos Arch. Czerniakowski and others (1984) drilled splits of a variety of calcite phases from chalk, including some vein samples, and concluded that isotopic fractionation had been minimal because the chalk was a hydrologically closed system. Oil in South Texas Austin Chalk reservoirs is interpreted as self sourced (Grabowski, 1984; Hunt and McNichol, 1984), indicating a dominantly closed system during oil maturation. Corbett and others (1991b) documented an early generation of fractures in the lower Austin Chalk (Atco) that are filled with calcite and clay and are interpreted as the product of natural hydrofracturing of the chalk and expulsion of fluids from the underlying Eagle Ford Formation. In contrast, calcite vein-fillings in southern Ellis County have $^{87}Sr/^{86}Sr$ of 0.7073 to 0.7074, close to the expected values for Cretaceous seawater (Reaser and Collins, 1988). This supports a hydrologically closed system for these veins, because waters that were derived from feldspar-bearing units such as the Woodbine or potentially the Eagle Ford Formation might be expected to acquire more ^{87}Sr from rubidium decay.

In Ellis County samples, oxygen in calcite is lighter with increasing permeability (fig. 34a). Carbon shows a possible weak trend of isotopically lighter carbon with increasing permeability (fig. 34b). Samples with the highest permeability are found in the units that characteristically exhibit the best preservation of fine structure in nannoplankton. It is possible that the porosity-occluding processes or pressure solution enhanced by clay-calcite grain contacts occurred in cool ocean water and resulted in precipitation of isotopically heavier calcite or preferential dissolution of isotopically lighter components, for example, plankton formed in warm near-surface water. It is also possible that units with higher porosity have undergone isotopic exchange with isotopically light fresh water; however, if this occurred, the exchange took place without significant calcite dissolution and reprecipitation.

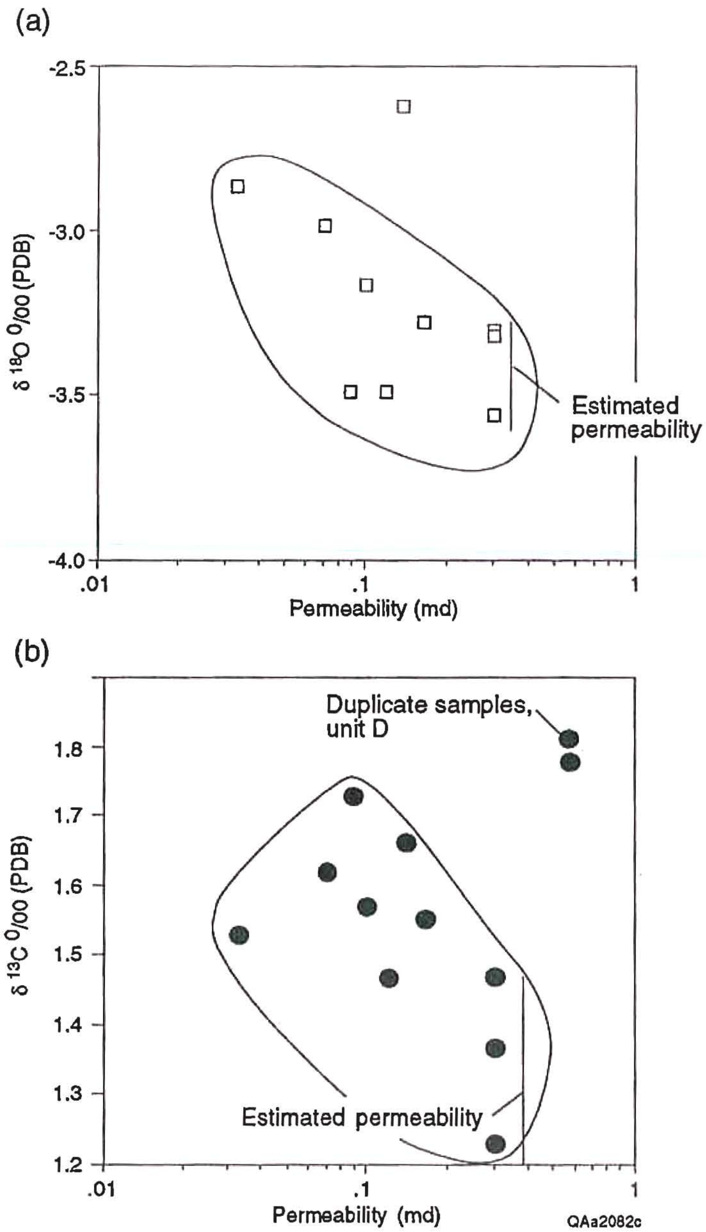

Figure 34. Relationship between chalk permeability and (a) $\delta^{18}O$ of calcite and (b) $\delta^{13}C$ of calcite, both showing a weak negative correlation. Permeabilities of 3 samples were estimated from figure 26.

Vertical Facies Variation in the Austin Chalk

Sedimentological features provide information about evolution of the Austin Chalk depositional environment (fig. 11). Interpretation of the depositional environment is based on the distribution of channels, firmground, cycle patterns, the insoluble content, and fauna.

A condensed section and accumulation of quartz, glauconite, and phosphate sand and pebbles marked minimum sediment accumulation during the rapid transgression that initiated chalk deposition. The initial phase of chalk deposition (unit A) is interpreted as a time when resedimentation of chalk was important. Resedimentation is reflected in chalk-filled channels. The paucity of macrofauna in this interval may also reflect reworking or rapid sedimentation of this unit. Resedimentation might have been favored by topographic irregularities or high depositional gradient on the shelf during initial chalk deposition. The sedimentologic conditions in which channels form in chalk have not been well documented in modern environments. In ancient sediments, channels are interpreted as a characteristic of near-shore and transitional areas (Scholle, 1977b). Schatzinger and others (1985) documented resedimentation via slumps, debris flow, and turbidites in chalks from the North Sea, possibly related to depositional topography at the Central Graben. Buchbinder and others (1988) documented glides, slumps, and debris flows in Eocene Chalks of Israel that formed in response to sedimentologically steepened slopes. Chalk-filled channels in Austin Chalk near Langtry, West Texas, are interpreted as distributary channels in an outer-shelf midfan setting (Lock, 1984).

In contrast, channels may reflect current energy. Basal scours defining cycles in the Cretaceous chalks of England are interpreted as the result of sea-level-driven fluctuation in tidal energy (ROCC Group, 1986; Robinson, 1986). Several horizons of 82-ft-deep (25-m), 492-ft-wide (150-m) chalk-filled channels in Turonian–Santonian chalks are mapped on sea-cliff exposures in Haute Normandie, France (Quine and Bosence, 1991). These channels are interpreted as the result of scours in structurally controlled straits of the Anglo–Paris Basin developed during sea-level lowstands.

Regional study of the widespread lower Austin Chalk and reexamination of its relationships with the Eagle Ford and with overlying units may help clarify the depositional environment of unit A in Ellis County. Chalk-marl cycles in unit A might result from deposition of chalk sediments supplied down channels alternating with interchannel marls. However, individual beds within unit A can be correlated 11 mi (18 km) along the west side of the SSC ring, suggesting that a dominant extrinsic forcing mechanism formed most chalk-marl alternations, which were then crosscut by small channels.

Deposition of Austin Chalk units B, C, and D is interpreted as occurring in the deepest water environment. Evidence for deep water is (1) minimum amounts and grain size of terrigenous detrital material, suggesting the most distal shoreline and (2) high organic content (0.007 percent) and disseminated pyrite content (nearly 1 percent), indicating disaerobic bottom conditions. Disaerobic conditions indicate separation of bottom waters from the surface and can develop in any water depth because of formation of several different water masses with different densities caused by temperature, salinity, or sediment load (Tucholke and Mountain, 1979; ROCC Group, 1986). Organic-rich chalks of the Niobrara Formation of the Western Interior Basin are interpreted as a product of anoxic conditions that developed midtransgression and midregression beneath a stratified water mass (Rodriguez and Pratt, 1985). In chalk sediments of Europe, anoxic sediments formed during highstands when deep ocean waters spilled up onto the shelves. The organic marls in units B and D may be partly analogous to these ocean anoxic events. An ocean anoxic event in the upper Coniacian of Yugoslavia (Jenkyns, 1991) or at the Coniacian–Santonian boundary (Hart and Ball, 1986) might correspond to units B or D. The base of the organic marls coincides with the B-12 bentonite where it was examined on the western side of the SSC ring; 9.3 mi (15 km) to the north in outcrop, organic marls occur several cycles below the bentonite. This relationship fits with the interpretation that the organic marls are depth related. In the deeper parts of the facies tract, toward the Dallas Basin, disaerobic conditions were established earlier. Unit C, which is characterized by low gamma-ray response of the marls, records an interval of cessation of stratified conditions. Unit D is gradational into the overlying middle Austin Chalk, as indicated by gradual decrease in gamma-ray response in the marls related to decreasing organic content.

The middle and upper Austin Chalk are characterized by an upward increase in the frequency of occurrence of winnowed packstone beds and firmgrounds. Many winnowing episodes are recorded only by remnant packstone-filled burrows. The more diverse faunal assemblage in the middle and upper Austin

Chalk, including *Gryphaea,* oysters, and small pelecypods, probably developed in response to more frequent, firmer bottom conditions. In some cycles (for example, in chalk I-6) firmgrounds are laterally correlative between cored wells to other firmgrounds, oyster beds, or intervals of packstone-filled burrows. In other cycles, for example marl E-6, a firmground recognized in the BE 3 core is equivalent to ordinary chalk with no evidence of winnowing 2.2 mi (3.5 km) away in the F 3 core, indicating that firmgrounds were of local extent. Limited lateral extent is also observed in outcropping packstone beds in the Lake Waxahachie spillway, which are equivalent to a number of thin-winnowed beds in unit K in the F 4 core 9.3 mi (15 km) away. Lateral heterogeneity in the upper Austin Chalk is also evidenced in the variable thickness trends of unit L, which is thickened along an east-west trend near the middle of the SSC ring. Upward-increasing winnowing and firmground formation and increased amounts of clay in chalk-marl cycles (fig. 29) in the middle and upper Austin Chalk are consistent with decreased water depth and basinward migration of the shoreline in response to falling sea level.

Detrital siliciclastic accumulation of the Ozan Formation resumed at the end of Austin Chalk deposition. In Ellis County, the top of the Austin Chalk is a bored hardground, indicating prolonged subaqueous nondeposition and sediment bypassing. Recent microfaunal dating of the chalk-marl contact (Marks and Stam, 1983) suggests that the age of this contact varies along the outcrop trend and that the amount of missing time at the contact is minor and unresolvable using faunal data.

In summary, subtle vertical facies changes in the Austin Chalk in Ellis County reflect (1) flooding (phosphate/glauconite/quartz-sand-rich condensed section and transition into chalk of unit T); (2) maximum relief (locally channeled, macrofauna-poor, strongly cyclic unit A); (3) deepest water (high-organic/low-detrital marls of units B and D); (4) shallowing (increased siliciclastic detrital as well as volcanic material and development of firmgrounds and oyster communities of units E through I of the middle Austin Chalk); (5) continued shoaling (local winnowed carbonate accumulations of units J, K, and L); (6) minor, possibly facies-controlled sediment bypassing (hardground formation); and (7) resumption of detrital siliciclastic accumulation (Ozan Formation).

Conclusions

The Austin Chalk was deposited in a deep-water shelf environment in which sediment supply was dominated by pelagic carbonate generated in situ. The dominant nannoplankton ooze limited bottom-dwelling populations to infaunal burrowers and specially adapted inoceramids. The stable depositional environment accounts for the lithologic homogeneity of the Austin Chalk. Subtle variability in the Austin Chalk is related to three kinds of environmental shifts: (1) chalk-marl alternation on a meter scale, (2) evolution of the depositional environment influencing sediment distribution patterns, and (3) changes in the amount and sources of allochthonous siliciclastic material (detrital and volcanogenic). These environmental changes have a variety of subtle effects on the mechanical properties of the Austin Chalk.

Abundant authigenic clay is interpreted as a product of alteration of volcanic ash codeposited with the chalk. The stratigraphic distribution of authigenic clay corresponds to disseminated minor amounts of biotite, quartz, and feldspar phenocrysts in most samples of the middle Austin Chalk. The ash contribution may influence the mechanical properties of the middle Austin Chalk.

Chalk-marl alternations are interpreted as production/dilution cycles. Concentration of macrofauna in marls suggests but does not prove that marls were formed at times of slower sedimentation (low productivity and/or low preservation of nannoplankton). Chalk-marl cycles vary slightly in thickness, the thickest cycles being in units A, K, and L. These thickness variations, or the ratio of chalk to marl bed thickness, potentially may influence fracture spacing.

Chalk sedimentation evolved during the highstand. The condensed section produced during flooding grades upward into unit A, which is interpreted as a locally channeled deposit. Channels may reflect conditions of higher topographic relief during transgression. Maximum flooding established deepest water conditions during deposition of units B, C, and D in the upper part of the lower Austin Chalk. The overlying middle and upper Austin Chalk contain increasing evidence of shallowing including firmgrounds, oyster communities, and local winnowed carbonate accumulations and increased detrital input. The increased abundance of calcite cement in the upper Austin Chalk is the product of stabilization of increased amounts of aragonitic skeletal material formed as a result of higher faunal diversity in firmground environments and is a possible variable decreasing matrix permeability.

FRACTURE SYSTEMS OF AUSTIN CHALK

Fractures play a significant role in moving ground water through the Austin Chalk and Ozan Formation because their unfractured bedrocks typically have low hydraulic conductivities. Predicting rates of ground-water flow and transport through fractures in low-permeability rock is a complex problem, requiring information on the characteristics of fractures and their three-dimensional networks. Important fracture characteristics include fracture geometry (strike, dip, length, height), connectivity (degree of contact among fractures), aperture, mineralization, and spacing. It is also important to determine the variation in fracture density and connectivity for different stratigraphic intervals as well as for structural features such as monoclines and faults.

This study focused on mapping and describing fractures in the Austin Chalk in the Ellis County area. Fractured marl of the Ozan Formation was not studied in the same detail as the Austin Chalk because Ozan outcrops are very sparse and weathered. The Ozan Formation is less brittle than the Austin Chalk and usually less fractured.

Description of Chalk Fractures

Fractures in outcrop and core from Ellis County include normal faults, veins, and joints (Collins and others, 1992). Normal fault planes are striated, polished, and locally calcite coated. Faults with less than 5 ft (1.5 m) of throw are the most common natural fracture type in core.

Veins are associated with faults. Some veins are gaps that developed along fault surfaces during fault movement. Others occur as parts of fracture swarms and as isolated features. They are generally only partly filled with calcite and thus have finite permeability. Veins typically have widths of as much as 2 inches (5 cm) and open apertures locally as wide as 0.8 inches (2 cm). Rare veins are as much as 8 inches (20 cm) wide. Crack-seal microstructures in vein-filling calcite indicate that veins experienced numerous crack-opening episodes. Some wide cavities are not connected by open pathways to other fractures because of infilling calcite, suggesting that convoluted and dead-end flow paths exist.

Joints are systematic and nonsystematic extension fractures that show no evidence of lateral movement parallel to fracture planes and that have small (<0.0098 inch [0.25 mm]) aperture. Many joints are the result of regional deformation. Others result from surficial processes such as unloading and weathering. Fractures lacking mineralization and having no evidence of slip are common in outcrop but rare in core. Quarries tend to be more fractured than natural outcrops as a result of mining operations. Fractures are also abundant in the near-surface weathering zone. In Ellis County, the weathered zone in Austin Chalk averages 12 ft (3.7 m) thick and locally is as thick as 45 ft (13.7 m). Systematic joints in weathered chalk are typically stained with limonite or hematite, and many are surrounded by halos of stained rock. Many fractures in the weathered zone are nonsystematic and do not exist below the base of the weathered zone.

Attributes of small faults, veins, and joints are described below in association with regional fracture sets or faults (fig. 2). Attributes that vary with structural position include size, width and aperture, attitude, orientation, spacing, and connectivity.

Fracture Stratigraphy

Compositional variations within the Austin Chalk influence fracture frequency (Corbett, 1982; Corbett and others, 1987) because chalk beds tend to have more fractures than marls. Moreover, chalk becomes less brittle as clay content increases. Outcrop data on fracture spacing and chalk strength were used by Corbett and others (1987) to infer that the upper and lower thirds of the Austin Chalk are more susceptible to fracture than the middle third. Our observations confirm this pattern but also show that important variations in brittleness exist within the three Austin Chalk intervals. We used the number of fractures per length of core for each stratigraphic unit (units T and A to L described above) to estimate fracture frequency (fig. 35). In 99 vertical and slant cores distributed over a 300 mi^2 (770 km^2) area, contrasts in fracture frequency are minor. Nevertheless, for wells and core intervals distant from

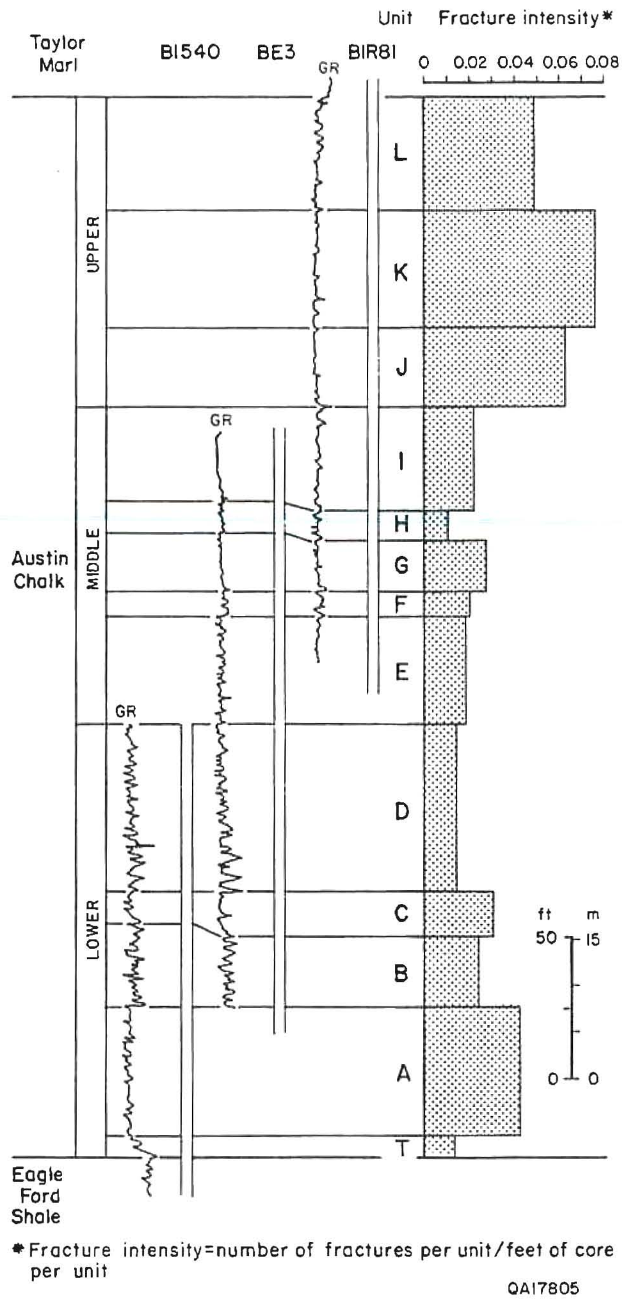

Figure 35. Stratigraphic subdivision of Austin Chalk, Ellis County, Texas, and regional fracture intensity for individual chalk units. Intensity is based on study of 369 fractures in 11,880 ft (3,621 m) of core not cut by large faults. GR = gamma ray log; single letters (E, G, H, etc.) designate informal chalk units; B1540, BE3, and BIR81 are boreholes at the SSC site. From Collins and others (1992).

faults, some units in the upper and lower Austin Chalk have more fractures than units in the middle part of the chalk (fig. 35). Greatest fracture intensity is found in lower unit A and upper units J, K, and L. The least fractured units are E through I in the middle zone, and units T, B, C, and D of the lower interval.

Chalk microfabrics show an interesting relationship to fracture intensity. The middle Austin Chalk has half the fracture intensity of the upper Austin Chalk and lower Austin Chalk unit A. The more ductile response to regional fracturing of the middle Austin Chalk has been related to smectite content (Corbett and others, 1987). However, in Ellis County, chalk beds in the middle Austin Chalk have a higher average clay content than does chalk in unit A, but a lower average chalk content than chalk beds in the upper Austin Chalk (fig. 28). Therefore, clay content is not a controlling mechanism on fracture intensity in SSC wells. It is possible, however, that distribution of authigenic clay might account for the reduced fracture intensity in the middle Austin Chalk. Authigenic clay coats on nannoplankton might allow slip on a microscopic scale, increasing ductility of the rock. This hypothesis could be tested by petrologic analysis of samples subjected to mechanical strain testing.

The match between microfabrics and fracture intensity is imperfect in that units B and D have excellent preservation of uncoated nannoplankton but fall in the low fracture intensity group. Possibly some other factor, such as high organic content in marls or weathering of the abundant disseminated pyrite, also affects the mechanical properties of the chalk in these units. This interpretation is supported by the weak response of these organic-rich units to outcrop weathering.

The higher disseminated ash contribution may be the sole or contributing cause of the regionally traceable low SP in the middle Austin Chalk. If this is true, similar increased authigenic clay might account for the more ductile behavior of this unit in other areas.

Regional Joints and Small Faults

In areas distant from large faults, widely spaced, isolated vertical joints and veins and small faults make up regional fracture patterns (Collins and others, 1992). Along the Balcones Fault Zone and along its projection in Ellis County, joints mostly strike in one of three directions: northeastward (N30°–60°E), eastward (N70°–100°E), and northward (N10°W–N20°E) (Collins, 1987; Reaser and Collins, 1988; Barquest, 1989; Muehlberger, 1990). Most faults and veins have similar strikes. Northwest-striking fractures have been reported from some parts of the fault zone (Mainster and Coppinger, 1987) but are uncommon in fresh rock in Ellis County; they are prevalent in some quarry exposures and in weathered outcrops. Vertical joints are rare in vertical cores, slant cores, and tunnels, suggesting that they also are uncommon in the subsurface. In core, small faults usually are the only fractures encountered (fig. 36).

In long outcrop traverses (550 to 1,650 ft [170 to 500 m]), spacing between fracture swarms or single faults ranges from 20 ft (6 m) to more than 300 ft (91 m) (fig. 37). In outcrops where fractures are more uniformly and closely spaced than this, surficial processes are commonly responsible.

For systematic regional joints and veins, heights (vertical trace lengths) are usually less than 10 ft (3 m). Joints and veins terminate vertically at chalk-bed margins, or less commonly, within chalk beds. Some joints cut several beds, whereas others cut only individual beds. The limited vertical extent of chalk joints should inhibit vertical fluid communication.

Trace length of joints in plan view is highly variable and, owing to limited outcrop size, is rarely possible to measure fully. The longest trace we measured was 33 ft (10 m), but most are in the range of 6 to 20 ft (2 to 6 m). Joints are commonly composed of segments arranged in relay and en echelon. Where segments overlap, fracture tips curve slightly and may intersect. Short traces and joint segmentation suggest that joint networks are poorly interconnected along strike.

In areas distant from large faults, fracture swarms are sparse but persistent. Swarms comprise a few to tens of closely spaced joints or veins. Swarms are as much as 10 ft (3 m) wide. One narrow 3-ft-wide (1-m) swarm near Rockett is composed of seven fractures with irregular spacing. Fractures in this swarm are partly open veins, with widths from 0.1 inch (0.25 cm) to 1.5 inches (3.8 cm). Portions of four veins have apertures greater than 0.2 inch (0.5 cm). Morphology of fracture-lining crystals shows that measured apertures are representative of the subsurface. Such exposures demonstrate that fracture swarms distant from folds and faults locally have attributes consistent with a capacity to transmit fluid.

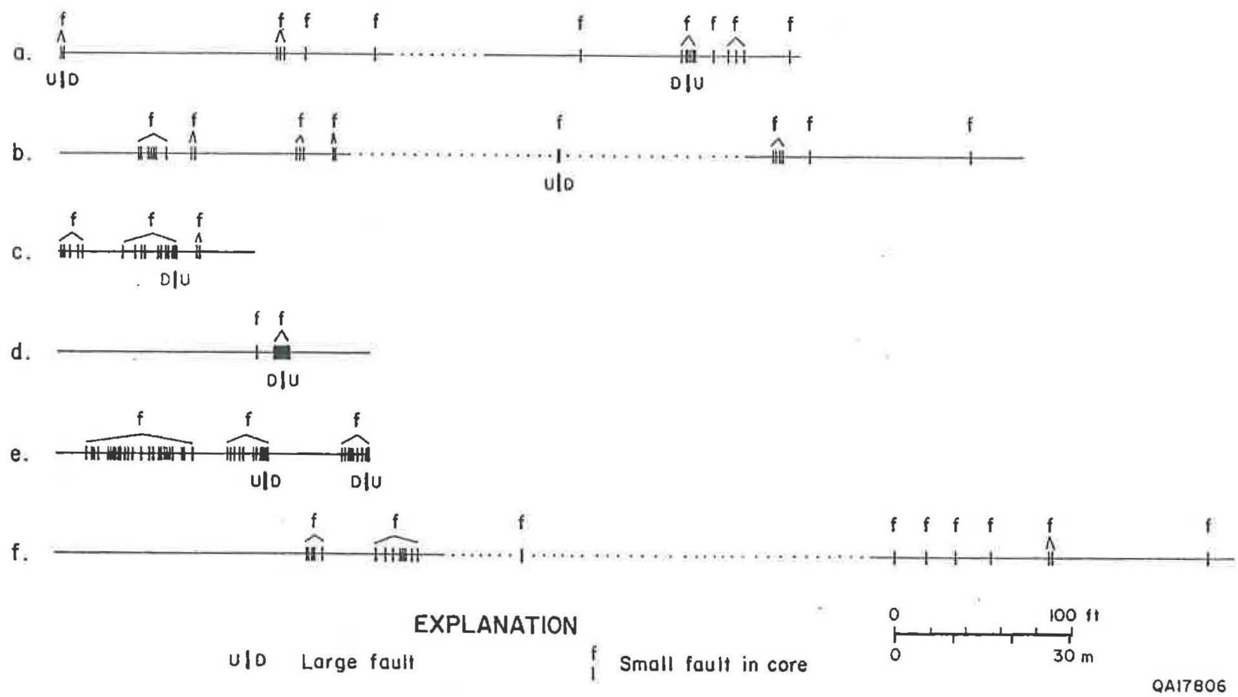

Figure 36. Scan lines showing fractures in slant core drilled at 45° to 55° in Austin Chalk, Ellis County, Texas. Fracture locations were projected from slant core hole to horizontal scan line. Scan lines a, b, and f were each constructed from two nearby slant holes. Scan lines a, b, c, d, and e cross large faults. Scan line f does not cross any large faults. From Collins and others (1992).

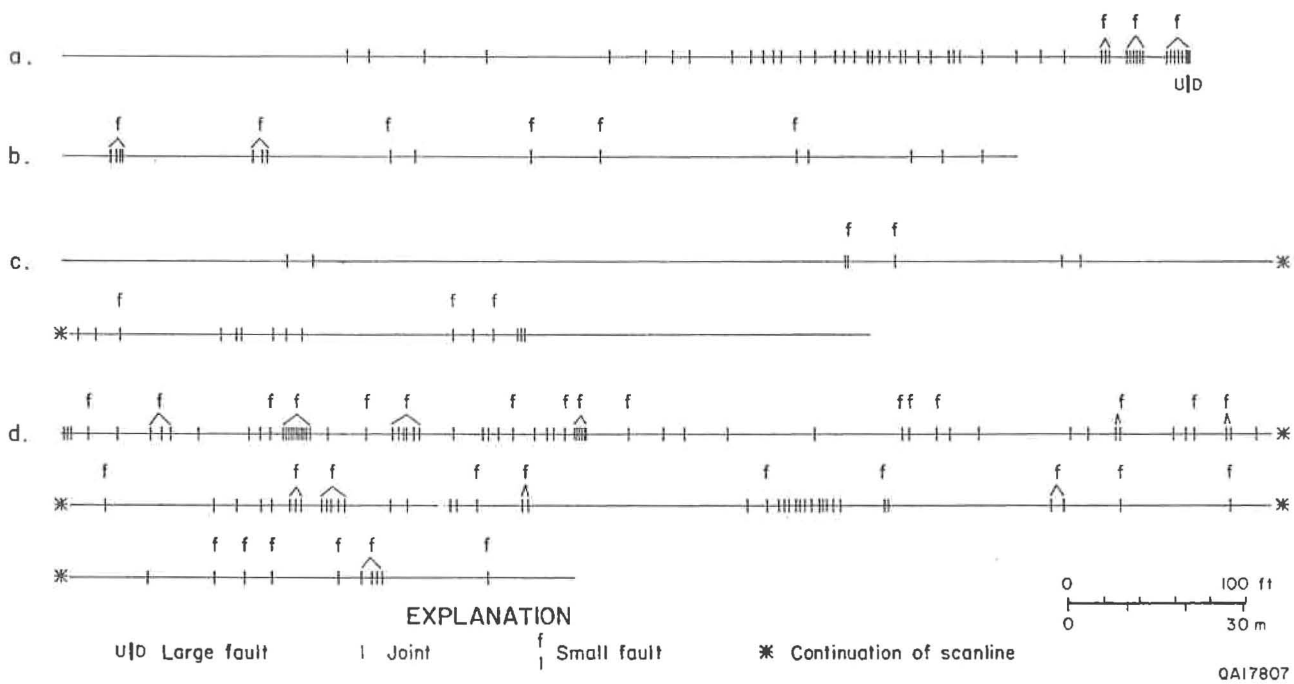

Figure 37. Scan lines showing fractures encountered along outcrop traverses. Line a is within unit L and is adjacent to a fault having about 60 ft (18 m) of throw. Lines b and c are in units A and B, respectively, and do not cross large faults or folds. Line d is in unit L and is in an overlap area between two en echelon faults. From Collins and others (1992).

Fault swarms and isolated small faults with throws between 3 ft (1 m) and less than 1 inch (2.5 cm) are more abundant than joint swarms. Lengths of some small faults exceed 1,500 ft (457 m). Fault swarms are composed of closely spaced faults that have attitudes and mineral fill similar to those of large faults. Swarms of small faults may be as wide as 10 ft (3 m). Widths of fault and joint swarms are similar. Locally, swarms are associated with nearly imperceptible (<0.5°) changes in bed dip. Such fault swarms locally grade into fold-related fractures.

Fault Zones

Normal faults are known to be loci of intense fracturing in the Austin Chalk (Collins and others, 1992). At a macroscopic scale, faults in Austin Chalk are considered to be planar and to have steep dips. In detail, however, fault surfaces are slightly curved and have downward-shallowing and downward-steepening segments. Faults in plan view have sinuous traces with variable wavelengths.

Normal faults are present throughout our study area in Ellis County (Reaser, 1961, 1991; Reaser and Collins, 1988; Werner, 1989). The largest faults have throws of 20 to 100 ft (6 to 30 m). They generally strike northeastward to east-northeastward and are downthrown toward the southeast and northwest. Fault dips range from 60° to 90°; dips of 40° to 80° are common among small faults. Distances between large faults range from 8,000 to 21,000 ft (2,440 to 6,400 m) (fig. 2). In these large faults, trace lengths are as much as 5 mi (8 km). Faults arranged en echelon result in longer trace lengths. Large and small faults are commonly associated with antithetic faults that locally have throws of comparable magnitude to main faults, defining graben. Graben are commonly less than 1,200 ft (366 m) wide. Corbett (1982) reported that highly fractured blocks are bounded by northwest-striking faults within northeast-striking graben near Waco, in McLennan County, Texas. They are ascribed to extension parallel to long axes of fault blocks, accommodating differing amounts of extension along traces of scissor-type faults.

Fracture Zonation Adjacent to Faults

Large normal faults are commonly surrounded by zones or halos of closely spaced faults, joints, and veins that strike about parallel to adjacent faults (Collins and others, 1992). Small faults, rather than joints, are most prevalent near master faults. In some areas, numerous veins occur in this zone. Where master faults juxtapose chalk against chalk, zones of minor faults appear to be equally well developed in both hanging wall and footwall blocks. We could not determine if these zones have constant width laterally and vertically along the fault plane.

Directly adjacent to fault surfaces are zones as much as 6 ft (1.8 m) wide of intensely faulted chalk (fig. 38, zone I). Subsidiary faults here have negligible slip; striations indicate dip-slip to slight oblique slip, consistent with movement on master faults. Minor faults are curved such that in plan view they have braided patterns; curvature has wavelengths of 1.6 to 3 ft (0.5 to 1 m); strikes vary as much as 60°. Locally, anastomosing fault arrays grade into breccia. Fractures are well connected both laterally and vertically owing to numerous intersecting and crosscutting fractures (fig. 38, zone I). Fracture spacing and network connectivity decrease away from master faults.

Adjacent to zones of curved minor faults are zones composed mostly of small faults and subsidiary veins and joints (fig. 38, zone II). These areas may be as wide as 20 to 90 ft (6 to 27 m). Slip on minor faults ranges from negligible to several inches. Fault spacing is between 0.5 and 13 ft (0.2 to 4 m). Fault trace lengths are between 3 and 30 ft (1 to 9 m).

There are few faults that strike at a high angle to master faults. Minor faults are less curved and less abundant than in zones closer to master faults. Therefore, cross-strike fracture connectivity is moderate to low. Cross-strike connections mainly result from intersections among antithetic and synthetic faults. Small faults generally end vertically within chalk beds rather than within marl beds or at contacts between chalk and marl; in one example, 80 percent of the faults terminate within chalk beds (fig. 38, zone II).

Domains of joints associated with faults and having spacing closer than typical regional patterns locally extend as much as 200 ft (60 m) away from master faults. Inner parts of these joint zones overlap

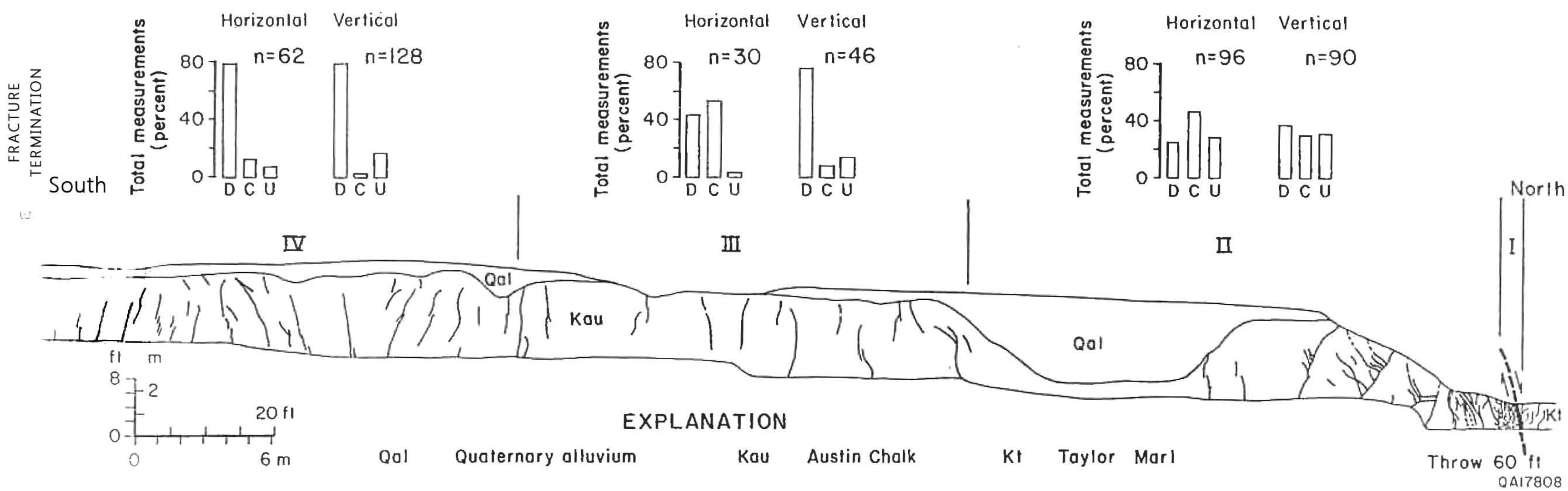

Figure 38. Cross section of fracture zonation in unit L on footwall block of large fault. Histograms indicate percentage of fracture terminations that are dead end (D) and connected (C) in horizontal and vertical directions. Characteristics of some fracture terminations are undetermined (U) because of limitations in size of streambed outcrop. Kau = Austin Chalk, Kt = Taylor Marl, Q_{al} = alluvium. Roman numerals designate zones discussed in text. From Collins and others (1992).

areas having numerous small faults (fig. 38, zones III and IV). Joints and veins are also concentrated near lateral (plan view) ends of minor faults. Joints extending beyond fault-tip lines (edge of slip surface or zero-fault-displacement contour on fault surface) may have been created in advance of growing fault tips.

Joint lengths are as much as 42 ft (13 m), but most are less than 20 ft (6 m). In beds 3 ft (1 m) thick, joints have average spacing of about 4.5 ft (1.4 m) (fig. 38, zones III and IV). Joints and veins are also concentrated near lateral (plan view) ends of minor faults. Joints extending beyond fault-tip lines (edge of slip surface or zero-fault-displacement contour on fault surface) may have been created in advance of growing fault tips.

Joint lengths are as much as 42 ft (13 m), but most are less than 20 ft (6 m). In beds 3 ft (1 m) thick, joints have average spacing of about 4.5 ft (1.4 m) (fig. 38, zones III and IV). This spacing is closer than that of regional joints distant from major faults. Strike-parallel connection between joint segments and average joint length increases toward master faults. As with regional joints, these fractures are poorly interconnected vertically. Of 135 vertical terminations of joints in the footwall block of a fault cutting unit L, 45 percent die out within chalk beds; 30 percent terminate within marl beds; the rest terminate at contacts between chalk and marl. Locally, joints terminate against faults, a relation that may indicate that joints grew in part after faults had formed.

Fractures Associated with Irregular Fault Surfaces

Fault surfaces commonly dip more steeply in chalk beds or chalk-rich intervals than in marl beds, resulting in localized areas of listric downward-flattening and downward-steepening fault profiles along faults that have steep dips overall. Outcrop- and quarry-wall-scale examples show that some downward-flattening fault segments have dips that decrease from 60° to 15° or less. Some small faults sole out as horizontal slip surfaces in marl beds. Corbett and others (1991a, b) reported that above downward-flattening faults, fractures are 1.5 times more abundant in hanging wall rocks than in footwall rocks. Fractures directly adjacent to downward-flattening segments of curved faults are predominantly faults having negligible aperture. There are few associated veins. Joints in open folds adjacent to faults strike parallel to fold hinges and are similar in appearance to those in monoclines. In such folds, fractures locally have as much as several inches of aperture. Fracture spacing may be as close as 1 ft (0.3 m) in fold hinges.

Downward-steepening faults and fault segments (Laubach and others, 1990, 1991) are widespread components of minor fault arrays in the Balcones Fault Zone. Within chalk, they locally vary in dip by as much as 10°. Locally, faults have abrupt ramps where fault segments having gentle dips in marl or shale intersect chalk beds. Fault surfaces dip as much as 45° more steeply in chalk than in marl. Faults with downward-steepening profiles also exist entirely within chalk or chalk-marl cycles that are predominantly chalk.

In brittle rocks, one manifestation of downward-steepening faults is a fault-bend graben or fracture zone above areas of maximum fault-surface curvature in hanging wall rocks (fig. 39). These upward-widening, wedge-shaped zones of fractures are composed of steeply dipping faults and veins. Faults commonly are associated with veins, and locally the faults themselves are dilated. Such zones are locally bounded by antithetic normal faults, defining graben. Graben common in the Balcones Fault Zone may be expressions of such zones.

In plan view, faults are locally curved by as much as 60°. In some outcrops, fracture intensity is not increased in footwall blocks adjacent to bends in map view. In hanging wall blocks, bends in fault traces that are convex toward downthrown blocks have more abundant fractures than other areas along strike, but these variations might be unrelated to fault-trace curvature. Fault-trace bends might be areas of enhanced fracture development on reservoir scales, but we found no convincing outcrop-scale examples. Lack of appropriate exposures prevented us from testing this idea in relation to large faults.

Fractures in Folds

Gentle to open folds occur adjacent to faults, as strike extensions of large faults, and as separate structures unrelated to exposed faults. Folds generally trend northeastward, about parallel to the fault

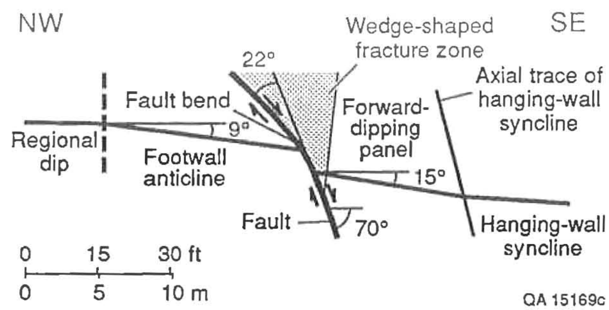

Figure 39. Diagram of angular relations and terminology of a downward-steepening fault in Cretaceous Georgetown and Edwards limestone, Austin region, Central Texas (from Collins and Laubach, 1990). Note wedge-shaped fracture zone.

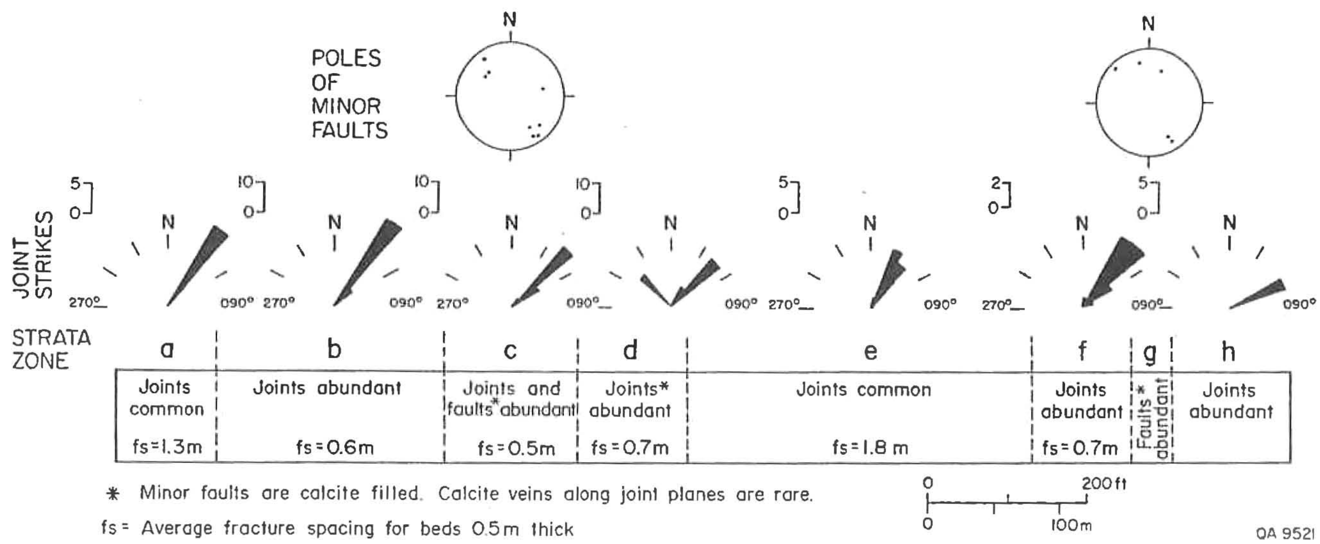

Figure 40. Fracture styles, geometries, and densities associated with a gentle flexure of Austin Chalk. Label "fs" denotes fracture spacing; "a" through "h" refer to fracture zones mapped along creek outcrop. Bar scales for rose diagrams are in number of joints per 10° interval. From Reaser and Collins (1988).

zone. Folds adjacent to faults occur in both hanging wall and footwall rocks. Hinges in footwall blocks are commonly abrupt and angular and have interlimb angles that range from 17° to 85°. Folds in hanging wall rocks above downward-flattening faults are gently tilted toward master faults, whereas beds near downward-steepening segments are commonly tilted in the direction of fault dip. In hanging wall blocks and folds that are strike extensions of faults, folds are broad monoclines having dips that range from less than 1° to 10° across areas as wide as 2,000 ft (609 m) (Collins and others, 1992).

Interlimb angles are commonly greater than 160°. Most monoclines face southeast. Folds distant from exposed faults are isolated symmetric to asymmetric, doubly plunging culminations that resemble folds near fault ends.

Folds adjacent to faults may result from conformance of hanging wall and footwall blocks to a curved fault surface or to strain related to fault displacement. Small-scale examples show that downward-flattening (listric) and downward-steepening faults have associated folds and fracture zones.

One monocline studied in detail has zones of small faults and joints as wide as 300 ft (91 m) that occur along the fold crest and flank (fig. 40). Average fracture spacing within zones is between 1.6 and 2.3 ft (0.5 and 0.7 m). Most of the fractures strike northeastward about parallel to the monocline hinge line. Some individual beds also contain cross fractures striking northwestward, causing local areas to have high fracture connectivity. Folds adjacent to faults also contain closely spaced fractures at the fold crests, which usually strike at low angles to the fold axis and master fault. Fracture spacing in folded chalk adjacent to faults is similar to spacing along axes of monoclines.

Overlapping Fault Traces

Areas between overlapping traces of large en echelon faults locally contain numerous fractures and fracture swarms (Collins and others, 1992). A 1,650-ft (500-m) traverse across the gap between en echelon traces of two faults that have 90 to 100 ft (27 to 30 m) of throw intersected 72 minor faults and numerous swarms of closely spaced joints in unit L (fig. 37, line d). Spacing of single small faults and fracture swarms is between 10 and 150 ft (3 and 46 m). Swarms of small faults are as much as 20 ft (6 m) wide and contain as many as 15 faults. Joint swarms that are as much as 40 ft (12 m) wide have fracture spacing of 2 to 5 ft (0.6 to 1.5 m). Areas between en echelon faults have about twice as many fractures per unit traverse length as would be expected in areas having only regional fracture abundance patterns, but few are found in local areas directly adjacent to large faults. However, in the gaps between en echelon faults, larger areas may be fractured than in the halo zones adjacent to large faults.

In areas between overlapping faults, multiple fracture sets are common. In contrast to the single predominant strike direction that typifies regional fractures, one area between fault strands has a mosaic of intermingled fracture swarms striking northward (N15°W–15°E), northeastward (N30°–55°E), and east-northeastward (N75°–90°E).

Implications for Ground-Water Flow

Fracture abundance and connectivity, two key elements that partly influence fluid movement through fractures, can be characterized stratigraphically and by the structural setting of the chalk.

The zone of weathered Austin Chalk that overlies unweathered bedrock across the Ellis County area is locally as much as 45 ft (14 m) thick. This weathered zone acts as an individual hydrologic unit although the zone is composed of the different Austin Chalk stratigraphic units. Within the weathered-chalk zone, joints are more abundant than in unweathered chalk, and small cavities and vugs are locally common along fractures and bedding planes. Unloading may cause fractures and bedding planes near the surface to be more permeable than fractures at greater depths and permeable bedding planes may aid in connecting fractures.

At a regional scale, unweathered Austin Chalk units have variable fracture frequencies that are unrelated to local large-scale structures such as folds and large faults. In Ellis County, fracture abundance in core is greatest in upper and lower units of the chalk (fig. 35). The greatest fracture intensity is found in lower unit A and upper units J, K, and L. The least fractured units are E through I in the middle zone, and units T, B, C, and D of the lower interval. These observations reflect the propensity of the chalk to fracture. They do not necessarily reflect actual fracture spacing. Slant core data and long outcrop traverses verify that fractures do not have uniform spacing within any given unit and that fracture swarms may occur away from large faults or folds (figs. 36 and 37). The variations in regional fracture density for the chalk units are the guide for separating unweathered Austin Chalk into four stratigraphic intervals (T and A, B to D, E to I, and J to L, fig. 35) for the hydrologic investigations described in following sections.

Areas of high fracture abundances and well-interconnected fractures also occur near faults and folds. These areas may act as preferred paths for ground-water flow. Halos or zones of fractured rocks surrounding large faults have well-interconnected fracture networks of considerable vertical and lateral extent. These networks extend vertically across bedding and may be in both hanging wall and footwall blocks. Fractured areas surrounding faults are relatively narrow, and the most highly interconnected parts are small faults that in many cases are at least partly coated with calcite.

Bending of brittle chalk can create fractures, so folds adjacent to curved faults, fault-propagation folds near lateral fault terminations, and areas between overlapping fault tips are local areas where abundant, well-interconnected fractures may occur. In Ellis County, exposed parts of large faults are nearly planar, but slight bends are loci of fracture zones. Small-scale examples show that these zones are common where faults steepen or flatten.

Hinges of folds have greater fracture frequency than fold limbs. Fractures are commonly joints or veins, which tend to be confined to individual chalk beds. Fold-related fractures in areas or stratigraphic intervals with numerous marly or shale interbeds tend to be confined to individual chalk beds, and fluid communication along fractures is vertically partitioned.

Greater density of minor faults and fracture swarms in areas where fault segments overlap could be due to strains caused by interacting faults and bending of rocks in lateral ramps (Peacock and Sanderson, 1991). Faults and fractures in this setting are not as large or as interconnected as those directly adjacent to faults.

RESULTS OF HYDROLOGIC STUDIES

Water Resources

Well Inventory

A total of 1,130 wells were located near the SSC in Ellis County (fig. 41), 419 of which were found on parcels on the SSC footprint (app. A), including the West Campus (fig. 42a) and East Campus (fig. 42b). The inventory of 108 wells on the West Campus corresponds to a well density of 9.1 wells/mi^2 (3.5 wells/km^2). Because an effort was made to compile a complete inventory on the SSC footprint, the 419 wells on the SSC footprint probably represent more than 99 percent of the actual population of wells on these land parcels. A few additional wells may eventually be found that were unrecorded or not readily seen. The inventory was not exhaustive for properties not on the SSC footprint.

The remaining 711 located wells not on identified SSC land parcels were inside and outside the SSC footprint (app. B). Wickham and Dutton (1991) found a well density of 7.3 wells/mi^2 (2.82/km^2) for the surficial aquifer in alluvium in the northeastern part of the SSC site. If the well density on the West Campus is representative of Ellis County, there might be more than 4,300 wells in the 475 mi^2 (1,277 km^2) area represented in figure 41. If so, the located wells not on the SSC footprint represent only about 26 percent of all in-use and abandoned wells. Well density, however, is not uniform. Wells were less abundant in the Ozan Formation than in Austin Chalk or alluvium, so more than 26 percent of the total off-site well population might have been located to date.

Of the 1,130 located wells,

- 811 (72 percent) were shallow dug wells less than 50 ft (15.24 m) in depth,
- 174 (15 percent) were drilled wells in the regional confined aquifers, at depths in excess of 420 ft (128 m),
- 45 (4 percent) were SSCL monitoring wells (fig. 2),
- 4 (<1 percent) were reportedly old oil or gas exploration wells, and
- the remaining 96 (8 percent) were either unmeasured or of unknown depth.

Of the 419 wells found on identified SSC-site parcels,

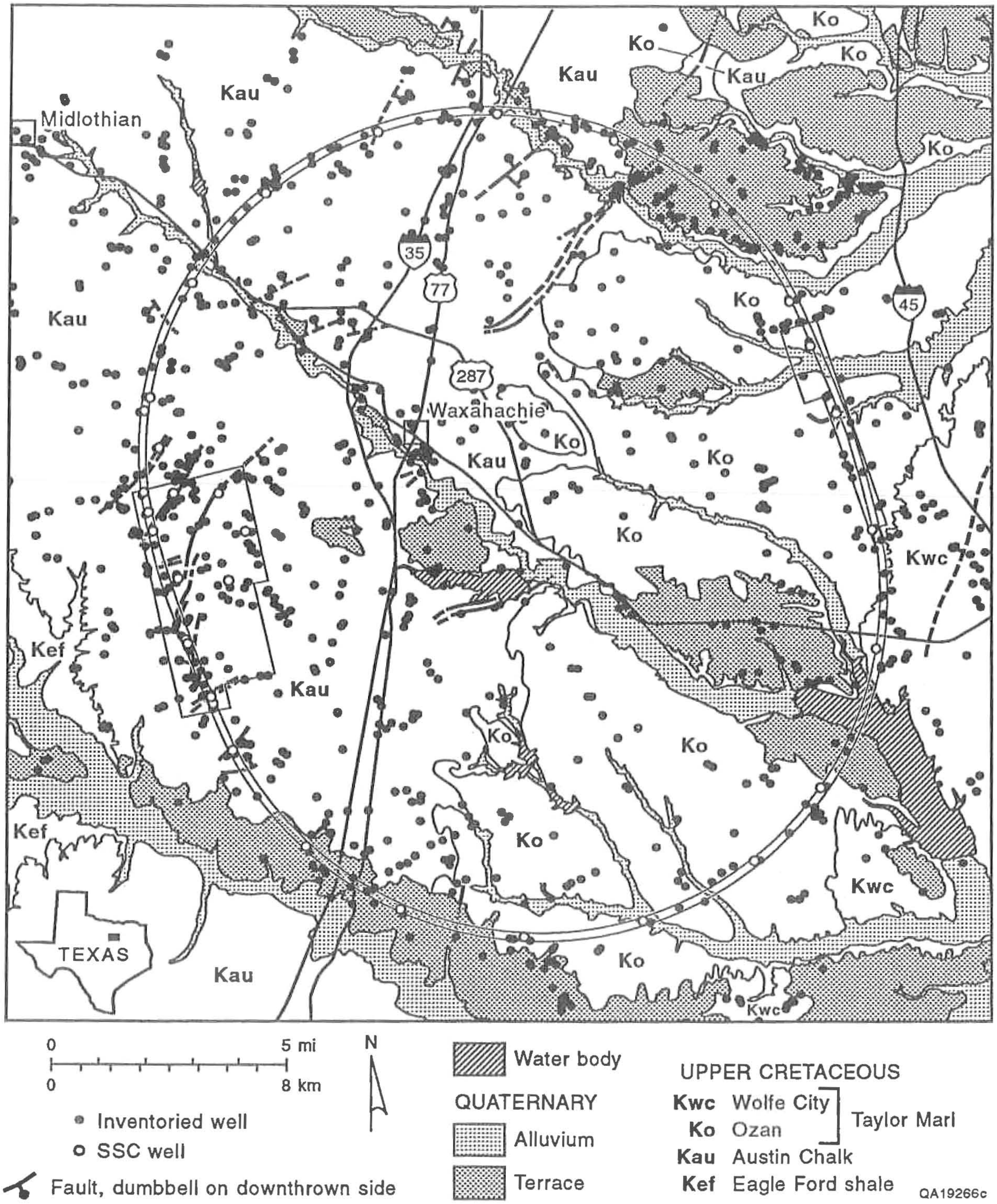

Figure 41. Inventory of water wells in the vicinity of the SSC project area.

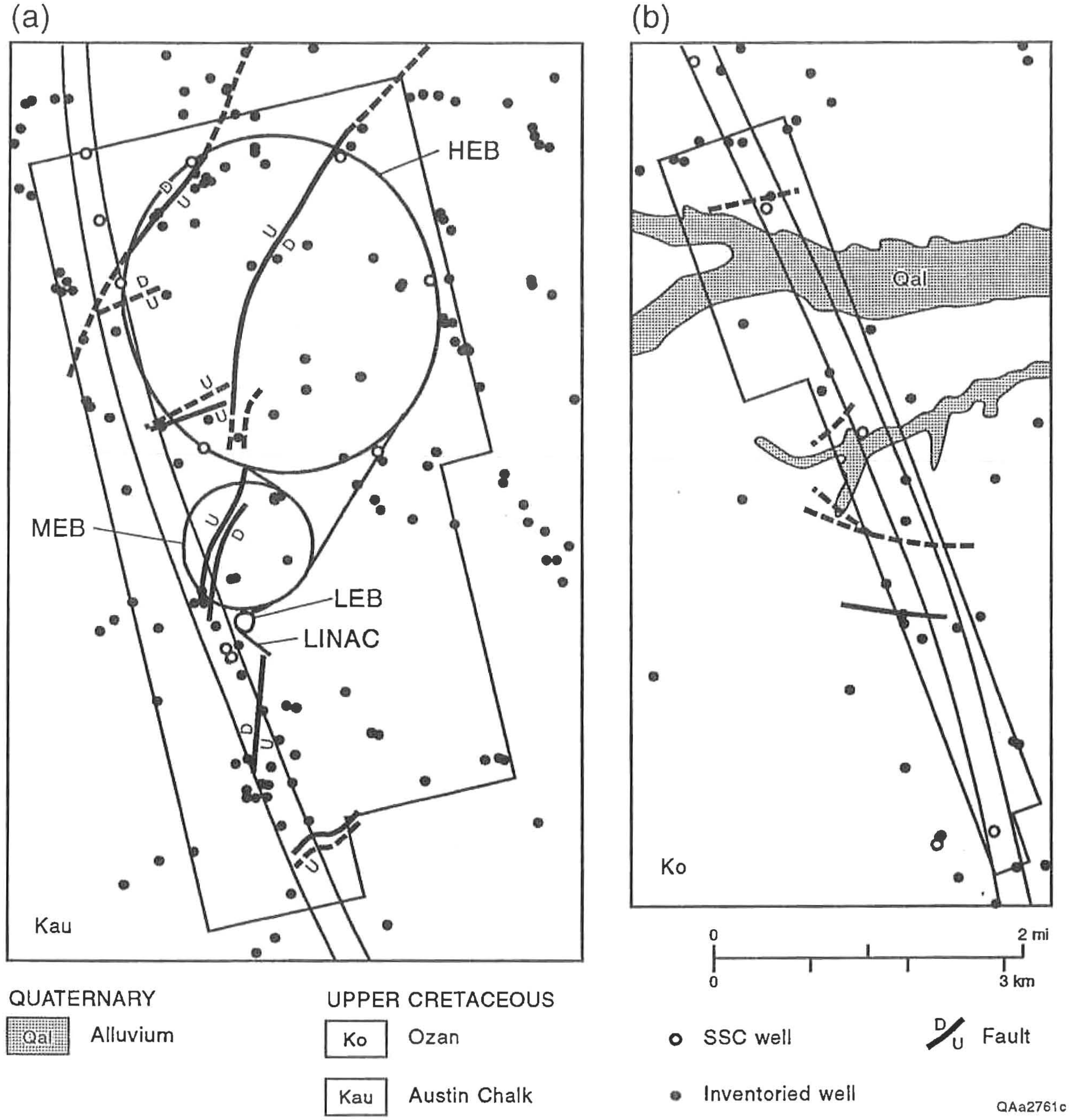

Figure 42. Location of inventoried wells (a) on the West Campus and (b) on the East Campus. Fault locations from The Earth Technology Corporation (1990a).

- 145 wells were on the West Campus and East Campus, including 109 (75 percent) that were shallow wells, 18 (12 percent) that were SSC monitor wells, and 15 (10 percent) that were deep, drilled wells, and
- 40 wells were within 150 ft (45.72 m) of the beam line projected at land surface (app. C).

Of the 40 wells within 150 ft (45.72 m) of the beam line, 17 were being used during 1991 and 1992 at the time of this survey (app. C). All but 42 of the 109 shallow wells on the West Campus and East Campus (fig. 42) have been filled with rock excavated from an SSC vertical shaft and capped with a concrete plug to ensure public health and safety and to remove openings to the surficial aquifer for entry of contaminants. The 42 wells were retained for historical interest and for possible use in monitoring ambient conditions of ground water.

Shallow-Well Characteristics

Depth of shallow, hand-dug wells averaged approximately 22.4 ft (6.83 m) and ranged from 5 to 50 ft (1.52 to 15.24 m). Borehole diameter measured at ground surface averaged 2.9 ft (0.88 m) and ranged from 0.6 to 14 ft (0.18 to 4.27 m). All wells have circular cross sections except for two, which were square. The square wells have dimensions of 4 by 4 ft (1.2 by 1.2 m) and 14 by 14 ft (4.3 by 4.3 m); the latter had railroad ties for casing and well screen. A variety of workmanship was evident among the wells with circular cross sections, from roughly hewn walls to perfectly rounded, smooth walls. Typical well completion in weathered Austin Chalk is open hole, with a surface collar extending 3 to 6 ft (0.9 to 1.8 m) through soil to the top of hard chalk. Some well collars were constructed of mortared brick or chalk cobbles. A few wells possess no collars above ground surface.

Diameters of dug wells in Austin Chalk typically increase with depth in order to increase the number of fractures intersected, the effective radius, and the storage capacity of the well, which compensate for the low yield from chalk with low hydraulic conductivity. In the 42 wells that were completely purged it was possible to estimate well radius from data on pumping rate and rate of drawdown. The radius of the well at a given depth is given by equation (8), assuming that the borehole is circular and that ground-water inflow is negligible compared to pumping rate:

$$r_w = \sqrt{\frac{Q\Delta t}{\pi \Delta d}} \tag{8}$$

where

r_w = radius of well at depth d,

Q = pumping rate,

Δt = change in time, and

Δd = change in head in well over Δt.

The 32 wells in chalk that were purged can be grouped into four shapes (fig. 43): jug, conical, shaft, and miscellaneous. The same physical properties of the Austin Chalk that make it especially suitable for tunneling make construction of such well shapes possible. "Jug" wells possess a narrow neck near land surface that widens at depth to another constant radius (fig. 43a). "Conical" wells have a narrow neck near ground surface that widens with depth at a constant slope to the flat well bottom (fig. 43b). "Shaft" wells have the simplest shape with a constant radius throughout depth (fig. 43c). Wells in chalk that intersected many water-producing fractures tend to have a constant radius, although not all "shaft" wells produce large amounts of water. A variety of shapes are grouped in the fourth category, such as telescoping shaft wells that were deepened with a different diameter than that at the top, and wells with a wide, variable radius at depth (fig. 43d). Some of the dug wells were deepened in an attempt to tap deeper ground water during droughts, such as occurred during 1952 to 1953, which caused the water table to fall below the base of shallow wells.

Wells in unconsolidated alluvium have the "shaft" profile. Large-diameter wells in alluvium were cased with unmortared brick and small-diameter wells were cased with plastic or steel pipe. Wells in marl, which typically also have a constant radius, were used more as cisterns than as ground-water production wells. The cisterns stored rainwater collected from the roof of a house or barn. Walls and floors of many wells in the marl were sealed with cement in an attempt to prevent poor-tasting

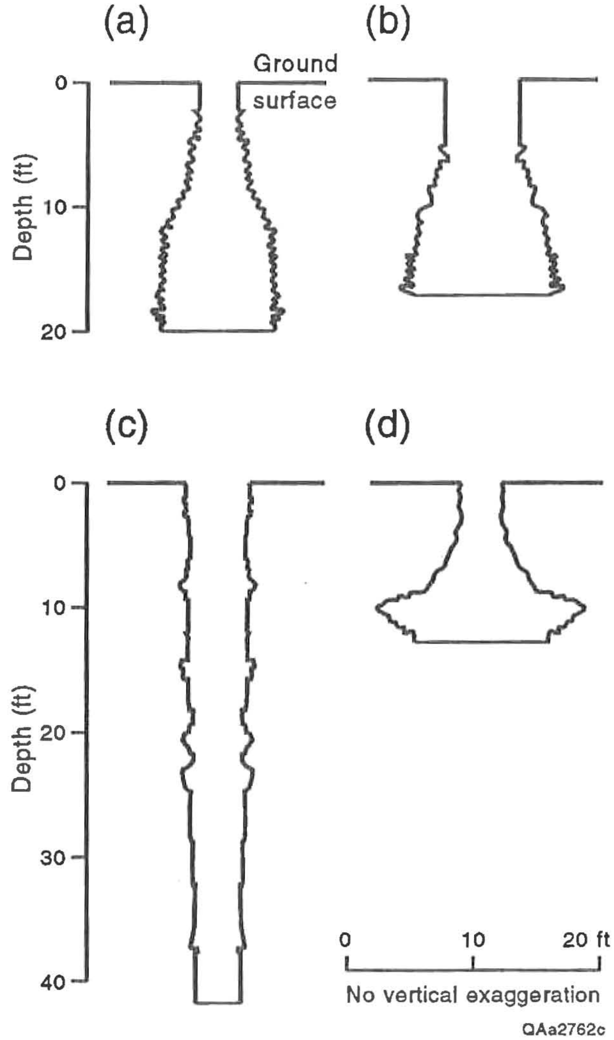

Figure 43. Comparison of typical shapes of dug wells. (a) "Jug" well with narrow neck at land surface, shoulder at mid-depth, and larger fixed radius at depth, (b) "conical" well with a flat bottom and walls with gradually increasing radius, (c) "shaft" wells with constant radius, and (d) a well with a markedly flared radius at depth.

"gyp" (i.e., gypsum, or sulfate-rich) ground water from seeping into the borehole. Several Austin Chalk wells also were used as cisterns during droughts with water carried from nearby streams and springs,

Most low-yield wells supplied small domestic and livestock water uses and were not used for large-scale irrigation. A dug well with unusually high specific capacity (50 gallons per minute per foot of drawdown [gpm/ft; 10.35 L s^{-1} m^{-1}]), located in Lone Elm, Texas, 2.4 mi (6.2 km) north of the West Campus, was reportedly used as a municipal supply well. Water consumption in rural households without indoor plumbing probably was approximately 10 gallons per day (gpd) (37.9 L/day) per person (Texas Department of Health, 1970), which most dug wells could easily supply. In comparison, average present-day water consumption at households in municipal areas is between 458 and 692 gpd (1,731 and 2,616 L/day) (Driscoll, 1986). These usage rates include as much or more water for lawn watering as for household consumption. Appendix G reports additional historical information related to shallow wells in Ellis County.

Only about 5 percent of the shallow wells on the SSC footprint provided domestic water supplies and another 8 percent supplied water for livestock or home gardens and yards during the 1991 to 1992 survey. These wells were generally in good condition, although most do not meet all the requirements of the Texas Department of Health (1970, p. 17) for a safe water-supply well:

- protection by a watertight, insect-proof seal,
- drainage of surface water directed away from the wellhead,
- use of surface casing to prevent polluted water from seeping into the well, and
- prevention of the growth of aquatic vegetation that might impart objectionable odors and tastes to well water by good well construction techniques.

At least 87 percent of the shallow wells on the SSC footprint were unused or abandoned. Prior to this survey, 26 percent had been filled and capped, but material used for fill is unknown. The remaining unused or abandoned wells were in varying states of disrepair. Many unused wells at occupied houses have been covered for safety and health. Covers on numerous other wells were missing, broken, or collapsed. Wells also were found that were partly collapsed or have broken casing at land surface. Abandoned large-diameter wells have been used for disposal of trash, such as household garbage, brick, wire, automobile tires, and roofing shingles. One well (600A-4) contained a kitchen sink and another (600A-5) even had a small car lodged in its wellhead.

As many as 2,700 shallow wells might be unused or abandoned in the entire study area within Ellis County if the average well density is 9.1 wells/mi^2 (3.5 wells/km^2), 72 percent of wells were shallow, and 87 percent of shallow wells were unused or abandoned. Because of the potential for rapid recharge and flow rate, the unconfined surficial aquifer in alluvium and in fractured, weathered bedrock is susceptible to contamination through these wells. There probably have been ground-water contamination problems caused by the misuse of wells, but no clear cases of pollution have been recorded. Wickham and Dutton (1991) reported that all tested wells in the alluvial aquifer overlying the northeast part of the SSC show some levels of coliform bacteria above Texas Department of Health standards for drinking water. Coliform bacteria also were found in abundance in shallow wells in weathered bedrock. Whether these results reflect endemic bacterial populations in the large-diameter wells or contamination throughout the aquifer was not determined.

Wells in the Regionally Confined Aquifers

Deep wells in the regionally confined aquifer system typically were drilled into the Upper Cretaceous Woodbine or Lower Cretaceous Paluxy and Twin Mountains Formations (table 1). Reported depths of wells ranged from 230 to 3,285 ft (70.1 to 1,001.3 m). There were more than 172 deep water-supply wells located in the inventory area in Ellis County, 50 of which were near the SSC site. The survey located 58 deep wells in use as private, municipal, or rural water-supply-company wells in the study area. Wells operated by the City of Palmer, Rockett Water Supply Corporation, City of Ennis, City of Bardwell, and City of Avalon serve local communities. A well operated by the Buena Vista Water-Supply Corporation lies within SSC Fee Simple Land on parcel 128. Sixty-four of the deep wells were not listed in the Texas Water Development Board computerized well file. It was difficult to ascertain depths of these wells. Depth of deep wells cannot readily be measured with pump, production pipe, and electric cable in the well. Most of the abandoned deep wells were cast with either 4- o

6-inch-diameter (nominal size) steel pipe, located inside a well house, and had a service frame erected above the wellhead. At least 58 of the deep water wells have been abandoned; current status of another 56 wells listed in Texas Water Commission files was not determined.

Other Wells in the SSC Area

Four reported oil or gas exploration wells were located or reported during the study. Well 272B-2 was a dry oil-exploration well and has been capped (M. Pinkard, personal communication, 1991). Another oil-test well on parcel 655 was reported by a neighbor but was not verified. Two wells on parcel 78 were reported as oil-test wells drilled during the 1950's (Thompson, 1967). No producing oil well was found in this inventory or reported by Nordstrom (1982). Oil was discovered in southeastern Ellis County in 1953 in the Wolfe City Formation (Upper Taylor Group) at a depth of 800 ft (245 m) in an oil field known as the Corsicana shallow field of Navarro and Ellis Counties (Hudnall, 1951; Thompson, 1967).

Water-Table Elevation

Surficial Aquifer

The water table is defined as the surface of ground water at which pore-water pressure is equal to atmospheric pressure. It is generally recognized by the height to which water will rise in a well bore. A map of the water table defines the elevation at which ground water is encountered in an unconfined aquifer.

The elevation of the water table above the base of the weathered zone delimits the saturated thickness of the surficial aquifer in weathered bedrock. Thickness of weathered bedrock beneath ground surface is related to topography, proximity to faults, and local rock characteristics. Thickness of the laterally extensive weathered zone averaged 12 ft (3.6 m) and was as much as 45 ft (14 m). Weathering locally can be especially deep along faults and fractures that allow circulation of ground water to depths greater than usual, such as the approximately 170-ft-deep (52-m) weathered zone detected in the M55 boring at the Medium Energy Booster (MEB) facility.

Water levels in the surficial aquifer varied seasonally, daily, and episodically. Seasonal change is shown by the difference in water-table elevation mapped in figures 44 and 45 and in hydrographs of individual wells (app. H). The water table was near the annual high stand in January 1992 (fig. 44) and was lower in September 1992 (fig. 45). At any given time, water levels closely mimic topography, with high elevations along upland surface-water divides and low elevations in valley floors beneath stream beds (figs. 44 and 45). The equipotential contours of the water-table maps form a "v" upstream in the creek valleys and bend downhill across the upland surface-water divides. Depth to water during 1991 averaged 8.1 ft (2.47 m) below land surface and ranged from 0 to 27.7 ft (0 to 8.44 m). Depth to water during 1992 averaged 8.5 ft (2.59 m) below land surface and ranged from 0 to 29.4 ft (0 to 8.96 m).

Amplitudes of daily cycles of water-level fluctuation typically were 0.05 ft (0.015 m) (fig. 46). Water levels decreased during the day to a minimum in the early evening, after which they rose to a maximum in early morning. This one-cycle-per-day behavior is most likely caused by evapotranspiration, by which evaporation and plant uptake is high during the day and low during the night. This was also documented in alluvium at the surficial aquifer by Wickham and Dutton (1991). Water levels in weathered chalk and marl did not appear to be affected by changes in atmospheric pressure or earth tides. Fluctuations in water level induced by changes in atmospheric pressure were semidiurnal (two cycles per day) whereas the observed fluctuations in the surficial aquifer were diurnal (one cycle per day). Earth tides owing to gravity of the moon typically result in water-level fluctuations of 0.03 to 0.06 ft (0.009 to 0.018 m) in confined aquifers. These effects are not expected in unconfined aquifers.

Wells in the weathered Austin Chalk often drained quickly after precipitation events. Water level at well 543A-1, which is representative of many shallow wells, fluctuated almost 10 ft (3.1 m) in 2 months (fig. 47a). These changes can be roughly correlated with rainfall, as measured about 1.1 mi (1.8 km) from well 543A-1 at an SSC environmental monitoring station (fig 47c). However, the relative amount of precipitation from different events does not fully correspond to the relative magnitude of

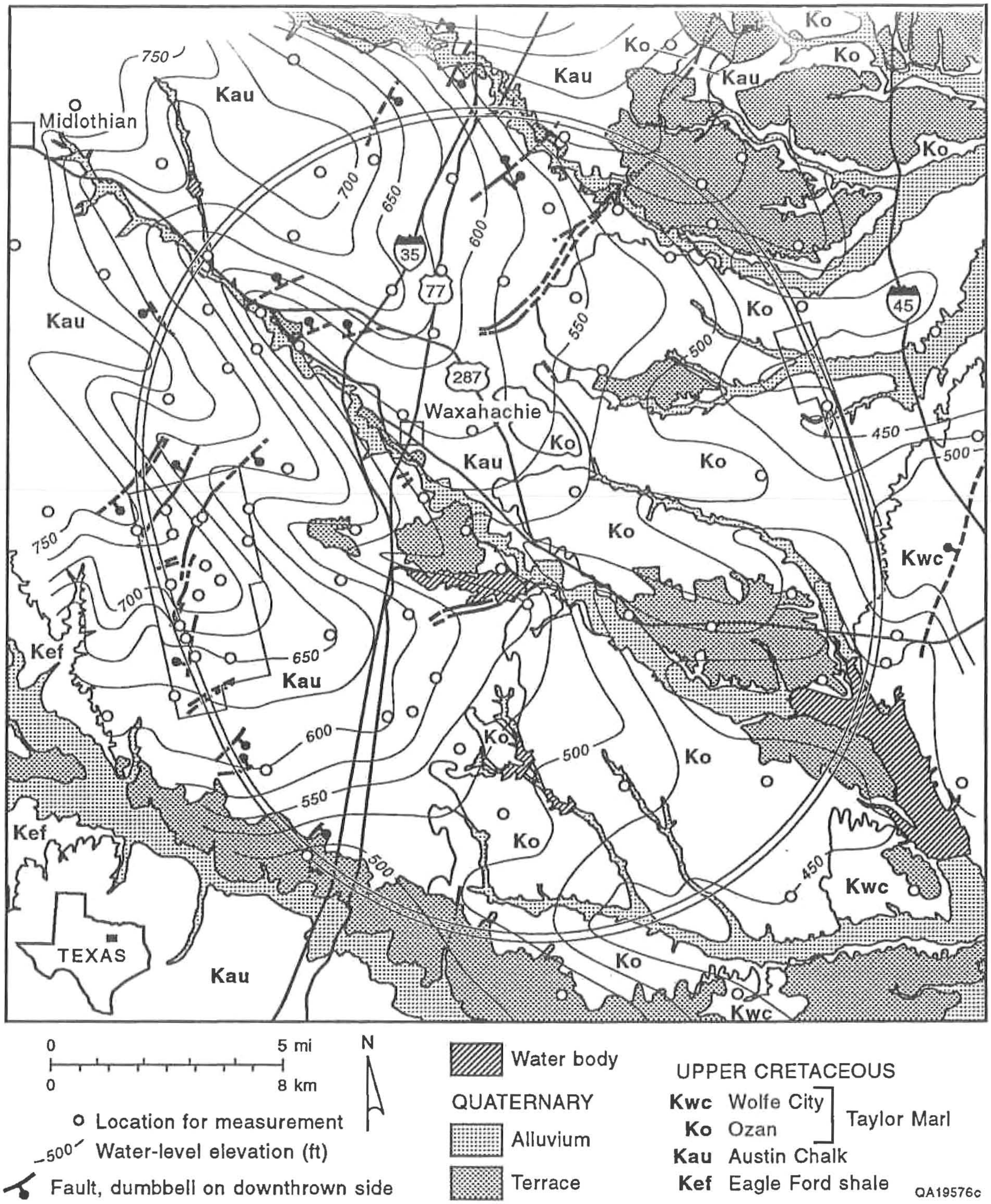

Figure 44. Water table mapped in weathered bedrock and alluvium in January 1992.

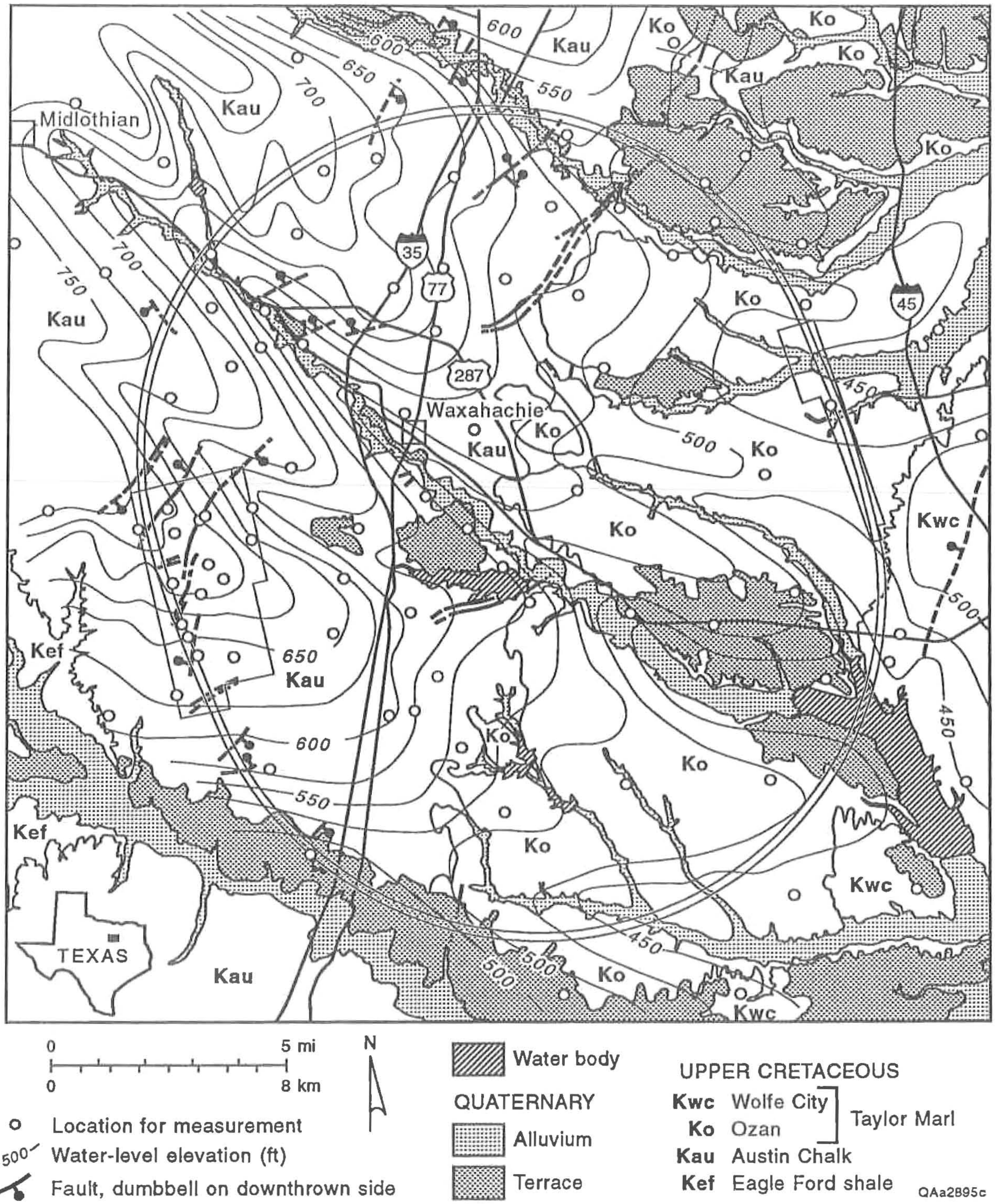

Figure 45. Water table mapped in weathered bedrock and alluvium in September 1992.

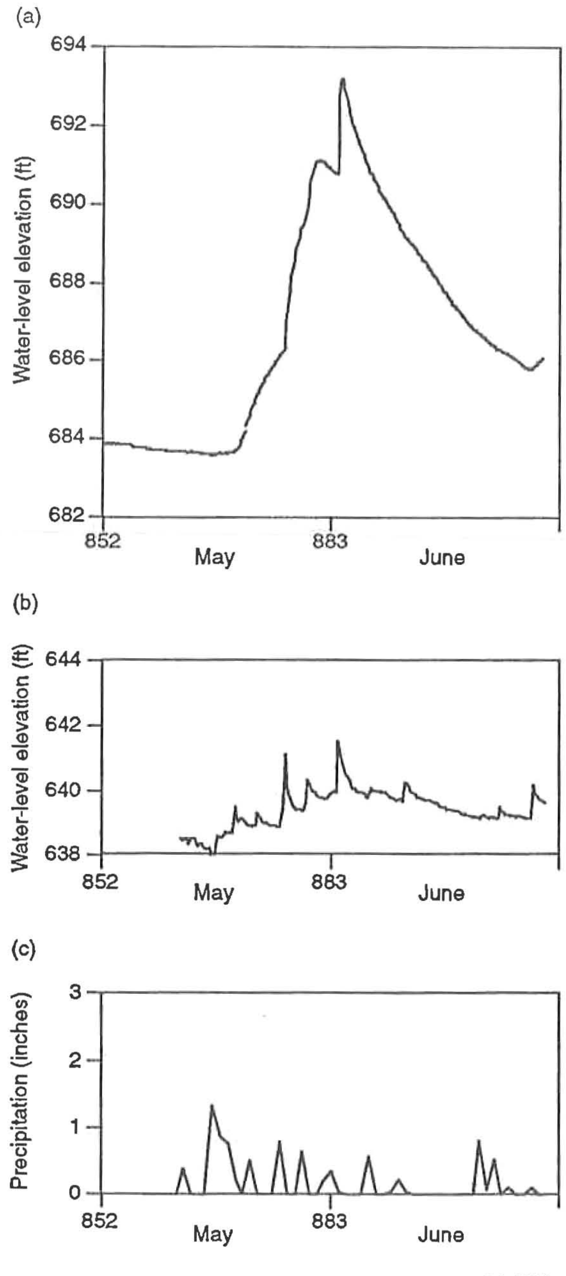

Figure 46. Hydrograph of well 543A-2 in weathered Austin Chalk showing daily fluctuations of approximately 0.05 ft (0.015 m). Data normalized to zero mean.

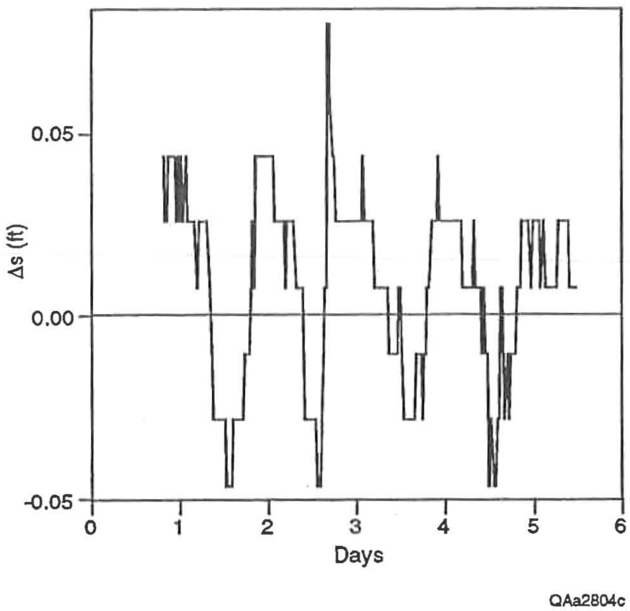

Figure 47. Hydrographs of water levels in (a) well 543A-1 in weathered Austin Chalk and (b) SSC monitoring well BI3. Hydrographs correspond to precipitation events (c) recorded at SSC magnet development laboratory from May through June 1992.

water-level change. The differences might reflect uneven spatial distribution of precipitation from thunderstorms. At some wells in local topographic lows, an increase in water level of as much as 10 to 15 ft (3.1 to 4.6 m) followed within an hour of precipitation. This probably reflects accumulation of runoff and direct recharge to the affected wells.

Ground Water in Unweathered Bedrock

Water-level hydrographs at the SSCL monitoring wells are presented in figure 48. The Earth Technology Corporation (1990e) recognized that hydraulic heads in the unweathered chalk, marl, and shale reflect ground-surface topography. Few of the water levels, however, had reached a static level as of the 1989 and 1990 measurements reported by The Earth Technology Corporation (1990e). Rates of water-level recovery after drawdown caused by well development or by later bailing and pumping generally followed one of three typical patterns:

- rapid, almost complete recovery to near equilibrium water level, giving a pattern of a sharp bend on a water-level hydrograph (fig. 48a–cc),
- gradual recovery at a rate that decreases with time, giving a pattern of a broad curve (fig. 48dd–jj), or
- negligible or very slow recovery that is nearly constant with time (fig. 48kk–oo).

By the end of 1992, water levels had nearly reached a steady level in all but three wells, BE1-90, BE1A, and B1697, which showed the third type of water-level response.

Water levels in BI3 respond to precipitation events (fig. 47b, c). There were suggestions of a possible annual cycle at wells BE10, BI3, BI6, BIR31, and BF6, with water levels as much as 8 to 10 ft (2.4 to 3 m) higher during January to April than during June to September (fig. 48e, l, o, r, and ii). Additional data, however, are needed to confirm the periodicity of fluctuations and to quantify how such fluctuations relate to recharge and discharge rates. In most wells in the unweathered bedrock, however, there were no detectable fluctuations in water level associated with precipitation events or

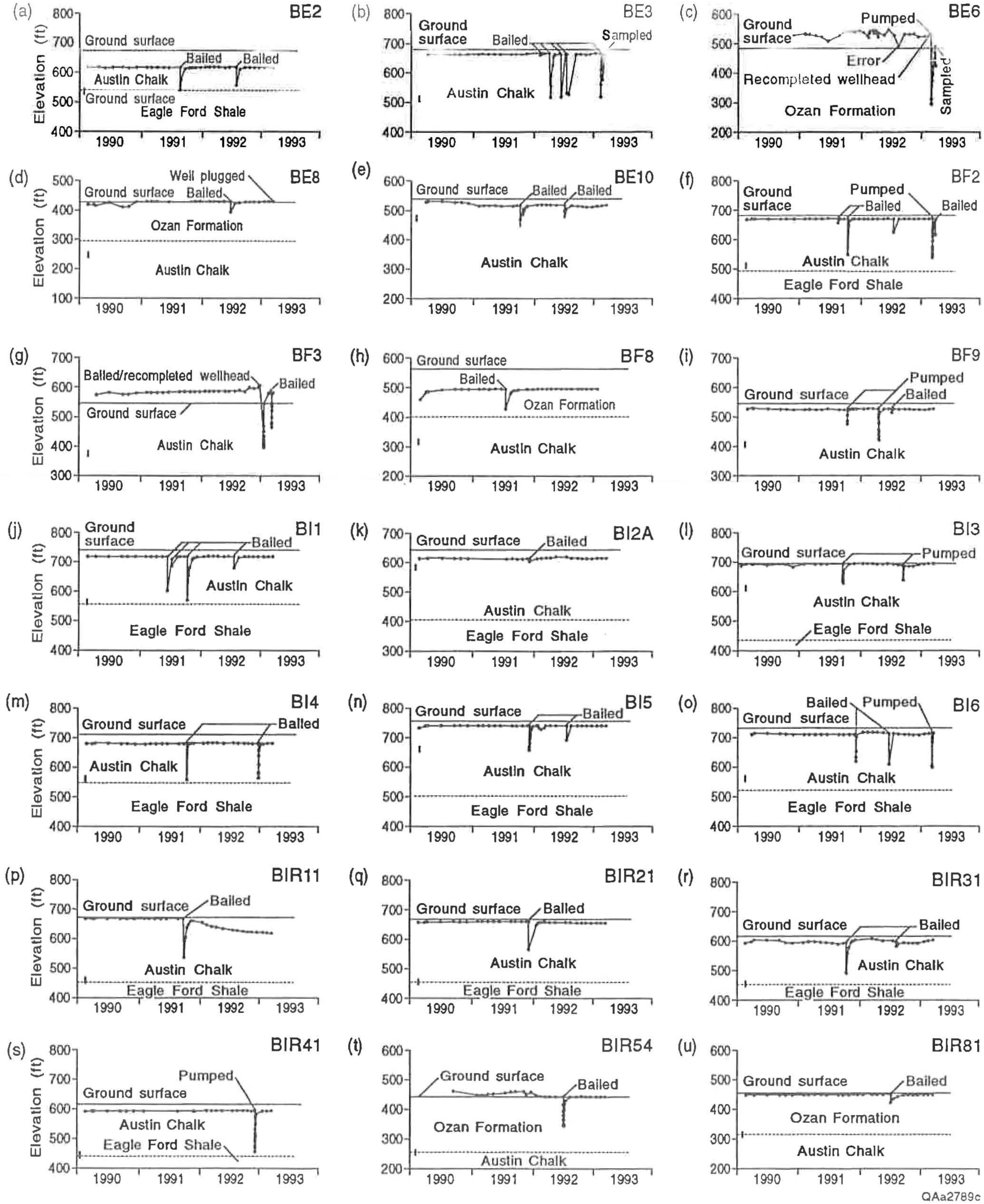

Figure 48. Water-level hydrographs in SSC monitoring wells, organized by three patterns of water-level recovery: rapid, almost complete recovery to near equilibrium water level (a–cc), gradual recovery at a rate that decreases with time (dd–jj), and negligible or very slow recovery that is nearly constant with time (kk–oo).

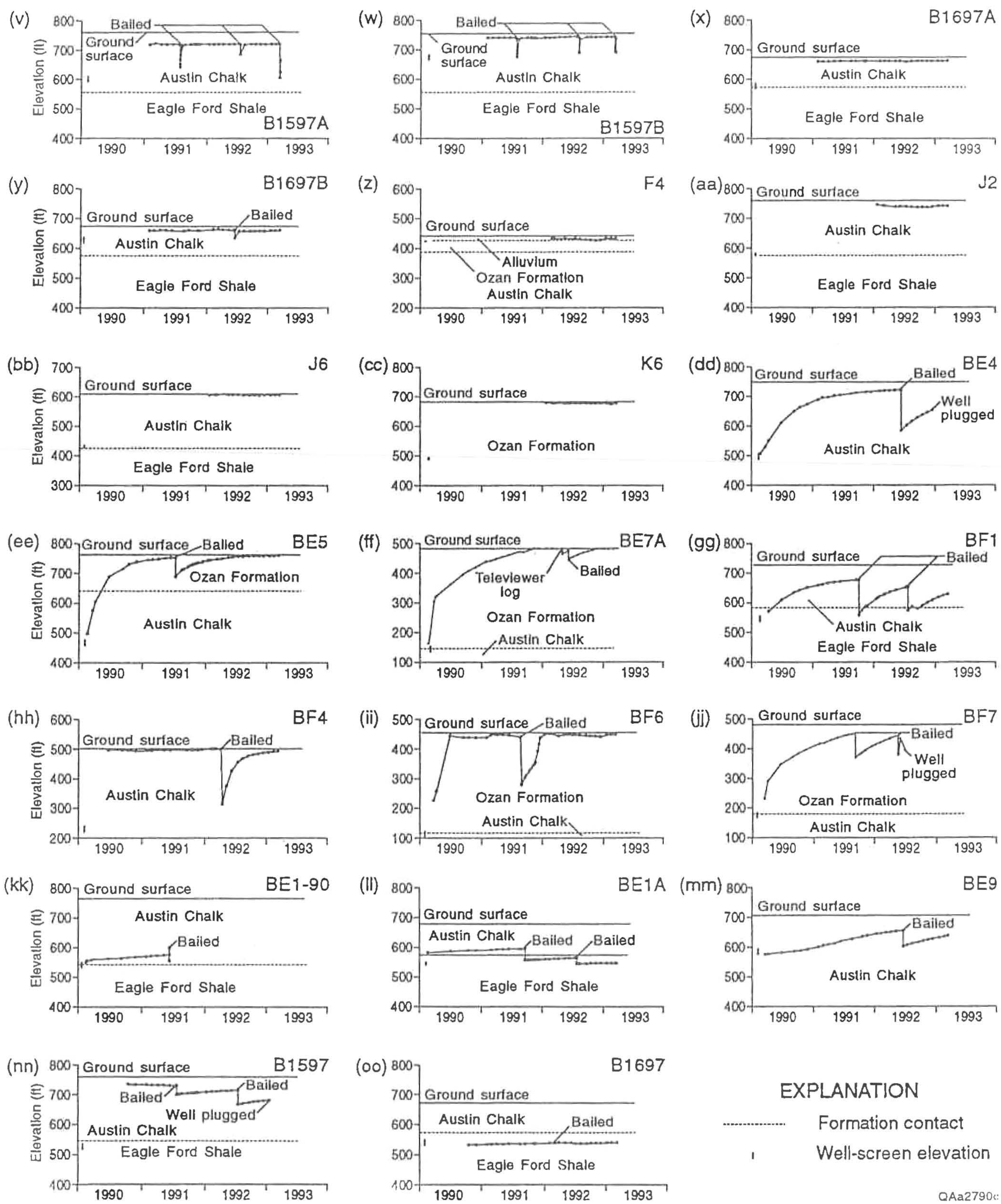

Figure 48 cont.

seasons. Daily fluctuations in water levels were observed in many wells; their association with changes in atmospheric pressure is discussed in a subsequent section.

Figure 49a updates The Earth Technology Corporation's (1990e) illustration of the relation between hydraulic head and ground-surface elevation. The three wells showing negligible apparent recovery, B1697, BE1A, and BE1-90, lie below the line. Two wells, BF3 and BE6, completed in Austin Chalk at the north and east sides of the SSC site (fig. 2), respectively, plot well above the line, reflecting the fact that water levels rise above ground surface in these artesian wells. Figure 49b presents a complementary picture of the relation between fluid pressure and depth of the well screen below ground surface. Fluid pressure was calculated for most wells from the height of the water column above the midpoint of the well screen and assuming a water weight of 0.433 psi/ft (9.795×10^{-3} MPa/m). Variation in water salinity is ignored. Again, the three wells that show negligible recovery appear highly underpressured for their depth, that is, they plot well to the left of the hydrostatic line, and the two artesian wells appear overpressured.

A graphical approach was used to evaluate whether regional data suggest there is vertical flow of ground water in the unweathered bedrock. There are enough data to describe the vertical gradient in hydraulic head at only a few locations, such as the exploratory borehole shaft (Robinson and others, 1993). Data are not yet sufficiently abundant, however, to prepare accurate, regional maps of the vertical gradient. The graphical approach plots the dynamic pressure increment, Δp, defined by Tóth (1978) as the difference between measured water pressure and that predicted for a given depth by the hydrostatic gradient (fig. 49b). It is a function of both ground-surface elevation and depth of the measuring point below ground surface (fig. 50a). Beneath recharge areas at the higher elevations of a drainage basin, the vertical component of ground-water flow is directed downward (fig. 50b), so water pressure at a given depth is less than hydrostatic and Δp values are negative (–). Beneath discharge areas at the lower elevations of a drainage basin, the vertical component of ground-water flow is directed upward, so water pressure at a given depth is greater than hydrostatic and Δp values are positive (+). Hydrostatic conditions with horizontal flow ($\Delta p = 0$) are found at the midline of simple

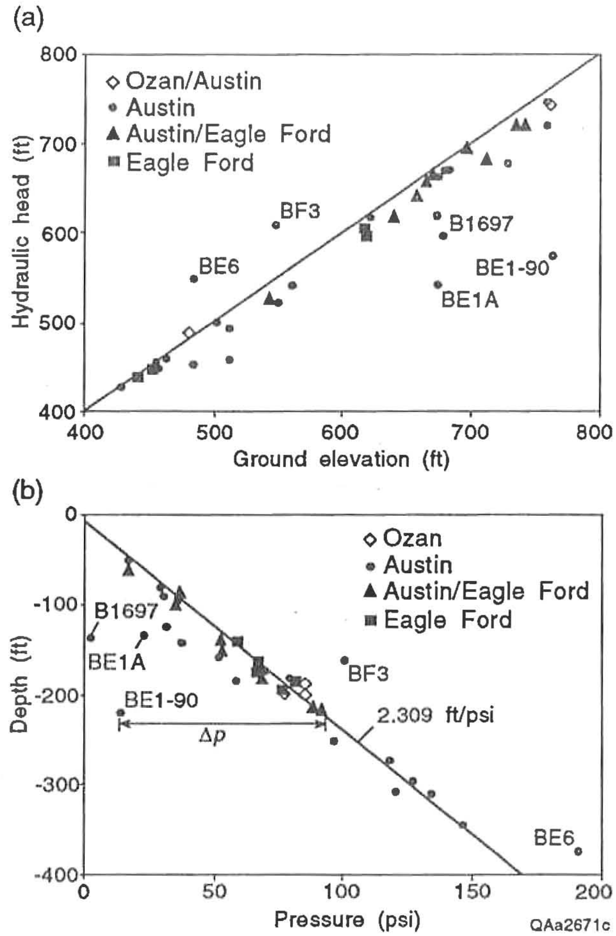

Figure 49. Relations between hydraulic head and ground-surface elevation (a) and fluid pressure and depth of the well screen below ground surface (b). Equation for line in (a) is y = x, with slope of one and intercept of zero. Slope of the line in (b) is 0.433 psi/ft (9.8×10^{-3} MPa/m), the specific weight of fresh water, and the depth-intercept is approximately 8 ft (~2.44 m), the average depth to water in weathered bedrock during 1991 and 1992. Δp is the dynamic pressure increment discussed in text.

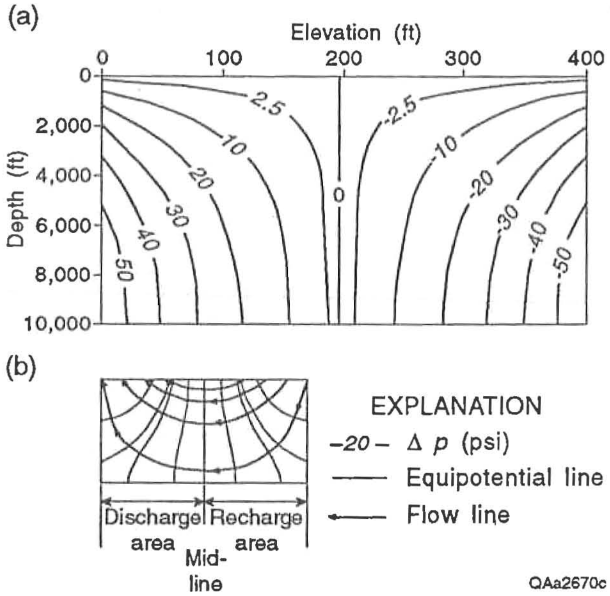

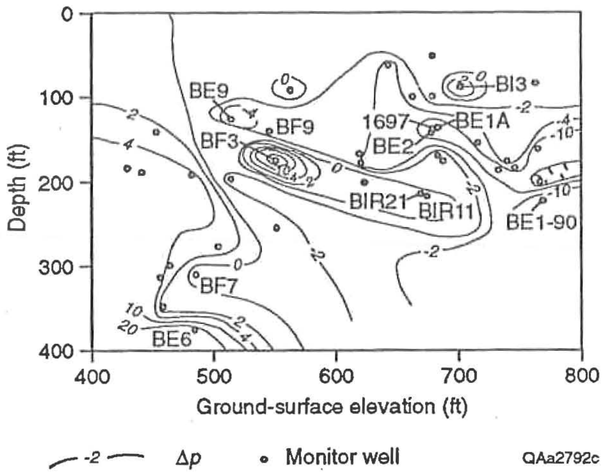

Figure 50. (a) Variation in dynamic pressure increment (Δp) as a function of ground-surface elevation and depth of the measuring point below ground surface. (b) Variation in dynamic pressure increment for the case of simple ground-water flow paths in a drainage basin having homogeneous hydrologic properties. Modified from Tóth (1978).

Figure 51. Variation in dynamic pressure increment (Δp) calculated from water levels in SSC monitoring wells.

drainage basins having homogeneous hydrologic properties (fig. 50b), but are displaced from the midline in more complex basins (Tóth, 1978).

The dynamic pressure increment based on water levels measured in SSCL monitoring wells is shown in figure 51. The picture is more complex than that for a simple drainage basin with homogeneous properties (fig. 50), but the differences offer useful insights into controls on vertical flow of ground water in the unweathered bedrock at the SSC site. The principal differences include

- nonsymmetrical distribution of positive and negative values of Δp,
- nonvertical orientation of the "hydrostatic" line ($\Delta p = 0$),
- anomalous distributions of wells with positive (BI3) or negative (BF7) Δp values amid a field of data of opposite sign, and
- inversions of Δp values, with Δp decreasing, increasing, and then decreasing again with increasing depth beneath ground surface at middle to high elevations.

Both artesian wells, BE6 and BF3, have large positive Δp values but plot at different locations (fig. 51). BE6 ($\Delta p = 32$) is located at a low elevation at the east side of the SSC site; its high positive Δp value is consistent with ground-surface elevation and depth of the well screen, according to the simple model shown in figure 50. BF3 ($\Delta p = 30$) is located on the south side of the valley of Red Oak Creek (figs. 2 and 9). Its depth is less than that of BE6 but it plots within a field of negative Δp values (fig. 51). Ground-water flow in the unweathered bedrock most likely is directed locally toward Red Oak Creek and not toward the southeast. The Δp value suggests a potential for vertical flow to be directed upward beneath the valley of Red Oak Creek. If data were sufficient to analyze local dynamic pressure increments within the Red Oak Creek watershed, the Δp value of BF3 might be found to plot as expected as a function of ground-surface elevation and well depth.

Well BI3 has a slightly positive Δp value (2.8) that is anolamous for its elevation and depth. As will be shown, hydraulic conductivity measured at BI3 is high and sampled ground water has high tritium and ^{14}C contents, which suggest that local ground-water flow is more rapid than at most other monitoring wells. Rapid recharge in fractured rock associated with faults in the area (fig. 2) implies a vertical component of ground-water flow. The high hydraulic conductivity associated with fracture might decrease the resistance of rock to flow of ground water and thus affect the gradient in hydraulic head in the vicinity of BI3. The other well with ^{14}C that is above the detection limit, BF9, has a Δp value of -3.6.

Several wells with anomalous Δp values are known to have well construction problems and unnatural chemical composition of water: BE1A, BE9, BIR11, BIR21, and BE2. Water levels in BE1A and BE9 have had negligible recovery of water level (fig. 48ll, mm), yielding small Δp values (–32 and –7.8, respectively). It is possible that formation damage related to well construction retards water inflow and pressure buildup at these wells. Correspondence between anomalous Δp values and possible well construction problems at the other wells is more problematical. Water-level changes at BIR11 and BIR21 (Δp = 2.6 and 0.4, respectively) and at BE2 (Δp = –20) appear normal and rapid. Wells BIR11 and BIR21 are near the exploratory borehole shaft, where vibrating-wire transducer data also indicate an upward-directed potential (Δp >0) for vertical flow (Robinson and others, 1993). The agreement between the two data sets suggests that the BIR11 and BIR21 water-level data are valid and not adversely affected by well construction. The area around the exploratory borehole shaft is situated on a local slope that is at an angle to the regional eastward dip of land surface. The difference between local and regional orientation of hydraulic-head gradient, like for the area around BF3, might account for the positive Δp values at BIR11 and BIR21 plotting within the negative Δp field (fig. 51).

Slow rate of water-level change does not necessarily yield an anomalously underpressured condition, and highly negative Δp values can arise even with rapid water-level recovery. BE2 (Δp = –20), with normal rates of water-level change, plots alongside wells B1697 and BE1A, which have extremely slow rates of water-level change, as previously stated, and very negative Δp values (–54 and –32, respectively). The Δp value for well BE1-90 was expected to be a large negative number consistent with the high ground-surface elevation and great depth of the well, although not as large as –78. It seems possible, therefore, that the negligible rate of recovery shown by BE1-90 (fig. 48kk), partly reflects a low hydraulic head in the regional field of ground-water flow.

Because water levels have been measured in the unweathered bedrock only in monitoring wells around the circumference of the SSC ring and on the West Campus, and because the wells are completed in different stratigraphic intervals of the Eagle Ford Formation, Austin Chalk, and Ozan Formation, a regional plan-view map of hydraulic head has not been made. The potentiometric surface of ground water in the unweathered bedrock of the West Campus area, however, is subparallel to the water table in weathered bedrock but has subdued relief. The regional gradient at depth would have a principal component directed eastward and local components directed from beneath surface-water divides toward valley floors. The magnitude of horizontal gradients in hydraulic head would be smaller at depth than in the shallow water table on the regional as well as the local scale.

Hydrologic Properties

Surficial Aquifer in Weathered Bedrock and Alluvium

Wickham and Dutton (1991) reported that hydraulic conductivity of Pleistocene alluvium ranged from 2.3 to 37.4 ft/d (0.70 to 11.4 m/d) and averaged 10.7 ft/d (3.26 m/d), on the basis of pumping tests in five test wells and large-diameter dug wells. Tests in the two large-diameter wells (wells 33 and 37) used by Wickham and Dutton (1991) were repeated during Phase II studies and analyzed by the 50-percent recovery method (Herbert and Kitching, 1981). Results of Phase I and Phase II interpreted tests were similar (table 11).

Values of hydraulic conductivity and transmissivity of the weathered Austin Chalk and Ozan Formation are summarized in table 12 on the basis of measurements during the Phase II studies. The

Table 11. Comparison of measured and simulated hydraulic conductivity (ft/d) in two large-diameter wells in alluvium.

Well	Wickham and Dutton (1991)	Simulation estimate	Phase II study
33	37.4	41.1	22.8
37	19.3	26.8	28.0

Table 12a. Results of hydrologic tests in shallow wells in the weathered zone of the Austin Chalk.

Map no.	Well	Transmissivity (ft^2/d)	Hydraulic conductivity (ft/d)
1	37-2.1	5.14	0.30
2	41A-1	5.35	0.41
3	86B-1	0.89	0.05
4	86C-1	0.17	0.01
5	94-7	0.11	0.01
6	104A-1	99.22	6.05
7	107A-4	148.89	12.47
8	144-1	0.23	0.01
9	156-1.1	152.24	7.65
9	156-1.2	51.79	2.89
10	215-1	22.93	1.42
11	244A-1	27.01	2.01
12	252-3	3.56	0.39
13	257-2.1	0.10	0.01
13	257-2.2	100.32	6.60
14	262A-2.1	46.57	1.52
14	262A-2.2	14.79	0.77
14	262A-2.3	31.48	0.87
15	276A-1	32.48	2.26
16	338-1	86.58	5.85
17	496-3	4.41	0.11
18	504B-1.1	0.52	0.08
18	504B-1.2	54.60	3.52
19	525-2	0.65	0.04
20	543A-1	2.19	0.10
21	543A-2	0.02	0.0015
22	543B-1	0.07	0.0045
23	A39-16-01	8.93	0.54
24	R55-27	39.38	1.97
25	R77-27	159.94	9.80
26	R77N-21	34.81	2.21
27	R287W-15	35.19	3.12
28	R287W-18	13.08	0.93
29	R664-16	29.50	1.49
30	R664-17	374.35	24.94
31	R813-11	30.79	2.17
32	R875-4	758.37	64.16
33	R876-4	55.57	1.89
34	R877-14	125.76	3.14
35	R878-2	71.73	2.55
36	R1446-8	68.83	3.94
37	R1446-25	2.41	0.22

Table 12b. Results of hydrologic tests in shallow wells in the weathered zone of the Ozan Formation.

Map no.	Well	Transmissivity (ft^2/d)	Hydraulic conductivity (ft/d)
38	38C-1	6.14	0.21
39	272B-1	0.40	0.03
40	R55-34	2.21	0.12
41	R287-33	16.63	0.95
42	R877-13.1	3.95	0.16
42	R877-13.2	2.98	0.11
43	R984-15	0.08	0.01

lowest hydraulic conductivity and transmissivity of the weathered Austin Chalk were found at well 543A-2 located on the West Campus inside the High Energy Booster (HEB) ring. The highest values were measured at well R875-4 located in Lone Elm, Texas, west of Waxahachie. Hydraulic conductivity ranged from 0.0015 to 64.16 ft/d ($10^{-8.28}$ to $10^{-3.65}$ m/s) and averaged 0.61 ft/d ($10^{-5.66}$ m/s) (fig. 52a). This is almost 20 times less than average hydraulic conductivity measured in alluvium by Wickham and Dutton (1991) (fig. 53). Transmissivity of the weathered Austin Chalk ranged from 0.02 to 758 ft^2/d (2.2×10^{-8} to 8.2×10^{-4} m^2/s).

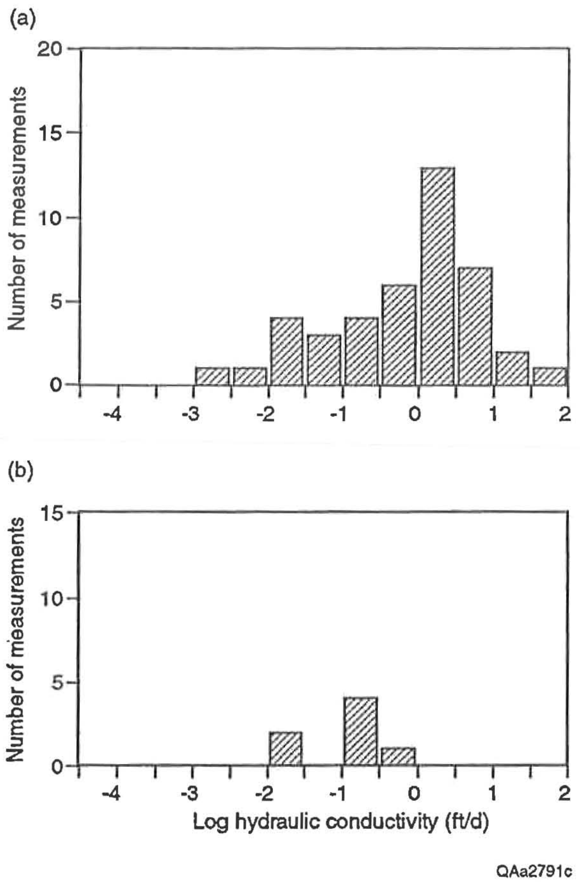

Figure 52. Histograms of hydraulic conductivity values measured in weathered Austin Chalk (a) and weathered Ozan Formation (b).

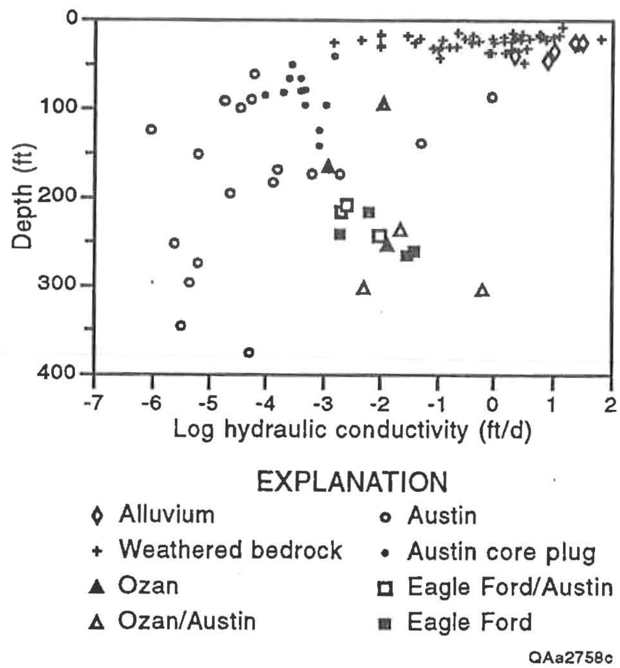

Figure 53. Variation in hydraulic conductivity with depth beneath ground surface in alluvium and in weathered and unweathered bedrock at the SSC site.

The lowest hydraulic conductivity and transmissivity values of the shallow, weathered Ozan Formation were found at well R984-15, located near Bardwell, Texas, and the highest values were measured at well R287-33, located approximately 3.5 mi (5.6 km) west of Ennis, Texas. Hydraulic conductivity ranged from 0.01 to 0.95 ft/d ($10^{-7.45}$ to $10^{-5.47}$ m/s) and averaged 0.10 ft/d ($10^{-6.45}$ m/s) (table 12; fig. 52b). Transmissivity of weathered Ozan ranged from 0.08 to 16.63 ft^2/d (8.6×10^{-8} to 1.8×10^{-5} m^2/s). One concern with measurement of hydrologic properties of the Ozan, however, is that test results might be inaccurate where wells or cisterns are fully cased by brick owing to the small aperture between bricks and to formation damage caused by well construction techniques (J. Yelderman, personal communication, 1991).

Hydrologic tests sequentially repeated at different initial water levels in wells 153-1, 257-2, 262A-2, and 504B-1 yielded different values of hydraulic conductivity in weathered Austin Chalk (table 13). In the three cases, a lower value of hydraulic conductivity was measured when the test started at a lower initial elevation of the water table (greater depth to water). This indicates that

- hydraulic conductivity decreases with depth in the weathered chalk,
- tests conducted at low initial water levels affect only the deeper, less permeable section of the weathered zone, and
- tests conducted at high initial water levels affect a greater section of the weathered chalk, yielding an average hydraulic conductivity weighted both by the proportional thickness of each strata of different hydraulic conductivity and by the effective hydraulic conductivity of intersected fractures.

Yelderman and others (1988), Barrett (1988), and Barquest (1989) studied ground-water flow in the Austin Chalk and Ozan Formation near Waco, Texas, approximately 67 mi (110 km) south of Waxahachie. Intensity of fracturing of chalk and marl owing to faulting along the Balcones Fault Zone is greater south of the SSC site. Hydraulic conductivity of the weathered zone studied near Waco, Texas, might on average be greater than that at the SSC site because of the more abundant fractures and greater fault displacement south of the Ellis County area along the Balcones Fault Zone. Calculated

Table 13. Results of hydrologic tests repeated at differing initial water levels in shallow wells in the weathered zone.

Well	Initial depth to water (ft)	Measured hydraulic conductivity (ft/day)
257-2	2.6	6.6
257-2	7.5	0.01
262A-2	2.6	0.87
262A-2	17.1	0.77
504B-1	14.35	3.52
504B-1	23.38	0.08

hydraulic conductivities cannot be directly compared between the Waco and SSC sites, however, because

- Barquest (1988) inaccurately applied Herbert and Kitching's (1981) method of interpreting aquifer tests,
- anisotropy ratios calculated by Barquest (1988) are invalid due to an error in the procedure proposed by Herbert and Kitching (1981), and
- there are few data on hydraulic conductivity of the Ozan Formation at the SSC site.

Barquest (1988) noted a decrease in fracture intensity with increasing depth beneath ground surface. Barquest (1988) also noted that total dissolved solids (TDS) was lower during winter and spring when water levels were high owing to seasonal recharge than during summer and fall when water levels were low. These observations are consistent with the decrease in hydraulic conductivity that occurs as water-level elevation and saturated thickness decrease. Poor water quality reflects less dilution by rapidly recharged rain water and greater extent of chemical reaction between ground water and soil minerals because of slow rates of flow in the deeper weathered zone. The slow flow rates inferred from higher TDS at low water levels were due to both a small saturated thickness (lower transmissivity) and to a low hydraulic conductivity with decreased fracture aperture and decreased abundance of fractures at depth in weathered bedrock. Whether there is a similar correlation between water quality and seasonal water level in weathered chalk and marl at the SSC site has not been studied.

Unweathered Bedrock

The only data on hydrologic properties of the unweathered chalk, marl, and shale come from packer tests by The Earth Technology Corporation (1990b), Phase II piezometer and pumping tests in SSCL monitoring wells, and tests of core from SSC boreholes. Pumping tests were performed at wells BI3 and BF9, where packer tests had shown high hydraulic conductivity (The Earth Technology Corporation, 1990e) and core had shown numerous fractures. A pumping test at BIR41 was unsuccessful because pumping rate exceeded ground-water inflow. At other wells in chalk, marl, and shale, Phase II estimates of hydraulic conductivity were based on piezometer (slug) tests, that is, the rate of water-level recovery in the well bore after an essentially instantaneous drawdown. The volume of rock over which hydrologic properties are averaged and the detection limit of the measurement vary between the packer, piezometer, pumping, and core-plug tests. Table 14 lists the test results.

As commonly observed for hydraulic-conductivity data, the frequency distribution of hydraulic-conductivity values in the Austin Chalk is approximately log-normal (fig. 54). Hydraulic conductivities measured in the Austin Chalk by packer, pumping, and piezometer tests range over 6 orders of magnitude from $10^{-6.0}$ to $10^{-0.07}$ ft/d ($10^{-11.5}$ to $10^{-5.5}$ m/s) (fig. 54a, b). Values from core-plug tests fall within this range (fig. 54c). Two obvious factors affect the range of hydraulic conductivity in Austin Chalk: variations in fracture intensity and in fracture aperture (de Marsily, 1986), and variations in matrix permeability of unfractured chalk owing to differences in chalk-marl ratio in the different Austin Chalk units. Hydraulic conductivity of intervals with fractures near faults lies between $10^{-3.88}$ and $10^{-0.23}$ ft/d ($10^{-9.34}$ to $10^{-5.68}$ m/s). The effect of fractures on hydraulic conductivity is clearly illustrated by the fact that hydraulic conductivities measured in plugs from BI3 core (table 8) were more than three orders of magnitude lower than those obtained from pumping tests (table 14). The pumping test result was influenced by fractures, but the core tests were not.

Table 14. Results of hydrologic tests in SSC monitoring wells.

Well	Analytical method	Transmissivity (ft^2/day)	Hydraulic conductivity (ft/day)
BE1A	Bouwer and Rice (1976)	7.53×10^{-6}	5.34×10^{-7}
	Ferris and Knowles (1954)	1.00×10^{-5}	7.09×10^{-7}
	Cooper and others (1967)	2.44×10^{-5}	1.73×10^{-6}
BE2	Bouwer and Rice (1976)	1.08×10^{-3}	3.74×10^{-5}
	Ferris and Knowles (1954)	4.10×10^{-4}	1.41×10^{-5}
	Cooper and others (1967)	2.81×10^{-3}	9.70×10^{-5}
BE3	Bouwer and Rice (1976)	3.43×10^{-3}	1.72×10^{-4}
	Ferris and Knowles (1954)	9.70×10^{-4}	4.85×10^{-5}
	Cooper and others (1967)	8.30×10^{-4}	4.15×10^{-5}
BE3*	Packer test	1.68×10^{-2}	7.94×10^{-4}
BE4.1	Bouwer and Rice (1976)	6.50×10^{-5}	2.32×10^{-6}
	Ferris and Knowles (1954)	1.75×10^{-5}	6.25×10^{-7}
BE4.2	Bouwer and Rice (1976)	4.46×10^{-5}	1.59×10^{-6}
	Ferris and Knowles (1954)	1.46×10^{-5}	5.23×10^{-7}
	Cooper and others (1967)	6.04×10^{-5}	2.16×10^{-6}
BE4*	Packer test	$<2.90 \times 10^{-3}$	$<1.45 \times 10^{-4}$
BE5.1	Bouwer and Rice (1976)	1.13×10^{-4}	4.35×10^{-6}
	Cooper and others (1967)	3.44×10^{-4}	1.32×10^{-5}
BE5.2	Bouwer and Rice (1976)	9.43×10^{-5}	3.63×10^{-6}
	Ferris and Knowles (1954)	2.51×10^{-5}	9.67×10^{-7}
	Cooper and others (1967)	1.93×10^{-4}	7.41×10^{-6}
BE6	Bouwer and Rice (1976)	1.34×10^{-3}	5.04×10^{-5}
	Ferris and Knowles (1954)	2.51×10^{-4}	9.49×10^{-6}
	Cooper and others (1967)	1.66×10^{-3}	6.27×10^{-5}
BE6*	Bouwer and Rice (1976)	1.88×10^{-3}	9.40×10^{-5}
	Packer test	1.31×10^{-1}	6.20×10^{-3}

Table 14 (cont.)

Well	Analytical method	Transmissivity (ft^2/day)	Hydraulic conductivity (ft/day)
BE7A.1	Bouwer and Rice (1976)	4.80×10^{-5}	1.95×10^{-6}
	Ferris and Knowles (1954)	1.63×10^{-5}	6.63×10^{-7}
	Cooper and others (1967)	no fit	
BE7A.2	Hvorslev (1951)	2.70×10^{-4}	1.10×10^{-5}
BE7A.3	Bouwer and Rice (1976)	1.22×10^{-4}	4.98×10^{-6}
	Ferris and Knowles (1954)	2.51×10^{-5}	1.02×10^{-6}
	Cooper and others (1967)	3.59×10^{-4}	1.46×10^{-5}
BE7A*	Bouwer and Rice (1976)	1.88×10^{-3}	9.40×10^{-5}
	Packer test	$<1.32 \times 10^{-3}$	$<6.20 \times 10^{-5}$
BE8	Bouwer and Rice (1976)	3.46×10^{-3}	1.32×10^{-4}
	Ferris and Knowles (1954)	6.46×10^{-4}	2.47×10^{-5}
	Cooper and others (1967)	9.75×10^{-3}	3.72×10^{-4}
BE8*	Bouwer and Rice (1976)	3.20×10^{-3}	1.60×10^{-4}
	Packer test	1.38×10^{-2}	6.52×10^{-4}
BE9.1	Bouwer and Rice (1976)	2.34×10^{-5}	9.06×10^{-7}
	Ferris and Knowles (1954)	7.27×10^{-6}	2.82×10^{-7}
	Cooper and others (1967)	5.65×10^{-5}	2.19×10^{-6}
BE9.2	Bouwer and Rice (1976)	2.10×10^{-5}	8.16×10^{-7}
	Ferris and Knowles (1954)	5.91×10^{-6}	2.29×10^{-7}
	Cooper and others (1967)	4.34×10^{-5}	1.68×10^{-6}
BE9*	Packer test	$<2.93 \times 10^{-3}$	$<1.39 \times 10^{-4}$
BE10	Bouwer and Rice (1976)	1.38×10^{-3}	5.12×10^{-5}
	Ferris and Knowles (1954)	2.54×10^{-4}	9.40×10^{-6}
	Cooper and others (1967)	2.11×10^{-3}	7.81×10^{-5}
BE10*	Bouwer and Rice (1976)	9.60×10^{-3}	4.80×10^{-4}
	Packer test	$<5.49 \times 10^{-3}$	$<2.60 \times 10^{-4}$

Table 14 (cont.)

Well	Analytical method	Transmissivity (ft^2/day)	Hydraulic conductivity (ft/day)
BF1.1	Bouwer and Rice (1976)	6.97×10^{-5}	3.03×10^{-6}
	Ferris and Knowles (1954)	2.28×10^{-5}	9.91×10^{-7}
	Cooper and others (1967)	1.84×10^{-4}	8.00×10^{-6}
BF1.2	Bouwer and Rice (1976)	6.08×10^{-5}	2.64×10^{-6}
	Ferris and Knowles (1954)	2.13×10^{-5}	9.26×10^{-7}
	Cooper and others (1967)	1.08×10^{-4}	4.70×10^{-6}
BF2.1	Bouwer and Rice (1976)	3.19×10^{-3}	1.33×10^{-4}
	Ferris and Knowles (1954)	1.34×10^{-3}	5.60×10^{-5}
	Cooper and others (1967)	4.94×10^{-3}	2.06×10^{-4}
BF2.2	Bouwer and Rice (1976)	3.21×10^{-3}	1.34×10^{-4}
	Ferris and Knowles (1954)	2.32×10^{-3}	9.68×10^{-5}
	Cooper and others (1967)	5.95×10^{-3}	2.48×10^{-4}
BF2.3	Bouwer and Rice (1976)	5.19×10^{-3}	2.16×10^{-4}
	Ferris and Knowles (1954)	1.33×10^{-3}	5.55×10^{-5}
	Cooper and others (1967)	1.05×10^{-2}	4.38×10^{-4}
BF2*	Packer test	$<2.90 \times 10^{-3}$	$<1.45 \times 10^{-4}$
BF3	Bouwer and Rice (1976)	1.61×10^{-2}	5.97×10^{-4}
	Ferris and Knowles (1954)	3.83×10^{-3}	1.42×10^{-4}
	Cooper and others (1967)	1.31×10^{-2}	4.86×10^{-4}
BF3*	Bouwer and Rice (1976)	1.48×10^{-2}	7.40×10^{-4}
	Packer test	$<1.98 \times 10^{-2}$	$<9.90 \times 10^{-4}$
BF4	Bouwer and Rice (1976)	1.54×10^{-4}	6.15×10^{-6}
	Ferris and Knowles (1954)	6.97×10^{-5}	2.79×10^{-6}
	Cooper and others (1967)	1.97×10^{-4}	7.89×10^{-6}
BF6	Bouwer and Rice (1976)	8.32×10^{-5}	3.08×10^{-6}
	Ferris and Knowles (1954)	8.25×10^{-6}	3.05×10^{-7}
	Cooper and others (1967)	1.89×10^{-4}	6.99×10^{-6}

Table 14 (cont.)

Well	Analytical method	Transmissivity (ft²/day)	Hydraulic conductivity (ft/day)
BF7.1	Bouwer and Rice (1976)	4.68×10^{-5}	1.87×10^{-6}
	Ferris and Knowles (1954)	1.25×10^{-5}	5.01×10^{-7}
	Cooper and others (1967)	4.81×10^{-5}	1.92×10^{-6}
BF7.2	Bouwer and Rice (1976)	5.61×10^{-5}	2.24×10^{-6}
	Ferris and Knowles (1954)	1.43×10^{-5}	5.72×10^{-7}
	Cooper and others (1967)	1.44×10^{-4}	5.76×10^{-6}
BF7*	Packer test	$<3.88 \times 10^{-1}$	$<1.84 \times 10^{-2}$
BF8	Bouwer and Rice (1976)	7.06×10^{-4}	2.25×10^{-5}
	Ferris and Knowles (1954)	2.77×10^{-4}	8.86×10^{-6}
	Cooper and others (1967)	1.10×10^{-3}	3.51×10^{-5}
BF8*	Bouwer and Rice (1976)	1.14×10^{-2}	5.70×10^{-4}
	Packer test	1.67×10^{-1}	7.90×10^{-3}
BF9*	Bouwer and Rice (1976)	4.20×10^{-2}	2.10×10^{-3}
	Packer test	2.11×10^{-0}	0.10×10^{-0}
BI1.1	Bouwer and Rice (1976)	1.28×10^{-3}	4.73×10^{-5}
	Ferris and Knowles (1954)	5.03×10^{-4}	1.86×10^{-5}
	Cooper and others (1967)	3.43×10^{-3}	1.27×10^{-4}
BI1.2	Bouwer and Rice (1976)	1.14×10^{-3}	4.22×10^{-5}
	Ferris and Knowles (1954)	7.43×10^{-4}	2.75×10^{-5}
	Cooper and others (1967)	2.55×10^{-3}	9.44×10^{-5}
BI1*	Packer test	$<2.80 \times 10^{-3}$	$<1.25 \times 10^{-4}$
BI2A	Bouwer and Rice (1976)	1.55×10^{-3}	5.83×10^{-5}
	Ferris and Knowles (1954)	1.48×10^{-4}	5.56×10^{-6}
	Cooper and others (1967)	2.49×10^{-3}	9.38×10^{-5}
BI2A*	Bouwer and Rice (1976)	2.40×10^{-2}	1.20×10^{-3}
	Packer test	$<1.79 \times 10^{-3}$	$<8.50 \times 10^{-5}$
BI3*	Bouwer and Rice (1976)	2.00×10^{-0}	0.10×10^{-0}
	Packer test	$1.20 \times 10^{+1}$	0.60×10^{-0}

Table 14 (cont.)

Well	Analytical method	Transmissivity (ft^2/day)	Hydraulic conductivity (ft/day)
BI4	Bouwer and Rice (1976)	1.54×10^{-4}	6.15×10^{-6}
	Ferris and Knowles (1954)	1.63×10^{-3}	6.52×10^{-5}
	Cooper and others (1967)	2.15×10^{-4}	8.61×10^{-6}
BI4*	Packer test	$<2.16 \times 10^{-3}$	$<1.08 \times 10^{-4}$
BI5	Bouwer and Rice (1976)	8.17×10^{-4}	3.41×10^{-5}
	Ferris and Knowles (1954)	6.55×10^{-4}	2.73×10^{-5}
	Cooper and others (1967)	2.03×10^{-3}	8.48×10^{-5}
BI5*	Packer test	$<2.72 \times 10^{-3}$	$<1.36 \times 10^{-4}$
BI6	Bouwer and Rice (1976)	5.18×10^{-2}	1.85×10^{-3}
	Ferris and Knowles (1954)	1.96×10^{-2}	7.00×10^{-4}
	Cooper and others (1967)	8.03×10^{-2}	2.87×10^{-3}
BI6*	Packer test	$<7.94 \times 10^{-4}$	$<3.97 \times 10^{-5}$
BIR11	Bouwer and Rice (1976)	3.19×10^{-3}	1.33×10^{-4}
	Ferris and Knowles (1954)	1.50×10^{-3}	6.24×10^{-5}
	Cooper and others (1967)	8.52×10^{-3}	3.55×10^{-4}
BIR21	Bouwer and Rice (1976)	2.69×10^{-3}	9.21×10^{-5}
	Ferris and Knowles (1954)	7.97×10^{-4}	2.73×10^{-5}
	Cooper and others (1967)	7.12×10^{-3}	2.44×10^{-4}
BIR21*	Packer test	$<2.26 \times 10^{-3}$	$<1.13 \times 10^{-4}$
BIR31	Bouwer and Rice (1976)	4.90×10^{-3}	1.61×10^{-4}
	Ferris and Knowles (1954)	1.69×10^{-3}	5.35×10^{-5}
	Cooper and others (1967)	1.31×10^{-2}	4.30×10^{-4}
BIR31*	Packer test	$<2.04 \times 10^{-3}$	$<1.02 \times 10^{-4}$
BIR41	Bouwer and Rice (1976)	1.80×10^{-2}	7.05×10^{-4}
	Ferris and Knowles (1954)	3.91×10^{-3}	1.63×10^{-4}
	Cooper and others (1967)	5.17×10^{-2}	2.15×10^{-3}

Table 14 (cont.)

Well	Analytical method	Transmissivity (ft^2/day)	Hydraulic conductivity (ft/day)
BIR41*	Packer test	6.24×10^{-2}	3.12×10^{-3}
BIR81	Bouwer and Rice (1976)	8.51×10^{-4}	3.55×10^{-5}
	Ferris and Knowles (1954)	7.54×10^{-4}	3.14×10^{-5}
	Cooper and others (1967)	7.12×10^{-5}	2.96×10^{-6}
BIR81*	Packer test	3.28×10^{-3}	1.64×10^{-4}
B1597A	Bouwer and Rice (1976)	3.05×10^{-3}	1.53×10^{-4}
	Ferris and Knowles (1954)	1.10×10^{-3}	5.50×10^{-5}
	Cooper and others (1967)	no fit	
B1597B	Bouwer and Rice (1976)	3.53×10^{-3}	1.76×10^{-4}
	Ferris and Knowles (1954)	1.20×10^{-3}	6.00×10^{-5}
	Cooper and others (1967)	no fit	

* Data from The Earth Technology Corporation (1990e)

Hydraulic conductivity measured in the Ozan Formation ranges from $10^{-5.7}$ to $10^{-1.7}$ ft/d ($10^{-11.2}$ to $10^{-7.1}$ m/s) (fig. 55a, b). Hydraulic conductivity measured in test intervals in the Eagle Ford or straddling the contact between the Eagle Ford Formation and Austin Chalk ranges from $10^{-6.3}$ to $10^{-1.4}$ ft/d ($10^{-11.7}$ to $10^{-6.9}$ m/s) (fig. 55c, d). There are too few successful or interpretable tests to characterize the statistical distribution for these formations.

Average hydraulic conductivity is almost 1,000 times lower in unweathered chalk, marl, and shale than in weathered bedrock (fig. 53). Hydraulic conductivity of unweathered but fractured chalk, however, can be as great as the average hydraulic conductivity of weathered bedrock. Figure 53 also suggests a tendency for a regional decrease in hydraulic conductivity with depth, which might be related to a decrease in fracture aperture with increasing depth.

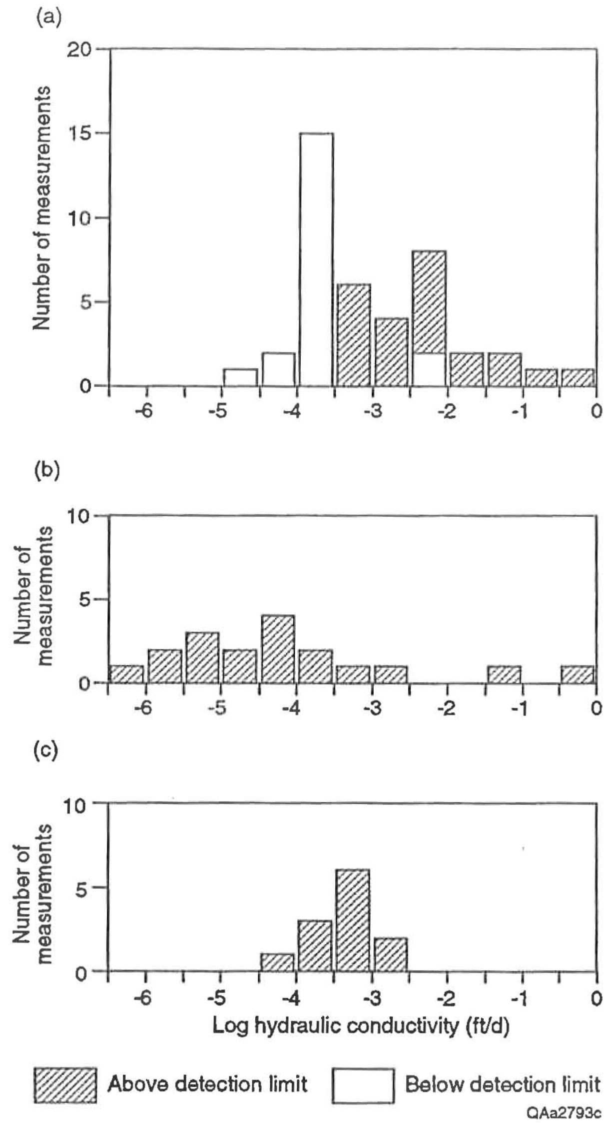

Figure 54. Histograms of hydraulic conductivity measured in unweathered Austin Chalk by (a) packer tests (The Earth Technology Corporation, 1990e), (b) Phase II piezometer and pumping tests, and (c) core-plug tests. Pumping tests in (b) were successful only at wells BI3 and BF9, as predicted by inspection of fractures in core and by results of previous packer tests. Packer-test results below detection limit reported as maximum value.

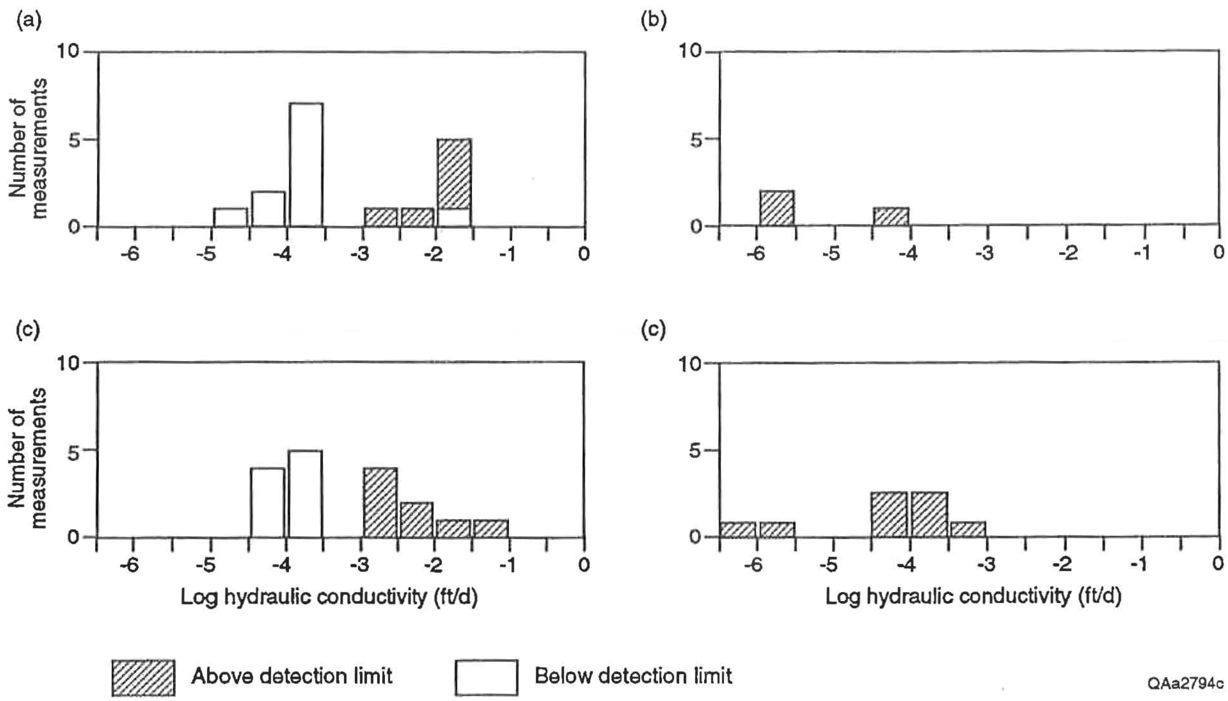

Figure 55. Histograms of hydraulic conductivity measured in (a) unweathered Ozan Formation by packer tests, (b) unweathered Ozan Formation by Phase II piezometer tests, (c) unweathered Eagle Ford Formation and Austin Chalk by packer tests, and (d) unweathered Eagle Ford Formation and Austin Chalk by Phase II piezometer tests. Packer tests were conducted by The Earth Technology Corporation (1990e). Histograms in (a) and (b) combine results from test intervals only in Ozan rock with results from test intervals that straddle the Ozan–Austin contact. Histograms in (c) and (d) combine results from test intervals only in Eagle Ford rock with results from test intervals that straddle the Eagle Ford–Austin contact. Packer-test results below detection limit reported as maximum value.

Figures 53 through 55 show results from packer, piezometer, pumping, and core-plug tests. Piezometer-test results generally agree with packer-test results, based on the 17 tests done in similar stratigraphic intervals (fig. 56). The packer tests were performed in unlined boreholes before casing was cemented in place. The screened interval in the cased monitoring well usually does not exactly match the packer-test interval. Figure 56 includes data in which the difference in test-interval midpoints between the two tests is less than 10 ft (3.05 m). The greatest discrepancy is for well BF7, where the hydraulic conductivity was higher in the uncased hole than in the completed monitor well. The lower hydraulic conductivity probably is due to wellface damage by cement in the screened interval. The midpoints of the test intervals used in well BE6 differ by 9 ft (2.74 m). Differences in strata possibly account for the two-order-of-magnitude difference in hydraulic conductivity. A downhole video log has not been made of BE6 so there are no direct data on formation damage; the water chemistry of this well was normal. No obvious explanation exists for the higher hydraulic conductivity at BI6 measured in the piezometer test compared to the packer test. Hydraulic conductivity was lower than the detection limit in half of the packer tests. Piezometer tests have a lower limit of measurement because the measurement period is longer, extending from tens to hundreds of days.

Average hydraulic conductivity of fractured chalk statistically differs between the subdivided units of the Austin Chalk (fig. 57). The F-ratio of between-means variance and within-groups pooled variance is 3.27, larger than the $F_{0.95}(3,38)$ statistic of ~2.84. Table 15 lists the data used in the analysis of variance. The differences in average hydraulic conductivity probably are due both to differences in fracture intensity between units (fig. 35) and correlated differences in fracture aperture. The Earth Technology Corporation (1990e) did not find significant variations in hydraulic conductivity between fractured and unfractured rock or between stratigraphic intervals. They did not sort out fractures associated with faults from other fractures, and included results measured at the packer-test detection limit. Fractures at faults with major displacements tend to be mineralized but more numerous and influenced each stratigraphic unit. Figure 57 includes The Earth Technology Corporation's (1990e) packer-test data but excludes measurements at faults and replaces four measurements below detection

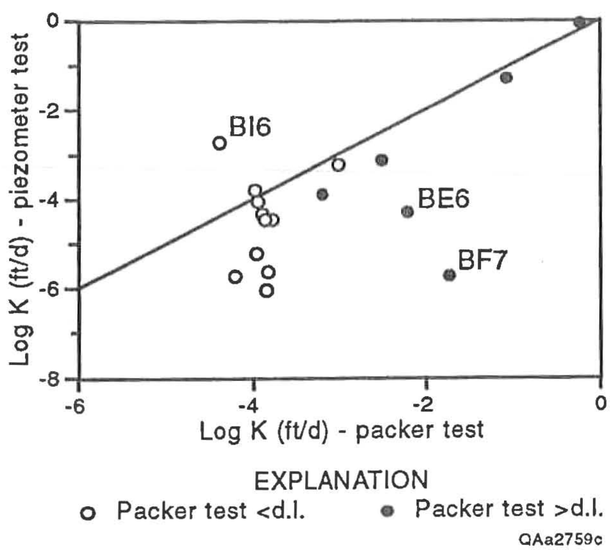

Figure 56. Comparison of hydraulic conductivity between packer and piezometer tests. Packer-test results below detection limit (d.l.) reported as maximum value (The Earth Technology Corporation, 1990e).

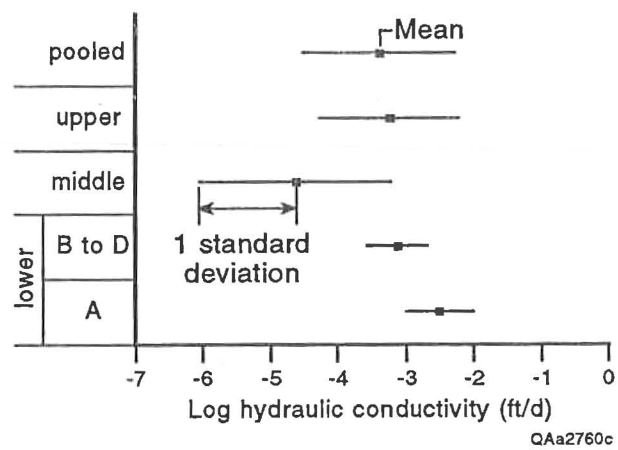

Figure 57. Comparison of mean and standard deviation of hydraulic conductivity between pooled and subdivided units of the fractured Austin Chalk for statistical analysis of variance. Subdivided units as defined in figure 35 include the lowermost Austin (unit A), upper part of the lower Austin (units B to D), middle Austin (units E to I), and upper Austin (units J to L). Square shows mean value of logarithm of hydraulic conductivity; extent of line either side of the square represents ±1 standard deviation. Data in table 15.

Table 15. Hydraulic conductivity data on fractured chalk used in analysis of variance calculation.

Well	Depth midpoint (ft)	Hydraulic conductivity (cm/s)	Hydraulic conductivity (ft/day)	Logarithm of hydraulic conductivity (ft/day)	Unit*
BE1-90	148.0	2.70×10^{-6}	7.65×10^{-3}	–2.12	A
BE3	164.4	2.80×10^{-7}	7.94×10^{-4}	–3.10	B–D
BE3	53.9	$<5.20 \times 10^{-8}$	1.47×10^{-4}	–3.83	M
BE4†	252.0	8.19×10^{-10}	2.32×10^{-6}	–5.63	M
BE4	74.0	$<5.10 \times 10^{-8}$	1.45×10^{-4}	–3.84	U
BE8†	177.7	4.65×10^{-8}	1.32×10^{-4}	–3.88	U
BE9†	125.2	3.20×10^{-10}	9.06×10^{-7}	–6.04	M
BF2	115.1	$<5.10 \times 10^{-8}$	1.45×10^{-4}	–3.84	B
BF3†	170.0	2.11×10^{-7}	5.97×10^{-4}	–3.22	B–D
BF4	142.0	1.80×10^{-7}	5.10×10^{-4}	–3.29	U
BIR12	200.5	9.20×10^{-7}	2.61×10^{-3}	–2.58	B
BIR32	195.4	2.90×10^{-7}	8.22×10^{-4}	–3.09	A
BIR41	135.0	1.60×10^{-6}	4.54×10^{-3}	–2.34	A
BIR81†	165.0	1.25×10^{-8}	3.55×10^{-5}	–4.45	U
BIR83	234.3	7.60×10^{-6}	2.15×10^{-2}	–1.67	U
BK1	155.1	4.50×10^{-7}	1.28×10^{-3}	–2.89	A–B
BK1	120.1	3.00×10^{-7}	8.50×10^{-4}	–3.07	B
se5.2e	218.7	1.50×10^{-6}	4.25×10^{-3}	–2.37	U

*Subdivided units as defined in figure 35 include the lowermost Austin (unit A), upper part of the lower Austin (units B to D), middle Austin (M: units E to J), and upper Austin (U: units K and L).
†Piezometer data; other data from packer tests by The Earth Technology Corporation (1990e).

limit with Phase II measurements by the piezometer test (as before, where the difference in test-interval midpoints between the two tests is less than 10 ft [3.05 m]). Excluding tests of fractures from near or at faults leaves a more homogeneous group of data within each stratigraphic unit.

Figure 58 shows a trend toward greater hydraulic conductivities with greater fault throw for faults having throws of 5 to 40 ft (1.5 to 12 m) (Collins and others, 1992). The difference is consistent with progressive development of an interconnected fracture system adjacent to faults. However, conductivity is lower than expected in fractured chalk near the three largest faults studied (fig. 58). Fractures in core from these fault zones are filled with calcite, suggesting that relatively low conductivities result from partial occlusion of fracture porosity (Collins and others, 1992).

Both greater fracture intensity and greater fracture aperture contribute to increased hydraulic conductivity of fractured Austin Chalk (fig. 59). There is a general relation between hydraulic conductivity and fracture intensity, expressed as the number of fractures observed per unit length of core studied (fig. 59). The slope of the data trend, however, is not as steep as that predicted from a theoretical relation between fracture intensity, fracture aperture, and hydraulic conductivity (Snow, 1968):

$$K = \frac{\rho g N b^3}{12\mu} \tag{9}$$

where K is hydraulic conductivity, ρ is fluid density, g is the gravitational constant, N is number of fractures per unit length, b is fracture aperture, and μ is dynamic viscosity. Equation (9) assumes a set of parallel and planar fractures of constant aperture and negligible flow of ground water through the matrix. If hydraulic conductivity and number of fractures per unit length are known (fig. 59), equation (9) can be solved for aperture width

$$b = \left(\frac{12\mu K}{\rho g N}\right)^{\frac{1}{3}} . \tag{10}$$

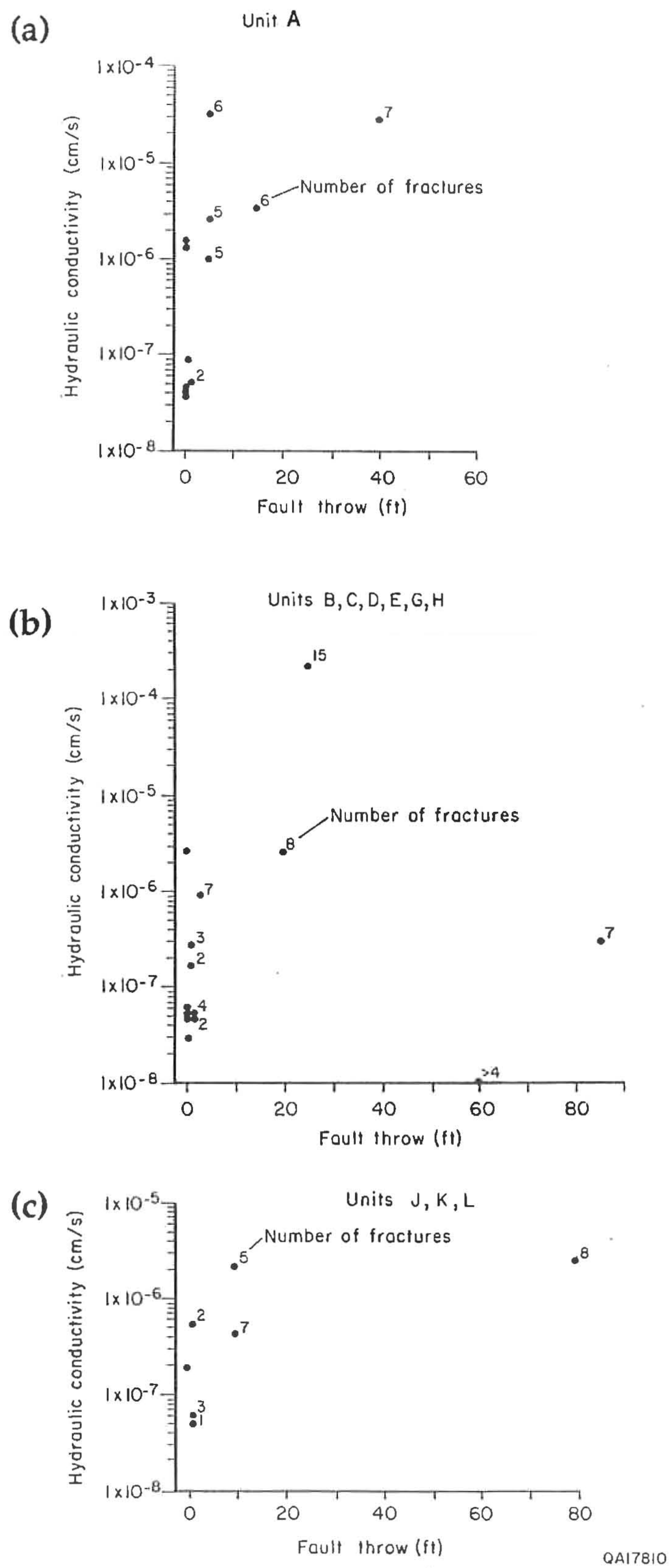

Figure 58. Relationship of hydraulic conductivity and fault offset in (a) lowermost Austin (unit A), (b) upper part of the lower Austin and middle Austin (units B to H), and (c) upper Austin (units J to L). Modified from Collins and others (1992).

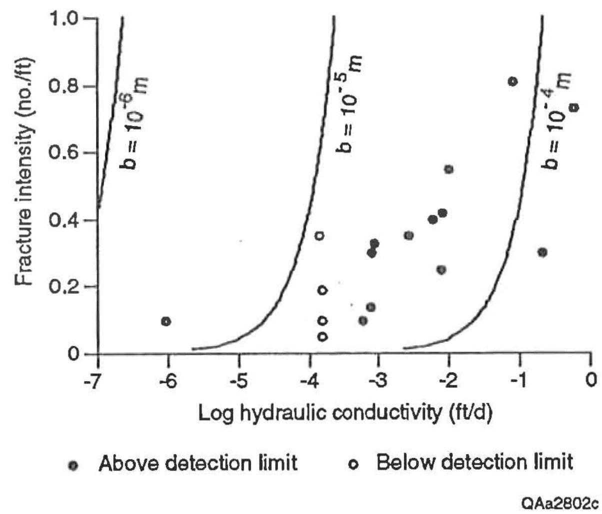

Figure 59. Variation of hydraulic conductivity with fracture intensity. Contours show fracture aperture predicted from cubic law.

Contours in figure 59 are calculated using equation (10). Given the number of fractures observed in core of the hydraulic-conductivity-test zones, calculated apertures range from 0.00003 to 0.0043 inches (0.0009 to 0.108 mm). The mean aperture is calculated to be 0.0011 inches (0.029 mm). These calculations agree with previously described estimates of fracture apertures in outcropping chalk, which were found to be less than 0.0098 inches (0.25 mm). Aperture of fractures should be greater at the outcrop than at depth because of the lack of overburden pressure.

Analysis of Water-Level Response to Atmospheric Pressure Changes

As water-level fluctuations are small, their radius of influence also is small. This limits the interpretation of hydrologic properties on the basis of the response of water level to atmospheric-pressure change. In tests of the low-permeability formations at the SSC site, hydraulic conductivity appears to be less influenced by hydrologic properties of the formation than by those of the sand pack in the well annulus or by wellface damage or stimulation. Additional study and analysis are required to verify whether elasticity and specific storage are representative of hydrologic properties or also affected by well construction.

Of 37 wells at which daily water-level fluctuations were monitored, only 11 could be used in an attempt to estimate aquifer properties (table 16) (BE2, BE3, BE7A, BF2, BF4, BF8, BF9, BI2A, B1697, B1697A, and B1697B).

Water-level fluctuations from these 11 wells and coincident atmospheric-pressure changes were analyzed as time series, following previously described methods to calculate a mean amplitude of fluctuations at both one and two cycles per day. Six of these 11 wells, however, yield high-pH water and had construction problems, which limit confidence in calculated results. Data from seven wells either were not collected (BF3) or were unusable (BE1A, BE5, BI4, BIR11, BIR21, and B1597) because of procedural or equipment problems such as lack of coincident atmospheric data, malfunction of equipment during monitoring period, use of a transducer insensitive to small water-level fluctuations, or presence of cement plugging the well screen. Nineteen wells (BE1-90, BE4, BE6, BE8, BE9, BE10, BF1,

Table 16. Summary of water-level fluctuations in SSC monitoring wells used to calculate barometric efficiency.

Well	Amplitude: Water level (ft) 1	Water level (ft) 2	Barometric pressure (ft) 1	Barometric pressure (ft) 2	Barometric efficiency 1	Barometric efficiency 2
Frequency (cycles/d)						
BE2	0.035	0.010	0.029	0.022	1.18	0.44
BE3	0.024	0.026	0.024	0.027	0.99	0.97
BE7A	0.010	0.004	0.024	0.023	0.40	0.19
BF2	0.030	0.011	0.035	0.023	0.85	0.47
BF4	0.009	0.006	0.018	0.028	0.49	0.23
BF8	0.012	0.004	0.030	0.023	0.40	0.17
BF9	0.025	0.015	0.035	0.027	0.71	0.57
BI2A	0.023	0.018	0:021	0.021	1.08	0.86
1697	0.034	0.012	0.030	0.028	1.12	0.42
1697A	0.061	0.029	0.055	0.036	1.11	0.80
1697B	0.063	0.030	0.054	0.032	1.17	0.94

Table 17. Summary of rock and hydrologic properties in SSC monitoring wells calculated on the basis of barometric efficiency.

Cycles/d	Uncorrected barometric efficiency 1	Uncorrected barometric efficiency 2	Corrected barometric efficiency 1	Corrected barometric efficiency 2	Hydraulic conductivity Calculated (ft/d)	Hydraulic conductivity Measured (ft/d)	Modulus of elasticity (MPa)	Specific storage (1/m)
BE2	1.18	0.44	1.18	0.89	1.46×10^{-3}	1.14×10^{-5}	6.29×10^{10}	1.42×10^{-6}
BE3	0.99	0.97	0.99	0.99	9.51×10^{-3}	5.24×10^{-5}	7.70×10^{11}	1.27×10^{-6}
BE7A	0.40	0.19	0.47	0.38	1.46×10^{-3}	1.52×10^{-6}	4.76×10^{9}	2.97×10^{-6}
BF2	0.85	0.47	0.98	0.95	1.46×10^{-3}	4.08×10^{-5}	1.48×10^{11}	1.31×10^{-6}
BF4	0.49	0.23	0.61	0.87	6.71×10^{-4}	1.87×10^{-6}	5.20×10^{10}	1.70×10^{-6}
BF8	0.40	0.17	0.46	0.34	1.46×10^{-3}	1.74×10^{-4}	4.01×10^{9}	3.15×10^{-6}
BF9	0.71	0.57	0.73	0.65	4.42×10^{-3}	6.40×10^{-4}	1.44×10^{10}	1.83×10^{-6}
BI2A	1.08	0.86	1.08	0.99	4.85×10^{-2}	1.78×10^{-5}	7.70×10^{11}	1.27×10^{-6}
1697[a]	1.12	0.42	1.12	0.92	1.31×10^{-3}	a	2.38×10^{11}	5.15×10^{-7}
1697A[a,b,c]	1.11	0.80	b	b	c	a	3.10×10^{10}	1.58×10^{-6}
1697B[a,b,c]	1.17	0.94	b	b	c	a	1.22×10^{11}	1.34×10^{-6}

[a] = No field test of hydraulic conductivity
[b] = Poor cross correlation
[c] = Unable to calculate

BF6, BF7, BI1, BI3, BI5, BI6, BIR31, BIR41, BIR54, BIR81, B1597A, B1597B) showed no water-level fluctuations, possibly because the test zone was locally unconfined, the well face in the screened zone was plugged or otherwise damaged, or hydraulic conductivity of the test zone was so low that flow of water between the well and formation did not occur in response to atmospheric-pressure change. Water level in well BE6 was above land surface and so was monitored by attaching a pressure transducer to the shut-in well head; the water column was not exposed to atmospheric-pressure changes. Well BI3 was inferred to be either unconfined or well connected to ground surface through fractures on the basis of the rapid water-level response, and so is not expected to be affected by barometric pressures. In most cases, however, the reason for the absence of fluctuations could not be determined. The 19 wells include only a few that yield high-pH water or show construction problems. Well damage is difficult to determine, especially behind the well pipe and screen, although the televiewer survey previously mentioned showed substantial damage or plugging in the screened interval at some wells.

Uncorrected barometric efficiency, which does not take into account a phase shift, was highly variable. Barometric efficiency based on the second harmonic of diurnal cycles was consistently lower than barometric efficiency based on the first harmonic (table 16). These values, however, should be similar because they measure the same physical phenomena. The difference suggested that borehole storage and formation permeability affect water-level response. In addition, four wells (BE2, BI2A, B1697, and B1697A) yielded first-harmonic barometric efficiencies greater than one, which is physically impossible if barometric pressure is the only force causing water-level fluctuations. Such values might reflect errors in measurement. For subsequent calculations, the first-harmonic barometric efficiency at these four wells was arbitrarily assumed to be 0.99.

Corrected water-level amplitudes were calculated by substituting phase shifts into the left-hand side of equation (4). Wave period, T_w (24 hr for 1 cycle/day and 12 hr for 2 cycles/day), and wave amplitudes, x_w and x_a, are known for each well. Corrected barometric efficiency showed greater agreement between diurnal and semidiurnal cycles than did uncorrected barometric efficiency (table 17). The right-hand side of equation (4) was used to solve for time lag, T_0, which allowed calculation of hydraulic conductivity using equation (5)

Modulus of elasticity (E_S) was solved using equation (2). Average modulus of elasticity for the Austin Chalk was approximately $10^{10.91}$ Pa (table 17). For comparison, The Earth Technology Corporation (1990c) determined average Young's modulus to be $10^{9.46}$ Pa. Young's modulus (E) is related to bulk modulus or elasticity (G), by Poisson's ratio (ν) (Ramsey, 1967, p. 287):

$$G = \frac{E}{2(1 - \nu)} . \tag{11}$$

The Earth Technology Corporation (1990c) reported ν to be 0.2 ± 0.09 for chalk. Using equation (11), elasticity of chalk should average $10^{9.26}$ Pa. The 45-fold higher value of elasticity calculated from water-level fluctuations suggests a somewhat lower compressibility than that based on laboratory measurements. Elasticity calculated from water-level fluctuations, therefore, appears to be uninfluenced by the unconsolidated sand pack in the well annulus, which would yield a smaller elasticity. Whether the field measurement of water-level fluctuations provides a different basis to measure elasticity of large samples of rock on the order of the length of well screen requires further study and analysis.

Specific storage was calculated from the 11 water-level hydrographs using equation (3). Calculated values were low (table 17), possibly indicating extreme confinement of ground water. Mean specific storage calculated for the Austin Chalk was $10^{-5.76}$ and mean specific storage for the Eagle Ford Formation was $10^{-6.29}$. Storativity has not been measured directly in test wells in unweathered bedrock at the SSC site, for example, by using paired pumping and observation wells, so there is no independent comparison for the value calculated using water-level fluctuations. Whether estimation of specific storage from the response of water-level fluctuations to atmospheric-pressure change is representative of in-situ specific storage also requires further study and analysis.

Hydraulic conductivity calculated from barometrically induced time lags averaged $10^{-2.1}$ ft/d ($10^{-7.56}$ m/s), within the upper range of bedrock hydraulic conductivity. The values from specific wells, however, were approximately 100 times greater than hydraulic conductivity calculated from piezometer-test data (table 17). The discrepancy most likely reflects the influence that the sand pack around the well screen has on the hydraulic conductivity calculated from the barometrically induced time lag. Piezometer tests are expected to be more accurate because they have a larger radius of influence owing to a larger pressure gradient between the well and the formation. Water-level fluctuations induced by atmospheric-pressure change were small in comparison and have a much smaller radius of influence, apparently not extending significantly past the sand pack. Therefore, hydraulic conductivity calculated from barometrically induced time lags at the SSCL monitoring wells probably reflects hydraulic conductivity of the sand pack alone or at best in combination with formation hydraulic conductivity.

Chemical Composition of Ground Water

Wickham and Dutton (1991) showed that ground water in the surficial alluvium was a calcium-bicarbonate hydrochemical facies (fig. 60), meaning that calcium and bicarbonate ions made up more than 50 percent of the total equivalent charge of cations and anions (Back, 1966). Concentrations of TDS in the surficial alluvium ranged from 542 to 758 mg/L (table 18).

Chemical composition of ground water in weathered bedrock of the Austin Chalk and Ozan Formation closely resembled that of ground water in surficial alluvium but had somewhat higher TDS and greater Na^+, Cl^-, and SO_4^{2-} (fig. 60, table 18). Hydrochemical facies in weathered bedrock ranged from calcium-bicarbonate to mixed-cation-bicarbonate and mixed-cation-sulfate types. Water collected from springs issuing from fractures in the Austin Chalk is a dilute calcium-bicarbonate type water (table 19). Samples S1, S2, S3, and S5 (table 19) from fractured Austin Chalk ionically resembled ground waters collected from wells in the weathered chalk. Sample S4, collected from the base of alluvium overlying chalk in Waxahachie (Hawkins Street Park), resembled ground waters from alluvium (samples 1 to 6, table 18).

Table 20 gives chemical composition of ground water from SSCL monitoring wells in unweathered bedrock. Naturally occurring waters at the SSC monitoring wells in table 20 are distinguished from

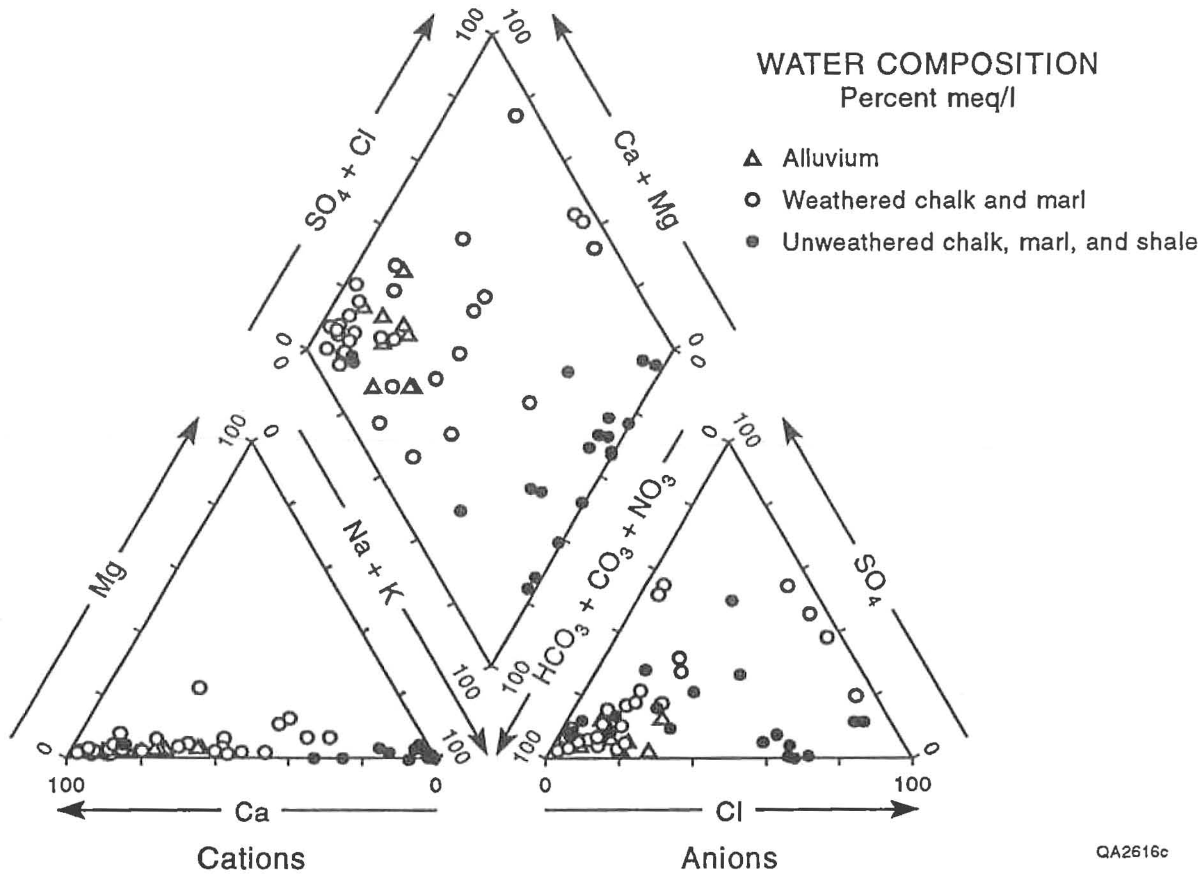

Figure 60. Trilinear diagram showing chemical composition of ground-water samples from alluvium (samples 1 through 6, table 18), weathered Austin Chalk and Ozan Formation (table 18), and unweathered Austin Chalk, Ozan Formation, and Eagle Ford Formation (table 20). NO_3 is significant in several samples from alluvium and weathered bedrock.

Table 18. Chemical analyses of ground waters from wells in vicinity of SSC site. Ionic concentrations in milligrams per liter (mg/L).

Map no.	Lab no.	Well name	Northing (ft)	Easting (ft)	Formation	Date	Temp. (°C)	pH	Na	K	Ca	Mg	Fe	SiO_2	Cl	SO_4
1	90-361	SSC1-1	6859059	2505577	Qal	8/ 8/90	22.5	6.8	37.1	1.4	134	2.7	0.12	18.5	43.6	26.7
1	90-611	SSC1-2	6859059	2505577	Qal	12/13/90	19.7	6.9	28.7	0.94	138	2.64	0.05	20.9	36.6	20.3
2	90-360	SSC2-1	6862400	2506780	Qal	7/19/90	21	6.7	73.6	1.2	120	4.3	<0.05	18.8	29.1	53.2
2	90-612	SSC2-2	6862400	2506780	Qal	12/12/90	19.5	6.9	72.3	0.73	112	4.05	<0.01	20.1	26.1	51.8
3	90-362	SSC3-1	6859779	2506845	Qal	8/ 8/90	21.3	7.1	36.7	1.5	101	2.5	0.12	16.7	13.2	9.7
4	90-615	SSC37-1	6854317	2513871	Qal	12/ 5/90	19.4	6.9	12.4	2.62	127	2.26	<0.01	18.6	13.3	9.54
5	90-614	SSC4-1	6857828	2508086	Qal	11/17/90	20.6	7.1	34.2	0.91	101	2.46	0.12	19.4	10.5	8.35
5	90-613	SSC4-2	6857828	2508086	Qal	11/29/90	19.6	7.1	38.3	0.92	96.3	2.53	<0.01	18.1	11.1	8.17
6	90-616	SSCGP6-1	6860263	2512217	Qal	12/6/90	19.8	6.8	27.9	0.58	153	2.96	<0.01	18	42.7	56.5
7	91-361	257	6818529	2450282	Kau	8/21/91	21.5	7.15	2.67	<1.39	103	1.98	*0.01	11	2.48	13.7
8	91-362	104A-1	6801607	2454070	Kau	8/19/91	20	7.08	15.2	4.12	139	1.78	0.1	12.5	13.7	22.7
9	92-120	107A-4-1	6842931	2454863	Kau	2/23/92	15	7.16	6	0.98	108	1.67	<0.01	10.2	3.2	8.7
10	91-360	144-1	6810290	2451115	Kau	8/22/91	19	7.2	3.96	*1.75	89	1.64	*0.01	10.1	3.72	15.3
11	92-109	215-1-1	6861042	2473197	Kau	1/22/92	16.5	6.8	103	4.8	131	5.9	*0.01	7.14	15.9	280
12	91-363	262A-2	6816101	2450549	Kau	8/20/91	18.5	7.12	24.1	8.62	112	2.63	*0.01	11.5	12.6	39.1
13	91-391	338-1	6812816	2455441	Kau	9/26/91	20	6.87	13	<1.4	103	1.82	*0.01	13	3.75	17
14	91-390	37-2	6800903	2458103	Kau	9/26/91	19.5	7.28	50.1	31.4	84.9	6.45	<0.02	12.7	28.1	102
15	91-376	496-3	6815417	2460029	Kau	9/17/91	18.5	7.44	43	3.57	86	22.5	<0.01	6.72	12.6	215
16	91-300	543A-1	6817418	2454348	Kau	7/10/91	18.5	7.4	6	1.1	99.3	1.66	*0.02	10.8	4.5	18.8
17	91-354	543A-2	6817930	2455295	Kau	8/ 7/91	19	7.76	13.6	2.98	107	6.77	*0.01	10.7	8.34	66.2
18	92-119	877-13-1	6787002	2504092	Kau	2/10/92	14	7	601	10.8	391	68.2	*0.01	20.1	640	1270
19	92-108	94-7-1	6831908	2450199	Kau	1/30/92	13.5	7.42	5.3	15.1	102	3.7	<0.01	7.94	5.49	19.6
20	92-121	A39-16-1-1	6811034	2470851	Kau	2/10/92	17	7	75.9	0.72	58.2	2.12	*0.01	5.5	15.9	47.2
21	92-112	R1446-25-1	6818419	2436483	Kau	1/22/92	13	7.01	33.3	17	91.5	3.4	0.07	14.7	32.2	38.1
22	92-122	R77-27-1	6795447	2479402	Kau	2/14/92	15	7	6.6	0.47	97.5	1.13	*0.01	10.5	7.6	10.5
23	92-113	R77N-21-1	6840741	2480676	Kau	1/24/92	16	7.42	9.8	2.9	99	2.2	*0.01	8.97	5.72	25.3
24	92-111	R875-4-1	6836198	2455295	Kau	1/30/92	17	6.8	4.4	4.46	90.3	1.7	*0.01	13.9	4.14	9.49
25	91-377	203-1	6841638	2523636	Ko	9/18/91	23	9.15	33.1	1.57	34.1	0.76	0.05	9.35	9.95	3.57
26	91-352	86C-1	6805374	2452035	Ko	8/13/91	19	7.53	11.5	2.88	93.2	1.25	8.37	11.8	12.5	<0.1
27	92-110	R813-11-1	6845445	2497090	Ko/Kau	1/31/92	16	6.81	92.4	1.1	109	2.4	<0.01	12.4	54.7	79.2
28	92-301	38C-1	6833012	2526301	Ko	4/7/92	19.5	7.64	255	2.16	80.8	13.6	<0.01	29.1	124	260
29	92-200	244A-1	6849115	2454442	Kau	3/9/92	17	7.97	22.6	<1.54	121	2.83	<0.01	7.72	15.5	60.3
30	92-202	252-3	6863667	2494451	Kau	2/28/92	17	7.6	296	2.81	1050	22.4	<0.01	11.4	850	636
31	92-302	272B-1	6844953	2523595	Ko	4/7/92	17.5	7.68	23.7	7.43	50.9	2.31	0.09	32.3	6.5	6.86
32	92-304	R55-34	6776005	2497887	Ko	4/7/92	19	7.6	863	8.34	379	52.2	<0.01	16.4	1080	1380
33	92-199	R287-33	6810258	2522838	Qal/Ko	3/9/92	17	8.05	25.2	5.44	82.1	4.43	<0.01	18.2	16.5	26.7
34	92-203	R664-16	6851985	2464078	Kau	3/9/92	17.3	7.32	32.7	13	82.7	2.96	<0.01	10.8	8.5	20.8
35	92-303	R876-4	6788036	2462703	Kau	4/7/92	19	7.9	59.6	1.61	78.4	2.19	<0.01	14.6	25.4	54.8
36	92-204	R877-14	6812815	2489214	Kau	2/20/92	20	7.87	6.8	<1.54	116	2.65	<0.01	13.7	4.3	16.1
37	92-198	R984-15	6787905	2520674	Ko	3/9/92	16	7.88	1470	16.8	771	185	<0.01	34.4	2240	2090
38	92-201	R1446-8	6823903	2463721	Kau	3/13/92	16	8.01	3.3	<1.54	111	1.41	<0.01	6.59	2.2	13.6

Table 18 (cont.)

Map no.	Lab no.	Well name	HCO_3	F	P	NO_3	B	Sr	Ba	Pb	Zn	Cu	Mn	Hg (µg/L)
1	90-361	SSC1-1	410	0.6	nm	nm	*0.06	0.57	0.12	<1	<0.1	<0.1	0.14	*0.015
1	90-611	SSC1-2	357	0.32	nm	33	0.04	0.58	0.11	<0.2	<0.02	<0.02	0.11	<0.5
2	90-360	SSC2-1	429	0.8	nm	nm	*0.08	1.07	0.06	<1	*0.1	<0.1	0.11	<0.010
2	90-612	SSC2-2	450	0.7	nm	19	0.07	0.98	0.05	<0.2	*0.02	<0.02	0.08	<0.5
3	90-362	SSC3-1	273	0.3	nm	nm	*0.06	0.67	0.1	<1	<0.1	<0.1	0.07	*0.014
4	90-615	SSC37-1	322	0.33	nm	55.6	0.04	0.64	0.08	<0.2	0.03	<0.02	<0.01	<0.5
5	90-614	SSC4-1	276	0.34	nm	88	0.07	0.68	0.08	<0.2	<0.02	<0.02	0.03	<0.5
5	90-613	SSC4-2	280	0.4	nm	89.7	0.08	0.69	0.09	<0.2	<0.02	<0.02	0.02	<0.5
6	90-616	SSCGP6-1	338	0.32	nm	63.7	0.06	0.91	0.07	<0.2	*0.02	<0.02	*0.01	<0.5
7	91-361	257	273.8	0.18	<0.2	10.1	*0.03	0.4	0.08	<0.2	*0.04	<0.02	*0.01	<0.5
8	91-362	104A-1	384	0.24	<0.2	17.5	0.04	0.56	0.08	<0.2	*0.02	<0.02	0.04	<0.5
9	92-120	107A-4-1	312	<0.1	<0.2	6	<0.04	0.38	*0.04	<0.2	*0.03	<0.02	<0.01	<0.5
10	91-360	144-1	237.5	0.19	<0.2	11.5	*0.02	0.43	*0.03	<0.2	*0.03	*0.02	<0.01	<0.5
11	92-109	215-1-1	288	0.33	<0.2	3.42	0.45	0.98	0.05	<0.2	*0.02	<0.02	0.11	<0.5
12	91-363	262A-2	314.3	0.22	<0.2	23.5	0.07	0.39	0.07	<0.2	*0.03	*0.02	<0.01	<0.5
13	91-391	338-1	314	0.38	<0.2	3.2	<0.01	0.59	0.07	<0.2	*0.04	<0.02	*0.02	<0.5
14	91-390	37-2	223	0.43	<0.2	57.6	0.39	0.82	*0.05	<0.2	*0.05	<0.02	<0.01	<0.5
15	91-376	496-3	188.6	0.89	<0.2	0.17	0.19	2.9	*0.03	<0.2	<0.02	<0.02	*0.01	<0.5
16	91-300	543A-1	292	0.42	<0.2	3.1	0.05	0.55	0.05	<0.2	<0.02	<0.02	0.04	<0.5
17	91-354	543A-2	236	*0.33	<0.2	44.3	0.06	0.84	*0.05	<0.2	*0.05	<0.02	*0.01	<0.5
18	92-119	877-13-1	183	2.61	<0.2	61.9	0.68	9.09	*0.04	<0.2	*0.05	<0.02	*0.01	<0.5
19	92-108	94-7-1	315	<0.1	<0.2	<0.1	*0.05	0.44	0.09	<0.2	<0.02	<0.02	<0.01	<0.5
20	92-121	A39-16-1-1	278	0.14	<0.2	7.77	0.09	0.51	*0.04	<0.2	*0.03	<0.02	<0.01	<0.5
21	92-112	R1446-25-1	290	<0.1	<0.20	0.68	0.15	0.39	0.04	<0.2	<0.02	<0.02	0.05	<0.5
22	92-122	R77-27-1	255	<0.1	<0.2	25.8	<0.04	0.38	0.05	<0.2	<0.02	<0.02	<0.01	<0.5
23	92-113	R77N-21-1	283	<0.1	<0.2	<0.1	0.07	0.42	0.08	<0.2	<0.02	<0.02	<0.01	<0.5
24	92-111	R875-4-1	261	0.17	<0.2	5.48	<0.04	0.31	0.05	<0.2	<0.02	<0.02	<0.01	<0.5
25	91-377	203-1	184	0.42	0.42	<0.1	0.1	0.2	*0.01	<0.2	<0.02	<0.02	0.05	<0.5
26	91-352	86C-1	314.3	0.42	*0.56	0.19	*0.04	0.52	0.07	<0.2	*0.02	<0.02	0.15	<0.5
27	92-110	R813-11-1	339	0.25	<0.2	36.1	*0.08	0.65	0.09	<0.2	0.08	<0.02	<0.01	<0.5
28	92-301	38C-1	491	1.3	<0.20	0.4	0.43	1.97	0.06	<0.02	<0.02	<0.02	*0.01	<0.50
29	92-200	244A-1	278	*0.2	<0.20	39.6	0.05	0.89	0.06	<0.02	<0.02	<0.02	<0.01	<0.50
30	92-202	252-3	217	<0.1	*0.26	1540	0.04	3.94	0.05	<0.02	0.33	*0.02	*0.03	<0.50
31	92-302	272B-1	216	*0.1	<0.20	<0.1	0.08	0.6	0.04	<0.02	<0.02	<0.02	0.23	<0.50
32	92-304	R55-34	178	<0.1	<0.20	7.2	0.54	7.97	0.04	<0.02	*0.02	<0.02	<0.01	<0.50
33	92-199	R287-33	243	*0.1	*0.22	23.7	0.1	0.47	0.09	<0.02	*0.03	<0.02	<0.01	<0.50
34	92-203	R664-16	299	*0.1	<0.20	24.9	0.13	0.29	0.05	<0.02	*0.04	<0.02	<0.01	<0.50
35	92-303	R876-4	281	<0.1	<0.20	11.5	0.23	0.47	0.05	<0.02	<0.02	<0.02	<0.01	<0.50
36	92-204	R877-14	319	<0.1	<0.20	15.4	0.04	0.54	0.1	<0.02	<0.02	<0.02	<0.01	<0.50
37	92-198	R984-15	257	0.7	<0.20	77.2	0.82	29.4	0.06	<0.02	*0.02	<0.02	<0.01	<0.50
38	92-201	R1446-8	253	<0.1	<0.20	60.6	0.04	0.39	0.07	<0.02	<0.02	<0.02	<0.01	<0.50

Table 18 (cont.)

Map no.	Lab no.	Well name	Ag	As	V	Co	Cr	Ni	Cd	Sb	Se	Be	Br	I
1	90-361	SSC1-1	<0.05	<0.1	<0.1	<0.1	<0.1	<0.25	<0.1	<0.25	<0.25	<0.1	<1	nm
1	90-611	SSC1-2	<0.025	<0.06	<0.02	<0.02	<0.02	<0.05	<0.02	<0.16	nm	<0.02	0.35	nm
2	90-360	SSC2-1	<0.05	<0.1	<0.1	<0.1	<0.1	<0.25	<0.1	<0.25	<0.25	<0.1	<1	nm
2	90-612	SSC2-2	<0.025	<0.06	<0.02	<0.02	<0.02	<0.05	<0.02	<0.16	nm	<0.02	0.28	nm
3	90-362	SSC3-1	<0.05	<0.1	<0.1	<0.1	<0.1	<0.25	<0.1	<0.25	<0.25	<0.1	<1	nm
4	90-615	SSC37-1	<0.025	<0.06	<0.02	<0.02	<0.02	<0.05	<0.02	<0.16	nm	<0.02	<0.1	nm
5	90-614	SSC4-1	<0.025	<0.06	<0.02	<0.02	<0.02	<0.05	<0.02	<0.16	nm	<0.02	<0.1	nm
5	90-613	SSC4-2	<0.025	<0.06	<0.02	<0.02	<0.02	<0.05	<0.02	<0.16	nm	<0.02	<0.1	nm
6	90-616	SSCGP6-1	<0.025	<0.06	<0.02	<0.02	<0.02	<0.05	<0.02	<0.16	nm	<0.02	<0.1	nm
7	91-361	257	*0.03	<0.06	<0.02	<0.02	<0.02	<0.05	<0.02	<0.16	<0.20	<0.02	<0.10	<0.1
8	91-362	104A-1	<0.025	<0.06	<0.02	<0.02	<0.02	<0.05	<0.02	<0.16	<0.20	<0.02	*0.11	<0.1
9	92-120	107A-4-1	<0.025	<0.06	<0.02	<0.02	<0.02	<0.05	<0.02	<0.16	<0.20	<0.02	<0.1	<0.1
10	91-360	144-1	<0.025	<0.06	<0.02	<0.02	<0.02	<0.05	<0.02	<0.16	<0.20	<0.02	*0.14	<0.1
11	92-109	215-1-1	<0.025	<0.06	<0.02	<0.02	<0.02	<0.05	<0.02	<0.16	<0.20	<0.02	<0.1	*0.12
12	91-363	262A-2	<0.025	<0.06	<0.02	<0.02	<0.02	<0.05	<0.02	<0.16	<0.20	<0.02	<0.10	0.41
13	91-391	338-1	<0.025	<0.06	<0.02	<0.02	<0.02	<0.05	<0.02	<0.16	<0.20	<0.02	<0.10	<0.1
14	91-390	37-2	<0.025	<0.06	<0.02	<0.02	<0.02	<0.05	<0.02	<0.16	<0.20	<0.02	<0.10	0.17
15	91-376	496-3	<0.025	<0.06	<0.02	<0.02	<0.02	<0.05	<0.02	<0.16	<0.16	<0.02	0.13	<0.1
16	91-300	543A-1	<0.025	<0.06	<0.02	<0.02	<0.02	<0.05	<0.02	<0.16	<0.20	<0.02	<0.1	0.22
17	91-354	543A-2	*0.03	<0.06	<0.02	<0.02	<0.02	<0.05	<0.02	<0.16	<0.20	<0.02	<0.10	*0.13
18	92-119	877-13-1	<0.025	<0.06	<0.02	<0.02	<0.02	<0.05	<0.02	<0.16	<0.20	<0.02	<0.1	0.23
19	92-108	94-7-1	<0.025	<0.06	<0.02	<0.02	<0.02	<0.05	<0.02	<0.16	<0.20	<0.02	*0.1	*0.12
20	92-121	A39-16-1-1	<0.025	<0.06	<0.02	<0.02	<0.02	<0.05	<0.02	<0.16	<0.20	<0.02	<0.1	<0.1
21	92-112	R1446-25-1	<0.025	<0.06	<0.02	<0.02	<0.02	<0.05	<0.02	<0.16	<0.20	<0.02	<0.1	0.36
22	92-122	R77-27-1	<0.025	<0.06	<0.02	<0.02	<0.02	<0.05	<0.02	<0.16	<0.20	<0.02	<0.1	<0.1
23	92-113	R77N-21-1	<0.025	<0.06	<0.02	<0.02	<0.02	<0.05	<0.02	<0.16	<0.20	<0.02	<0.1	<0.1
24	92-111	R875-4-1	<0.025	<0.06	<0.02	<0.02	<0.02	<0.05	<0.02	<0.16	<0.20	<0.02	<0.1	*0.12
25	91-377	203-1	<0.025	<0.06	<0.02	<0.02	<0.02	<0.05	<0.02	<0.16	<0.16	<0.02	<0.1	<0.1
26	91-352	86C-1	<0.025	<0.06	<0.02	*0.06	<0.02	<0.05	<0.02	<0.16	<0.20	<0.02	*0.11	2.64
27	92-110	R813-11-1	<0.025	<0.06	<0.02	<0.02	<0.02	<0.05	<0.02	<0.16	<0.20	<0.02	<0.1	*0.11
28	92-301	38C-1	<0.025	<0.06	<0.02	<0.02	<0.02	<0.05	<0.02	<0.16	<0.20	<0.20	0.7	*0.1
29	92-200	244A-1	<0.025	<0.06	<0.02	<0.02	<0.02	<0.05	<0.02	<0.16	<0.20	<0.20	<0.1	<0.1
30	92-202	252-3	<0.025	<0.06	<0.02	<0.02	<0.02	<0.05	<0.02	<0.16	*0.31	<0.20	2.5	*0.2
31	92-302	272B-1	<0.025	<0.06	<0.02	<0.02	<0.02	<0.05	<0.02	<0.16	<0.20	<0.20	<0.1	0.3
32	92-304	R55-34	<0.025	<0.06	<0.02	<0.02	<0.02	<0.05	<0.02	<0.16	<0.20	<0.20	2.7	<0.1
33	92-199	R287-33	<0.025	<0.06	<0.02	<0.02	<0.02	<0.05	<0.02	<0.16	<0.20	<0.20	<0.1	<0.1
34	92-203	R664-16	<0.025	<0.06	<0.02	<0.02	<0.02	<0.05	<0.02	<0.16	<0.20	<0.20	<0.1	*0.1
35	92-303	R876-4	<0.025	<0.06	<0.02	<0.02	<0.02	<0.05	<0.02	<0.16	<0.20	<0.20	<0.1	0.7
36	92-204	R877-14	<0.025	<0.06	<0.02	<0.02	<0.02	<0.05	<0.02	<0.16	<0.20	<0.20	<0.1	<0.1
37	92-198	R984-15	<0.025	<0.06	*0.03	<0.02	<0.02	<0.05	<0.02	<0.16	*0.22	<0.20	4.4	<0.1
38	92-201	R1446-8	<0.025	<0.06	<0.02	<0.02	<0.02	<0.05	<0.02	<0.16	<0.20	<0.20	<0.1	<0.1

* = Near detection limit.; nm = Not measured.

Table 19. Chemical analyses of miscellaneous spring waters in Ellis County. Ionic concentrations in milligrams per liter (mg/L).

Map no.	Lab no.	Spring name	Location	Formation	Date	Temp. (°C)	pH	Na	K	Ca	Mg	Fe	SiO_2	Cl	SO_4
S1	92-061	Hawkins	Midlothian	Kau	1/11/92	21.0	7.35	22.3	8.16	104	2.09	*.01	10.4	24.6	38.0
S2	92-062	Unnamed	Waxahachie	Qal	1/11/92	18.6	6.87	102	1.83	199	3.97	0.08	16.7	116	129
S3	92-063	Unnamed	Mountain Pk.	Kau	1/11/92	19.0	7.41	7.7	<1.54	88.7	1.15	<0.01	9.0	4.91	14.9
S4	92-064	Brach	Boz	Kau	1/10/92	17.0	7.54	8.6	<1.54	92.9	1.48	*0.02	9.73	18.6	[illegible]
S5	92-065	Mamouth	Mountain Pk.	Kau	1/11/92	18.5	7.13	10.7	<1.54	99.6	1.21	0.01	9.68	7.9	19.7
S5	92-1093	Mamouth	Mountain Pk.	Kau	11/13/92	20.6	7.34	24.8	18.1	111	2.9	0.07	10.8	42	47.3

Map no.	Lab no.	HCO_3	F	P	NO_3	B	Sr	Ba	Pb	Zn	Cu	Mn	Hg (µg/L)
S1	92-061	290	<0.1	<0.2	11.4	0.05	0.48	0.06	<0.2	<0.02	<0.02	*0.01	<0.5
S2	92-062	498	0.13	<0.2	18.5	0.54	1.02	0.10	<0.2	<0.02	<0.02	0.08	<0.5
S3	92-063	257	<0.1	<0.2	2.77	*0.02	0.46	*0.02	<0.2	<0.02	<0.02	<0.01	<0.5
S4	92-064	268	1.19	<0.2	3.0	*0.02	0.44	*0.02	<0.2	<0.02	<0.02	<0.01	<0.5
S5	92-065	281	<0.1	<0.2	6.05	*0.01	0.41	0.05	<0.2	<0.02	<0.02	<0.01	<0.5
S5	92-1093	299	0.34	<0.2	<0.8	*0.1	0.5	0.06	<0.2	<0.02	<0.02	<0.01	<0.50

Map no.	Lab no.	Ag	As	V	Co	Cr	Ni	Cd	Sb	Se	Be	Br	I
S1	92-061	<0.025	<0.06	<0.02	<0.02	<0.02	<0.05	<0.02	<0.16	<0.2	<0.02	<0.1	0.43
S2	92-062	<0.025	<0.06	<0.02	<0.02	<0.02	<0.05	<0.02	<0.16	<0.2	<0.02	<0.1	0.39
S3	92-063	<0.025	<0.06	<0.02	<0.02	<0.02	<0.05	<0.02	<0.16	<0.2	<0.02	<0.1	0.4
S4	92-064	<0.025	<0.06	<0.02	<0.02	<0.02	<0.05	<0.02	<0.16	<0.2	<0.02	<0.1	0.53
S5	92-065	<0.025	<0.06	<0.02	<0.02	<0.02	<0.05	<0.02	<0.16	<0.2	<0.02	<0.1	0.4
S5	92-1093	<0.025	<0.06	<0.02	<0.02	<0.02	<0.05	<0.02	<0.16	<0.20	<0.20	<0.25	<0.1

* Near detection limit.
nm Not measured.

Table 20. Chemical analyses of ground waters from SSC monitor wells. Samples largely free of cement contamination. Ionic concentrations in milligrams per liter (mg/L).

Lab no.	Well name	Northing (ft)	Easting (ft)	Form-ation	Date	Temp. (°C)	pH	Na	K	Ca	Mg	Fe	SiO_2	Cl	SO_4
91-304	B1597A	6821000	2447707	Kau	7/23/91	20.1	9.55	3,880	244	29.9	37.1	*0.01	5.56	5,340	1,010
92-646	B1597A-2	"	"	"	7/15/92	20.5	9.93	3,690	163	25.8	20.6	<0.01	6.73	5,090	1,070
	B1597A	"	"	"	3/3/93	–	9.08	–	–	–	–	–	–	–	–
93-142	B1597A	"	"	"	3/8/93	21.3	9.26	2,680	110	16.7	17.9	<0.01	5.56	3,430	678
91-305	B1597B-1	6821000	2447707	Kau	7/23/91	21.5	8.73	1,640	86.6	39.7	41.3	<0.01	8.75	2,250	441
93-141	B1597B	"	"	"	8/4/92	–	9.05	1,310	54.6	22.8	27.2	<0.01	10.3	1,670	359
92-679	B1597B	"	"	"	3/3/93	–	8.90	–	–	–	–	–	–	–	–
	B1597B	"	"	"	3/8/93	21.3	8.73	1,120	53.6	28.3	26.4	<0.01	13	1,450	306
92-592	B1697-1	6830681	2447602	Kau	6/17/92	21.5	8.18	1,730	12.2	36.1	14.2	<0.01	11.1	2,250	461
92-593	B1697B-1	6830667	2447603	Kau	6/17/92	20	8.94	1,170	38.6	56.3	53.9	<0.01	7.91	1,990	177
91-251	BE190-1	6818656	2448230	Kef	6/12/91	24	8.61	397	2.19	2.62	0.71	*0.02	12.1	130	126
93-111	BE3	6863768	2473856	Kau	2/24/93	18.2	8.2	350	7.2	4.2	1.67	<0.01	14	151	64.9
93-175	BE6	6817710	2532149	Kau	3/23/93	18.5	7.56	6,430	27.7	274	107	1.09	16	10,450	9.59
92-594	BE8-1	6771737	2506652	Kau	6/18/92	22	7.87	2,220	19.6	148	50.2	0.07	11	3,610	178
91-652	BE10	6790888	2458827	Kau	10/8/91	20	7.89	272	3.8	39.5	6.53	0.6	18.5	154	66.5
92-632	BE10-2	"	"	"	7/2/92	22.5	8.2	339	4.9	12.2	5.5	*0.01	13.7	180	84.1
91-649	BF1	6832267	2448113	Kef	10/8/91	19.7	8.02	381	29.5	6.8	1.15	0.06	9.73	90.3	75.1
92-649	BF1-2	"	"	"	7/22/92	22	7.89	760	3	8.4	2.3	0.09	12.7	370	18
91-351	BF2-1	6856397	2461093	Kau	8/15/91	21	9.41	524	37.8	1.33	1.89	*0.02	7.42	506	86.7
92-642	BF2-2	"	"	"	7/14/92	20.5	8.29	598	14.2	6.2	4.2	*0.02	12.1	597	58.8
	BF2	"	"	"	3/3/93	–	7.84	–	–	–	–	–	–	–	–
	BF2	"	"	"	3/11/93	–	8.23	–	–	–	–	–	–	–	–
93-176	BF2	"	"	"	3/23/93	19.9	8.22	660	5.6	10.3	4.43	*0.01	10.5	662	42.9
93-104	BF3	6866038	2487723	Kau	1/12/93	15	7.83	2,550	21.7	90.7	39.3	0.09	10.4	4,050	6.16
90-363	BF9	6779852	2467146	Kau	9/17/91	19.2	–	599	4.3	25.3	12.5	0.18	12.6	736	6.9
91-651	BF9	"	"	"	10/10/91	25	7.85	619	39.5	25.2	11.2	*0.03	14.6	750	5.8
92-292	BF9-02	"	"	"	4/15/92	21.5	8.06	555	4.2	21	11.1	0.07	19.3	645	9.63
92-631	BF9-2	"	"	"	7/2/92	21.5	7.79	563	6.3	22.5	11.7	*0.03	14.5	658	10.2
91-252	BI1-1	6816498	2448982	Kau/Kef	6/11/91	20.3	9.08	419	11.6	1.79	0.79	*0.01	18.3	189	182
92-643	BI1-2	"	"	"	7/14/92	22	8.95	465	11.9	2	1.1	*0.02	13.8	220	135
91-350	BI3-2	"	"	"	8/ 5/91	23	7.4	16.1	1.88	94.8	3.04	*0.01	12.1	5.86	20.9
91-379	BI3-3	"	"	"	9/17/91	19.2	–	18.1	1.22	94.9	3.02	<0.01	9.99	6.29	19.7
91-365	BI4-1	6820765	2451277	Kau	8/21/91	21.8	7.75	192	11.1	23.1	2.54	*0.02	10.5	43.7	129
92-116	BI5	6816744	2459586	Kau	12/3/91	19	8.57	443	36.7	8.2	7.1	*0.01	12.6	454	37.4
92-644	BI5-2	"	"	"	7/15/92	20.5	8.33	466	28.1	9.4	8	*0.01	11.7	501	34.3
92-117	BI6-1	6810785	2451903	Kau	12/3/91	18	9.46	296	11.5	1.4	0.2	0.07	18.9	33.1	158
92-591	BI6-3	"	"	"	6/17/92	21	10.49	114	10.8	0.3	<0.32	0.13	44.5	16.7	49.9
	BI6	"	"	"	3/3/93	–	9.06	–	–	–	–	–	–	–	–
	BI6	"	"	"	3/3/93	–	8.9	–	–	–	–	–	–	–	–
	BI6	"	"	"	3/3/93	–	9.02	–	–	–	–	–	–	–	–
	BI6	"	"	"	3/4/93	–	8.92	–	–	–	–	–	–	–	–
91-353	BIR31-1	6796867	2455942	Kau/Kef	7/23/91	20.2	8.09	337	6.2	4.79	1.14	*0.01	13.3	69.6	100
92-680	BIR31-2	"	"	"	8/4/92	21	8.2	418	4.1	3.9	0.9	*.02	12.3	130	89.7
92-1094	BIR-41	6796272	2456007	Kau/Kef	12/2/92	19	8.74	414	32.6	1.9	*0.4	*0.01	12.7	94.3	116
92-629	BIR54-2	6831583	2527673	Ko/Kau	7/1/92	22	7.85	2,210	7.1	42.5	16.3	*0.02	19.5	3,270	13.2
92-630	BIR81-2	6839299	2524447	Ko/Kau	7/1/92	22	8.03	1,080	64.7	180	27.9	0.19	14.2	725	1,730

Table 20 (cont).

Lab no.	Well name	HCO_3	F	P	NO_3	B	Sr	Ba	Pb	Zn	Cu	Mn	Hg (µg/L)
91-304	B1597A	745.6	2.6	<0.2	17.1	4.71	5.85	0.1	<0.2	*0.02	<0.02	<0.01	<0.5
92-646	B1597A-2	128	3.11	<0.20	3.76	4.46	6.48	0.13	<0.20	*0.05	0.1	<0.01	<0.50
	B1597A	–	–	–	–	–	–	–	–	–	–	–	–
93-142	B1597A	215	3.74	*0.25	0.57	5.87	5.87	0.11	<0.02	<0.02	<0.02	<0.01	–
91-305	B1597B-1	495.4	1.81	<0.2	6.5	3.18	5.27	0.07	<0.2	0.08	<0.02	0.09	<0.5
93-141	B1597B	285	1.85	<0.12	6.77	3.75	5.07	0.04	<0.02	*0.07	<0.02	<0.01	–
92-679	B1597B	236	1.83	<0.20	1.90	3.56	4.69	0.05	<0.20	*0.02	0.08	<0.01	<0.50
	B1597B	–	–	–	–	–	–	–	–	–	–	–	–
92-592	B1697-1	385	1.97	<0.20	1.68	4.93	3.44	0.12	<0.20	<0.02	<0.02	0.05	<0.50
92-593	B1697B-1	26.7	1.42	<0.20	1.64	2.83	7.11	0.2	<0.20	0.09	<0.02	<0.01	<0.50
91-251	BE190-1	623	6.67	*0.85	0.28	5.31	0.26	*0.01	<0.2	<0.02	<0.02	<0.01	<0.5
93-111	BE3	575	6.06	17.8	*0.11	2.82	0.67	0.05	<0.02	<0.02	<0.02	<0.01	–
93-175	BE6	255	1.26	21.7	<0.80	5.08	44.8	1.85	<0.02	<0.02	<0.02	*0.02	–
92-594	BE8-1	172	1.15	<0.20	1.31	3.43	7.11	0.59	<0.20	*0.02	<0.02	0.06	<0.50
91-652	BE10	555	3.5	0.18	3.76	3.73	1.21	0.09	<0.2	*0.02	*0.02	0.04	<0.5
92-632	BE10-2	564	3.3	<0.20	2.3	4.66	1.26	0.13	<0.20	0.06	<0.02	<0.01	<0.50
91-649	BF1	890.8	3.28	0.66	<0.10	2.93	0.35	*0.03	<0.2	*0.03	<0.02	*0.03	<0.5
92-649	BF1-2	1,320	2.01	*0.65	1.51	5.79	0.76	0.09	<0.20	*0.02	<0.02	0.09	<0.50
91-351	BF2-1	393	5.27	<0.2	1.42	3.68	0.46	*0.03	<0.2	<0.02	*0.02	<0.01	<0.5
92-642	BF2-2	479	4.28	<0.20	<0.8	5.28	0.94	0.06	<0.20	*0.02	<0.02	<0.01	<0.50
	BF2	–	–	–	–	–	–	–	–	–	–	–	–
	BF2	–	–	–	–	–	–	–	–	–	–	–	–
93-176	BF2	542	4.59	0.3	*0.2	5.02	1.26	0.07	<0.02	*0.02	<0.02	*0.02	–
93-104	BF3	296	2.22	<0.12	<0.8	5.59	12.4	0.72	<0.02	<0.02	<0.02	0.07	–
90-363	BF9		3.0			3.9	2.90	0.32	<1	<0.1	<0.1	*0.02	*0.010
91-651	BF9	665.7	3.93	1.51	<0.10	4.2	2.1	0.19	<0.2	0.19	<0.02	*0.01	<0.5
92-292	BF9-02	439	2.5	<0.20	<0.1	4.07	2.17	0.24	<0.02	<0.02	<0.02	*0.01	<0.50
92-631	BF9-2	448	2.34	<0.20	1.11	4.26	2.7	0.31	<0.20	0.09	<0.02	*0.02	<0.50
91-252	BI1-1	541	5.1	<0.2	0.26	5.23	0.23	*0.03	<0.2	*0.02	<0.02	<0.01	<0.5
92-643	BI1-2	548	5.41	<0.20	<0.8	6.02	0.41	0.06	<0.20	0.05	<0.02	<0.01	<0.50
91-350	BI3-2	283	0.5	<0.2	9	0.07	0.79	0.06	<0.2	*0.04	<0.02	*0.01	<0.5
91-379	BI3-3	303	0.45	<0.2	6.06	0.1	0.89	0.07	<0.2	*0.04	<0.02	*0.01	<0.5
91-365	BI4-1	340	2.15	<0.2	0.4	1.04	0.62	*0.03	<0.2	<0.02	<0.02	*0.03	<0.5
92-116	BI5	386	3.53	<0.2	<0.1	6.13	1.52	0.11	<0.2	<0.02	<0.02	<0.01	<0.5
92-644	BI5-2	410	2.97	<0.20	1.06	6.15	1.95	0.14	<0.20	*0.02	<0.02	<0.01	<0.50
92-117	BI6-1	370	1.94	<0.2	0.60	1.25	0.08	*0.01	<0.2	<0.02	<0.02	<0.01	<0.5
92-591	BI6-3	109	1.01	<0.20	<0.80	0.39	<0.01	0.1	<0.20	0.05	<0.02	<0.01	<0.50
	BI6	–	–	–	–	–	–	–	–	–	–	–	–
	BI6	–	–	–	–	–	–	–	–	–	–	–	–
	BI6	–	–	–	–	–	–	–	–	–	–	–	–
	BI6	–	–	–	–	–	–	–	–	–	–	–	–
91-353	BIR31-1	707.3	3.54	*0.2	1.06	2.84	0.28	*0.02	<0.2	*0.02	*0.02	<0.01	<0.5
92-680	BIR31-2	749	4.6	<0.20	1.99	4.16	0.4	0.07	<0.20	0.06	<0.02	<0.01	*0.58
92-1094	BIR-41	731	2.55	<0.20	<0.8	2.58	0.34	*0.04	<0.02	*0.04	*0.02	<0.01	<0.50
92-629	BIR54-2	673	1.81	<0.20	2.3	3.51	4.67	0.14	<0.20	<0.02	<0.02	*0.01	<0.50
92-630	BIR81-2	431	2.61	<0.20	<0.80	3.9	3.9	0.19	<0.20	*0.02	<0.02	0.07	<0.50

Table 20 (cont.)

Lab no.	Well name	Ag	As	V	Co	Cr	Ni	Cd	Sb	Se	Be	Br	I
91-304	B1597A	*0.04	<0.06	<0.02	<0.02	0.15	<0.05	<0.02	<0.16	<0.20	<0.02	0.86	0.17
92-646	B1597A-2	<0.025	<0.06	<0.02	<0.02	<0.02	<0.05	<0.02	<0.16	<0.20	<0.02	0.95	0.6
	B1597A	–	–	–	–	–	–	–	–	–	–	–	–
[illegible]-142	B1597A	-	<0.06	<0.02	<0.02	*0.04	<0.05	<0.02	<0.16	<0.14	<0.20	0.9	*0.21
91-305	B1597B-1	<0.025	<0.06	<0.02	<0.02	<0.02	<0.05	<0.02	<0.16	<0.20	<0.02	0.39	0.22
93-141	B1597B	–	<0.06	<0.02	<0.02	*0.05	<0.05	<0.02	<0.16	<0.14	<0.20	0.29	*0.13
92-679	B1597B	<0.025	<0.06	<0.02	<0.02	<0.02	<0.05	<0.02	<0.16	<0.02	<0.02	*0.28	0.51
	B1597B	–	–	–	–	–	–	–	–	–	–	–	–
92-592	B1697-1	<0.025	<0.06	<0.02	<0.02	<0.02	<0.05	<0.02	<0.16	<0.20	<0.02	1.45	0.67
92-593	B1697B-1	<0.025	<0.06	<0.02	<0.02	<0.02	<0.05	<0.02	<0.16	<0.20	<0.02	1.45	0.36
91-251	BE190-1	<0.025	<0.06	<0.02	<0.02	<0.02	<0.05	<0.02	<0.16	<0.20	<0.02	0.48	0.27
93-111	BE3	–	<0.06	<0.02	<0.02	<0.02	<0.05	<0.02	<0.16	<0.14	<0.20	0.35	0.53
93-175	BE6	–	*0.08	<0.02	<0.02	<0.02	<0.05	<0.02	<0.16	<0.14	<0.20	38.7	12.0
92-594	BE8-1	<0.025	<0.06	<0.02	<0.02	<0.02	<0.05	<0.02	<0.16	<0.20	<0.02	11.9	3.2
91-652	BE10	<0.025	0.1	*0.02	*0.02	*0.02	<0.05	<0.02	<0.16	<0.20	<0.02	0.83	0.19
92-632	BE10-2	<0.025	<0.06	<0.02	<0.02	<0.02	<0.05	<0.02	<0.16	<0.20	<0.02	0.99	0.54
91-649	BF1	<0.025	*0.06	<0.02	<0.02	<0.02	<0.05	<0.02	<0.16	<0.20	<0.02	0.37	0.34
92-649	BF1-2	<0.025	<0.06	<0.02	<0.02	<0.02	<0.05	<0.02	<0.16	<0.20	<0.02	6.48	1.11
91-351	BF2-1	*0.04	<0.06	<0.02	<0.02	<0.02	<0.05	<0.02	<0.16	<0.20	<0.02	4.41	2.02
92-642	BF2-2	<0.025	<0.06	<0.02	<0.02	<0.02	<0.05	<0.02	<0.16	<0.20	<0.02	1.81	1.25
	BF2	–	–	–	–	–	–	–	–	–	–	–	–
	BF2	–	–	–	–	–	–	–	–	–	–	–	–
93-176	BF2	–	<0.06	<0.02	<0.02	<0.02	<0.05	<0.02	<0.16	<0.14	<0.20	2.55	0.89
93-104	BF3	–	<0.06	<0.02	<0.02	<0.02	<0.05	<0.02	<0.16	<0.14	<0.20	14.8	5.03
90-363	BF9	<0.05	<0.1	<0.1	<0.1	<0.1	<0.25	<0.1	<0.25	<0.25	<0.1	2.4	–
91-651	BF9	<0.025	<0.06	<0.02	<0.02	<0.02	<0.05	<0.02	<0.16	<0.20	<0.02	2.43	1.08
92-292	BF9-02	<0.025	<0.06	<0.02	<0.02	<0.02	<0.05	<0.02	<0.16	<0.20	<0.20	2.35	0.91
92-631	BF9-2	<0.025	<0.06	<0.02	<0.02	<0.02	<0.05	<0.02	<0.16	<0.20	<0.02	3.1	1.08
91-252	BI1-1	<0.025	<0.06	<0.02	<0.02	<0.02	<0.05	<0.02	<0.16	<0.20	<0.02	0.98	0.45
92-643	BI1-2	<0.025	<0.06	<0.02	<0.02	<0.02	<0.05	<0.02	<0.16	<0.20	<0.02	1.84	1.59
[illegible]-350	BI3-2	*0.03	<0.06	<0.02	<0.02	<0.02	<0.05	<0.02	<0.16	<0.20	<0.02	*0.11	0.45
91-379	BI3-3	<0.025	<0.06	<0.02	<0.02	<0.02	<0.05	<0.02	<0.16	<0.16	<0.02	<0.1	<0.1
91-365	BI4-1	<0.025	<0.06	<0.02	<0.02	<0.02	<0.05	<0.02	<0.16	<0.20	<0.02	0.23	*0.13
92-116	BI5	<0.025	<0.06	<0.02	<0.02	<0.02	<0.05	<0.02	<0.16	<0.20	<0.02	1.12	0.49
92-644	BI5-2	<0.025	<0.06	<0.02	<0.02	<0.02	<0.05	<0.02	<0.16	<0.20	<0.02	1.89	0.55
92-117	BI6-1	<0.025	<0.06	<0.02	<0.02	<0.02	<0.05	<0.02	<0.16	<0.20	<0.02	*0.1	<0.1
92-591	BI6-3	<0.025	<0.06	<0.02	<0.02	<0.02	<0.05	<0.02	<0.16	<0.20	<0.02	<0.25	0.33
	BI6	–	–	–	–	–	–	–	–	–	–	–	–
	BI6	–	–	–	–	–	–	–	–	–	–	–	–
	BI6	–	–	–	–	–	–	–	–	–	–	–	–
	BI6	–	–	–	–	–	–	–	–	–	–	–	–
91-353	BIR31-1	<0.025	<0.06	<0.02	<0.02	<0.02	<0.05	<0.02	<0.16	<0.20	<0.02	0.51	0.22
92-680	BIR31-2	<0.025	<0.06	<0.02	<0.02	<0.02	<0.05	<0.02	<0.16	<0.20	<0.02	<0.25	0.46
92-1094	BIR-41	<0.025	<0.06	<0.02	<0.02	<0.02	<0.05	<0.02	<0.16	<0.20	<0.20	0.57	<0.1
92-629	BIR54-2	<0.025	<0.06	<0.02	<0.02	<0.02	<0.05	<0.02	<0.16	<0.20	<0.02	13.7	4.05
92-630	BIR81-2	<0.025	<0.06	<0.02	<0.02	<0.02	<0.05	<0.02	<0.16	<0.20	<0.02	2.69	0.84

* Near detection limit.
– Not measured.

waters with anomalous pH and ionic composition in table 21. Only the good-quality data on the natural waters have been included in further interpretation. Locations of samples are shown in figure 2.

Ground water from unweathered bedrock, collected at the SSCL monitoring wells, tends to have the highest TDS and a large proportion of samples were sodium-chloride hydrochemical types (fig. 60). Figure 61 shows that Na^+ and Cl^- concentrations in ground waters from the SSCL monitoring wells lie along or above the seawater dilution line. Similarly, the Br^-/Cl^- ratio of the ground waters generally is similar to that of seawater (fig. 62); two samples (B1597A and B1597B) were depleted in bromide relative to chloride ionic concentrations. The Na^+, Cl^-, and Br^- ions are assumed to reflect natural variations and not to be due to salt that might have been added to the cement grout to shorten its hardening time.

Data on Cl^- and SO_4^{2-} composition of Austin Chalk rock samples are consistent with the analyses of waters sampled from SSCL monitoring wells (table 22). For comparing data sets, concentration units were converted from mg/Kg-rock to mg/L-water by dividing the former by gravimetric moisture content data, assuming that data reflect the ionic concentrations in pore water. Average Cl^- concentration estimated from rock samples is 2,730 mg/L and standard deviation is 3,050 mg/L (table 22b). Average sulfate concentration estimated from rock samples is 3,310 mg/L and standard deviation is 2,390 mg/L. Coefficients of variation are very large. Concentrations might somewhat overestimate actual pore water concentrations because rock samples might have partly dried before laboratory determination of moisture content. The chloride concentration in water samples from the Austin Chalk averages 1,800 mg/L; its standard deviation is 2,820 mg/L (table 22a). Average sulfate concentration in water samples from the Austin Chalk is 255 mg/L and its standard deviation is 370 mg/L. Average chloride concentrations based on rock and water samples are not statistically different. Average sulfate concentration based on rock samples is significantly higher than that based on water samples. Core handling and laboratory technique might have caused oxidation of disseminated pyrite, increasing concentration of dissolved sulfate.

Carbon-14 (^{14}C) and tritium (^{3}H) are naturally occurring, radioactive isotopes in ground water that are commonly used for determining age of water since recharge. ^{14}C has a half life of 5,730 yr.

Table 21. Chemical analyses of ground waters from SSC monitoring wells. Samples affected by CaOH fluid with pH generally greater than 10.5 and negligible Mg content. Ionic concentrations in milligrams per liter (mg/L).

Lab no.	Well name	Northing (ft)	Easting (ft)	Formation	Date	Temp. (°C)	pH	Na	K	Ca	Mg	Fe	SiO_2	Cl	SO_4
91-380	BE1A	6826452	2449328	Kef	9/17/91	19.5	10.72	502	79.2	2.9	0.16	0.07	10.5	219	575
92-648	BE1A-2	"	"	"	7/22/92	24	10.5	545	81.2	1	<0.32	0.06	17	243	655
	BE1A	"	"	"	8/4/92	dry hole									
91-366	BE2-1	6845874	2452651	Kau/Kef	8/20/91	20	10.05	277	9	1.2	<0.32	0.05	9.73	176	158
92-647	BE2-2	"	"	"	7/22/92	20.5	11.37	283	9.6	6.2	<0.32	*0.01	6.14	205	111
	BE4	6863177	2501591	Kau	6/16/92	20.8	11.939	-	-	-	-	-	-	-	-
	BE4	"	"	"	6/16/92	20.8	11.79	-	-	-	-	-	-	-	-
91-301	BE5	6844515	2521980	Kau	9/11/91	21.9	12.12	1,920	744	7.74	<0.32	*0.03	95.6	2,360	203
	BE7A	6787639	2526782	Ko/Kau	6/18/92	-	11.59	-	-	-	-	-	-	-	-
	BE9	6772657	2478167	Kau	6/19/92	22.0	10.65	-	-	-	-	-	-	-	-
92-293	BF4	6855729	2513455	Kau	4/16/92	21.0	12.21	542	382	54.5	<0.36	<0.01	24.2	727	95.5
91-364	BF6-1	6803761	2532364	Ko/Kau	8/22/91	25	12.52	1,240	1250	392	<0.32	*0.02	2.14	1,130	20.3
91-650	BF7	6778921	2519286	Ko/Kau	10/10/91	16.9	7.54	2,580	106	783	<0.32	<0.02	0.73	3,770	17.5
92-633	BF7-2	"	"	"	7/2/92	23	12.14	3,570	76.7	1,020	<0.32	<0.01	1.3	5,630	35.5
91-602	BF8	6769591	2492774	Kau	6/11/91	22.5	11.43	3,140	142	119	<0.32	0.05	24.2	4,560	268
92-115	BI2A	6821089	2456444	Kau	12/3/91	17	11.88	119	80.1	47.9	<0.06	*0.02	27.6	21.8	164
91-349	BI3-1	6810744	2457868	Kau	8/ 5/91	23	11.49	90.7	5.81	90.7	<0.32	*0.01	13	22	25.9
	BI3	"	"	"	8/7/91	23	11.45	-	-	-	-	-	-	-	-
	BI3	"	"	"	8/7/91	23	12.12	-	-	-	-	-	-	-	-
92-641	BI3-4	"	"	"	7/14/92	23	11.64	54	6.7	111	<0.32	<0.01	14.6	11.7	49.5
92-118	BI6-2	6810785	2451903	Kau	12/4/91	18	12.3	136	42.3	69.1	<0.06	*0.01	14.6	14.6	60.7
91-389	BIR11	6803737	2452815	Kau/Kef	9/27/91	21.5	11.55	306	27.8	6.3	<0.32	0.38	52.8	46.6	190
92-114	BIR21	6803468	2453022	Kau/Kef	5/12/91	20	11.99	133	305	28.9	<0.06	0.13	8.26	17.7	117
91-303	B1597-1	6821000	2447707	Kef	7/23/91	20.5	11.83	2,820	347	16.6	<0.32	*0.02	26.5	3,840	516
92-645	B1597-2	"	"	"	7/15/92	20.5	12.10	7,980	875	103	<0.32	<0.01	7.61	11,500	1,110

Table 21 (cont.)

Lab no.	Well name	HCO_3‡	F	P	NO_3	B	Sr	Ba	Pb	Zn	Cu	Mn	Hg (µg/L)
91-380	BE1A	158	6.9	<0.2	<0.1	5.26	0.36	0.02	<0.2	<0.02	<0.02	<0.01	<0.5
92-648	BE1A-2	144	6.67	<0.20	<0.8	5.61	0.35	*0.02	<0.20	*0.02	<0.02	<0.01	<0.50
	BE1A	-	-	-	-	-	-	-	-	-	-	-	-
91-366	BE2-1	165	6.52	<0.2	*0.1	4.23	0.2	*0.02	<0.2	<0.02	*0.02	<0.01	<0.5
92-647	BE2-2	40.1	5.71	<0.20	<0.8	4.31	1.04	0.11	<0.20	*0.03	<0.02	<0.01	<0.5
	BE4	-	-	-	-	-	-	-	-	-	-	-	-
	BE4	-	-	-	-	-	-	-	-	-	-	-	-
91-301	BE5	2,320	3.22	<0.2	0	2.53	3.07	0.21	<0.2	0.14	<0.02	0.01	<0.5
	BE7A	-	-	-	-	-	-	-	-	-	-	-	-
	BE9	-	-	-	-	-	-	-	-	-	-	-	-
92-293	BF4	69.6	3.5	<0.2	<0.1	1.10	3.35	0.10	<0.2	<0.02	<0.02	<0.01	<0.5
91-364	BF6-1	73	0.59	<0.2	<0.1	0.09	8.2	0.94	<0.2	*0.05	<0.02	<0.01	<0.5
91-650	BF7	272.7	13.8	<0.2	1.33	<0.01	17.7	1.47	<0.2	0.2	<0.02	<0.01	<0.5
92-633	BF7-2	209	0.34	<0.20	<0.80	0.31	7.11	1.49	<0.20	0.49	*0.03	<0.01	<0.5
91-302	BF8	35.6	1.67	<0.2	63	2.67	8.2	0.23	<0.2	<.02	<0.02	<0.01	<0.5
92-115	BI2A	44.5	1.54	<0.2	*0.13	1.3	1.6	*0.02	<0.2	<0.02	<0.02	<0.01	<0.5
91-349	BI3-1	31.1	2.81	<0.2	24.3	0.3	0.82	*0.04	<0.2	*0.02	<0.02	<0.01	<0.5
	BI3	-	-	-	-	-	-	-	-	-	-	-	-
	BI3	-	-	-	-	-	-	-	-	-	-	-	-
92-641	BI3-4	38.9	1.03	<0.20	<0.8	0.2	0.69	0.17	<0.20	0.08	<0.02	<0.01	<0.5
92-118	BI6-2	47.4	1.46	<0.2	*0.18	0.37	0.64	0.1	<0.2	*0.03	<0.02	<0.01	<0.5
91-389	BIR11	74.3	3.28	<0.2	0.29	1.67	0.33	*0.03	<0.2	<0.02	*0.02	<0.01	<0.5
92-114	BIR21	78.9	1.23	<0.2	2.08	0.11	2.57	0.3	<0.2	0.08	*0.03	<0.01	<0.5
91-303	B1597-1	81	1.54	<0.2	9	0.74	0.78	0.05	<0.2	*0.04	<0.02	0.01	<0.5
92-645	B1597-2	87.6	1.07	<0.20	3.14	0.73	2.99	0.3	<0.20	<0.02	0.62	<0.01	<0.5

Table 21 (cont.)

Lab no.	Well name	Ag	As	V	Co	Cr	Ni	Cd	Sb	Se	Be	Br	I
91-380	BE1A	<0.025	<0.06	<0.02	<0.02	<0.02	<0.05	<0.02	<0.16	<0.16	<0.02	0.6	0.33
92-648	BE1A-2	<0.025	<0.06	<0.02	<0.02	<0.02	<0.05	<0.02	<0.16	<0.20	<0.02	0.57	0.67
	BE1A	-	-	-	-	-	-	-	-	-	-	-	-
91-366	BE2-1	*0.03	<0.06	<0.02	<0.02	<0.02	<0.05	<0.02	<0.16	<0.20	<0.02	1.29	0.53
92-647	BE2-2	<0.025	<0.06	<0.02	<0.02	<0.02	<0.05	<0.02	<0.16	<0.20	<0.02	1.2	0.81
	BE4	-	-	-	-	-	-	-	-	-	-	-	-
	BE4	-	-	-	-	-	-	-	-	-	-	-	-
91-301	BE5	*0.03	<0.06	<0.02	<0.02	<0.02	<0.05	<0.02	<0.16	<0.20	<0.02	7.88	2.92
	BE7A	-	-	-	-	-	-	-	-	-	-	-	-
	BE9	-	-	-	-	-	-	-	-	-	-	-	-
92-293	BF4	<0.025	<0.06	<0.02	<0.02	<0.02	<0.05	<0.02	<0.16	<0.20	<0.02	0.91	1.02
91-364	BF6-1	*0.04	<0.06	<0.02	<0.02	<0.02	<0.05	<0.02	<0.16	<0.20	<0.02	3.68	1.42
91-650	BF7	0.07	<0.06	<0.02	<0.02	0.09	<0.05	<0.02	<0.16	<0.20	<0.02	11.6	4.34
92-633	BF7-2	<0.025	<0.06	<0.02	<0.02	<0.02	<0.05	<0.02	<0.16	<0.20	<0.02	23.3	6.03
91-302	BF8	*0.03	<0.06	<0.02	<0.02	*0.02	<0.05	<0.02	<0.16	<0.20	<0.02	16.5	4.76
92-115	BI2A	<0.025	<0.06	*0.02	<0.02	*0.02	<0.05	<0.02	<0.16	<0.20	<0.02	<0.1	0.21
91-349	BI3-1	<0.025	<0.06	*0.02	<0.02	<0.02	<0.05	<0.02	<0.16	<0.20	<0.02	*0.14	*0.15
	BI3	-	-	-	-	-	-	-	-	-	-	-	-
	BI3	-	-	-	-	-	-	-	-	-	-	-	-
92-641	BI3-4	<0.025	<0.06	<0.02	<0.02	<0.02	<0.05	<0.02	<0.16	<0.20	<0.02	<0.25	0.26
92-118	BI6-2	<0.025	<0.06	*0.02	<0.02	<0.02	<0.05	<0.02	<0.16	<0.20	<0.02	*0.1	0.17
91-389	BIR11	<0.025	<0.06	0.07	<0.02	0.04	<0.05	<0.02	<0.16	<0.20	<0.02	1.18	1.01
92-114	BIR21	<0.025	<0.06	<0.02	<0.02	0.07	<0.05	<0.02	<0.16	<0.20	<0.02	*0.19	0.4
91-303	B1597-1	<0.025	<0.06	<0.02	<0.02	0.27	<0.05	<0.02	<0.16	<0.20	<0.02	1.11	0.54
92-645	B1597-2	<0.025	<0.06	<0.02	<0.02	<0.02	<0.05	<0.02	<0.16	<0.20	<0.02	1.77	1.22

* Near detection limit.
‡ HCO_3^- estimate for samples inaccurate owing to interference by OH^-.
\- Not measured.

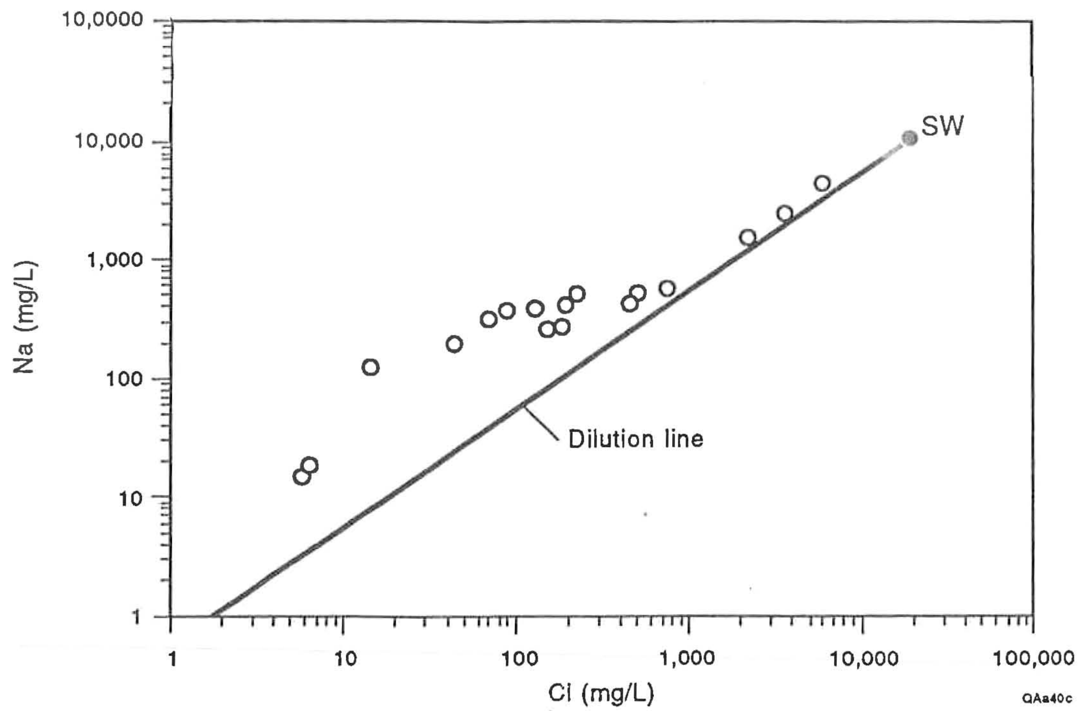

Figure 61. Variation of Na^+ with Cl^- in ground waters from SSC monitoring wells and in seawater. Mixing of seawater and rainwater follows the dilution line.

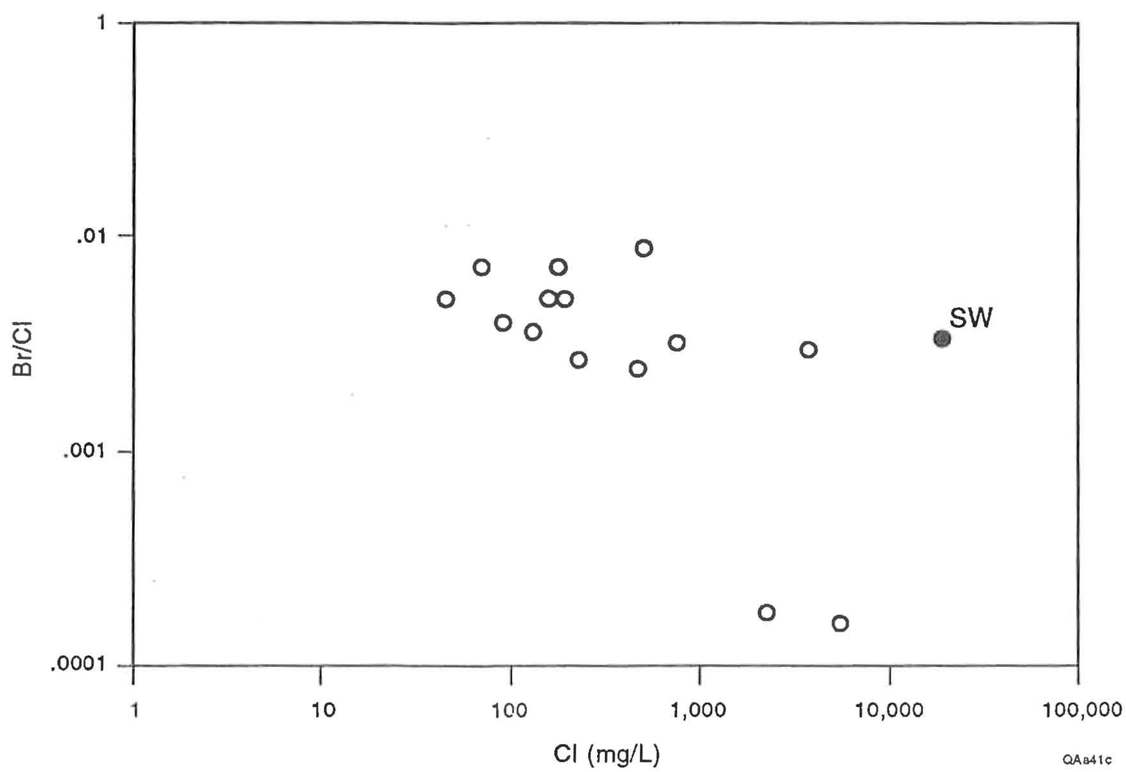

Figure 62. Variation of Br^-/Cl^- ratio with Cl^- in ground waters from SSC monitoring wells compared to seawater.

Table 22. Summary of dissolved Cl^- and SO_4^{2-} concentrations in rock and water samples.

a. Water samples from SSC monitoring wells

		Cl^- (mg/L)	SO_4^{2-} (mg/L)
Average	Ozan Formation	1997.5	871.6
	Austin Chalk	1795.9	255.5
	Eagle Ford Formation	210.5	289.8
Standard deviation	Ozan Formation	1799.6	1214.0
	Austin Chalk	2823.0	370.6
	Eagle Ford Formation	109.0	300.6

b. Rock samples from Austin Chalk*

Borehole number	Cl^- (mg/kg)	SO_4^{2-} (mg/kg)	Moisture content (%)	Cl^- (mg/L)†	SO_4^{2-} (mg/L)†
PB1925	100.	156.	11.7	854.7	1333.3
PB1965	50.	225.	9.6	520.8	2343.8
PB2226	350.	161.	12.4	2822.6	1298.4
PB2266	180.	344.	10.1	1782.2	3405.9
PBIR15	50.	580.	12.2	409.8	4754.1
PBIR16	95.	668.	15.0	633.3	4453.3
PBIR47	30.	205.	11.6	258.6	1767.2
PBN35	30.	148.	9.1	329.7	1626.4
PBN57	880.	240.	10.1	8712.9	2376.2
PBIR85	875.	637.	8.9	9831.5	7157.3
PBIR88	900.	164.	12.2	7377.0	1344.3
PBN40-2	170.	961.	10.6	1603.8	9066.0
PBN40-E	225.	372.	8.5	2647.1	4376.5
PBN40-U	170.	426.	8.5	2000.0	5011.8
PBN50-3	150.	479.	13.6	1102.9	3522.1
PBN50-U	210.	43.	12.3	1707.3	349.6
PBN55-E	600.	546.	10.3	5825.2	5301.0
PBN50-U	70.	14.	10.0	700.0	140.0
Average	285.3	353.8	10.9	2728.9	3312.6
Standard deviation	307.3	251.5	1.8	3048.4	2389.1

* Data provided by Charles Daugherty, March 1993
† mg/L = (mg/kg) /moisture content

Tritium (^3H) has a half-life of 12.43 yr (Mann and others, 1982). One tritium unit (TU) is equivalent to a tritium/hydrogen ratio of 10^{-18} and a radioactivity of 3.2 picocuries per liter (pCi/L). Tritium concentration in precipitation was elevated by atmospheric testing of nuclear weapons starting in 1952 and continuing through the early 1960's. Elevated tritium content since has been used as a ground-water tracer to differentiate water recharged before 1952 from younger waters. Assuming that pre-1952 precipitation had an original background concentration of approximately 5 TU, its present-day activity would be less than 0.54 TU (1.7 pCi/L). Any tritium in a ground-water sample above 0.54 TU (1.7 pCi/L), therefore, implies that the water contains some component of more recent or post-1952 precipitation (Fontes, 1980). The U.S. Environmental Protection Agency maximum concentration limit for drinking water is 6,250 TU (20,000 pCi/L) (De Zuane, 1990). The level of dissolved tritium generally found in water, therefore, is very far below the standard for drinking water.

Carbon-14 content measured at BI3 (table 23) was very high, 97 ± 0.7 percent of Modern atmospheric carbon-14 activity (pmc). Carbon-14 content measured in ground water from BF9 was low, 2.1 ± 0.2 pmc, but above detection limit. BI3 and BF9 were the two SSCL monitoring wells that had high enough yield to allow sufficient pumping to obtain a representative sample of ground water from the formation for carbon-14 analysis.

The tritium concentrations in water samples from surficial alluvium were low but above background, ranging from 3.58 to 11.1 TU (11.5 to 35.5 pCi/L) (Wickham and Dutton, 1991). Tritium analyses of water samples from SSCL monitoring wells show a range of tritium concentrations from 0 to approximately 7 TU (0 to 22.4 pCi/L) at well BI3 (table 23). Tritium was 2.93, 2.03, and 0.55 TU (9.4, 6.5, and 1.8 pCi/L) at wells BI4, B1597B, and B1697B, respectively. These samples are from shallow depths and/or fractured zones. The range of tritium content in ground water from these wells was slightly lower than in the alluvial aquifer. The ^{14}C and ^3H data suggest that ground water in surficial alluvium and locally in fractured or shallow bedrock, such as at BI3, was recharged within the last 40 to 50 years. The above-background tritium values suggest that fracturing might influence ground-water flow at wells BI4, B1597B, and B1697B. Ground water in bedrock with less well interconnected fractures, such as at BF9, is older, possibly recharged within the past 15,000 to 20,000 yr. Ten samples were essentially

Table 23. Ambient (preoperational) content of various radioactive and stable isotopes in ground water from SSC monitoring wells.

Isotope	BE10	BF1	BF2	BI1	BI5	BIR31	D.L.
^{3}H	0.01	0.37		0.43	0.23	-0.02	0.09
^{7}Be	bdl	bdl	bdl	bdl	bdl	bdl	18
^{22}Na	bdl	bdl	bdl	bdl	bdl	bdl	10
^{40}K	14±2	8.9±0.6	18±2	5.9±0.4	7.1±0.3	11±2	—
^{45}Ca	bdl	bdl	bdl	bdl	bdl	bdl	5
^{54}Mn	bdl	bdl	bdl	bdl	bdl	bdl	10
^{60}Co	bdl	bdl	bdl	bdl	bdl	bdl	10
Ra (total)	bdl	bdl	bdl	bdl	2±1	bdl	1
^{228}Th	bdl	bdl	bdl	bdl	bdl	bdl	0.6
^{230}Th	bdl	bdl	bdl	bdl	bdl	bdl	0.6
^{232}Th	bdl	0.6±0.4	bdl	bdl	bdl	bdl	0.6
^{137}Cs	bdl	bdl	bdl	bdl	bdl	bdl	5

	1597A	1597B	1697	1697B	BIR81	BI4	BE190	BI3	BF9
^{3}H	2.03	0.	0.07	0.55	0.22	2.93	0.12	6.8, 7.0	0.08
^{14}C	—	—	—	—	—	—	—	97±0.7	2.3
^{13}C	—	—	—	—	—	—	—	—	-2.6

D.L. = Detection limit
bdl = Below detection limit
— = Not measured

less than 0.4 TU (1.3pCi/L) and five were less than 0.1 TU (0.3 pCi/L). These 10 results probably reflect the absence of "bomb"-related tritium originating from meteoric recharge during the past 40 to 50 years.

All ground water is expected to show minute levels of radioactive constituents related to the rock and soil (De Zuane, 1990). Table 23 gives results of analyses of ^{7}Be, ^{22}Na, ^{45}Ca, ^{54}Mn, ^{60}Co, ^{40}K, ^{137}Cs, total radium, and isotopic thorium in water samples from 6 of the SSCL monitoring wells and ^{3}H in 14 of the SSCL monitoring wells. The six samples were selected for analysis after excluding samples from wells with cement problems or where the screen interval is far below the collider tunnel elevation. These radioactive isotopes might be generated in ground water by SSC operation. There is interest, therefore, in establishing ambient concentrations before SSC operation. A natural constituent of silicate minerals such as many clays and feldspar, ^{40}K is found in all samples in concentrations from 6 to 18 pCi/L. Radium, one of the decay products of uranium, which is present in trace quantities in most rocks and ground water, was measured at 2 ± 1 pCi/L in BI5, just above the detection limit of 1 pCi/L. Another natural decay product of uranium, ^{232}Th, was measured at 0.6 ± 0.4 pCi/L in the sample from BF1, also at the detection limit of 0.6 pCi/L. The other radionuclides of beryllium, sodium, calcium, manganese, cobalt, and cesium are generally not present in detectable quantities in these natural waters.

Bottom-Hole Temperature

Table 24 lists bottom-hole temperature measured in SSCL monitoring wells in 1991 and 1992 and compares plumbed and design depths of the wells. The regression of bottom-hole temperature versus depth (fig. 63) on the basis of measurements from problem-free wells is

$$\text{Temperature } (^\circ\text{C}) = 18.6 + 0.0303\ (^\circ\text{C/m}) \bullet \text{Depth (m)}. \qquad (12)$$

The intercept predicts a ground-surface temperature of 65.5°F (18.6°C), close to the 66°F (18.9°C) 1931–1965 average of air temperature in Waxahachie. Data used in the regression excluded measurements in

Table 24. Bottom-hole temperature measured in SSC monitoring wells in 1991 and 1992, including comparison of design and plumbed depths.

Well	Elev. top casing (ft)	Elev. bottom casing (ft)	Design total depth (ft)	Plumbed depth (ft)	Design – plumbed depth (ft)	Ground-surface elev. (ft)	Well-head height (ft)	Depth below ground surface (ft)	Aug. 1991 Bottom temp. (°C)	Aug. 1992 Bottom temp. (°C)
BE 1-90	766.0	533.1	232.9			763.1	2.9	230.0	–	
BE1A	681.2	540.0	141.2	145.0	–3.8	679.0	2.2	139.0	19.5	19.8
BE2	675.7	523.1	152.6	155.0	–2.4	674.1	1.6	151.0	20.0	20.1
BE3	680.0	503.5	176.5	–	–3.5	679.5	0.5	176.0	19.8	–
BE4	551.6	287.8	263.8	260.0	3.8	549.8	1.8	248.6	20.3	20.5
BE5	463.9	156.5	307.4	320.0	–12.6	462.5	1.4	306.0	21.7	21.7
BE6	487.2	100.2	387.0	–	–	484.2	3.0	384.0	–	–
BE7A	457.3	134.8	322.5	320.0	2.5	454.8	2.5	320.0	23.0	22.9
BE8	430.7	236.5	194.2	–	–	428.0	2.7	191.5	–	–
BE9	513.6	378.0	135.6	137.0	–1.4	512.0	1.6	134.0	20.0	20.0
BE10	562.7	461.8	100.9	100.0	0.9	560.8	1.9	99.0	19.8	19.9
BF1	730.6	533.7	196.9	200.0	–3.1	727.7	2.9	194.0	–	20.7
BF2	684.5	500.1	184.4	162.0	22.4	683.1	1.4	183.0	19.9	20.0
BF3	550.1	365.4	184.7	–	–	548.4	1.7	183.0	–	–
BF4	504.3	217.7	286.6	280.0	6.6	501.7	2.6	284.0	–	20.3
BF6	457.9	101.3	356.6	350.0	6.6	456.3	1.6	355.0	23.4	23.2
BF7	484.5	166.1	318.4	280.0	38.4	483.3	1.2	317.2	22.7	22.7
BF8	514.7	307.7	207.0	207.0	0.0	512.2	2.5	204.5	20.3	21.2
BF9	545.0	395.0	150.0	150.0	0.0	543.3	1.7	148.3	20.2	20.4
BI1	744.0	551.4	192.6	195.0	–2.4	741.4	2.6	190.0	20.3	20.2
BI2A	642.1	570.2	71.9	65.4	6.5	639.9	2.2	69.7	19.4	19.2
BI3	698.9	600.7	98.2	100.0	–1.8	696.7	2.2	96.0	19.2	19.2
BI4	713.8	550.0	163.8	164.7	–0.9	710.9	2.9	160.9	20.3	20.2
BI5	662.0	550.4	111.6	112.0	–0.4	658.4	3.6	108.0	19.5	19.2
BI6	735.7	552.1	183.6	170.0	13.6	734.1	1.6	182.0	20.2	20.1

Table 24 (cont).

Well	Elev. top casing (ft)	Elev. bottom casing (ft)	Design total depth (ft)	Plumbed depth (ft)	Design – plumbed depth (ft)	Ground–surface elev. (ft)	Well–head height (ft)	Depth below ground surface (ft)	Aug. 1991 Bottom temp. (°C)	Aug. 1992 Bottom temp. (°C)
BIR11	672.5	405.2	267.3	265.0	2.3	670.2	2.3	265.0	21.4	21.3
BIR21	667.1	442.8	224.3	195.0	29.3	665.3	1.8	222.5	20.4	20.5
BIR31	620.2	322.5	297.7	280.0	17.7	617.5	2.7	295.0	21.6	22.3
BIR41	621.3	392.7	228.6	220.0	8.6	618.7	2.6	226.0	21.1	21.3
BIR54	442.6	19.3	423.3	320.0	103.3	440.3	2.3	421.0	–	21.9
BIR81	454.0	47.2	406.8	385.0	21.8	452.2	1.8	405.0	22.3	22.3
B1597	759.4	515.0	244.4	106.0	138.4	757.6	1.8	104.4	19.7	19.4
B1597A	760.2	590.2	170.0	170.0	0.0	758.2	2.0	168.0	20.1	20.0
B1597B	760.0	668.0	92.0	90.0	2.0	758.0	2.0	90.0	19.5	19.3
B1697	676.7	528.7	148.0	138.0	10.0	674.7	2.0	146.0	20.0	19.8
B1697A	676.9	570.2	106.7	100.0	6.7	675.2	1.7	105.0	–	19.2
B1697B	676.7	616.0	60.7	58.0	2.7	675.0	1.7	59.0	19.1	19.3

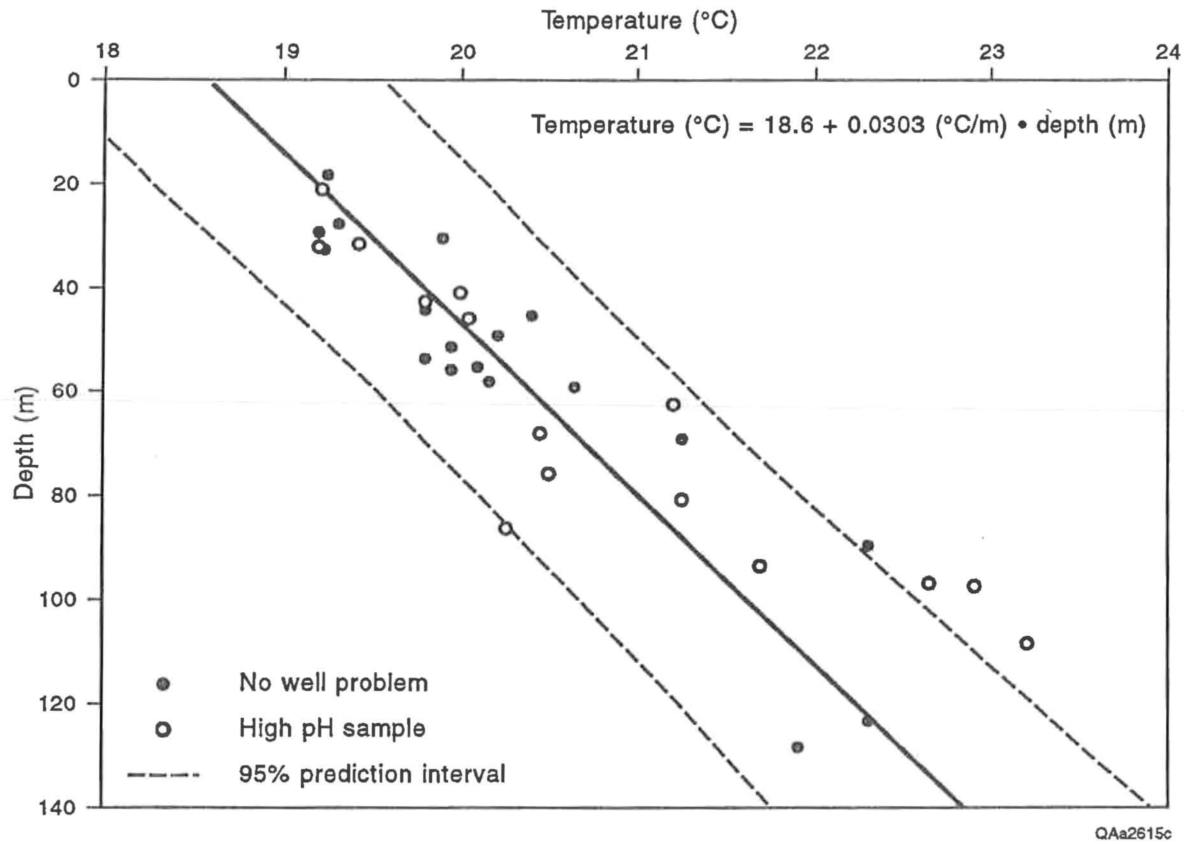

Figure 63. Regression of bottom-hole temperature versus depth at SSC monitoring wells. There is a 95 percent probability that the actual temperature at a given depth lies within the range of the prediction interval calculated for that depth.

wells with known well construction problems or in wells yielding water samples with a high pH. Pooling all data (table 25) would slightly decrease the intercept and increase the slope. The calculated slope shown in figure 63 represents an estimate of the geothermal gradient: 1.7°F/100 ft (30.3°C/km). This agrees with regional trends in geothermal gradient of 1.5°F/100 ft to 1.8°F/100 ft (27.3°C/km to 32.7°C/km) (DeFord and others, 1976). It is somewhat cooler, however, than the gradient of 2.1°F/ 100 ft (38.3°C/km) calculated by Dutton (1987) from bottom-hole temperatures at seven much deeper wells in the East Texas Basin.

Spring Flow and Water Temperature

Table 25 summarizes measurements of water temperature and stream flow in gallons per minute (gpm) measured at several springs in the vicinity of the SSC. Water temperatures ranged from 62.6°F to 69.8°F (17°C to 21°C); three samples measured 65.3°F to 66.2°F (18.5°C to 19°C). The coolest was Brach Springs (S4) and the warmest was Hawkins Spring in Midlothian (S1). Reference to the geothermal-gradient data (fig. 63) suggests that ground water with a temperature of less than or equal to 66.2°F (19°C) circulates only to shallow depths of less than approximately 65 to 100 ft (20 to 30 m). The geothermal-gradient data suggest that the Hawkins Spring water (69.8°F [21°C]) might have circulated to a depth of approximately 250 ft (77 m). There would be some cooling as the ground water rises to the spring at land surface and mixes with water circulating at shallow depths. This places the depth of circulation into the Eagle Ford Shale. The chemical composition of the Hawkins Spring water, however, closely resembles the chemical composition of shallow Austin Chalk water and shows no evidence of contact with such a distinctly different mineralogy and lithology as the Eagle Ford Formation. Depth of circulation of ground water feeding Hawkins Spring remains an unresolved question.

Table 25. Temperature and flow rate in springs in the vicinity of the SSC.

Map no.	Spring	Date	Flow rate (gpm)	Temperature (°C)
S1	Hawkins Spring	1/11/92	nm	21.0
S1	Hawkins Spring	2/10/92	nm	21.0
S1	Hawkins Spring	3/25/92	212	20.5
S1	Hawkins Spring	4/16/92	nm	20.8
S1	Hawkins Spring	5/12/92	90	21.0
S1	Hawkins Spring	6/18/92	106	20.05
S1	Hawkins Spring	7/28/92	465	20.2
S1	Hawkins Spring	11/13/92	150	20.6
S2	Hawkins Street Spring	1/11/92	nm	18.6
S3	Armstrong Creek	1/11/92	nm	19.0
S3	Armstrong Creek	2/10/92	nm	19.5
S3	Armstrong Creek	3/25/92	135	19.0
S3	Armstrong Creek	5/12/92	low	19.3
S4	Brach Spring	1/10/92	nm	17.0
S4	Brach Spring	3/25/92	725 to 885	17.3
S4	Brach Spring	3/25/92	725	17.3
S4	Brach Spring	6/18/92	463	21.19
S4	Brach Spring	7/28/92	432	24.8
S4	Brach Spring	11/13/92	low	21.85
S5	Mammouth Spring	1/11/92	nm	18.5
S5	Mammouth Spring	2/10/92	nm	17.5
S5	Mammouth Spring	3/25/92	138	17.5
S5	Mammouth Spring	5/12/92	nm	19.3
S5	Mammouth Spring	6/18/92	nm	18.1
S5	Mammouth Spring	7/28/92	nm	18.4

nm = not measured

DISCUSSION OF GROUND-WATER HYDROLOGY

This section presents a conceptual model of ground-water flow in weathered and unweathered chalk and marl. The conceptual model represents a synthesis of the results of hydrological studies and analyses of stratigraphy and fracture characteristics. Further tests and models are discussed as tools for interpreting rates and modes of the hydrological processes that control the occurrence, movement, and chemical composition of ground water at the SSC site.

Conceptual Model of Hydrology of Weathered and Unweathered Bedrock

It is generally understood that the position of the water table in an unconfined aquifer is determined by the balance between recharge, discharge, and flow rate. The shape of the water table (figs. 44 and 45) and water-level hydrographs (fig. 48, app. H) suggest that:

- Precipitation over the upland drainage divides percolates into the ground and moves downward through the soil zone and weathered bedrock and alluvium to recharge shallow ground water at the water table.
- The water table fluctuates seasonally, daily, and episodically in response to recharge from precipitation and to discharge by evapotranspiration, flow to springs and seeps, and pumping of wells. The magnitude of water-level changes most likely decreases with depth and is less in unweathered bedrock than in the weathered zone.
- Typical of flow in limestone terrain (LeGrand and Stringfield, 1966), ground water percolates along vertical fractures and horizontal bedding-plane joints and through the more permeable sedimentary layers. Vertical movement is retarded by unfractured, low-permeability beds. Ground water in the weathered section follows an arcuate flow path generally eastward but bending toward discharge points in the valley bottom and stream banks. Wickham and Dutton (1991, figs. 22 and 23) depicted such ground-water paths in the surficial aquifer in alluvium.
- At the margins of incised stream valleys, ground water issues in springs and seeps from bedding plane joints as well as discrete vertical fractures. Perennial streams can be fed even during

mild droughts until the water table falls below the elevation of the springs and seeps, leading to testimony that such springs have "not gone dry in living memory." Brach Spring, which feeds part of Greathouse Branch; Mammouth Spring, which feeds Armstrong Creek; and Hawkins Spring, which feeds Waxahachie Creek in Midlothian, Texas, are notable examples of fracture-controlled discharge in weathered chalk.

As discussed earlier, the weathered zone averages 12 ft (3.6 m) thick in the Austin Chalk. Unloading and weathering can result in an increase in hydraulic conductivity by 2 to 4 orders of magnitude (Davis, 1969). The gain in porosity and hydraulic conductivity in limestone is generally greater than in other less ductile rocks. Because the amount of weathering decreases with depth, apparent fracture intensity also decreases (Zdankus, 1974; Barker and Herbert, 1989; Barquest, 1989). When fractures control hydrologic properties, there can be a concomitant decrease in hydraulic conductivity with depth (LeGrand, 1954; Davis and De Wiest, 1966; LeGrand and Stringfield, 1966; Rasmuson and Neretnieks, 1986). Hydraulic conductivity of the Austin Chalk decreases with depth at the SSC site in both the weathered zone (table 13) and unweathered bedrock (fig. 53). At a given depth hydraulic conductivity varies over several orders of magnitude.

Because of the decrease in hydraulic conductivity with increasing depth below ground surface, only a small amount of the ground water moving through the surficial weathered bedrock moves downward into unweathered, low-permeability bedrock. The important exception to this occurs in zones of interconnected fractures. Vertical circulation of ground water in such zones locally deepens the weathered zone, such as was found at the M55 boring at the SSC's MEB. Deep vertical circulation is more likely in chalk than in marl because fractures in chalk remain open to greater depth. Because of the association of greater hydraulic conductivity with fracture aperture and fracture intensity (fig. 59), and the variation of fracture intensity and hydraulic conductivity with stratigraphic units of the Austin Chalk (figs. 35 and 57), fracture-controlled inflow into the SSC excavations might be predicted from mapping their location in the upper and lowermost parts of the Austin Chalk and in proximity to faults. The collider tunnel runs through the lowermost Austin Chalk from the vicinity of the MEB northward almost to N25 (fig. 64). In the vicinity of Waxahacie Creek between N25 and N30, the

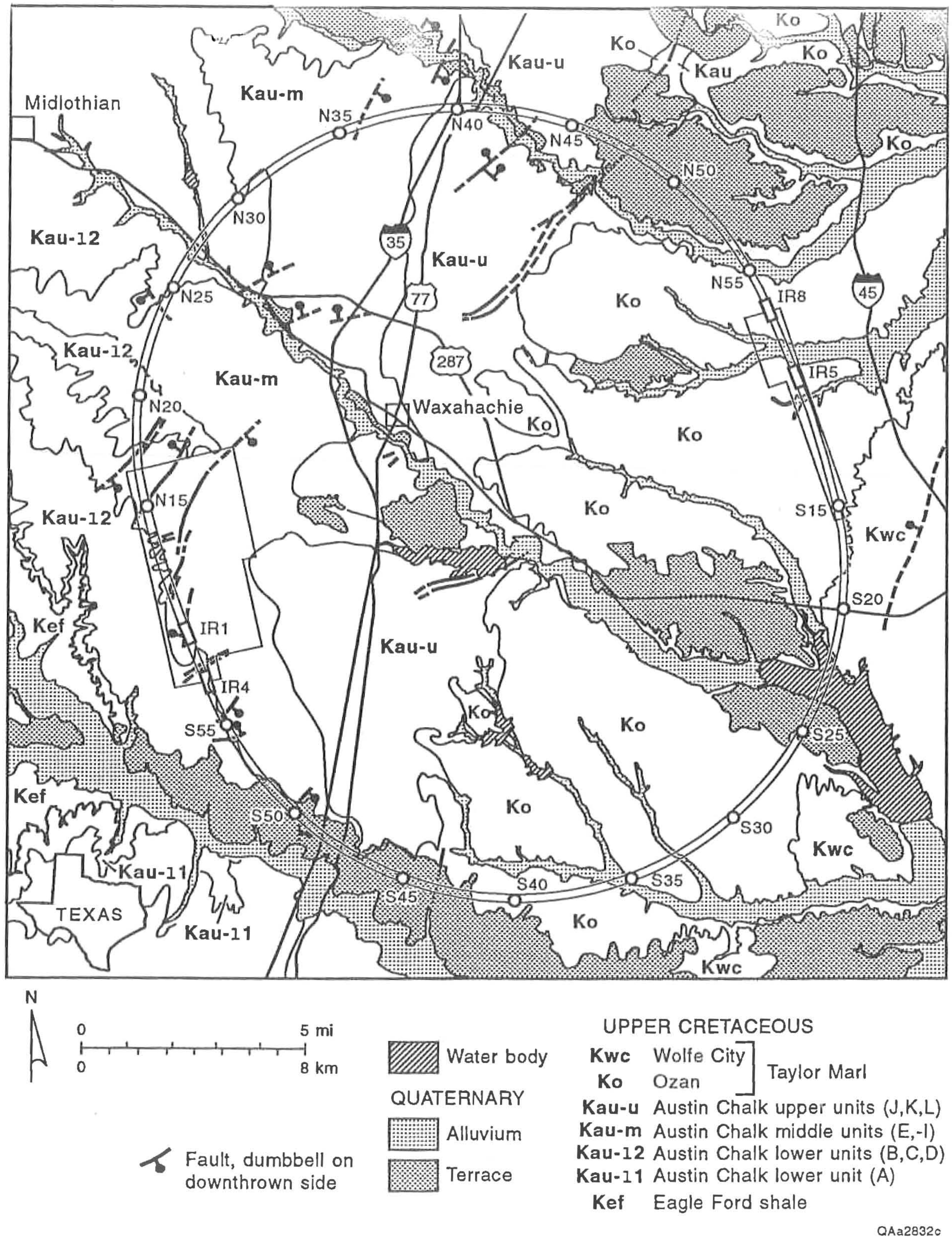

Figure 64. Generalized geologic map of the SSC project area showing outcrop of informal stratigraphic subdivisions of the Austin Chalk and locations of service areas and interaction halls.

tunnel is beneath the outcrop of the lowermost Austin Chalk, where more abundant fractures might connect recharge sources of water and the collider tunnel. The tunnel boring machine encountered significant ground-water inflow from a fracture zone in this tunnel segment (D. Goss, personal communication, 1993). The collider tunnel crosses through the upper Austin in the vicinity of N55 on the northeast side of the ring and in the vicinity of S40 to the southeast and lies beneath the outcrop of the upper Austin Chalk in the vicinity of interstate highway 35 north and south of Waxahachie (fig. 64).

Water that moves into the unweathered chalk through interconnected fractures, whether in concentrated zones or not, follows flow paths controlled by local hydraulic-head gradients and the anisotropic hydraulic conductivity. Although data are insufficient to draw a plan-view map of the potentiometric surface in weathered bedrock, it can be assumed to resemble the water table in weathered bedrock and alluvium, because both are controlled by rates of recharge across upland drainage divides and rates of discharge in low-lying areas (figs. 49a and 51). Some ground water in the unweathered bedrock moves toward discharge points in stream valleys, where it might be discharged either directly to surface streams or to alluvium and weathered bedrock that floor the valley. The remaining ground water moves generally southeastward underneath the Ozan Formation following the regional gradient. Hydraulic head along the eastern side of the SSC ring, as measured in SSCL monitoring wells BE6 and BIR54, completed in the upper Austin Chalk, is near or above land surface. This indicates the local vertical gradient in hydraulic head is directed upward (fig. 51), that is, there is a potential for ground water to flow from the Austin Chalk into the overlying Ozan Formation. The hydraulic head and dynamic pressure increment are consistent with the potential energy of water recharged to the west in the Austin Chalk outcrop. Regional flow paths through the unweathered chalk beneath the marl are assumed to be mainly through interconnected fractures rather than the unfractured matrix, although this has not been directly observed. Such a fracture pattern, however, is oriented toward the northeast. This, in turn, should impart a northeasterly anisotropy to regional values of hydraulic conductivity in the Austin Chalk.

The amount of ground-water recharge into the low-permeability, unfractured part of the Austin Chalk and Ozan Formation in the SSC area has not been measured directly but can be inferred within reasonable limits by combining physical-hydrogeological and geochemical data with results of modeling studies. This is discussed in the following sections.

To be consistent with this conceptual model of ground-water flow, chemical composition of ground water in weathered and unweathered chalk and marl is expected to be affected by

- rate and chemical composition of precipitation, which is the source of recharge,
- reaction of recharge (meteoric) water with minerals that make up the formations, and
- displacement and mixing with sodium, chloride, and other dissolved salts inherited from seawater (connate water, White, 1965), which was trapped in pores at or soon after the time of deposition of the chalk and marl.

As will be shown, additional reactions such as pyrite oxidation and ion exchange also affect water composition. The possibility of mixing with sodium, chloride, and other dissolved connate salts was suggested by the first water sample collected from the unweathered bedrock, sample BF9-1 (table 20). This water was dominated by Na^+ and Cl^- ions, unlike the calcium-bicarbonate hydrochemical facies typical of alluvium and weathered chalk and marl (fig. 60). Na^+, Cl^-, and Br^- ions are present in the samples from unweathered bedrock in nearly the same relative proportions as in seawater (figs. 61 and 62). The concentration of chloride in water samples from both fractured and unfractured rock sampled at SSCL monitoring wells has the same mean and variance as the concentration of chloride in rock samples from the Austin Chalk (table 22). The difference in their absolute concentrations might reflect the amount of flushing of connate water by recharged meteoric water (precipitation). The amount of flushing of connate salts in unweathered bedrock presumably is related to the interconnectedness and regional hydraulic conductivity of fractures between the sample point and the recharge zone. The ratio between ground water and seawater in the ionic concentrations of Na^+, Cl^-, and Br^-, therefore, might be an estimate of cumulative flushing of pore water by circulating meteoric water over the time that the stratigraphic section has been in its present hydrological setting.

Age of ground water obviously is related to distance from the recharge area and rate of flow. Fracture zones are capable of moving small amounts of water very quickly. The volume of flow depends on fracture aperture and fracture abundance. High tritium (^3H) content in ground water at depths of approximately 90 ft (27 m) or more in chalk is evidence of rapid vertical flow, which most likely occurs through fractures. In comparing samples from equivalent depths and distances from the outcrop, those with above-zero ^3H or ^{14}C activities must reflect more rapid flow along more permeable paths such as fracture zones. Inferences of rates of ground-water flow cannot be made with confidence on the basis of samples without detectable tritium, but the absence of measurable tritium activity must represent sufficient time of travel, at least 40 to 50 years, for "bomb" tritium to decay in activity to below detection limits. This might reflect

- rapid velocity of flow in fractured zones over a long distance from the recharge area,
- slow velocity of flow through rock with low hydraulic conductivity owing to poorly interconnected fractures or fracture with small apertures, or
- slow velocity of flow through unfractured, low-permeability bedrock.

Simulation of Ground-Water Flow

Approach

Numerical modeling was used as a tool to interpret and better understand the parameters that control regional ground-water flow paths and travel times at the SSC site and to evaluate the conceptual model. Weathered and fractured zones with enhanced permeability were included to assess the effect of these features on flow paths and travel times. Data from pumping, slug, packer, and core tests were used to define hydraulic properties initially assigned in the models (tables 12 to 14). The models were calibrated with water-level data from monitoring wells and wire-line piezometer data near a test shaft excavated by the SSC project. This section discusses results of two cross-sectional models (fig. 9): a NE-SW profile across the West Campus (A-A′), and a longer NW-SE profile across Ellis County (B-B′).

West Campus Model

The goal of modeling ground-water flow in the West Campus model was to estimate

- amount of flow between weathered and unweathered bedrock,
- movement of water between Austin Chalk and Eagle Ford Formation,
- flow paths, including the effect of fracture zones, and
- residence times and ages of ground water.

Profile A–A′ (fig. 9) was positioned to be roughly perpendicular to the regional slope of land surface and to extend from low-lying area of Chambers Creek to the upland area of the West Campus. It thus simulates local components of ground-water flow related to topographic relief. The position of the profile was chosen to include three monitoring wells and the SSC exploratory test shaft for calibration data.

Several hydrologic units were included in profile A–A′ (fig. 65):

- surficial aquifers, including weathered Austin Chalk and Quaternary alluvium,
- a fault zone in the vicinity of SSCL monitoring well BI3,
- unweathered and unfractured rock of the middle Austin Chalk (units E to J), upper part of the lower Austin Chalk (units B, C, and D), and lowermost Austin Chalk, and
- part of the Eagle Ford Formation.

The upper part of the Austin Chalk (units K through L) is absent along profile A–A′ (fig. 64).

Assignment of Hydrologic Properties

The general head boundary package of MODFLOW (McDonald and Harbaugh, 1988) was used to prescribe the upper boundary as a constant head. The head value for the general head boundary was placed at the mean water level of the shallow, surficial aquifers which is approximately 8 ft (2.44 m) below ground surface. The general head boundary allows inflow and outflow at the upper boundary. This simulates recharge and discharge.

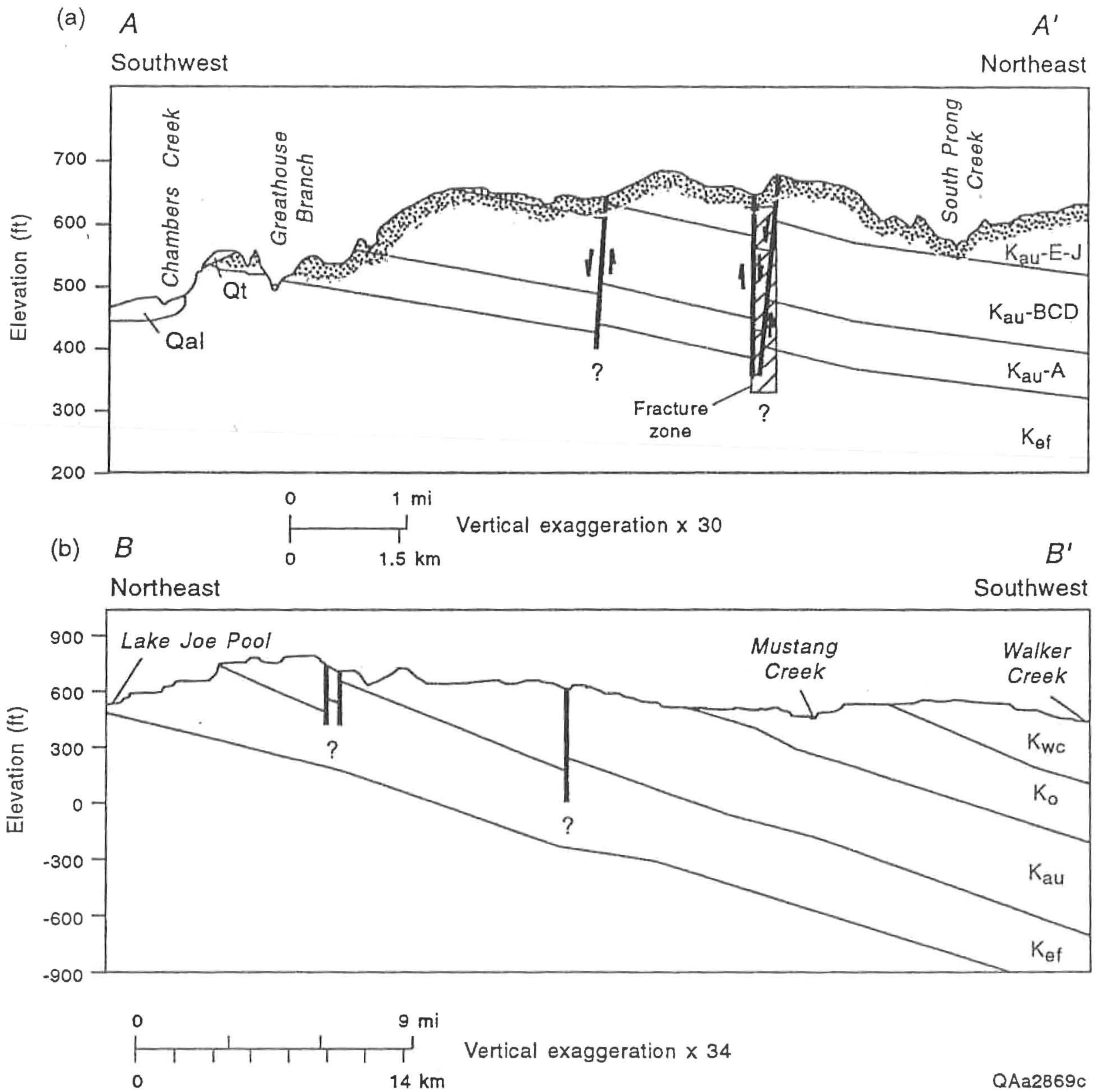

Figure 65. Distribution of finite-difference blocks used in numerical simulation of ground-water flow in the West Campus model (a) and Ellis County model (b). Profiles A–A′ and B–B′ located in figure 9. K_{ef} – Cretaceous Eagle Ford Formation. K_{au} – Austin Formation. K_{au}-A – lowermost unit A of the Austin Formation. K_{au}-BCD – Austin Formation units B, C, and D. K_{au}-E-J – middle Austin units E to J. K_o – Ozan Formation. K_{wc} – Wolfe City Formation.

Bottom and side boundaries initially were set as no-flow boundaries. The side boundaries were placed at surface-water divides to justify the hydrologic-model assumptions and were located far from the West Campus area of interest to minimize the effects of those assumptions on model results. The bottom of the cross section was placed in the Eagle Ford Formation and was assumed to be a no-flow boundary.

Hydrologic properties of different hydrologic units are summarized in table 26. The weathered zone was subdivided into two layers to incorporate the observed decrease in hydraulic conductivity with depth (table 13). The upper layer was 20 ft (6.1 m) thick and was assigned the geometric mean of the hydraulic conductivity on the basis of aquifer tests in weathered chalk (0.61 ft/d [$10^{-5.67}$ m/s]). The lower, less permeable layer was 10 ft thick (3.05 m) and was assigned a hydraulic conductivity of 0.17 ft/d ($10^{-6.21}$ m/s). Vertical hydraulic conductivity of the weathered zone was assumed to be 100 times less than the horizontal hydraulic conductivity. The fracture zone was assigned a hydraulic conductivity of 0.15 ft/d ($10^{-6.28}$ m/s) on the basis of the results of the pumping test at well BI3. Porosity of fractured chalk in the weathered zone and fracture zone was assumed to be between 1 to 3 percent (Freeze and Cherry, 1979). Because MODFLOW does not consider fractures as explicit features, hydraulic conductivity of the weathered and fractured zones assumes that a fracture network can be modeled as a porous medium with a hydraulic conductivity equivalent to that of the fractures. This approach should be valid, as calculations showed that a single productive fracture does not account for the water-level hydrograph from the test at BI3 (table 14). However, there is likely to be a wide range of fracture sizes represented by a mean hydraulic conductivity (equation 10, fig. 59). Simulated travel time and particle paths in the fracture zone thus might be misrepresented by the porous-media flow model.

Hydraulic conductivities for the Austin Chalk layers (table 26) were assigned values according to core-plug data (table 8, fig. 53). Core-plug data provided measurements generally below the limits of the packer test method, although the scale of the measured material is inches instead of feet. A hydraulic conductivity of 10^{-6} ft/d ($10^{-11.45}$ m/s) was assumed for the Eagle Ford Formation because all of the packer tests in shale included permeable fractures. This value compared well with hydraulic

Table 26. Hydrologic properties used as initial and calibrated values in West Campus and Ellis County models.

Hydrologic unit	Hydraulic conductivity (ft/day)	Hydraulic conductivity (m/s)	Porosity
Weathered zone:			
top	6.10×10^{-1}	2.15×10^{-6}	0.030
bottom	0.70×10^{-1}	0.62×10^{-6}	0.030
Fracture zone	1.50×10^{-1}	0.53×10^{-6}	0.030
Wolfe City Formation	2.83×10^{-4}	9.98×10^{-10}	0.350
Ozan Formation (initial)	8.96×10^{-6}	0.32×10^{-10}	0.350
Ozan Formation (final)	3.21×10^{-6}	1.13×10^{-11}	0.350
Austin Chalk (all)	5.71×10^{-5}	2.01×10^{-10}	0.266
middle (unit E)	3.24×10^{-5}	1.14×10^{-10}	0.212
upper lower (units BCD)	1.70×10^{-4}	6.00×10^{-10}	0.329
lower (unit A)	1.10×10^{-4}	3.88×10^{-10}	0.309
Eagle Ford Formation	1.00×10^{-6}	3.53×10^{-12}	0.100

K_h / K_v (initial) = 0.01
K_h / K_v (final) = 0.0085

Table 27. Piezometer measurements for model calibration.

Piezometer	Hydraulic-head elevation (ft)	Land-surface elevation (ft)	Tip/Screen elevation (ft)
West Campus model			
BI5	642.3	662.0	560.4
BI3	694.9	698.9	610.7
BIR11	667.4	672.5	455.2
Exploratory borehole shaft			
p1	661.2	665.5	532.6
p2	659.2	665.4	552.2
p3	660.6	666.0	574.0
p4	660.4	666.7	574.7
p5	655.7	665.6	572.6
p8	664.9	665.6	440.6
Ellis County model			
BE6	530.2	487.5	110.2

conductivity measured on core plugs taken from the Eagle Ford Formation near Waco, Texas (Bradley and Yelderman, 1993). Porosity of 10 percent was assumed for the Eagle Ford.

Wickham and Dutton (1991) found that $10^{-5.29}$ ft/d ($10^{-9.74}$ m/s) is an upper limit of reasonable estimates for vertical hydraulic conductivity of unweathered Austin Chalk and Ozan Formation, on the basis of numerical modeling results. This is 0.01 times the estimated mean horizontal hydraulic conductivity, which is a generally accepted ratio of vertical-to-horizontal anisotropy. Anisotropy of all zones was set initially to 0.01 and adjusted during calibration.

Calibration

Calibration involved adjusting assigned values of hydraulic conductivity and the anisotropy ratio (K_v/K_h) of each zone to optimize by a trial-and-error method the match between simulated and observed hydraulic heads. Hydraulic head at three wells (table 27) and interpretations of chemical data were available for evaluating the match. Vertical hydraulic conductivity was treated as an unknown, while measured values of horizontal hydraulic conductivity were honored as much as possible. Hydraulic head measured at well BI5 was used to establish the anisotropy ratio in the Austin Chalk. A vertical to horizontal anisotropy ratio (K_v/K_h) of 0.0085 gave the best match. This is close to the 0.01 initial estimate of anisotropy.

Hydraulic head and flow velocity calculated in the model were compared to both isotopic and hydraulic-head data. Hydraulic conductivity at the fracture zone was adjusted on the basis of each comparison. The backward particle tracking capability of MODPATH was used to place a particle at the screened interval of the well and follow the particle back to the point of recharge at ground surface. This represents one possible solution of flow paths and travel times for recharge to the BI3 well. With the fracture zone assigned a hydraulic conductivity of 0.15 ft/d ($10^{-6.28}$ m/s) on the basis of measurements at BI3, travel time from ground surface to the well was calculated to be 758 years. Carbon-14 and tritium data, however, suggested that time of ground-water travel from ground surface to well BI3 was less than 50 years. A travel time of about 50 years was obtained by setting hydraulic conductivity of the fracture zone to 4.0 ft/d ($10^{-4.85}$ m/s). A slightly lower value of hydraulic conductivity, 1.4 ft/d ($10^{-5.31}$ m/s), was required to match simulated and measured hydraulic head (table 27). A reasonable estimate of hydraulic conductivity of the fracture zone, therefore, is between 1.4 and 4 ft/d ($10^{-5.31}$ and $10^{-4.85}$ m/s), higher than the hydraulic-conductivity estimate of 0.15 ft/d ($10^{-6.28}$ m/s) determined in pumping tests at well BI3 (table 14).

Data on water pressure from wire-line piezometers at the exploratory borehole shaft (Robinson and others, 1993), along with water levels measured at well BIR11 (fig. 48p), clearly show an upward-directed gradient of hydraulic head in the unweathered Austin Chalk and Eagle Ford Formation (fig. 66). This feature is more likely related to local topography and variations in hydraulic conductivity than to position in the regional flow path across Ellis County, as indicated by the local value of the dynamic pressure increment (fig. 51). The test shaft location projected on the cross-sectional model lies in a topographic low. In this setting the numerical model results reasonably match measured vertical profile in hydraulic head and the measured water level at well BIR11.

Unique solutions cannot be simulated by a numerical model if hydrologic information is sparse. In this case, parameter values are largely unknown. Certain hydrologic properties are assigned either on the basis of a single measurement or an educated guess. To evaluate whether the estimates are reasonably close to actual values, sensitivity of model results was analyzed by observing the effect of

- changes in anisotropy ratio between vertical and horizontal hydraulic conductivity,
- hydraulic conductivities of the different zones,
- conductance used in the general head boundary package of MODFLOW, which controls recharge and discharge rates, and
- different conditions at the lateral boundaries of the model.

Simulated hydraulic heads were compared with measured values at wells BIR11, BI5, and BI3 (table 27).

Hydraulic head at well BIR11 was most sensitive to vertical-to-horizontal anisotrophy ratio and less sensitive to hydraulic conductivity in the lower and middle Austin Chalk (fig. 67a). Hydraulic head at wells BIR11 and BI5 were insensitive to general head boundary conductance and to the

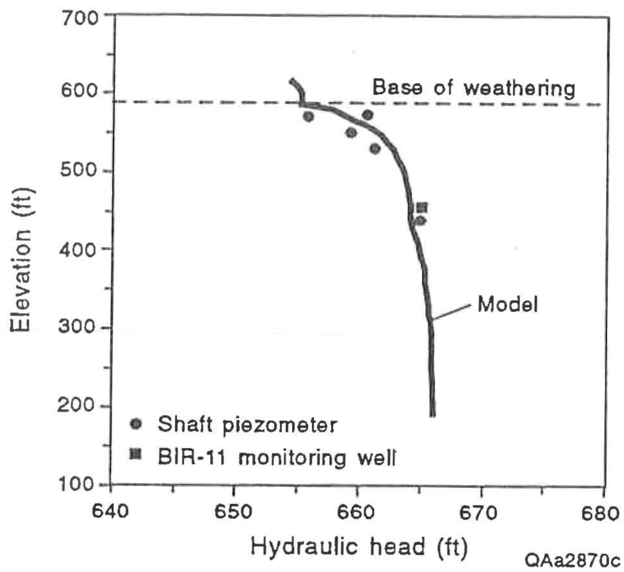

Figure 66. Comparison between simulation results, wire-line piezometer data from the exploratory borehole shaft (Robinson and others, 1993), and water-level data measured at monitoring well BIR11.

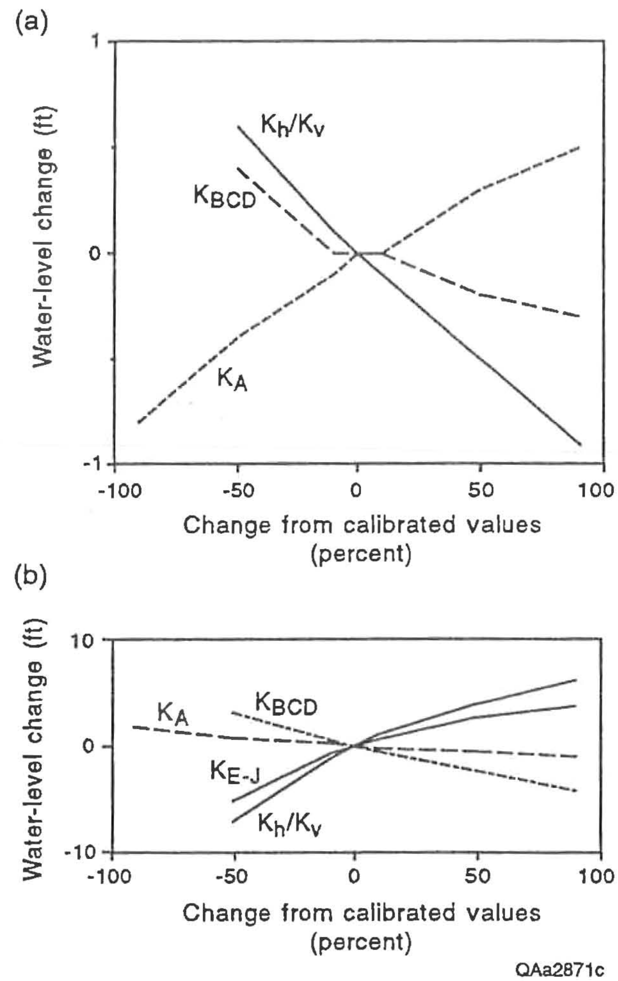

Figure 67. Sensitivity of simulated water level to uncertainty in hydrologic properties in the West Campus model, expressed for model blocks corresponding to monitoring wells BIR11 (a) and BI5 (b). Note 10-fold scale difference between (a) and (b). K_A is hydraulic conductivity of lower Austin Chalk unit A. K_{BCD} is hydraulic conductivity of units B, C, and D. $K_{E\text{-}J}$ is hydraulic conductivity of the middle Austin Chalk units E through J. K_h/K_v is ratio of horizontal hydraulic conductivity to vertical hydraulic conductivity.

hydraulic conductivities of the weathered zone and Eagle Ford Formation. Simulated hydraulic head was more sensitive to the various parameters at the test shaft than at well BI5 (fig. 67b). Hydraulic head at well BI3 was sensitive to hydraulic conductivity of the fractured zone but insensitive to hydraulic conductivity of the weathered zone and to anisotropy ratio assigned in the fractured zone. Hydraulic head in unfractured rock adjacent to the fractured zone remained nearly unchanged while hydraulic conductivity in the fractured zone was changed over two orders of magnitude. This treats ground-water flow in the fracture zone as separate from flow in the unfractured bedrock.

The boundary on the South Prong Creek side of the model was changed from a zero-flux boundary to a specified head boundary. Vertical gradient in hydraulic head at the boundary was varied from –10 to 10. Over this range, simulated ground-water flow was affected only between the boundary and South Prong Creek, which showed that the West Campus area of the model was not influenced by the boundary.

Results

Using MODPATH, particles were proportionally placed according to constant head fluxes in the top cells and allowed to travel through the model. These particles indicated ground-water flow paths. The majority of particles (>99 percent) remained within the weathered zone (fig. 68b). This was determined by comparing the amount of recharge and the amount of flow leaving the weathered zone into the unweathered zone. Flow paths are influenced both by hydraulic conductivity of the various zones of the model and by hydraulic-head gradients. The latter are controlled largely by distribution and amount of recharge across the varied topography of the modeled area. Hydraulic-head values indicate predominantly horizontal flow paths across most of the profile with nearly vertical flow paths beneath the upland and low-lying areas at the ends of the model (fig. 68a). The head distribution suggested a network of local, intermediate, and regional scale flow systems (Tóth, 1963, 1978). Where topographic relief is low, hydraulic head contours are farther apart, residence time is longer, and flow velocity is slower. With greater relief, hydraulic-head gradients are steeper and flow

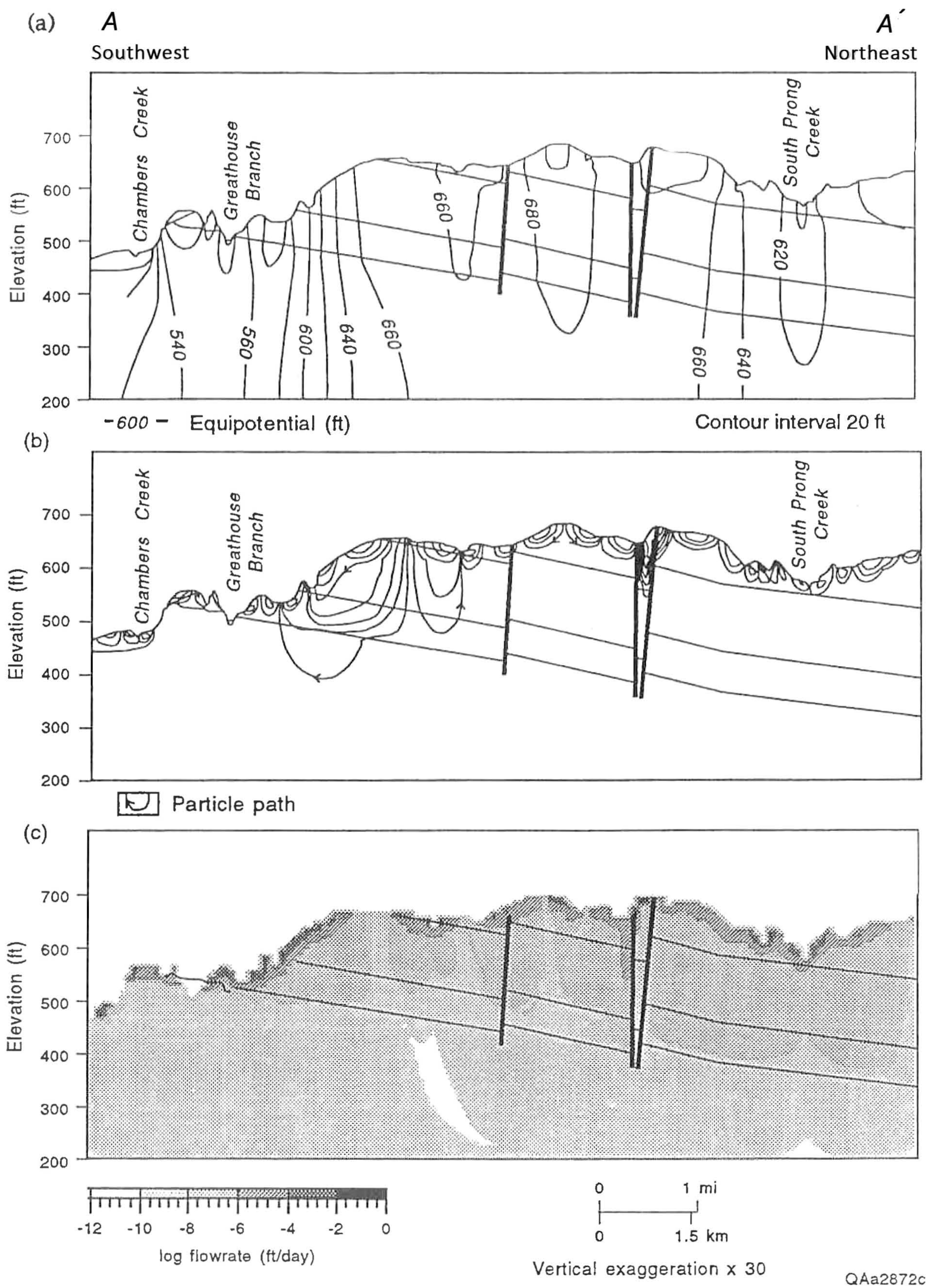

Figure 68. Results from West Campus model simulation: (a) equipotential contours, (b) particle paths, and (c) flow rates. Contour interval in (a) is 20 ft (~6 m). Direction of flow in (b) is indicated for only a few particle paths for the sake of clarity; flow direction is generally from topographically high areas to low areas. Formation contacts are as labeled in figure 65a.

velocity is faster. Hydraulic-head gradient indicated downward-directed flow beneath topographic highs and upward-directed flow beneath topographic lows (figs. 68a, b). Vertically averaged upward-directed gradients varied from 0 to 0.1. The recharge rate, calculated by summing the fluxes into the model divided by area of the land surface was 0.08 ft/yr (2.4 cm/yr), less than 1 percent of precipitation. This is consistent with results given by Dutton and Wickham (1992), who estimated recharge in more permeable, surficial alluvium to be a few percent of precipitation.

The fastest flow rates, of course, coincided with the permeable weathered zone and ranged from 10^{-2} to 10^{-6} ft/d ($10^{-7.45}$ to $10^{-11.45}$ m/s) (fig. 68c). Slower flow rates were simulated in the unweathered and unfractured rock and ranged from 10^{-6} to 10^{-8} ft/d ($10^{-11.45}$ to $10^{-13.45}$ m/s). The lowest flow rates, 10^{-8} to 10^{-10} ft/d ($10^{-13.45}$ to $10^{-15.45}$ m/s) were simulated in the Eagle Ford Formation and also in the Austin Chalk beneath areas of little topographic relief. The fracture zone allowed higher flow rates to penetrate deeper into the chalk and shale.

Residence time showed a log-normal distribution (fig. 69). The smallest residence time was in the weathered zone, where the geometric mean of particle travel time was 5 to 10 years, depending on the porosity used (1 to 3 percent) and length of path to discharge point. Particles circulated deeply in the fracture zone with travel times of 100 to 1,500 years, depending on assigned hydraulic conductivity of the fracture zone, as previously mentioned. From recharge points across the broad surface-water divide, several particles circulated to greater depth into the low-permeability, unweathered chalk. Travel time in the unweathered zone was substantially longer with a geometric mean travel time of 921,000 yr. This flow rate is consistent with the conceptual model of incomplete flushing of seawater from the chalk and marl.

Ground-water recharge to the weathered chalk was approximately 1 inch/yr (24.4 mm/yr), approximately 3 percent of precipitation. Net movement of ground water downward from the weathered zone into the unweathered chalk was 0.001 inches/yr (0.027 mm/yr). Net discharge of ground water from the unweathered chalk downward into the Eagle Ford Shale was negligible, 0.1×10^{-6} inches/yr (4×10^{-6} mm/tr). This indicates that 0.11 percent of flow in the weathered zone is lost to

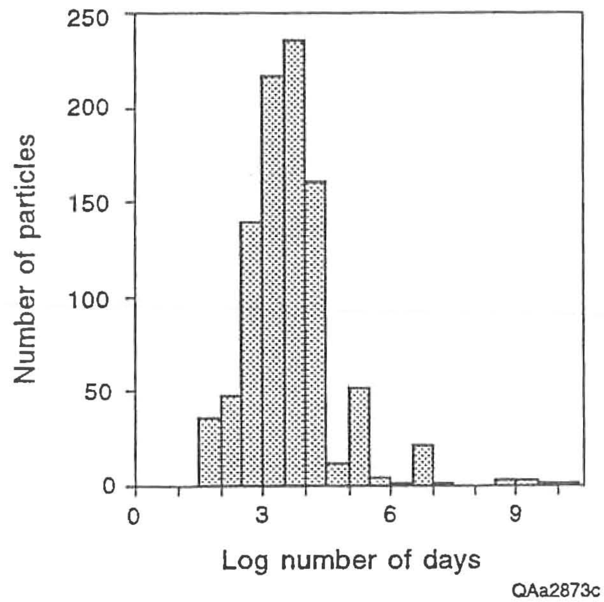

Figure 69. Distribution of residence times of particles under steady-state flow condition simulated in West Campus model. Residence time appears log-normally distributed. Although water chemical composition suggests locally long residence time, the long residence time ($10^{10.5}$ days = 86.6 million years) of a few particles is not geologically reasonable.

the deeper, unweathered bedrock, and that only 0.01 percent of ground water in the unweathered chalk moves into the Eagle Ford Formation.

Ellis County Model

The goal of modeling ground-water flow in the Ellis County model was to investigate

- the contrast between horizontal and vertical hydraulic conductivity that is required to reproduce artesian pressure in Austin Chalk at the east side of the SSC site,
- flow between the Ozan Formation and Austin Chalk and between Austin Chalk and Eagle Ford Formation,
- recharge and discharge areas,
- particle path lines, and
- residence time and age of ground water.

Profile B–B′ of the Ellis County model (fig. 9) lies along a surface-water divide between Red Oak Creek and Waxahachie Creek and passes through the East Campus. It thus simulates the regional movement of ground water from west to east following the regional gradient in hydraulic head related to topographic relief. The profile incorporates monitoring well BE6 for calibration data. The model includes four hydrologic units representing the Austin Chalk, Eagle Ford, Ozan, and Wolfe City Formations. Weathered bedrock and alluvium were not included; therefore, the East Campus model simulates ground-water flow only through unweathered bedrock.

Assignment of Hydrologic Properties

Hydrologic Properties used in the West Campus model were assigned in the Ellis County model (table 26). Hydraulic conductivity and porosity of Wolfe City Formation were assigned values typical of sandstone (Freeze and Cherry, 1979). Boundary conditions were represented the same way as in the West Campus model. The general head boundary package of MODFLOW (McDonald and Harbaugh, 1998) was used to prescribe the upper boundary at a constant head, because the weathered zone was not explicitly included, the general head boundary simulates movement of water between the weathered and unweathered zones. The head value for the general head boundary was placed at the mean water level of the shallow, surficial aquifers which is approximately 8 ft (2.44m) below ground surface.

Calibration

Model calibration involved adjusting horizontal and vertical hydraulic conductivities of the Austin Chalk and Ozan Formation. Calibration data were limited to hydraulic head measured at well BE6 (model column 123, layer 25). Ozan Formation hydraulic conductivity was adjusted to match the 46 ft (14.02 m) of artesian head (head above ground surface) at well BE6. The final ratio of hydraulic conductivity between the Austin Chalk and Ozan Formation was 17.8.

Sensitivity of simulated hydraulic head was analyzed by observing the effect of

- changes in anisotropy ratio of vertical-to-horizontal hydraulic conductivity,
- contrast in hydraulic conductivities between the Austin Chalk and Ozan Formation,
- hydraulic conductivity of the Wolfe City and Eagle Ford Formations, and
- conductance used in the general head boundary package of MODFLOW, which controls recharge and discharge rates.

Hydraulic head at well BE6 was sensitive to the ratio in vertical-to-horizontal hydraulic conductivity, contrast in hydraulic conductivities between the Austin Chalk and Ozan Formation, and the conductance term for the general head boundary condition (fig. 70). Hydraulic head at BE6 was relatively insensitive to hydraulic conductivity of the Wolfe City and Eagle Ford Formations.

Results in the Ellis County model were more sensitive to the conductance term in the general-head-boundary package of MODFLOW than in the West Campus model, due to a lack of a weathered zone included in the Ellis County model. The vertical conductance term was assigned on the basis of the vertical hydraulic conductivity of the block to which it was applied and lower values of vertical conductance were used in the Ellis County model than in the West Campus model. Flow rates in and out

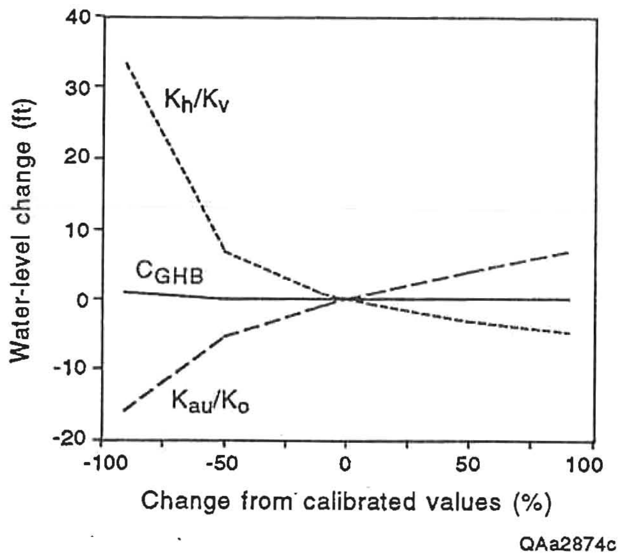

Figure 70. Sensitivity of simulated water level to uncertainty in hydrologic properties in the Ellis County model. Comparison is for model block corresponding to monitoring well BE6. K_h/K_v is ratio of horizontal to vertical hydraulic conductivity. C_{GHB} is conductance term of the general head boundary. K_{au}/K_o is contrast in hydraulic conductivity between Austin Chalk and Ozan Formation.

of the imaginary blocks of the general head boundary represent inflow to an outflow from the unweathered bedrock in the Ellis County model.

Sensitivity to the right-hand boundary condition was investigated by changing the boundary from specified-flux (no-flow) to specified- (constant-) head conditions. The effect of different vertical gradients in hydraulic head and of different vertical hydraulic conductivities (K_V) were simulated with the different boundary condition.

Results

General results resemble those of the West Campus model. Hydraulic-head values indicate predominantly horizontal or intrastratal flow paths across most of the profile, with obvious local, intermediate, and regional scale flow systems (fig. 71a). A plot of the difference between hydraulic head in a block and ground-surface elevation shows areas with artesian pressure (fig. 71c). Artesian pressure developed predominantly in the chalk where it lies beneath the lower-permeability marl, in the vicinity of the "BE6" block (column 123 and layer 25), agreeing with measurements at BE6. Artesian pressure at the down-gradient end of the model might be affected by the no-flow boundary condition, which forces water upward. The boundary lies, however, at some distance from the East Campus area of interest and has no effect on results there.

The Ellis County model simulated ground-water flow entirely within unweathered bedrock. Particle travel times in the low-permeability, unweathered Austin Chalk had a geometric mean of 1.7 m.y., ranging from 0.21 to 244 m.y. Mean travel time in the unweathered Ozan and Eagle Ford Formations was longer, approximately 27 m.y. Near the chalk-marl boundary at the outcrop, some particles placed in the chalk outcrop followed a short flow path beneath the marl and discharged upward at the topographic low representing Mustang Creek (fig. 71b). Flow from a weathered zone downward into unweathered bedrock was

- Wolfe City Sand — 7.4×10^{-4} inches/yr (1.9×10^{-2} mm/yr),
- Austin Chalk — 1.4×10^{-4} inches/yr (3.4×10^{-3} mm/yr),

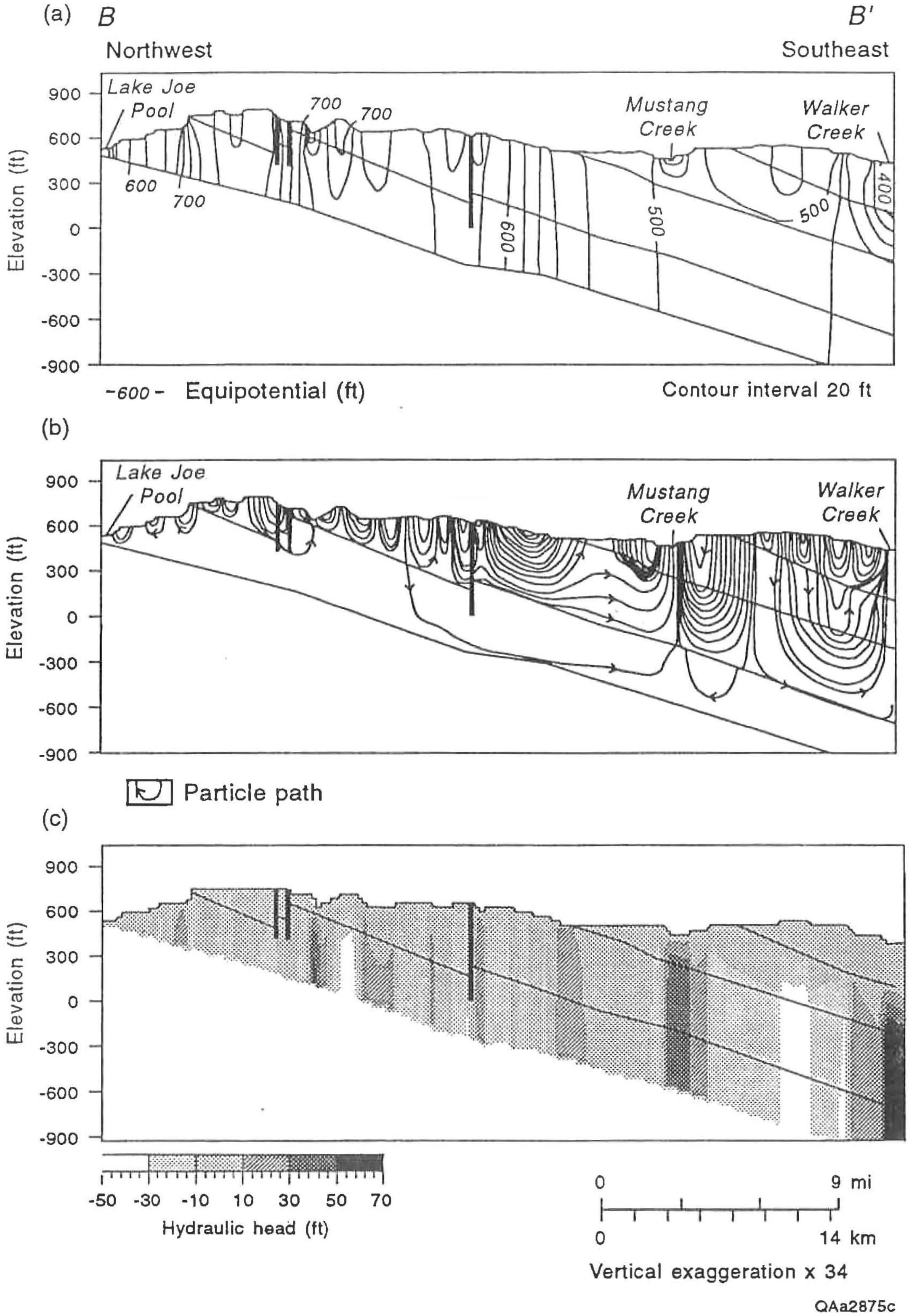

Figure 71. Results from Ellis County model simulation: (a) equipotential contours, (b) particle paths, and (c) difference between ground-surface elevation and simulated hydraulic head in model blocks. Contour interval in (a) is 20 ft. Direction of flow in (b) is indicated for only a few particle paths for the sake of clarity; flow direction is generally from topographically high areas to low areas. Head differences greater than zero in (c) indicate areas of artesian pressure with hydraulic head above ground surface. Formation contacts are as labeled in figure 65b.

- Ozan Formation— 6.6×10^{-6} inches/yr (1.7×10^{-4} mm/yr, and
- Eagle Ford Formation— 1.2×10^{-6} inches/yr (3.1×10^{-5} mm/yr).

Cross-formational flow into the Wolfe City was high due to the greater hydraulic conductivity of sandstone compared to hydraulic conductivity of chalk, marl, or shale. The net cross-formation flow of ground water between the Austin and Ozan was directed upward, with 72 percent of the 1.4×10^{-5} inches/yr (3.4×10^{-4} mm/yr) occurring beneath the western part of the Ozan Formation outcrop, west of Mustang Creek. Flow downward from the Austin to the Eagle Ford was 1.6×10^{-6} inches/yr (4.0×10^{-5} mm/yr).

The response of simulated hydraulic head in the "BE6" block to changes in the boundary's hydraulic-head gradient was linear over the range of gradients examined (fig. 72). Changing the gradient from –1 to 1 (both direction and magnitude) produced a range in hydraulic head of as much as 30 ft (9.1 m) at the "BE6" block. Vertical hydraulic gradient in hydraulic head at the model boundary and vertical hydraulic conductivities of Austin Chalk and Ozan Formation marl were varied together to maintain the agreement between simulated and observed hydraulic heads at well BE6 (fig. 73). The ratio of vertical hydraulic conductivities that allows a match in hydraulic heads is asymptotically related to the vertical gradient at the boundary, and actual field conditions might be found at any position along the line shown in figure 73.

Model Limitations

Due to the paucity of calibration data along model profiles, these models are limited to use as interpretive tools and do not predict specific ground-water flow paths or velocities. Results might be verified with additional field measurements. Limitations involve

- the assumption that fractured rock can be treated equivalent to a porous medium,
- the possibility that northeast strike of faults and fractures might impose a spatial anisotropy to hydraulic conductivity, which was ignored,
- the assumption that ground-water flow is restricted to the plane of the profile model, and

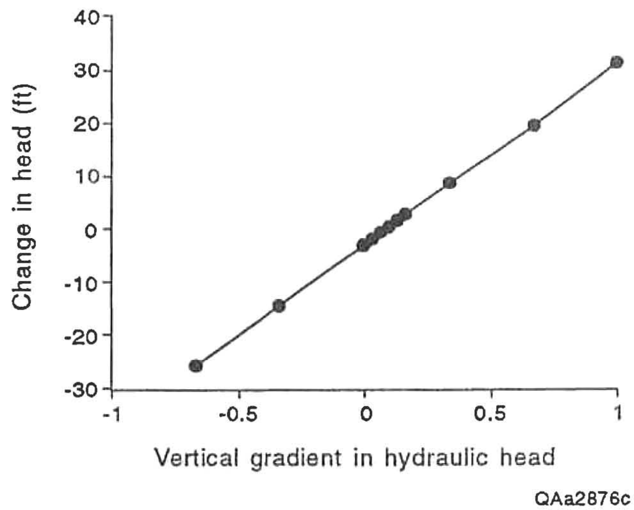

Figure 72. Effect of vertical gradient in hydraulic head at the downdip boundary of the Ellis County model (C′) on hydraulic head in finite-difference block (123, 25) corresponding to monitoring well BI6.

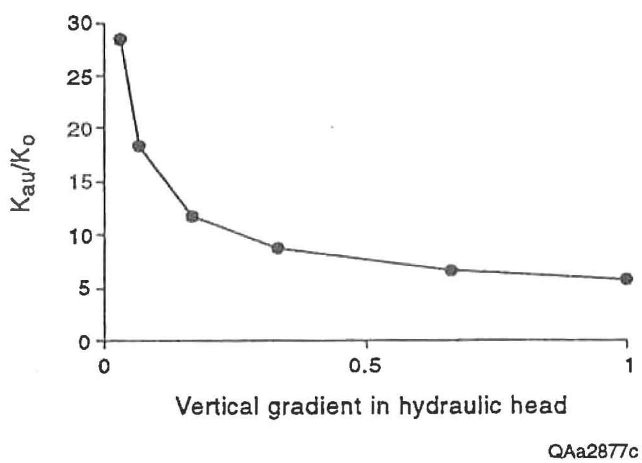

Figure 73. Contrast in hydraulic conductivity between Austin Chalk (K_{au}) and Ozan Formation (K_o) required for Ellis County model results to match artesian head of 40 ft 12.2 m) measured at BE6, as a function of vertical gradient in hydraulic head specified at the downdip boundary C′).

- the uncertainty in parameter values.

The most limiting assumption, at least in a local sense, is that fractured zones with great density of fractures, such as was included in the West Campus model, do not influence flow on a regional scale, as simulated in the Ellis County model. The fracture zone in the West Campus model shows that concentrated and interconnected fractures can substantially increase flow velocity and circulation depths and decrease travel times.

Representing ground-water flow through fracture zones is difficult if detailed information on orientation and lateral extent of the zone is not available. For instance, the fracture zone depicted in the West Campus model likely extends perpendicular from the cross section. If this is the case, ground water might actually be flowing in and out of the plane of the cross section as its own flow system, compromising an important assumption of the conceptual model. This limitation might account for the differences in permeabilities between model estimates using travel times and hydraulic head and the field measured value. Structurally, the graben feature at well BI3 is strictly interpretive, generated to accommodate the 50 ft (15.2 m) throw of the fault. The geometry of the fracture zone may be completely different.

Conclusions Based on Flow Models

A numerical ground-water flow model was constructed to evaluate poorly known hydrologic parameters, predict ground-water circulation paths, estimate ground-water travel times, and examine the connection between the weathered and unweathered zones. With limited field data, two profile models were constructed to investigate a ground-water flow system in an aquitard. Model results suggest that

- horizontal hydraulic conductivity is a little more than 100 times greater than vertical hydraulic conductivity,
- hydraulic conductivity of the Austin Chalk is 18 times greater than hydraulic conductivity of the Ozan Formation on a regional scale,

- best value of hydraulic conductivity for simulating flow in a fracture zone on the West Campus is between 1.4 and 4.0 ft/d ($10^{-5.31}$ and $10^{-4.85}$ m/s), as constrained by age of ground water inferred on the basis of tritium content and by measured hydraulic heads.

Execution of the calibrated model showed that

- 99 percent of ground water flows through the weathered zone,
- ground-water residence time in the weathered zone is 5 to 10 years,
- less than 3 percent of precipitation is recharged,
- average ground-water residence time in unweathered rock is 1 million years,
- deep and rapid ground-water circulation occurs in fracture zones,
- vertical gradients in hydraulic head range from 0 to 0.1,
- ground water that is recharged at the Austin Chalk outcrop either discharges to creeks that cross the outcrop, or flows downdip and eventually discharges upward through the Ozan Formation,
- ground-water velocity in weathered bedrock ranges from 10^{-2} to 10^{-6} ft/d ($10^{-7.45}$ to $10^{-11.45}$ m/s), and
- ground-water velocity in unweathered bedrock ranges from 10^{-6} to 10^{-8} ft/d ($10^{-11.45}$ to $10^{-13.45}$ m/s).

Ground-water velocities in unfractured rock are very slow and should retard the transport of radionuclides. However, where bedrock is intensely fractured, rapid flow velocities and transit times of less than 50 years can be obtained. Therefore, it is very important to identify fracture zones and to quantify their hydraulic properties in the vicinity of expected sources of radioactivated ground water.

Controls on Chemical Composition

Geochemical models PHRQPITZ (Plummer and others, 1988) and PHREEQE (Parkhurst and others, 1980) were used to simulate reactions hypothesized to control chemical composition of ground water, including

- mixing of recharged rainwater (meteoric water) with sodium, chloride, and other dissolved salts inherited from (connate) seawater (White, 1965) trapped in pores in low-permeability rock, and
- reaction of mixed water with minerals such as calcite that make up the formations.

Initial simulations showed that there must be additional reactions besides solution of calcite to match observed SO_4^{2-}, Ca^{2+}, Mg^{2+}, and Na^+ concentrations. Pyrite oxidation was assumed to be responsible for adding SO_4^{2-}. Ion exchange was assumed to provide a sink for Ca^{2+} and Mg^{2+} and a source for Na^+. Initial geochemical simulations using PHRQPITZ considered dilution of seawater (Nordstrom and others, 1979) with pure water (total dissolved solids = 0 mg/L). Subsequent simulations were made using PHREEQE to study pyrite oxidation and cation exchange reactions. The following reactions were simulated using PHREEQE and are listed in sequence (reactions in PHREEQE and PHRQPITZ are calculated on the basis of unit volume so that concentration units per liter are implied in the following:

- Dilution of seawater by rain water, with rainwater composition interpolated from Junge and Werby (1958) and additional data.
- Oxidation of pyrite and equilibration with pyrite, goethite, calcite, and dolomite.
- Exchange of adsorbed Na^+ for dissolved Ca^{2+} and Mg^{2+} ions.

Mixing of seawater and freshwater equilibrated with the calcite results primarily in minor changes in ion ratios until the percentage of freshwater nears 90 percent. Simulated cation and anion concentrations change gradually with dilution, then decrease rapidly when seawater has been diluted to less than 10 percent (fig. 74). HCO_3^- remains relatively constant at low or zero oxygen concentration because it is buffered by calcite (fig. 74b). At higher oxygen concentration (2.5×10^{-4} moles oxygen), both SO_4^{2-} and HCO_3^- remain relatively constant in dilution with concentrations buffered by pyrite and calcite. However, simple dilution and equilibration with calcite does not account for relatively high SO_4^{2-} and Na^+ and low Ca^{2+} and Mg^{2+} concentrations in ground water sampled at the SSC site. In most cases, chemical composition of ground water sampled at the SSC site in unweathered chalk and marl approximately coincides with mixtures of less than 5 percent seawater and between 95 percent and 100 percent freshwater.

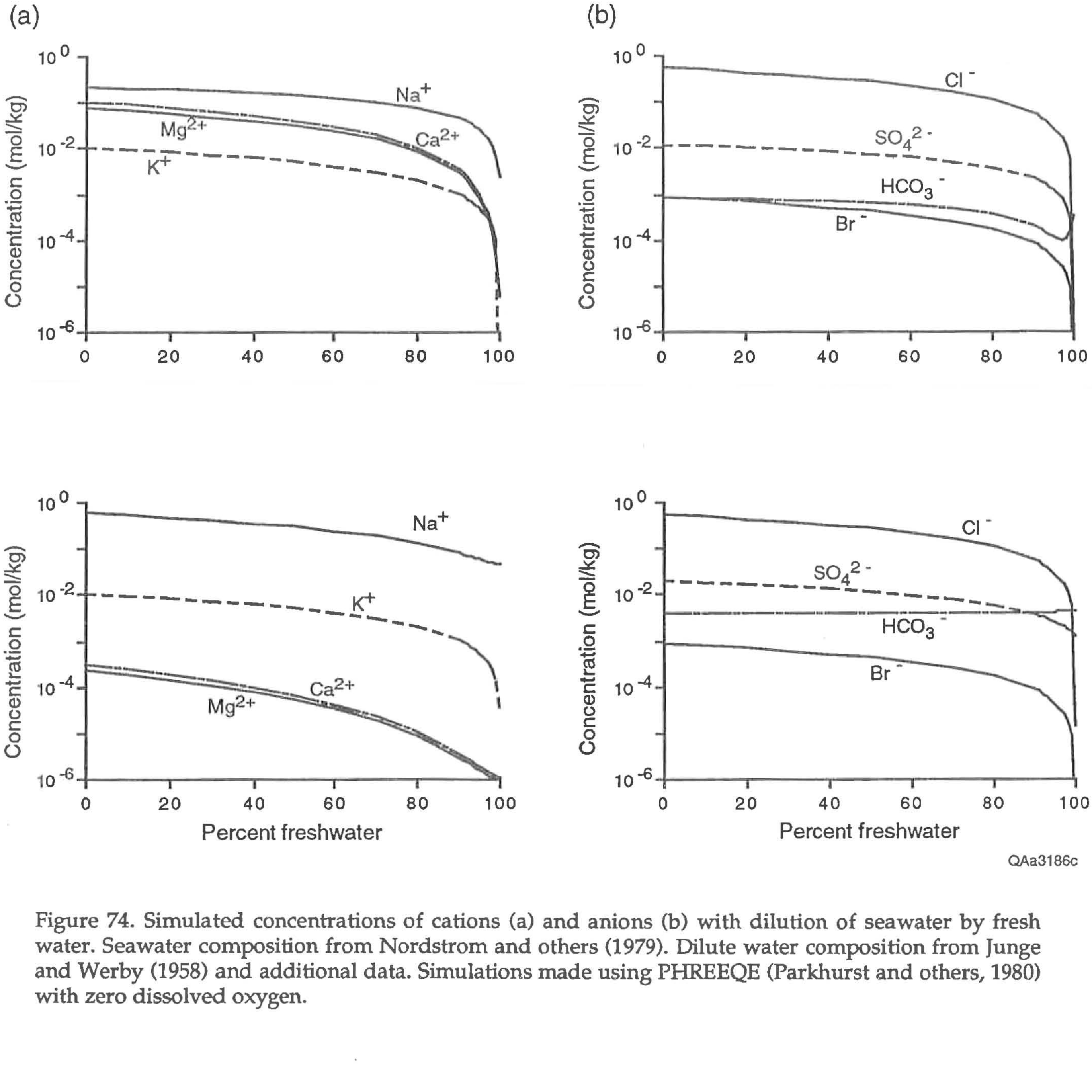

Figure 74. Simulated concentrations of cations (a) and anions (b) with dilution of seawater by fresh water. Seawater composition from Nordstrom and others (1979). Dilute water composition from Junge and Werby (1958) and additional data. Simulations made using PHREEQE (Parkhurst and others, 1980) with zero dissolved oxygen.

The amount of pyrite oxidation was determined by the amount of dissolved oxygen present. Pyrite oxidation releases SO_4^{2-} and H^+ ions, which in turn reacts with the calcite to release Ca^{2+} as in equations (13) and (14)

$$2FeS_2 + 5H_2O + 7.5O_2 = 2FeO(OH) + 8H^+ + 4SO_4^{2-} \tag{13a}$$

$$K_{eq} = \frac{\left[H^+\right]^8 \left[SO_4^{2-}\right]^4}{\left[O_2\right]^{7.5}} \tag{13b}$$

$$8CaCO_3 + 8H^- = 8Ca^{2+} + 8HCO_3^- \tag{14a}$$

$$K_{eq} = \frac{\left[\mathrm{Ca}^{2+}\right]^8 \left[\mathrm{HCO}_3^-\right]^8}{\left[\mathrm{H}^+\right]^8} \tag{14b}$$

Dissolved oxygen (DO) and the equilibrium constant (K_{eq}) as defined in equation (13b) control the amount of pyrite oxidation. DO concentrations were varied from 0 to 2.5×10^{-4} moles (~8 mg/L), which represents the range of DO from that in a closed system where all dissolved oxygen has been consumed to that in water in equilibrium with the atmosphere at 25°C (Drever, 1988). The amount of dissolved oxygen is higher in typical lake water than in ground water that is not in direct contact with the atmosphere.

Cation exchange was simulated by simple reactions

$$2Na^+ + Ca\text{-}clay = Ca^{2+} + Na\text{-}clay \tag{15a}$$

$$K_{eq} = \frac{\left[q_{Na}\right]\left[C_{Ca}\right]}{\left[C_{Na}\right]^2\left[q_{Ca}\right]} \tag{15b}$$

$$2Na^+ + Mg\text{-}clay = Mg^{2+} + Na\text{-}clay \tag{16a}$$

$$K_{eq} = \frac{[q_{Na}][C_{Mg}]}{[C_{Na}]^2[q_{Mg}]} \tag{16b}$$

where C stands for the concentration of the dissolved ion and q stands for the adsorbed concentration. Ca^{2+} released in reaction (13a) is exchanged for Na^+ adsorbed on smectite in the Austin Chalk and Ozan Formation according to reaction (15a). Dissolved magnesium, presumably derived from seawater, also is exchanged for adsorbed Na^+ according to reaction (16a). The equilibrium constants expressed in equations (15b) and (16b) were varied by trial and error to bound the observed concentrations of dissolved ions in ground waters from the SSCL monitoring wells. Both equilibrium constants were varied over the same range, with a log K_{eq} value from 3×10^{-5} to 3.5.

There are, of course, an infinite number of combinations of DO and cation exchange capacity (CEC) that might account for any individual chemical analysis between the bounds. Sample data are bounded by simulated reaction paths with

- DO of zero and exchangeable Ca^{2+}/Na^+ ratio of 3×10^{-5} and
- DO of 2.5×10^{-4} and exchangeable Ca^{2+}/Na^+ ratio of 3.5.

The results indicated that the Ca^{2+}/Na^+ ratio is more sensitive to cation exchange than to pyrite oxidation coupled with calcite solution (fig. 75). At small concentrations of dissolved oxygen, pyrite oxidation slightly affects SO_4^{2-} and Ca^{2+} concentrations. Ca^{2+}/Cl^- and Na^+/Cl^- ratios increase with increasing dissolved oxygen because of the progress of reactions (13a), (14a), and (15) (figs. 76 and 77). Dissolved SO_4^{2-} increases and the Cl^-/SO_4^{2-} ratio decreases with increased dissolved oxygen (fig. 78). Dissolved SO_4^{2-} is controlled mainly by pyrite oxidation and is not greatly affected by the cation exchange.

The fairly good match between observed and simulated chemical composition supports the conclusion that ground waters in the Austin Chalk and Eagle Ford Formation in the Waxahachie area have undergone four geochemical processes:

- **mixing of ground water derived from rainfall (95 to 100 percent) and seawater (0 to 5 percent),**
- **equilibration of the resulting mixture with the surrounding rock,**

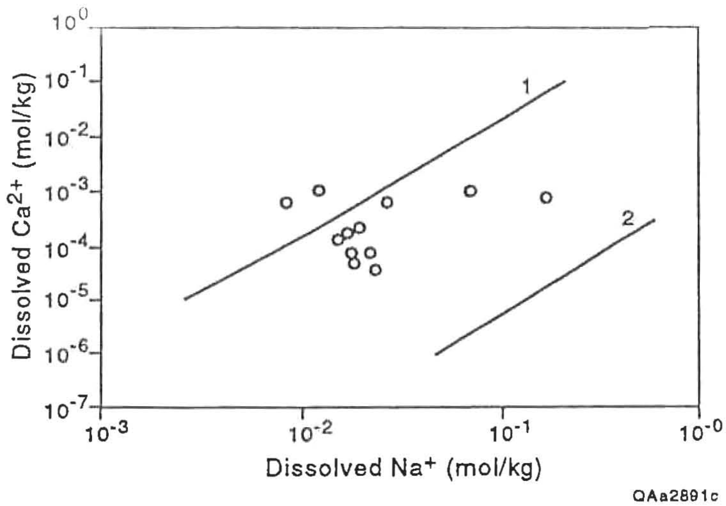

Figure 75. Comparison of measured and simulated concentrations of dissolved calcium and sodium in ground water at the SSC site. Bounding lines defined by the exchangeable Ca^{2+}/Na^{+} ratios of 3×10^{-5} (line 1) and 3.5 (line 2), dissolved oxygen of zero, and dilution of seawater by rainwater. Ca^{2+} and Na^{+} concentrations are more sensitive to Ca^{2+}/Na^{+} adsorbed-ion ratio than to dissolved oxygen concentration.

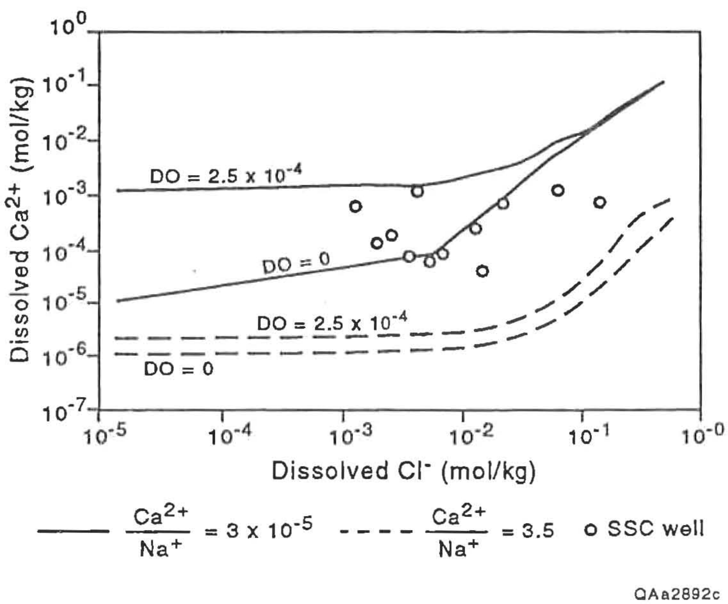

Figure 76. Comparison of measured and simulated ionic concentrations of Ca^{2+} as a function of dilution of seawater. Bounding lines defined by the exchangeable Ca^{2+}/Na^{+} ratios of 3×10^{-5} and 3.5, dissolved oxygen (DO) concentrations of 0 and 0.00025 mol/kg, and dilution of seawater by rainwater. Ca^{2+}/Na^{+} adsorbed-ion ratio is the primary control and dissolved oxygen is a secondary control.

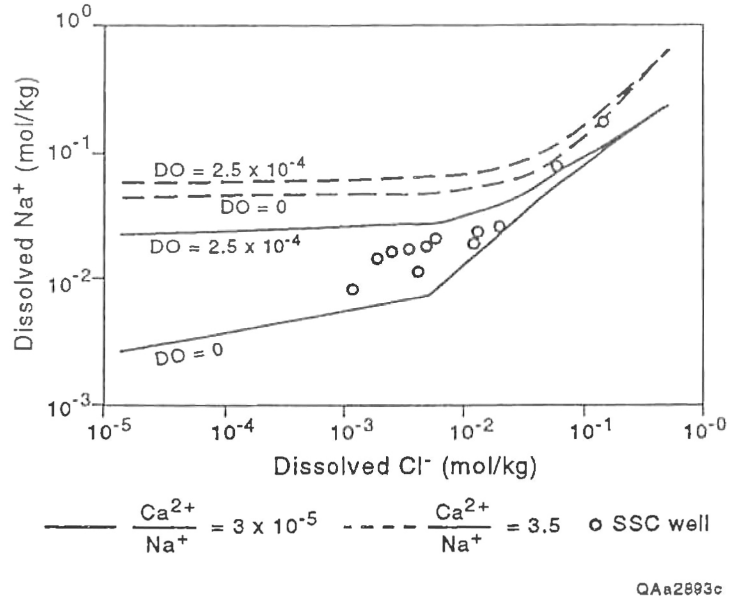

Figure 77. Comparison of measured and simulated ionic concentrations of Na^+ as a function of dilution of seawater. Bounding lines defined by exchangeable Ca^{2+}/Na^+ ratios of 3×10^{-5} and 3.5, dissolved oxygen (DO) concentrations of 0 and 0.00025 mol/kg, and dilution of seawater by rainwater. Note that positions of bounding lines defined by the exchangeable Ca^{2+}/Na^+ ratio are switched (compare to fig. 76).

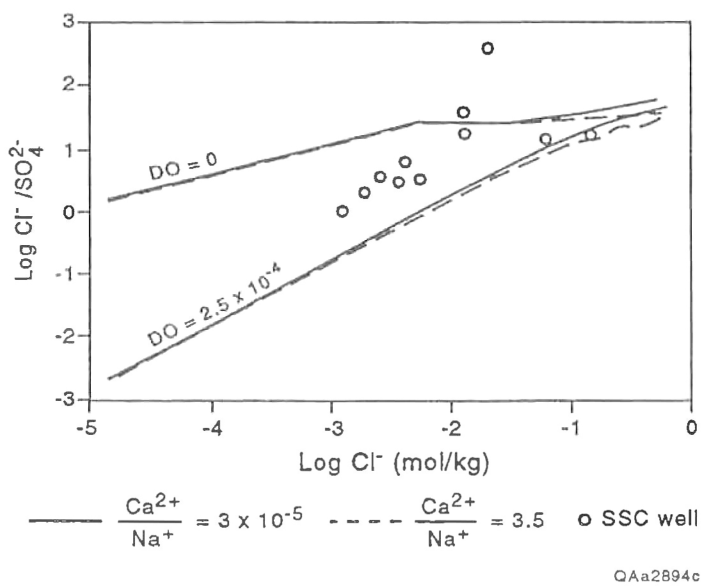

Figure 78. Comparison of measured and simulated Cl^-/SO_4^{2-} ratio as a function of dilution of seawater. Dissolved oxygen concentration is the main control on Cl^-/SO_4^{2-} ratio. Results are sensitive to exchangeable cations only at high salinity.

- **oxidation of pyrite with dissolved oxygen ranging between 0.0 to 2.5×10^{-4} moles/liter,** accompanied by related solution of calcite, and
- cation exchange in which adsorbed Na^+ in smectite is replaced by dissolved Ca^{2+} and Mg^{2+}.

Calcite solution is probably diffuse because there is no widespread occurrence of large vugs or solution cavities in the Austin Chalk. The scatter of data shown in figures 75 to 78 indicates that ground waters have been influenced by the above reactions to different extents in different places and stratigraphic units. Defining a unique set of reaction coefficients on the basis of cation or sulfate concentrations is not possible. The concentration of dissolved chloride, however, should indicate the relative amount of seawater dilution and, therefore, of ground-water flow. Since the upper Cretaceous section has been exposed in Ellis County to precipitation during part or most of the Tertiary and Quaternary Periods, there has been enough recharge and circulation of meteoric water to flush most seawater from pores in the low-permeability rock. However, flushing is incomplete, possibly because the rock is inhomogeneous with fractured zones having high permeability and unfractured rock having low permeability. In such situations, solute concentration might be controlled more by diffusion than by advective displacement (Domenico and Robbins, 1985). At low concentrations, Cl^- might be influenced by diffusion of solutes from unfractured rock as well as by advective flow within fractures.

APPLICATION TO GROUND-WATER FLOW AROUND INTERACTION HALLS

On the basis of the preceding geologic and hydrologic results and interpretation, it is possible to study in detail ground-water flow at specific sites around the SSC. The purpose of this study is to determine the size of the zone in which ground water would be captured, that is, drawn into the large excavations of interaction halls and adjacent tunnel segments owing to the local hydraulic-head gradient imposed by these openings. Additional studies are needed to locate optimum locations of ground-water monitoring wells and to predict travel time between specific SSC elements and a monitoring well.

The occurrence and movement of ground water in the vicinity of an interaction hall was studied in three tasks:

- calculation of the effect of drainage boreholes on effective permeability and total ground-water discharge into hall,
- modeling of ground-water flow and of capture-zone size over a range of assumed hydrogeologic properties, and
- analysis of the development and thickness of a possible "dry" zone adjacent to walls.

After excavation and construction, discharge to the experimental hall will result in a decline in hydraulic head and pore pressure in both weathered and unweathered bedrock within some distance from the hall. The amount of the hydraulic-head decline depends on the hydraulic conductivity of rock, the number and size of the drainage boreholes installed in the walls, and the effect of wall treatments such as application of a geotextile-material cover and shotcrete. Calculation of the capture zone around an interaction hall, therefore, is a complex, three-dimensional problem of ground-water flow that requires a numerical model. To develop a reasonable model in a minimum of time, it was necessary to simplify the description of hydrologic properties in the area around the interaction hall because it was not reasonable to account for the hydrologic details of each borehole. To estimate the effective radius of the ground-water capture zone, it is necessary to evaluate the discharge into the experimental hall and the effect of drainage design on equivalent hydraulic conductivity. This procedure also is used to evaluate how discharge and radius of influence are affected by drainage design.

Hydrogeologic Setting of Interaction Halls

Experimental halls IR5 and IR8 are located in the East Campus (fig. 64) and will house proton collision detectors during the 40-year life of the SSC project. This analysis focuses on IR8; similar findings are expected for ground-water flow around IR5. One main difference between the two settings is the elevation of the contact between Austin Chalk and the Ozan Formation. Construction of hall IR8 is designed to be 113.8 ft wide, 344.5 ft long, and 160 ft deep (34.7, 105, and 48.77 m, respectively). The top of the hall is about 32.8 ft (10 m) below the ground surface (The Earth Technology Corporation, 1990e). Almost 90 percent of the height of the interaction hall will be in the Ozan Formation; the bottom 6 m extends into Austin Chalk at IR8. Top of the Eagle Ford Formation lies approximately 460 ft (140 m) below the floor of hall IR8.

The experimental hall connects tunnel segments and will be surrounded by many boreholes to promote drainage of the rock adjacent to the interaction hall. The present design is for the boreholes to be drilled 120 ft (36.6 m) into hall walls at a slight upward angle.

Water levels in the shallow, weathered zone and deep unweathered bedrock generally mimic land surface (figs. 44, 45, and 49a). Recharge to and discharge from the unweathered marl occurs through the weathered zone. The water table in surficial weathered bedrock is regionally about 8 ft (2.44 m) below ground surface and in the East Campus within 4 ft (1.22 m) of ground surface. Downward-directed gradients in hydraulic head were predicted beneath topographic highs and upward gradients beneath topographic lows (fig. 51) so that water is recharged on upland hills and discharged to local seeps and streams (figs. 44, 45, 51, and 71b). Major topographic highs and lows are assumed to be ground-water divides in the ground-water flow system. Part of the ground-water flow in the Austin Chalk beneath the East Campus is derived from recharge on the chalk outcrop to the west of the East Campus (fig. 71b). The recharged ground water moves from the outcrop area and flows eastward beneath the Ozan Formation. Hydraulic head measured at well BE6, which has a screened interval in the uppermost Austin Chalk, is as much as 46 ft (14 m) above ground surface (fig. 48c). Variation in hydraulic head at wells BE6 and BIR81 during the period from 1990 through 1992 was less than 1 ft (0.3 m) (fig. 48c, u).

Analysis of Effect of Drainage Boreholes

This section quantifies the effect of drainage boreholes on effective permeability and ground-water discharge into an interaction hall, specifically IR8. The objectives are to assess the contribution of drainage holes to the total flow rate and to estimate the total discharge from the walls of the interaction hall. An analytical solution is developed that relates total discharge and effective permeability to the number and spacing of boreholes. Formulations were made for north and south walls, both with and without the large collider tunnel, and for the east and west walls. The solutions define the relative contribution of each borehole.

Discharge from a Single Drainage Hole

Assuming that average pressure (p_e) at a large radius from the drainage hole is constant and that pressure at the interior surface of the hole is zero, the governing equation for a drainage hole can be written as

$$r\frac{\partial^2 p}{\partial r^2}+\frac{\partial p}{\partial r}=0 \qquad r_w<r<r_e\,, \tag{17}$$

subject to the following boundary conditions

$$p(r_w)=0\,, \tag{17a}$$

$$p(r_e)=p_e\,, \tag{17b}$$

where r is the radial coordinate, r_w and r_e are the interior and exterior radii, respectively, of the drainage hole, and p_e is the average pressure on the exterior boundary. The solution of equation (17) is

$$p(r)=p_e\frac{\ln(r/r_w)}{\ln(r_e/r_w)}\,. \tag{18}$$

Discharge, q, of ground water from a drainage hole of unit length can be obtained from the following equation

$$q=2\pi Kr\frac{\partial p}{\partial r} \tag{19}$$

where K is the conductivity of rock. Substituting equation (18) into (19) yields

$$q = 2\pi K \frac{p_e}{\ln(r_e / r_w)} \tag{20}$$

Assuming a linear distribution of pressure along the borehole and zero gauge (atmospheric) pressure on the wall surface of the experimental hall, average pressure on the exterior boundary is

$$p_e = \frac{p_c}{L} x \tag{21}$$

where L is the horizontal length of the drainage holes and

$$p_c = \gamma z \tag{22}$$

where γ is the specific weight of water and z is the vertical coordinate of drainage hole (depth from ground surface).

Discharge from Multiple Boreholes

Drainage holes drilled into the wall of the experimental hall generally enhance the drainage of the rock. These drainage holes are closely distributed (fig. 79), and the pressure distribution around these holes overlaps; therefore, it is necessary to analyze their total discharge. In general, according to (20), the general pressure distribution around a borehole resembles

$$p = \frac{q}{2\pi K} \ln r \tag{23}$$

where r is the radial distance as measured from the center of the well. According to the linearity of Laplace's equation (17), the sum of n of these terms for n boreholes is also the solution of (17). Muskat (1982) provides a general equation of pressure distribution for multiple boreholes:

$$p_j = c + \frac{q_j}{2\pi K} \ln r_j + \frac{1}{2\pi K} \sum_{i \neq j} q_i \ln d_{ij} \tag{24}$$

$$p_e = c + \frac{1}{2\pi K} \Sigma q_i \ln R \tag{25}$$

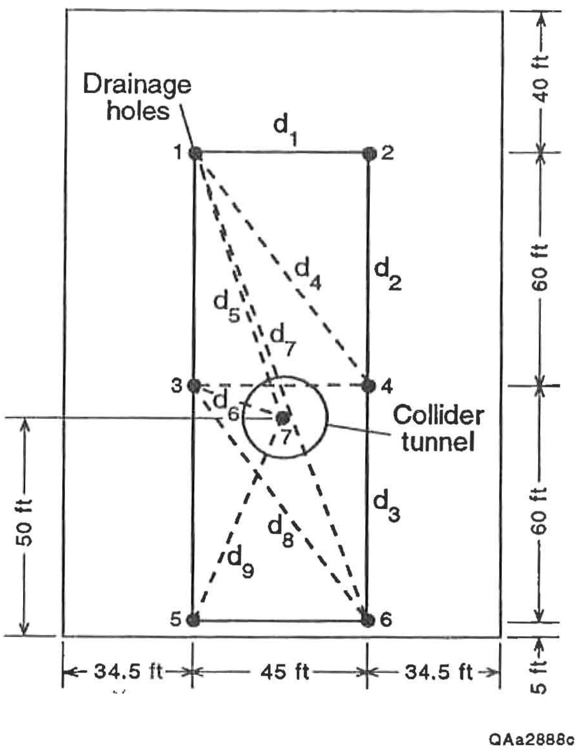

Figure 79. Location of and distances between drainage boreholes on north wall of interaction hall IR8.

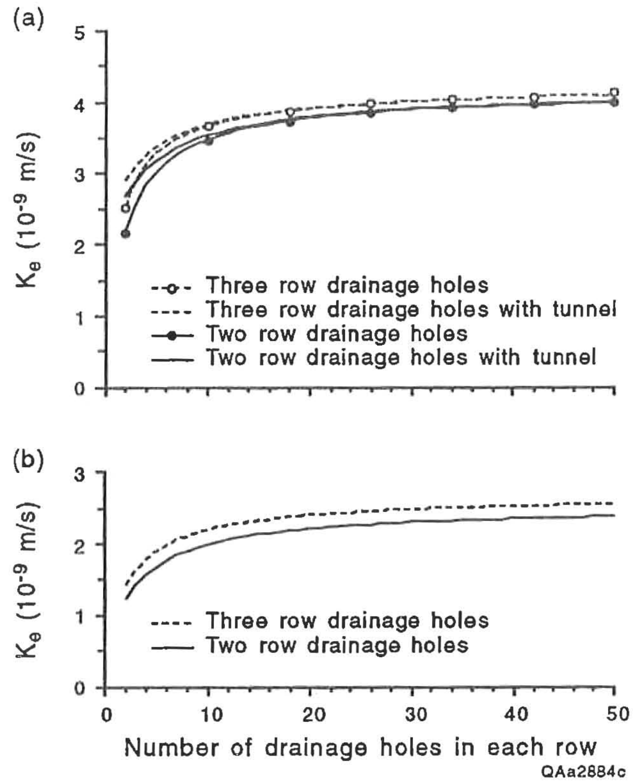

Figure 80. Discharge rate in interaction hall IR8 as a function of number of drainage holes on north and south walls (a) and east and west walls (b). Discharge calculated by program MWELL.

where p_j is pressure in borehole j, c is an unknown constant, q_i and q_j are the discharge of boreholes i and j, respectively, d_{ij} is the distance between two boreholes i and j (fig. 79), R is the radius of the external boundary of the individual and overlapping areas of affected pressure around all of these holes, and p_e is the average pressure at this boundary. Assuming that p_e is known and $p_j = 0$ for $j = 1, 2, 3, \ldots\ldots$ n at the inner boundary of a drainage borehole ($r_j = r_n$), because the borehole is inclined toward the hall and freely drains, to solve for flow rate q_j ($j = 1, 2, 3, \ldots\ldots$ n), equation (24) is rewritten as

$$2\pi K(p_j - c) = q_j \ln r_j + \sum_{i \neq j} q_i \ln d_{ij} \qquad i, j = 1, 2, 3, \ldots\ldots n. \tag{26}$$

There are n + 1 combinations of equations (24) and (25) corresponding to n + 1 unknowns q_j and c. Because $p_j = 0$ for $j = 1, 2, 3, \ldots$n, we can solve for c from (25) and substitute it into (26) to obtain the following equations

$$2\pi K p_e = q_j \ln(R / r_j) + \sum_{i \neq j} q_i \ln(R / d_{ij}) \qquad i, j = 1, 2, 3, \ldots\ldots n. \tag{27}$$

Solving equation (27) gives flow rates for all of the drainage holes.

Equation (27) is based on the concept of an aquifer of infinite areal extent, or very deep boreholes. Because the water table at experimental hall IR8 is located about 8.5 ft (2.5 m) below surface, the above equations are not suitable for our problem. Using superposition, however, hypothetical "image" boreholes suitably located above the discontinuity or boundary allow analysis of the pressure distribution and flow rate as if the aquifer were of an infinite areal extent. Assuming that water table is a no-flow boundary, and using the same size and distribution of the real boreholes below the water table as "image boreholes," the equations (24) and (25) can be changed to

$$p_j = c + \frac{q_j}{2\pi K}(\ln r_j + \ln r_{j^*}) + \frac{1}{2\pi K}\sum_{i \neq j}^{m} q_i(\ln d_{ij} + \ln d_{i^* j}) \tag{28}$$

and

$$p_e = c + \frac{1}{\pi K}\sum_{i=1}^{m} q_i(\ln R) \tag{29}$$

where d_{i^*j} is the distance between the nodes i^* (image borehole) and j (real borehole).

Equation (28) is rewritten as:

$$2\pi K(p_j - c) = 2q_j \ln r_j + \sum_{i \neq j} q_i (\ln d_{ij} + \ln d_{i^*j}) \ . \tag{30}$$

According to design, all drainage boreholes are declined and water can freely flow out. Thus, we consider the pressure in the drainage borehole zero, that is,

$$p_j = 0,\ j = 1, 2, 3, \ldots\ldots n \tag{31}$$

then equation (30) can be written as

$$2\pi K p_e = q_j \ln \frac{R^2}{r_j^2} + \sum_{i \neq j} q_i \ln \frac{R^2}{d_{ij} d_{i^*j}},\ i, j = 1, 2, 3, \ldots\ldots n\ . \tag{32}$$

Equation (32) can also be written as a matrix form

$$\begin{bmatrix} C_{11} & C_{12} & C_{13} & \cdots & C_{1n} \\ C_{21} & C_{22} & C_{23} & \cdots & C_{2n} \\ C_{31} & C_{32} & C_{33} & \cdots & C_{3n} \\ \cdot\cdot & \cdot\cdot & \cdot\cdot & \cdots & \cdot\cdot \\ C_{n1} & C_{n2} & C_{n3} & \cdots & C_{nn} \end{bmatrix} \begin{Bmatrix} q_1 \\ q_2 \\ q_3 \\ \cdot\cdot \\ q_n \end{Bmatrix} = \begin{Bmatrix} 2\pi K p_e \\ 2\pi K p_e \\ 2\pi K p_e \\ \cdots \\ 2\pi K p_e \end{Bmatrix} \tag{33}$$

where

$$C_{ij} = \ln \frac{R^2}{r_i^2} \ for\ i = j \tag{34}$$

and

$$C_{ij} = \ln \frac{R^2}{d_{ij} d_{i^*j}} \ for\ i \neq j \tag{35}$$

where n is the total number of real boreholes. It is also noted that $d_{ij} = d_{ji}$ and $d_{i^*j} = d_{j^*i}$. Using these relationships, therefore, the computation of coefficients in equation (33) can be largely reduced.

According to equations (32) to (35), a computer code MWELL was developed to evaluate the flow rate of multi-borehole systems. The code consists of two parts—one is to generate the geometric matrix based on the borehole locations and the other is to solve for flow rates using the regular Gauss elimination method. The listing of code MWELL is documented in Bureau of Economic Geology quality-assurance files.

After obtaining the flow rate of an individual layer, total discharge can be defined as

$$q_d = \sum_{j=1}^{n} q_j \ . \tag{36}$$

Water pressure is assumed to be linearly distributed along each borehole, and the average value can be determined using (21) with an average length of the drainage holes (for example, 120 ft [36.58 m]). The total flux from the borehole and the tunnel then can be written as

$$Q_d = q_d L \tag{37}$$

where L is the length of the drainage hole in horizontal direction.

Calculation of Flow Rate for Experimental Hall

Figure 79 illustrates one possible distribution of drainage holes on either the northern or southern wall of an experimental hall such as IR8. The spacing of drainage holes in the vertical direction is 60 ft (18.28 m), and the horizontal distance between the holes in the x-direction is 45 ft (13.71 m). Two cases are considered: (1) the collider tunnel is treated as a drainage hole with a very large radius and (2) the collider tunnel is considered to have an impermeable lining such as precast concrete. According to figure 79, the distance between nodes is

$$\begin{aligned}
d_4 &= \sqrt{d_1^2 + d_2^2} \\
d_5 &= \sqrt{(d_2 + d_3 - d)^2 + d_1^2 / 4} \\
d_6 &= \sqrt{(d_3 - d)^2 + d_1^2 / 4} \\
d_7 &= \sqrt{(d_2 + d_3)^2 + d_1^2} \\
d_8 &= \sqrt{d_3{}^2 + d_1^2} \\
d_9 &= \sqrt{d^2 + d_1^2 / 4}
\end{aligned} \tag{38}$$

For case 1 of a leaky tunnel, given the geometry shown in figure 79, d_1 = 45 ft (13.72 m), $d_2 = d_3$ = 60 ft (18.28 m), r_i = 0.417 ft (0.127 m) for i = 1, 2, 3, . . 6, and r_7 = 18 ft (5.48 m) for the collider tunnel. The average exterior boundary pressure, p_e, is 95.14 ft (29 m). The radius of exterior boundary, R, is 328.08 ft

(100 m), set to include the entire area with effected pressure around all of the drainage holes. Equation (38) is used to calculate the other distances, d_i, for i = 4, 5, 6, 7. Assuming the tunnel acts as a drainage borehole with a large radius, proportional flow rate out of each drainage hole is:

$$q_1 : q_2 : q_3 : q_4 : q_5 : q_6 : q_7 = 1 : 1 : 0.84 : 0.84 : 1.32 : 1.32 : 3.09. \tag{39}$$

These ratios show that the relative rate of ground-water discharge from the collider tunnel (q_7) might be about 3.1 times that out of the uppermost drainage holes. The middle and the bottom drainage holes account for less discharge because of the large effect of the nearby collider tunnel.

For case 2, which assumes that precast concrete lining and grout effectively make the tunnel wall impermeable, the flow rate, q_7, is zero, and proportional flow rate out of the other drainage boreholes is

$$q_1 : q_2 : q_3 : q_4 : q_5 : q_6 : q_7 = 1 : 1 : 1.03 : 1.03 : 1.27 : 1.27 : 0 . \tag{40}$$

These ratios show that when the collider tunnel wall is impermeable, the top and middle rows of drainage boreholes provide almost the same flow rate, and the bottom row of drainage boreholes provides slightly higher flow rate.

Discharge and Distribution of Drainage Holes

Discharge from drainage holes is dependent on the number of drainage holes, hydraulic conductivity of rock, and the radius of drainage holes. Darcy's law states that the flow rate proportionately increases with conductivity, K (equation [20]). The computer code MWELL uses equation (33) to calculate the variation of flow rate with number and location of drainage boreholes.

Figure 80 shows total discharge as a function of number of drainage holes in each row, assuming the radius of the exterior boundary, R, is 328.08 ft (100 m), the radius of drainage holes, r_w, is 0.417 ft (0.127 m), average pressure, p_e, is 95.12 ft (29.0 m), and hydraulic conductivity, K is 1.64×10^{-4} ft/d (5.8×10^{-10} m/ s). Drainage holes might be arrayed, for example, in rows of two or three. When there are few drainage holes per row or per elevation, increasing the number of drainage holes markedly increases the flow rate. Figure 80a shows that the difference between the two- and three-row drainage design is small in the north and south walls, suggesting that two-row drainage holes may be most cost-effective for maximizing ground-water inflow and drainage-zone size when few drainage holes per row are used. Adding a few columns of boreholes allows two rows to yield the same discharge as three rows.

Figure 80a also shows that when only a few drainage boreholes (<10) are used in the north and south walls, the assumption of whether or not the collider tunnel wall remains permeable has a significant effect on calculated discharge. Positioning the elevation of rows of drainage holes relative to the tunnel would be important. With an increased number of drainage boreholes in either two or three rows, however, the contribution of the tunnel significantly decreases even if its wall is permeable.

Discharge from two and three rows of drainage holes in the east and west walls is shown in figure 80b; those results ignore shafts and tunnels behind the eastern and the western walls. The difference in discharge between two- and three-row designs is greater for the east and west walls than for the north and south walls, which include the collider tunnel, because of the difference in expanse of the walls. When the number of drainage holes in each row is small for east and west walls, the three-row design may provide a better solution (for example, using a 3×6 drainage hole arrangement, $q_{3\times6} = 6.7 \times 10^{-8}$ m^3 s^{-1} m^{-1}, and using a 2×9 arrangement, $q_{2\times9} = 6.4 \times 10^{-8}$ m^3 s^{-1} m^{-1}).

Equivalent Hydraulic Conductivity

To determine the position of the water table and discharge into the experimental hall after excavation, it is necessary to estimate the equivalent hydraulic conductivity of rock. Ground-water flow rate near the hall will be increased by the effect of the drainage holes. Because a three-dimensional analysis would be difficult, the drainage holes are treated as small openings uniformly distributed in the rock, as if they proportionately increase the hydraulic conductivity of the bedrock.

To define hydraulic conductivity of the rock equivalent to the effect of the boreholes, consider the flow balance

$$q_d L + q_s = q_{se} \tag{41}$$

where q_d is the total radial flow rate from all drainage holes per unit length, q_s is the lateral flow rate from rock with the conductivity K, L is the length of the drainage boreholes, and q_{se} is the flow rate from the rock with the equivalent conductivity K_e. Assuming that the outer radius of the drainage-hole area equals half the distance between two drainage holes, the flow rate, q_s, is

$$q_s = K \frac{\partial p}{\partial x} A_s \tag{42}$$

where A_s is the surface area of the experimental hall walls, excluding borehole and tunnel cross-sectional areas, and x is the coordinate perpendicular to the wall surface. Similarly, an expression for q_{se} is

$$q_{se} = K_e \frac{\partial p}{\partial x} A \tag{43}$$

where K_e is the equivalent conductivity, and A is the surface area including the drainage holes and the tunnel on the walls of the experimental hall. Assuming $p = zx/L$ and substituting it into (41), (42), and (43), the equivalent conductivity is (with $A_s/A \cong 1$):

$$K_e = K + \frac{q_d L^2}{Az} . \tag{44}$$

Equation (44) shows that the equivalent conductivity is a nonlinear function of drainage hole length and a linear function of flow rate, q_d, which depends on the number of boreholes in that layer, the radius of drainage holes, r_e, and on whether the tunnel acts as a drainage hole. Figure 81 illustrates equivalent hydraulic conductivity as a function of number of the drainage holes and varying with effect of the tunnel. The calculation assumes that the water table is drawn down, relative to the original water-table position, to half the height of the excavation. Equivalent hydraulic conductivity is about

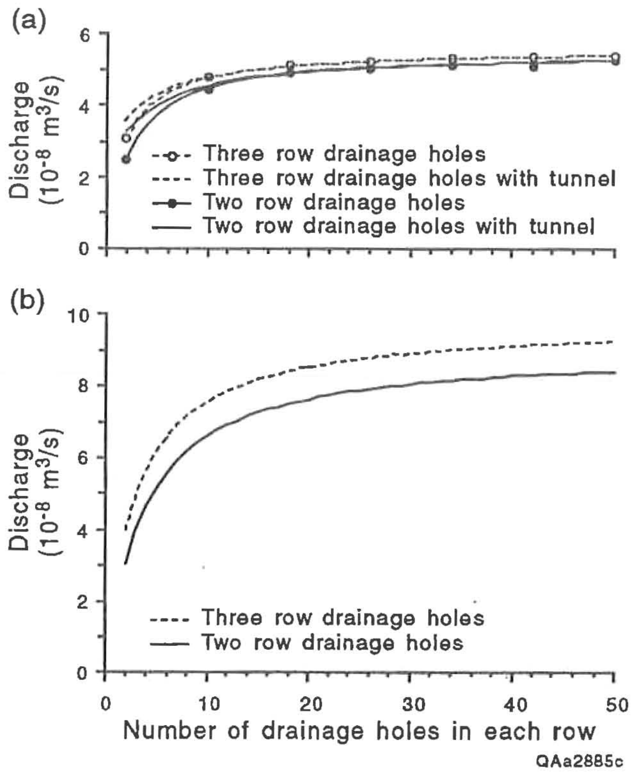

Figure 81. Equivalent hydraulic conductivity (K_e) as a function of number of drainage holes in the southern or northern walls (a) and in the eastern or western walls (b). As total number of boreholes decreases, K_e approaches K_{Ozan}, the hydraulic conductivity of undisturbed Ozan Formation.

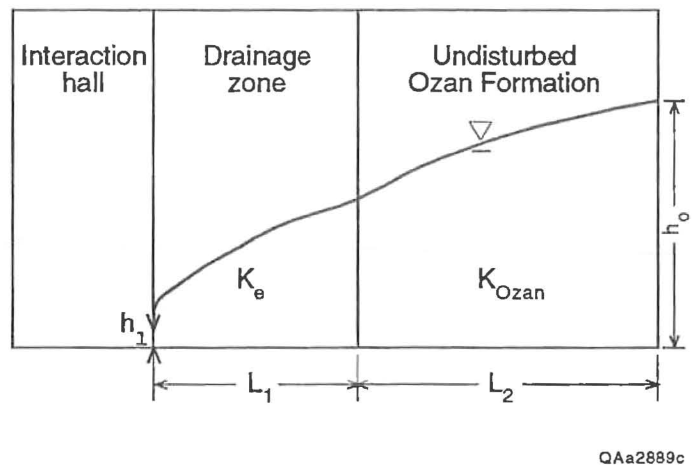

Figure 82. Profile of unconfined water table in porous media with two different effective hydraulic conductivities. K_e is equivalent hydraulic conductivity determined by drainage boreholes, and K_{Ozan} is hydraulic conductivity of undisturbed bedrock. L_1 is length of drainage boreholes, and L_2 is distance beyond the drainage zone to the limit of the zone of influence of the interaction hall on hydraulic head.

10 times greater than the hydraulic conductivity of bedrock beyond the influence of the drainage boreholes (1.64×10^{-4} ft/d [5.8×10^{-10} m/s]). Whether the tunnel wall is permeable or not accounts for only a minor difference in effective hydraulic conductivity (fig. 81a). Equivalent hydraulic conductivity in the northern and the southern walls is higher than that in the eastern and western walls because of the small surface area and proportionately large number of drainage holes on the northern and southern walls. Because L, z, and K are constant, only the term q_d/A makes a difference according to equation (44) (fig. 81a, b).

Flow from the Wall Surface

Ground-water discharge from the wall surface will be limited by hydraulic conductivity of the rock, hydraulic gradient, and hydraulic conductivity of material used to cover the rock face, assuming that saturated conditions are maintained. Because of the drainage holes, the region behind the wall can be divided into two domains of differing effective hydraulic conductivity (fig. 82). Water level remains constant at a distance L_2 from the domain of the drainage holes, which is at a distance (L_1) of 120 ft (36.58 m) from the interaction hall. The unknown distance ($L_1 + L_2$), the radius of influence on hydraulic head, has a large effect on the calculated discharge. Flow rate for different values of L_2 were calculated, with $K_e = 10^{-3.21}$ ft/d ($10^{-8.66}$ m/s) for the northern and southern walls, and $K_e = 10^{-3.25}$ ft/d ($10^{-8.62}$ m/s) for the eastern and western walls. A 2×2 arrangement of drainage boreholes was assumed for the northern and southern walls, and a 3×6 arrangement was assumed for the eastern and western walls. As a preliminary analysis, discharge (Bear, 1972) is given by:

$$q_s = \frac{h_o^2 - h_l^2}{2[L_1 / K_1 + L_2 / K_2]} \tag{45}$$

where q_s is flow rate per unit width of wall, h_o is the original hydraulic head, h_l is the water table at the seepage face (set = 0 here), L_1 is the width of the domain with drainage holes, and L_2 is the distance across rock without drainage holes to the point where hydraulic head is unafftected by the interaction hall. The total flow rate, Q_s, is

$$Q_s = q_s W \tag{46}$$

where W is the width of the wall surface. Assuming h_o = 170 ft (51.82 m) and h_l = 0 ft, figure 83 gives flow rate, q_s, as a function of the distance L_2 and number of boreholes. At a given discharge rate, the radius of influence is greater beyond the eastern and western walls and is similar to that beyond the northern and southern walls. When L_2 is large, the tunnel makes an insignificant contribution to total discharge even when its walls are assumed to be permeable.

Summary

The radius of influence and zone of capture of ground water by an interaction hall depends on the amount of ground-water inflow and hydraulic conductivity around the hall. Ground-water flow into experimental halls consists of radial flow into drainage holes and possibly the collider tunnel and lateral flow from the walls and floor of the experimental hall. Solving for total inflow rate is a three-dimensional problem because those flow components affect each other and depend on tunnel size, the locations of drainage holes, size of drainage holes, the conductivity of the rock around the experimental hall, permeability of material covering the walls and floor, and water-table elevation. Three-dimensional flow simulations would involve a large computation beyond the scope of this study. Because the height of the experimental hall is about the same as its width, simulations without accounting for drainage holes would greatly underestimate discharge. To simplify the problem, an analytical solution combining interacting effects of drainage boreholes and possibly the tunnel is considered to determine effective hydraulic conductivity around the interaction hall and to calculate the flow rate.

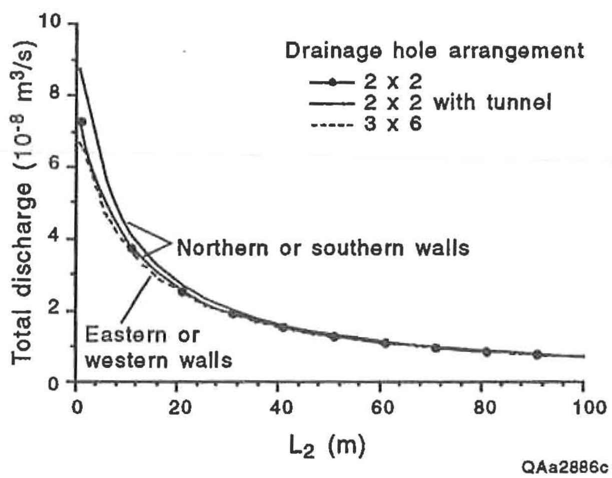

Figure 83. Total ground-water discharge into the experimental hall as the function of L_2, the distance beyond the drainage zone to the limit of the zone of influence of the interaction hall on hydraulic head. L_2 increases and discharge decreases with time after interaction hall is excavated.

Analysis of ground-water flow at the experimental hall IR8 shows that

- Discharge from drainage holes on the N-S or the E-W walls is different (fig. 83). The collider tunnel yields the highest flow rate if hydraulic conductivity of precast concrete is not much less than that of bedrock (equation [40]). The uppermost drainage holes provide the second highest flow rate, and two middle holes produce the least because of the effect of the tunnel. When the tunnel wall is considered impermeable, the bottom row of drainage holes provides the greatest discharge whereas the top and middle rows have similar, lower discharge.
- The distribution of drainage holes might be limited to two rows on northern and southern walls, each with more columns of boreholes (fig. 80a), and located at the middle and the bottom of the wall. This design would increase the discharge and drawdown. Boreholes high on the wall might be left above the water table and become ineffective.
- When only a few drainage boreholes are used in the N-S walls, a tunnel with a permeable wall functions as a large drainage borehole; however, its discharge decreases with increase in number of drainage boreholes.
- Equivalent hydraulic conductivity depends on the number of holes (fig. 81). However, incremental gain in hydraulic conductivity falls off when there are too many holes.
- Total flow rate is larger from the eastern and western walls than from the southern and northern walls (fig. 83), especially when L_2 is very small. For the case where permeability of the tunnel wall is assumed to be similar to that of bedrock, flow rate in N-S walls is higher, although tunnel discharge is reduced as the distance of influence, L_2, becomes large.

Flow rates from the drainage holes and the collider tunnel depend on the number of holes and the size and permeability of the tunnel wall. Based on multi-well theory, an arrangement of drainage holes of 2×2 or 2×3 (three in horizontal direction) can be used for the northern and southern walls, and an arrangement of drainage holes of 3×6 (6 holes in horizontal direction) can be used for the eastern and the western walls for efficient draining of water. The equivalent hydraulic conductivity in the region containing drainage holes may change significantly when the number of drainage holes is large.

Evaluation of Capture-Zone Size

A two-dimensional numerical model was constructed to determine the size of the capture zone around interaction hall IR8. The model was oriented generally north-south along the long axis of the hall, as shown by line C–C′ (fig. 9). Sensitivity of the capture-zone estimate to uncertainty in estimates of hydraulic conductivity and dimensions of the zone with drainage boreholes and to the hydraulic conductivity of the Ozan Formation was determined. Results of transient simulations made with different parameter values were compared at a simulation time of 20 years for the sensitivity analysis.

Model Design and Calibration

MODFLOW, a three-dimensional, block centered, finite-difference ground-water flow model (McDonald and Harbaugh, 1988), was used to simulate ground-water flow. All simulations used the strongly implicit procedure to solve the finite-difference equations. Convergence for hydraulic-head changes was 0.001 ft (0.0003 m). MODPATH (Pollock, 1989) was used to calculate ground-water pathlines.

A two-dimensional model grid was aligned approximately north-south along line C–C′ (fig. 9) from Red Oak Creek to Bone Branch through the long axis of the interaction hall. One hundred and twenty columns and 22 layers of varying lengths and widths were used; node width was least near the hall and increased away from the hall. The thickness of the top layer, layer 1, represented the distance from land surface elevation to base of the marl. Thickness of the top layer was assigned cell by cell to reflect surface topography. The remaining 21 layers were in the chalk. Layer 2 was uniformly 19.7 ft (6 m) thick and represented the thickness of chalk exposed in the hall. Layers 3 to 22 were all uniformly 16.4 ft (5 m) thick. The base of the model, 347.8 ft (106 m) below the top of the chalk, was twice the depth of the hall and was assigned as a no-flow boundary. This distance is generally accepted as the distance at which the influence of an excavation is minor. The top layer was considered unconfined and the remaining layers were confined. Water levels in the unconfined layer were allowed to fall below the top of the layer, that is, saturated thickness varied. The general head boundary

(GHB) package of MODFLOW was used to represent flow between the uppermost layer of the model and the weathered zone, which was not explicitly included in the model. The vertical conductivity of the Ozan Formation ($10^{-7.05}$ ft/d [$10^{-12.5}$ m/s]) multiplied by unit distance was assigned as the GHB conductance term. Lateral boundaries were set at apparent hydrologic boundaries at topographically low elevations in the valleys of Bone Branch to Red Oak Creek and were considered no-flow boundaries. The model was executed as steady-state and transient simulations.

Hydraulic conductivity was assigned on the basis of tests of SSC monitoring well BIR81 (tables 14 and 28) and were assumed to be representative throughout the model domain. Wickham and Dutton (1991) showed that the ratio of horizontal hydraulic conductivity to vertical hydraulic conductivity, called the anisotropy ratio, needs to be ≥100 to accurately simulate bedrock leakage to a surficial aquifer overlying bedrock. An anisotropy ratio of 116 was determined by calibration of the Ellis County model. Freeze and Cherry (1979) reported that whereas the anisotropy ratio calculated from measurements of oriented core samples of clays and shale seldom exceeds 10 and is usually less than 3, the anisotropy ratio calculated on a regional or field scale is commonly ≥100.

A qualitative calibration was performed to ensure that model results were consistent with results of the West Campus and Ellis County regional models and seemed physically reasonable and to ensure that simulated hydraulic head roughly matched measured water level at monitoring well BIR81. The model was initially executed as a steady-state model without the interaction hall to establish a pre-excavation baseline. The calibrated model then was adjusted to include the drawdown and change in hydraulic conductivity imposed by the interaction hall.

Table 28. Parameters used in calculating inflow from drainage boreholes.

	North/South	East/West
Height (ft)	160	160
Width (ft)	113.8	344.5
Exterior boundary (R, ft)	95.12	164.04
Radius of drainage holes (r_w, ft)	0.417	0.417
Average pressure (p_e, ft)	95.12	95.12
Hydraulic conductivity (K, ft/d)	1.64×10^{-4}	1.64×10^{-4}

Effects of the interaction hall on ground-water flow were studied with transient simulations. Parameters such as recharge and discharge, were kept constant. The hall was assumed to be instantaneously excavated, that is, the hall was excavated at time = 0 in the transient model. A seepage face was assumed to form 32.8 ft (10 m) above the bottom of the hall; above the seepage face the bedrock would be unsaturated. Seepage-face height was varied as part of the sensitivity analysis. The nine finite-difference blocks within the interaction hall were reset to constant-head blocks, with hydraulic head assigned 32.8 ft (10 m) above the hall bottom. Flux through the constant-head blocks representing the walls and floor of the interaction hall represented the amount of flow into the hall. The zone with drainage boreholes was included as a zone of increased equivalent horizontal hydraulic conductivity in the Ozan Formation. Vertical conductivity of the Ozan remained unchanged within the drainage zone.

Model Results

The pre-excavation, steady-state model shows recharge moving downward beneath the surface-water divide, laterally beneath the flanks of the interstream area, and upward beneath the valleys of Red Oak Creek and Bone Branch (fig. 84a). This reflects the conceptual model and boundary conditions imposed on the numerical simulation.

Response of hydraulic head in the interaction hall vicinity is slow. For example, >100,000 yr is required to approach a steady-state solution. Water-level decline is slow in the drainage zone and very slow in the marl (fig. 85a). The slow response appears to be confirmed by preliminary data from wireline piezometers at the S30 shaft excavation (Roy Cook, personal communication, 1993). Drawdown in the chalk is faster, and its influence extends much farther than in the marl (fig. 85b). The rate of drawdown is faster in the zone with drainage boreholes and slower farther from the interaction hall in undisturbed marl (fig. 86a).

The large interaction hall markedly changes particle pathlines (compare fig. 84a and b). The hall functions as a drain, collecting water from around the hall of marl and chalk. Water entering the

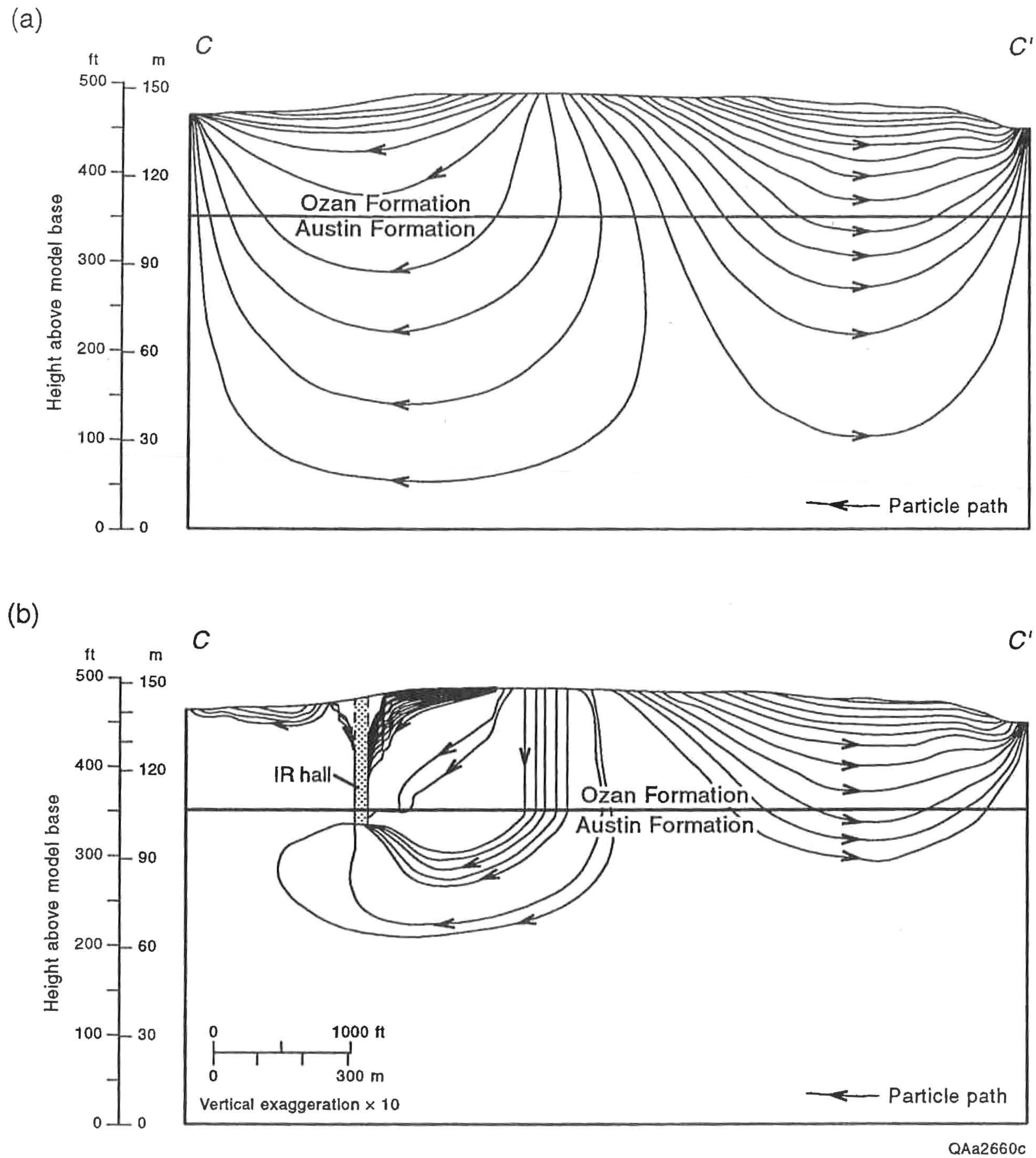

Figure 84. Particle paths simulated in the interaction hall model along profile C–C′ (fig. 9). (a) Pre-excavation at steady state and (b) post-excavation particle paths after 20 years.

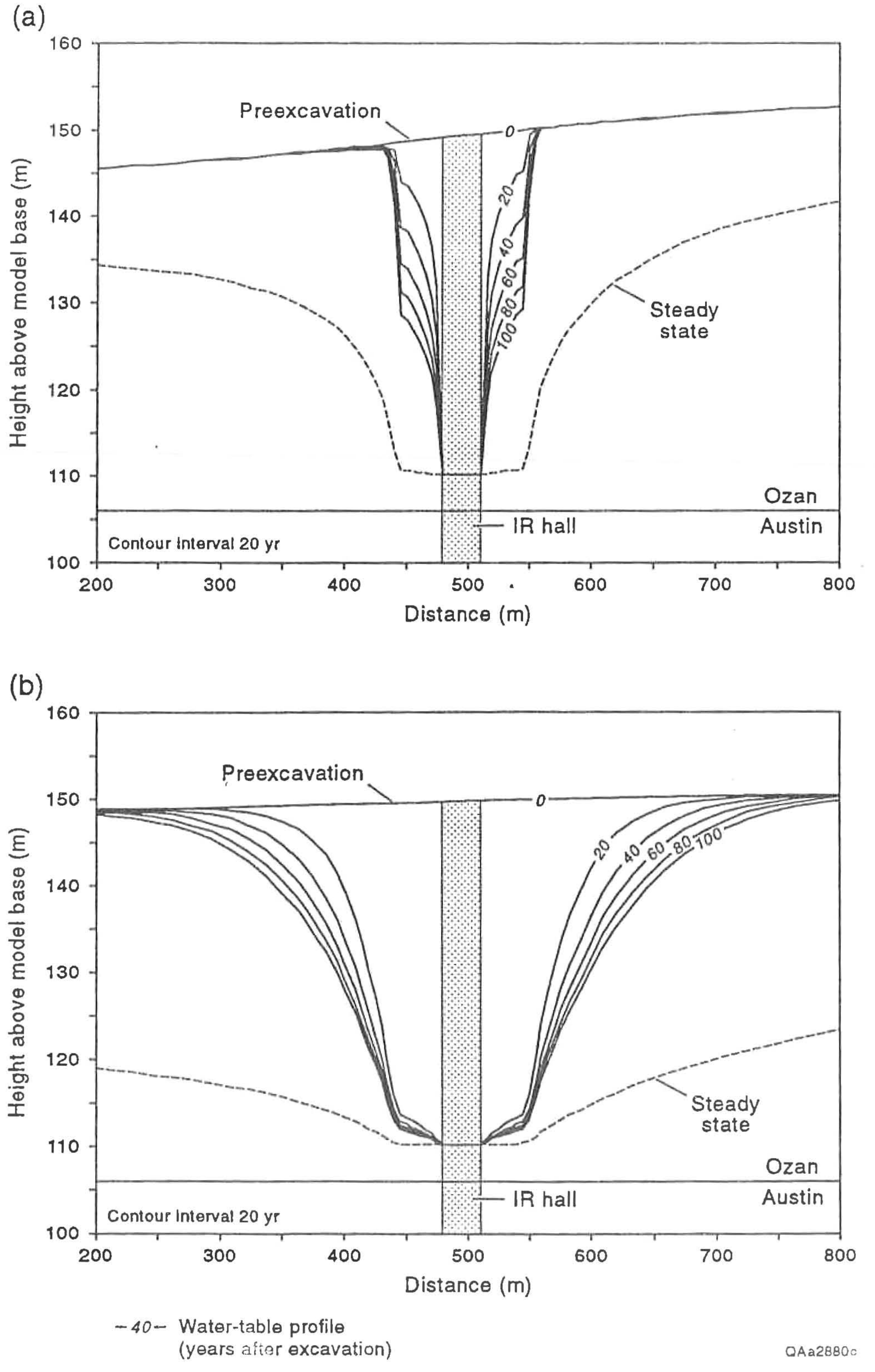

Figure 85. Profiles of decline in (a) unconfined water table in Ozan Formation (layer 1) and (b) confined potentiometric surface in Austin Chalk (layer 2). Steady state profile develops after approximately 100,000 yr. Distance is from south end of profile C-C' (fig. 9).

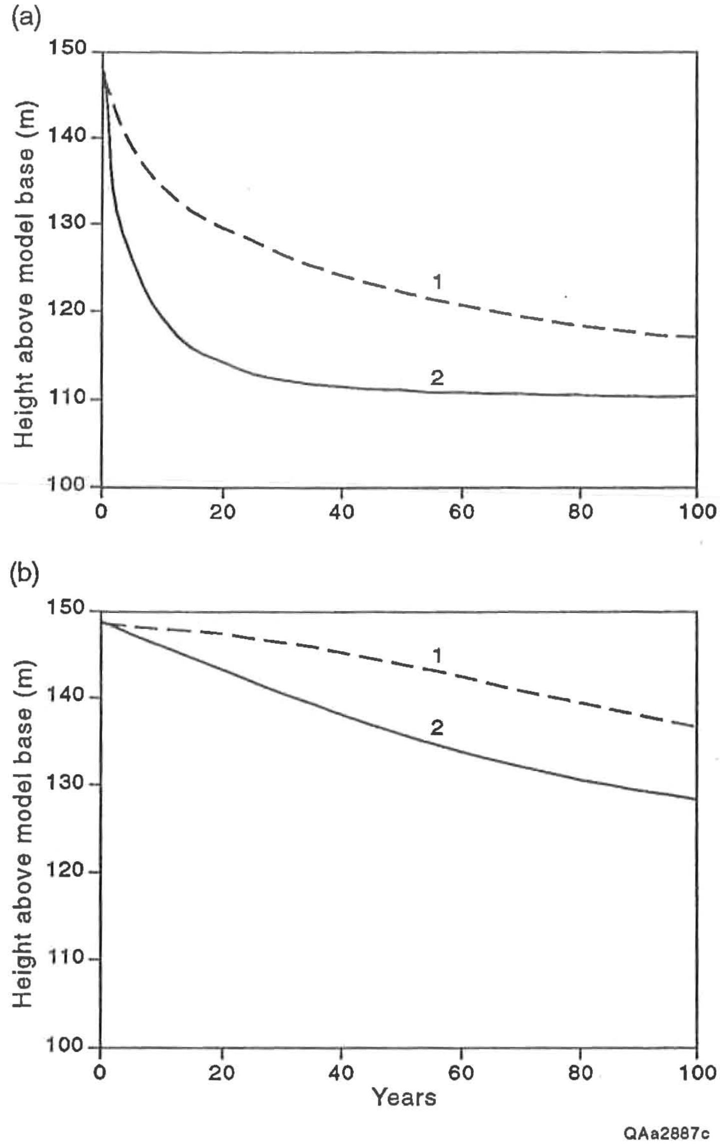

Figure 86. Hydrographs showing rates of water-level drawdown for (a) block (1, 35) located within the drainage zone just outside the interaction hall and (b) block (1, 42) located just outside the drainage zone. Line 1 shows drawdown for an equivalent hydraulic conductivity (K_e) approximately 10 times hydraulic conductivity of the Ozan Formation (K_{Ozan}). Line 2 shows drawdown for K_e approximately 100 times K_{Ozan}.

hall from the seepage face on the hall walls is ~10 times the inflow through the chalk floor. At 20 yr, flow rate into the hall from the walls is $10^{-0.24}$ ft^3/d ($10^{-6.73}$ m^3/s), while flow rate into the hall from the bottom is $10^{-1.34}$ ft^3/d ($10^{-7.82}$ m^3/s).

Sensitivity

Hydraulic conductivity of the Ozan Formation was initially assigned on the basis of tests at monitoring well BIR81. Alternatively, estimates of a geometric mean of hydraulic conductivity might be used, which would be higher than the actual measured value from BIR81. The geometric mean commonly is assumed to be the "expected value" of hydraulic conductivities on a regional scale and is therefore used where site-specific data are absent. The sensitivity-analysis approach allows the effect of this uncertainty on predicted growth of the ground-water capture zone to be evaluated.

Sensitivity of simulated hydraulic head in the marl to uncertainty in hydraulic conductivity of the marl is slight (fig. 87a). When hydraulic conductivity is increased by two orders of magnitude, water-level decline is more in the marl and less in the drainage zone. Hydraulic-head drawdown in the chalk also is relatively unaffected by uncertainty in hydraulic conductivity of the marl, particularly within the drainage zone (fig. 87b).

Figure 88 compares the size of the zone of ground-water capture for three cases:

- no drainage boreholes, such that the hydraulic conductivity is constant with distance from the interaction hall;
- equivalent hydraulic conductivity, calculated by equation (44) and previously assumed parameter values, is approximately 10 times greater than the undisturbed hydraulic conductivity of the Ozan Formation as measured at BIR81 (1.64×10^{-4} ft/d [5.8×10^{-10} m/s]); and
- additional boreholes or changed configuration of boreholes increases equivalent hydraulic conductivity to approximately 100 times greater than the undisturbed hydraulic conductivity of the Ozan Formation.

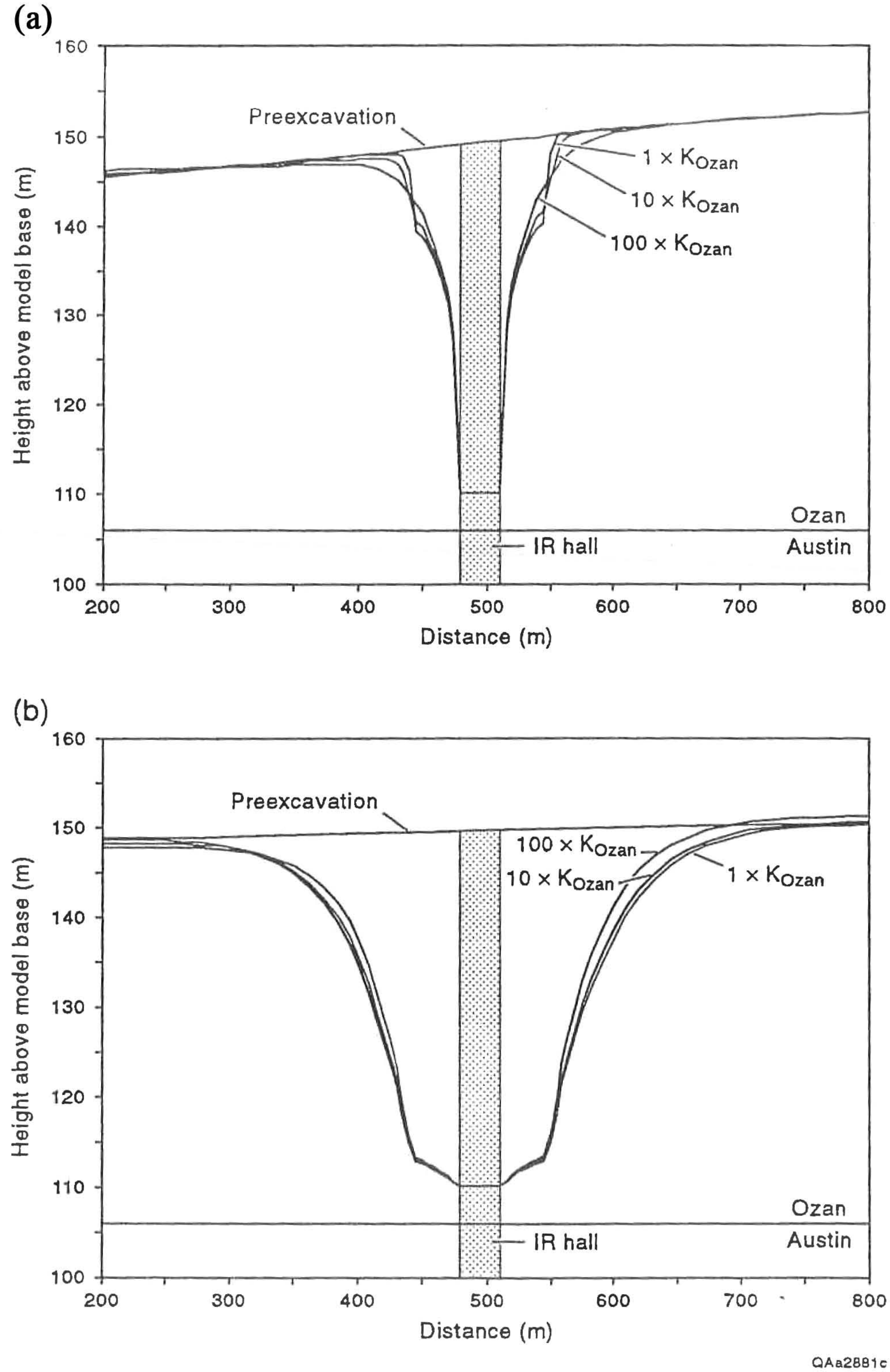

Figure 87. Sensitivity of (a) unconfined water table in Ozan Formation (layer 1) and (b) confined potentiometric surface in Austin Chalk (layer 2) to uncertainty of hydraulic conductivity of marl. $K_{Ozan} = 1.64 \times 10^{-4}$ ft/d (5.8×10^{-10} m/s). Profiles predicted at 20 yr after excavation. Distance is from south end of profile C–C′ (fig. 9). Equivalent hydraulic conductivity (K_e) of drainage zone held constant while K_{Ozan} varied. With $K_{Ozan} < K_e$, the slope of the water table markedly changes at the edge of the drainage zone.

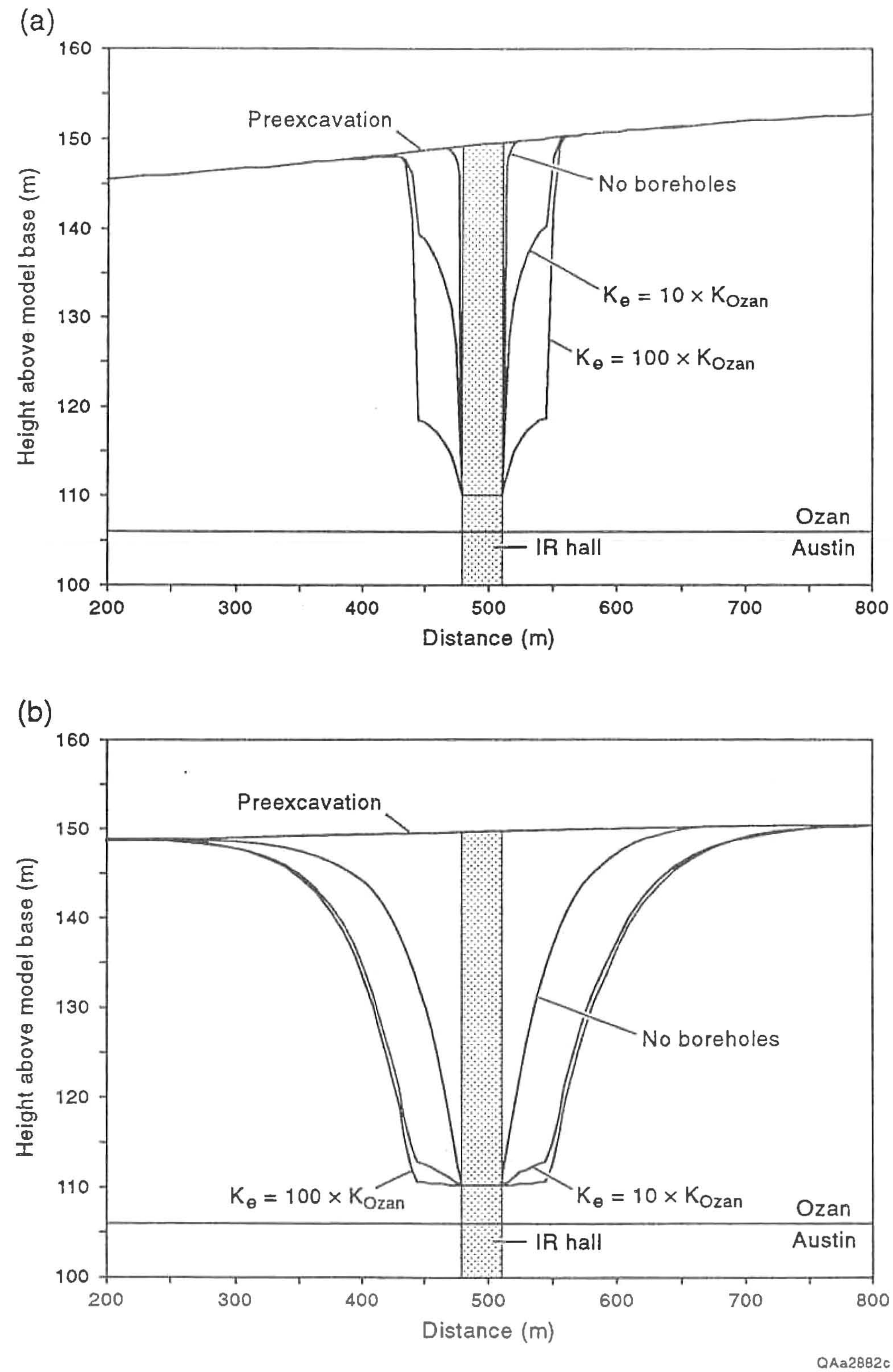

Figure 88. Profile of (a) unconfined water table simulated in Ozan Formation and (b) confined potentiometric surface in Austin Chalk. Profiles differ between simulations with no drainage boreholes ($K_e = K_{Ozan}$), with drainage boreholes giving an equivalent hydraulic conductivity (K_e) approximately 10 times the hydraulic conductivity of the Ozan Formation (K_{Ozan}), and with K_e approximately 100 times K_{Ozan}. Profiles predicted at 20 yr after excavation. Distance from south end of profile C-C' (fig. 9).

Including a drainage zone markedly increases the zone of capture of ground-water and increases the drawdown of hydraulic-head in the Ozan, although the greatest effect is within the drainage zone (fig. 88a). This indicates that drainage borehole spacing might be specified on the basis of the rate at which marl should be dewatered as well as the size of the ground-water capture zone. The drainage zone also effects hydraulic head in the chalk (fig. 88b), although the effect of a 10-fold difference in equivalent hydraulic conductivity is less in the Austin (layer 2) than in the Ozan (layer 1). The rate of water-level decline, of course, increases with the higher equivalent hydraulic conductivity (fig. 86b).

Hydraulic head in the Austin Chalk is much more sensitive to vertical hydraulic conductivity of the drainage zone in the Ozan than is hydraulic head in the Ozan. Increased vertical hydraulic conductivity allows greater vertical flow of ground water through the Ozan, which keeps head high in the Austin Chalk in the zone around the interaction hall. Increase in length of the drainage zone from 115 to 200 ft (35 to 60 m) extended drawdown farther and increased the ground-water capture zone, but hydraulic head within much of the drainage zone was higher than with shorter boreholes (fig. 89).

The model was insensitive to GHB conductance because the amount of flow between the weathered and unweathered zones is small. The GHB cells were turned off, and no effect was observed on results.

Model Limitations

This model serves mainly as an interpretive tool because there are few data for calibration. There is no information concerning local heterogeneities or abundance and size of fractures in the unweathered bedrock. The model assumes that the interaction hall is a long trench in the east-west direction, perpendicular to the simple, two-dimensional model, and calculates flow to the hall in rectangular (Cartesian) coordinates. Since the east-west width of the hall is finite, flow to the hall at large distances may actually be radial. Radial flow conditions would let water-level change be less sensitive to parameter uncertainties. However, during the lifetime of the project, flow to the hall is probably accurately modeled with a Cartesian cross section since water-level decline is limited in extent.

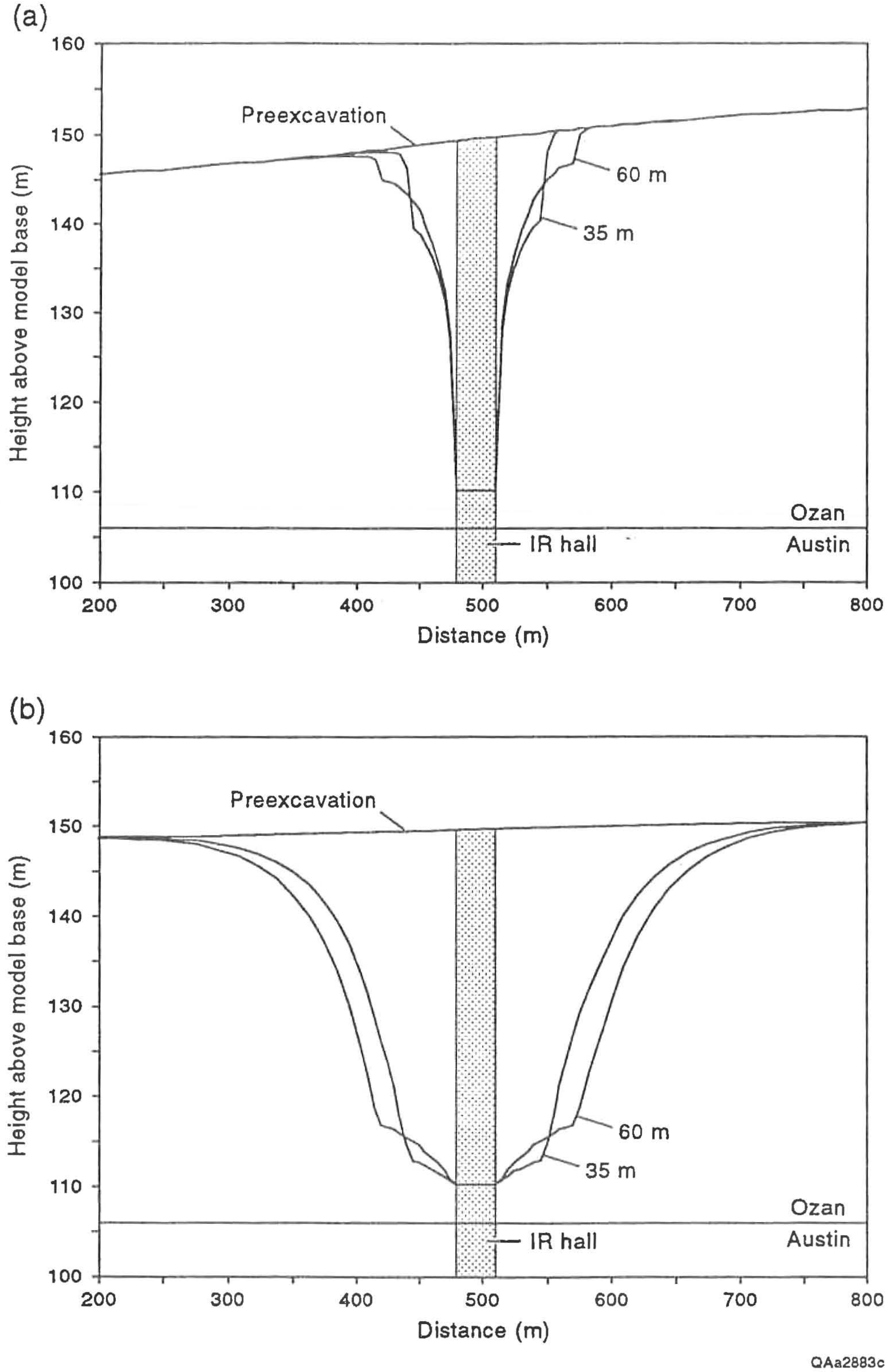

Figure 89. Sensitivity to length of drainage boreholes of (a) unconfined water table simulated in Ozan Formation (layer 1) and (b) confined potentiometric surface in Austin Chalk (layer 2). The zone of capture closely corresponds to the length of the 35- and 60-m-long drainage boreholes. Profiles predicted at 20 yr after excavation. Distance from south end of profile C-C' (fig. 9).

The seepage face was inferred to be 32.8 ft (10 m) above the bottom of the hall. The actual height of the seepage face that might develop is unknown and hard to predict with confidence. Seepage-face locations can be found by trial-and-error steady-state solutions (Freeze and Cherry, 1979), but this requires calibration data such as a measured water level near the excavation. An additional complication is the decrease in seepage-face height as the section drains. If detailed information of seepage face location is required, models that rigorously solve for seepage face position, such as FREESURF (Neuman and Witherspoon, 1970; Neuman, 1976) or AQUIFEM-N (Townley, 1990) must be used.

Initial conditions assumed a steady-state distribution of hydraulic head. As seen in transient results, more than 100,000 yr might be required to reach equilibrium. Since Bone Branch and Red Oak Creek were incised during the Pleistocene, present-day water levels in the marl are possibly not in equilibrium. Although this suggests that hydraulic head used for the initial condition in the simulation were not at steady state, it does not affect the conclusions of the transient simulation because ground-water flow is only affected close to the hall.

Conclusions

The excavation of an interaction hall will affect local ground-water flow. Hall IR8 will act as a hydrologic drain, lowering water level in the marl and chalk, and collecting ground water from at least 115 ft (35 m) away in the marl and 492 ft (150 m) in the chalk. The effect of the hall on water levels in the marl is most sensitive to the hydraulic conductivity of the drainage zone. Head in the chalk is most sensitive to hydraulic conductivity of the drainage zone and to vertical hydraulic conductivity of the marl. The predicted equivalent hydraulic conductivity of the drainage zone is effective in draining the marl; however, drainage rates are sensitive to equivalent hydraulic conductivity. The number of drainage boreholes drilled into marl might be determined on the basis of required drainage rate as much as on the basis of capture-zone size. The effect of the Austin Chalk on dewatering the Ozan

Formation in the vicinity of the interaction hall is small during the life of the project and only becomes significant with greater time.

Prediction of "Dry" Zone

Change in pore-water pressure adjacent to the tunnel wall and its effect on the capture of ground water are considered in this section. It seemed possible, if not likely, that the low hydraulic conductivity of chalk and marl, combined with the forced circulation of dehumidified air in the collider tunnel and interaction hall, might cause water to be partly replaced by air in pores of the rock adjacent to tunnel and interaction hall. Use of a geotextile cover on walls of the interaction hall and precast concrete lining on tunnel walls in marl, however, might limit exposure of the rock to air. This analysis, therefore, applies mainly to drying of tunnel walls in chalk. To the extent that the interaction hall wall or tunnel walls in marl are exposed to conditions with less than 100 percent humidity or a less than saturated liner, then the following conclusions might apply.

The tunnel and hall wall might act either as a sink or a barrier to flow, depending on whether an unsaturated section develops at the wall. Because the tunnels and halls probably will be ventilated with dehumidified air, the relative humidity of the air in the tunnels and halls will be much lower than that in the surrounding rock. The study of the zone adjacent to the tunnel and hall walls involved two analyses: (1) evaluation of computer codes to numerically simulate the process and (2) analytical evaluation of the process.

Evaluation of Two-Phase Computer Codes

Two computer codes that simulate two phase (air and water) flow were considered. The Princeton code simulates one-dimensional isothermal flow and transport code in porous media (Celia and Binning, 1992) and the Los Alamos code titled WAFE (acronym for Water, Air, and Fire in Earth) simulates two-dimensional, nonisothermal flow in porous and fractured media (Travis, 1980). These simulations would not converge because the flow problem was too nonlinear.

The one-dimensional domain was defined to extend 16.4 ft (5 m) into the wall of the tunnel. Although material properties for chalk or marl were not available, properties for these materials were approximated by those of clay (Scanlon and others, 1991)

$$\theta_s = 0.51 \qquad \theta_r = 0.1 \qquad \alpha = 0.014 \qquad m = 0.1803 \tag{47}$$

where θ_s is saturated water content (equivalent to porosity), θ_r is residual water content, and α and m are fitting parameters for water retention and hydraulic conductivity functions, respectively, described by van Genuchten (1978) and Mualem (1976) and used in the Princeton code. Water retention and hydraulic conductivity functions described by Brooks and Corey (1964) and Mualem (1976) were used in the Los Alamos code. Because the sum of liquid and gas-phase saturations is equal to one, the gas phase saturation curve is simply one minus the liquid-phase saturation curve. Estimates of the saturated (liquid) hydraulic conductivity of the chalk and marl range from $10^{-1.55}$ to $10^{-3.55}$ ft/d (10^{-7} to 10^{-9} m/s). The air hydraulic conductivity was calculated by multiplying the liquid hydraulic conductivity by 55.26, the ratio of air viscosity to liquid viscosity (Bird and others, 1960). The modeled domain was initially saturated and a temperature of 59°F (15°C) was assumed. The relative humidity in the tunnel was assumed to be 50 percent. The lower boundary for ψ, the matric potential, at the tunnel wall (3.08×10^4 ft [9.4×10^3 m]) corresponded to a relative humidity of 50 percent in the tunnel and was calculated according to the Kelvin equation

$$\psi = \frac{-RT}{V_w} \ln\left(\frac{RH}{100}\right) \tag{48}$$

where R is gas constant, T is Kelvin temperature, V_w is the molar volume of water, and RH is relative humidity. The upper boundary was assigned a constant positive liquid pressure of 82.0 ft (25 m) to correspond to the height of the water table above the modeled domain. The upper and lower air boundaries were set to atmospheric pressure. The time period for the simulation was 10 yr. The 16.4-ft-long (5-m) section was subdivided into 0.0033-ft-long (0.001-m) grid blocks. Attempts to reduce the nonlinearity of the problem by increasing the constant matric potential along the lower boundary from 3.08×10^4 to 0.3 ft (9.4×10^3 to 1 m) did not suffice to make the simulations converge.

Analytical Solution

Because the numerical codes would not converge, an analytical solution was developed to solve the problem. The analytical solution is much simpler than the numerical solution and assumes the following:

- steady-state flow,
- rock and tunnel temperature are the same,
- $\frac{\partial \sigma}{\partial x} \rightarrow 0$ close to the wall, where σ is saturation in the rock and x is distance from the wall, and
- the tunnel is ventilated and relative humidity is constant.

Analysis Including Gravity

To evaluate vertical flow into the tunnel, the gravity term is included in the following analysis. At steady state the water flux (Q) is constant and is equal to the saturated hydraulic conductivity (K_0). If an unsaturated section develops, the water plus vapor flux must sum to Q.

$$\frac{-k(\sigma)}{\mu_w}\left(\frac{\partial y(\sigma)}{\partial x} + \rho_w g\right) - D\frac{\partial C}{\partial x} = Q = -K_0 \tag{49}$$

where k is intrinsic permeability, μ_w is water viscosity, σ is saturation (θ/θ_s), ρ_w is water density, g is gravitational acceleration, D is molecular diffusivity of water vapor in air, C is vapor density

$$C = C_s(T) f(\sigma) \tag{49a}$$

where C_s is the saturated vapor density and f is the vapor pressure lowering due to capillarity, and K_0 is saturated liquid hydraulic conductivity. The parameters K, ψ, and D are functions of the saturation (σ). Using the chain rule, equation (49) can be expanded to the following

$$\frac{-k_0 k_r(\sigma)}{\mu_w}\left(\frac{\partial y(\sigma)}{\partial x}\frac{\partial \sigma}{\partial x} + r_w g\right) - D(\sigma) C_s \frac{\partial f}{\partial \sigma}\frac{\partial \sigma}{\partial x} = -K_0 \tag{50}$$

where k_0 is saturated permeability and k_r is relative permeability. Solving equation (50) for $\frac{\partial \sigma}{\partial x}$,

$$\frac{\partial \sigma}{\partial x} = \frac{K_0(1-k_r(\sigma))}{D(\sigma)C_s \frac{\partial f}{\partial \sigma} + \frac{k_r(\sigma)k_0}{m_w}\frac{\partial y}{\partial \sigma}} \tag{51}$$

A thin boundary layer (Δx_{bl}) is assumed to exist at the wall across which the vapor density drops to the tunnel value. In addition, $\frac{\partial \sigma}{\partial x} = 0$ at $x = 0.0033$ ft (0.001 m). The governing equation (49) reduces to:

$$k_0 k_r(\sigma)\frac{\rho_w g}{\mu_w} + D(\sigma)C_s \frac{[f(\sigma) - f_{tunnel}]}{\Delta x_{bl}} = K_0 \tag{52}$$

$$R + f_{tunnel} = Rk_r(\sigma) + f(\sigma) \text{ where } R = \frac{K_0 Dx_{bl}}{D(\sigma)C_s}. \tag{53}$$

First, σ is solved at the tunnel wall using equation (53) and then equation (51) is integrated to obtain the variation in σ with distance from the wall.

Analysis Excluding Gravity

To evaluate lateral flow into the tunnel or interaction hall, the gravity term is excluded. Equations (49) to (53) are rewritten without the gravity term.

$$\frac{-k(\sigma)}{m_w}\left(\frac{\partial \psi(\sigma)}{\partial x}\right) - D\frac{\partial C}{\partial x} = Q = -K_0 \tag{54}$$

$$\frac{-k_0 k_r(\sigma)}{m_w}\left(\frac{\partial \psi(\sigma)}{\partial \sigma}\frac{\partial \sigma}{\partial x}\right) - D(\sigma)C_s \frac{\partial f}{\partial \sigma}\frac{\partial \sigma}{\partial x} = -K_0$$

$$\frac{\partial \sigma}{\partial x} = \frac{K_0}{D(\sigma)C_s \frac{\partial f}{\partial \sigma} + \frac{k_r(\sigma)k_0}{\mu_w}\frac{\partial \psi}{\partial \sigma}} \tag{55}$$

$$D(\sigma)C_s \frac{[f(\sigma) - f_{tunnel}]}{\Delta x_{bl}} = K_0 \tag{56}$$

$$R + f_{tunnel} = f(\sigma), \text{ where } R = \frac{K_0 \Delta x_{bl}}{D(\sigma) C_s} \qquad (57)$$

Parameter Estimation

There are no exact measurements available for many of the parameters required for this analysis. The boundary layer thickness was assumed to be 0.0033 ft (0.001 m). A temperature of 59°F (15°C) was used in the analysis. The saturated vapor density at this temperature is approximately 10^{-5} g cm^3. Hanks and Ashcroft (1980) suggest that only limited error is introduced if the molecular diffusivity of water vapor in air is considered a constant (0.2 cm^2/s). The relative humidity of the tunnel was set to 50 percent. The saturated hydraulic conductivity was set initially to $10^{-1.55}$ ft/d (10^{-7} m/s). Sensitivity of the results to variations in the hydraulic conductivity was examined (fig. 90). The following expressions were used to write equation (53) in terms of known variables to solve for σ at the wall:

$$f(\sigma) = e^{\frac{-V_w \psi(\sigma)}{RT}} \qquad (58)$$

$$\psi = \frac{\rho_w g}{a} \{ (\frac{\sigma - \sigma_r}{1 - \sigma_r})^{-1/m} - 1 \}^{1-m} \text{ van Genuchten (1978)} \qquad (59)$$

$$k_r(\sigma) = \frac{\mu_w}{\rho_w g} (\frac{\sigma - \sigma_r}{1 - \sigma_r})^{0.5} (1 - [1 - (\frac{\sigma - \sigma_r}{1 - \sigma_r})^{1/m}]^m)^2 \text{ van Genuchten (1980)}. \qquad (60)$$

Results

The results of calculated saturation at the rock face and the integrated distance to saturated conditions are presented as a function of hydraulic conductivity (fig. 90), which varies spatially and is poorly known at the interaction halls. Water content at the rock face falls away from saturation asymptomatically as hydraulic conductivity is decreased, but saturation remains relatively constant at approximately 29 percent at hydraulic conductivities less than $10^{-2.55}$ ft/ d ($<10^{-8}$ m/s). At the larger

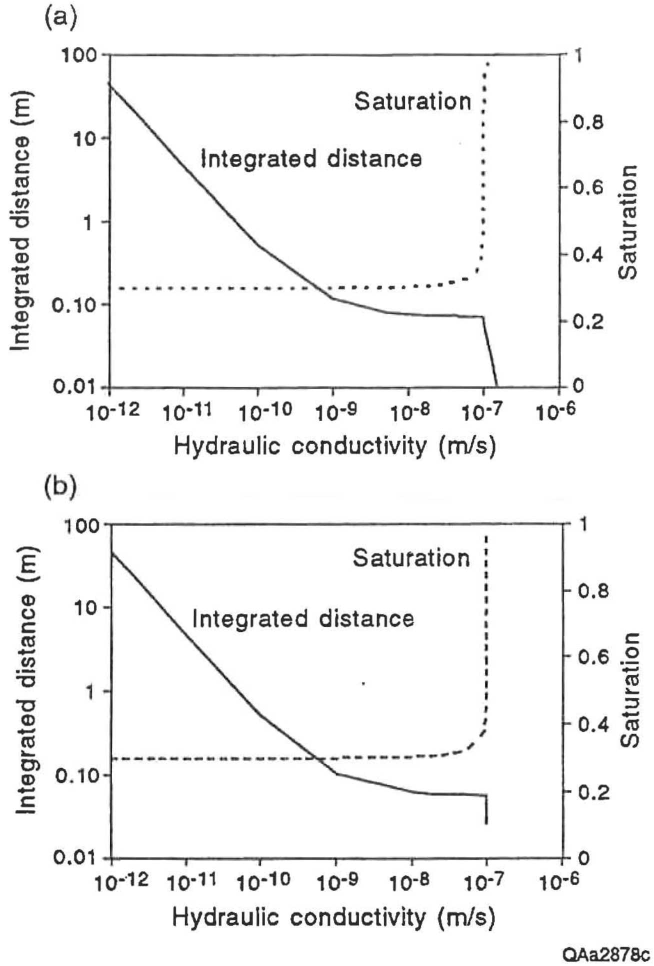

Figure 90. Water saturation at the rock face and distance from rock face to saturated conditions as a function of saturated hydraulic conductivity, (a) with and (b) without gravity effect. Diffusivity (D) is 2 cm^2/s.

hydraulic conductivities, the capacity of the rock to transmit water always exceeds potential evaporation rates and the rock face remains saturated and wet. Distance from the rock face to saturation remains less than a few inches (<10 cm) at hydraulic conductivities greater than $10^{-2.55}$ ft/d (>10^{-8} m/s) but increases logarithmically at lower hydraulic conductivities because liquid flux is so small. At hydraulic conductivities greater than $10^{-1.55}$ ft/d (>10^{-7} m/s), the integrated distance to saturation is slightly less when gravity is considered (fig. 90a) than when it is not (fig. 90b). This indicates that the cross-sectional height of the envelope of partly water-saturated rock is slightly less than the cross-sectional width because of the vertical gravity-driven flow of water.

This analysis does not indicate how long this saturation profile will take to develop. If the relative humidity in the tunnel is close to 100 percent or concrete or other wall liners have permeability much lower than that of the rock, then pores will remain saturated and there will be no vapor flux. Water flux from the wall under high humidity will be controlled by the saturated hydraulic conductivity, as discussed in previous sections.

Possible unsaturated conditions in rock adjacent to tunnel or interaction hall walls affect the potential for movement of different radioactive isotopes. Tritiated ground water, for example, can move both as a vapor phase and a liquid phase, whereas other isotopes that might be generated in rock near the interaction hall are nonvolatile and move only in solution. It is possible, therefore, that nonvolatile radioisotopes might be concentrated at the capillary fringe at some distance from the wall, as estimated in figure 90, while tritium might move in water vapor into the tunnel and interaction hall. Additional study is necessary to quantify the probable flux of radioactive isotopes.

SUMMARY

Introduction

The focus of this report is on ground water in weathered and unweatherd Austin Chalk and Ozan and Eagle Ford Formations in the vicinity of the Superconducting Super Collider site in Ellis County, Texas. Major topics discussed include the structural stratigraphic, and mineralogic controls on fracture intensity and fracture characteristics; influence of fractures on hydrogeologic properties and ground-water flow; the role of springs and seeps in the local hydrological cycle; regional hydrologic controls on artesian conditions; paleohydrologic and mineralogic controls on chemical composition of ground water; sources of ground water and ground-water residence time; inventory of in-use and abandoned water wells; effects of SSCL construction on ground-water flow; and methods used to conduct the geologic and hydrologic studies. The studies were conducted between December 1990 and March 1993. Studies included

- inventorying 1,130 wells, including 419 wells on footprint parcels and 40 wells within 150 ft of accelerator beam line;
- monitoring water levels at more than 120 public, private, and SSCL project wells and description of the three-dimensional distribution of hydraulic head and flow potential;
- hydrologic testing at 29 SSCL project wells and 43 private wells;
- sampling ground water at the 37 SSCL project wells and at 38 private wells and analyses of chemical and isotopic composition;
- studying petrographically the stratigraphic controls on fracture intensity;
- defining the mineralogic and paleohydrologic controls on water chemical composition and interpretation of ground-water ages;
- modeling of ground-water flow in Austin Chalk, Eagle Ford, and Ozan Formations to evaluate hydrologic interpretations and to estimate difficult-to-measure hydrologic properties; and
- delineating the ground-water capture zone around SSCL particle-interaction halls.

Petrology of the Austin Chalk in the Ellis County Area

The Austin Chalk at the SSC site is a 400- to 500-ft-thick (121.1- to 151.4-m) sequence of chalk beds alternating with thinner marl beds. Matrix porosity and permeability are low, but the unit is fractured both in fault zones and in more widely spaced regional fracture systems. This study focused on understanding the stratigraphic and mineralogic controls on the distribution of these fractures.

The Austin Chalk accumulated as a nannoplankton ooze in a deep-water shelf environment. The stable depositional environment accounts for the lithologic homogeneity of the Austin Chalk. Variability in chalk-marl cycle patterns, texture, fauna, and the amount and sources of clay affect the mechanical properties of the Austin Chalk (for example, fracture spacing and weathering characteristics). Cycles in the Austin Chalk are defined by repetitive alternation of carbonate-dominated chalks and marls. Marl beds have a consistently higher acid-insoluble content (18 to 26 percent) than do adjacent chalk beds, which have an average insoluble content of 8 to 15 percent. Clay minerals include smectite, kaolinite, and illite.

Clay origin as well as distribution influence the mechanical properties and log-response character of the chalk and marl. In the lower and upper Austin Chalk, detrital clay and sand are recognized in most chalk and marl beds, except in discrete beds of altered volcanic ash. The middle Austin Chalk, with its low-SP response, is traditionally interpreted as a high-clay unit. In Ellis County, however, the middle Austin Chalk does not have a markedly higher clay content than other units but the source and microdistribution of clay are different. Clay coats on nannoplankton grains are interpreted as devitrified volcanic ash that was codeposited with the chalk. The authigenic clay is associated with volcanic biotite, quartz, and feldspar. The middle Austin Chalk typically has lower porosity, greater ductility, lower fracture intensity, and lower average hydraulic conductivity compared to the upper and lower Austin Chalk. These properties are controlled by clay distribution around and between individual coccoliths rather than by total clay content.

Thirteen subsurface units are delineated on the basis of gamma-ray patterns, core description, and fracture intensity. Units T, A, B, C, and D correlate approximately with the lower Austin Chalk. Units E through I are approximately equivalent to the low-SP middle Austin Chalk, and units J, K, and L correspond to the upper Austin Chalk. Subsurface units projected to ground surface form the basis of a geologic map, structural cross sections, and a three-dimensional stratigraphic model. The structural cross sections were used for hydrologic modeling. From structural cross sections, part of the upper Austin Chalk is found to be missing from the previously defined stratigraphic section. Adding this interval to the cross section, however, has little impact on the interpretation of the structure or stratigraphy at collider tunnel depth, but slightly increases stratigraphic dips along the eastern part of the ring.

Fracture Systems of the Austin Chalk

Fractures probably are the primary conduit of ground-water flow in the Austin Chalk and Ozan and Eagle Ford Formations because unfractured bedrock typically has low hydraulic conductivity. This study focused on mapping and describing fractures in outcrop and core in the Austin Chalk in the Ellis County area. Fractured marl of the Ozan Formation and fractured shale of the Eagle Ford Formation were not studied in the same detail as the Austin Chalk because unweathered Ozan outcrops are sparse. The Ozan Formation is less brittle than the Austin Chalk and usually is less fractured.

The zone of weathered Austin Chalk is locally as much as 45 ft (14 m) thick in the Ellis County area. Joints are more abundant than in unweathered chalk and small cavities and vugs are locally common along fractures and bedding planes. Unloading might cause fractures and bedding planes near the surface to be more permeable than fractures at greater depths. Permeable bedding planes might aid in connecting vertical fractures.

Deeper, unweathered Austin Chalk units have variable fracture frequencies in areas away from large faults. In Ellis County, fracture intensity is highest in upper (units J, K, and L) and lower (unit A) units of the chalk. The least fractured units are E through I in the middle zone, and units T and B, C, and D of the lower interval. Slant-core data and long outcrop traverses verify that fractures do not have uniform spacing within any given unit and that fracture swarms occur away from large faults or folds.

Areas of high fracture abundances and well-interconnected fractures occur near faults and folds. Fractured areas surrounding faults are relatively narrow, and the most highly interconnected parts are small faults that in many cases are at least partly coated with calcite. Halos or zones of fractured rocks surrounding large faults have well-interconnected fracture networks of considerable vertical and lateral extent. These networks extend vertically across bedding and might be in both hanging wall and footwall blocks. Bending of brittle chalk can create fractures, so folds adjacent to curved faults, fault-propagation folds near lateral fault terminations, and areas between overlapping fault tips are areas where abundant, well-interconnected fractures might occur. Hinges of folds have greater fracture frequency than fold limbs. In Ellis County, exposed parts of large faults are nearly planar, but slight bends are loci of fracture zones. Small-scale examples show that these zones are common where faults steepen or flatten.

Fractures are commonly joints or veins, which tend to be confined to individual chalk beds. Fold-related fractures in areas or stratigraphic intervals with numerous marly or shale interbeds tend to be confined to individual chalk beds, and fluid communication along fractures is vertically partitioned.

Water Resources

A total of 1,130 wells are located near the SSC in Ellis County, 419 of which are on parcels on the SSC footprint. The inventory of 108 wells on the West Campus corresponds to a well density of 9.1 wells/mi^2 (3.5 wells/km^2). If the well density on the West Campus is representative of Ellis County, there might be more than 4,300 wells in the 475 mi^2 area (1,277 km^2). Most (72 to 75 percent) of the wells are shallow dug wells less than 50 ft (<15.24 m) in depth, and 10 to 15 percent are drilled water-supply wells in the regional confined aquifers at depths generally in excess of 420 ft (>128 m). Only 40 wells lie within 150 ft (45.72 m) of the beam line projected at land surface. Of these, 17 are being used as of this 1991–1992 survey. About 5 percent of the shallow wells on the SSC footprint are used for domestic water supplies and another 8 percent supply water for livestock or home gardens and yards. At least 87 percent of the shallow wells on the SSC footprint are unused or abandoned and as many as 2,700 shallow wells might be unused or abandoned in the entire study area within Ellis County. Most abandoned wells are in disrepair and have been used for disposal of trash. Because of the potential for rapid recharge and flow rate, the unconfined surficial aquifer in alluvium and in fractured, weathered bedrock is susceptible to contamination through these abandoned wells.

Deep wells in the regionally confined aquifer system typically are drilled into the Upper Cretaceous Woodbine or Lower Cretaceous Paluxy and Twin Mountains Formations. Reported depths of wells range from 230 to 3,285 ft (70.1 to 1001.3 m). Wells operated by the City of Avalon, City of Bardwell, Buena Vista Water Supply Corporation, City of Ennis, City of Palmer, and Rockett Water Supply Corporation serve communities near the SSC. At least 58 of the deep water wells in the study area have been abandoned.

Water-Table Elevation

The position of the water table or potentiometric surface fluctuates seasonally, daily, and episodically as the balance changes between rate of recharge from precipitation and rates of discharge by evapotranspiration, flow to springs and seeps, and pumping of wells. At any given time, water levels closely mimic topography, with high elevations along upland surface-water divides and low elevations in valley floors beneath stream beds. Depth to water averaged 8.1 to 8.5 ft (2.47 to 2.59 m) below land surface during 1991 and 1992, respectively. Water levels in wells in the weathered Austin Chalk generally rise and fall quickly after precipitation events. The magnitude of water-level changes decreases with depth and generally is less in unweathered bedrock than in the surficial aquifer in alluvium and weathered bedrock. In most deep wells in the unweathered bedrock there were no detectable fluctuations in water level associated with precipitation events or seasons, indicating very low recharge rates. Water level in SSCL monitoring well BI3, however, responds rapidly to precipitation events, and there are suggestions of a possible annual cycle at wells BE10, BI3, BI6, BIR31, and BF6, where water levels are as much as 8 to 10 ft (2.4 to 3 m) higher during January to April than during June to September. Additional data, however, are needed to confirm the periodicity of fluctuations and to quantify how such fluctuations relate to recharge and discharge rates.

The dynamic pressure increment (Δp), calculated from water levels measured in SSCL monitoring wells, is used to evaluate potential for vertical flow of ground water. Artesian wells such as BE6 and BF3 have large positive Δp values and indicate local and regional potentials for upward-directed flow. Among wells with very negative Δp values, BE2 shows a normal rate of water-level recovery but plots alongside wells B1697 and BE1A, which have extremely slow rates of water-level recovery. These data suggest that low hydraulic heads occur naturally beneath upland recharge areas.

Hydrologic Properties

Hydraulic conductivity of the weathered Austin Chalk averages 0.61 ft/d ($10^{-5.66}$ m/s) and decreases with depth. Hydrologic tests conducted at low initial water levels affect only the deeper, less permeable section of the weathered zone, and tests conducted at high initial water levels yield a higher hydraulic conductivity weighted both by the hydraulic conductivities of different strata and by the effective hydraulic conductivity of intersected fractures. The potential for transport of contaminants by ground water in the weathered chalk, therefore, varies seasonally with water-table elevation.

Average hydraulic conductivity of unweathered chalk, marl, and shale is almost 1,000 times lower than hydraulic conductivity of weathered bedrock, but hydraulic conductivity of unweathered, fractured chalk can be as great as the average hydraulic conductivity of weathered bedrock. Hydraulic conductivity measured in the unweathered Austin Chalk ranges over 6 orders of magnitude from $10^{-6.0}$ to $10^{-0.07}$ ft/d ($10^{-11.5}$ to $10^{-5.5}$ m/s). Factors that affect the range of hydraulic conductivity in Austin Chalk are (1) variations in fracture intensity and fracture aperture and (2) variations in chalk-marl ratio and microdistribution of clay. Analysis of variance shows that average hydraulic conductivity of fractured chalk statistically differs between the subdivided units of the Austin Chalk, a different conclusion than previously made. Hydraulic conductivity of fractured zones near faults tends to increase with greater fault throw for faults having throws of 5 to 40 ft (1.5 to 12 m). The increase reflects the interconnection of fractures adjacent to faults. Lower than expected hydraulic conductivity of fractured rock near the three largest fault zones results from partial occlusion of fracture porosity by calcite vein filling. Fracture apertures in the Austin Chalk calculated using a cubic-law relationship range from 0.00003 to 0.0043 inches (0.0009 to 0.108 mm) and average 0.0011 inches (0.029 mm).

Specific storage is calculated at 11 SSCL monitoring wells from the water-level response to atmospheric-pressure changes. Calculated barometric efficiencies are low, possibly indicating extreme confinement of ground water. Mean specific storage calculated for the Austin Chalk is $10^{-5.76}$ and mean specific storage for the Eagle Ford Formation is $10^{-6.29}$. Storativity has not been measured directly in test wells in unweathered bedrock at the SSC site, so there is no independent comparison for the value calculated using water-level fluctuations. Determining whether estimation of specific storage from the response of water-level fluctuations to atmospheric-pressure change is representative of in situ specific storage requires further study and analysis.

Geothermal Gradient

Bottom-hole temperature increases with depth. The intercept of the regression matches the 66°F (18.9°C) 1931–1965 average of air temperature in Waxahachie. The calculated slope estimates a geothermal gradient of 1.7°F/100 ft (30.3°C/km), which agrees with the regional trend in geothermal gradient.

Chemical Composition of Ground Water

Ground water in weathered bedrock of the Austin Chalk and Ozan Formation ranges from calcium-bicarbonate to mixed-cation-bicarbonate and mixed-cation-sulfate types. Water collected from springs issuing from fractures in the Austin Chalk also is a dilute calcium-bicarbonate type water resembling ground waters collected from wells in the weathered chalk. Ground water from unweathered bedrock tends to have the highest TDS, and a large proportion of samples were sodium-chloride hydrochemical types. Na^+ and Cl^- concentrations lie along or above the seawater dilution line. Similarly, the Br^-/Cl^- ratio of the ground waters generally is similar to that of seawater. Geochemical models are used to simulate reactions hypothesized to control chemical composition of ground water. Simulated reactions include (1) dilution by recharged rainwater of sodium, chloride, and other dissolved salts inherited from seawater trapped in pores in low-permeability rock and (2) reactions of the diluted mixture with minerals such as calcite, pyrite, and clays (ion exchange) that make up the formations. The ratio of conservative ions such as Cl^- and Br^- between ground water and seawater, therefore, might be an estimate of how much recharged water has circulated through the rock, displacing and diluting ancient seawater, since the stratigraphic section has been in its present hydrological setting. Although most seawater has been displaced from pores in low-permeability rock, flushing is incomplete. The amount of flushing of marine salts presumably is related to the interconnectedness and hydraulic conductivity of fractures. In such situations, solute concentration might be controlled by diffusion from unfractured rock as well as by advective flow within fractures.

BI3 and BF9 are the two SSCL monitoring wells that have high enough yield to provide a ground-water sample for carbon-14 (^{14}C) analysis. Carbon-14 content measured at BI3 is 97 ± 0.7 percent of Modern atmospheric ^{14}C activity (pmc). Carbon-14 content measured in ground water from BF9 is 2.1 ± 0.2 pmc, but above detection limit. Tritium (^{3}H) concentrations in water samples from alluvium and weathered bedrock are low but above background, ranging from 3.58 to 11.1 TU (11.45 to 35.5 pCi/L). Tritium concentrations of water samples from SSCL monitoring wells range from 0 to approximately 7 TU (0 to 22.4 pCi/L). The ^{14}C and ^{3}H data suggest that ground water in shallow or fractured bedrock, such as at BI3, was recharged within the last 40 to 50 yr. High ^{3}H content in ground water at depths of approximately 90 ft (27 m) or more in chalk is evidence of rapid vertical flow, which most likely occurs through fractures. The above-background ^{3}H values suggest that fractures also might influence ground-water flow at wells BI4, B1597B, and B1697B. Inferences of rates of ground-water flow cannot be made with confidence on the basis of samples without detectable ^{3}H, but ^{3}H activity of less than 0.4 TU (<1.3 pCi/L) in 10 samples must represent sufficient time of travel, at least 40 to 50 yr, for "bomb" tritium to decay in activity to below detection limits. Ground water in bedrock with less well interconnected fractures, such as at BF9, is older, possibly recharged within the past 15,000 to 20,000 yr on the basis of limited ^{14}C data. Numerical model results suggest an average age of ground water in unweathered, unfractured bedrock of 1 m.y.

All ground water is expected to show minute levels of radioactive constituents such as ^{40}K, radium, and ^{23}???, which are derived from the rock and soil through which the water passes. Radioactive isotopes of beryllium, sodium, calcium, manganese, cobalt, and cesium were not detected in these naatural waters but might be generated by SSCL accelerator operation.

Ground-Water Flow Paths

The physical and chemical hydrogeologic studies indicate that recharge from precipitation over the upland drainage divides percolates into the ground and moves downward through the soil zone and weathered bedrock to the water table. Beneath the water table in the weathered zone, ground water percolates along vertical fractures and horizontal bedding-plane joints and through the more permeable sedimentary layers. Vertical movement can be retarded by unfractured beds of low permeability. Because of the decrease in hydraulic conductivity with increasing depth below ground surface, only a small fraction of recharged ground water, estimated to be only 1 percent by numerical models, moves downward into unweathered bedrock. The important exception to this occurs in zones of interconnected fractures. Deep vertical circulation is more likely in fractured chalk than in marl because fractures in chalk remain open to greater depth.

Regional flow paths through the unweathered chalk are assumed to be mainly through interconnected fractures rather than through unfractured matrix. The strike of fractures, however, imparts a northeasterly anisotropy to regional values of hydraulic conductivity in the Austin Chalk that might influence direction of ground-water flow. Ground water flows generally southeastward but flow paths bend toward discharge points in the valley bottoms and stream banks. At the margins of incised stream valleys, ground water discharges in springs and seeps from bedding plane joints and vertical fractures. Perennial streams can be fed during droughts until the water table falls below the elevation of the springs and seeps, leading to testimony that such springs have "not gone dry in living memory." Notable examples of fracture-controlled springs in weathered chalk include Brach Spring, which feeds part of Greathouse Branch, Mammouth Spring, which feeds Armstrong Creek, and Hawkins Spring, which feeds Waxahachie Creek in Midlothian, Texas.

Water temperatures at such springs ranged from 62.6° to 69.8°F (17° to 21°C). The coolest temperatures suggest that ground water circulated only to shallow depths of less than approximately 65 to 100 ft (20 to 30 m). The warmest temperatures suggest that ground water might have circulated to a depth of approximately 250 ft (77 m). This places the depth of circulation near Hawkins Spring into the Eagle Ford Shale. The chemical composition of the Hawkins Spring water, however, closely resembles the chemical composition of shallow Austin Chalk water and shows no evidence of contact with such a distinctly different mineralogy and lithology as the Eagle Ford Formation. Depth of circulation of ground water feeding Hawkins Spring remains an unresolved question.

Ground-water velocities in unfractured rock are very slow and should retard the transport of radionuclides. However, where bedrock is intensely fractured, rapid flow velocities and transit times of less than 50 yr can be obtained. Therefore, it is important to identify fracture zones and to quantify their hydraulic properties in the vicinity of expected sources of radioactivated ground water.

Simulation of Ground-Water Flow

Numerical modeling is used as a tool to interpret and better understand the parameters that control regional ground-water flow paths and travel times and to evaluate the conceptual hydrologic model. A "West Campus" model investigates local flow rates and flow paths in weathered and unweathered Austin Chalk and in fractured zones. An "Ellis County" model evaluates regional flow paths within unweathered Ozan Formation, Austin Chalk, and Eagle Ford Formation and determines the hydrogeologic control of artesian pressure in Austin Chalk at the eastern side of the SSC site.

Hydraulic properties are initially assigned on the basis of data from hydrologic tests and adjusted by matching simulated hydraulic head with water-level data from SSCL monitoring wells and exploratory-borehole-shaft piezometers. Model calibration provides estimates of hydrologic properties that cannot be readily measured and indicates that (1) horizontal hydraulic conductivity is a little more than 100 times greater than vertical hydraulic conductivity, (2) average hydraulic conductivity of the Austin Chalk is 8 times greater than averace hydraulic conductivity of the Ozan

Formation, (3) hydraulic conductivities between 1.4 and 4.0 ft/ d ($10^{-5.31}$ and $10^{-4.85}$ m/ s) in a fracture zone on the West Campus yield flow velocities that are consistent with tritium data and simulated hydraulic heads that match measured values, and (4) vertical gradients in hydraulic head range from 0 to 0.1. In addition, model results suggest that (1) less than 3 percent of precipitation is recharged, (2) 99 percent of ground water flows through the weathered zone and less than 1 percent moves downward into unweathered bedrock, (3) ground-water residence time in the weathered zone is 5 to 10 yr, (4) average ground-water residence time in unweathered rock is 1 m.y., (5) ground-water circulation is deep and rapid in fracture zones, (6) ground water that is recharged at the Austin Chalk outcrop either discharges to creeks that cross the outcrop or flows downdip and eventually discharges upward through the Ozan Formation, and (7) ground-water velocity ranges from 10^{-2} to 10^{-6} ft/d ($10^{-7.45}$ to $10^{-11.45}$ m/s) in weathered bedrock and from 10^{-6} to 10^{-8} ft/d ($10^{-11.45}$ to $10^{-13.45}$ m/s) in unweathered bedrock. These models can be modified for other purposes, for example, to locate optimum locations of ground-water monitoring wells and to predict travel time between specific SSCL facilities and a monitoring well.

Effect of SSCL Excavations on Ground-Water Flow

An "Interaction Hall" model estimates the size of the zone in which ground water will be captured, that is, drawn into the large excavations of interaction halls and adjacent tunnel segments owing to the local hydraulic-head gradient imposed by these openings. Construction of hall IR8, for example, is designed to be 113.8 ft wide, 344.5 ft long, and 160 ft deep beneath ground surface (34.7, 105, and 48.77 m, respectively). The interaction hall will be surrounded by near-horizontal boreholes to promote drainage of the rock adjacent to the interaction hall.

The amount of ground-water inflow and hydraulic-head decline after excavation depends on the hydraulic conductivity of rock, the number and size of the drainage boreholes installed in the walls, and the effect of wall treatments such as application of a geotextile-material cover and shotcrete. To simplify the problem, an analytical solution combining mutual effects of drainage boreholes and the tunnel is developed to determine effective conductivity of the zone influenced by drainage holes, calculate discharge, and evaluate how discharge and capture zones are affected by design of drainage boreholes.

These calculations show that (1) total flow rate is larger from the long eastern and western walls than from the short southern and northern walls, especially early in the history of the excavation when the radius of influence is small, (2) the collider tunnel might yield a greater flow rate than other boreholes if the hydraulic conductivity of its concrete lining is not much less than the hydraulic conductivity of the bedrock, (3) the uppermost and middle rows of drainage holes yield the second and highest and least flow rates, respectively, and (4) the number of drainage boreholes drilled into marl might be determined on the basis of required drainage rate as much as on the basis of capture-zone size.

Hydrologic properties initially are assigned in the numerical model on the basis of tests of SSCL monitoring well BIR81 and results of West Campus and Ellis County model simulations, but are varied to evaluate sensitivity of model results to the assumed values. The model is executed first as a steady-state model to establish a pre-excavation baseline, then is modified to include the change in hydraulic conductivity imposed by construction of the interaction hall. Model results show that the interaction-hall excavation acts as a hydrologic drain, lowering water level in the marl and chalk, and capturing ground water from at least 115 ft (35 m) away in the marl and 492 ft (150 m) in the chalk. Calculation of water levels near the interaction hall is sensitive to the vertical and horizontal hydraulic conductivity of the drainage zone.

Use of a geotextile cover or shotcrete on walls of the interaction hall and precast concrete lining on tunnel walls in marl limits exposure of bedrock to air. Painting chalk walls with a sealant also influences hydrologic conditions behind the wall. Tunnel walls might become dry, nonetheless, owing to the low hydraulic conductivity of chalk and marl and forced circulation of air. Drying of tunnel walls might limit movement of captured ground water into the excavations. It is possible that volatile isotopes such as ^{3}H might move in water vapor while nonvolatile radioisotopes such as ^{22}Na might be concentrated at the capillary fringe at some distance from the wall. Additional study is necessary to quantify the probable flux of volatile and nonvolatile radioactive isotopes.

ACKNOWLEDGMENTS

This work was funded by the Texas National Research Laboratory Commission (TNRLC) under interagency contracts IAC(92-93)-0301 and IAC 94-0108. We appreciate the cordial cooperation of many Ellis County residents in allowing our inventory of wells, tests of hydrologic properties, and collection of water samples. We benefited from the assistance of M. Smith and G. Bryant of the TNRLC in coordinating our field investigations with other activities at the SSC. Chemical analyses were performed at the BEG Mineral Studies Laboratory, University of Miami Tritium Laboratory, Beta Analytic, Inc., and Controls for Environmental Pollution, Inc. Drafts of this report were reviewed by S. Atkin, D. Goss, and S. Nance. Word processing was by S. Lloyd, editing by A. Masterson. Illustrations were drafted by M. Bailey, S. Krepps, J. Lardon, K. Prewitt, J. Robinson, M. Saenz, and T. Weaver under supervision of R. Dillon. Report assembly was by J. Coggin.

REFERENCES

Anderson, M. P., and Woessner, W. W., 1992, Applied groundwater modeling, simulation of flow and advective transport: San Diego, Academic Press, Inc., 381 p.

Back, W., 1966, Hydrochemical facies and ground-water flow patterns in the northern part of the Atlantic coastal plain: U.S. Geological Survey Professional Paper 498-A, 42 p.

Baher, H., 1990, Analog and digital signal processing: New York, John Wiley & Sons, 474 p.

Barker, J. A., 1985, Generalized well function evaluation for homogeneous and fissured aquifers: Journal of Hydrology, v. 76, p. 143–154.

__________ 1989, Programs to simulate and analyze pumping tests in large-diameter wells: Wallingford, England, British Geological Survey Technical Report, Hydrogeology Series WD/89/24, 34 p.

Barker, J. A., and Herbert, R., 1989, Nomograms for the analysis of recovery tests on large-diameter wells: Quarterly Journal of Engineering Geology, London, v. 22, p. 151–158.

Barquest, B. A., 1989, A hydrogeologic assessment of the Austin Chalk outcrop belt, Central Texas: Baylor University, Master's thesis, 174 p.

Barrett, D. P., 1988, A hydrogeologic assessment of the Ozan Formation, Central Texas: Baylor University, Master's thesis, 141 p.

Barrier, J., 1980, A revision of the stratigraphic distribution of some Cretaceous coccoliths in Texas: Journal of Paleontology, v. 54, p. 289–308.

Beall, A. O., 1964, Stratigraphy of the Taylor Formation (Upper Cretaceous), East-Central Texas: Baylor Geological Studies Bulletin No. 6, 35 p.

Bear, J., 1972, Dynamics of fluids in porous media: New York, American Elsevier, 764 p.

Bird, R. B., Stewart, W. E., and Lightfoot, E. N., 1960, Transport phenomena: New York, John Wiley & Sons, 780 p.

Bottjer, D. J., 1985, Trace fossils and paleoenvironments of two Arkansas Upper Cretaceous discontinuity surfaces: Journal of Paleontology, v. 59, p. 282–298.

Bottjer, D. J., and Bryant, W. A., 1980, Paleoenvironmental analysis of disconformity and condensed bed at contact of Austin and Taylor Groups (Upper Cretaceous), east-central and northeast Texas (abs.): AAPG Bulletin, v. 64, p. 679.

Boulton, N. S., and Streltsova, T., 1976, The drawdown near an abstraction well of large diameter under non-steady conditions in an unconfined aquifer: Journal of Hydrology, v. 30, p. 29–46.

Bouwer, Herman, 1989, The Bouwer and Rice slug test—an update: Ground Water, v. 27, p. 304–309.

Bouwer, Herman, and Rice, R. C., 1976, A slug test method for determining hydraulic conductivity of unconfined aquifers with completely or partially penetrating wells: Water Resources Research, v. 12, no. 3, p. 423–428.

Bradley, R. G., and Yelderman, J. C., Jr., 1993, The hydrogeology of the Lake Waco Formation: Eagle Ford Group, Central Texas (abs.): Geological Society of America Abstracts with Programs, v. 25, no. 1, p. 31.

Bromehead, C. E. N., 1942, The early history of water supply: Geographical Journal, v. 99, p. 142–151 and 185–196.

Brooks, C., Rogers, C. A., Mayberry, J. H., McSpadden, J. O., Jr., Mitchell, W. D., and Huntsinger, J. W., 1964, Soil survey of Ellis County, Texas: Washington, D.C., U.S. Department of Agriculture, Soil Conservation Service, 76 p.

Brooks, R. H., and Corey, A. T., 1964, Hydraulic properties of porous media: Colorado State University, Fort Collins, Colorado, Hydrology Papers, 27 p.

Brown, C. M., 1981, Regional stratigraphy of the Austin Chalk and its relationship to petroleum occurrence and potential in Burleson County: Baylor University, Bachelor's thesis, 78 p.

Brown, E., Skougstad, M. W., and Fishman, M. J., 1970, Methods for collection and analysis of water samples for dissolved minerals and gases: U.S. Geological Survey Techniques of Water-Resources Investigations, book 5, chapter A1, 160 p.

Buchanan, T. J., and Somers, W. P., 1969, Discharge measurements at gauging stations: U.S. Geological Survey Techniques of Water-Resources Investigations, book 3, chapter A8, 65 p.

Buchbinder, B., Benjamini, C., Mimran, Y., and Gvirtzman, G., 1988, Mass transport in Eocene pelagic chalk on the northwestern edge of the Arabian Platform, Shefela area, Israel: Sedimentology, v. 35, no. 2, p. 257-274.

Carslaw, H. S. and Jaeger, J. C., 1959, Conduction of heat in solids; London, Oxford University Press, 510p.

Celia, M. A., and Binning, P., 1992, A mass conservative numerical solution for two-phase flow in porous media with application to unsaturated flow: Water Resources Research, v. 28, p. 2819-2828.

Chachadi, A. G., and Mishra, G. C., 1992, Analysis of unsteady flow to a large-diameter well experiencing well loss: Ground Water, v. 30, p. 369–375.

Champlin, M. A., 1976, Geology of the Mertens quadrangle, Ellis, Hill, and Navarro Counties, Texas: The University of Texas at Arlington, Master's thesis, 90 p.

Chapuis, R. P., 1989, Shape factors for permeability tests in boreholes and piezometers: Ground Water, v. 27, no. 5, p. 647–654.

_________ 1992, Using Cooper-Jacob approximation to take account of pumping well pipe storage effects in early drawdown data of a confined aquifer: Ground Water, v. 30, p. 331–336.

Charvat, W. A., 1985, The nature and origin of the bentonite rich Eagle Ford rocks, Central Texas: Baylor University, Master's thesis, 220 p.

Cloud, K. W., 1975, The diagenesis of the Austin Chalk: The University of Texas at Dallas, Master's thesis, 70 p.

Collins, E. W., 1987, Characterization of fractures in limestone, northern segment of the Edwards aquifer and Balcones Fault Zone, central Texas: Gulf Coast Association of Geological Societies Transaction, v. 37, p. 43–54.

Collins, E. W., and Laubach, S. E., 1990, Faults and fractures in the Balcones Fault Zone, Austin region, central Texas: Austin Geological Society Guidebook 13, 34 p.

Collins, E. W., Hovorka, S. D., and Laubach, S. E., 1992, Fracture systems of the Austin Chalk, north-central Texas, *in* Schmoker, J. W., Coalson, E. B., and Brown, C. A., eds., Geological studies relevant to horizontal drilling: examples from western North America: Rocky Mountain Association of Geologists, p. 129–142.

Connorton, B. J., and Reed, R. N., 1978, A numerical model for the prediction of long term well yield in an unconfined chalk aquifer: Quarterly Journal of Engineering Geology, London, v. 11, p. 127–138.

Cooper, H. H., Jr., and Jacob, C. E., 1946, A generalized graphical method for evaluating formation constants and summarizing well field history: American Geophysical Union Transactions, v. 27, p. 526–534.

Cooper, H. H., Jr., Bredehoeft, J. D., and Papadopulos, I. S., 1967, Response of a finite-diameter well to an instantaneous charge of water: Water Resources Research, v. 3, no. 1, p. 263–269.

Corbett, K. P., 1982, Structural stratigraphy of the Austin Chalk: Texas A&M University, Master's thesis, 111 p.

Corbett, K. P., Friedman, M., and Spang, J., 1987, Fracture development and mechanical stratigraphy of Austin Chalk, Texas: American Association of Petroleum Geologists Bulletin, v. 71, no. 1, p. 17–28.

Corbett, K. P., Friedman, Melvin, Wiltschko, D. V., and Hung, J. H., 1991a, Controls on fracture development, spacing, and geometry in the Austin Chalk Formation, Central Texas: considerations for exploration and production: Dallas Geological Society Field Trip No. 4, 49 p.

_________ 1991b, Characteristics of natural fractures in the Austin Chalk outcrop trend, *in* Chuber, Stewart, ed., Austin Chalk exploration symposium: South Texas Geological Society, p. 3–11.

Czerniakowski, L. A., Lohmann, K. C., and Wilson, J. L., 1984, Closed-system marine burial diagenesis: isotopic data from the Austin Chalk and its components: Sedimentology, v. 31, p. 863–877.

Dallas Geological Society, 1965, Geology of Dallas County, 211 p.

Davis, S. N., 1969, Porosity and permeability of natural materials, *in* De Wiest, R. J. M., ed., Flow through porous media: New York, Academic Press, p. 53–89.

Davis, S. N., and De Wiest, R. J. M., 1966, Hydrogeology: New York, John Wiley & Sons, Inc., 463 p.

Dawson, W. C., McNulty, C. L., and Reaser, D. F., 1983, Stratigraphic and structural overview of Upper Cretaceous rocks exposed in the Dallas vicinity: SEPM Annual Meeting, Dallas Geological Society, 99 p.

Dawson, W. C., and Reaser, D. F., 1985, Ichnology and paleoenvironments of the Middle and Upper Austin Chalk (Upper Cretaceous), Northeastern Texas, *in* McNulty, C. L., and McPherson, J. G., eds., Southwest Section American Association of Petroleum Geologists Transactions: Fort Worth Geological Society, p. 47–57.

Dawson, W. C., Reaser, D. F., and Cooper, J. E., 1985, Bentonites: potential key beds in the Marlbrook Formation (Campanian), Ellis County, Texas: The Texas Journal of Science, v. 36, p. 259–266.

DeFord, R. K., Kehle, R. O., and Connolly, E. T., 1976, Geothermal gradient map of North America: American Association of Petroleum Geologists and U.S. Geological Survey, scale 1:5,000,000.

deMarsily, Ghislain, 1986, Quantitative hydrogeology: San Diego, Academic Press, 440 p.

DeZuane, John, 1990, Handbook of drinking water quality standards and controls: New York, Van Nostrand Reinhold, 523 p.

DHV, 1979, Shallow wells: Amersfoort, The Netherlands, DHV Consulting Engineers, 192 p.

Domenico, P. A., and Robbins, G. A., 1985, The displacement of connate water from aquifers: Geological Society of America Bulletin, v. 96, p. 328–335.

Dracher, R., 1936, Grundwasserstromung (Flow of Groundwater): Wien, Julius Springer, 141 p.

Dravis, J. J., Jr., 1980, Sedimentology and diagenesis of the Upper Cretaceous Austin Chalk Formation, South Texas and northern Mexico: Rice University, Ph.D. dissertation, 532 p.

Dravis, J. J., 1991, Regional depositional setting and porosity evolution of the Austin Chalk Formation, South Texas, *in* Chuber, Stewart, ed., Austin Chalk Exploration Symposium: South Texas Geological Society, p. 17–23.

Drever, J. I., 1988, The geochemistry of natural water (2d ed.): Englewood Cliffs, New Jersey, Prentice Hall, Inc., 388 p.

Duffield, C. M., and Rumbaugh, J. O., III, 1989, AQTESOLV Aquifer Test Solver Version 1.00 Documentation: Reston, Virginia, Geraghty and Miller Modeling Group, 134 p. and program disks.

Durham, C. O., Jr., 1957, The Austin Group in Central Texas: Columbia University, Ph.D. dissertation, 54 p.

Durham, C. O., and Hall, S. B., 1991, The Austin Chalk—bed by bed through Central Texas, *in* Chuber, Stewart, ed., Austin Chalk exploration symposium: South Texas Geological Society, p. 25–40.

Dutton, S. P., 1987, Diagenesis and burial history of the lower Cretaceous Travis Peak Formation, East Texas: The University of Texas at Austin, Bureau of Economic Geology Report of Investigations No. 164, 58 p.

Einsele, G., 1982, Limestone-marl cycles (periodites): Diagenesis, significance, causes—a review, *in* Einsele, G., and Seilacher, A., eds., Cyclic and event stratification: New York, Springer-Verlag, p. 8–53.

Ewing, T. E., and Caran, S. C., 1982, Late Cretaceous vulcanism in south and central Texas—stratigraphic, structural and seismic models (abs.): AAPG Bulletin, v. 66, no. 9, p. 1429.

Ewing, T. E., 1986, Balcones volcanoes in South Texas; exploration methods and examples, *in* Dutton, L. A., and others, eds., Contributions to the geology of South Texas 1986, South Texas Geological Society, p. 368–379.

Feltz, H. R., and Hanshaw, B. B., 1963, Preparation of water samples for carbon 14 dating: U.S. Geological Survey Circular 480, 3 p.

Fenske, P. R., 1977a, Radial flow with discharging-well and observation-well storage: Journal of Hydrology, v. 32, p. 87–96.

__________ 1977b, Type curves for recovery of a discharging well with storage: Journal of Hydrology, v. 33, p. 341–348.

Ferris, J. G., and Knowles, D. B., 1954, The slug test for estimating transmissibility: U.S. Geological Survey Ground Water Notes No. 26, 7 p.

Fontes, J. C., 1980, Environmental isotopes in ground-water hydrology, Chapter 3, *in* Fritz, P., and Fontes, J. C., eds., Handbook of environmental isotope geochemistry: New York, Elsevier, p. 75–140.

Freeze, R. A., and Cherry, J. A., 1979, Groundwater: Englewood Cliffs, New Jersey, Prentice-Hall, Inc., 604 p.

Fürsich, F. T., Kennedy, W. J., and Palmer, T. J., 1981, Trace fossils at a regional discontinuity surface: the Austin/Taylor (Upper Cretaceous) contact in central Texas: Journal of Paleontology, v. 55, p. 537–551.

Geological Society of America, Rock-Color Chart Committee, 1979, Rock-color chart, unpaginated.

Gleason, J. D., Friedman, I., and Hanshaw, B. B., 1969, Extraction of dissolved carbonate species from natural water for carbon-isotope analysis: U.S. Geological Survey Professional Paper 650-D, p. D-248–D-250.

Grabowski, G. J., Jr., 1984, Generation and migration of hydrocarbons in Upper Cretaceous Austin Chalk, south-central Texas, *in* Palacas, J. G., ed., Petroleum geochemistry and source rock potential of carbonate rocks: American Association of Petroleum Geologists Studies in Geology 18, p. 97–115.

Hall, S. A., 1990, Channel trenching and climatic change in the southern U.S. Great Plains: Geology, v. 18, p. 342–345.

Hallam, A. A., 1986, The origin of minor limestone/shale cycles: Geology, v. 14, p. 609–612.

Hallgarth, W. E., 1959, A foraminiferal study of the relationship of the Buditt Marl to the Austin Chalk and Taylor Marl in the vicinity of Austin, Texas: University of Tulsa, Master's thesis, 31 p.

Hancock, J. M., and Kauffman, E. G., 1979, The great transgressions of the Late Cretaceous: Journal of the Geological Society of London, v. 136, p. 175–186.

Hanks, R. J., and Ashcroft, G. L., 1980, Applied soil physics: New York, Springer-Verlag, 159 p.

Hardcastle, B. J., 1987, Wells ancient and modern—an historical review: Quarterly Journal of Engineering Geology, v. 20, p. 231–238.

Hart, M. B., and Ball, K. C., 1986, Late Cretaceous anoxic events, sea level changes and the evolution of planktonic foraminifera, *in* Summerhayes, C. P., ed., North Atlantic paleoceanography, Geological Society Special Publications, 21, p. 67–78.

Hassan, A., 1982, Methodologies for extraction of dissolved inorganic carbon for stable carbon isotope studies: evaluation and alternatives: U.S. Geological Survey, Water Resources Investigations 82-6, 51 p.

Herbert, R., 1990, Interpreting recovery data from pumping tests: Quarterly Journal of Engineering Geology, London, v. 23, p. 267–268.

Herbert, R., and Kitching, R., 1981, Determination of aquifer parameters from large-diameter dug well pumping tests: Ground Water, v. 19, p. 593–599.

Hudnall, J. S., 1951, Corsicana-Powell Field, Navarro County, Texas *in* Occurrence of oil and gas in northeast Texas: The University of Texas, Bureau of Economic Geology Publication 5116, p. 96–104.

Hunt, J. M., and McNichol, A. P., 1984, The Cretaceous Austin Chalk of South Texas; a petroleum source rock, *in* Palacas, J. G., ed., Petroleum geochemistry and source rock potential of carbonate rocks, American Association of Petroleum Geologists Studies in Geology 18, p. 117–125.

Hvorslev, M. J., 1951, Time lag and soil permeability in ground-water observations: Vicksburg, Mississippi, U.S. Army Corps of Engineers Bulletin, no. 36, 50 p.

Jacob, C. E., 1940, On the flow of water in an elastic artesian aquifer: American Geophysical Union Transactions, v. 21, p. 574–586.

Jenkyns, H. C., 1991, Impact of Cretaceous sea level rise and anoxic events on the Mesozoic carbonate platform of Yugoslavia: American Association of Petroleum Geologists Bulletin, v. 75, p. 1007–1017.

Johnson, E. E., Inc., 1966, Ground water and wells: St. Paul, Minnesota, Edward E. Johnson, Inc., 440 p.

Junge, C. E., and Werby, R. T., 1958, The concentration of chloride, sodium, potassium, calcium, and sulfate in rain water over the United States: Journal of Meteorology, v. 15, p. 417–425.

Kennedy, W. T., 1975, Trace fossils in carbonate rocks, *in* Frey,R.W., ed., The study of trace fossils: New York, Springer-Verlag, p. 377-398.

Kharaka, Y. K., Gunter, W. D., Aggarwal, P. K., Perkins, E. H., and DeBraal, J. D., 1988, SOLMINEQ.88: a computer program for geochemical modeling of water-rock interactions: U.S. Geological Survey Water-Resource Investigations Report 88-4227, 420 p.

Koger, Curtis, 1981, Depositional and diagenetic history of the Austin Chalk, Central Texas, and its relationship to petroleum potential: Baylor University, Master's thesis, 151 p.

Kruseman, G. P., and De Ridder, N. A., 1983, Analysis and evaluation of pumping test data (3d ed.): Wageningen, The Netherlands, International Institute for Land Reclamation and Improvement, Bulletin 11, 200 p.

Kumaraswamy, P., 1973, Laminar inflow theory for hard-rock open wells: Indian Geohydrology, v. 9, no. 2, p. 53–65.

Lai, R. Y. S., Karadi, G. M., and Williams, R. A., 1973, Drawdown at time-dependent flowrate: Water Resources Bulletin, v. 9, no. 5, p. 892–900.

Lai, R. Y. S., and Su, C., 1974, Nonsteady flow to a large well in a leaky aquifer: Journal of Hydrology, v. 22, p. 333–345.

Larkin, T. J., and Bomar, G. W., 1983, Climatic atlas of Texas: Austin, Texas Department of Water Resources, LP-192, 151 p.

Laubach, S. E., Vendeville, B. C., and Reynolds, S. J., 1990, Downward-steepening normal faults (abs.): Geological Society of America Abstracts with Programs, v. 22, p. A272–A273.

__________ 1991, Patterns in the development of extensional fault-block shapes from comparison of outcrop-scale faults and experimental physical models, *in* Larsen, R. M., ed., Structural and tectonic modeling and its application to petroleum geology: Norwegian Petroleum Society Special Publication, p. 95–101.

LeGrand, H. E., 1949, Sheet structure, a major factor in the occurrence of ground water in the granites of Georgia: Economic Geology, v. 44, p. 110–118.

LeGrande, H. E., and Stringfield, V. T., 1966, Development of permeability and storage in the Tertiary limestones of the southeastern states, U.S.A.: International Association of Scientific Hydrology Bulletin, v. 11, p. 61–73.

Lin-Hua, Song, and Atkinson, T. C., 1991, Chemical reaction between concrete and natural groundwaters and its implications for the commissioning of observation boreholes in chalk: Quarterly Journal of Engineering Geology, v. 24, p. 221–229.

Lock, B. E., 1984, Channels in resedimented chalks, Cretaceous Gulf coastal province of Texas and Mexico: Gulf Coast Geological Society Transactions, v. 34, p. 373.

Longoria, J. F., 1991, Microfacies analysis as a lithocorrelation tool applied to the Austin/Anachacho problem: surface and subsurface of Bexar County, *in* Chuber, Stewart, ed., Austin Chalk Exploration Symposium: South Texas Geological Society, p. 89–99.

Mainster, M. A., and Coppinger, W. W., 1987, Transverse fracture trends developed in Austin Chalk outcrops within the Balcones Fault Zone, Bexar, Comal, and Guadalupe Counties, Texas (abs.): Geological Society of America Abstracts with Programs, v. 19, p. 756.

Mann, W. B., Unterweger, M. P., and Coursey, B. M., 1982, Comments on the NBS tritiated-water standards and their use: International Journal of Applied Radiation and Isotopes, v. 33, p. 383–386.

Marks, P., and Stam, P., 1983, The Austin Chalk–Taylor Clay in Texas and the Santonian–Campanian boundary: Cretaceous Research, v. 4, p. 271–279.

Martinez, Norma, 1982, A regional subsurface study of the Austin Chalk, South Texas: Baylor University, Master's thesis, 113 p.

McDonald, M. G., and Harbaugh, A. W., 1988, A modular three-dimensional finite-difference ground-water flow model: Techniques of Water-Resources Investigations of the U.S. Geological Survey, book 6, chapter A1, variously paginated.

McNulty, C. L., Jr., 1965, Lithology of the Eagle Ford–Austin contact in northeast Texas: The Texas Journal of Science, v. 17, p. 46–55.

Miller, M. A., 1978, Stratigraphic relations of the Austin Chalk (Upper Cretaceous) in Central Texas: Baylor University, Master's thesis, 81 p.

Miller, R., 1982, Public health lessons from prehistoric times: World Water, v. 5, p. 22–25.

Mishra, G. C., and Chachadi, A. G., 1985, Analysis of flow to a large-diameter well during the recovery period: Ground Water, v. 23, p. 646–651.

Mualem, Y., 1976, A new model for predicting the hydraulic conductivity of unsaturated porous media: Water Resources Research, v. 12, p. 513–521.

Muehlberger, W. R., 1990, Regional fracture patterns in the Austin area, Central Texas, *in* Collins, E. W., and Laubach, S. E., eds., Faults and fractures in the Balcones Fault Zone, Austin, p. 29–34.

Muskat, M., 1982, The flow of homogenous fluids through porous media: Boston, Massachusetts, International Human Resources Development Corporation, 763 p.

Neuman, S. P., 1976, User's guide for FREESURF I: Tucson, Arizona, University of Arizona, Department of Hydrology and Water Resources, 22 p.

Neuman, S. P., and Witherspoon, P. A., 1970, Finite element method of analyzing steady seepage with a free surface: Water Resources Research, v. 6, no. 3, p. 889–897.

Nordstrom, D. K., et al., 1979, A comparison of computerized chemical models for equilibrium calculations in aqueous systems, *in* Jenne, E. A., ed., Chemical modeling in aqueous systems: American Chemical Society Symposium Series 93, p. 857–892.

Nordstrom, P. L., 1982, Occurrence, availability, and chemical quality of ground water in the Cretaceous aquifers of North-Central Texas: Austin, Texas Department of Water Resources, Report 269, 61 p.

Papadopulos, I. S., and Cooper, H. H., 1967, Drawdown in a well of large diameter: Water Resources Research, v. 3, no. 1, p. 241–244

Parkhurst, D. L., Thorstenson, D. C., and Plummer, L. N., 1980, PHREEQE—a computer program for geochemical calculation, U.S. Geological Survey, Water Resources Investigation 80-96, 210 p.

Patel, S. C., and Mishra, G. C., 1983, Analysis of flow to a large-diameter well by a discrete kernel approach: Ground Water, v. 21, p. 573–579.

Peacock, D. C. P., and Sanderson, D. J., 1991, Displacements, segment linkage, and relay ramps in normal fault zones: Journal of Structural Geology, v. 13, p. 721–734.

Peck, A. J., 1960, The water table as affected by atmospheric pressure: Journal of Geophysical Research, v. 65, no. 8, p. 2383–2388.

Pessagno, E. A., 1969, Upper Cretaceous stratigraphy of the western Gulf Coast area of Mexico, Texas, and Arkansas: Geological Society of America Memoir 111, 138 p.

Phillips, S., 1987, Shelf sedimentation and depositional sequence stratigraphy of the Upper Cretaceous Woodbine–Eagle Ford Groups, East Texas: Cornell University, Ph.D. dissertation, 507 p.

Plummer, L. N., Parkhurst, D. L., Fleming, G. W., and Dunkle, S. A., 1988, A computer program incorporating Pitzer's equations for calculation of geochemical reactions in brines. U.S. Geological Survey, Water Resources Investigation 88-4153, 301 p.

Podell, Mark, Lewallwn, Kyle, and Krystinik, L. F., 1993, The origin of the "Waco Channel" in the greater Giddings Field area (abs.), *in* Crick, R. E., ed., 1993 Southwest Section Geological Convention, American Association of Petroleum Geologists Transactions and Abstracts, p. 95.

Pollastro, R. M., and Martinez, C. J., 1985, Mineral, chemical, and textural relationships in rhythmic-bedded, hydrocarbon-productive chalk of the Niobrara Formation, Denver Basin, Colorado: The Mountain Geologist, v. 22, p. 55–63.

Pollock, D. W., 1989, Documentation of computer programs to compute and display pathlines using results from the U.S. Geological Survey modular three-dimensional finite-difference ground-water flow model: Washington, D.C., Scientific Software Group, variously paginated.

Price, M., 1985, Introducing groundwater: London, George Allen & Unwin Publishers, Ltd., 191 p.

Quine, Mark, and Bosence, Dan, 1991, Stratal geometries, facies, and sea-floor erosion in Upper Cretaceous Chalk, Normandy, France: Sedimentology, v. 38, p. 1113–1152.

Rajagopalan, S. P., 1983, Analysis of dug-well test data: Journal of Hydrology, v. 64, p. 175–188.

Ramsey, J. G., 1967, Folding and fracturing of rocks: New York, McGraw-Hill, International Series in the Earth and Planetary Sciences, 568 p.

Rasmuson, A., and Neretnieks, I., 1986, Radionuclide transport in fast channels in crystalline rock: Water Resources Research, v. 22, no. 8, p. 1247–1256.

Reaser, D. F., 1957, Geology of the Ferris quadrangle, Dallas and Ellis Counties, Texas: Field and Laboratory, v. 25, no. 4, p. 83–93.

__________ 1961, Balcones Fault system: Its northeast extent: American Association of Petroleum Geologists Bulletin, v. 45, p. 1759–1762.

__________ 1989, Geology of the Texas site for the Superconducting Super Collider (SSC), *in* Field Trip Guide to the Annual Meeting of the South-Central Section of the Geological Society of America, 108 p.

__________ 1991, Structural features near proposed site for the Superconducting Super Collider in North-Central Texas, *in* Chuber, S., ed., Austin Chalk Exploration Symposium: Abstracts and short papers of the South Texas Geological Society, p. 119–122.

Reaser, D. F., and Collins, E. W., 1988, Style of faults and associated fractures in Austin Chalk, northern extension of the Balcones Fault Zone, Central Texas: Gulf Coast Association of Geological Societies Transactions, v. 38, p. 267–276.

Research on Cretaceous Cycles (ROCC) Group, 1986, Rhythmic bedding in Upper Cretaceous pelagic carbonate sequences: Varying sedimentary response to climatic forcing: Geology, v. 14, p. 153–156.

Robinson, N. D., 1986, Fining-upward microrhythms with basal scours in the chalk of Kent and Surrey, England and their stratigraphic importance: Newsletters on Stratigraphy, v. 17, p. 21–28.

Robinson, R. A., Kucker, M. S., and Brouillette, R. P., 1993, Construction behavior of the first underground opening of the Superconducting Super Collider project, in Bowerman, L. D., and Monsees, J. E., eds., 1993 Rapid Excavation and Tunneling Conference (RETC) Proceedings, p. 607–629.

Rodriguez, T. E., and Pratt, L. M., 1985, High-resolution stratigraphic correlation and geochemical analyses, Cretaceous Niobrara Formation, northwestern Denver-Julesurg Basin (abs.): American Association of Petroleum Geologists Bulletin, v. 69, p. 863.

Rushton, K. R., and Holt, S. M., 1981, Estimating aquifer parameters for large-diameter wells: Ground Water, v. 19, p. 505–509.

Rushton, K. R., and Singh, V. S., 1984, Drawdowns in large-diameter wells due to decreasing abstraction rates: Ground Water, v. 21, p. 670–677.

Sakthivadivel, R., and Rushton, K. R., 1989, Numerical simulation of large diameter wells with a seepage face: Journal of Hydrology, v. 107, p. 43–55.

Sammel, E. A., 1974, Aquifer tests in large-diameter wells in India: Ground Water, v. 12, p. 265–272.

Scanlon, B. R., Wang, F. P., and Richter, B. C., 1991, Field studies and numerical modeling of unsaturated flow in the Chihuahuan Desert, Texas: The University of Texas at Austin, Bureau of Economic Geology Report of Investigations No. 199, 56 p.

Schatzinger, R. A., Feazel, C. T., and Henry, W. E., 1985, Evidence of resedimentation in chalk from the Central Graben, North Sea, *in* Crevello, P. D., ed., Deep-water carbonates: buildups, turbidites, debris flows, and chalks; a core workshop: Society of Sedimentary Geology Core Workshop 6, p. 342–385.

Schlanger, S. O., and Douglas, R. G., 1974, The pelagic ooze-chalk-limestone transition and its implications for marine stratigraphy, *in* Hsü, K. J., and Jenkyns, H. C., eds., Pelagic sediments on land and under the sea: International Association Sedimentologists Special Publication no. 1, p. 177–184.

Schneebeli, G., 1966, Hydraulique Souterraine: Paris, Eyrolles, 362 p.

Scholle, P. A., 1977a, Chalk diagenesis and its relation to petroleum exploration: oil from chalks, a modern miracle?: American Association of Petroleum Geologists Bulletin, v. 61, no. 7, p. 982-1009.

_________ 1977b, Current oil and gas production from North American Upper Cretaceous Chalks: U.S. Geological Survey Circular 767, 51 p.

_________ 1977c, Deposition, diagenesis, and hydrocarbon potential of "deeper-water" limestones: American Association of Petroleum Geologists Education Course Note Series no. 7, 27 p.

Scholle, P. A., Arthur, M. A., and Ekdale, A. A., 1983, Pelagic environment, *in* Scholle, P. A., Bebout, D. G., and Moore, C. H., Carbonate depositional environments: American Association of Petroleum Geologists Memoir 33, p. 620–691.

Scholle, P. A., and Cloud, K., 1977, Diagenetic patterns of the Austin Group and their control of petroleum potential, *in* Bebout, D. G., and Loucks, R. G., eds., Cretaceous carbonates of Texas and Mexico—applications to subsurface exploration: The University of Texas at Austin, Bureau of Economic Geology Report of Investigations No. 89, p. 257–259.

Seewald, K. O., 1959, Stratigraphy of the Austin Chalk, McLennan County, Texas: Baylor University, Master's thesis, 42 p.

Singh, V. S., and Gupta, C. P., 1986, Hydrogeological parameter estimation from pump tests on a large diameter well: Journal of Hydrology, v. 87, p. 223–232.

Smith, C. I., 1955, Stratigraphy of the upper Austin in the vicinity of Dallas, Texas: Louisiana State University, Master's thesis, 30 p.

Snow, D. T., 1968, Rock fracture spacings, openings, and porosities: Journal of Soil Mechanics and Foundation Division, American Society of Civil Engineers, Proceedings, v. 94, p. 73–91.

SPSS, 1990, Statistical data analysis, operations guide for Macintosh: Chicago, Statistical Package for the Social Sciences, Inc., 159 p.

Surles, M. A., Jr., 1983, Nature and significance of the Austin–Taylor unconformity on the western margin of the East Texas Basin: Baylor University, Bachelor's thesis, 65 p.

Taggart, J. N., 1953, Problems in correlation of terraces along the Trinity River in Dallas County, Texas: Southern Methodist University, Master's thesis, 21 p.

Texas Department of Health, 1970, Individual home water supplies: Texas, 46 p.

The Earth Technology Corporation, 1990a, Bedrock geology of the Superconducting Super Collider site: Long Beach, California, Project No. 87-888-0017, Report No. SSC-GR-65, variously paginated.

_________ 1990b, Geomechanical characterization of Austin Chalk Formation at the Superconducting Super Collider site: Long Beach, California, Project No. 87-888-0017, Report No. GR-67, variously paginated.

_________ 1990c, Groundwater monitor wells at the Superconducting Super Collider site, May 1989 to May 1990: Long Beach, California, Project No. 87-888-0017, Report No. SSC-GR-64, variously paginated.

__________ 1990d, Groundwater monitor wells at the Superconducting Super Collider site, November 1990 addendum (includes vibration monitoring borings): Long Beach, California, Project No. 87-888-0017, Report No. SSC-GR-64A, variously paginated.

__________ 1990e, Hydrogeologic conditions at the Superconducting Super Collider site: Long Beach, California, Project No. 87-888-0017, Report No. SSC-GR-63, variously paginated.

__________ 1990f, Thickness of Chambers Creek terrace near Lumkins, Texas: Long Beach, California, Project No. 87-888-0017, Report No. SSC-GR-62, variously paginated.

Theis, C. V., 1935, The relation between the lowering of the piezometric surface and the rate and duration of discharge of a well using groundwater storage: American Geophysical Union Transaction, v. 16, p. 519–524.

Thompson, G. L., 1967, Ground-water resources of Ellis County, Texas: Austin, Texas Water Development Board Report 62, 115 p.

Thornhill, S. A., 1982, Austin Chalk and its petroleum potential: south-central Texas: Baylor University, Master's thesis, 161 p.

Todd, D. K., 1959, Ground water hydrology: New York, John Wiley & Sons, Inc., 336 p.

Tóth, Jósef, 1963, A theoretical analysis of groundwater flow in small drainage basins: Journal of Geophysical Research, v. 68, no. 16, p. 4795–4812.

__________ 1978, Gravity-induced cross-formation flow of formation fluids, Red Earth Region, Alberta, Canada: analysis, patterns, and evolution: Water Resources Research, v. 14, no. 5, p. 805–843.

Townley, L. R., 1990, AQUIFEM-N: a multi-layered finite element aquifer flow model, user's manual and description: Perth, Western Australia, CSIRO Division of Water Resources.

Travis, B. J., 1980, WAFE: A model for two-phase, multicomponent mass and heat transport in porous/fractured media: Los Alamos National Laboratory Report LA-10488-MS, draft.

Tucholke, B. E., and Mountain, G. S., 1979, Seismic stratigraphy, lithostratigraphy, and paleosedimentation patterns in the western North Atlantic, *in* Talwani, M., Hay, W. W., and Ryan, W. B. F., eds. Deep drilling results in the Atlantic Ocean; continental margins and paleoenvironment: American Geophysical Union, Maurice Ewing Series No. 3, p. 58–86.

Tucker, D. R., and Henecy, D. P., 1987, Mini-shelves in the Taylor Shale: stratigraphy of the late Cretaceous and early Tertiary units of Bastrop County, Texas: Gulf Coast Association of Geological Societies Transactions 32, p. 263–276.

U.S. Army Corps of Engineers, 1992, Results of tests of video camera investigation: monitor wells—Superconducting Super Collider: U.S. Army Corps of Engineers, Southwestern Division Laboratory, Report no. SWDED-GL 15561, prepared for SSC Laboratory Environment Safety and Health Oversight Office, 46 p.

U.S. Environmental Protection Agency, 1975, Manual of individual water supply systems: Washington, D.C., EPA-430/9-74-007, 155 p.

van Genuchten, M. Th., 1978, Calculating the unsaturated hydraulic conductivity with a new closed-form analytical model: Princeton University, Department of Civil Engineering, Water Resources Program Research Report 78-WR-08, 63 p.

_________ 1980, A closed-form equation for predicting the hydraulic conductivity of unsaturated soils: Soil Science Society of America Journal, 44, p. 892–898.

Walton, W. C., 1970, Groundwater resource evaluation: New York, McGraw-Hill, 664 p.

Watt, S. B., and Wood, W. E., 1976, Hand dug wells and their construction: London, International Technology Publications, Ltd., p. 234.

Weeks, Edwin, 1979, Barometric fluctuations in wells tapping deep unconfined aquifers: Water Resources Research, v. 15, no. 5, p. 1167–1176.

Werner, M., 1989, Discussion of faulting in Superconducting Super Collider supplemental environmental impact statement: Long Beach, California, The Earth Technology Corporation, report no. SSC-GR-76, variously paginated.

White, D. E., 1965, Saline waters of sedimentary rocks: American Association of Petroleum Geologists Memoir, v. 4, p. 342–366.

Wickham, M. K., and Dutton, A. R., 1991, Transient simulation of ground-water flow and particle path lines: hydrogeologic case study of Pleistocene alluvium overlying the Superconducting Super Collider site, Ellis County, Texas: The University of Texas at Austin, Bureau of Economic Geology, contract report prepared for the Texas National Research Laboratory Commission under contract no. (90-91)-1650, August 1, 1991, 117 p.

Wikramaratna, R. S., 1985, A new type-curve method for the analysis of pumping tests in large-diameter wells: Water Resources Research, v. 21, no. 2, p. 261–264.

Wood, W. W., 1976, Guidelines for collection and field analysis of ground-water samples for selected unstable constituents: U.S. Geological Survey, Techniques of Water-Resources Investigations, book 1, chapter D2, 24 p.

Yelderman, J. C., Jr., Barrett, D. P., and Barquist, B. A., 1988, The effects of structure and weathering fractures on shallow groundwater systems, in Proceedings of the 1988 International Symposium on fracture flow: Atlanta, Georgia State University, p. 487–500.

Young, Keith, 1986, Cretaceous marine inundations of the San Marcos Platform, Texas: Cretaceous Research, v. 7, p. 117–140.

Young, Keith, Barker, D. S., and Jonas, E. C., 1975, Stratigraphy of the Austin Chalk in the vicinity of Pilot Knob: South Central Section Geological Society of America field trip guidebook, 18 p.

Young, Keith, and Woodruff, C. M., Jr., 1985, Austin Chalk in its type area—stratigraphy and structure: Austin Geological Society, Guidebook 7, 88 p.

Zdankus, N. T., 1974, Analysis of shallow hard rock well pumping and recovery test data: Ground Water, v. 12, no. 5, p. 310–317.

Appendix A. Inventory of Water Wells on SSC Footprint, Including West and East Campuses

Appendix A. SSC well inventory data base

Well ID	Map no.	NAD 83 northing (ft)	NAD 83 easting (ft)	Beam distance (ft)	Within ease-ment	Ground surface elev. (ft)	Well depth (ft)	Water level elev. (ft)	Date meas M/D/Y	Forma-tion	Diameter surface casing (ft)	Casing material	Well use	Wellhead condition
1B-1	28	6803223	2472236	1,900	n	583	-	-	-	-	-	-	-	-
1F-1	28	6788363	2457628	3,200	n	600	0	-	-	Kau	-	brick	abandoned	filled
2-1	95	6787360	2531035	3,750	n	460	22.4	451	4/17/91	Ko	2.2	brick	unused	uncovered/pump
8A-1	28	6792142	2459901	1,800	y	580	14.9	573.4	4/18/91	Kau	3.7	brick	unused	uncovered
8A-2	28	6786067	2461360	100	y	583	42.4	676.9	4/18/91	Kau	3	brick	unused	formica board cover
8A-3	28	6790888	2458827	0	y	550	128	540.9	2/28/91	Kau	0.2	pvc	monitor	steel cover
8B-1	28	6790636	2457838	750	y	570	21.9	553.9	4/16/91	Kau	4.1	brick	unused	uncovered
8B-2	28	6786583	2458993	1,800	n	575	16.6	570.4	4/18/91	Kau	2.5	brick	unused	uncovered
11-1	28	6792255	2459402	1,400	n	570	21.1	556.9	4/23/91	Kau	3	brick	unused	wood cover
14-1	29	6778883	2462074	4,200	n	522	-	-	-	-	-	steel	-	housed
15-1	43	6781959	2467155	1,700	n	530	-	-	-	Kau	-	brick	unused	steel & stove on top
16A-1	28	6793255	2454122	3,000	n	612	10.4	604.8	3/27/91	Kau	3.5	brick	unused	covered w/ 4 ft trestles
17C-1	82	6782443	2523123	200	y	-	-	-	-	-	-	-	abandoned	filled
17C-2	82	6782467	2523143	200	y	-	-	-	-	-	-	-	abandoned	filled
18D-1	82	6778921	2519286	0	y	485	350	419.4	2/27/91	Ko/Kau	0.2	pvc	abandoned	filled
19C-1	28	6793749	2454722	2,200	n	568	-	-	2/27/92	Kau	-	brick	abandoned	windmill over top
19D-1	27	6796272	2456007	0	y	619	226	594.4	1/29/91	Kau/Ksb	0.3	pvc	monitor	steel cover
21A-1	27	6795266	2455271	1,150	y	610	14	-	-	Kau	3	brick	abandoned	filled w/ tire & wire
21B-1	27	6796867	2455942	0	y	618	295	596.3	2/28/91	Kau/Ksb	0.3	pvc	monitor	steel cover
27A-1	93	6805785	2534801	1,850	n	485	-	478.3	5/15/91	Kwc	2.2	brick	unused	cement (collapsing)
28-1	27	6800108	2462259	7,100	y	682	-	-	-	-	0.3	steel	unused	pump on wellhead
28-2	27	6800087	2462376	7,200	y	682	12.6	671.7	3/27/91	Kau	5.5	none	unused	uncovered
30-1	27	6799388	2459736	4,500	y	615	20.3	610.9	3/21/92	Kau	2.1	brick	domestic	pump on wellhead
32E-1	26	6802379	2456945	2,800	y	648	19.4	644.9	3/27/91	Kau	2.5	brick	unused	uncovered
33-1	93	6806882	2534146	1,100	n	493	10.7	487.8	4/17/91	Kwc	6	brick	unused	wood cover
35-1	93	6807684	2533198	100	y	493	44.6	484	4/17/91	Kwc	2.5	concrete	lawn	covered
37-1	27	6800913	2457927	3,400	y	657	24.9	648.7	3/27/91	Kau	1.5	brick	unused	uncovered
37-2	27	6800903	2458103	3,550	y	657	20.5	647.1	3/27/91	Kau	1.8	brick	unused	wood cover
38B-1	26	6802373	2456943	2,800	y	650	30.5	646.9	3/19/91	Kau	2.5	brick	unused	pump on wellhead
38C-1	90	6833012	2526301	600	y	465	30.3	463.5	4/16/91	Ko	2.7	brick	unused	uncovered
38C-2	90	6833600	2526634	50	y	460	19.7	458.8	8/11/92	Ko	2	brick	unused	no crown, plywood top
38C-3	90	6831583	2527673	25	y	440	421	447.3	2/27/91	Ko/Kau	0.3	pvc	monitor	steel cover
38C-4	90	6832735	2526767	250	y	465	20.2	458.7	8/11/92	Ko	2	brick	unused	plywood cover
39-1	25	6811183	2453076	875	y	735	10.6	729	3/19/91	Kau	2.5	brick	unused	housed, wood cover
41A-1	26	6809024	2454407	200	y	740	16.8	732.7	3/19/91	Kau	3	brick	unused	uncovered
41A-2	26	6809111	2454573	50	y	740	19.5	730.3	3/19/91	Kau	2.9	brick	unused	uncovered
41A-3	26	6809136	2454394	150	y	745	1,700?	-	-	-	0.5	steel	lawn	pump on wellhead
46B-1	25	6813045	2461329	2,000	n	670	-	-	-	-	0.1	steel	abandoned	uncovered
46C-1	25	6814377	2460930	1,275	y	645	13	642.4	3/21/91	Kau	2.5	brick	unused	uncovered
46C-2	25	6814443	2460842	1,175	y	645	-	-	-	Kau	-	-	-	-
46C-3	25	6814433	2460729	1,075	y	645	-	-	-	-	0.3	steel	domestic	pump on wellhead
46C-4	25	6814624	2460432	750	y	650	-	-	-	Kau	-	-	-	-
46C-5	25	6813302	2457175	1,900	y	735	-	734.7	3/21/92	-	-	steel	unused	housed
46E-1	25	6816828	2463014	3,400	n	640	30.5	636	5/23/91	Kau	3	brick	unused	steel gate cover
46E-2	25	6816667	2463088	3,400	n	645	-	-	-	Kau	3	brick	unused	heavy cement cover
47-1	-	not located	-	-	-	-	-	-	-	-	-	-	-	-
50B-1	93	6805552	2535270	2,300	n	490	25.3	486.6	4/17/91	Kwc	2.3	brick	lawn	wood cover
52B-1	26	6809745	2462184	4,400	n	715	20.4	705.3	3/21/91	Kau	2.3	brick	unused	housed, uncovered
52B-2	25	6810019	2462266	4,200	n	720	2.5	-	-	Kau	4.5	none	abandoned	uncovered
57-1	93	6809908	2533240	150	y	470	5	-	-	Ko	2	brick	abandoned	filled

Appendix A. (continued)

Well ID	Utility	Other ID	Relative depth	Notes	Owner	City	State
1B–1	well	-	shallow	northwest corner	Ludlow	Waxahachie	TX
1F–1	well	-	shallow	near road	Ludlow	Waxahachie	TX
2–1	well	-	shallow	5 ft from east end house	Griffin	Ennis	TX
8A–1	well	-	shallow	hand dug near old house	Chapman	Waxahachie	TX
8A–2	well	-	shallow	near old house	Chapman	Waxahachie	TX
8A–3	well	BE 10	deep	SSCL well	Chapman	Waxahachie	TX
8B–1	well	-	shallow	SW of old house in pasture	Chapman	Waxahachie	TX
8B–2	well	-	shallow	NW side of house	Chapman	Waxahachie	TX
11–1	well	-	shallow	in pasture by pecan tree	Rogers	Waxahachie	TX
14–1	well	-	deep	between house and access road	McNeely	Boston	MA
15–1	well	-	shallow	at abandoned house	Kirkland	Waxahachie	TX
16A–1	well	-	shallow	in pasture beneath wood pile	Wakeland	Waxahachie	TX
17C–1	well	-	shallow	by side porch	Farmer	Bardwell	TX
17C–2	well	-	shallow	by back door	Farmer	Bardwell	TX
18D–1	well	BF 7	deep	SSCL well	Walker	Bardwell	TX
19C–1	well	-	shallow	beneath windmill near creek	Worshan	Duncanville	TX
19D–1	well	BIR 41	deep	SSCL well	Worshan	Duncanville	TX
21A–1	well	-	shallow	near barn and old shed	Wheeler	Waxahachie	TX
21B–1	well	BIR 31	deep	SSCL well	TNRLC	-	-
27A–1	well	-	shallow	NW corner behind house	Gibson	Dallas	TX
28–1	well	-	deep	near old barn	Glass	Dallas	TX
28–2	well	-	shallow	behind eastern house	Glass	Dallas	TX
30–1	well	-	shallow	near center of pasture by creek	Morrison	Waxahachie	TX
32E–1	well	-	shallow	NE part of pasture	Allen	Waxahachie	TX
33–1	well	-	shallow	behind house north of barn	Kohn	Dallas	TX
35–1	well	-	shallow	in front yard	Bates	Ennis	TX
37–1	well	-	shallow	in sidewalk in backyard	Dunaway	Trophy Club	TX
37–2	well	-	shallow	N side of house	Dunaway	Trophy Club	TX
38B–1	well	-	shallow	behind house	Ackley	Waxahachie	TX
38C–1	well	-	shallow	just off road near creek/pond	Ackley	Waxahachie	TX
38C–2	well	-	shallow	50 ft from road, W of dirt road	Ackley	Waxahachie	TX
38C–3	well	BIR 54	deep	SSCL well	Ackley	Waxahachie	TX
38C–4	well	-	shallow	near road	Ackley	Waxahachie	TX
39–1	well	-	shallow	in white shed S of house	Ackley	Waxahachie	TX
41A–1	well	-	shallow	by house	Wilburn	Waxahachie	TX
41A–2	well	-	shallow	E of house by white well shed	Wilburn	Waxahachie	TX
41A–3	well	-	deep	behind house	Wilburn	Waxahachie	TX
46B–1	well	-	deep	S end of property	Aday	Waxahachie	TX
46C–1	well	-	shallow	by stream on SE corner	Aday	Waxahachie	TX
46C–2	spring	-	spring	in clump on trees	Aday	Waxahachie	TX
46C–3	well	-	deep	in metal shed along drive	Aday	Waxahachie	TX
46C–4	spring	-	spring	N of barns	Aday	Waxahachie	TX
46C–5	well	-	deep	in well case with well frame	Aday	Waxahachie	TX
46E–1	well	-	shallow	by pumphouse	Aday	Waxahachie	TX
46E–2	well	-	shallow	-	Aday	Waxahachie	TX
47–1	-	-	-	reported to be in rear of lot	Nelson	Waxahachie	TX
50B–1	well	-	shallow	N side of house	Nesuda	Mesquite	TX
52B–1	well	-	shallow	behind house in shed	Pigg	Bryan	TX
52B–2	well	-	shallow	SW side of barn	Pigg	Bryan	TX
57–1	well	-	shallow	southeast, 200 ft from road	Reeves	Lancaster	TX

Appendix A. SSC well inventory data base

Well ID	Map no.	NAD 83 northing (ft)	NAD 83 easting (ft)	Beam distance (ft)	Within ease-ment	Ground surface elev. (ft)	Well depth (ft)	Water level elev. (ft)	Date meas M/D/Y	Forma-tion	Diameter surface casing (ft)	Casing material	Well use	Wellhead condition
60–1	65	6853193	2511144	3,700	n	496	19.6	490.2	4/5/91	Qt	3	brick	unused	cement cover
60–2	65	6853427	2511087	3,600	n	497	27	489.1	4/5/91	Qt	0.6	ceramic	unused	pump on wellhead
62A–1	61	6769591	2492774	0	y	515	232	494.7	2/28/91	Kau	0.2	pvc	abandoned	filled
62C–1	61	6769711	2490631	100	y	508	19.8	500.2	4/18/91	Ko	2.5	cement	unused	concrete cover
62C–2	61	6769694	2490887	100	y	512	20 ?	-	-	Ko	-	-	-	-
62D–1	61	6768390	2490682	1,200	n	535	-	-	-	-	-	-	-	-
63–1	93	6809679	2533506	400	y	475	15.8	465.2	4/17/91	Ko	10	cement	unused	wood cover
64–1	60	6773897	2492154	4,600	n	473	0	-	-	-	-	-	abandoned	filled
69–1	64	6863562	2500462	100	y	505	31.7	487	5/14/91	Kau	3	corr. steel	lawn	housed
72A–1	93	6809550	2533023	50	y	470	35.9	463.3	5/16/91	Ko	2.4	concrete	unused	cement cover
75–1	43	6779852	2467146	100	y	543	167.5	524.7	2/28/91	Kau	0.2	pvc	monitor	steel cover
76–1	43	6781879	2467221	1,650	n	530	15.3	517.8	4/30/91	Kau	3.2	brick	livestock	cement cover
77–1	43	6783055	2469164	3,850	n	575	-	-	-	Kau	-	-	-	-
78A–1	92	6810408	2534146	1,050	y	490	-	-	-	-	-	-	abandoned	plugged at top
78A–2	92	6810232	2533781	950	y	492	-	-	-	-	0.7	steel	abandoned	plugged ?
79–1	92	6812449	2533170	200	y	475	0	-	-	-	-	-	abandoned	filled
79–2	92	6812454	2533192	200	y	475	0	-	-	-	-	-	abandoned	filled
80C–1	44	6777981	2467777	1,000	n	500	8.2	493.7	4/16/91	Qt	2.8	brick	unused	uncovered
86A–1	44	6775650	2472131	200	y	500	12.4	496.7	4/18/91	Qt	3.1	brick	unused	uncovered
86A–2	44	6775700	2472120	200	y	510	16.7	507.7	4/18/91	Qt	14	concrete	unused	uncovered
86B–1	26	6803416	2452944	50	y	665	20.5	660.7	3/20/91	Kau	3.5	brick	unused	uncovered
86B–2	26	6803737	2452815	0	y	673	265	667.7	2/28/91	Kau/Ksb	0.3	pvc	monitor	steel cover
86B–3	26	6803467	2453022	0	y	665	312.6	657.8	2/28/91	Kau/Ksb	0.3	pvc	monitor	steel cover
86C–1	26	6805374	2452035	150	y	687	29.1	674.4	6/12/91	Kau	3	none	unused	uncovered
86C–2	26	6804633	2452460	50	y	682	12.8	678.1	6/12/91	Kau	3	none	abandoned	uncovered
86C–3	26	6803922	2453269	300	y	660	17.6	654.8	3/20/91	Kau	2	brick	unused	wire to block hole
86E–1	44	6774707	2474096	0	y	524	50	-	-	Qt	0.2	pvc	monitor	monitor well cover
88B–1	14	6805828	2451954	50	y	690	29.4	674.4	3/19/91	Kau	2.8	brick	unused	covered w/ metal pan
90-1	9	6847307	2449734	3,050	n	685	8.5	681.9	4/3/91	Kau	2.5	concrete	unused	metal fence
94–1	11	6831342	2444540	3,150	y	739	-	-	-	-	0.5	steel	unused	pump on wellhead
94–2	11	6830701	2447604	0	y	675	105	661.6	3/1/91	Kau/Ksb	0.2	pvc	monitor	steel cover
94–3	11	6830681	2447602	0	y	675	164	535.8	3/1/91	Ksb	0.2	pvc	monitor	steel cover
94–4	11	6830667	2447603	0	y	675	59	661.5	3/1/91	Kau	0.2	pvc	monitor	steel cover
94–5	11	6828317	2440477	7,200	n	805	-	620.9	5/21/91	-	0.4	steel	unused	uncovered
94–6	11	6832267	2448113	300	y	731	221	663.5	2/28/91	Ksb	0.2	pvc	monitor	steel cover
94–7	11	6831908	2450199	2,400	n	725	15.6	720.1	5/21/91	Kau	3	brick	unused	uncovered
94–8	11	6832353	2450947	3,100	n	730	24.7	722.7	5/21/91	Kau	4	brick	unused	housed
95A–1	11	6830255	2450906	3,312.5	n	710	-	-	-	Kau	-	brick	-	covered
101–1	69	6768505	2500489	1,300	n	512	17	-	-	Ko	5.4	brick	unused	uncovered
103C–1	27	6799738	2454419	50	y	633	38.9	620.7	3/28/91	Kau	2	brick	unused	wood cover w/ screen
104A–1	27	6801607	2454070	100	y	640	19.7	635.9	3/20/91	Kau	2.5	cement	unused	uncovered
104B–1	26	6802863	2453360	0	y	655	-	-	-	Kau	-	-	unused	under porch
106A–1	14	6804457	2450458	2,000	y	680	47.6	671.4	11/19/91	Kau	2.3	brick	unused	wood cover with trash
107A–1	21	6843232	2453725	2,400	n	691	450 ?	-	-	Kwb?	-	steel	unused	housed
107A–2	21	6844119	2453405	1,700	n	678	0	-	-	-	-	-	abandoned	filled
107A–3	21	6843067	2454337	3,100	n	681	27.8	673.4	4/4/91	Kau	1.6	brick	unused	cement slab
107A–4	21	6842931	2454863	3,600	n	675	16.9	667	4/4/91	Kau	3.5	brick	unused	uncovered
107A–5	21	6845874	2452651	0	y	674	211	617.9	2/28/91	Kau/Ksb	0.2	pvc	monitor	steel cover
107C–1	12	6819904	2451487	800	y	730	3	-	-	Kau	3	cement	abandoned	covered w/ livestock pan
107C–2	12	6820365	2451437	400	y	730	0	-	-	Kau	-	-	abandoned	uncovered

Well ID	Utility	Other ID	Relative depth	Notes	Owner	City	State
60–1	well	-	shallow	behind barn	Prude	Palmer	TX
60–2	well	-	shallow	in small shed in field	Prude	Palmer	TX
62A–1	well	BF 8	deep	SSCL well	Odom	Waxahachie	TX
62C–1	well	-	shallow	in pasture N side of house	Odom	Waxahachie	TX
62C–2	well	-	shallow	in shed by office, SW of drive	Odom	Waxahachie	TX
62D–1	well	-	shallow	-	Odom	Waxahachie	TX
63–1	well	-	shallow	in front of house	Holt	Ennis	TX
64–1	well	-	shallow	by metal barn	Thompson	Waxahachie	TX
69–1	well	-	shallow	SE of house	Lockhart	Red Oak	TX
72A–1	well	-	shallow	W of house by sheds	Potter	Ennis	TX
75–1	well	BF 9	deep	SSCL well	Dana	DeSoto	TX
76–1	well	-	shallow	under windmill, E of trailer	Price	Waxahachie	TX
77–1	well	-	shallow	SW corner of house	Hill	Denison	TX
78A–1	well	-	deep	oil, plugged 30 yrs ago	Reynal	Ennis	TX
78A–2	well	-	deep	oil, plugged 30 yrs ago	Reynal	Ennis	TX
79–1	well	-	shallow	N side of house	Maliska	Ennis	TX
79–2	well	-	shallow	N side of barn	Maliska	Ennis	TX
80C–1	well	-	shallow	S of old barn	Bynum	Forreston	TX
86A–1	well	-	shallow	near creek	Underwood	Waxahachie	TX
86A–2	well	-	shallow	near creek	Underwood	Waxahachie	TX
86B–1	well	-	shallow	N of old house	Underwood	Waxahachie	TX
86B–2	well	BIR 11	deep	SSCL well	Underwood	Waxahachie	TX
86B–3	well	BIR 21	deep	SSCL well	Underwood	Waxahachie	TX
86C–1	well	-	shallow	NW corner of property	Underwood	Waxahachie	TX
86C–2	well	-	shallow	on west end, 1/2 way down road	Underwood	Waxahachie	TX
86C–3	well	-	shallow	E of barn	Underwood	Waxahachie	TX
86E–1	well	E-9	shallow/50 ft	just of road	Underwood	Waxahachie	TX
88B–1	well	-	shallow	in field	Underwood	Waxahachie	TX
90-1	well	-	shallow	50 ft SW of house, in creek	Davis	Midlothian	TX
94–1	well	-	deep	windmill on top	Meadows	Dallas	TX
94–2	well	B 1697A	deep	SSCL well	Meadows	Dallas	TX
94–3	well	B 1697	deep	SSCL well	Meadows	Dallas	TX
94–4	well	B 1697B	shallow/59 ft	SSCL well	Meadows	Dallas	TX
94–5	well	-	deep	windmill	Meadows	Dallas	TX
94–6	well	BF 1	deep	SSCL well	Meadows	Dallas	TX
94–7	well	-	shallow	by barn	Meadows	Dallas	TX
94–8	well	-	shallow	in shed	Meadows	Dallas	TX
95A–1	well	-	shallow	in drive	-	-	TX
101–1	well	-	shallow	SW corner of burned barn	McConnell	Italy	TX
103C–1	well	-	shallow	E side of house	Bratcher	Waxahachie	TX
104A–1	well	-	shallow	10 yards SW of house	Coker	Waxahachie	TX
104B–1	well	-	shallow	under porch	Coker	Waxahachie	TX
106A–1	well	JK-33-41-501	shallow	behind house	Sparks	Waxahachie	TX
107A–1	well	-	deep	N side of house	May	Midlothian	TX
107A–2	well	-	shallow	in creek bed behind barn	May	Midlothian	TX
107A–3	well	-	shallow	N of road, E of house, by road	May	Midlothian	TX
107A–4	well	-	shallow	SE corner of property, by tree	May	Midlothian	TX
107A–5	well	BE 2	deep	SSCL well	May	Midlothian	TX
107C–1	well	-	shallow	S part of lot by metal tanks	May	Midlothian	TX
107C–2	well	-	shallow	along creek, in bad shape	May	Midlothian	TX

Appendix A. SSC well inventory data base

Well ID	Map no.	NAD 83 northing (ft)	NAD 83 easting (ft)	Beam distance (ft)	Within ease-ment	Ground surface elev. (ft)	Well depth (ft)	Water level elev. (ft)	Date meas M/D/Y	Forma-tion	Diameter surface casing (ft)	Casing material	Well use	Wellhead condition
107C-3	12	6820765	2451277	0	y	700	184.5	679.2	3/1/91	Kau	0.2	pvc	monitor	steel cover
111A-1	74	6842231	2518412	4,300	n	485	-	-	-	-	-	cement	unused	cement
111B-1	74	6844515	2521980	0	y	464	335	446.6	3/1/91	Kau	0.2	pvc	monitor	steel cover
114-1	73	6850839	2520638	2,100	n	483	-	-	-	-	-	-	-	-
117C-1	21	6847575	2453051	350	y	610	13.8	608.4	5/10/91	Qal	2.6	corr. steel	unused	uncovered
118B-1	92	6815191	2532217	400	n	502	0	-	-	-	-	-	abandoned	filled
120-1	21	6848802	2454040	260	n	620	1,100?	-	-	-	0.2	steel	-	housed
120-2	21	6848660	2453570	470	n	600	48.9	585.3	3/26/92	Kau	2.4	concrete	unused	concrete cover
121A-1	20	6857250	2461575	285	n	660	-	-	-	-	-	-	-	-
121F-1	20	6857255	2461420	400	y	670	-	-	-	-	-	-	-	-
128C-1	14	6805288	2451743	150	y	690	2,606	640	4/1/75	Kctm	0.5	steel	municipal	pump on wellhead
128D-1	13	6816234	2446726	2,000	y	750	2,564	-26	1/21/77	Kctm	0.3	steel	municipal	pump on wellhead
134-1	20	6856397	2461093	25	y	683	208	671.5	2/28/91	Kau	0.2	pvc	monitor	steel cover
137	-	not located	-	-	-	-	-	-	-	-	-	-	-	-
141-1	12	6818656	2448230	0	y	763	257.4	571.6	2/28/91	Ksb	0.2	pvc	abandoned	filled
144-1	13	6810290	2451115	700	y	720	30.8	712.6	3/20/91	Kau	2.5	cement	unused	cement cover
145-1	13	6811529	2450459	250	y	700	6.4	699.5	5/15/91	Kau	2.7	brick	unused	uncovered
153B-1	13	6810785	2451903	730	y	734	231	712.6	2/28/91	Kau	0.2	pvc	monitor	steel cover
156-1	13	6814794	2448849	250	y	743	22.8	739.5	11/19/91	Kau	3.5	brick	abandoned	uncovered, at grade
156-2	13	6812380	2447886	1,800	y	685	-	-	-	Kau	-	brick?	unused	bolted shut
156-3	13	6812172	2448000	1,700	y	685	727	-	-	Kwb	0.4	steel	abandoned	
156-4	13	6814526	2447699	1,350	y	705	27.9	704.7	11/21/91	Kau	3	brick	abandoned	
156-5	13	not located	-	-	-	-		-	-	-	-	-	abandoned	
156-6	13	not located	-	-	-	-	-	-	-	-	-	-	abandoned	
156-7	13	not located	-	-	-	-	-	-	-	-	-	-	abandoned	-
156-8	13	not located	-	-	-	-	-	-	-	-	-	-	abandoned	-
157A-1	49	6864865	2479147	400	n	643	0	-	-	-	-	-	abandoned	filled
159-1	48	6867686	2478150	2,400	n	655	28.7	649.4	4/4/91	Kau	4.3	brick	abandoned	fenced
159-2	48	6867861	2477988	2,600	n	664	26.1	652.3	4/4/91	Kau	2	brick	abandoned	fenced
160-1	64	6859407	2511400	1,300	n	511	21.3	503.5	4/5/91	Qt	4	brick	unused	wood cover
161-1	72	6858827	2515152	3,400	n	502	35.6	498.4	4/8/91	Qt	0.2	pvc	monitor	good
162A-1	73	6854485	2514277	350	n	496	0	-	-	-	-	-	abandoned	filled
162A-2	73	6855071	2515277	720	n	497	44.83(60)*	494.5	2/28/92	Qt/Ko	0.2	pvc	monitor	monitor well cover
162C-1	90	6832679	2529368	1,950	n	455	1	-	-	-	-	brick	abandoned	filled
163A-1	90	6829848	2532271	3,600	n	472	17.6	458.7	5/7/91	Ko	3	brick	unused	wood cover
163A-2	90	6831822	2533761	5,700	n	470	0	-	-	-	-	-	abandoned	filled
163A-3	90	6828432	2529228	200	y	480	0	-	-	-	-	brick	abandoned	filled
163B-1	90	6829885	2529166	700	y	475	0	-	-	-	-	-	abandoned	filled
166-1	83	6776416	2513854	1,150	n	453	15.4	443.3	5/2/91	Ko	3	brick	unused	cement cover
167A-1	83	6777638	2514928	1,600	n	485	11.6	477.3	5/17/91	Ko	2.7	brick	unused	wood cover
169-1	69	6768548	2500736	1,500	n	512	-	-	-	-	-	-	-	pump on wellhead
169-2	69	6768468	2500733	1500	n	512	0	-	-	-	-	-	abandoned	filled
172-1	92	6816354	2532872	450	y	510	9.7	505.4	10/9/91	Kwc	5	wood	unused	wood cover
172-2	92	6817710	2532149	0	y	484	419	532.5	2/27/91	Kau	0.2	pvc	monitor	steel cover
173-1	83	6774304	2512878	200	y	465	20?	-	-	Ko?	-	-	-	-
174-1	49	6865478	2482569	350	n	600	-	-	-	Kau	-	-	unused	housed
174-2	49	6865563	2482353	250	y	610	-	-	-	Kau	-	-	unused	wire covers wellhead
177-1	73	6851961	2514650	1,850	n	485	17.5	471	4/8/91	Qt	2.7	-	domestic	-
178A-1	92	6816574	2534053	1,700	n	522	22	503.4	4/23/91	Kwc	2.5	brick	unused	wood cover
178A-2	92	6816465	2533899	1,500	n	519	28.1	509.7	4/23/91	Ko	3	brick	animals	uncovered

Well ID	Utility	Other ID	Relative depth	Notes	Owner	City	State
107C–3	well	BI 4	deep	SSCL well	May	Midlothian	TX
111A–1	cistern	-	shallow	at house	Harper	Palmer	TX
111B–1	well	BE 5	deep	SSCL well	Harper	Palmer	TX
114–1	well	BEG 117	deep	at house	Michael	Nokomis	IL
117C–1	well	-	shallow	30-40 ft from end of dam	Ratzman	Midlothian	TX
118B–1	well	-	shallow	SE side of house	Mittelbach	Dallas	TX
120–1	well	-	deep	near old house	Pierce	Midlothian	TX
120–2	well	-	shallow	near creek	Pierce	Midlothian	TX
121A–1	well	-	-	next to barn	Alford	Waxahachie	TX
121F–1	cistern	-	shallow	in back lot	Alford	Waxahachie	TX
128C–1	well	JK-33-41-501	deep	public water well	Buena Vista Water Co.	Waxahachie	TX
128D–1	well	JK-33-41-203	deep	by water tanks	Buena Vista Water Co.	Waxahachie	TX
134–1	well	BF 2	deep	SSCL well	Glass	Dallas	TX
137	well	-	-	reportedly covered	Phillips	Waxahachie	TX
141–1	well	BE 1-90	deep	SSCL well	Morris	Mesquite	TX
144–1	well	-	shallow	S of red barn, 75 yards	Howard	Waxahachie	TX
145–1	well	-	shallow	N of barn	Vargas	Waxahachie	TX
153B–1	well	BI 6	deep	SSCL well	Wesson	Waxahachie	TX
156–1	well	-	shallow	behind house	Hitt	Dallas	TX
156–2	well	-	shallow	N side of house	Hitt	Dallas	TX
156–3	well	JK-33-41-202	deep	behind house	Hitt	Dallas	TX
156–4	well	-	shallow	by tank	Hitt	Dallas	TX
156–5	well	-	-	listed on UFS map	Hitt	Dallas	TX
156–6	well	-	-	listed on UFS map	Hitt	Dallas	TX
156–7	well	-	-	listed on UFS map	Hitt	Dallas	TX
156–8	well	-	-	listed on UFS map	Hitt	Dallas	TX
157A–1	well	-	shallow	by old barn	O'Brien	Red Oak	TX
159–1	well	-	shallow	W of stock pen	Estes	Dallas	TX
159–2	well	-	shallow	E of road, W of trailer	Estes	Dallas	TX
160–1	well	BEG-33	shallow	S of house, windmill	Newton	Fort Worth	TX
161–1	well	SSC-2	shallow	monitor well	BEG(Dunavant Lse)	Rockett-Red Oak	TX
162A–1	well	BEG-118	shallow	on homesite	McClain	Palmer	TX
162A–2	well	F-4	shallow	along side of road	SSC	-	-
162C–1	well	-	shallow	in old shed	McClain	Palmer	TX
163A–1	well	-	shallow	near pond	Wilson	Dallas	TX
163A–2	well	-	shallow	near corral	Wilson	Dallas	TX
163A–3	cistern	-	shallow	-	Wilson	Dallas	TX
163B–1	well	-	shallow	by dead tree	Wilson	Dallas	TX
166–1	well	-	shallow	at rear of house	Jurik	Ennis	TX
167A–1	well	-	shallow	behind abandoned house	Armstrong	Abilene	TX
169–1	well	-	deep?	N of abandoned house	Carroll	Mesquite	TX
169–2	well	-	shallow	-	Carroll	Mesquite	TX
172–1	well	-	shallow	SW corner of old barn	Vrana	Ennis	TX
172–2	well	BE 6	deep	SSCL well	Vrana	Ennis	TX
173–1	well	-	shallow	attached to carport	Tatum	Corsica	TX
174–1	well	-	-	in shed	Austin, Sr.	Dallas	TX
174–2	well	-	shallow	-	Austin, Sr.	Dallas	TX
177–1	well	BEG 74	shallow	near old homesite	Alderdice	Waxahachie	TX
178A–1	well	-	shallow	W of house by tree	Slovacek	Ennis	TX
178A–2	well	-	shallow	W of barn	Slovacek	Ennis	TX

Appendix A. SSC well inventory data base

Well ID	Map no.	NAD 83 northing (ft)	NAD 83 easting (ft)	Beam distance (ft)	Within ease-ment	Ground surface elev. (ft)	Well depth (ft)	Water level elev. (ft)	Date meas M/D/Y	Forma-tion	Diameter surface casing (ft)	Casing material	Well use	Wellhead condition
178B-1	92	6816936	2534796	2,500	n	520	5.8	516.9	4/23/91	Kwc	2.5	brick	abandoned	uncovered
181-1	26	6806241	2453113	1,075	y	685	0	-	-	-	-	-	abandoned	filled w/ garbage
181-2	26	6806249	2452996	1,100	y	688	12.4	685.7	4/8/92	Kau	2.5	brick	abandoned	uncovered
185D-1	61	6768448	2495421	1,100	n	525	-	-	-	Ko	-	-	-	-
188-1	91	6825118	2528988	1,150	y	480	0	-	-	-	-	-	abandoned	filled
188-2	91	6824880	2529028	1,150	y	480	-	-	-	Ko	-	-	abandoned	housed
191A-1	90	6826209	2528450	1,300	n	465	0	-	-	-	-	-	abandoned	filled
200-1	68	6775995	2510642	2,400	n	472	-	-	-	-	-	-	-	cement cover
200-2	68	6776448	2509737	3,400	n	473	-	-	-	-	-	-	-	-
201-1	68	6773414	2510083	300	n	460	25.6	449.4	5/23/91	Ko	2.5	brick	garden	uncovered
202A-1	64	6862464	2503560	50	y	540	21.4	470.5	5/15/91	Qt	2.8	brick	unused	uncovered
202A-2	64	6862595	2503843	300	y	540	24.8	466	5/15/91	Qt	2	brick	unused	metal cover
202A-3	64	6862391	2503384	50	y	532	-	-	-	-	-	-	unused	housed
202B-1	64	6863177	2501591	50	y	550	287	496.1	2/27/91	Kau	0.2	pvc	monitor	steel cover
202B-2	64	6861696	2502530	1,000	n	530	22	515.5	12/9/92	-	-	brick	unused	uncovered
203-1	75	6841638	2523686	250	y	427	16.2	425	4/23/91	Ko	2.1	brick	unused	cement cover
204LL-1	89	6835078	2528050	1,600	y	450	15	-	-	Ko	-	brick	abandoned	partially filled
211-1	88	6842092	2525175	1,200	y	478	0	-	-	-	3	brick	abandoned	filled
211-2	75	6841666	2523179	200	y	470	17.5	467	4/23/91	Ko	2.2	brick	unused	uncovered
211-3	75	6840725	2520046	3,500	n	474	9.1	-	-	Ko	2.1	brick	abandoned	uncovered
211-4	75	6835344	2523685	2,000	y	480	0	-	-	-	-	brick	abandoned	filled
211-5	89	6839299	2524447	0	y	452	405	448.1	2/27/91	Ko/Kau	0.3	pvc	monitor	steel cover
211-6	89	6839563	2524567	225	y	460	20	457	3/12/92	Ko	2.5	brick	abandoned	steel cover
215-1	33	6861042	2473197	2,400	n	693	19.6	689	4/4/91	Kau	1.7	brick	unused	rock covers wellhead
215-2	33	6863137	2472842	300	n	694	17.5	689	4/4/91	Kau	2.3	brick	unused	uncovered
215-3	33	6863768	2473856	150	y	680	266.9	667	2/24/91	Kau	0.2	pvc	monitor	steel cover
215-4	33	6862191	2475887	2,200	n	650	20	650	3/11/92	Kau	3	brick	abandoned	uncovered
217-1	33	6861915	2472621	1,400	n	693	1,100	-	-	Kwb	-	steel	municipal	pump on wellhead
220-1	33	6860566	2466774	0	y	715	0	-	-	-	-	-	abandoned	filled
225-1	25	6811790	2452073	950	y	730	0	-	-	-	-	-	abandoned	filled
227-1	33	6861708	2469494	300	y	708	14.4	701.8	5/8/91	Kau	3	brick	unused	wood cover
227-2	33	6861771	2468873	50	y	710	0	-	-	-	3	brick	abandoned	filled
228-1	33	6860600	2466430	200	n	723	270.5	-	-	Kau/Ksb	0.2	pvc	monitor	steel cover
228-2	-	not located		-	-	-	-	-	-	-	-	-	-	buried?
229A-1	19	6859171	2462466	1,400	n	712	-	-	-	-	-	-	abandoned	livestock pan cover
229C-1	33	6859856	2466754	125	n	722	17.3	716.9	10/22/91	Kau	3	brick	unused	tree trunk cover
231-1	9	6848176	2450339	3,000	n	696	17.7	688.2	4/3/91	Kau	3	brick	lawn	covered
231-2	9	6848181	2450357	3,000	n	696	700?	-	-	-	-	steel	abandoned	under carport
235B-1	10	6841288	2448642	1,500	n	732	-	-	-	-	0.3	steel	unused	uncovered
235D-1	9	6843773	2451328	0	y	702	26.6	696.1	5/20/92	Kau	3	brick	unused	uncovered
237-1	10	6835965	2448588	25	y	761	0	-	-	-	-	-	abandoned	filled
238-1	10	6837159	2449111	2,300	n	768	185.5	745.1	2/28/92	Kau	0.2	pvc	monitor	monitor well cover
241-1	10	6835079	2444665	3,600	n	740	750	-	-	Kwb	0.4	steel	domestic	housed
241-2	10	6835553	2447733	700	y	755	13.9	749.7	4/3/91	Kau	2.2	brick	unused	fenced
243-1	10	6836546	2451148	2,400	n	725	-	-	-	Kau	-	brick	-	-
244A-1	21	6849115	2454442	0	y	622	13.9	619	4/4/91	Kau	1.9	brick	unused	wood cover
245A-1	21	6847215	2456682	2,900	n	610	38.4	598.7	5/16/91	Kau	3.5	corr. steel	unused	uncovered
245B-1	20	6853217	2457801	25	y	695	20.9	690.5	5/16/91	Kau	2.5	ceramic	unused	uncovered
245D-1	20	6854469	2459365	300	n	711	7.6	707.2	4/4/91	Kau	2.2	brick	unused	wood cover
245E-1	20	6857728	2458136	2,900	n	731	14.8	728.3	4/4/91	Kau	1.5	brick	unused	concrete cover

Well ID	Utility	Other ID	Relative depth	Notes	Owner	City	State
178B–1	well	-	shallow	in pasture along road	Slovacek	Ennis	TX
181–1	well	-	shallow	-	Orr	Houston	TX
181–2	well	-	shallow	-	Orr	Houston	TX
185D–1	seep	-	shallow	-	Central TX Farm Land	Geneva Switzerland	
188–1	well	-	shallow	in gulley to NE	Roberts	Palmer	TX
188–2	pump	-	shallow	by pump house for pond	Roberts	Palmer	TX
191A–1	well	-	shallow	in back yard by trees	Young	Ennis	TX
200–1	well	-	shallow	W of house	-	-	-
200–2	well	-	shallow	heavy cement lid, access?	Ira Gorman	-	-
201–1	well	-	shallow	50 yrd NNE of house	Hebeler	Dallas	TX
202A–1	well	BEG-120	shallow	near old house, under windmill	Dobkins	Waxahachie	TX
202A–2	well	BEG-121	shallow	NW side of house	Dobkins	Waxahachie	TX
202A–3	well	BEG-119	shallow	at SW side of house	Dobkins	Waxahachie	TX
202B–1	well	BE 4	deep	SSCL well	Dobkins	Waxahachie	TX
202B–2	well	-	shallow	-	Dobkins	Waxahachie	TX
203–1	cistern	-	shallow	behind house, next to garage	Hunter	Dallas	TX
204LL–1	well	-	shallow	in trees	Solens	Chatsworth	CA
211–1	well	-	shallow	E side of old house	Schmolder	Ferris	TX
211–2	well	-	shallow	along road	Schmolder	Ferris	TX
211–3	well	-	shallow	along road	Schmolder	Ferris	TX
211–4	well	-	shallow	along road by small tree	Schmolder	Ferris	TX
211–5	well	BIR 81	deep	SSCL well	Schmolder	Ferris	TX
211–6	well	-	shallow	at edge of field	Schmolder	Ferris	TX
215–1	well	-	shallow	W of metal shed	Atkins	Dallas	TX
215–2	well	-	shallow	75 yrds E of narrow dirt road	Atkins	Dallas	TX
215–3	well	BE 3	deep	SSCL well	Atkins	Dallas	TX
215–4	well	-	shallow	under windmill by creek	Atkins	Dallas	TX
217–1	well	JK-33-34-104‡	deep	water tower	Rockett WSC	Red Oak	TX
220–1	well	-	shallow	E of house	Chapman	Chapman Ranch	TX
225–1	well	-	shallow	by shed at old home site	Robertson	Waxahachie	TX
227–1	well	-	shallow	W of house	Smith	Waxahachie	TX
227–2	well	-	shallow	opposite end of property	Smith	Waxahachie	TX
228–1	well	F-2	deep	100 ft from SE corner	Arrianga(SSC)	Dallas	TX
228–2	well	-	shallow?	100 ft from NE corner	Arrianga	Dallas	TX
229A–1	well	-	shallow	in pasture	Finch	Waxahachie	TX
229C–1	well	-	shallow	near barn, under windmill	Black Champ/Hamen	Waxahachie	TX
231–1	cistern	-	shallow	in backyard, SE of house	Mayes	Midlothian	TX
231–2	well	-	deep	under carport slab	Mayes	Midlothian	TX
235B–1	well	-	deep	NE of house	Getzendaner	Waxahachie	TX
235D–1	well	-	shallow	near fence	Getzendaner	Waxahachie	TX
237–1	well	-	shallow	in field	Rutherford	Waxahachie	TX
238–1	well	J-2	deep	1987 monitor well	SSC	-	-
241–1	well	JK-33-33-704	deep	near house	McAlpin	Midlothian	TX
241–2	well	-	shallow	NW of old homestead	McAlpin	Midlothian	TX
243–1	well	-	shallow	behind house	-	-	-
244A–1	well	-	shallow	on front porch of house	Roten	Alvarado	TX
245A–1	well	-	shallow	in field by big stump	Midlothian	TX	
245B–1	well	-	shallow	in pasture	Seale	Midlothian	TX
245D–1	well	-	shallow	behind house	Seale	Midlothian	TX
245E–1	well	-	shallow	S of house, by porch	Seale	Midlothian	TX

Appendix A. SSC well inventory data base

Well ID	Map no.	NAD 83 northing (ft)	NAD 83 easting (ft)	Beam distance (ft)	Within ease-ment	Ground surface elev. (ft)	Well depth (ft)	Water level elev. (ft)	Date meas M/D/Y	Forma-tion	Diameter surface casing (ft)	Casing material	Well use	Wellhead condition
245E-2	20	6856375	2457953	2,050	n	715	988	127	4/10/84	Kwb	0.5	steel	unused	pump on wellhead
247-1	57	6864517	2492788	1,100	n	508	-	-	-	-	0.4	steel	unused	housed
247-2	57	6864546	2492726	1,100	n	508	26	502.7	5/9/91	Qt	1.6	plastic	animals	wood cover
248A-1	20	6852485	2453647	2,700	n	640	780	242	11/7/75	Kwb	0.5	steel	unused	uncovered
248A-2	20	6850881	2455767	0	y	665	550	525	0/0/54	Kwb	0.4	steel	unused	uncovered
248A-3	20	6852973	2454975	~2,000	n	639	600	479	0/0/64	Kwb	0.3	steel	abandoned	-
250-1	12	6823634	2451820	2,400	y	710	18.7	703.7	5/16/91	Kau	-	brick	unused	uncovered
250-2	12	6824432	2450332	2,900	y	715	-	-	-	Kau	-	-	-	-
250-3	12	6823187	2450989	2,200	n	733	0	-	-	-	-	-	abandoned	filled
252-1	57	6863169	2494789	2,000	n	505	22.6	492.5	4/5/91	Qal	3	brick	animals	cover being made
252-2	57	6863606	2494187	1,750	n	520	28.1	509.3	4/5/91	Qt	2.5	brick	animals	steel cover
252-3	57	6863667	2494451	1,600	n	527	25.4	510.1	4/5/91	Kau	2	brick	animals	uncovered
252-4	57	6864322	2495064	900	n	540	23	533.3	4/5/91	Kau	3	brick	animals	55 gal. drum cover
253-1	57	6864425	2496887	350	n	543	22.5	535.3	5/17/91	Kau	1.2	corr. steel	lawn	55 gal. drum cover
256-1	57	6864517	2498203	100	y	542	22.8	533.9	5/17/91	Kau	2.5	cement	unused	steel sheet cover
257-1	12	6818871	2450208	450	y	740	-	-	-	-	-	steel	unused	pump on wellhead
257-2	12	6818529	2450282	700	y	745	17.8	740.2	3/14/91	Kau	3.1	brick	unused	uncovered
257-3	12	6818783	2450135	400	y	740	-	-	-	-	-	-	-	-
260A-1	13	6817400	2450848	1,656	y	752	-	-	-	Kau	-	brick	abandoned	-
262A-1	25	6817071	2453467	4,000	y	710	0	-	-	-	-	-	abandoned	filled
262A-2	13	6816101	2450549	1,600	y	747	36.3	737.1	3/15/91	Kau	2.2	brick	unused	uncovered
262B-1	25	6813969	2455387	3,650	y	743	0	-	-		-	-	abandoned	filled
265B-1	57	6864347	2498551	50	y	540	30?	-	-	-	-	brick	unused	in/near pumphouse
267C-1	12	6818549	2451468	1,700	y	745	-	742.6	3/21/91	Kau	3	brick	unused	uncovered
271A-1	12	6822821	2446576	1,050	n	755	852	435?	1/27/70	Kwb	0.6	steel	dairy farm	pump on wellhead
271A-2	12	6822868	2447067	450	n	738	870	-	2/27/92	Kwb	-	steel	dairy farm	pump on wellhead
272A-1	75	6841681	2522098	1,100	n	475	29.1	465.7	5/12/91	Ko	3	brick	unused	cement cover
272B-1	74	6844953	2523595	1,600	n	500	17	495.8	5/17/91	Ko	3.7	brick	unused	uncovered
272B-2	74	6844182	2522964	700	y	500	-	-	-	-	-	-	abandoned	capped/plugged
273-1	73	6851418	2516039	1,200	n	484	15	-	-	Qt	0.1	steel	abandoned	plugged
274B-1	11	6826412	2446735	900	y	725	-	-	-	-	0.5	steel	unused	pump on wellhead
274B-2	11	6826418	2446808	600	y	725	25.8	703.7	5/9/91	Kau	4	none	unused	uncovered
274B-3	11	6826830	2445805	1,800	y	750	0	-	-	-	-	none	abandoned	filled
274C-1	11	6826452	2449328	1,700	n	681	140	593.6	3/1/91	Ksb	0.3	pvc	monitor	steel cover
275-1	73	6850249	2518477	0	y	480	15.3	475.6	5/10/91	Qt	3	brick	lawn	steel cover
275-2	73	6850372	2518655	200	y	470	0	-	-	Qt	-	brick	abandoned	filled
275-3	73	6850366	2518675	200	y	465	-	-	-	Qt	-	-	-	-
276A-1	13	6816427	2447127	1,550	y	752	19.7	742.2	3/14/91	Kau	5.5	brick	unused	uncovered
276A-2	13	6816236	2447368	1,400	y	750	17	740.2	3/14/91	Kau	5	brick	unused	uncovered
276A-3	13	6816498	2448982	25	y	741	211	720.4	3/1/91	Kau/Ksb	0.3	pvc	monitor	steel cover
276A-4	13	6816172	2446953	1,797	y	752	20.3	742.5	5/19/92	Kau	3.5	brick	unused	wire/wood in wellhead
276B-1	12	6821755	2445345	2,350	n	785	2,556	-274	3/14/90	Kctm	-	steel	municipal	pump on wellhead
276B-2	12	6822712	2445692	1,900	n	780	26.1	774	5/16/91	Kau	3.1	brick	unused	uncovered
276B-3	12	6822662	2445556	2,000	n	780	21.6	773.2	5/16/91	Kau	3.1	brick	unused	uncovered
295C-1	92	6816002	2530904	750	y	450	-	-	-	Ko	-	-	-	housed
296-1	91	6824702	2530973	600	y	480	15.8	-	2/25/92	Ko	3	brick	unused	wood box cover
304-1	91	6820618	2532914	1,550	y	505	24	-	-	-	-	brick	abandoned	filled
304-2	91	6820719	2532789	1,550	y	504	19.3	495.3	8/11/92	Ko	3.6	brick	unused	uncovered
305B-1	93	6803761	2532364	375	y	456	380	449.8	2/27/91	Kau	0.2	pvc	monitor	steel cover
306B-1	44	6777618	2468772	500	y	513	15.4	-	4/16/91	Qt	1.8	brick	unused	housed

Appendix A. (continued)

Well ID	Utility	Other ID	Relative depth	Notes	Owner	City	State
245E–2	well	JK-33-33-302	deep	windmill	Seale	Midlothian	TX
247–1	well	-	deep?	NW of treatment plant	-	-	-
247–2	well	-	shallow	-	-	-	-
248A–1	well	JK-33-33-501	deep	by shed behind house	McElroy	Dallas	TX
248A–2	well	JK-33-33-503	deep	on hill, in bushes	McElroy	Dallas	TX
248A–3	well	JK-33-33-502	deep	approximate location	McElroy	Dallas	TX
250–1	well	-	shallow	at house	McLaughlin	Cedar Hill	TX
250–2	seep	-	shallow	middle of property	McLaughlin	Cedar Hill	TX
250–3	well	-	shallow	behind house	McLaughlin	Cedar Hill	TX
252–1	well	-	shallow	near fence line	Carter	Waxahachie	TX
252–2	well	-	shallow	N of barn	Carter	Waxahachie	TX
252–3	well	-	shallow	in pasture, near road	Carter	Waxahachie	TX
252–4	well	-	shallow	in pasture	Carter	Waxahachie	TX
253–1	well	-	shallow	150 ft S of house	Robbins	Red Oak	TX
256–1	well	-	shallow	W of garage	Cantrell	Red Oak	TX
257–1	well	-	deep	NW of house, by pole	Schaefer	Waxahachie	TX
257–2	well	-	shallow	SW corner of property	Schaefer	Waxahachie	TX
257–3	-	-	-	-	Schaefer	Waxahachie	TX
260A–1	well	-	shallow	in field	-	-	-
262A–1	well	-	shallow	near drainage	Hastings	Waxahachie	TX
262A–2	well	-	shallow	NW corner of property	Hastings	Waxahachie	TX
262B–1	well	-	shallow	in field behind mobile home	Hastings	Waxahachie	TX
265B–1	well	-	shallow	E of house	Watson	Lancaster	TX
267C–1	well	-	shallow	by old house	Willeford	Red Oak	TX
271A–1	well	JK-33-41-205	deep	between trailers	Tamminga	Waxahachie	TX
271A–2	well	JK-33-41-204	deep	by barn	Tamminga	Waxahachie	TX
272A–1	well	-	shallow	behind house	Pinkard	Richardson	TX
272B–1	well	-	shallow	at old homestead	Pinkard	Richardson	TX
272B–2	well	-	deep?	on hill, middle of property	Pinkard	Richardson	TX
273–1	well	BEG 87	shallow	-	Evans	Palmer	TX
274B–1	well	-	deep	near old barns	Dillard	Waxahachie	TX
274B–2	well	-	shallow	near burned house	Dillard	Waxahachie	TX
274B–3	well	-	shallow	by pole	Dillard	Waxahachie	TX
274C–1	well	BE 1A	deep	SSCL well	Dillard	Waxahachie	TX
275–1	well	BEG 111	shallow	NW side of house	Pierce	Palmer	TX
275–2	well	BEG 116	shallow	in trees by road	Pierce	Palmer	TX
275–3	spring	-	-	E side of old house	Pierce	Palmer	TX
276A–1	well	-	shallow	E of old house	Loftis	Waxahachie	TX
276A–2	well	-	shallow	SE of house	Loftis	Waxahachie	TX
276A–3	well	BI 1	deep	SSCL well	Loftis	Waxahachie	TX
276A–4	well	-	shallow	-	Loftis	Waxahachie	TX
276B–1	well	-	deep	water tower	Loftis	Waxahachie	TX
276B–2	well	JK-33-41-205‡	shallow	E of house by corral	Loftis	Waxahachie	TX
276B–3	well	-	shallow	W of house	Loftis	Waxahachie	TX
295C–1	well	-	-	near creek	-	-	-
296–1	cistern	-	shallow	W of house	Alcala	Palmer	TX
304–1	cistern	-	shallow	near barn	Mitchell	Ennis	TX
304–2	cistern	-	shallow	-	Mitchell	Ennis	TX
305B–1	well	BF 6	deep	SSCL well	Dunkerley	Ennis	TX
306B–1	well	-	shallow	E of ranch entrance	Lewis	Forreston	TX

Appendix A. SSC well inventory data base

Well ID	Map no.	NAD 83 northing (ft)	NAD 83 easting (ft)	Beam distance (ft)	Within ease-ment	Ground surface elev. (ft)	Well depth (ft)	Water level elev. (ft)	Date meas M/D/Y	Forma-tion	Diameter surface casing (ft)	Casing material	Well use	Wellhead condition
310-1	44	6776383	2468386	1,750	n	522	0	-	-	-	-	-	abandoned	filled
311-1	44	6777287	2469031	600	y	522	0	-	-	-	-	-	abandoned	filled
320-1	15	6796435	2450621	5,000	n	660	20.7	648	9/25/91	Kau	3	brick	unused	-
320-2	15	6795542	2449582	6,250	n	610	-	-	-	Kau	2-3	brick	unused	uncovered
329-1	20	6857035	2462019	150	y	670	40?	-	-	Kau	-	-	abandoned	heavy cement cover
329-2	20	6857219	2462172	125	y	680	40?	-	-	Kau	-	-	abandoned	heavy cement cover
331-1	20	6857262	2463532	825	n	713	15.9	709.5	2/10/92	Kau	2.7	brick	-	-
338-1	25	6812816	2455441	2,600	y	723	15.8	721.3	3/21/91	Kau	3	brick	unused	uncovered
338-2	25	6812012	2454328	2,000	y	741	24.4	716.6	8/5/92	Kau	3	brick	unused	uncovered
339-1	73	6850736	2520464	1,900	n	480	-	-	-	Qt	-	-	domestic	covered
340-1	19	6858285	2462760	300	y	690	-	-	-	-	-	-	unused	under metal pan
342A-1	20	6857949	2462664	150	y	685	-	684.9	-	-	-	steel	abandoned	filled?
344-1	27	6800744	2454625	250	y	655	8.3	651.2	3/27/91	Kau	3	brick	unused	cement cover
344-2	27	6800153	2455278	600	y	650	13	643.8	3/27/91	Kau	3	none	abandoned	cement cover
344-3	27	not located	-	-	-	-	-	-	-	-	-	-	abandoned	-
344-4	27	not located	-	-	-	-	-	-	-	-	-	-	abandoned	-
345-1	15	not located	-	-	-	-	-	-	-	-	-	-	-	-
350-1	27	6797901	2455624	100	y	630	0	-	-	-	-	-	abandoned	filled
357-1	27	6797337	2455718	0	y	628	181.61(185)*	617.7	2/28/92	Kau	0.2	pvc	monitor	monitor well cover
378B-1	48	6866038	2487723	0	y	548	208	584.7	2/27/91	Kau	0.2	pvc	monitor	steel cover
379A-1	49	6865007	2481659	750	n	615	15	dry	4/4/91	Kau	-	brick	abandoned	filled to 15 ft
379A-2	49	6865025	2482963	825	n	610	940	400 ?	0/0/45	Kwb	0.3	steel	abandoned	housed
381-1	48	6866746	2485468	700	y	552	25.6	547.5	4/4/91	Kau	2.5	concrete	domestic	concrete cover
381-2	48	6866838	2485391	700	n	-	-	-	-	Kau	-	-	-	uncovered
383-1	82	6778384	2516207	1,300	n	475	0	-	-	-	-	-	abandoned	filled
389-1	14	6805332	2449785	1,750	y	698	25.0?	693.6	3/29/91	Kau	3	brick	abandoned	partially covered
390-1	-	not located	-	-	-	-	-	-	-	-	-	-	-	-
392B-1	27	6801775	2455213	1,200	y	670	17.7	663	3/28/91	Kau	1.4	brick	unused	uncovered
392B-2	27	6801807	2454984	1,000	y	667	22.7	659.8	3/28/91	Kau	4	brick	unused	uncovered, fenced
393A-1	44	6775771	2474764	1,300	n	513	-	-	-	-	2.5	brick	animals	covered
396-1	53	6769895	2484360	750	y	502	0	-	-	-	-	brick	abandoned	filled
397-1	44	6773759	2474781	400	y	502	0	-	-	-	-	-	abandoned	filled
397-2	44	6773782	2474745	400	y	502	30	-	-	Qt	-	-	domestic	pump on wellhead
398A-1	52	6772657	2478167	0	y	512	162.3	408.5	2/28/91	Kau	0.2	pvc	monitor	steel cover
398B-1	-	not located	-	-	-	510	1,050	210	7/15/65	Kwb	0.3	steel	unused	-
399-1	57	6864774	2493361	750	n	542	0	-	-	-	-	-	abandoned	filled
433-1	57	6865042	2497092	300	y	550	28.5	536.3	4/23/91	Kau	1.3	corr. steel	lawn	wood cover
434-1	15	6801857	2450508	1,500	y	685	-	-	-	-	0.1	steel	unused	pipes in hole
435-1	57	6864037	2497079	,650	n	540	15.7	532.8	4/5/91	Kau	2	brick	domestic	concrete cover
436-1	27	6799872	2453246	1100	y	645	30.1	628.8	3/28/91	Kau	3	brick	unused	sheet metal cover
436-2	27	6799949	2453662	700	y	615	25.8	610	3/27/91	Kau	3	brick	unused	metal w/ cement
437B-1	27	6798691	2454274	600	y	615	18.4	599.8	3/27/91	Kau	2.3	brick	domestic	housed
438-1	27	6798989	2454277	500	y	615	6	-	3/27/91	Kau	4.5	none	unused	uncovered
438-2	27	6799044	2454080	650	y	615	13.1	611.9	3/27/91	Kau	2	brick	unused	uncovered
441-1	27	6798881	2453642	600	y	625	-	-	-	-	3	brick	-	-
462-1	12	6821068	2444688	3,100	n	792	-	-	-	Kau	-	brick	unused	cement cover
462-2	12	6821303	2445172	2,600	n	792	-	-	-	Kau	-	brick	unused	-
464-1	57	6864389	2497214	300	n	544	26.7	534.1	4/5/91	Kau	2.5	corr. steel	lawn	wood cover
465-1	24	6823125	2458688	2,900	n	620	17.2	603.7	3/20/91	Kau	3	brick	unused	covered
465-2	24	6823216	2459130	3,200	n	640	31.8	624.7	3/20/91	Kau	3.5	brick	unused	covered

Appendix A. (continued)

Well ID	Utility	Other ID	Relative depth	Notes	Owner	City	State
310–1	well	-	shallow	NW of barn	Williams	Forreston	TX
311–1	well	-	-	near trees	Evans	Forreston	TX
320–1	well	-	shallow	windmill	Ed Dawson	-	-
320–2	well	-	-	-	-	-	-
329–1	well	-	shallow	-	Yarbrough	Midlothian	TX
329–2	well	-	shallow	middle of property	Yarbrough	Midlothian	TX
331–1	well	-	shallow	-	Jumper	Waxahachie	TX
338–1	well	-	shallow	along creek by FM66	Parten	Waxahachie	TX
338–2	well	-	shallow	near homesite	SSC?	-	-
339–1	well	BEG 109	shallow	by home	Michael	Nokomis	IL
340–1	well	-	shallow	by tree with large pan	Finham	Waxahachie	TX
342A–1	well	-	deep	next to creek by street car	Alford	Dallas	TX
344–1	well	-	shallow	N end of property	Seabolt	Irving	TX
344–2	well	-	shallow	SE corner	Seabolt	Irving	TX
344–3	well	-	shallow?	-	Seabolt	Irving	TX
344–4	well	-	shallow?	-	Seabolt	Irving	TX
345–1	well	-	shallow?	in western pasture	Caddel	Waxahachie	TX
350–1	well	-	shallow	in backyard	Williams	Waxahachie	TX
357–1	well	J-6	deep	1987 monitor well	SSC	-	-
378B–1	well	BF 3	deep	SSCL well	Wannack	Red Oak	TX
379A–1	well	-	shallow	SW corner of house	Bowers	Waxahachie	TX
379A–2	well	JK-33-34-203	deep	in pasture near two roads	Bowers	Waxahachie	TX
381–1	well	-	shallow	-	Sargent	Waxahachie	TX
381–2	spring	-	spring	spring fed catfish ponds	Sargent	Waxahachie	TX
383–1	well	-	shallow	near house	Dolezal	Ennis	TX
389–1	well	-	shallow	behind house	Gaston	Waxahachie	TX
390–1	well	-	deep?	-	Price	Forreston	TX
392B–1	well	-	shallow	behind house	Elliott	Waxahachie	TX
392B–2	well	-	shallow	W of barn	Elliott	Waxahachie	TX
393A–1	well	-	shallow	SE corner of house	Goosby	Dallas	TX
396–1	well	-	shallow	behind house	Fort	HuntintonBeach	CA
397–1	well	-	shallow	windmill near house	Harrison	Mesquite	TX
397–2	well	-	shallow	next to house	Harrison	Mesquite	TX
398A–1	well	BE 9	deep	SSCL well	Singleton	Cedar Hill	TX
398B–1	well	JK-33-50-101	deep	-	Singleton	Cedar Hill	TX
399–1	well	-	shallow	near back door of old house	Gibbons	Red Oak	TX
433–1	well	-	shallow	S of shed	Gregory	Red Oak	TX
434–1	well	-	deep	by old house	Dickerson	Ovilla	TX
435–1	well	-	shallow	W of small house	Zurmon	Lancaster	TX
436–1	well	-	shallow	E of house	Sherman	Waxahachie	TX
436–2	well	-	shallow	W of creek	Sherman	Waxahachie	TX
437B–1	well	-	shallow	behind trailer	Williams	Waxahachie	TX
438–1	well	-	shallow	SW corner of land	Patterson	Waxahachie	TX
438–2	well	-	shallow	W side of creek opposite house	Patterson	Waxahachie	TX
441–1	well	-	shallow	under windmill	Sims	Waxahachie	TX
462–1	well	-	shallow	in front of house	Morgan	Waxahachie	TX
462–2	well	-	shallow	by house	Morgan	Waxahachie	TX
464–1	well	-	shallow	W of garage	McElroy	Red Oak	TX
465–1	well	-	shallow	in pasture W of house	Winningham	Waxahachie	TX
465–2	well	-	shallow	behind house	Winningham	Waxahachie	TX

Appendix A. SSC well inventory data base

Well ID	Map no.	NAD 83 northing (ft)	NAD 83 easting (ft)	Beam distance (ft)	Within ease-ment	Ground surface elev. (ft)	Well depth (ft)	Water level elev. (ft)	Date meas M/D/Y	Forma-tion	Diameter surface casing (ft)	Casing material	Well use	Wellhead condition
472D-1	95	6791789	2529135	0	y	465	35 ?	-	-	Qt	-	-	domestic	buried
473A-1	95	6793296	2529523	300	n	450	34.9	441.8	4/17/91	Qt	3.3	brick	domestic/lawn	concrete cover
473C-1	95	6792888	2528273	1,250	n	467	-	-	-	-	-	-	-	concrete cover
482B-1	92	6817185	2530155	1,670	n	480	200	489.7	2/28/92	Ko	0.2	pvc	monitor	monitor well cover
483-1	92	6817336	2529991	2,187	n	490	-	-	-	-	-	-	-	-
484A-1	92	6817281	2529996	2,187	n	485	-	-	-	-	-	-	-	-
492-1	25	6816848	2460223	650	n	630	300 ?	624.2	3/29/91	Kau	0.5	steel	lawn	uncovered
494-1	91	6824303	2529669	775	y	460	-	-	-	Kau	-	-	-	submerged in pond
496-1	25	6815303	2460122	400	y	650	3	-	-	Kau	3	brick	abandoned	cover
496-2	25	6815246	2460322	600	y	637	40.1	622.5	3/19/91	Kau	5.5	none	lawn	housed
496-3	25	6815417	2460029	300	y	650	44.5	646	3/19/91	Kau	2.4	cement	unused	cement cover
498-1	91	6819899	2529064	2,400	n	650	-	-	-	-	-	-	abandoned	filled
504A-1	27	6797677	2454791	550	y	600	9.8	594	3/27/91	Kau	3	brick	unused	uncovered
504A-2	27	6797665	2454811	550	y	600	25 ?	593.4	3/27/91	Kau	3	brick	unused	bolted steel cover
504B-1	15	6796648	2451805	3,600	n	655	32.1	632.4	10/10/91	Kau	3	brick	abandoned	steel culvert cover
510-1	27	6798687	2453933	1,000	y	620	36.8	610.6	3/27/91	Kau	2.5	brick	domestic	metal cover
514-1	27	6800043	2461763	6,600	y	667	5	-	-	Kau	6.5	none	abandoned	uncovered
519A-1	40	6807130	2464117	7,000	n	629	19	628	5/15/91	Kau	3	brick	abandoned	cement cover
519A-2	26	6807118	2463769	7,000	n	672	2	-	-	Kau	-	brick	abandoned	partially filled
519A-3	40	6806352	2464358	7,000	n	660	19.1	655.7	5/15/91	Kau	2.5	cement	abandoned	-
519A-4	40	6807533	2464530	7,000	n	675	0	-	-	-	-	brick	abandoned	filled
519B-1	26	6808378	2463083	5,800	n	692	2	-	-	-	-	-	abandoned	filled
519C-1	26	6809021	2462864	6,400	n	676	21.4	676	5/15/91	Kau	2.5	brick	unused	uncovered
519C-2	26	6808072	2463676	6,400	n	676	16.1	675.9	5/15/91	Kau	2.5	brick	unused	cement cover
519C-3	26	6809017	2462866	600	n	705	3	-	-	-	-	-	abandoned	filled
519C-4	26	6808290	2460575	3,600	n	669	0	-	-	-	-	-	abandoned	filled
522-1	24	6820568	2452430	750	y	725	-	-	-	-	0.5	steel	unused	pump on wellhead
525-1	26	6809077	2457754	750	y	722	19.2	712.8	3/22/91	Kau	2	brick	unused	uncovered
525-2	25	6810512	2456766	50	y	740	25.4	731.2	3/22/91	Kau	2.2	brick	unused	uncovered
525-3	25	6810422	2458030	300	y	693	20.6	689.9	3/22/91	Kau	3	brick	unused	wood cover
525-4	25	6810744	2457868	0	y	697	282	694.2	1/30/91	Kau	0.2	pvc	monitor	metal cover
525-5	26	6809545	2457199	25	y	707	0	-	-	-	-	-	abandoned	filled
526A-1	24	6818597	2452376	2,375	y	731	886	485	11/11/77	-	0.3	steel	-	-
529B-1	24	6822391	2453418	800	y	700	25.5	694.6	3/14/91	Kau	2.3	brick	unused	uncovered
529D-1	24	6822344	2452759	750	y	670	35.5	647.6	3/14/91	Kau	3	brick	lawn	housed
531B-1	24	6820681	2453840	1,000	y	715	-	-	-	-	-	-	-	-
541-1	25	6816595	2458533	1,050	y	650	-	-	-	Kau	-	-	-	uncovered
541-2	25	6816653	2458581	1,000	y	660	7.6	656.4	3/21/91	Kau	3.5	brick	domestic	covered
541-3	25	6816629	2458577	1,000	y	660	47.7	655.7	3/21/91	Kau	3	cement	domestic	cement cover w/ lid
541-4	24	6818594	2460261	750	n	635	0	-	-	-	-	-	abandoned	filled
541-5	25	6816744	2459586	0	y	658	280	641.4	2/28/91	Kau	0.2	pvc	monitor	steel cover
543A-1	25	6817418	2454348	4,000	y	695	33.3	686.6	3/14/91	Kau	3.2	brick	unused	uncovered
543A-2	25	6817930	2455295	3,600	y	704	24.9	693.3	3/14/91	Kau	2.8	brick	unused	uncovered
543A-3	25	6817495	2457580	1,750	y	660	-	-	-	Kau	-	-	-	-
543B-1	24	6818980	2459925	1,000	n	650	22.9	641.7	3/14/91	Kau	1.9	brick	unused	uncovered
543B-2	24	6819124	2459844	1,000	n	650	0	-	-	Kau	-	-	abandoned	filled
546A-1	24	6821408	2456788	450	y	650	0	-	-	-	-	-	abandoned	filled
553-1	27	6799104	2455146	100	y	640	18.2	635.4	3/28/91	Kau	2.5	brick	unused	wood cover
555-1	13	6811757	2448668	1,250	y	702	-	-	-	-	-	-	-	-
556A-1	25	6810773	2459911	1,750	y	692	25.2	688.5	3/19/91	Kau	4.8	brick	unused	wood & wire

Well ID	Utility	Other ID	Relative depth	Notes	Owner	City	State
472D–1	well	-	shallow	buried S of yellow house	Moore	Ennis	TX
473A–1	well	-	shallow	behind red barn	Bozek	Ennis	TX
473C–1	well	-	shallow?	S corner of front yard	Bozek	Ennis	TX
482B–1	well	K-6	deep	1987 monitor well	SSC	-	-
483–1	well	JK-33-43-201	deep	-	-	-	-
484A–1	well	JK-33-43-203	deep	-	-	-	-
492–1	well	-	deep	across pond opposite house	Graham	Waxahachie	TX
494–1	well	-	shallow	submerged in stock pond	Seabolt	Ennis	TX
496–1	well	-	shallow	beside house	Parten	Waxahachie	TX
496–2	well	-	shallow	in metal shed	Parten	Waxahachie	TX
496–3	well	-	shallow	in middle of front lot	Parten	Waxahachie	TX
498–1	well	-	shallow?	20 ft E of pond	Evans	Ennis	TX
504A–1	well	-	shallow	near creek below house	Wakeland	Waxahachie	TX
504A–2	well	-	shallow	near creek below house	Wakeland	Waxahachie	TX
504B–1	well	-	shallow	near road, edge of property	-	-	-
510–1	well	-	shallow	W side of house	Wakeland	Waxahachie	TX
514–1	well	-	shallow	E of barn	Vincent	Waxahachie	TX
519A–1	well	-	shallow	in field under windmill	Yancey	Dallas	TX
519A–2	well	-	shallow	E of house	Yancey	Dallas	TX
519A–3	well	-	shallow	in field, 500 yards S of house	Yancey	Dallas	TX
519A–4	well	-	shallow	behind eastern house	Yancey	Dallas	TX
519B–1	well	-	shallow	N of house	Yancey	Dallas	TX
519C–1	well	-	shallow	in field, N of house, windmill	Yancey	Dallas	TX
519C–2	well	-	shallow	in field, N of house	Yancey	Dallas	TX
519C–3	well	-	shallow	-	Yancey	Dallas	TX
519C–4	well	-	shallow	by old stump	Yancey	Dallas	TX
522–1	well	-	deep	by service frame	Colosina	Duncanville	TX
525–1	well	-	shallow	E of house	Strickland	Dallas	TX
525–2	well	-	shallow	in center of property, on hill	Strickland	Dallas	TX
525–3	well	-	shallow	on E side of property	Strickland	Dallas	TX
525–4	well	BI 3	deep	SSCL well	Strickland	Dallas	TX
525–5	well	-	shallow	west of pond	Strickland	Dallas	TX
526A–1	well	JK-33-41-2A	deep	-	Crownover	Waxahachie	TX
529B–1	well	-	shallow	in field E of house	Currie	Irving	TX
529D–1	well	-	shallow	off road	Currie	Irving	TX
531B–1	well	-	deep?	in white pump house	Crownover	Waxahachie	TX
541–1	spring	-	spring	in creek	Norton	Waxahachie	TX
541–2	well	-	shallow	by creek, NW of house	Norton	Waxahachie	TX
541–3	well	-	shallow	by creek, NW of house	Norton	Waxahachie	TX
541–4	well	-	shallow	NE part of field, windmill	Norton	Waxahachie	TX
541–5	well	BI 5	deep	SSCL well	Norton	Waxahachie	TX
543A–1	well	-	shallow	at old home site	Walker	Waxahachie	TX
543A–2	well	-	shallow	at old farm site	Walker	Waxahachie	TX
543A–3	spring	-	spring	bubbling fracture	Walker	Waxahachie	TX
543B–1	well	-	shallow	at top of hill	Walker	Waxahachie	TX
543B–2	well	-	shallow	-	Walker	Waxahachie	TX
546A–1	well	-	shallow	behind house	Betzel	DeSoto	TX
553–1	well	-	shallow	W of old house	Wafer	Waxahachie	TX
555–1	well	-	deep?	in front of house	Hernandez	Waxahachie	TX
556A–1	well	-	shallow	E of house	Welch	Waxahachie	TX

Appendix A. SSC well inventory data base

Well ID	Map no.	NAD 83 northing (ft)	NAD 83 easting (ft)	Beam distance (ft)	Within ease-ment	Ground surface elev. (ft)	Well depth (ft)	Water level elev. (ft)	Date meas M/D/Y	Forma-tion	Diameter surface casing (ft)	Casing material	Well use	Wellhead condition
556A-2	25	6810238	2459607	1,775	y	689	13.7	687.6	3/19/91	Kau	5	brick	unused	sheet metal cover
560-1	10	6835121	2443686	4,600	y	740	-	-	-	-	-	-	abandoned	housed
563-1	21	6848762	2453570	550	y	615	30?	-	-	Qal	-	-	unused	cement cover
568-1	27	6798677	2453656	600	y	625	22.3	615	3/28/91	Kau	1.6	brick	unused	wood cap, wired
571-1	91	6825058	2531707	1,450	n	475	19.1	465.3	4/17/91	Ko	2	brick	abandoned	wood cover
577-1	75	6841062	2521255	1,900	y	470	24	459.1	8/11/92	Ko	2.8	brick	unused	housed, covered
577-2	75	6840941	2521579	1,900	y	459	13.8	445.2	8/11/92	Ko	3.1	brick	unused	housed, covered
578B-1	73	6854235	2513894	800	n	492	24.5	484.8	4/5/91	Qt	2	brick	unused	cement cover
578B-2	73	6855729	2513455	50	y	502	310	495.6	2/27/91	Kau	0.2	pvc	abandoned	filled
583-1	92	6817404	2530238	1,900	n	495	14.7	494.5	5/15/91	Ko	2.6	brick	domestic	-
583-2	92	6817442	2530288	1,900	n	495	20	486.8	5/15/91	Ko	2.4	brick	unused	uncovered
586-1	14	6809281	2449313	1,250	y	712	41.3	692.3	5/19/92	Kau	5	brick	unused	cement pad over half
591-1	61	6766959	2495118	2,600	n	540	6	-	-	Qt	-	-	abandoned	partially filled
591-2	61	6766814	2495641	2,600	n	550	6	-	-	Qt	-	-	abandoned	partially filled
591-3	61	6767120	2495075	2,400	n	540	8	-	-	Qt	-	-	abandoned	filled
593B-1	61	6766889	2492902	2,600	n	542	-	-	-	-	-	-	unused	-
596A-1	-	not located	-	-	-	-	-	-	-	-	-	-	-	-
599-1	14	6809698	2450457	0	y	715	1	-	-	Kau	3	cement	garbage	cover
599-2	14	6809698	2450508	0	y	715	-	-	-	Kwb	0.5	steel	domestic	pump in hole
600A-1	12	6821000	2447707	0	y	758	168	743	3/1/91	Kau	0.2	pvc	monitor	steel cover
600A-2	12	6821000	2447707	0	y	758	256	434.4	3/1/91	Kau	0.2	pvc	abandoned	filled
600A-3	12	6821000	2447707	0	y	758	90	723.7	3/1/91	Kau	0.2	pvc	monitor	steel cover
600A-4	12	6819517	2445757	2,250	y	782	24.7	771.9	3/22/91	Kau	2.5	brick	unused	uncovered
600A-5	12	6819716	2445396	2,600	y	780	3.5	-	-	Kau	4.5	none	abandoned	small car on top
605-1	26	6808798	2457964	1,100	y	725	-	-	-	Kau	-	-	-	capped
612A-1	20	6857468	2461678	400	y	775	33.9	756.3	4/4/91	Kau	2.5	concrete	domestic	housed
616-1	26	6808909	2458005	1,031	y	711	-	-	-	Kau	-	-	abandoned	filled
618A-1	26	6808429	2459107	2,250	y	700	5	-	-	Kau	3.5	none	abandoned	uncovered, filled
620	-	not located	-	-	-	-	-	-	-	-	-	-	-	-
622-1	26	6806864	2454852	600	y	702	35.8	696.8	3/19/91	Kau	3.2	brick	unused	cement cap
631-1	10	6837585	2449901	900	n	745	16.8	737.7	4/3/91	Kau	2.5	brick	lawn	cement cap
631-2	10	6837852	2449803	700	n	745	15.4	739.1	4/3/91	Kau	5	brick	unused	wood cover
644-1	95	6787639	2526782	25	y	455	350	417.1	2/27/91	Ko/Kau	0.2	pvc	monitor	steel cover
668B-1	24	6822058	2457199	1,200	y	630	17.5	616.5	3/21/91	Kau	2.2	cement	unused	livestock pan cover
672-1	24	6821089	2456444	0	y	640	261.5	611.7	6/27/90	Kau	0.2	steel	monitor	steel cover
678-1	13	6816838	2446774	1,800	y	755	135.9	755	3/14/91	Kau	0.3	steel	unused	uncovered
695-1	68	6771737	2506652	0	y	428	220	429.1	2/28/91	Kau	0.2	pvc	monitor	steel cover
712-1	12	6820069	2451911	900	y	735	22	726	3/14/91	Kau	2.5	brick	lawn	wood cover
712-2	12	6820159	2451762	800	y	730	3	-	-	Kau	3	brick	abandoned	uncovered, junk fill
712-3	12	6820061	2451739	850	y	730	0	-	-	Kau	-	cement	abandoned	wire fill
715B-1	12	6822383	2450977	1,625	n	710	805	500	8/20/82	Kwb	0.3	steel	-	-
726-1	24	6824757	2455345	3,200	n	630	20.4	616.7	3/15/91	Kau	3	cement	animals	housed
727-1	24	6821101	2453483	550	y	780	-	-	-	-	-	-	-	sheet metal & bush
727-2	24	6821242	2453455	500	y	725	-	-	-	-	-	-	-	-
728-1	24	6823267	2452399	1,800	y	705	94.8	681.6	5/9/91	Kau	0.4	pvc	animals	metal can cover
728-2	24	6823298	2452440	1,800	y	705	50 ?	-	-	Kau	0.4	pvc	animals	uncovered
731-1	24	6825848	2454126	4,200	n	650	21.9650.3		4/24/91 Kau	2	brick	unused	uncovered	
752-1	24	6825356	2453877	3,650	y	640	35.7	623	3/14/91	Kau	~3	cement	unused	uncovered
754-1	24	6825428	2453086	3,800	y	754	0	-	-	-	-	-	abandoned	filled
758-1	-	not located	-		-	-	0	-	-	-	-	-	abandoned	filled

Appendix A. (continued)

Well ID	Utility	Other ID	Relative depth	Notes	Owner	City	State
556A–2	well	-	shallow	in pasture, windmill	Welch	Waxahachie	TX
560–1	well	-	shallow	W of house	McAlpin	Midlothian	TX
563–1	well	-	shallow	100 yards S of house, by creek	Pickard	Midlothian	TX
568–1	well	-	shallow	W of house	Yowell	Waxahachie	TX
571–1	well	-	shallow	SE corner of barn	Davis	Irving	TX
577–1	well	JK-33-35-502	shallow	-	Everett	Waxahachie	TX
577–2	well	-	shallow	-	Everett	Waxahachie	TX
578B–1	well	BEG-37	shallow	at house	Farrar	Dallas	TX
578B–2	well	BF 4	deep	SSCL well	Farrar	Dallas	TX
583–1	well	-	shallow	on back porch	-	-	-
583–2	well	-	shallow	E of house	-	-	-
586–1	well	-	shallow	-	-	-	-
591–1	well	-	shallow	in pasture	Southard	Avalon	TX
591–2	well	-	shallow	in pasture	Southard	Avalon	TX
591–3	well	-	shallow	-	Southard	Avalon	TX
593B–1	well	-	shallow	in front of house	Riddle	Avalon	TX
596A–1	well	-	shallow	dug well near barn	Head	Waxahachie	TX
599–1	cistern	-	shallow	W side of trailer	Oropeza	Waxahachie	TX
599–2	well	-	deep	E side of trailer	Oropeza	Waxahachie	TX
600A–1	well	B 1597 A	deep	SSCL well	Strauss	Dallas	TX
600A–2	well	B 1597	deep	SSCL well	Strauss	Dallas	TX
600A–3	well	B 1597 B	deep	SSCL well	Strauss	Dallas	TX
600A–4	well	-	shallow	-	Strauss	Dallas	TX
600A–5	well	-	shallow	NW corner of property	Strauss	Dallas	TX
605–1	well	-	-	in front yard	Davis	Lincoln	NM
612A–1	well	-	shallow	NW of house near creek	Gary	Waxahachie	TX
616–1	well	-	shallow	-	-	-	-
618A–1	well	-	shallow	W of red barn	Scholz	Papua, New Guinea	
620	well	-	-	-	Crenshaw	Waxahachie	TX
622–1	cistern	-	shallow	W of house	Kientzle	Waxahachie	TX
631–1	well	-	shallow	in front of house	Butler	Midlothian	TX
631–2	well	-	shallow	behind house in pasture	Butler	Midlothian	TX
644–1	well	BE 7A	deep	SSCL well	Kriska	Bardwell	TX
668B–1	well	-	shallow	in back part of property	Couch	Dallas	TX
672–1	well	BI 2A	deep	SSCL well	Couch	Dallas	TX
678–1	well	-	deep	behind garage	Franks	Waxahachie	TX
695–1	well	BE 8	deep	SSCL well	Jett	Italy	TX
712–1	well	-	shallow	inside house, back porch	Crouch	Waxahachie	TX
712–2	well	-	shallow	NW of house	Crouch	Waxahachie	TX
712–3	well	-	shallow	NW of house	Crouch	Waxahachie	TX
715B–1	well	JK-33-41-206	deep	-	Fisher	Waxahachie	TX
726–1	well	-	shallow	by creek	Peterson	Waxahachie	TX
727–1	well	-	shallow	-	Roper	Dallas	TX
727–2	well	-	shallow	SW corner	Roper	Dallas	TX
728–1	well	-	deep	by barn	Bryant	Waxahachie	TX
728–2	well	-	shallow	by barn	Bryant	Waxahachie	TX
731–1	well	-	shallow	-	Kvale	Waxahachie	TX
752–1	well	-	shallow	behind wood pump house	Crawford	Waxahachie	TX
754–1	well	-	shallow	-	Glenney	Grand Prairie	TX
758–1	cistern	-	shallow	near stock tank,not on SSC	Rogers	Cedar Hill	TX

Appendix A. SSC well inventory data base

Well ID	Map no.	NAD 83 northing (ft)	NAD 83 easting (ft)	Beam distance (ft)	Within ease- ment	Ground surface elev. (ft)	Well depth (ft)	Water level elev. (ft)	Date meas M/D/Y	Forma- tion	Diameter surface casing (ft)	Casing material	Well use	Wellhead condition
758–2	-	not located	-		-	-	-	-	-	-	-	-	-	-
759–1	91	6820338	2535991	4,400	n	540	-	-	-	-	-	-	-	-
761–1	93	6802344	2534360	1,800	n	468	22.4	452.9	4/23/91	Kwc	3	brick	unused	sheet metal
761–2	93	6802239	2534123	1,600	n	464	16.3	454.8	4/23/91	Kwc	3.1	brick	animals	uncovered
761–3	94	6801940	2533936	1,500	n	466	35.6	449.1	4/23/91	Kwc	2.5	brick	unused	cement cover
761–4	94	6801916	2533953	1,500	n	466	24.6	448.1	4/23/91	Kwc	3	brick	unused	housed
762–1	94	6801380	2533061	700	y	465	0	-	-	-	-	-	abandoned	filled
762–2	94	6801515	2532983	1,050	y	465	0	-	-	-	-	-	abandoned	filled
762–3	94	6801380	2533000	650	y	465	100 ?	-	-	Ko?	0.5	steel	domestic	pump on wellhead
767–1	44	6776592	2472217	700	n	510	-	-	-	Qt	-	brick	unused	cement cover
778–1	88	6842306	2525513	1,600	y	482	17.9	479.5	5/22/91	Ko	3	brick	unused	cement cover
781	88	not located	-	-	-	-	-	-	-	-	-	-	-	-
798B–1	88	6843984	2525984	3,280	n	450	0	-	-	Ko	-	-	-	filled
803–1	88	6843002	2526762	3,000	n	480	0	-	-	-	-	-	abandoned	filled
803–2	88	6842972	2526769	3,000	n	480	0	-	-	-	-	-	abandoned	filled
806B–1	96	6785630	2524495	800	n	485	-	-	-	-	-	-	unused	plywood cover
808B–1	24	6824634	2453017	3,000	y	690	100.1	657.5	3/15/91	Kau	0.5	steel	lawn	pump, in garage
810	73	not located	-	-	-	-	-	-	-	Ko	-	-	-	-
B063–1	96	6785110	2525554	400	y	480	0	-	-	-	-	-	abandoned	filled

Appendix A. (continued)

Well ID	Utility	Other ID	Relative depth	Notes	Owner	City	State
758–2	cistern	-	shallow	-	Rogers	Cedar Hill	TX
759–1	well	-	shallow	near house	Dixon	Ennis	TX
761–1	well	-	shallow	behind house	Hitchcock	Ennis	TX
761–2	well	-	shallow	S of house	Hitchcock	Ennis	TX
761–3	well	-	shallow	behind house	Hitchcock	Ennis	TX
761–4	well	-	shallow	behind house	Hitchcock	Ennis	TX
762–1	well	-	shallow	W of house	Reznik	Dallas	TX
762–2	well	-	shallow	in front of barn	Reznik	Dallas	TX
762–3	well	-	deep	W of house in pasture	Reznik	Dallas	TX
767–1	well	-	shallow	450 ft N of road in clearing	Hobratschk	Vernon	TX
778–1	well	-	shallow	by trailer	Donley	Palmer	TX
781	well	-	shallow	not on SSC footprint	Livesay	Palmer	TX
798B–1	well	-	shallow	by pond	Houghtelling	Palmer	TX
803–1	well	-	shallow	behind trailer, capped	Swaim	Palmer	TX
803–2	well	-	shallow	behind trailer, capped	Swaim	Palmer	TX
806B–1	well	-	shallow	behind trailer	Forston	Ennis	TX
808B–1	well	-	deep	in garage	Settlemeyer	Waxahachie	TX
810	spring	-	spring	not located	Oates	Palmer	TX
B063–1	well	-	shallow	-	Dobecka	Ennis	TX

Appendix A. Column heading explanation.

Well ID	First number is UFS parcel number; digit after hyphen is well number
Map no.	Number of aerial map on which well is located
NAD 83 northing and easting	Coordinates defining well location
Beam distance	Distance of well from beam alignment
Within easement	Is well within campus boundaries or within easement defined on aerial photos?
Ground surface elev.	Ground-surface elevation above mean sea level at wellhead
Well depth (ft)	Depth of well from ground surface
Water level elev.	Elevation above mean sea level of water level in well
Date meas (M/D/Y)	Date water-level measurement taken (month/day/year)
Formation	Geologic unit in which well is completed or screened Qal alluvium Qt terrace deposits Kau Austin Chalk Ko "lower Taylor Marl," Ozan Formation Kwc "middle Taylor Marl," Wolfe City Formation Ksb Eagle Ford Shale Kwb Woodbine Formation Kctm Twin Mountains Formation
Diameter surface casing	Diameter of well casing at top of well
Casing material	Description of surface casing construction materials
Well use	Use of the well
Wellhead condition	Description of cover on well and well maintenance
Utility	Designation as well, cistern, spring, or seep
Other ID	State or SSC designation for well
Relative depth	Qualitative characterization distinguishing shallow (<50 ft) dug well from deep (>200 ft) well of unmeasured depth in regional aquifer

Symbols:

-	Not applicable or data not collected
?	Unverified report
*	Measured depth/drilled depth
†	Well not located
‡	Possible match to well listed in state data base

Appendix B. Inventory of Water Wells Not Located on SSC Footprint

Appendix B. Table 1. Off-ring well inventory located on 7.5-minute topographic maps. See explanation of column headings and symbols at end of table.

Well ID	Topographic quadrangle	NAD 83 northing (ft)	NAD 83 easting (ft)	Ground surface elev. (ft)	Well depth (ft)	Water level elev. (ft)	Date meas. M/D/Y	Form-ation	Diameter surface casing (ft)	Casing material	Well use	Wellhead condition
A19—13—1	Midlothian	6864268	2459818	720	14.5	717.7	4/4/91	Kau	2	brick	unused	in metal pipe
A19—14—1	Midlothian	6863308	2459422	737	22.4	732.4	4/4/91	Kau	2.5	brick	lawn	covered w/boards
A19—14—2	Midlothian	6863145	2459413	737	23	732.2	4/4/91	Kau	2	brick	lawn	covered w/boards
A20—09—1	Midlothian	6856335	2457559	700	25.9	697.8	5/16/91	Kau	2.4	brick	unused	uncovered
A20—13—1	Midlothian	6857924	2459083	725	-	-	-	Kau	-	-	-	-
A20—16—1	Midlothian	6850743	2459801	691	19.2	686.9	4/4/91	Kau	2.3	brick	unused	uncovered
A20—20—1	Midlothian	6850983	2460362	690	-	-	-	Kau	-	-	aban'd	-
A24—14—1	Midlothian	6823235	2459692	620	-	-	-	Kau	-	-	-	-
A25—21—1	Boz	6816328	2463781	620	20	-	-	Kau	3	brick	aban'd	uncovered
A27—23—1	Boz	6797963	2463617	670	-	-	-	Kau	-	-	-	-
A38—19—1	Forreston	6820399	2473802	622	-	-	-	Kau	-	-	-	-
A39—03—1	Boz	6812681	2464620	650	-	-	-	Kau	-	brick	aban'd	-
A39—08—1	Boz	6810673	2467408	620	5.8	616.6	5/23/91	Kau	4.8	brick	unused	uncovered
A39—15—1	Forreston	6813724	2471222	560	-	-	-	Kau	-	-	-	-
A39—16—1	Forreston	6811034	2470851	621	22.7	615.7	5/23/91	Kau	2.5	brick	unused	covered
A39—17—1	Forreston	6817040	2472275	600	20.7	590	5/24/91	Kau	2.3	brick	unused	cement cover
A40—07—1	Boz	6804581	2467626	660	36.2	653.5	5/23/91	Kau	3	brick	unused	cement cover
A40—11—1	Boz	6804067	2469603	662	17.3	658.2	5/23/91	Kau	3	brick	unused	uncovered
A40—13—1	Forreston	6809607	2470507	643	30	638.3	5/23/91	Kau	2.5	brick	unused	covered
A40—14—1	Forreston	6806183	2470991	662	30.5	656.3	5/23/91	Kau	2.5	brick	unused	cement cover
A40—14—2	Forreston	6806201	2471096	661	836	-	-	Kwb	0.5	steel	aban'd	pump on wellhead
A40—21—1	Forreston	6809907	2475495	598	-	-	-	Kau	-	-	-	-
A41—05—1	Boz	6801087	2467779	625	-	-	-	Kau	-	-	aban'd	-
A41—05—2	Boz	6801131	2467784	625	-	-	-	Kau	-	brick	aban'd	-
A41—05—3	Boz	6800542	2467846	625	-	-	-	Kau	-	-	aban'd	-
A41—09—1	Boz	6801923	2469419	652	29	647.6	5/23/91	Kau	2.2	brick	unused	uncovered
A41—16—1	Boz	6795734	2470445	605	14.6	602.1	5/24/91	Kau	2.4	brick	unused	uncovered
A41—16—2	Boz	6795749	2470487	605	-	-	-	Kau	-	brick	aban'd	steel cover
A48—02—1	Lancaster	6870592	2477709	608	-	-	-	Kau	-	-	-	-
A48—02—2	Lancaster	6870534	2477992	600	-	-	-	Kau	-	-	-	-
A61—16—1	Avalon	6766308	2494506	550	-	-	-	Qt	-	-	-	-
A68—21—1	Cryer Creek	6777471	2510261	470	0	-	-	Ko	-	-	aban'd	filled?
A77—13—1	Palmer	6824513	2519019	506	-	-	-	Ko	-	brick	-	-
A77—13—2	Palmer	6824557	2519219	504	-	-	-	Ko	-	brick	-	fenced, no crown
A81—03—1	Ennis West	6789776	2513088	495	1200	-	-	-	-	steel	municipal	-
A81—12—5	Ennis West	6787947	2517644	503	24.9	486.4	5/17/91	Ko	2.7	brick	unused	wood cover
A89—20—1	Palmer	6835076	2528048	451	-	-	-	Ko	-	brick	-	housed
A90—22—1	Palmer	6830953	2535734	460	-	-	-	Ko	-	brick	-	-
A91—06—1	Ennis West	6822611	2527217	500	-	-	-	Ko	-	steel	municipal	-
A96—01—1	Ennis West	6784169	2525468	483	-	-	-	Ko	-	brick	aban'd	partially collapsed
A96—06—1	Ennis West	6783710	2526414	475	-	-	-	Ko	-	-	-	-
R34—1	Ennis West	6794012	2539871	482	-	-	-	Kwc	-	-	-	-
R34—2	Ennis West	6793812	2539904	482	-	-	-	Kwc	-	-	-	-
R34—3	Ennis West	6788208	2543382	477	29.8	455.2	10/17/91	Kwc	3.5	brick	unused	uncovered, loose bricks
R34—4	Ennis West	6788911	2544525	473	-	-	-	Kwc	-	-	-	-
R34—5	Avalon	6758161	2491151	489	-	-	-	Qt	-	-	-	-
R34—6	Avalon	6754329	2477885	520	-	-	-	Kau	-	-	-	-
R34—7	Italy	6753189	2466717	560	-	-	-	Kau	-	-	-	-
R34—8	Ennis West	6782250	2516865	488	-	-	-	Ko	-	-	-	-

Appendix B. Table 1. (continued)

Well ID	Utility	Other ID	Relative depth	Notes	Owner	City	State
A19—13—1	well	-	shallow	-	Roy Shipley	-	-
A19—14—1	well	-	shallow	-	Roy Shipley	-	-
A19—14—2	well	-	shallow	-	Roy Shipley	-	-
A20—09—1	well	-	shallow	-	-	-	-
A20—13—1	-	-	-	-	-	-	-
A20—16—1	well	-	shallow	-	-	-	-
A20—20—1	well	-	-	-	-	-	-
A24—14—1	well	-	shallow	-	-	-	-
A25—21—1	well	-	shallow	-	-	-	-
A27—23—1	well	-	-	-	-	-	-
A38—19—1	well	-	-	-	-	-	-
A39—03—1	well	-	shallow	-	-	-	-
A39—08—1	well	-	shallow	-	-	-	-
A39—15—1	-	-	-	-	-	-	-
A39—16—1	well	-	shallow	-	Robert Browning	Waxahachie	TX
A39—17—1	well	-	shallow	-	-	-	-
A40—07—1	well	-	shallow	-	-	-	-
A40—11—1	well	-	shallow	-	-	-	-
A40—13—1	well	-	shallow	-	-	-	-
A40—14—1	well	-	shallow	-	-	-	-
A40—14—2	well	JK-33-42-404	deep	-	-	-	-
A40—21—1	well	-	shallow?	-	-	-	-
A41—05—1	well	-	deep	-	-	-	-
A41—05—2	well	-	shallow	-	-	-	-
A41—05—3	well	-	shallow?	windmill	-	-	-
A41—09—1	well	-	shallow	-	-	-	-
A41—16—1	well	-	shallow	windmill	-	-	-
A41—16—2	well	-	shallow	-	-	-	-
A48—02—1	well	-	-	-	-	-	-
A48—02—2	well	-	-	-	-	-	-
A61—16—1	well	-	-	public water supply well	-	-	-
A68—21—1	well	-	shallow	-	-	-	-
A77—13—1	well	-	shallow	-	-	-	-
A77—13—2	well	-	shallow	-	-	-	-
A81—03—1	well	JK-33-43-701	deep	rural water supply well	-	-	-
A81—12—5	well	-	shallow	-	-	-	-
A89—20—1	well	JK-33-35-803‡	shallow	-	-	-	-
A90—22—1	well	-	shallow	-	-	-	-
A91—06—1	well	JK-33-43-204	deep	-	Boyce Water Supply	-	-
A96—01—1	well	JK-33-43-801	shallow	-	-	-	-
A96—06—1	well	-	-	-	-	-	-
R34—1	well	-	shallow	-	-	-	-
R34—2	well	-	shallow	-	-	-	-
R34—3	well	-	shallow	-	Marusak	Ennis	TX
R34—4	well	-	shallow	-	-	-	-
R34—5	well	-	shallow	-	-	-	-
R34—6	well	-	shallow	-	-	-	-
R34—7	well	-	shallow	-	-	-	-
R34—8	well	-	shallow	-	-	-	-

Appendix B. Table 1. Off-ring well inventory located on 7.5-minute topographic maps. See explanation of column headings and symbols at end of table.

Well ID	Topographic quadrangle	NAD 83 northing (ft)	NAD 83 easting (ft)	Ground surface elev. (ft)	Well depth (ft)	Water level elev. (ft)	Date meas. M/D/Y	Form-ation	Diameter surface casing (ft)	Casing material	Well use	Wellhead condition
R45—1	Ennis West	6809699	2546560	515	-	-	-	Kwc	-	-	-	-
R45—2	Ennis West	6810163	2546104	530	-	-	-	Kwc	-	-	-	filled? trash
R45—3	Ennis West	6814905	2544837	532	-	-	-	Kwc	-	-	-	-
R45—4	Ennis West	6814693	2542978	545	-	-	-	Kwc	-	-	-	-
R45—5	Ennis West	6819384	2539991	550	-	-	-	Kwc	-	-	-	-
R45—6	Ennis West	6819140	2539583	555	-	-	-	Kwc	-	-	-	-
R45—7	Ennis West	6820580	2538886	548	-	-	-	Kwc	-	-	-	-
R45—8	Ennis West	6820512	2538156	553	-	-	-	Kwc	-	-	-	-
R45—9	Ennis West	6819336	2539261	502	-	-	-	Kwc	-	-	-	-
R45—10	Ennis West	6809459	2544001	540	-	-	-	Kwc	-	-	-	-
R45—11	Ennis West	6808685	2544461	545	-	-	-	Kwc	-	-	-	-
R45—12	Ennis West	6811182	2543500	550	-	-	-	-	-	steel	municipal	water tower
R45—13	Ennis West	6815636	2541636	555	-	-	-	Kwc	-	-	-	-
R45—14	Ennis West	6817285	2545840	540	-	-	-	Kwc	-	-	-	-
R45—15	Ennis West	6817847	2544362	551	-	-	-	-	-	steel	municipal	water tower
R45—16	Ennis West	6819065	2535772	539	-	-	-	Kwc	-	brick	-	-
R45—17	Ennis West	6820248	2537859	550	-	-	-	Kwc	-	-	-	-
R45—18	Ennis West	6812918	2544120	552	-	-	-	Kwc	-	brick	-	-
R45—19	Ennis West	6813452	2543644	552	-	-	-	Kwc	-	brick	-	-
R45—20	Ennis West	6811537	2544817	532	-	-	-	Kwc	-	-	-	-
R45—21	Ennis West	6811131	2545102	530	-	-	-	Kwc	-	-	-	-
R45—22	Ennis West	6809136	2546296	530	-	-	-	Kwc	-	-	-	-
R55—1	Forreston	6813452	2543644	545	-	-	-	Kau	-	-	-	-
R55—2	Forreston	6811537	2544817	525	-	-	-	-	-	steel	-	housed
R55—3	Forreston	6811131	2545102	519	-	-	-	Ko	-	brick	-	covered
R55—4	Forreston	6783911	2485934	522	-	-	-	Kau	-	brick	-	covered, junk heap
R55—5	Forreston	6799808	2481831	580	35.1	572.5	8/28/91	Kau	2.9	brick	-	covered
R55—6	Forreston	6800680	2480951	587	-	-	-	Kau	-	-	-	-
R55—7	Forreston	6801594	2480723	594	-	-	-	Kau	-	-	-	-
R55—8	Forreston	6805834	2477952	623	-	-	-	Kau	-	-	-	housed
R55—9	Forreston	6790879	2485296	541	23	535.3	8/28/91	Kau	2.3	brick	-	cement cover
R55—10	Forreston	6783922	2490075	520	-	-	-	Ko	-	brick	unused	cement cover, garbage filled
R55—11	Forreston	6783510	2489943	520	21.1	510.9	8/28/91	Ko	2.6	-	-	-
R55—12	Forreston	6783785	2490248	521	17.1	512.4	8/28/91	Ko	3	-	-	-
R55—13	Avalon	6761890	2497426	532	25.3	522	10/10/91	Qt	3	cement	-	-
R55—14	Avalon	6759016	2499243	515	-	-	-	Qt	-	-	-	-
R55—15	Avalon	6756539	2500492	498	-	-	-	Qt	-	-	-	-
R55—16	Avalon	6753228	2503426	517	-	-	-	Qt	-	-	-	-
R55—17	Avalon	6752684	2503147	470	32.2	461	10/10/91	Qt	3	-	-	-
R55—18	Avalon	6761373	2496498	522	-	-	-	Qt	-	-	-	-
R55—19	Forreston	6784326	2489784	522	-	-	-	Ko	-	-	-	-
R55—20	Forreston	6785235	2484843	530	-	-	-	Kau	-	-	-	-
R55—21	Avalon	6766565	2492893	540	-	-	-	Qt	-	-	-	-
R55—22	Avalon	6764055	2495638	548	-	-	-	Qt	-	-	-	-
R55—23	Avalon	6754861	2506034	500	-	-	-	Qt	-	-	-	-
R55—24	Avalon	6763057	2496637	531	-	-	-	Qt	-	-	-	housed
R55—25	Avalon	6762952	2496379	528	-	-	-	Qt	-	brick	-	-
R55—27	Forreston	6806987	2478583	608	24	603.3	11/19/91	Kau	3	brick	-	-
R55—28	Forreston	6806736	2478476	609	-	-	-	Kau	-	-	-	-

Appendix B. Table 1. (continued)

Well ID	Utility	Other ID	Relative depth	Notes	Owner	City	State
R45—1	well	-	shallow	-	-	-	-
R45—2	well	-	shallow	-	-	-	-
R45—3	well	-	shallow	-	-	-	-
R45—4	well	-	shallow	-	-	-	-
R45—5	well	-	shallow	-	-	-	-
R45—6	well	-	shallow	-	-	-	-
R45—7	well	-	shallow	-	-	-	-
R45—8	well	-	-	windmill	-	-	-
R45—9	well	-	shallow	-	-	-	-
R45—10	well	-	shallow	-	-	-	-
R45—11	well	-	shallow	-	-	-	-
R45—12	well	-	deep	water tower	-	-	-
R45—13	well	-	shallow	-	-	-	-
R45—14	well	-	shallow	-	-	-	-
R45—15	well	-	deep	water tower	-	-	-
R45—16	well	-	shallow	-	-	-	-
R45—17	well	-	shallow	-	-	-	-
R45—18	well	-	shallow	-	-	-	-
R45—19	well	-	shallow	-	-	-	-
R45—20	well	-	shallow	-	-	-	-
R45—21	well	-	shallow	-	-	-	-
R45—22	well	-	shallow	-	-	-	-
R55—1	well	-	-	windmill on topo map gone	-	-	-
R55—2	well	-	deep?	-	-	-	-
R55—3	well	-	shallow	-	-	-	-
R55—4	well	-	shallow	-	-	-	-
R55—5	well	-	shallow	-	Davis	-	-
R55—6	well	-	shallow	-	-	-	-
R55—7	well	-	shallow	-	-	-	-
R55—8	well	-	shallow	-	-	-	-
R55—9	well	-	shallow	-	-	-	-
R55—10	well	-	shallow	in front of church	-	-	-
R55—11	well	-	shallow	Nash Community Center	-	Nash	TX
R55—12	well	-	shallow	-	Jenkins	-	-
R55—13	well	-	shallow	-	Gomez	Avalon	TX
R55—14	well	-	shallow	-	Gillespie	-	-
R55—15	well	-	shallow	-	-	-	-
R55—16	well	-	shallow	-	-	-	-
R55—17	well	-	shallow	-	Martinez	Italy	TX
R55—18	well	-	shallow	-	-	Avalon	TX
R55—19	well	-	shallow	-	-	-	-
R55—20	well	-	shallow	in field	-	-	-
R55—21	well	-	shallow	in empty lot	-	-	-
R55—22	well	-	shallow	-	-	-	-
R55—23	well	-	shallow	-	-	-	-
R55—24	well	-	shallow	-	-	-	-
R55—25	well	-	shallow	-	-	-	-
R55—27	well	-	shallow	-	Washington	Waxahachie	TX
R55—28	well	-	shallow	in front of house	-	-	-

Appendix B. Table 1. Off-ring well inventory located on 7.5-minute topographic maps. See explanation of column headings and symbols at end of table.

Well ID	Topographic quadrangle	NAD 83 northing (ft)	NAD 83 easting (ft)	Ground surface elev. (ft)	Well depth (ft)	Water level elev. (ft)	Date meas. M/D/Y	Form-ation	Diameter surface casing (ft)	Casing material	Well use	Wellhead condition
R55—29	Forreston	6808868	2478678	600	-	-	-	Kau	-	brick	-	-
R55—30	Forreston	6809216	2478513	590	-	-	-	Kau	-	steel	municipal	-
R55—31	Forreston	6810589	2482566	560	-	-	-	Kau	-	cement	-	-
R55—32	Forreston	6808534	2478372	601	-	-	-	Kau	-	-	-	-
R55—33	Avalon	6774320	2495492	475	deep	-	-	-	0.17?	steel	-	-
R55—34	Avalon	6776005	2497887	482	19.9	481.2	2/25/92	Ko	2.9	brick	-	-
R55—35	Avalon	6767407	2487683	517	27	499.4	1/21/92	Qt	2.5	brick	unused	wood cover
R55—36	Avalon	6775745	2484589	502	23.7	491.6	1/21/92	Ko	2.5	brick	unused	metal plate cover
R55—37	Avalon	6774875	2484022	516	deep	-	-	-	0.17?	steel	-	-
R55—38	Avalon	6776068	2485628	501	deep	-	-	-	0.17?	steel	-	-
R55—39	Avalon	6762119	2497750	532	deep?	-	-	-	0.17?	steel	-	-
R55—40	Avalon	6761517	2496802	526	deep	-	-	-	0.17?	steel	-	small water tower
R55—41	Forreston	6782383	2486336	518	-	-	-	Ko	-	-	-	-
R55—42	Forreston	6782581	2486829	512	-	-	-	Ko	-	-	-	-
R55—43	Forreston	6787124	2495307	487	-	-	-	Ko	-	-	-	-
R55—44	Forreston	6790600	2498433	513	-	-	-	Ko	-	-	-	-
R55—45	Forreston	6781561	2495477	519	shallow	-	-	Ko	-	brick	-	-
R55—46	Avalon	6776433	2498939	490	shallow	-	-	Ko	-	-	-	wood cover
R55—47	Avalon	6775684	2497412	483	-	-	-	Ko	-	brick	aban'd	collapsed
R55—48	Forreston	6778162	2478737	540	-	-	-	Kau	-	-	-	-
R55—49	Forreston	6780660	2482895	542	-	-	-	Kau	-	brick	-	housed
R55—50	Forreston	6780105	2481351	534	-	-	-	Kau	-	brick	-	-
R55—51	Forreston	6778966	2479565	545	-	-	-	Kau	-	brick	aban'd	-
R55—52	Forreston	6778515	2483191	518	-	-	-	Kau	-	-	-	-
R55—53	Forreston	6778538	2484013	512	-	-	-	Kau	-	-	-	-
R55—54	Forreston	6781308	2484141	543	-	-	-	Ko/Kau	-	-	-	pump on wellhead
R55—55	Avalon	6776348	2489115	494	-	-	-	Ko	-	-	-	-
R55—56	Avalon	6777793	2483854	509	-	-	-	Kau	-	-	-	-
R66—1	Boz	6804736	2449044	665	-	-	-	-	-	steel	municipal	pump on wellhead
R66—2	Forreston	6821571	2470242	642	29.8	635.3	8/28/91	Kau	3	-	-	locking cover, grated
R66—3	Forreston	6821393	2470336	642	-	-	-	Kau	-	-	-	-
R66—4	Forreston	6821449	2470134	642	-	-	-	-	-	steel?	-	-
R66—5	Boz	6801898	2431837	560	-	-	-	Ksb	-	-	unused	collapsed
R66—6	Boz	6788991	2436268	540	-	-	-	Qt/Ksb	-	-	-	-
R66—7	Boz	6790001	2436938	515	-	-	-	Qt/Ksb	-	-	-	-
R66—8	Boz	6790232	2437358	508	-	-	-	Qt/Ksb	-	-	-	-
R66—9	Boz	6804723	2444200	710	-	-	-	Kau	-	-	-	uncovered
R66—10	Boz	6818809	2465973	630	-	-	-	Kau	-	-	-	-
R66—11	Boz	6803705	2443156	711	-	-	-	Kau	-	-	-	-
R66—12	Boz	6805052	2444040	721	728	381.2	6/16/65	Kwb	0.4	steel	unused	plugged
R66—13	Boz	6801777	2443014	677	-	-	-	Kau	-	-	filled	filled
R66—14	Boz	6799902	2439682	630	-	-	-	Kau/Ksb	-	-	lawn?	-
R66—15	Boz	6799932	2440033	630	-	-	-	Kau/Ksb	-	-	-	-
R66—16	Forreston	6822119	2471814	610	-	-	-	Kau	-	-	-	-
R66—17	Boz	6819169	2466044	631	-	-	-	Kau	-	-	-	-
R66—18	Boz	6819598	2465873	631	-	-	-	Kau	-	-	-	-
R77—1	Forreston	6796666	2475375	609	26	599.9	10/23/91	Kau	1.5	brick	unused	-
R77—2	Forreston	6805043	2475812	622	-	-	-	-	-	steel?	-	-
R77—3	Forreston	6804887	2475985	622	32	613.3	9/18/91	Kau	3	brick	-	-

Appendix B. Table 1. (continued)

Well ID	Utility	Other ID	Relative depth	Notes	Owner	City	State
R55—29	well	-	shallow	S of house	-	-	-
R55—30	well	JK-33-42-105	deep	rural water supply	-	-	-
R55—31	well	-	shallow	-	-	-	-
R55—32	well	-	shallow	S of barn	-	-	-
R55—33	well	JK-33-50-201	deep	windmill	-	-	-
R55—34	well	-	shallow	-	-	-	-
R55—35	well	-	shallow	-	Odom	-	-
R55—36	well	-	shallow	-	Russo	Forreston	TX
R55—37	well	-	deep	windmill	-	-	-
R55—38	well	-	deep	windmill	-	-	-
R55—39	well	-	deep	windmill	-	-	-
R55—40	well	JK-33-50-501	deep	behind gas station	-	-	-
R55—41	well	-	shallow?	-	-	-	-
R55—42	well	-	shallow?	-	-	-	-
R55—43	well	-	shallow?	-	-	-	-
R55—44	well	-	shallow?	-	-	-	-
R55—45	well	-	shallow	-	-	-	-
R55—46	well	-	shallow	-	-	-	-
R55—47	well	-	shallow	-	-	-	-
R55—48	well	-	shallow?	-	-	-	-
R55—49	well	-	shallow?	-	-	-	-
R55—50	well	-	shallow?	-	-	-	-
R55—51	well	-	shallow?	-	-	-	-
R55—52	well	-	shallow?	windmill	-	-	-
R55—53	well	-	shallow?	windmill	-	-	-
R55—54	well	-	shallow?	-	-	-	-
R55—55	well	-	shallow?	-	-	-	-
R55—56	well	-	shallow?	in flood plain	-	-	-
R66—1	well	JK-33-41-502	deep	-	Casa Grande Water Co.	-	-
R66—2	well	-	shallow	-	-	-	-
R66—3	well	-	shallow	-	-	-	-
R66—4	well	-	deep	-	-	-	-
R66—5	well	-	shallow	-	-	-	-
R66—6	well	-	shallow	-	Winton	Desoto/Oak Cliff	TX
R66—7	well	-	shallow	-	-	-	-
R66—8	well	-	-	windmill	-	-	-
R66—9	well	-	shallow	behind house	-	-	-
R66—10	well	-	shallow	at house near park	-	-	-
R66—11	well	-	-	windmill	-	-	-
R66—12	well	JK-33-41-401	deep	former deep well pulled 1989	Sullivan	Waxahachie	TX
R66—13	well	-	shallow	E side of house	Vickers	-	-
R66—14	well	-	shallow	behind trailer for lawn	-	-	-
R66—15	well	-	shallow	behind garage	-	-	-
R66—16	well	-	shallow	E of house	-	-	-
R66—17	well	-	shallow	behind house	-	-	-
R66—18	well	-	-	windmill	-	-	-
R77—1	well	-	shallow	-	Stanton	Waxahachie	TX
R77—2	well	-	-	under windmill	-	-	-
R77—3	well	-	shallow	-	Odom	Nena	TX

Appendix B. Table 1. Off-ring well inventory located on 7.5-minute topographic maps. See explanation of column headings and symbols at end of table.

Well ID	Topographic quadrangle	NAD 83 northing (ft)	NAD 83 easting (ft)	Ground surface elev. (ft)	Well depth (ft)	Water level elev. (ft)	Date meas. M/D/Y	Form-ation	Diameter surface casing (ft)	Casing material	Well use	Wellhead condition
R77—4	Forreston	6794351	2478028	595	17	591.9	1/15/92	Kau	3	brick	-	wood cover
R77—5	Forreston	6795359	2479011	583	20.1	581.8	1/29/92	Kau	2.5	brick	-	-
R77—6	Forreston	6794524	2476661	611	20.8	604.4	10/23/91	Kau	2.4	brick	unused	-
R77—7	Forreston	6786826	2477204	581	-	-	-	Kau	-	-	-	-
R77—8	Forreston	6786688	2478329	564	-	-	-	Kau	-	-	-	-
R77—9	Forreston	6783295	2479981	550	-	-	-	-	-	steel?	-	-
R77—10	Forreston	6779977	2474211	535	-	-	-	Kau	-	-	-	-
R77—11	Forreston	6784507	2474021	555	20	551	10/23/91	Kau	-	brick	-	-
R77—12	Forreston	6785765	2480163	564	-	-	-	Kau	-	-	-	-
R77—13	Forreston	6786322	2480031	552	-	-	-	Kau	-	-	-	-
R77—14	Forreston	6784459	2471606	561	-	-	-	Kau	-	-	-	-
R77—15	Italy	6774412	2469728	495	-	-	-	Qt	-	-	-	-
R77—16	Forreston	6781095	2476306	550	-	-	-	Kau	-	-	-	-
R77—18	Forreston	6818165	2475890	611	-	-	-	Kau	-	-	-	-
R77—19	Forreston	6817605	2475741	610	-	-	-	Kau	-	-	-	-
R77—20	Forreston	6795642	2479058	612	21.9	602.8	10/23/91	Kau	2.2	brick	unused	-
R77—21	Avalon	6773541	2472146	490	-	-	-	Qt	-	-	-	-
R77—22	Forreston	6779439	2473595	548	-	-	-	Kau	-	-	-	-
R77—23	Waxahachie	6827337	2477106	550	1200	-	-	Kwb	-	steel	unused	-
R77—24	Forreston	6792967	2474936	585	20	584.2	1/15/92	Kau	3	brick	unused	wood cover
R77—25	Forreston	6793663	2475852	593	-	-	-	Kau	-	brick	unused	-
R77—27	Forreston	6795447	2479402	575	16	573.3	1/29/92	Kau	3	brick	unused	-
R77—28	Avalon	6777873	2477876	539	-	-	-	Kau	-	cement	-	-
R77—29	Avalon	6776821	2476509	530	-	-	-	Kau	-	-	-	-
R77—30	Forreston	6794156	2475142	598	-	-	-	Kau	-	-	-	-
R77—31	Avalon	6769354	2479303	509	-	-	-	Qt	-	-	unused	metal cover
R77N—1	Waxahachie	6854735	2482108	600	-	-	-	-	-	steel?	-	-
R77N—2	Waxahachie	6855928	2482712	620	-	-	-	Kau	-	-	-	housed?
R77N—3	Waxahachie	6859508	2482838	629	-	-	-	Kau	-	-	-	pump on wellhead
R77N—4	Waxahachie	6859420	2482519	631	-	-	-	Kau	-	wood?	-	wood crown
R77N—5	Waxahachie	6859059	2482437	634	32	626.7	8/30/91	Kau	2.5	cement	-	uncovered
R77N—6	Waxahachie	6858689	2482436	631	-	-	-	Kau	-	-	-	-
R77N—7	Waxahachie	6853813	2481989	603	-	-	-	Kau	-	steel	-	-
R77N—8	Waxahachie	6851316	2481596	600	-	-	-	Kau	-	brick	-	-
R77N—9	Waxahachie	6851992	2482735	590	-	-	-	Kau	-	-	-	housed
R77N—10	Waxahachie	6848371	2481265	625	26.2	616.9?	10/9/91	Kau	3	brick	unused	-
R77N—11	Waxahachie	6840471	2480538	620	47.6	615.4	10/9/91	Kau	3	-	-	-
R77N—12	Waxahachie	6845953	2481262	634	-	-	-	Kau	-	-	-	-
R77N—13	Waxahachie	6845101	2481141	640	-	-	-	Kau	-	-	-	-
R77N—14	Waxahachie	6844646	2480921	640	-	-	-	Kau	-	-	-	under deck
R77N—15	Waxahachie	6829214	2478947	578	-	-	-	Kau	-	-	-	-
R77N—16	Waxahachie	6851361	2482258	598	-	-	-	Kau	-	brick	-	housed
R77N—17	Waxahachie	6858699	2482436	637	-	630.8	8/30/91	Kau	1.9	-	-	-
R77N—18	Lancaster	6877894	2485192	618	-	-	-	Kau	-	-	-	flush with surface
R77N—19	Lancaster	6882672	2487796	641	15.7	637.4	10/23/91	Kau	3	metal	unused	-
R77N—20	Waxahachie	6830708	2477240	580	11.1	573.8	10/24/91	Kau	2.3	brick	unused	-
R77N—21	Waxahachie	6840741	2480676	620	21.2	615.2	11/15/91	Kau	3	-	-	heavy steel cover
R77N—22	Waxahachie	6848275	2481033	626	24.2	608.7	11/15/91	Kau	2.5	brick	unused	flush with surface
R77N—23	Waxahachie	6836847	2480339	613	-	-	-	Kau	-	-	-	-

Appendix B. Table 1. (continued)

Well ID	Utility	Other ID	Relative depth	Notes	Owner	City	State
R77—4	well	-	shallow	pump on wellhead	Jansky	Waxahachie	TX
R77—5	well	-	shallow	-	-	-	-
R77—6	well	-	shallow	-	Adamson	Waxahachie	TX
R77—7	well	-	shallow	-	-	-	-
R77—8	well	-	shallow	-	-	-	-
R77—9	well	-	-	under windmill	-	-	-
R77—10	well	-	shallow	-	-	-	-
R77—11	well	-	shallow	under windmill	Garoosi	-	-
R77—12	well	-	-	in pasture	-	-	-
R77—13	well	-	-	in Onion Creek	-	-	-
R77—14	well	-	-	windmill	-	-	-
R77—15	well	-	-	in flood plain	-	-	-
R77—16	well	-	shallow	-	-	-	-
R77—18	well	-	shallow	in field	-	-	-
R77—19	well	-	-	windmill and tank	-	-	-
R77—20	well	-	shallow	-	Adamson	Waxahachie	TX
R77—21	well	-	shallow	-	-	-	-
R77—22	well	-	shallow	-	-	-	-
R77—23	well	JK-33-34-701‡	deep	-	City of Waxahachie	Waxahachie	TX
R77—24	well	-	shallow	-	Futch	Waxahachie	TX
R77—25	well	-	shallow	-	Brown	Waxahachie	TX
R77—27	well	-	shallow	in front yard	Hinds	Waxahachie	TX
R77—28	well	-	shallow	-	-	-	-
R77—29	well	-	shallow	-	-	-	-
R77—30	well	-	shallow	near brick pumphouse	-	-	-
R77—31	well	-	shallow	-	-	-	-
R77N—1	well	-	shallow	under windmill	-	-	-
R77N—2	well	-	-	-	-	-	-
R77N—3	well	-	shallow	pump?	-	-	-
R77N—4	well	-	shallow	-	-	-	-
R77N—5	well	-	shallow	-	Appellon	-	-
R77N—6	well	-	shallow	-	-	-	-
R77N—7	well	-	shallow	-	-	-	-
R77N—8	well	-	shallow	-	-	-	-
R77N—9	well	-	shallow	-	-	-	-
R77N—10	well	-	shallow	-	-	-	-
R77N—11	well	-	shallow	-	Buchanan	-	-
R77N—12	well	-	shallow	-	-	-	-
R77N—13	well	-	shallow	-	-	-	-
R77N—14	well	-	shallow	under deck	-	-	-
R77N—15	well	-	shallow?	-	-	-	-
R77N—16	well	-	shallow?	in creek bed	-	-	-
R77N—17	well	-	shallow	in flood plain	Appellon	-	-
R77N—18	well	-	shallow	-	-	-	-
R77N—19	well	-	shallow	augered to 50 ft	Bice	Red Oak	TX
R77N—20	well	-	shallow	-	Fred Stones Realty	-	-
R77N—21	well	-	shallow	heavy steel cover	-	-	-
R77N—22	well	-	shallow	under windmill	Childrens Home	-	-
R77N—23	well	-	shallow	at house near High School	-	-	-

Appendix B. Table 1. Off-ring well inventory located on 7.5-minute topographic maps. See explanation of column headings and symbols at end of table.

Well ID	Topographic quadrangle	NAD 83 northing (ft)	NAD 83 easting (ft)	Ground surface elev. (ft)	Well depth (ft)	Water level elev. (ft)	Date meas. M/D/Y	Form-ation	Diameter surface casing (ft)	Casing material	Well use	Wellhead condition
R77N—24	Waxahachie	6829543	2478241	580	-	-	-	Kau	-	-	-	fastened wood cover
R77N—25	Waxahachie	6847861	2481550	623	900	373	6/16/65	Kwb	0.4	steel	dom.	-
R77N—26	Waxahachie	6859673	2482592	630	-	-	-	Kau	-	-	-	-
R77N—27	Waxahachie	6855808	2482224	611	-	-	-	Kau	-	-	-	-
R77N—28	Waxahachie	6856825	2483669	628	3088	-	-	Kctm	1.1	steel	municipal	-
R77N—29	Waxahachie	6868927	2490919	552	-	-	-	Kau	-	-	-	-
R77N—30	Waxahachie	6859429	2481295	640	-	632.6	4/7/92	Kau	2.5	brick	unused	garbage inside
R77N—31	Waxahachie	6867505	2490170	515	-	-	-	Qal	-	cement	unused	covered
R287—1	Midlothian	6842490	2460194	595	25.8	578.6	4/4/91	Kau	1.8	brick	aban'd	tire on board
R287—2	Midlothian	6845827	2459487	639	-	-	-	Kau	-	-	-	-
R287—3	Midlothian	6842568	2460073	590	-	-	-	Kau	-	-	lawn	-
R287—4	Midlothian	6843240	2458304	640	-	-	-	Kau	-	-	-	-
R287—5	Midlothian	6843290	2456923	655	-	-	-	Kau	-	-	-	-
R287—6	Midlothian	6854769	2449510	684	-	-	-	-	-	steel	-	-
R287—7	Ennis West	6800836	2517351	480	-	-	-	-	0.3	steel	-	housed
R287—8	Ennis West	6800914	2518921	471	-	-	-	Qt	-	-	-	-
R287—9	Ennis West	6802164	2521513	460	-	-	-	Qal	-	-	-	housed
R287—10	Ennis West	6801301	2523385	473	-	-	-	Qt	-	-	-	housed
R287—11	Ennis West	6799645	2524657	449	-	-	-	Qt	-	-	-	-
R287—12	Ennis West	6799612	2524938	449	-	-	-	Qt	-	-	lawn	-
R287—13	Ennis West	6799492	2529935	458	-	-	-	Qt/Ko	-	-	-	collar
R287—14	Ennis West	6801634	2523117	473	-	-	-	Qt	-	-	-	-
R287—15	Waxahachie	6833736	2489023	592	-	-	-	Kau	-	-	-	-
R287—16	Waxahachie	6833452	2485826	590	-	-	-	-	-	steel	municipal	-
R287—17	Forreston	6822367	2497168	528	-	-	-	Ko	-	-	-	housed
R287—18	Forreston	6821299	2495143	556	-	-	-	Ko	-	-	-	-
R287—19	Forreston	6820764	2494302	563	-	-	-	Ko	-	-	-	-
R287—20	Ennis West	6806267	2513697	495	43.1	478.6	8/30/91	Qt	2.5	cement	unused	uncovered
R287—21	Ennis West	6806349	2515476	491	-	-	-	Qt	-	-	-	-
R287—22	Ennis West	6806723	2518570	501	-	-	-	Qt	-	-	-	-
R287—23	Ennis West	6814640	2519960	512	-	-	-	Ko	-	-	-	-
R287—24	Ennis West	6819708	2519927	490	-	-	-	Ko	-	-	-	-
R287—25	Ennis West	6820183	2519345	490	-	-	-	Ko	-	-	-	-
R287—26	Ennis West	6819926	2519011	491	-	-	-	Ko	-	-	-	-
R287—27	Ennis West	6822446	2519261	506	-	-	-	Ko	-	-	-	-
R287—28	Ennis West	6822922	2519940	507	-	-	-	Ko	-	-	-	-
R287—29	Ennis West	6823145	2520505	507	-	-	-	Ko	-	-	-	-
R287—30	Ennis West	6814604	2527187	483	-	-	-	Ko	-	-	-	-
R287—31	Ennis West	6814479	2526980	480	-	-	-	Ko	-	-	-	-
R287—32	Ennis West	6811207	2521604	495	-	-	-	Qt	-	-	-	-
R287—33	Ennis West	6810258	2522838	501	24.9	482.5	10/23/91	Qt/Ko	4	brick	-	-
R287—34	Ennis West	6803037	2535835	470	-	-	-	Kwc	-	-	-	-
R287—35	Ennis West	6796294	2538000	481	-	-	-	Kwc	-	-	-	-
R287—36	Ennis West	6794905	2539595	490	-	-	-	Kwc	-	-	-	-
R287—37	Ennis West	6806166	2520735	491	-	-	-	Qt	-	-	-	-
R287—38	Ennis West	6806204	2513578	492	-	-	-	Qt	-	-	-	covered
R287—39	Forreston	6808395	2503690	480	17.2	466.6	10/9/91	Qt	3	cement	-	-
R287—40	Forreston	6817944	2491068	530	-	-	-	Kau	-	-	-	-
R287—41	Forreston	6822016	2497902	532	15.7	522.7	10/9/91	Ko	4	brick	-	garbage in well

Appendix B. Table 1. (continued)

Well ID	Utility	Other ID	Relative depth	Notes	Owner	City	State
R77N—24	well	-	shallow	next to office/house	-	-	-
R77N—25	well	JK-33-34-402	deep	windmill in trees	J. Howe Leasing	Waxahachie	TX
R77N—26	well	-	shallow	-	-	-	-
R77N—27	well	-	-	windmill	-	-	-
R77N—28	well	JK-33-34- 207, 209	deep	water supply, four tanks	Rockett WSC	Red Oak	TX
R77N—29	well	-	-	windmill	-	-	-
R77N—30	well	-	shallow	-	-	-	-
R77N—31	well	-	shallow	-	-	-	-
R287—1	well	-	shallow	-	-	-	-
R287—2	well	-	-	windmill	-	-	-
R287—3	well	-	shallow	lawn	-	-	-
R287—4	well	-	shallow	-	-	-	-
R287—5	well	-	shallow	-	-	-	-
R287—6	well	-	deep?	-	-	-	-
R287—7	well	-	deep	under windmill	-	-	-
R287—8	well	-	-	-	-	-	-
R287—9	well	-	-	-	-	-	-
R287—10	well	-	-	-	-	-	-
R287—11	well	-	shallow	-	-	-	-
R287—12	well	-	shallow	-	-	-	-
R287—13	well	-	shallow	-	-	-	-
R287—14	well	-	shallow	-	-	-	-
R287—15	well	-	deep?	windmill	-	-	-
R287—16	well	-	deep	deep well	City of Waxahachie	Waxahachie	TX
R287—17	well	-	shallow	-	-	-	-
R287—18	well	JK-33-42-201‡	-	-	-	-	-
R287—19	well	-	shallow	-	-	-	-
R287—20	well	-	shallow	-	-	-	-
R287—21	well	-	-	-	-	-	-
R287—22	well	-	shallow	near racetrack	-	-	-
R287—23	well	-	shallow	under windmill	-	-	-
R287—24	well	-	shallow	-	-	-	-
R287—25	well	-	shallow	-	-	-	-
R287—26	well	-	shallow	-	-	-	-
R287—27	well	-	shallow	-	-	-	-
R287—28	well	-	shallow	-	-	-	-
R287—29	well	-	shallow	-	-	-	-
R287—30	well	-	shallow	-	-	-	-
R287—31	well	-	shallow	-	-	-	-
R287—32	well	-	shallow	-	-	-	-
R287—33	well	-	shallow	-	Henderson	-	-
R287—34	well	-	shallow	-	-	-	-
R287—35	well	-	shallow	-	-	-	-
R287—36	well	-	-	windmill	-	-	-
R287—37	well	-	-	-	-	-	-
R287—38	well	-	shallow	-	-	-	-
R287—39	well	-	shallow	-	-	-	-
R287—40	well	-	shallow	-	-	-	-
R287—41	well	-	shallow	garbage in well	-	-	-

Appendix B. Table 1. Off-ring well inventory located on 7.5-minute topographic maps. See explanation of column headings and symbols at end of table.

Well ID	Topographic quadrangle	NAD 83 northing (ft)	NAD 83 easting (ft)	Ground surface elev. (ft)	Well depth (ft)	Water level elev. (ft)	Date meas. M/D/Y	Form-ation	Diameter surface casing (ft)	Casing material	Well use	Wellhead condition
R287—42	Forreston	6819038	2503179	547	-	-	-	Ko	-	-	-	-
R287—43	Forreston	6808558	2503473	485	-	-	-	Qt	-	-	-	very crumbly cover
R287—44	Forreston	6808197	2502913	483	22.4	461.8	10/9/91	Qt	2.2	cement	-	-
R287—45	Forreston	6809756	2502308	490	-	-	-	Ko	-	-	-	-
R287—46	Forreston	6807440	2504217	473	12.6	467	10/9/91	Qt/Qal	2.5	brick	unused	-
R287—47	Forreston	6807350	2504428	473	13.1	467.2	10/9/91	Qt/Qal	3	brick	domestic	-
R287—48	Ennis West	6799922	2525912	460	-	-	-	Qt/Ko	-	cement	-	-
R287—49	Ennis West	6800015	2527032	460	39.8	440.2	10/23/91	Qt/Ko	4	cement	-	wood cover
R287—50	Ennis West	6809862	2524013	497	-	-	-	Qt	-	-	-	-
R287—51	Forreston	6813273	2496670	501	-	-	-	Qal	-	-	-	-
R287—52	Ennis West	6799576	2525522	450	-	-	-	Qt/Ko	-	brick	unused	cover bolted down
R287—53	Midlothian	6843037	2455964	666	-	-	-	Kau	-	-	-	-
R287—54	Forreston	6809339	2503043	480	-	-	-	Ko	-	cement	-	housed
R287—55	Ennis West	6805948	2519367	501	-	-	-	Qt	-	brick	-	-
R287W—1	Midlothian	6843556	2463669	620	-	-	-	Kau	-	-	-	housed (deteriorated)
R287W—2	Waxahachie	6833741	2473056	587	-	-	-	Kau	-	-	aban'd	trash inside, dry
R287W—3	Waxahachie	6833589	2472115	553	-	-	-	Kau	-	-	-	-
R287W—4	Waxahachie	6832568	2472883	560	-	-	-	Kau	-	-	-	-
R287W—5	Midlothian	6860084	2434577	720	8.5	dry	10/16/91	Kau	-	-	unused	overgrown, dry
R287W—6	Midlothian	6860243	2434176	718	-	-	-	Kau	-	-	aban'd	overgrown
R287W—7	Midlothian	6859316	2433967	750	-	-	-	Kau	-	-	aban'd	-
R287W—8	Midlothian	6860605	2435769	705	-	-	-	Kau	-	-	-	overgrown
R287W—9	Midlothian	6859646	2435189	735	-	-	-	Kau	-	-	-	-
R287W—10	Midlothian	6849955	2448949	690	-	-	-	Kau	-	-	-	-
R287W—11	Midlothian	6849289	2445074	690	-	-	-	-	-	steel?	-	-
R287W—12	Midlothian	6849830	2445001	700	-	-	-	Kau	-	-	-	-
R287W—13	Midlothian	6849426	2443249	725	-	-	-	Kau	-	-	-	-
R287W—14	Midlothian	6849625	2443156	725	-	-	-	-	-	steel?	unused	-
R287W—15	Midlothian	6847090	2442447	725	16.2	723.5	11/19/91	Kau	2.5	brick	-	-
R287W—16	Midlothian	6853515	2442085	730	-	-	-	-	-	steel?	municipal	-
R287W—18	Midlothian	6860167	2448815	733	20.6	730.4	11/19/91	Kau	3	brick	-	-
R287W—19	Midlothian	6858992	2449050	732	-	-	-	Kau	-	-	-	-
R287W—20	Midlothian	6861569	2449188	718	-	-	-	-	-	steel?	-	-
R287W—21	Midlothian	6861722	2448655	727	-	-	-	Kau	-	-	-	-
R287W—22	Midlothian	6861992	2448652	722	-	-	-	Kau	-	-	-	-
R287W—23	Midlothian	6862695	2449023	728	-	-	-	Kau	-	-	-	-
R287W—24	Midlothian	6845067	2439507	753	-	-	-	Kau	-	-	-	-
R287W—25	Midlothian	6844809	2439630	740	-	-	-	Kau	-	-	-	-
R287W—26	Midlothian	6844342	2461398	622	-	-	-	Kau	-	-	-	-
R287W—27	Midlothian	6844949	2461733	610	-	-	-	Kau	-	-	-	-
R287W—28	Midlothian	6858316	2441560	680	-	-	-	Kau	-	-	-	housed
R308—1	Italy	6750951	2443038	725	-	-	-	Kau	-	-	-	-
R308—2	Italy	6750346	2443364	715	-	-	-	Kau	-	-	-	-
R308—3	Italy	6747847	2444741	672	-	-	-	Kau	-	-	-	-
R528—1	Waxahachie	6825751	2480329	530	-	-	-	Qt	-	cement	-	-
R528—2	Waxahachie	6825837	2480096	530	-	-	-	Qt	-	-	-	-
R528—3	Waxahachie	6826184	2479306	525	-	-	-	Qt	-	-	-	-
R528—4	Waxahachie	6825296	2481211	555	-	-	-	Kau	-	-	-	-
R528—5	Waxahachie	6826425	2480558	530	-	-	-	Kau	-	-	-	-

Appendix B. Table 1. (continued)

Well ID	Utility	Other ID	Relative depth	Notes	Owner	City	State
R287—42	well	-	shallow	-	-	-	-
R287—43	well	-	shallow	-	-	-	-
R287—44	well	-	shallow	near windmill	-	-	-
R287—45	well	-	shallow	well/cistern	-	-	-
R287—46	well	-	shallow	tall crown	Honza	-	-
R287—47	well	-	shallow	-	Honza	-	-
R287—48	well	-	shallow	-	-	-	-
R287—49	well	-	shallow	-	Spanel	Ennis	TX
R287—50	well	-	shallow	-	-	-	-
R287—51	well	-	-	windmill	-	-	-
R287—52	well	-	shallow	cover bolted down	-	-	-
R287—53	well	-	-	-	-	-	-
R287—54	well	-	shallow	pumphouse near RR	-	-	-
R287—55	well	-	shallow	in pasture near two trees	-	-	-
R287W—1	well	-	shallow	in poorly kept shed	-	-	-
R287W—2	well	-	shallow	dry, trash in bottom	-	-	-
R287W—3	well	-	shallow	-	-	Waxahachie	TX
R287W—4	well	-	shallow	-	-	-	-
R287W—5	well	-	shallow	under windmill	Joseph?	Midlothian	TX
R287W—6	well	-	shallow	-	-	-	-
R287W—7	well	-	-	-	-	-	-
R287W—8	well	-	-	under windmill	-	-	-
R287W—9	well	-	-	under windmill	-	-	-
R287W—10	well	JK-33-33-504‡	-	under windmill	-	-	-
R287W—11	well	-	deep	under windmill	-	-	-
R287W—12	well	-	shallow	-	-	-	-
R287W—13	cistern	-	shallow	cistern behind house	Duvall	-	-
R287W—14	well	-	deep	behind house, not working	Duvall	-	-
R287W—15	well	-	shallow	in field	Griffith	Midlothian	TX
R287W—16	well	-	deep	rural water supply well	-	-	-
R287W—18	well	-	shallow	-	Tucker	-	-
R287W—19	well	-	shallow	-	Tucker	-	-
R287W—20	well	-	deep?	in back lot	-	-	-
R287W—21	well	-	shallow	behind house	-	-	-
R287W—22	well	-	shallow	near barn	-	-	-
R287W—23	well	-	shallow	N side of house	-	-	-
R287W—24	well	-	shallow	-	-	-	-
R287W—25	well	-	-	windmill	-	-	-
R287W—26	well	-	-	-	-	-	-
R287W—27	well	-	shallow	in shed N of house	-	-	-
R287W—28	well	-	shallow	pumphouse	-	-	-
R308—1	well	-	shallow	-	-	-	-
R308—2	well	-	shallow	-	-	-	-
R308—3	well	-	shallow	-	-	-	-
R528—1	well	-	shallow	-	-	-	-
R528—2	well	-	shallow	-	-	-	-
R528—3	well	-	shallow	-	-	-	-
R528—4	well	-	shallow	-	-	-	-
R528—5	well	-	shallow	-	-	-	-

Appendix B. Table 1. Off-ring well inventory located on 7.5-minute topographic maps. See explanation of column headings and symbols at end of table.

Well ID	Topographic quadrangle	NAD 83 northing (ft)	NAD 83 easting (ft)	Ground surface elev. (ft)	Well depth (ft)	Water level elev. (ft)	Date meas. M/D/Y	Form-ation	Diameter surface casing (ft)	Casing material	Well use	Wellhead condition
R528—6	Waxahachie	6829960	2482157	580	-	-	-	Kau	-	-	-	-
R528—7	Waxahachie	6831468	2479056	605	-	-	-	Kau	-	-	-	-
R528—8	Waxahachie	6833419	2474944	610	-	-	-	Kau	-	-	-	-
R663—1	Midlothian	6850086	2431795	770	11.4	768.5	10/23/91	Kau	2.2	brick	yard	-
R663—2	Midlothian	6857508	2433348	777	-	-	-	-	-	steel	municipal	-
R663—3	Midlothian	6853749	2438496	700	-	-	-	Kau	-	-	-	-
R663—4	Midlothian	6841370	2432114	809	-	-	-	Kau	-	-	-	-
R664—2	Waxahachie	6842516	2470197	663	-	-	-	Kau	-	-	-	-
R664—3	Waxahachie	6842276	2470192	663	-	-	-	Kau	-	-	-	-
R664—4	Waxahachie	6841357	2470184	665	-	-	-	Kau	-	-	aban'd	-
R664—5	Waxahachie	6838525	2469980	622	-	-	-	-	-	steel?	-	-
R664—6	Waxahachie	6847609	2470096	682	-	-	-	Kau	-	-	-	-
R664—7	Midlothian	6858444	2469014	680	-	-	-	Kau	-	-	-	-
R664—8	Waxahachie	6859319	2470129	670	-	-	-	Kau	-	-	-	-
R664—9	Waxahachie	6859720	2469778	670	-	-	-	Kau	-	-	-	-
R664—10	Waxahachie	6845771	2475642	660	27	656.4	8/29/91	Kau	2	-	-	-
R664—11	Waxahachie	6848048	2475619	658	-	-	-	Kau	-	-	-	-
R664—12	Midlothian	6855212	2468681	697	-	-	-	Kau	-	-	-	-
R664—13	Cedar Hill	6872012	2464369	707	20.9	693.9	10/16/91	Kau	1.5	brick	unused	-
R664—14	Cedar Hill	6872433	2464387	690	15.7	686.7	10/16/91	Kau	3	cement	unused	overgrown
R664—15	Lancaster	6875788	2507309	554	47	534.8	10/17/91	Kau	2.9	brick	unused	brick crumbling
R664—16	Midlothian	6851985	2464078	682	24.1	676	10/23/91	Kau	3	brick	unused	-
R664—17	Waxahachie	6839197	2470173	635	28.1	621.9	4/1/92	Kau	2.1	brick	unused	-
R664—18	Waxahachie	6839781	2472737	605	-	-	-	Kau	-	-	-	-
R664—19	Waxahachie	6843275	2472165	649	-	-	-	Kau	-	-	-	-
R664—20	Waxahachie	6840262	2472782	610	-	-	-	Kau	-	-	lawn?	-
R664—21	Midlothian	6868510	2463067	741	-	-	-	Kau	-	-	-	-
R664—22	Cedar Hill	6869369	2461673	720	-	-	-	Kau	-	-	-	-
R664—23	Cedar Hill	6869717	2460728	738	-	-	-	Kau	-	-	-	-
R664—24	Cedar Hill	6874745	2464313	673	-	-	-	Kau	-	-	-	-
R664—25	Waxahachie	6839430	2472406	620	-	-	-	Kau	-	-	-	-
R664—26	Waxahachie	6858782	2470235	668	-	-	-	Kau	-	cement	-	-
R664—27	Waxahachie	6836543	2470319	580	-	-	-	Kau	-	cement	-	-
R813—1	Waxahachie	6841693	2487498	600	-	-	-	Kau	-	-	-	-
R813—2	Waxahachie	6848087	2489616	570	-	-	-	Kau	-	-	aban'd?	-
R813—3	Waxahachie	6853825	2498659	530	-	-	-	Ko	-	-	-	-
R813—4	Waxahachie	6857422	2502078	495	-	-	-	Ko	-	-	-	-
R813—5	Waxahachie	6849676	2501971	551	-	-	-	Ko	-	-	-	-
R813—6	Waxahachie	6848096	2487447	570	-	-	-	Kau	-	-	-	-
R813—7	Waxahachie	6846998	2488738	560	-	-	-	Kau	-	-	-	-
R813—8	Waxahachie	6846997	2488728	560	8.1	557.4	10/23/91	Kau	2.5	-	-	-
R813—9	Waxahachie	6849264	2497160	580	-	-	-	Kau	-	-	lawn	housed
R813—10	Waxahachie	6845619	2497237	560	19.3	550.3	10/23/91	Ko	4	brick	unused	-
R813—11	Waxahachie	6845445	2497090	560	21.2	554.8	3/31/92	Ko	2.5	brick	unused	housed, wood cover
R813—12	Waxahachie	6845527	2500563	545	-	-	-	Ko	-	-	-	uncovered
R813—13	Waxahachie	6850447	2507978	530	12.2	521.2?	9/25/91	Kau	3	brick	-	-
R813—14	Waxahachie	6861147	2502321	514	-	-	-	Kau	-	-	-	-
R813—15	Waxahachie	6856315	2502091	511	18.2	504.7	10/9/91	Kau/Ko	3	cement	-	-
R813—16	Palmer	6842539	2539023	445	34.5	420.5	10/17/91	Ko	2	brick	unused	-

Appendix B. Table 1. (continued)

Well ID	Utility	Other ID	Relative depth	Notes	Owner	City	State
R528—6	well	-	shallow	-	-	-	-
R528—7	well	-	shallow	-	-	-	-
R528—8	well	-	shallow	-	-	-	-
R663—1	well	-	shallow	artesian flow to creek	Kemp	Midlothian	TX
R663—2	well	-	deep	Midlothian water tower	City of Midlothian	Midlothian	TX
R663—3	well	-	shallow	in creek	-	-	-
R663—4	well	-	shallow	-	-	-	-
R664—2	well	-	deep	-	-	-	-
R664—3	well	-	shallow	-	-	-	-
R664—4	well	-	shallow	-	-	-	-
R664—5	well	-	deep	windmill	-	-	-
R664—6	well	-	shallow	in house	-	-	-
R664—7	well	-	shallow	near creek	-	-	-
R664—8	well	-	shallow	near creek	-	-	-
R664—9	well	-	shallow	-	-	-	-
R664—10	well	-	shallow	-	-	-	-
R664—11	well	-	shallow	by ballfield	-	-	-
R664—12	well	-	-	-	-	-	-
R664—13	well	-	shallow	-	Mckinny	Ovilla	TX
R664—14	well	-	shallow	-	Mckinny	Ovilla	TX
R664—15	well	-	shallow	reported pesticide contamination	Horne	Red Oak	TX
R664—16	well	-	shallow	-	Black Champ Ranch	Waxahachie	TX
R664—17	well	-	shallow	in trees	-	-	-
R664—18	well	-	shallow	near stream	-	-	-
R664—19	well	-	shallow	in trees near frontage rd.	-	-	-
R664—20	well	-	shallow	on frontage road/creek	-	-	-
R664—21	well	-	-	-	-	-	-
R664—22	well	-	-	-	-	-	-
R664—23	well	-	-	-	-	-	-
R664—24	well	-	-	-	-	-	-
R664—25	well	-	shallow	-	-	-	-
R664—26	well	-	shallow	pump near creek	-	-	-
R664—27	well	-	shallow	-	-	-	-
R813—1	well	-	shallow	-	-	-	-
R813—2	well	-	shallow	-	-	-	-
R813—3	well	-	shallow	-	-	-	-
R813—4	well	-	shallow	-	-	-	-
R813—5	well	-	shallow	-	Hopkins	-	-
R813—6	well?	-	-	-	-	-	-
R813—7	well	-	-	-	-	-	-
R813—8	well	-	-	-	-	-	-
R813—9	well	-	-	-	-	-	-
R813—10	well	-	-	windmill ruins	Maxwell	Waxahachie	TX
R813—11	well	-	shallow	-	-	-	-
R813—12	well	-	shallow	-	-	-	-
R813—13	well	-	shallow	-	Fuller	-	-
R813—14	well	-	shallow	-	-	-	-
R813—15	well	-	shallow	-	Clopton	-	-
R813—16	well	-	shallow	-	Wilson	Palmer	TX

Appendix B. Table 1. Off-ring well inventory located on 7.5-minute topographic maps. See explanation of column headings and symbols at end of table.

Well ID	Topographic quadrangle	NAD 83 northing (ft)	NAD 83 easting (ft)	Ground surface elev. (ft)	Well depth (ft)	Water level elev. (ft)	Date meas. M/D/Y	Formation	Diameter surface casing (ft)	Casing material	Well use	Wellhead condition
R813—17	Waxahachie	6854353	2491764	587	-	-	-	Kau	-	-	unused	large concrete cover
R813—18	Waxahachie	6855879	2493939	570	23.5	565.1	2/11/92	Kau	2.5	brick	unused	flush with surface
R813—19	Palmer	6842802	2539689	445	-	-	-	Ko	-	-	-	-
R813—20	Waxahachie	6860354	2499099	511	-	-	-	Kau	-	-	-	-
R813—21	Waxahachie	6857639	2502390	486	-	-	-	Qt/Kau	-	-	-	filled
R813—22	Waxahachie	6846024	2489844	555	-	-	-	Kau	-	-	-	-
R813—23	Palmer	6845187	2528424	465	1394	402	17/21/85	-	0.4	steel	municipal	-
R813—24	Palmer	6844412	2533482	462	1472	325	5/18/09	Kwb	0.7	steel	unused	collapsed, 1965
R813—25	Waxahachie	6861872	2496018	521	-	-	-	Qt/Kau	-	brick	-	-
R813—26	Waxahachie	6844377	2489218	554	-	-	-	Kau	-	-	-	-
R813—27	Waxahachie	6849453	2497764	582	17.4	578	11/19/91	Kau	3	brick	-	-
R813—28	Waxahachie	6831268	2480462	601	-	-	-	Kau	-	-	-	-
R875—1	Midlothian	6835436	2450987	745	19.8	735.6	7/25/91	Kau	3	brick	unused	cement cover
R875—2	Midlothian	6835685	2450963	742	15.4	733.2	7/25/91	Kau	2.7	brick	unused	uncovered
R875—3	Midlothian	6835836	2452491	716	-	-	-	-	-	steel	unused	housed
R875—4	Midlothian	6836198	2456915	675	20.4	660.8	7/25/91	Kau	4.5	cement	unused	cement cover
R875—5	Midlothian	6836486	2456861	675	-	-	-	Kau	-	-	aban'd	covered
R875—6	Midlothian	6836279	2457034	681	-	-	-	Kau	-	-	unused	pump on wellhead
R875—7	Midlothian	6836386	2456822	668	9.1	662.9	7/25/91	Kau	2.5	cement	domestic	housed
R875—8	Midlothian	6836892	2457415	666	0	-	-	Kau	-	filled	-	filled
R875—9	Midlothian	6837580	2460925	638	19.8	632.7	9/17/91	Kau	3	brick	-	-
R875—10	Midlothian	6838118	2465866	570	28.7	555	10/10/91	Kau	3	cement	-	housed
R875—11	Midlothian	6833960	2441079	760	deep	-	-	Kau	-	-	-	-
R875—12	Midlothian	6833714	2439913	775	deep	-	-	Kau	-	-	-	-
R875—13	Midlothian	6836371	2456513	680	shallow	-	-	Kau	-	-	-	-
R875—14	Midlothian	6837185	2457886	650	-	-	-	Kau	-	-	-	-
R875—15	Midlothian	6838441	2458055	631	-	-	-	Kau	-	brick	-	-
R875—16	Midlothian	6836682	2434653	823	20.8	814.3	12/19/92	Kau	4	brick	aban'd	broken wellhead, trash
R876—1	Boz	6790951	2464373	607	-	-	-	-	-	steel	-	-
R876—2	Boz	6791190	2464350	607	-	-	-	Kau	-	brick	-	-
R876—3	Boz	6786116	2468174	583	-	-	-	Kau	-	brick	-	-
R876—4	Boz	6788036	2462703	603	33.8	595.1	7/25/91	Kau	2.4	brick	unused	covered
R876—5	Boz	6788149	2462902	605	-	-	-	-	-	steel	unused	housed
R876—6	Boz	6790073	2463581	602	17.2	597.5	7/25/91	Kau	2.3	brick	unused	wood cover
R876—7	Boz	6789815	2463715	601	-	-	-	-	-	steel	unused	pump on wellhead
R876—8	Forreston	6822319	2474779	606	-	-	-	Kau	-	-	-	-
R876—9	Boz	6801063	2467681	625	10	624	9/18/91	Kau	3	brick	unused	-
R876—10	Boz	6794314	2458562	590	-	-	-	Kau	-	cement	-	-
R876—11	Boz	6783370	2469407	582	-	-	-	Kau	-	-	-	-
R877—1	Forreston	6803507	2494762	560	-	-	-	Kau	-	brick	-	covered
R877—2	Forreston	6808734	2491952	562	94.7	546.9	7/25/91	Kau	0.4	steel	unused	uncovered
R877—3	Forreston	6808378	2489051	591	-	-	-	Kau	-	brick	unused	-
R877—4	Forreston	6808070	2488636	591	-	-	-	Kau	-	-	unused	metal lid
R877—5	Forreston	6807402	2484609	565	-	-	-	Kau	0.5	steel	unused	-
R877—6	Forreston	6797730	2487918	588	-	-	-	Kau	-	-	unused	housed
R877—7	Forreston	6795873	2485347	592	-	-	-	Kau	-	brick	-	-
R877—8	Forreston	6801140	2497817	540	12.9	dry	10/9/91	Ko	-	-	unused	junk in bottom, dry
R877—9	Forreston	6793129	2502808	540	-	-	-	Ko	-	-	-	-
R877—10	Forreston	6795687	2500882	522	13.2	509.5	2/19/92	Ko	-	-	-	-

Appendix B. Table 1. (continued)

Well ID	Utility	Other ID	Relative depth	Notes	Owner	City	State
R813—17	well	-	-	-	-	-	-
R813—18	well	-	-	-	-	-	-
R813—19	well	-	-	-	-	-	-
R813—20	well	-	shallow	-	-	-	-
R813—21	well	-	shallow	-	-	-	-
R813—22	well	-	shallow	-	-	-	-
R813—23	well	JK-33-35-504	deep	Well #2	City of Palmer	Palmer	TX
R813—24	well	JK-33-35-501	deep	-	City of Palmer	Palmer	TX
R813—25	well	-	shallow	-	-	-	-
R813—26	well?	-	shallow	old windmill	-	-	-
R813—27	well	-	shallow	30 feet off road in field	-	-	-
R813—28	well	-	shallow	-	Criddle	Waxahachie	TX
R875—1	well	-	shallow	-	-	-	-
R875—2	well	-	shallow	-	-	-	-
R875—3	well	-	deep	-	-	-	-
R875—4	well	-	shallow	-	-	-	-
R875—5	well	JK-33-33-802‡	-	-	-	-	-
R875—6	well	-	deep	pump in well	-	-	-
R875—7	well	-	shallow	-	-	-	-
R875—8	well	-	shallow	-	-	-	-
R875—9	well	-	shallow	near windmill	Cox	-	-
R875—10	well	-	shallow	-	-	-	-
R875—11	well	-	deep	-	-	-	-
R875—12	well	-	deep	-	-	-	-
R875—13	well	-	shallow	-	-	-	-
R875—14	well	-	shallow	-	-	-	-
R875—15	well	-	-	-	-	-	-
R875—16	well	-	-	-	-	-	-
R876—1	well	-	deep	-	-	-	-
R876—2	well	-	shallow	-	-	-	-
R876—3	well	-	shallow	-	-	-	-
R876—4	well	-	-	-	Bradbury	Waxahachie	TX
R876—5	well	JK-33-41-801‡	deep	-	-	-	-
R876—6	well	-	-	-	-	-	-
R876—7	well	-	deep	-	-	-	-
R876—8	well	-	shallow	not located on map	-	-	-
R876—9	well	-	shallow	under old windmill	-	-	-
R876—10	well	-	shallow	behind pavillion, creek	-	-	-
R876—11	well	-	-	-	-	-	-
R877—1	well	-	shallow	-	-	-	-
R877—2	cistern	-	deep/94′	poor-quality water	-	-	-
R877—3	well	-	shallow	-	-	-	-
R877—4	well	-	shallow	-	-	-	-
R877—5	well	JK-33-42-401‡	deep	-	-	-	-
R877—6	well	-	shallow	-	-	-	-
R877—7	well	-	shallow	-	-	-	-
R877—8	well	-	shallow	dry, junk in bottom	Cline	-	-
R877—9	well	-	shallow	dry	-	-	-
R877—10	well	-	shallow	-	-	-	-

Appendix B. Table 1. Off-ring well inventory located on 7.5-minute topographic maps. See explanation of column headings and symbols at end of table.

Well ID	Topographic quadrangle	NAD 83 northing (ft)	NAD 83 easting (ft)	Ground surface elev. (ft)	Well depth (ft)	Water level elev. (ft)	Date meas. M/D/Y	Form-ation	Diameter surface casing (ft)	Casing material	Well use	Wellhead condition
R877—11	Forreston	6797897	2499505	522	-	-	-	Ko	-	-	unused	tree growing out of well
R877—12	Forreston	6787367	2503864	489	-	-	-	Ko	-	-	-	-
R877—13	Forreston	6787002	2504092	492	29.3	487.3	8/28/91	Ko	2.5	-	aban'd	-
R877—14	Forreston	6812815	2489214	541	47.5	525.9	10/10/91	Kau	3	cement	-	-
R877—15	Forreston	6817294	2485396	545	23.6	538.6	11/14/91	Qt	2.5	brick	-	-
R877—16	Forreston	6820956	2480130	562	33.3	540.5	10/23/91	Kau	3	cement	unused	housed
R877—17	Waxahachie	6823882	2479729	545	47.5	528.9	9/18/91	Kau	-	brick	unused	-
R877—18	Forreston	6812489	2491447	488	-	-	-	Qal/Kau	-	brick	-	-
R877—19	Cryer Creek	6762972	2515598	465	5	-	-	Qt/Kwc	-	cement	aban'd	filled
R877—20	Cryer Creek	6762401	2517892	465	17.1	451.6	10/10/91	Kwc	3	-	-	-
R877—21	Forreston	6801304	2497459	540	17.7	528.3	10/10/91	Ko	4	-	-	-
R877—22	Cryer Creek	6762657	2517607	465	-	-	-	Kwc	-	-	-	-
R877—23	Cryer Creek	6759482	2510155	482	-	-	-	Qt	-	-	-	-
R877—24	Cryer Creek	6759626	2510725	481	-	-	-	Qt	-	-	-	-
R877—25	Cryer Creek	6759658	2510935	481	-	-	-	Qt	-	-	-	-
R877—26	Forreston	6814856	2480667	576	-	-	-	Qt	-	-	-	-
R877—27	Forreston	6812228	2481715	545	-	-	-	Qt	-	cement	-	-
R877—28	Forreston	6812467	2481133	550	-	-	-	Qt	-	cement	-	-
R877—29	Forreston	6812779	2481904	550	-	-	-	Qt	-	cement	-	-
R877—30	Forreston	6821404	2479860	569	-	-	-	Kau	-	-	-	-
R877—31	Forreston	6820394	2479762	560	-	-	-	Kau	-	brick	-	-
R877—32	Forreston	6819707	2481066	540	-	-	-	Kau	-	-	-	-
R877—33	Forreston	6820428	2480087	551	-	-	-	Kau	-	cement	-	-
R877—34	Forreston	6797491	2489645	521	-	-	-	Qal/Kau	-	-	-	-
R877—35	Forreston	6796801	2489702	519	-	-	-	Qal/Kau	-	-	-	-
R877—36	Forreston	6780391	2507675	485	-	-	-	Ko	-	brick	-	pump in well
R877—37	Ennis West	6783577	2510122	479	-	-	-	Ko	-	-	-	-
R877—38	Forreston	6797839	2499389	520	<30	514.4	6/10/92	Kau	0.3	pvc	unused	cinder block cover
R878—1	Waxahachie	6836862	2504705	520	-	-	-	Ko	-	brick	aban'd	filled with bricks
R878—2	Waxahachie	6831180	2490791	575	34.4	574.3	9/16/91	Kau	3	brick	unused	wood cover
R878—3	Waxahachie	6830106	2491409	563	-	-	-	Ko	-	brick	unused	housed
R878—4	Waxahachie	6831586	2494025	564	-	-	-	Ko	-	-	-	housed
R878—5	Waxahachie	6833399	2497627	552	-	-	-	Ko	-	brick	unused	-
R878—6	Waxahachie	6833081	2499402	535	0	-	-	Ko	-	-	aban'd	filled
R878—7	Waxahachie	6833519	2501872	501	12.7	491.4	6/13/91	Kau	2.5	brick	unused	wood cover
R878—8	Waxahachie	6833519	2501872	501	16.4	492.3	6/13/91	Kau	2.2	brick	unused	wood cover
R878—9	Waxahachie	6833797	2502227	495	8.6	490.4	6/13/91	Qt	1.3	cement	unused	rubber mat cover
R878—10	Waxahachie	6834008	2502282	500	20.9	494.5	6/13/91	Qt/Kau	2	brick	garden	thick wood cover
R878—11	Waxahachie	6833300	2501515	510	-	-	-	Kau	-	-	-	-
R878—12	Waxahachie	6836997	2502362	525	16.6	516.6	6/13/91	Ko	2.1	brick	domestic	plywood cover
R878—13	Waxahachie	6837512	2502169	526	-	-	-	Ko	-	brick	-	-
R878—14	Waxahachie	6840738	2502122	538	13.9	532.5	6/13/91	Ko	3.7	brick	domestic	wooden cover
R878—15	Waxahachie	6846538	2502758	552	32.7	537.6	6/13/91	Ko	3	brick	domestic	chicken wire cover
R878—16	Palmer	6840471	2518783	460	-	-	-	Ko	-	brick	-	tipping crown
R878—17	Palmer	6838409	2516313	495	0	-	-	Ko	-	-	aban'd	filled
R878—18	Waxahachie	6828974	2485742	578	17.6	574.1	9/16/91	Kau	3	-	-	-
R878—19	Waxahachie	6839984	2495121	547	-	-	-	Ko	-	-	-	-
R878—20	Waxahachie	6840127	2499094	548	-	-	-	Ko	-	-	used	-
R878—21	Waxahachie	6837557	2493431	556	-	-	-	Kau	-	-	-	-

Appendix B. Table 1. (continued)

Well ID	Utility	Other ID	Relative depth	Notes	Owner	City	State
R877—11	well	-	shallow	-	-	-	-
R877—12	well	-	shallow	-	-	-	-
R877—13	well	-	shallow	-	-	-	-
R877—14	well	-	shallow	-	-	-	-
R877—15	well	-	shallow	near brick pumphouse	-	-	-
R877—16	well	-	shallow	-	Peel	-	-
R877—17	well	-	shallow	-	-	-	-
R877—18	well	-	shallow	-	Pigg	-	-
R877—19	well	-	shallow	-	-	-	-
R877—20	well	-	shallow	-	Gorman	-	-
R877—21	well	-	shallow	-	-	-	-
R877—22	well	-	shallow	-	-	-	-
R877—23	well	-	shallow	in pasture	-	-	-
R877—24	well	-	shallow	-	-	-	-
R877—25	well	-	shallow	-	-	-	-
R877—26	well	-	shallow	-	-	-	-
R877—27	well	-	shallow	-	-	-	-
R877—28	well	-	shallow	-	-	-	-
R877—29	well	-	shallow	-	-	-	-
R877—30	well	-	shallow	-	-	-	-
R877—31	well	-	shallow	-	-	-	-
R877—32	well	-	shallow	-	-	-	-
R877—33	well	-	shallow	-	-	-	-
R877—34	well	-	shallow	-	-	-	-
R877—35	well	-	shallow	-	-	-	-
R877—36	well	-	shallow	pump, east of house	-	-	-
R877—37	well	-	shallow	homestead site	-	-	-
R877—38	well	-	shallow	drilled, north of barn	-	-	-
R878—1	well	-	shallow	-	-	-	-
R878—2	well	-	shallow	windmill	Williams	Waxahachie	TX
R878—3	well	-	shallow	-	-	-	-
R878—4	well?	-	-	-	-	-	-
R878—5	well	-	shallow	-	-	-	-
R878—6	well	-	shallow	-	-	-	-
R878—7	well	-	shallow	-	Wesson Ranch	-	-
R878—8	well	-	shallow	-	-	-	-
R878—9	well	-	-	-	-	-	-
R878—10	well	-	shallow	-	-	-	-
R878—11	well	-	-	-	-	-	-
R878—12	well	-	shallow	-	Mays	-	-
R878—13	well	-	shallow	-	-	-	-
R878—14	well	-	shallow	-	Brundige	-	-
R878—15	well	-	shallow	-	-	-	-
R878—16	well	-	shallow	-	-	-	-
R878—17	well	-	shallow	-	-	-	-
R878—18	well	-	shallow	-	Morrison	-	-
R878—19	well	-	shallow	-	-	-	-
R878—20	well	-	shallow	-	-	-	-
R878—21	well	-	shallow	-	-	-	-

Appendix B. Table 1. Off-ring well inventory located on 7.5-minute topographic maps. See explanation of column headings and symbols at end of table.

Well ID	Topographic quadrangle	NAD 83 northing (ft)	NAD 83 easting (ft)	Ground surface elev. (ft)	Well depth (ft)	Water level elev. (ft)	Date meas. M/D/Y	Form-ation	Diameter surface casing (ft)	Casing material	Well use	Wellhead condition
R878—22	Waxahachie	6836932	2500455	525	16	516.6	9/16/91	Ko	2.5	cement	-	-
R878—23	Waxahachie	6836521	2500375	524	27.5	513.6	9/16/91	Ko	3	brick	-	-
R878—24	Waxahachie	6830739	2491996	571	26	554.7?	9/16/91	Ko	3	brick	-	housed
R878—25	Palmer	6841405	2518850	483	-	-	-	-	-	-	-	-
R878—26	Waxahachie	6833262	2502641	490	-	-	-	Kau	-	-	-	hand pump on wellhead
R878—27	Waxahachie	6829600	2489881	565	-	-	-	Kau	-	-	-	-
R878—28	Waxahachie	6827629	2484108	586	-	-	-	Kau	-	-	-	pump on wellhead
R878—29	Waxahachie	6839769	2505038	500	-	-	-	Ko	-	brick	-	-
R878—30	Waxahachie	6837235	2507441	511	-	-	-	Qt/Ko	-	cement	-	-
R879—1	Waxahachie	6828460	2494079	543	-	-	-	Ko	-	brick	unused	-
R879—2	Waxahachie	6827020	2491482	530	-	-	-	Ko	-	brick	unused	-
R879—3	Waxahachie	6828351	2503481	536	25?	-	-	Ko	-	brick	unused	wood cover
R879—4	Waxahachie	6828349	2508512	532	1304	280	0/0/58	Kwb	0.3	steel	unused	housed
R879—5	Palmer	6827969	2509017	535	-	-	-	-	-	steel	municipal	steel cover
R879—6	Waxahachie	6826546	2504056	531	-	-	-	Ko	-	-	unused	-
R879—7	Palmer	6825037	2511447	522	1303	203.3	7/30/65	-	-	steel	gin	-
R879—8	Ennis West	6821316	2513363	500	-	-	-	Ko	-	brick	-	-
R879—9	Waxahachie	6824791	2491836	546	-	-	-	Kau	-	-	-	-
R879—10	Waxahachie	6825246	2491984	542	-	-	-	Kau	-	-	-	-
R879—11	Palmer	6824587	2519238	505	17.5	504.5	2/19/92	Ko	2	-	-	-
R879—12	Palmer	6824513	2519019	505	-	-	-	Ko	-	-	-	-
R879—13	Palmer	6828902	2544096	485	14.9	475.2	10/17/91	Kwc	3.2	brick	unused	-
R879—14	Palmer	6829707	2544400	492	15.8	482.2	10/17/91	Kwc	3.5	cement	unused	-
R879—15	Ennis West	6821581	2537353	549	-	-	-	Kwc	-	-	-	-
R879—16	Palmer	6824720	2535904	527	-	-	-	Ko	-	cement	-	-
R879—17	Palmer	6824109	2514918	520	-	-	-	Ko	-	-	-	-
R879—18	Palmer	6828100	2512320	517	1321	142	12/26/73	-	-	-	-	-
R879—19	Palmer	6833252	2511331	488	-	-	-	Ko	-	-	-	-
R879—20	Waxahachie	6833864	2507555	502	-	-	-	Qt	-	-	used	-
R879—21	Palmer	6830004	2544423	485	-	-	-	Kwc	-	brick	-	-
R879—22	Palmer	6830242	2544369	497	-	-	-	Kwc	-	-	-	cement cover
R984—1	Ennis West	6789707	2513076	511	-	-	-	-	-	steel?	municipal	covered?
R984—2	Forreston	6794344	2505230	522	-	-	-	Ko	-	-	-	-
R984—3	Ennis West	6789766	2520932	478	14.4	469.7	5/17/91	Ko	2.7	brick	-	-
R984—4	Ennis West	6789516	2520478	478	-	-	-	Ko	-	-	-	covered
R984—5	Ennis West	6789727	2513486	515	-	-	-	Ko	-	-	-	-
R984—6	Ennis West	6779253	2531359	467	-	-	-	Kwc	-	-	-	-
R984—7	Cryer Creek	6762221	2522365	470	-	-	-	Kwc	-	cement	-	-
R984—8	Cryer Creek	6761851	2522361	475	-	-	-	Kwc	-	-	-	-
R984—9	Cryer Creek	6762468	2522811	471	-	-	-	Kwc	-	-	-	-
R984—10	Cryer Creek	6766411	2526455	461	-	-	-	Qt	-	-	-	-
R984—11	Cryer Creek	6774437	2523779	455	12.5	446.6	9/19/91	Ko	4.5	brick	unused	-
R984—12	Cryer Creek	6774505	2522998	461	-	-	-	Ko	-	-	-	-
R984—13	Cryer Creek	6779270	2531365	461	-	-	-	Ko	-	-	-	-
R984—14	Ennis West	6788662	2520019	486	17.1	478.6	5/17/91	Ko	3.9	brick	unused	-
R984—15	Ennis West	6787905	2520674	487	16.5	478.8	5/17/91	Ko	3.6	brick	unused	-
R984—16	Cryer Creek	6775315	2525048	460	-	-	-	Ko	-	-	-	-
R984—17	Ennis West	6790129	2513219	508	-	-	-	Ko	-	-	-	housed
R984—18	Cryer Creek	6763504	2524570	464	-	-	-	Qt	-	cement	-	broken cement collar

Appendix B. Table 1. (continued)

Well ID	Utility	Other ID	Relative depth	Notes	Owner	City	State
R878—22	well	-	shallow	-	Schmidt	Waxahachie	TX
R878—23	well	-	shallow	-	-	-	-
R878—24	well	-	shallow	-	Williams	-	-
R878—25	well	-	shallow	-	-	-	-
R878—26	well	-	shallow	-	-	-	-
R878—27	well	-	shallow	-	-	-	-
R878—28	well	-	shallow	-	-	-	-
R878—29	well	-	-	-	-	-	-
R878—30	well	-	-	-	-	-	-
R879—1	well	-	shallow	-	-	-	-
R879—2	well	-	shallow	-	-	-	-
R879—3	cistern	-	shallow	may be filled in	-	-	-
R879—4	well	JK-33-34-901	deep	-	Muirhead	Waxahachie	TX
R879—5	well	JK-33-35-702	deep	Plant 1	Boyce Water Supply	-	-
R879—6	well	-	deep?	under windmill	-	-	-
R879—7	well	JK-33-35-701‡	deep	near gin	-	-	-
R879—8	well	-	shallow	-	-	-	-
R879—9	well	-	shallow	-	-	-	-
R879—10	well	-	shallow	-	-	-	-
R879—11	well	-	shallow	in empty lot	-	-	-
R879—12	well	-	shallow	in empty lot	-	-	-
R879—13	cistern	-	shallow	-	Aycock	Ennis	TX
R879—14	well	-	shallow	conduit pipe	Landsfeld	Ennis	TX
R879—15	well	-	-	windmill	-	-	-
R879—16	well	-	shallow	-	-	-	-
R879—17	well	-	-	windmill	-	-	-
R879—18	well	JK-33-35-702‡	shallow	-	-	-	-
R879—19	well	-	shallow	-	-	-	-
R879—20	well	-	shallow	-	-	-	-
R879—21	well	-	shallow	-	-	-	-
R879—22	well	-	shallow	-	-	-	-
R984—1	well	JK-33-43-702	deep	-	Rural Bardwell Water Supply	-	-
R984—2	well	-	shallow	-	-	-	-
R984—3	well	-	shallow	-	-	-	-
R984—4	well	-	shallow	-	-	-	-
R984—5	cistern	-	shallow	-	-	-	-
R984—6	well	-	-	-	-	-	-
R984—7	well	-	shallow	-	-	-	-
R984—8	well	-	shallow	-	-	-	-
R984—9	well	-	shallow	-	-	-	-
R984—10	well	-	shallow	-	-	-	-
R984—11	well	-	shallow	-	Jackson	-	-
R984—12	well	-	shallow	-	-	-	-
R984—13	well	-	-	windmill	-	-	-
R984—14	well	-	shallow	-	Placek?	-	-
R984—15	well	-	shallow	-	Betik	-	-
R984—16	well	-	shallow	-	-	-	-
R984—17	well	-	-	-	-	-	-
R984—18	well	-	shallow	-	-	-	-

Appendix B. Table 1. Off-ring well inventory located on 7.5-minute topographic maps. See explanation of column headings and symbols at end of table.

Well ID	Topographic quadrangle	NAD 83 northing (ft)	NAD 83 easting (ft)	Ground surface elev. (ft)	Well depth (ft)	Water level elev. (ft)	Date meas. M/D/Y	Form-ation	Diameter surface casing (ft)	Casing material	Well use	Wellhead condition
R984—19	Cryer Creek	6762742	2523772	468	-	-	-	Kwc	-	-	-	-
R984—20	Cryer Creek	6760228	2519858	482	-	-	-	Kwc	-	-	-	-
R985—1	Ennis West	6780296	2533783	461	-	-	-	Kwc	-	-	-	-
R985—2	Cryer Creek	6775202	2537916	425	21.8	422.7	9/19/91	Kwc	3.5	brick	unused	-
R985—3	Ennis West	6782479	2533516	466	-	-	-	Kwc	-	-	-	-
R1367—1	Midlothian	6863852	2436751	725	-	-	-	Kau	-	-	-	-
R1367—2	Midlothian	6867071	2438366	770	17.4	760.2	10/16/91	Kau	2	brick	unused	-
R1367—3	Midlothian	6867241	2438335	770	8	763	10/16/91	Kau	1.8	brick	unused	-
R1367—4	Midlothian	6863114	2447840	750	-	-	-	Kau	-	cement	-	tightly covered
R1367—5	Midlothian	6864000	2446466	762	-	-	-	Kau	-	-	-	-
R1367—6	Cedar Hill	6872203	2448403	772	-	-	-	Kau	-	-	-	-
R1367—7	Cedar Hill	6873547	2450306	772	-	-	-	Kau	-	-	-	-
R1367—8	Midlothian	6864419	2436768	717	-	-	-	Kau	-	-	-	-
R1367—9	Midlothian	6864331	2436910	713	-	-	-	Kau	-	-	-	-
R1367—10	Midlothian	6862476	2436292	715	-	-	-	Kau	-	-	-	-
R1367—11	Midlothian	6864344	2438753	740	-	-	-	Kau	-	-	-	-
R1367—12	Midlothian	6863208	2456491	732	-	-	-	Kau	-	-	-	-
R1367—13	Cedar Hill	6871964	2449013	744	-	-	-	Kau	-	-	-	-
R1446—1	Boz	6818282	2435445	740	-	-	-	Kau	-	brick	unused	-
R1446—2	Midlothian	6827791	2456966	675	-	-	-	Kau	-	brick	aban'd	fenced
R1446—3	Midlothian	6825988	2455542	663	-	-	-	-	-	steel?	unused	housed
R1446—4	Midlothian	6828039	2453383	680	-	-	-	Kau	-	brick?	unused	housed
R1446—5	Midlothian	6830647	2451865	719	-	-	-	-	-	steel	unused	housed
R1446—6	Midlothian	6830549	2451947	719	820	299	6/21/69	Kau	-	brick	lawn	covered
R1446—7	Midlothian	6830545	2451697	714	-	-	-	Kau	-	brick	aban'd	covered, no access
R1446—8	Midlothian	6823903	2463721	669	21.2	664	11/14/91	Kau	2.3	brick	-	-
R1446—9	Boz	6822986	2462147	650	17.9	649.4	11/14/91	Kau	1.8	brick	-	-
R1446—10	Boz	6823063	2460310	645	-	-	-	Kau	-	-	-	housed behind house
R1446—11	Boz	6813565	2438178	700	-	-	-	Kau	-	-	aban'd	garbage
R1446—12	Boz	6813734	2437276	700	-	-	-	Kau	-	-	-	-
R1446—13	Boz	6816288	2435899	765	23.4	756.5	11/14/92	Kau	3.5	brick	-	-
R1446—14	Boz	6820212	2440691	750	-	-	-	Kau	-	-	-	-
R1446—15	Boz	6820485	2442564	790	-	-	-	Kau	-	-	-	-
R1446—16	Boz	6819769	2444048	770	-	-	-	Kau	-	-	-	-
R1446—17	Boz	6812476	2443329	740	-	-	-	Kau	-	-	-	-
R1446—18	Boz	6821501	2463561	631	13.6	625.8	10/24/91	Kau	1.8	brick	unused	metal cover
R1446—19	Boz	6821591	2463240	635	-	-	-	-	0.2	steel	-	-
R1446—20	Boz	6821890	2463099	642	-	-	-	Kau	-	brick	unused	pump and cover on wellhead
R1446—21	Boz	6822159	2462999	652	-	-	-	Kau	3	brick	unused	covered
R1446—22	Midlothian	6826320	2463131	700	-	-	-	Kau	-	-	unused	bolted shut, no access
R1446—23	Midlothian	6826497	2463217	700	-	-	-	Kau	-	-	-	-
R1446—25	Boz	6818419	2436483	762	13.6	757.3	11/14/91	Kau	4.5	-	-	-
R1446—26	Boz	6817901	2434907	738	-	-	-	Kau	-	-	-	-
R1446—27	Waxahachie	6825009	2470834	635	-	-	-	Kau	-	-	lawn?	-
R1446—28	Waxahachie	6825944	2471216	630	-	-	-	Kau	-	-	-	molded cover
R1446—29	Waxahachie	6826761	2470061	600	-	-	-	Kau	-	-	-	-
R1446—30	Waxahachie	6826946	2470551	610	-	-	-	-	-	steel?	-	-
R1446—31	Boz	6821718	2431759	695	-	-	-	Kau	-	-	-	-
R1446—32	Boz	6821458	2431538	710	-	-	-	Kau	-	-	-	-

Appendix B. Table 1. (continued)

Well ID	Utility	Other ID	Relative depth	Notes	Owner	City	State
R984—19	well	-	shallow	windmill	-	-	-
R984—20	well	-	-	windmill	-	-	-
R985—1	well	-	shallow	-	-	-	-
R985—2	well	-	shallow	-		-	-
R985—3	well	-	shallow	-	-	-	-
R1367—1	spring	-	shallow	Hawkin's Spring	-	-	-
R1367—2	well	-	shallow	-	Box Crow Cement	Midlothian	TX
R1367—3	well	-	shallow	-	Box Crow Cement	Midlothian	TX
R1367—4	well	-	shallow	-	-	-	-
R1367—5	well	-	shallow	-	-	-	-
R1367—6	well	-	shallow	-	-	-	-
R1367—7	well	-	shallow	-	-	-	-
R1367—8	well	-	shallow	near drainage	-	-	-
R1367—9	well	-	shallow	near drainage	-	-	-
R1367—10	well	-	shallow	east of house	-	-	-
R1367—11	well	-	shallow	in pasture E of house	-	-	-
R1367—12	well	-	-	-	-	-	-
R1367—13	well	-	-	-	-	-	-
R1446—1	well	-	shallow	-	-	-	-
R1446—2	well	-	shallow	-	-	-	-
R1446—3	well	-	deep	-	-	-	-
R1446—4	well	-	shallow	-	-	-	-
R1446—5	well	JK-33-33-803‡	deep	-	-	-	-
R1446—6	cistern	-	shallow	-	-	-	-
R1446—7	well	-	shallow	-	-	-	-
R1446—8	well	-	shallow	-	-	-	-
R1446—9	well	-	shallow	-	-	-	-
R1446—10	well	-	shallow	probably in shed?	-	-	-
R1446—11	well	-	shallow	-	-	-	-
R1446—12	well	-	shallow	-	-	-	-
R1446—13	well	-	shallow	-	-	-	-
R1446—14	well	-	shallow	-	-	-	-
R1446—15	well	-	shallow	-	-	-	-
R1446—16	well	-	shallow	-	-	-	-
R1446—17	well	-	shallow	-	-	-	-
R1446—18	well	-	shallow	-	Walker	-	-
R1446—19	well	-	deep	2-inch diameter, windmill	Walker	-	-
R1446—20	well	-	shallow	-	Walker	-	-
R1446—21	cistern	-	shallow	-	Walker	-	-
R1446—22	well	-	shallow	-	Ackerly	-	-
R1446—23	well	-	deep	N side of house	-	-	-
R1446—25	well	-	shallow	-	Dunn	-	-
R1446—26	well	-	shallow	-	-	-	-
R1446—27	well	-	shallow	W side of house	-	-	-
R1446—28	well	-	shallow	-	-	-	-
R1446—29	well	-	-	windmill in pasture near drainage	-	-	-
R1446—30	well	-	deep	near house	-	-	-
R1446—31	well	-	-	-	-	-	-
R1446—32	well	-	-	windmill and storage tank	-	-	-

Appendix B. Table 1. Off-ring well inventory located on 7.5-minute topographic maps. See explanation of column headings and symbols at end of table.

Well ID	Topographic quadrangle	NAD 83 northing (ft)	NAD 83 easting (ft)	Ground surface elev. (ft)	Well depth (ft)	Water level elev. (ft)	Date meas. M/D/Y	Form-ation	Diameter surface casing (ft)	Casing material	Well use	Wellhead condition
R1446—33	Midlothian	6828865	2456302	690	-	-	-	Kau	-	-	-	wire fence on wellhead
R1493—1	Boz	6794050	2443987	620	31	614	9/25/91	Kau	2.5	brick	unused	-
R1493—2	Boz	6794047	2443767	620	deep	-	-	-	-	-	-	-
R1722—1	Ennis West	6815565	2531649	488	-	-	-	-	-	-	aban'd	-
BEG-12	Palmer	6856763	2516593	496	20.4	492.8	4/8/91	Qt	2.5	concrete	aban'd	-
BEG-30	Palmer	6850389	2524025	480	22	465.4	12/6/90	Qt	6	-	domestic	-
BEG-31	Palmer	6862413	2513286	514	23.2	506.7	4/8/91	Qt	2.5	-	domestic	-
BEG-32	Palmer	6861572	2513423	512	33	505.6	4/8/91	Qt	2.81	-	domestic	-
BEG-34	Palmer	6853264	2511174	496	20.4	487.7	9/6/90	Qt	3.5	-	aban'd	-
BEG-35	Palmer	6853796	2510895	498	27	487.7	12/6/90	Qt	0.5	-	aban'd	-
BEG-36	Palmer	6850792	2516725	482	23.5	471.4	4/8/91	Qt	2.7	-	domestic	-
BEG-38	Palmer	6853649	2509703	490	15.5	485.4	4/8/91	Qt	2	-	aban'd	-
BEG-39	Palmer	6853953	2508612	495	36.2	485	9/6/90	Qt	1.33	-	domestic	-
BEG-40	Palmer	6853792	2508822	485	50	480.9	4/8/91	Qt	2.5	-	aban'd	-
BEG-41	Palmer	6862811	2517504	496	29.7	482	4/8/91	Qt	2.5	-	aban'd	-
BEG-42	Palmer	6863300	2517996	490	22.1	470.5	4/8/91	Qt	3.5	-	unused	-
BEG-43	Palmer	6862415	2519095	483	12.1	dry	10/4/90	Qt	3.4	-	unused	-
BEG-44	Palmer	6859278	2522731	485	30.7	471.8	9/7/90	Qt	1.3	-	unused	-
BEG-45	Palmer	6859503	2524524	474	24.8	461.9	4/8/91	Qt	2.8	-	aban'd	-
BEG-46	Palmer	6859020	2525084	470	14.2	467	4/8/91	Qt	3.9	-	aban'd	-
BEG-47	Waxahachie	6853843	2507053	470	20.6	472.2	4/8/91	Qt	1.2	-	unused	-
BEG-48	Waxahachie	6853693	2507133	460	13.3	465.9	10/1/90	Qt	1.2	-	domestic	-
BEG-49	Palmer	6856798	2508771	510	29	-	-	Qt	3	-	aban'd	-
BEG-50	Waxahachie	6856113	2506917	506	33	490.3	10/2/90	Qt	0.5	-	domestic	-
BEG-51	Waxahachie	6856304	2507139	509	34.7	489.6	10/2/90	Qt	2.6	-	domestic	-
BEG-52	Waxahachie	6856143	2507098	508	8.8	507.5	10/2/90	Qt	2.5	-	unused	-
BEG-53	Waxahachie	6856353	2507631	512	29.4	492.4	10/2/90	Qt	0.95	-	domestic	-
BEG-54	Waxahachie	6856543	2507742	512	34.4	493.3	10/2/90	Qt	2.5	-	aban'd	-
BEG-55	Waxahachie	6856704	2507994	513	29.6	495.8	10/2/90	Qt	2.5	-	aban'd	-
BEG-56	Waxahachie	6856415	2506647	505	29.6	485.1	10/2/90	Qt	1.2	-	unused	-
BEG-57	Waxahachie	6856395	2506858	506	31.7	487.4	10/2/90	Qt	1.2	-	unused	-
BEG-58	Waxahachie	6855712	2506645	503	28.6	487.7	10/2/90	Qt	2.5	-	domestic	-
BEG-59	Waxahachie	6855994	2506586	504	29.5	488.4	4/8/91	Qt	1	-	domestic	-
BEG-60	Waxahachie	6858429	2504341	511	-	-	-	Qt	-	-	unused	-
BEG-61	Waxahachie	6858358	2504260	510	34.1	479.7	10/3/90	Qt	2.5	-	domestic	-
BEG-62	Waxahachie	6858348	2504240	505	-	-	-	Qt	-	-	unused	-
BEG-63	Waxahachie	6858329	2503999	499	-	-	-	Qt	-	-	-	-
BEG-64	Waxahachie	6858319	2503908	490	17.1	481.9	10/3/90	Qt	2.7	-	domestic	-
BEG-65	Waxahachie	6858279	2503788	485	26	460.8	4/8/91	Qt	2.5	-	domestic	-
BEG-66	Waxahachie	6858157	2504551	512	38.4	480.8	10/3/90	Qt	2.6	-	unused	-
BEG-67	Waxahachie	6858177	2504792	512	41.9	482.6	10/3/90	Qt	2.5	-	domestic	-
BEG-68	Waxahachie	6858226	2504943	512	30.6	484.2	4/8/91	Qt	2.5	-	aban'd	-
BEG-69	Waxahachie	6857837	2503978	500	27	479.1	10/3/90	Qt	2.5	-	domestic	-
BEG-70	Waxahachie	6858589	2504481	512	39.4	479.7	4/9/91	Qt	2.5	-	unused	-
BEG-71	Palmer	6852894	2511143	495	22	488.7	4/8/91	Qt	3	-	unused	-
BEG-72	Palmer	6852995	2510672	490	-	-	-	Qt	-	-	aban'd	-
BEG-73	Palmer	6852196	2513013	482	14	472.4	10/3/90	Qt	2	-	unused	-
BEG-75	Waxahachie	6858759	2504854	516	42.1	483.5	3/4/91	Qt	2.5	-	unused	-
BEG-76	Palmer	6862928	2518606	465	5.4	463	10/4/90	Qt	4	-	aban'd	-

Appendix B. Table 1. (continued)

Well ID	Utility	Other ID	Relative depth	Notes	Owner	City	State
R1446—33	well	-	shallow	-	-	-	-
R1493—1	well	-	shallow	-	Dawson	-	-
R1493—2	well	-	deep	probably drilled, artesian	Dawson	-	-
R1722—1	well	-	shallow	front yard	Prachyl	Ennis	TX
BEG-12	well	-	shallow	concrete casing broken	Campbell	Rockett-Red Oak	TX
BEG-30	well	-	shallow	household water	Windham	-	-
BEG-31	well	-	shallow	Huerta (tenant)	Adams	Rockett-Red Oak	TX
BEG-32	well	-	shallow	-	Pederson	Rockett-Red Oak	TX
BEG-34	well	-	shallow	behind shop	Prude	Palmer	TX
BEG-35	well	-	shallow	not used in 2 years, in field	Prude	Palmer	TX
BEG-36	well	-	shallow	always pumping	Evans	Palmer	TX
BEG-38	well	-	shallow	behind aban'd house	Prude?	Palmer	TX
BEG-39	well	-	shallow	-	Prude	Palmer	TX
BEG-40	well	-	shallow	near spring	Prude	Palmer	TX
BEG-41	well	-	shallow	near old structures	Weatherford	-	-
BEG-42	well	-	shallow	in front yard	Weatherford	-	-
BEG-43	well	-	shallow	dry well	Weatherford	-	-
BEG-44	well	-	shallow	did not produce	McLean	Palmer	TX
BEG-45	well	-	shallow	Goulart (tenant), S of house	Windham	Palmer	TX
BEG-46	well	-	shallow	in field S of road	Moffitt	Palmer	TX
BEG-47	well	-	shallow	near street	Trewin	Palmer	TX
BEG-48	well	-	shallow	water lawn	Ponder	Palmer	TX
BEG-49	well	-	shallow	surface casing skewed	Brodsky	Palmer	TX
BEG-50	well	-	shallow	water lawn, horses	Mudge	Palmer	TX
BEG-51	well	-	shallow	supplies household water	Xedis	Palmer	TX
BEG-52	well	-	shallow	bad odor, film	Xedis	Palmer	TX
BEG-53	well	-	shallow	water lawn, horses	Van Zandt	Palmer	TX
BEG-54	well	-	shallow	vacant lot off of Van Zandt	-	Palmer	TX
BEG-55	well	-	shallow	in old orchard E of Van Zandt	-	Palmer	TX
BEG-56	well	-	shallow	behind barn in l k yard	Byrne	Palmer	TX
BEG-57	well	-	shallow	-	Smart	Palmer	TX
BEG-58	well	-	shallow	water lawn, horses	Snodgrass	Palmer	TX
BEG-59	well	-	shallow	water lawn, pump broken	Dow	Palmer	TX
BEG-60	well	-	shallow	locked cover, contact realtor	Haak	Rockett-Red Oak	TX
BEG-61	well	-	shallow	supplies household water	Runnels	Rockett-Red Oak	TX
BEG-62	well	-	shallow	-	-	Rockett-Red Oak	TX
BEG-63	well	-	shallow	unable to contact owners	-	Rockett-Red Oak	TX
BEG-64	well	-	shallow	supplies household water	Dunavant	Rockett-Red Oak	TX
BEG-65	well	-	shallow	water lawn, garden	Ross	Rockett-Red Oak	TX
BEG-66	well	-	shallow	behind old schoolhouse	Green	Rockett-Red Oak	TX
BEG-67	well	-	shallow	in field behind schoolhouse	Green	Rockett-Red Oak	TX
BEG-68	well	-	shallow	in field near #67	-	Rockett-Red Oak	TX
BEG-69	well	-	shallow	supplies household water	Blair	Rockett-Red Oak	TX
BEG-70	well	-	shallow	in back yard	Donica	Rockett-Red Oak	TX
BEG-71	well	-	shallow	in front yard	E. Prude	Rockett-Red Oak	TX
BEG-72	well	-	shallow	no access, covered by old roof	E. Prude	Rockett-Red Oak	TX
BEG-73	well	-	shallow	-	Mc Donald	Rockett-Red Oak	TX
BEG-75	well	-	shallow	in living room	Donica	Rockett-Red Oak	TX
BEG-76	well	-	shallow	in field E of road to house	Weatherford	Rockett-Red Oak	TX

Appendix B. Table 1. Off-ring well inventory located on 7.5-minute topographic maps. See explanation of column headings and symbols at end of table.

Well ID	Topographic quadrangle	NAD 83 northing (ft)	NAD 83 easting (ft)	Ground surface elev. (ft)	Well depth (ft)	Water level elev. (ft)	Date meas. M/D/Y	Form-ation	Diameter surface casing (ft)	Casing material	Well use	Wellhead condition
BEG-77	Palmer	6850714	2525709	472	35	456.4	10/4/90	Qt	0.5	-	domestic	-
BEG-78	Palmer	6856107	2527729	471	35.7	461.6	4/8/91	Qt	2.6	-	unused	-
BEG-79	Palmer	6855478	2527006	470	12.6	dry	10/4/90	Qt	-	-	aban'd	-
BEG-80	Palmer	6855489	2526665	470	29.4	457.6	10/4/90	Qt	4	-	aban'd	-
BEG-81	Palmer	6859806	2523714	481	37.6	466.7	10/4/90	Qt	3	-	unused	-
BEG-82	Palmer	6859626	2523603	485	27	474.8	4/8/91	Qt	2.3	-	unused	-
BEG-83	Palmer	6859447	2523696	484	6.2	dry	10/4/90	Qt	3	-	aban'd	-
BEG-84	Palmer	6860319	2523085	480	28.9	457.6	10/4/90	Qt	2	-	aban'd	-
BEG-85	Palmer	6860659	2523186	467	31.9	438.3	10/4/90	Qt	2	-	aban'd	-
BEG-86	Palmer	6851489	2515134	480	16.8	464.5	10/4/90	Qt	3	-	domestic	-
BEG-88	Palmer	6855016	2508385	506	-	-	-	Qt	-	-	-	-
BEG-89	Waxahachie	6864779	2507297	512	22.4	499.5	4/8/91	Qt	3	-	unused	-
BEG-90	Palmer	6854796	2524249	475	9.4	473.5	4/8/91	Qt	3	-	domestic	-
BEG-91	Palmer	6855082	2525632	470	6.63	470	4/8/91	Qt	2.8x1.9	-	domestic	-
BEG-92	Palmer	6857371	2530287	457	29.1	441.7	10/16/90	Qt	2.5	-	unused	-
BEG-93	Palmer	6857278	2531118	460	28.4	440.5	10/16/90	Qt	3	-	unused	-
BEG-94	Palmer	6857416	2531950	440	47.7	422.8	10/16/90	Qt	2.5	-	domestic	-
BEG-95	Palmer	6857638	2531349	457	-	-	-	Qt	-	-	domestic	-
BEG-96	Palmer	6857029	2530686	462	25.5	443.7	10/16/90	Qt	2.5	-	domestic	-
BEG-97	Palmer	6853876	2529915	468	13.9	460.1	4/8/91	Qt	5	-	unused	-
BEG-98	Palmer	6856515	2528451	464	22	450.2	10/17/90	Qt	2.5	-	unused	-
BEG-99	Palmer	6856815	2528653	466	28.7	452.2	10/17/90	Qt	2.5	-	domestic	-
BEG-100	Palmer	6857236	2528794	464	-	-	-	Qt	-	-	domestic	-
BEG-101	Palmer	6857497	2528625	460	21.6	450.8	4/8/91	Qt	2.5	-	domestic	-
BEG-102	Palmer	6857777	2528786	460	27.8	451.4	4/8/91	Qt	2.5	-	unused	-
BEG-103	Palmer	6857016	2531878	450	25.1	442.8	4/8/91	Qt	2.5	-	unused	-
BEG-104	Palmer	6858068	2528366	410	43.4	400.5	1/21/91	Qt	2.5	-	aban'd	-
BEG-105	Palmer	6858408	2528587	412	10.55	410.3	1/21/91	Qt	2.5	-	aban'd	-
BEG-106	Palmer	6858677	2529259	409	32.8	395.2	10/17/90	Qt	2.5	-	unused	-
BEG-107	Palmer	6856397	2527840	465	22.9	459	4/9/91	Qt	2.5	-	unused	-
BEG-108	Palmer	6854285	2530618	461	24.8	451.3	4/8/91	Qt	2.3	-	unused	-
BEG-110	Palmer	6852125	2523029	482	-	-	-	Qt	~2.5	brick	aban'd	-
BEG-112	Waxahachie	6858827	2505979	520	-	502.5	4/8/91	Qt	2.5	-	aban'd	-
BEG-113	Palmer	6857715	2532461	470	-	458.7	3/4/91	Qt	2.5	-	aban'd	-
BEG-114	Palmer	6857395	2532250	465	-	-	-	Qt	-	-	aban'd	-
BEG-115	Palmer	6850348	2517715	481	-	-	-	Qt	-	-	domestic?	-
SSC-1	Palmer	6862194	2516103	505	39.1	494.6	4/8/91	Qt	0.166	pvc	monitor	housed
SSC-4	Palmer	6852059	2522874	482	46.2	475.2	4/8/91	Qt	0.33	pvc	monitor	housed

Appendix B. Table 1. (continued)

Well ID	Utility	Other ID	Relative depth	Notes	Owner	City	State
BEG-77	well	-	shallow	household water	Almand	Palmer	TX
BEG-78	well	-	shallow	-	Wadley	Palmer	TX
BEG-79	well	-	shallow	dry well	Wadley	Palmer	TX
BEG-80	well	-	shallow	at old windmill	Wadley	Palmer	TX
BEG-81	well	-	shallow	behind house	Hamm	Ferris	TX
BEG-82	well	-	shallow	in horse corral	Hamm	Ferris	TX
BEG-83	well	-	shallow	in horse corral, dry	Hamm	Ferris	TX
BEG-84	well	-	shallow	in field behind house	Hamm	Ferris	TX
BEG-85	well	-	shallow	in field behind house	Hamm	Ferris	TX
BEG-86	well	-	shallow	supplies two houses	Spahr	-	-
BEG-88	well	-	shallow	-	Wyckoff	Palmer	TX
BEG-89	well	-	shallow	pump but not used	Buell	-	-
BEG-90	well	-	shallow	pump but not used	Epps	Palmer	TX
BEG-91	well?	-	shallow	flowing well/spring	Bardwell	Palmer	TX
BEG-92	well	-	shallow	-	Ramirez	-	-
BEG-93	well	-	shallow	-	Browder	Palmer	TX
BEG-94	well	-	shallow	-	Moseley	-	-
BEG-95	well	-	shallow	-	Prigeon	Palmer	TX
BEG-96	well	-	shallow	-	Schmidt	Palmer	TX
BEG-97	well	-	shallow	debris in bottom of well	Miller	Palmer	TX
BEG-98	well	-	shallow	in back yard	Gutierrez	Palmer	TX
BEG-99	well	-	shallow	waters 30 to 40 fruit trees	Fowler	-	-
BEG-100	well	-	shallow	-	Noisam	Palmer	TX
BEG-101	well	-	shallow	-	Houston	Rockett-Red Oak	TX
BEG-102	well	-	shallow	pump in well	Veterans Admin.	-	-
BEG-103	well	-	shallow	under garage shed	Ferguson	-	-
BEG-104	well	-	shallow	in horse pasture	Blocker	Palmer	TX
BEG-105	well	-	shallow	full of debris	Whited	Palmer	TX
BEG-106	well	-	shallow	-	Floyd	-	-
BEG-107	well	-	shallow	on corner, easy access	Elliott	-	-
BEG-108	well	-	shallow	flows at ground level at times	McKeever	Palmer	TX
BEG-110	well	-	shallow	brick surface casing collapsed	Cox or Windham?	-	-
BEG-112	well	-	shallow	behind aban'd structures	-	Rockett-Red Oak	TX
BEG-113	well	-	shallow	on vacant property	-	-	-
BEG-114	well	-	shallow	dirt-filled, has surface casing	-	-	-
BEG-115	well	-	shallow	probably small-diameter well	Campbell	Rockett-Red Oak	TX
SSC-1	well	-	shallow	monitor well	BEG (Adams lease)	Rockett-Red Oak	TX
SSC-4	well	-	shallow	monitor well	BEG (Cox lease)	Rockett-Red Oak	TX

Appendix B. Table 2. Off-ring well inventory from State data base, located on 7.5-minute topographic maps.

Well ID	Topographic quadrangle	NAD 83 northing (ft)	NAD 83 easting (ft)	Ground surface elev. (ft)	Well depth (ft)	Water level elev. (ft)	Date meas. M/D/Y	Form-ation	Diameter surface casing (ft)	Casing material	Well use	Wellhead condition
JK33-33-102	Midlothian	6862172	2433209	753	2,512	753	-/-/65	Kctm	0.5	steel	municipal	good
JK33-33-103	Midlothian	6862016	2434692	753	699	753	11/30/56	Kwb	0.33	steel	abandoned	-
JK33-33-104	Midlothian	6859026	2438105	753	698	-	-	Kwb	-	steel	abandoned	-
JK33-33-105	Midlothian	6862030	2432920	735	2,354	735	7/8/68	Kctm	0.55	steel	municipal	-
JK33-33-106	Midlothian	6863005	2431660	735	735	735	4/21/72	Kwb	0.38	steel	industrial	-
JK33-33-107	Midlothian	6861096	2434371	745	743	745	6/4/68	Kwb	0.38	steel	abandoned	-
JK33-33-201	Midlothian	6859506	2448832	726	619	726	-/-/57	Kwb	0.33	steel	domestic/stock	-
JK33-33-202	Midlothian	6855295	2448812	700	754	700	6/24/65	Kwb	0.38	steel	domestic/stock	-
JK33-33-203	Midlothian	6867339	2444736	783	2,530	1,120	11/13/86	Ktm	0.55	steel	municipal	-
JK33-33-401	Midlothian	6842571	2431503	839	642	839	8/3/63	Kwb	0.38	steel	domestic/stock	-
JK33-33-402	Midlothian	6852512	2431900	815	762	815	10/17/63	Kwb	0.38	steel	domestic	-
JK33-33-403	Midlothian	6844759	2431813	850	786	850	9/-/63	Kwb	0.33	steel	domestic	-
JK33-33-404	Midlothian	6852544	2438476	763	2,490	763	11/11/86	Ktm	0.38	steel	municipal	-
JK33-33-504	Midlothian	not located	-	690	550	-	-	Kgr	-	steel	-	-
JK33-33-601	Midlothian	6845884	2469594	650	1,017	650	10/13/69	Kwb	0.46	steel	domestic	-
JK33-33-701	Midlothian	6836090	2432997	832	1,425	832	-/-/64	Kpa	-	steel	domestic	-
JK33-33-702	Midlothian	6835623	2433151	835	695	835	-/-/65	Kwb	-	steel	stock	-
JK33-33-703	Midlothian	6835332	2432974	835	620	835	3/31/61	Kwb	0.46	steel	stock	-
JK33-33-705	Midlothian	6835510	2437046	788	2,475	788	6/-/69	Kctm	0.58	steel	irrigation	-
JK33-33-706	Midlothian	6835404	2437488	788	2,505	-	-	Kctm	0.33	steel	irrigation	-
JK33-34-101	Waxahachie	6854215	2477134	652	902	652	-/-/56	Kwb	0.33	steel	domestic/stock	-
JK33-34-102	Waxahachie	6851877	2477881	625	-	-	-	-	-	-	-	-
JK33-34-103	Waxahachie	6851877	2477881	625	1,020	625	8/2/85	Kwb	0.38	steel	domestic	-
JK33-34-201	Waxahachie	6856855	2483694	630	41	-	-	Kau	2	brick?	domestic/stock	-
JK33-34-202	Waxahachie	6863159	2485668	622	1,000	622	7/22/65	Kwb	0.38	steel	domestic	-
JK33-34-204	Waxahachie	6859457	2482648	638	968	638	7/22/65	Kwb	0.38	steel	domestic/stock	-
JK33-34-205	Waxahachie	6868393	2484385	590	967	590	4/9/70	Kwb	0.38	steel	domestic/stock	-
JK33-34-206	Waxahachie	6856507	2490358	595	1,191	595	7/3/71	Kwb	0.25	steel	municipal	good
JK33-34-208	Waxahachie	6865057	2485149	570	1,035	570	5/22/86	Kwb	0.29	steel	-	-
JK33-34-209	Waxahachie	6856855	2483694	628	1,110	628	7/5/88	Ktr	0.33	steel	municipal	good
JK33-34-210	Waxahachie	6854378	2488193	615	3,085	615	12/20/84	Ktr	0.5	steel	municipal	good
JK33-34-211	Waxahachie	6853784	2485758	615	1,180	-	-	Ktr	0.58	steel	municipal	good
JK33-34-301	Waxahachie	6859845	2506540	525	3,285	525	3/12/75	Kctm	0.58	steel	municipal	good
JK33-34-302	Waxahachie	6856896	2501112	500	30	500	3/18/75	Kau/Qt	2.5	brick	domestic	-
JK33-34-306	Waxahachie	6860196	2498582	515	20	515	3/18/75	Kau	3.5	concrete	domestic	-
JK33-34-401	Waxahachie	6845785	2480896	630	50	-	-	-	2.5	concrete	nursery	-
JK33-34-403	Waxahachie	6848537	2470330	632	876	632	5/-/63	Kwb	0.38	steel	domestic	-
JK33-34-405	Waxahachie	6853368	2479342	627	952	627	3/5/63	Kwb	0.38	steel	commercial	-
JK33-34-502	Waxahachie	6841488	2495178	558	1,080	-	-	Kwb	0.38	steel	domestic	-
JK33-34-601	Waxahachie	6850758	2507014	530	1,302	530	7/23/65	Kwb	0.38	steel	domestic	-
JK33-34-702	Waxahachie	6826011	2478548	525	2,950	525	2/18/53	Kctm	0.5	steel	unused	-
JK33-34-703	Waxahachie	6824930	2478332	540	2,950	540	3/16/48	Kctm	0.67	steel	observation	-
JK33-34-704	Waxahachie	6828114	2476322	551	2,878	551	3/16/65	Kctm	0.72	steel	municipal	good

Appendix B. Table 2 (continued)

Well ID	Utility	Relative depth	Notes	Owner	City	State
JK33-33-102	well	deep	City well no. 2	Midlothian	Midlothian	TX
JK33-33-103	well	deep	City well no. 1	Midlothian	Midlothian	TX
JK33-33-104	well	deep	never used	GC&SF RR	Midlothian	TX
JK33-33-105	well	deep	City well no. 4	Midlothian	Midlothian	TX
JK33-33-106	well	deep	-	Elevator Ind.	Midlothian	TX
JK33-33-107	well	deep	commercial	V.L. Hice	Midlothian	TX
JK33-33-201	well	deep	-	J.B. Gaither	Midlothian	TX
JK33-33-202	well	deep	-	Webster&Dunn	Midlothian	TX
JK33-33-203	well	deep	municipal	Sardis-Lone Elm	Midlothian	TX
JK33-33-401	well	deep	-	Frank Tennery	Midlothian	TX
JK33-33-402	well	deep	-	Marvin Byrd	Midlothian	TX
JK33-33-403	well	deep	-	O.Ray Jobe	Midlothian	TX
JK33-33-404	well	deep	Well no. 3	Sardis-Lone Elm	Midlothian	TX
JK33-33-504	well	deep	-	-	Midlothian	TX
JK33-33-601	well	deep	-	B. Barnard	Midlothian	TX
JK33-33-701	well	deep	-	Hi-View Hereford	Dallas	TX
JK33-33-702	well	deep	-	Hi-View Hereford	Dallas	TX
JK33-33-703	well	deep	-	Hi-View Hereford	Dallas	TX
JK33-33-705	well	deep	-	Hi-View Hereford	Dallas	TX
JK33-33-706	well	deep	-	Hi-View Hereford	Dallas	TX
JK33-34-101	well	deep	-	Bernard Dale	Waxahachie	TX
JK33-34-102	well	-	-	-	-	-
JK33-34-103	well	deep	-	Bekins A-1 Movers	Waxahachie	TX
JK33-34-201	well	shallow	4 dug wells, near R77N-28	T.C. Buie	Waxahachie	TX
JK33-34-202	well	deep	-	E.K. Burks	Waxahachie	TX
JK33-34-204	well	deep	-	W.J. Byrne	Waxahachie	TX
JK33-34-205	well	deep	stock	Glenn Stephenson	Red Oak	TX
JK33-34-206	well	deep	-	North Texas Corp.	Dallas	TX
JK33-34-208	well	deep	-	Tufco	Waxahachie	TX
JK33-34-209	well	deep	near R77N-28	Rockett WSC	Red Oak	TX
JK33-34-210	well	deep	Well no. 6	Rockett WSC	Red Oak	TX
JK33-34-211	well	deep	Well no. 6A	Rockett WSC	Red Oak	TX
JK33-34-301	well	deep	Well no. 1	Rockett WSC	Red Oak	TX
JK33-34-302	well	shallow	dug well	Hayden Jackson	Waxahachie	TX
JK33-34-306	well	shallow	dug well	Maye Rockett	Waxahachie	TX
JK33-34-401	well	shallow	9 wells	Naughton's Nursery	Waxahachie	TX
JK33-34-403	well	deep	-	V.L. Herndon	Waxahachie	TX
JK33-34-405	well	deep	commercial	Stuckey's	Waxahachie	TX
JK33-34-502	well	deep	-	J.M. Edmondson	Waxahachie	TX
JK33-34-601	well	deep	-	C.W. Melton	Waxahachie	TX
JK33-34-702	well	deep	City well no. 1, flowed until 1932	City of Waxahachie	Waxahachie	TX
JK33-34-703	well	deep	City well no. 3	City of Waxahachie	Waxahachie	TX
JK33-34-704	well	deep	City well no. 4	City of Waxahachie	Waxahachie	TX

Appendix B. Table 2. Off-ring well inventory from State data base, located on 7.5-minute topographic maps.

Well ID	Topographic quadrangle	NAD 83 northing (ft)	NAD 83 easting (ft)	Ground surface elev. (ft)	Well depth (ft)	Water level elev. (ft)	Date meas. M/D/Y	Form-ation	Diameter surface casing (ft)	Casing material	Well use	Wellhead condition
JK33-34-707	Waxahachie	6831136	2472431	550	-	-	-	-	-	-	-	-
JK33-34-706	Waxahachie	6838742	2470884	603	839	353	6/17/65	Kwb	-	steel	-	-
JK33-34-711	Waxahachie	6825682	2478424	525	1,521	-	-	Kwb/Ktr	-	steel	abandoned	-
JK33-34-712	Waxahachie	6826969	2479642	535	2,907	535	-/-/32	Ktr	0.67	steel	municipal	plugged
JK33-34-802	Waxahachie	6835584	2493825	572	1,180	572	-/-/55	Kwb	-	steel	domestic/stock	-
JK33-34-803	Waxahachie	6832025	2485711	580	1,091	580	7/30/65	Kwb	0.38	steel	domestic/stock	-
JK33-35-401	Palmer	6848252	2512215	528	1,295	528	8/6/65	Kwb	0.67	steel	domestic/stock	-
JK33-35-405	Palmer	not located	-	625	-	-	-	-	-	-	-	-
JK33-35-503	Palmer	6844934	2533256	467	1,522	467	7/6/65	Kwb	0.33	steel	municipal	-
JK33-35-801	Palmer	6829299	2523568	460	18	460	8/9/65	-	2.5	brick	unused	-
JK33-35-803	Palmer	6835076	2528048	451	-	451	6/21/65	-	-	steel	-	-
JK33-35-902	Palmer	6837106	2540656	538	140	538	8/6/65	Ko/Kau	0.33	steel	domestic	-
JK33-41-206	Boz	6822364	2450954	731	805	731	8/20/82	Kwb	0.38	steel	stock	-
JK33-41-402	Boz	6806720	2443446	710	690	710	10/23/62	Kwb	0.38	steel	domestic/stock	-
JK33-41-503	Boz	6804277	2448480	640	758	640	4/1/74	Kwb	0.46	steel	domestic	-
JK33-41-802	Boz	6784494	2452182	532	632	532	6/16/65	Kwb	0.38	steel	stock	-
JK33-41-3A	Boz	6820345	2462270	728	50	-	-	Kau	2.5	concrete	-	-
JK33-42-104	Forreston	6809618	2476313	585	1,019	585	7/19/65	Kwb	0.38	steel	domestic/stock	-
JK33-42-201	Forreston	6821299	2495143	557	1,285	557	5/21/70	Kwb	0.38	steel	domestic/stock	-
JK33-42-301	Forreston	6811529	2499032	492	30	474	1/10/64	Qal/Ko	2.5	concrete	-	-
JK33-42-401	Forreston	6806385	2478147	622	1,026	622	7/30/63	Kwb	0.38	steel	domestic/stock	-
JK33-42-405	Forreston	6797126	2474910	608	2,900	608	1/21/77	Kctm	0.58	steel	municipal	-
JK33-42-702	Forreston	6779659	2472520	550	2,850	550	1/21/77	Kctm	0.58	steel	municipal	-
JK33-42-704	Forreston	6791205	2470910	621	36	621	6/19/63	Kau	2.5	concrete	domestic	-
JK33-42-706	Forreston	6785211	2479193	557	35	dry	9/5/61	Kau	2.5	concrete	domestic	-
JK33-42-901	Forreston	6793129	2502808	513	1,238	513	7/20/65	Kwb	0.33	steel	municipal	-
JK33-43-101	Ennis West	6813122	2516159	527	1,370	380	11/7/75	Kwb	0.25	steel	municipal	-
JK33-43-201	Ennis West	6817415	2529924	490	-	-	-	-	-	-	-	-
JK33-43-203	Ennis West	6817335	2529945	490	-	-	-	-	-	-	-	-
JK33-43-301	Ennis West	6819328	2537919	555	1,350	555	8/10/65	Kwb	0.38	steel	municipal	-
JK33-43-302	Ennis West	6823127	2546026	521	230	521	3/17/65	Kwc	0.5	iron	domestic	-
JK33-43-401	Ennis West	6806723	2518570	503	1,350	503	-/-/50	Kwb	0.67	steel	dom/ind	-
JK33-43-601	Ennis West	6802786	2536309	450	-	-	-	-	-	-	-	-
JK33-43-602	Ennis West	6803431	2543444	510	1,806	510	1/22/64	Kwb	0.5	steel	municipal	-
JK33-43-802	Ennis West	6784493	2526674	479	1,525	479	1/15/80	Ktr	0.33	steel	municipal	-
JK33-43-901	Ennis West	6779031	2543588	446	1,659	446	7/23/64	Kwb	0.58	steel	abandoned	-
JK33-43-902	Ennis West	6787565	2544752	467	-	-	-	-	-	-	-	-
JK33-50-202	Avalon	6774359	2495525	550	3,204	550	1/27/76	Kwb	0.58	steel	municipal	-
JK33-50-301	Avalon	6777218	2500527	500	990	-	-	Kwb	0.17	steel	domestic	-
JK33-50-401	Avalon	6754349	2475625	500	1,050	500	-/-/59	Kwb	0.33	steel	domestic	-
JK33-50-503	Avalon	6752628	2496940	460	1,185	460	4/29/65	Kwb	0.38	steel	domestic	-
JK33-50-601	Avalon	6748442	2505393	421	-	-	-	-	-	-	-	-
JK33-50-901	Avalon	6747215	2506463	420	-	-	-	-	-	-	-	-

Appendix B. Table 2 (continued)

Well ID	Utility	Relative depth	Notes	Owner	City	State
JK33-34-707	well	deep	-	City of Waxahachie	Waxahachie	TX
JK33-34-706	well	deep	-	W.H. Prather	Waxahachie	TX
JK33-34-711	well	deep	mineral well	City of Waxahachie	Waxahachie	TX
JK33-34-712	well	deep	City well no. 2, plugged	City of Waxahachie	Waxahachie	TX
JK33-34-802	well	deep	closed in 1965	Ted Almand	Waxahachie	TX
JK33-34-803	well	deep	-	M.G. Bennett	Waxahachie	TX
JK33-35-401	well	deep	-	Hart Farm	Waxahachie	TX
JK33-35-405	well	deep	-	-	-	-
JK33-35-503	well	deep	City well no. 2	City of Palmer	Palmer	TX
JK33-35-801	well	shallow	-	J.&S. Macalik	Palmer	TX
JK33-35-803	well	deep	A-89-20-1‡, industrial	McClain	Palmer	TX
JK33-35-902	well	deep	-	Don L. Griffith	Palmer	TX
JK33-41-206	well	deep	-	Tom Fisher	Waxahachie	TX
JK33-41-402	well	deep	-	E.C. Dawson	Waxahachie	TX
JK33-41-503	well	deep	-	Vern Mayes	Waxahachie	TX
JK33-41-802	well	deep	-	Barron Kidd	Dallas	TX
JK33-41-3A	well	shallow	-	M.I. Norton	Waxahachie	TX
JK33-42-104	well	deep	-	C.O. Bigham	Waxahachie	TX
JK33-42-201	well	deep	R287-18‡, domestic, stock	J.J. King	Waxahachie	TX
JK33-42-301	well	shallow	-	Frank Martin	Waxahachie	TX
JK33-42-401	well	deep	R877-5‡	James Lewis	Waxahachie	TX
JK33-42-405	well	deep	-	Nash-Forreston	Forreston	TX
JK33-42-702	well	deep	-	Nash-Forreston	Forreston	TX
JK33-42-704	well	shallow	-	J.A. Rudd	Forreston	TX
JK33-42-706	well	shallow	-	Leland Calvert	Waxahachie	TX
JK33-42-901	well	deep	c/o H Odom	Howard Co-op	Waxahachie	TX
JK33-43-101	well	deep	E-Log Q60	Boyce WSC	Waxahachie	TX
JK33-43-201	-	deep	E-Log	-	-	-
JK33-43-203	-	deep	E-Log	-	-	-
JK33-43-301	well	deep	municipal	H.R. Stroube	Corsicana	TX
JK33-43-302	well	deep	-	Guy Killough	Ennis	TX
JK33-43-401	well	deep	-	K.Gin, W.R. Crittondon	Waxahachie	TX
JK33-43-601	well	-	-	-	-	TX
JK33-43-602	well	deep	City well no. 3	City of Ennis	Ennis	TX
JK33-43-802	well	deep	City well no. 2	City of Bardwell	Bardwell	TX
JK33-43-901	well	deep	-	M&S Construction	Milford	TX
JK33-43-902	well	-	-	-	-	TX
JK33-50-202	well	deep	-	City of Avalon	Avalon	TX
JK33-50-301	well	deep	-	Ma-Griffith	Ennis	TX
JK33-50-401	well	deep	-	D.L. Rollins	Italy	TX
JK33-50-503	well	deep	-	D.D. Betts	Italy	TX
JK33-50-601	well	-	-	-	-	TX
JK33-50-901	well	-	-	-	-	TX

Appendix B. Column heading explanation.

Well ID	First number is UFS parcel number; digit after hyphen is well number
Topographic quadrangle	USGS 7.5-minute topographic map on which well is located
NAD 83 northing and easting	Coordinates defining well location
Beam distance	Distance of well from beam alignment
Within easement	Is well within campus boundaries or within easement defined on aerial photos?
Ground surface elev.	Ground-surface elevation above mean sea level at wellhead
Well depth (ft)	Depth of well from ground surface
Water level elev.	Elevation above mean sea level of water level in well
Date meas (M/D/Y)	Date water-level measurement taken (month/day/year)
Formation	Geologic unit in which well is completed or screened. Qal alluvium Qt terrace deposits Kau Austin Chalk Ko "lower Taylor Marl," Ozan Formation Kwc "middle Taylor Marl," Wolfe City Formation Ksb Eagle Ford Shale Kwb Woodbine Formation Kctm Twin Mountains Formation
Diameter surface casing	Diameter of well casing at top of well
Casing material	Description of surface casing construction materials
Well use	Use of the well
Wellhead condition	Description of cover on well and well maintenance
Utility	Designation as well, cistern, spring, or seep
Other ID	State or SSC designation for well
Relative depth	Qualitative characterization distinguishing shallow (<50 ft) dug well from deep (>200 ft) well of unmeasured depth in regional aquifer

Symbols

-	Not applicable or data not collected
?	Unverified report
*	Measured depth/drilled depth
†	Well not located
‡	Possible match to well listed in state data base

Appendix C. List of Water Wells Located within 150 ft (45.72 m) of SSC Beamline

Appendix C. List of wells within 150 ft of beam alignment, excluding SSC monitoring wells.

ID	Map no.	Beam distance (ft)	Ground surface elev. (ft)*	Well depth (ft)	Diameter surface casing (ft)	Well use
104-B-1	26	0	655	-	-	unused
220-1	33	0	715	0	-	abandoned
235-D-1	9	0	702	26.6	696.1	unused
244-A-1	21	0	622	13.9	619	unused
248-A-2	20	0	665	550	525	unused
275-1	73	0	480	15.3	475.6	lawn
472-D-1	95	0	465	35 ?	-	domestic
599-1	14	0	715	1	-	abandoned
599-2	14	0	715	-	-	domestic
237-1	10	25	761	0	-	abandoned
245-B-1	20	25	695	20.9	690.5	unused
525-5	26	25	707	0	-	abandoned
38-C-2	90	50	460	19.7	458.8	unused
41-A-2	26	50	740	19.5	730.3	unused
72-A-1	93	50	470	35.9	463.3	unused
86-B-1	26	50	665	20.5	660.7	unused
86-C-2	26	50	682	12.8	678.1	abandoned
88-B-1	14	50	690	29.4	674.4	unused
103-C-1	27	50	633	38.9	620.7	unused
202-A-1	64	50	540	21.4	470.5	unused
202-A-3	64	50	532	-	-	unused
227-2	33	50	710	0	-	abandoned
265-B-1	57	50	540	30.0?	-	unused
525-2	25	50	740	25.4	731.2	unused
8-A-2	28	100	583	42.4	676.9	unused
35-1	93	100	493	44.6	484	lawn
62-C-1	61	100	508	19.8	500.2	unused
62-C-2	61	100	512	20?	-	-
69-1	64	100	505	31.7	487	lawn
104-A-1	27	100	640	19.7	635.9	unused
256-1	57	100	542	22.8	533.9	unused
350-1	27	100	630	0	-	abandoned
553-1	27	100	640	18.2	635.4	unused
229-C-1	33	125	722	17.3	716.9	unused
329-2	20	125	680	40?	-	abandoned
41-A-3	26	150	745	1,700?	-	lawn
57-1-1	93	150	470	5	-	abandoned
86-C-1	26	150	687	29.1	674.4	unused
128-C-1	14	150	690	2,606	640	municipal
329-1	20	150	670	40?	-	abandoned
342-A-1	20	150	685	-	684.9	abandoned

Appendix D. Methods of Analyzing Hydrologic Tests in Large-Diameter Wells in Unconfined Aquifers

Appendix D. Methods of Analyzing Hydrologic Tests in Large-Diameter Wells in Unconfined Aquifers

ABSTRACT

Aquifer tests in large-diameter, hand-dug wells are difficult to interpret because of wellbore storage effects. Many analytical methods assume the well to be a line sink and thus cannot be used to analyze tests in wells with substantial storage. One analytical solution that considers wellbore storage is valid only for relatively permeable aquifers. Several authors have proposed numerical and empirical solutions that determine hydrologic properties in low-yield aquifers using large-diameter wells. Unfortunately, numerical modeling can be time consuming, and empirical methods can be difficult to validate and confusing to implement. However, slug tests are simple and common techniques developed for analyzing aquifer tests in single piezometers that can also be used for analyzing tests in large-diameter, hand-dug wells. With slug tests, water is "instantaneously" added or removed, and the water-level recovery observed. These tests are easily performed and are explained and derived in many published sources.

To show that slug tests can be accurately used with hand-dug wells, a numerical model, empirical solutions, and different slug test analysis methods were used to evaluate aquifer tests in 12 wells with diameters ranging from 1.5 to 10 ft (0.46 to 3.05 m). The wells are located in the Austin Chalk outcrop in Ellis County, North-Central Texas. The test procedure involved (1) pumping the well for approximately 1 hr to lower the water level no more than 10 percent of the saturated thickness and (2) measuring the rate of water-level recovery. Slug test analysis methods that rely on early-time recovery data compared favorably with numerical and empirical methods. This result shows that slug tests are easily implemented and interpreted for determining hydraulic conductivity in aquifers using large-diameter wells in low-yield aquifers.

INTRODUCTION

Shallow (<50 ft [<15 m]) hand-dug wells are common in many parts of the world in aquifers in alluvial deposits and the weathered section of less permeable carbonate, crystalline, and basaltic bedrock. Evaluation of hydrologic properties and water resources in rural areas must rely on tests in such wells. If a shallow aquifer hosts many hand-dug wells, new wells do not need to be drilled for tests, saving considerable time and expense in characterizing hydrologic properties of the aquifer. However, aquifer tests in large-diameter wells are difficult to interpret with standard techniques because of wellbore storage effects. Wellbore storage is the volume of water "stored" in the wellbore. When a well is pumped, the volume of water produced is a combination of ground-water inflow from the aquifer and water from wellbore storage. If ground-water inflow is small, most of the water produced from the well is from wellbore storage, and drawdown with time will be linear if pumping rate is held constant. Many methods do not consider wellbore storage. For example, the Theis (1935) method assumes that a well can be represented as a line sink and thus does not consider storage effects of the wellbore. The Hantush (1964, p. 340) solution for a finite-diameter well assumes that the rate of flow out of the well equals the rate of flow into the well and therefore also neglects wellbore storage.

Papadopulos and Cooper (1967) and others recognized the limitations of the Theis method and Hantush solution and attempted to quantify wellbore storage. Papadopulos and Cooper (1967) presented an analytical solution for estimating transmissivity and storativity from drawdown data in a well with storage in a confined aquifer. They solved the flow equation for transient radial ground-water flow to a well in a homogeneous, isotropic, confined aquifer (Jacob, 1950) with a boundary condition that set the rate of discharge from the well as the sum of the rate of ground-water flow into the well and the rate of decrease in volume of water within the well

$$2\pi r_w T \frac{\partial s(r_w, t)}{\partial r} - \pi r_c^2 \frac{\partial s_w(t)}{\partial t} = -Q \qquad \text{for } t>0 \qquad \text{(D1)}$$

where T is transmissivity of the aquifer, t is time since start of pumping, s is drawdown in the aquifer at distance r and time t, s_w is drawdown in well at time t, Q is constant discharge from well, r_w is radius of the well, and r_c is radius of the casing (fig. D1). Papadopulos and Cooper (1967) presented type curves for use in analyzing drawdown data. Practical application of their approach requires a relatively permeable aquifer. For example, Papadopulos and Cooper (1967) stated that their analytical solution cannot be used unless

$$t > 250 \frac{r_c^2}{T}. \tag{D2}$$

For a well casing radius of 2 ft and an aquifer transmissivity of 5 ft^2/day (0.46 m^2/day), approximately 40 days of pumping are required before an accurate estimate of transmissivity can be obtained. The analytical solution is clearly not useful for analyzing aquifer tests in wells with large wellbore storage effects.

The limitation of Papadopulos and Cooper's (1967) solution led to the development of numerical and empirical methods that estimate aquifer properties in less permeable formations. Rushton and Redshaw (1979), Singh and Gupta (1986), and Barker (1989), among others, proposed different numerical methods. Other methods involved numerical modeling to develop empirical equations describing aquifer properties. Two such methods were published by Herbert and Kitching (1981) and Barker and Herbert (1989). Numerical modeling can be time consuming, especially if a model must be written and verified, and the resulting empirically derived solutions for finding hydraulic conductivity can be confusing to use. For example, confusing notation and typographical errors in Herbert and Kitching's (1981) paper can cause errors in calculated hydraulic conductivities (R. Herbert, 1991, personal communication). In addition, numerically derived solutions are extremely difficult to re-derive and verify.

Apparently overlooked in the literature is the use of slug tests, which also consider wellbore storage and use water-level recovery for analysis (Hvorslev, 1951; Cooper and others, 1967; Bouwer and Rice, 1976; Bouwer, 1989). Slug tests are commonly used to estimate hydrologic properties with solitary piezometers or wells and to characterize formations of low permeability. A slug test involves instantaneously adding or removing a slug of water in a well and observing the water-level response.

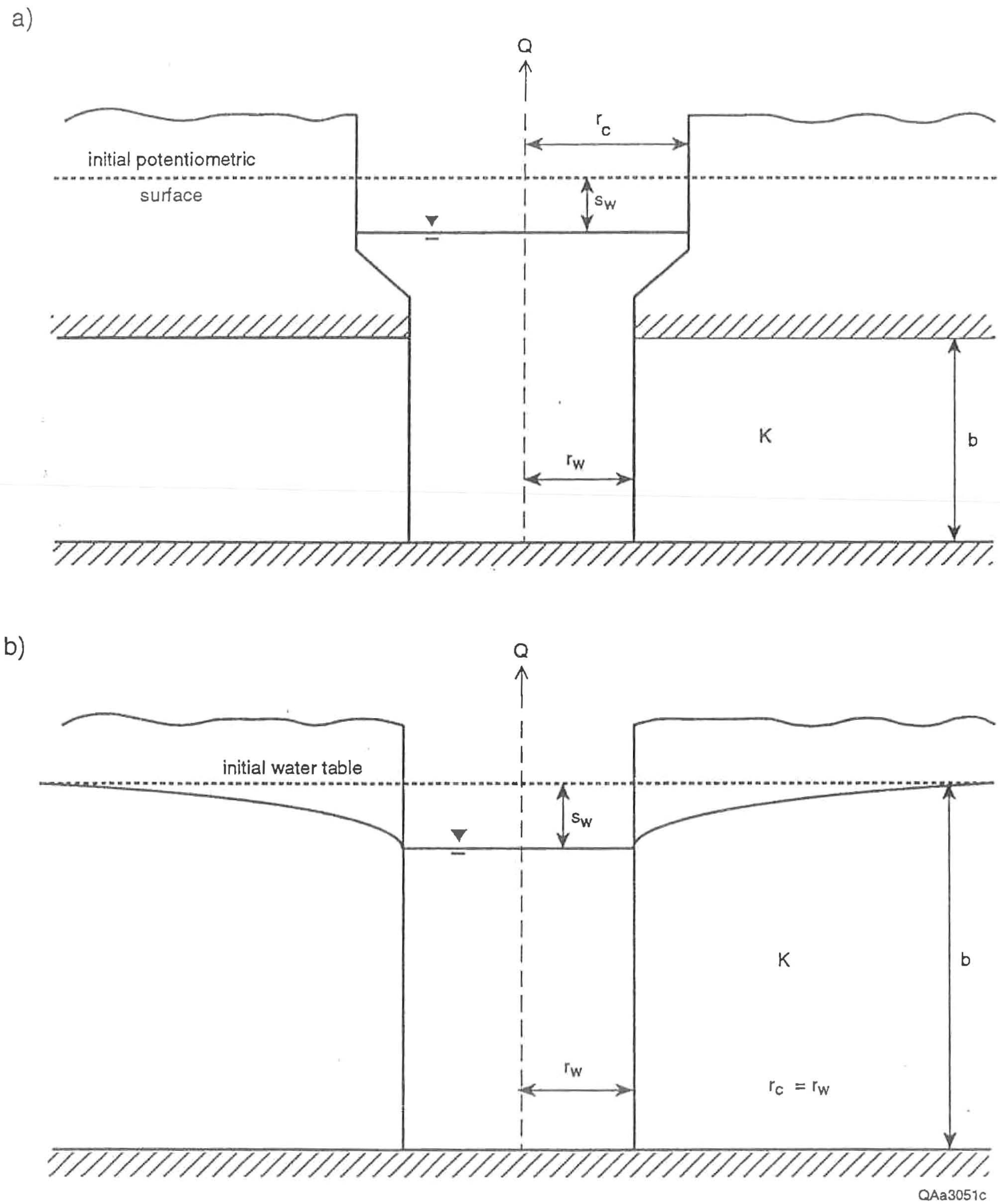

Figure D1. Drawdown in a large-diameter well in (a) a confined aquifer and (b) an unconfined aquifer. Q = discharge from the well, r_w is radius of the well, s_w is drawdown in the well, K is hydraulic conductivity, and b is aquifer thickness.

Slug tests are easy to perform and analyze and are familiar to most hydrologists. Barker and Herbert (1989) mentioned that slug test analysis methods should be used to interpret tests of very slow recovery that cannot be analyzed with their method. Fenske (1977) found that as pumping time became short relative to recovery time, his type recovery curves approached the slug test curves of Cooper and others (1967). However, no one has investigated whether slug test analysis methods can be substituted for numerical models and empirical methods in estimating hydrologic properties of large-diameter wells where Papadopulos and Cooper's (1967) analytical solution is not valid.

To compare slug test analysis methods with numerical and empirical solutions, 12 aquifer tests were conducted in weathered Austin Chalk in Ellis County, North-Central Texas. Aquifer test results were analyzed with a finite-difference numerical model written for this study, Herbert and Kitching's (1981) 50-percent recovery method, Barker and Herbert's (1989) 25- and 50-percent recovery methods, and Hvorslev's (1951), Bouwer and Rice's (1976), and Cooper and others' (1967) slug test analysis methods. This paper shows that piezometer tests are just as accurate at estimating hydraulic conductivity in large-diameter wells as the more complicated and potentially confusing numerical and empirical methods.

Methods

Herbert and Kitching (1981) described the validity of estimating aquifer properties from recovery data in large-diameter wells. They observed that in low-permeability formations very little of the water pumped from the well is contributed from the aquifer during water-level drawdown and that all flow into the well during recovery is derived from the aquifer. Therefore, results estimated from measured recovery more accurately represent aquifer properties than those estimated from drawdown.

Because many hand-dug wells are located in unconfined aquifers, care must be taken to keep water-level drawdown in the well small in order to approximate horizontal confined flow conditions. With small drawdowns, ground-water flow to the well is predominantly horizontal and the vertical component of flow near the wellbore is reduced. If the drawdown is small compared to the saturated thickness of the aquifer, ground-water flow equations for confined conditions can be used to describe flow in unconfined aquifers (Jacob, 1950). Herbert and Kitching's (1981) test design involves pumping the well for approximately 1 hr so that total drawdown is less than 10 percent of the saturated thickness of the aquifer. Water levels are then measured during recovery. For the procedure described, Herbert and Kitching (1981) stated that

- well losses and turbulence will not affect results because flow into the well will be at a low rate due to the 1 hr pumping period and 10-percent drawdown, and
- because well losses are negligible, the drawdown-time relationship of the confined and unconfined systems will be nearly identical.

In Ellis County, Texas, there are more than 800 hand-dug wells with diameters ranging from 1.5 to 10 ft (0.46 to 3.05 m) and depths ranging from 5 to 50 ft (1.52 to 15.24 m). These wells develop ground-water resources in the surficial weathered section of low-permeability, Upper Cretaceous Austin Chalk and Taylor Marl. These wells also develop ground-water in Pleistocene and Holocene alluvial deposits. Water-level recovery data collected at these wells were used to estimate aquifer properties of the chalk, marl, and alluvium. The test procedure involved (1) pumping the well for 1 hr at a constant rate so that total drawdown did not exceed 10 percent of the saturated aquifer thickness and (2) measuring recovering water levels. A pressure transducer and data-logger were used to record changes in water levels in the well. Well geometry and pumping rate were measured during the test.

Water-level recovery data were analyzed with a finite-difference model, Herbert and Kitching's (1981) 50-percent recovery method, Barker and Herbert's (1989) 25- and 50-percent recovery methods, and Hvorslev's (1951), Bouwer and Rice's (1976), and Cooper and others' (1967) slug test analysis methods.

An implicit finite-difference numerical model was written to simulate confined radial ground-water flow to large-diameter wells. The model was constructed following instructions by Herbert and Kitching (1981), Rushton and Holt (1981), Rushton and Redshaw (1979), and Wang and Anderson (1982). The model was validated by reproducing water-level drawdown and recovery from a program based on Papadopulos and Cooper's (1967) analytical solution Barker (1989), (fig. D2a). Aquifer

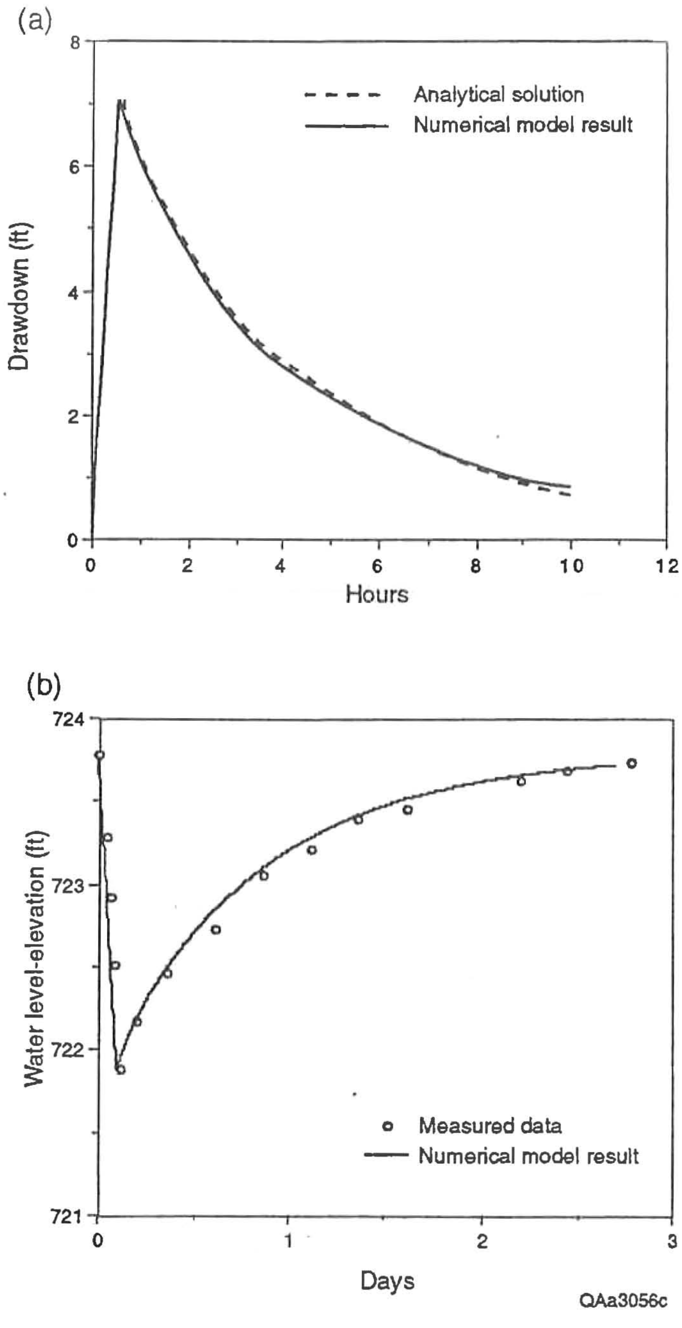

Figure D2. Comparison of water-level drawdown and recovery predicted by the finite-difference model to (a) a numerical solution of Papadopulos and Cooper's (1967) analytical solution (Barker, 1989) and (b) an aquifer test at a large-diameter well in Austin Chalk.

parameters were numerically estimated by trial-and-error adjustment of hydraulic conductivity in the model until numerical results matched the observed drawdown and recovery of water levels (for example, fig. D2b).

Analysis with Herbert and Kitching's (1981) 50-percent recovery method involved measuring the elapsed time of water-level recovery to 50 percent of the maximum water-level drawdown. The 50-percent recovery time, well and aquifer geometry, and pumping duration were used to find transmissivity with an empirically derived equation.

Analysis with Barker and Herbert's (1989) 25- and 50-percent recovery methods involved measuring the elapsed time of water-level recovery to 25- and 50-percent of the maximum water-level drawdown. These recovery times, well and aquifer geometry, and pumping duration were used to find transmissivity with numerically derived nomograms based on Papadopulos and Cooper's (1967) analytical solution.

Analysis with Hvorslev's (1951) method for interpreting slug tests involved finding the time lag′ from a semi-log plot of relative water-level recovery (amount recovered/initial drawdown) versus time. The time lag, well geometry, and a shape factor describing the screened portion of the well (well intake) in contact with the aquifer were used to calculate hydraulic conductivity.

Hvorslev's (1951) method allows different shape factors to be used depending on the geometry of the well and the aquifer setting. For instance a shape factor, c, commonly presented in textbooks (Freeze and Cherry, 1981; Domenico and Schwartz, 1990) describes partial well completion in aquifer material (fig. D3a) as an ellipsoid (Dachler, 1936)

$$c = \frac{2\pi L}{\ln\left(L / r_w\right)}. \tag{D3}$$

For hand-dug wells in unconfined aquifers, r_w is the radius of the well and L is the distance from the static water level to the bottom of the well. Since water in the surficial, weathered bedrock tested for this paper is unconfined, the upper boundary is a no-flow boundary. Therefore, a shape factor for a well intake extended at an impermeable boundary (fig. D3b) may be more accurate. Dachler (1936, as cited

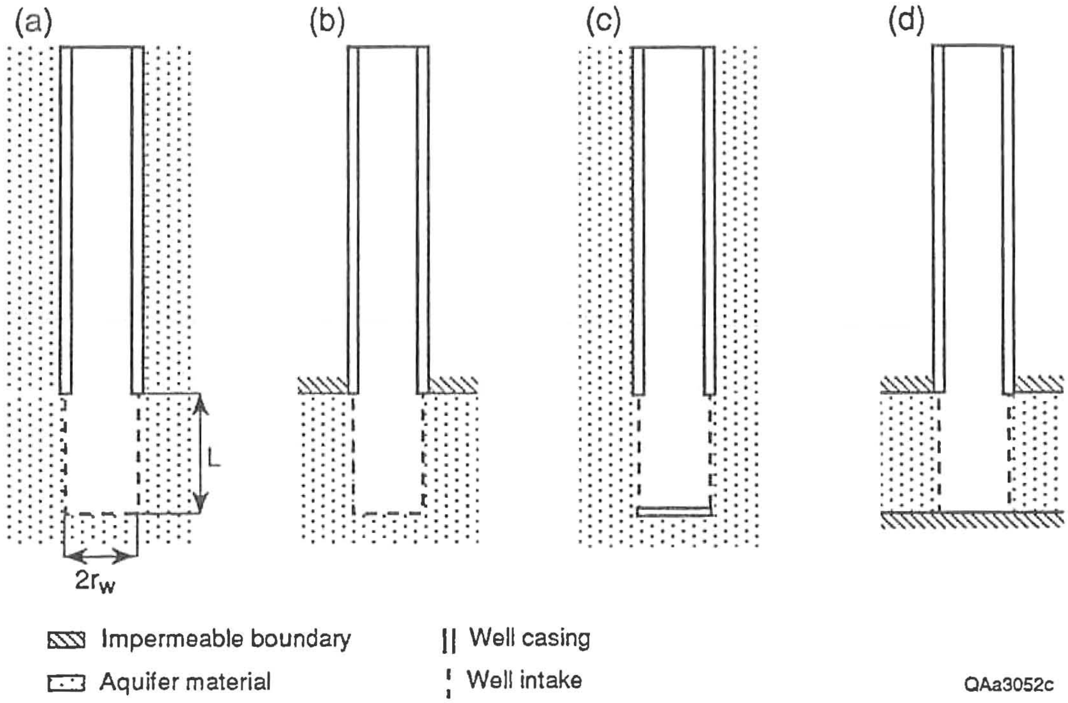

Figure D3. Piezometer geometries and aquifer settings for the slug test analysis methods of (a) Hvorslev (1951) with simplified ellipsoid shape factor (Dachler, 1936) and spherical shape factor (Schneebeli, 1966), (b) Hvorslev (1951) with semi-ellipsoid shape factor (Dachler, 1936), (c) Bouwer and Rice (1976), and (d) Cooper and others (1967).

by Hvorslev, 1951) derived such a shape factor that describes the well intake as a semi-ellipsoid

$$c = \frac{2\pi L}{ln\left(\dfrac{L}{r_w} + \sqrt{1 + \left(\dfrac{L}{r_w}\right)^2}\right)}. \tag{D4}$$

Both of these shape factors are accurate for well geometries where L/r_w >16 and less accurate for 8 <L/r_w <16. For L/r_w < 8, vertical flow components become large and compromise the solution.

Well geometries of large-diameter hand-dug wells commonly have L/r_w values less than 8. Therefore, a shape factor for shallow, large-diameter wells is required. Chapius (1989) reviewed numerically derived shape factors and presented an analytical shape factor by Schneebeli (1966) that approximates the cylindrical well intake with a sphere of equal surface area (fig. D3c)

$$C = 4\pi r_w \left(\frac{L}{2r_w} + \frac{1}{4}\right)^{\frac{1}{2}}. \tag{D5}$$

(Chapius [1989] incorrectly presented Schneebeli's [1966] shape factor. However, Chapius [1989] used the correct equation for all plots and analysis in the paper.) Chapius (1989) concluded that this shape factor gave reasonable results for 0 <L/r_w <16.

Analysis with Bouwer and Rice's (1976) method for interpreting slug tests involved finding the slope of early time recovery for a semi-log plot of recovery against recovery time. This rate and well and aquifer geometries were used to find an effective radius of influence and hydraulic conductivity. If L/r_w << 4 (fig. D3c), flow through the well bottom may be significant enough to compromise the solution. AQTESOLV 1.00 (Duffield and Rumbaugh, 1989), an aquifer test solver for personal computers, was used to analyze test data with the Bouwer and Rice (1976) method.

Analysis with Cooper and others' (1967) method for interpreting slug tests involves using type curves to match recovery data. The match point and well and aquifer geometries were used to find transmissivity. The method assumes a fully penetrating well in a confined aquifer (fig. D3d). AQTESOLV 1.00 (Duffield and Rumbaugh, 1989), was used to analyze test data with the Cooper and others' (1967) method.

For the purpose of analysis, all wells tested in this study were assumed to be fully penetrating and well depth was assumed to represent aquifer thickness.

Results and Discussion

Results of slug test analysis methods (Hvorslev, 1951 [with Dachler's (1936) ellipsoid shape factor]; Cooper et al., 1967; Bouwer and Rice, 1976) compare favorably to results of the finite-difference model and the two numerically derived solutions (Herbert and Kitching, 1981; Barker and Herbert, 1989) over a range of more than 6 orders of magnitude (table D1, fig. D4). Hydraulic conductivities of individual wells, calculated by different methods vary by a factor of 5 to 10. Eleven of the 12 tests lie below the limit of Papadopulos and Cooper's (1967) analytical solution (fig. D5). This limit was determined by solving equation D1 for a pumping period of 1 hr. Figure D5, in conjunction with figure D4, shows that slug test analysis methods can be used to interpret aquifer tests for a large range of well radii and transmissivities over which the analytical solution is not applicable.

There is generally little difference in hydraulic conductivities calculated with Hvorslev's (1951) method using the shape factors of Hvorslev (1951), Dachler (1936), or Schneebeli (1954) for fully penetrating wells (table D1, fig. D6). This suggests that there is little flow into the well bottom and that flow to the well is mostly horizontal. This is a reasonable interpretation given the nature of the strata tested in this study. Thickness of the Austin Chalk weathered section averages 12 ft (3.66 m) and locally is as thick as 45 ft (13.72 m) (Collins and others, 1992). Fracture intensity and hydraulic conductivity of the weathered section decreases rapidly from land surface until less conductive ($10^{-4.24}$ ft/day [$10^{-4.76}$ m/day]), unweathered chalk is reached. This behavior is commonly observed in other fractured aquifers (Davis and Turk, 1964; Rasmuson and Neretnieks, 1986). Since the depths of the hand-dug wells average 22.4 ft (6.83 m), well bottoms are likely completed in unweathered chalk. Therefore, little or no flow would be expected to move through the well bottom. Hand-dug wells in weathered Taylor Marl would also likely be completed in unweathered rock. Many of the wells in

Table D1. Hydraulic conductivity results obtained by various methods.

Well	L/r_w	Hydraulic conductivity, K (in ft/d) Numerical model	50-% method[a]	25-% method[b]	50-% method[b]	Dachler simplified ellipsoid[c]	Dachler semi-ellipsoid[c]	Schneebeli sphere[c]	Slug test[d]	Slug test[e]
144-1	18.32	0.0007	0.01	< 0.01	< 0.01	0.003	0.003	0.003	0.002	0.01
86C-1	8.60	0.0045	0.01	< 0.02	< 0.02	0.012	0.013	0.011	0.007	0.02
R877-13.1	20.00	0.04	0.16	< 0.02	0.02	0.08	0.09	0.09	0.06	0.11
37-2.1	6.21	0.28	0.30	0.11	0.11	0.22	0.25	0.21	0.14	0.40
R877-33	13.35	0.45	0.95	0.85	1.70	0.73	0.79	0.71	0.47	2.57
R664-16	7.64	0.61	1.49	0.28	0.28	1.38	1.53	1.28	0.98	4.43
R877-14	31.05	0.54	3.14	0.82	1.64	1.43	1.49	1.62	0.87	2.14
262A-2.2	3.93	2.56	0.77	3.11	4.92	0.70	0.86	0.68	0.57	5.21
R1446-8	17.11	3.40	3.94	13.97	11.10	6.77	7.30	6.88	2.81	6.03
187A-4	6.28	32.96	12.47	49.90	52.25	15.42	15.41	12.38	8.06	9.22
BEG-37	8.28	53.21	19.30	41.78	52.60	44.57	44.58	37.68	30.90	60.58
R875-4	5.03	114.82	64.16	148.80	470.56	179.06	179.24	141.38	103.28	NA

[a] Herbert and Kitching (1981)

[b] Barker and Herbert (1989)

[c] Hvorslev (1951)

[d] Bouwer and Rice (1976)

[e] Cooper and others (1967)

NA – not analyzable

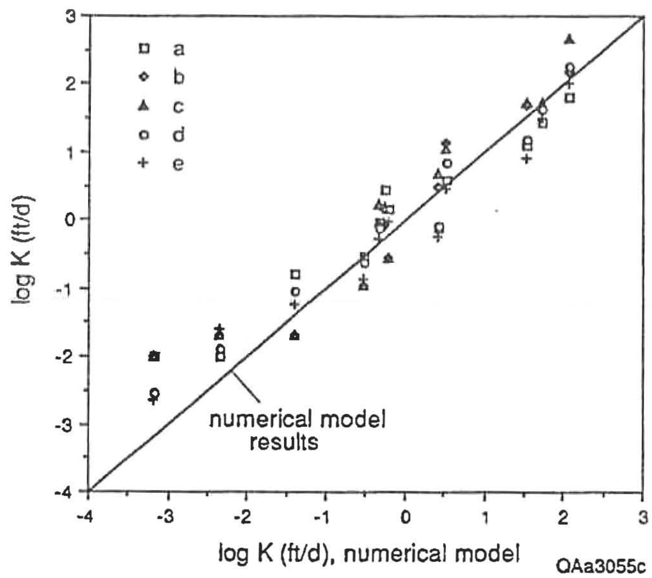

Figure D4. Comparison of hydraulic conductivity (*K*) estimated with the numerical model to hydraulic conductivity calculated with the empirical methods of (a) Herbert and Kitching's (1981) 50-percent method, (b) Barker and Herbert's (1989) 25-percent method, (c) Barker and Herbert's (1989) 50-percent method, and the slug test analysis methods of (d) Hvorslev (1951), (e) Bouwer and Rice (1976), and (f) Cooper and others (1967).

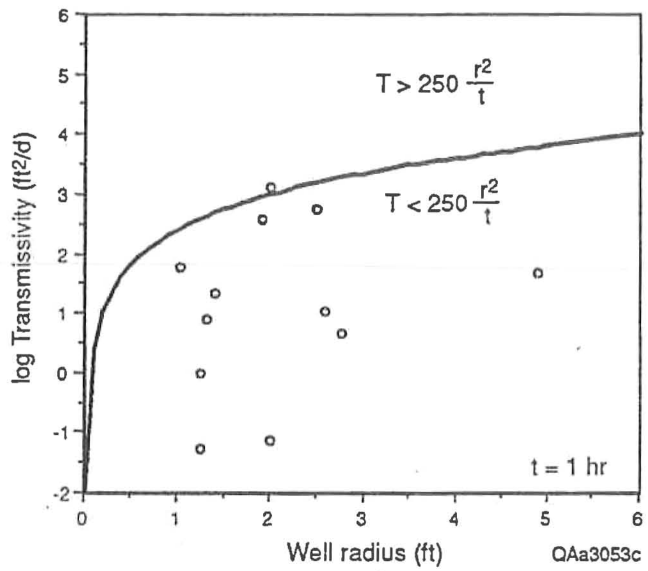

Figure D5. Relation of aquifer-test results shown in figure 4 to the lower limit of applicability of Papadopulos and Cooper's (1967) analytical solution. If a point lies below the curve, it may be possible to use the analytical solution to interpret the aquifer test.

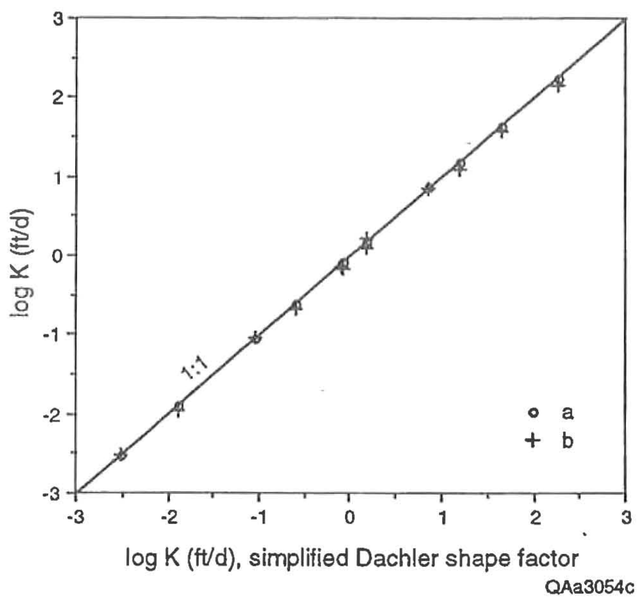

Figure D6. Comparison of hydraulic conductivity calculated using Hvorslev's (1951) method with different shape factors. The plot shows hydraulic conductivity calculated using an ellipsoid shape factor (Dachler, 1936) to hydraulic conductivity using (a) a spherical shape factor (Schneebeli, 1966) and (b) a semi-ellipsoid shape factor (Dachler, 1936).

alluvial deposits in the study area are dug through the entire thickness of the alluvium to unweathered chalk or marl (Wickham and Dutton, 1991; Dutton and Wickham, 1992).

Of the slug test analysis methods, Hvorslev's (1951) method using Schneebeli's (1954) shape factor may give the only reasonable estimate for hydraulic conductivity in a shallow, partially penetrating, large-diameter well. Partial penetration is more likely in deep alluvial deposits or in aquifers of greater thickness.

Slug tests require an instantaneous addition or removal of water. In reality, a finite amount of time is required to add or remove the water. In this study, a pumping duration of 1 hr was used to remove the water. For aquifer tests in which the time of recovery was much longer than the pumping time, a pumping duration of 1 hr was sufficiently "instantaneous" for the slug test analysis methods. However, some ground-water inflow occurred during the pumping period in the more permeable strata. In these cases, only early-time recovery data and the Hvorslev (1951) and Bouwer and Rice (1976) methods were used to calculate hydraulic conductivity. Cooper and others' (1967) method relies on curve matching over the entire recovery period and, therefore, is less reliable when inflow to the well occurs during the pumping period.

The pumping period of 1 hr is based on Herbert and Kitching's (1981) test method with the assumption that well loss is negligible with this pumping period. Herbert and Kitching's (1981) numerically derived solution requires a 1 hr pumping period since the rate of recovery depends upon the duration and rate of pumping (Singh, 1981). Barker and Herbert's (1989) and the slug test analysis methods have no such pumping time requirement. Therefore, shorter pumping times could be used to obtain more accurate results with the slug test analysis methods.

In general, if substantial inflow is observed while a large-diameter well is being pumped, the analytical solution of Papadopulos and Cooper (1967) should be used to interpret the test. However, if this requirement is not met, slug test analysis methods can be used to accurately determine hydraulic conductivity.

CONCLUSION

Slug test analysis methods of Hvorslev (1951), Bouwer and Rice (1976), and Cooper and others (1967) can be used to interpret aquifer tests in large-diameter wells where Papadopulos and Cooper's (1967) analytical solution cannot be applied. The slug test analysis methods compared favorably with numerically derived solutions of Herbert and Kitching (1981) and Barker and Herbert (1989) and to results from an implicit finite-difference numerical model. Hydraulic conductivities calculated with the Hvorslev (1951) method for different shape factors were very similar, indicating that flow to the wells was mostly horizontal. This is a reasonable interpretation because the hand-dug wells tested probably penetrate the total thickness of the weathered zone. However, for a shallow, partially penetrating, large-diameter well, Hvorslev's (1951) method using Schneebeli's (1954) shape factor for $0 < L/r_w < 8$ may give the only reasonable estimate of hydraulic conductivity when using slug test analysis methods.

The aquifer test procedure should involve (1) pumping the well at a constant rate for 1 hr so that total drawdown does not exceed 10 percent of the saturated thickness and (2) recording the recovering water levels. This testing procedure allows wells in confined and unconfined aquifers to be analyzed with the same methods. A 1-hr pumping period is required for Herbert and Kitching's (1981) analysis, but not for the others. Therefore, longer and shorter pumping periods can be used. Early-time recovery should be used for any analysis with the Hvorslev (1951), Bouwer and Rice (1976), and Cooper (1967) slug test analysis methods, especially if there is inflow to the well during the pumping period.

Conventional slug test analysis methods are preferable because numerical modeling can be time-consuming and because numerically derived solutions in the literature may be difficult to re-derive, are poorly documented, and may contain errors. In addition, slug tests are easy to perform and analyze and are familiar to most hydrologists.

REFERENCES

Barker, J. A., 1989, Programs to simulate and analyze pumping tests in large-diameter wells: Wallingford, England, British Geological Survey Technical Report, Hydrogeology Series WD/89/24, 34 p.

Barker, J. A., and Herbert, R., 1989, Nomograms for the analysis of recovery tests on large-diameter wells: Quarterly Journal of Engineering Geology, London, v. 22, p. 151–158.

Bouwer, H., 1989, The Bouwer and Rice slug test-an update: Ground Water, v. 27, p. 304–309.

Bouwer, H., and Rice, R. C., 1976, A slug test for determining hydraulic conductivity of unconfined aquifers with completely or partially penetrating wells: Water Resources Research, v. 12, no. 3, p. 423–428.

Chapius, R. P., 1989, Shape factors for permeability tests in boreholes and piezometers: Ground Water, v. 27, no. 5, p. 647–654.

Collins, E. W., Hovorka, S. D., and Laubach, S. E., 1992, Fracture systems of the Austin Chalk, North-Central Texas, *in* Schmoker, J. W., Coalson, E. B., and Brown, C. A., eds., Geological studies relevant to horizontal drilling: examples from western North America: Rocky Mountain Association of Geologists, p. 75–88.

Cooper, H. H., Jr., Bredehoeft, J. D., and Papadopulos, I. S., 1967, Response of a finite-diameter well to an instantaneous charge of water: Water Resources Research, v. 3, no. 1, p. 263–269.

Dachler, R., 1936, Grundwasserstromung (Flow of Groundwater): Wien, Julius Springer, 141 p.

Davis, S. N., and Turk, L. J., 1964, Optimum depth of wells in crystalline rocks: Ground Water, v. 2, p. 6–11.

Domenico, P. A., and Schwartz, F. W., 1990, Physical and chemical hydrogeology: New York, John Wiley and Sons, 824 p.

Duffield, G. M., and Rumbaugh, J. O., III, 1989, AQTESOLV, Aquifer Test Solver Version 1.00 Documentation: Reston, Virginia, Geraghty and Miller Modeling Group, 134 p.

Dutton, A. R., and Wickham, M. K., 1992, Simulation of ground-water particle paths in a Pleistocene alluvial terrace overlying the Superconducting Super Collider (SSC) site, Texas: GSA Abstracts with Programs, v. 24, no. 1, p. 9.

Fenske, P. R., 1977, Type curves for recovery of a discharging well with storage: Journal of Hydrology, v. 33, p. 341–348.

Freeze, R. A., and Cherry, J. A., 1979, Groundwater: Englewood Cliffs, New Jersey, Prentice-Hall, Inc., 604 p.

Hantush, M. S., 1964, Hydraulics of wells, *in* Chow, V. T., ed., Advances in Hydroscience, 1: New York, Academic Press, p. 281–432.

Herbert, R., and Kitching R., 1981, Determination of aquifer parameters from large-diameter dug well pumping tests: Ground Water, v. 19, p. 593–599.

Hvorslev, M. J., 1951, Time lag and soil permeability in ground-water observations: Vicksburg, Mississippi, U.S. Army Corps of Engineers, 50 p.

Jacob, C. E., 1950, Flow of ground water, *in* Rouse, H., ed., Engineering hydraulics: Proceedings of the fourth Hydraulics Conference, Iowa Institute of Hydraulic Research, June 12–15, 1949, New York, John Wiley, 1039 p.

Papadopulos, I. S., and Cooper, H. H., Jr., 1967, Drawdown in a well of large diameter: Water Resources Research, v. 3, p. 241–244.

Rasmuson, A., and Neretnieks, I., 1986, Radionuclide transport in fast channels in crystalline rock: Water Resources Research, v. 22, no. 8, p. 1247–1256.

Rushton, K. R., and Holt, S. M., 1981, Estimating aquifer parameters for large-diameter wells: Ground Water, v. 19, p. 505–509.

Rushton, K. R., and Redshaw, S. C., 1979, Seepage and groundwater flow: numerical analysis by analog and digital methods: New York, John Wiley, 339 p.

Schneebeli, G., 1966, Hydraulique Souterraine: Eyrolles, Paris, 362 p.

Singh, V. S., 1981, Discussion of "Determination of aquifer parameters from large-diameter hand dug well pumping tests": Ground Water, v. 20, no. 5, p. 616.

Singh, V. S., and Gupta, C. P., 1986, Hydrogeological parameter estimation from pump tests on a large diameter well: Journal of Hydrology, v. 87, p. 223–232.

Theis, C. V., 1935, The relation between the lowering of the piezometric surface and the rate and duration of discharge of a well using ground-water storage: Transactions of the American Geophysical Union, v. 16, p. 519–524.

Wang, H. F., and Anderson, M. P., 1982, Introduction to groundwater modeling; finite difference and finite element methods: San Francisco, W. H. Freeman, 237 p.

Wickham, M. K., and Dutton, A. R., 1991, Hydrogeology and water resources of a Pleistocene alluvial terrace overlying the Superconducting Super Collider (SSC) site, Texas (abs.): Geological Society of America, Abstracts with Programs, v. 23, no. 5, p. A216.

Appendix E. Finite-Difference Modeling of Ground-Water Flow to a Large-Diameter Borehole

Appendix E. Finite-Difference Modeling of Ground-Water Flow to a Large-Diameter Borehole

INTRODUCTION

Numerical modeling of ground-water flow can be a useful tool in interpreting aquifer tests, especially if the system is too complex for existing analytical solutions. In the case of large-diameter wells, borehole storage and nonuniform well radius are complicating factors that a numerical model can easily simulate. In order to facilitate aquifer test interpretation, a block centered, finite-difference radial flow model was developed to simulate ground-water flow to large-diameter wells. The model recognizes horizontal and vertical flow, layering of hydraulic conductivity, nonuniform well radius, and variable pumping rate.

DERIVATION OF THE FINITE DIFFERENCE SOLUTION

Numerous authors have used finite-difference models to describe ground-water flow to wells. Rushton and Redshaw (1979) demonstrated how finite-difference models could be used to simulate radial flow to a well. Herbert and Kitching (1981) and Rushton and Holt (1981) also have considered radial finite-difference models, but specifically for flow to large-diameter wells. The flow equation describing radial flow to a well can be expressed in cylindrical coordinates as

$$\frac{1}{r}\frac{\partial}{\partial r}\left(r\,K(r,z)\,\frac{\partial h}{\partial r}\right) + \frac{\partial}{\partial z}\left(K(r,z)\,\frac{\partial h}{\partial z}\right) = S_s\,\frac{\partial h}{\partial t} + W, \qquad \text{(E1)}$$

where h is the hydraulic head, K is hydraulic conductivity, r is the radial coordinate, z is the vertical coordinate, S_S is specific storage, and W is a source/sink term. A finite-difference grid was assembled by taking a one radian slice of a cylinder around a well and performing a volumetric flow budget on each cell (fig. E1). Darcy's law,

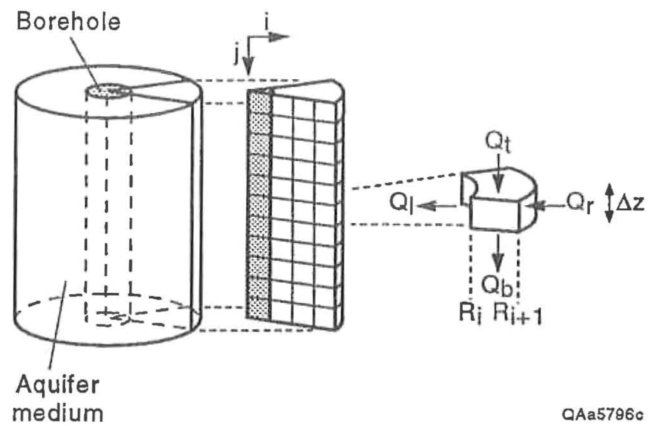

Figure E1. Construction of the radial finite-difference grid.

$$Q = -KA\frac{\partial h}{\partial L} \tag{E2}$$

where Q is volumetric flow rate and L is distance, was used to quantify flow for each side of the cell in the r and z directions.

Flow into the element through the top at time t is

$$Q_t = K_v\left[\frac{r_i^2+1 - r_i^2}{2}\right]\left[\frac{\left(h_{i,j+1}^t - h_{i,j}^t\right)}{Dz}\right], \tag{E3}$$

where K_v is vertical hydraulic conductivity, r_i is the radius to inside of cell i, r_{i+1} is the radius to outside of cell i, $h_{i,j}$ is head in cell i, j, and Δz is layer thickness.

Likewise, flow out through the bottom at time t is

$$Q_b = K_v\left[\frac{r_i^2+1 - r_i^2}{2}\right]\left[\frac{\left(h_{i,j}^t - h_{i,j-1}^t\right)}{\Delta z}\right]. \tag{E4}$$

Flow through the right-hand face of the element at time t is

$$Q_r = K_h \left[r_i \Delta z \right] \left[\frac{\left(h^t_{i+1,j} - h^t_{i,j} \right)}{\Delta r} \right], \qquad \text{(E5)}$$

where K_h is horizontal hydraulic conductivity and Δr is radial spacing, while flow through the left-hand face at time t is

$$Q_l = K_h \left[r_i \Delta z \right] \left[\frac{\left(h^t_{i,j} - h^t_{i-1,j} \right)}{\Delta r} \right]. \qquad \text{(E6)}$$

By equating flow in and out of the cell to

$$S_s \Delta z \frac{\left(r^2_{i+1} - r^2_i \right)}{2} \left[\frac{\left(h^{t+1}_{i,j} - h^t_{i,j} \right)}{\Delta t} \right], \qquad \text{(E7)}$$

which represents a change in water storage in the aquifer, a water budget is obtained.

By solving for h^{t+1}, the drawdowns at time t+1 can be determined from the drawdowns at time t

$$h^{t+1}_{i,j} = h^t_{i,j} + \frac{\Delta t}{S_s \Delta z} \frac{2}{\left(r^2_{i+1} - r^2_i \right)} \left(Q_t - Q_b + Q_r - Q_l \right) \qquad \text{(E8)}$$

and the explicit finite-difference equation for transient ground-water flow is derived.

Boundary conditions must be specified in order to simulate flow to a well. The top, bottom, and inner sides of the model are no-flow boundaries in which water is not allowed to enter or exit the model. The outer side is a constant head boundary in which the water level remains constant. The well face is treated as a specified head boundary whose position is determined by pumping and ground-water inflow rates. Pumping is simulated by decreasing the head in the borehole cells according to well radius and pumping rate. With each iteration, the total flow across the well face is calculated, computed into a head change based on well radius, and added to the head in the well.

In order to ensure that the numerical model converges to a correct solution, small time steps are used during the simulation, the magnitude of which depends on well geometry and aquifer parameters (Rushton and Redshaw, 1979):

$$\Delta t = \frac{0.025\, r_w^2\, S}{T}. \tag{E9}$$

USE OF PROGRAM

The finite-difference model has been programmed to allow the user to represent a large array of formations and well construction. The model allows the user to define layer thickness and radial distances and to input different horizontal and vertical hydrological properties for each layer. The user can also define variable borehole geometry. Changes in pumping rate are read from a separate file. The Fortran code is presented at the conclusion of this section in addendum E1.

To use the code, the user first assigns the appropriate hydrologic, well, and test parameters in a formatted input file (addendum E2) according to layer and radial column (fig. E2). In order to use the variable pumping capability, the pumping rate should be chosen as "9999." for the input file. This flags the program to use a formatted pumping rate input file (addendum E3). An output file of input parameters and time versus drawdown is created.

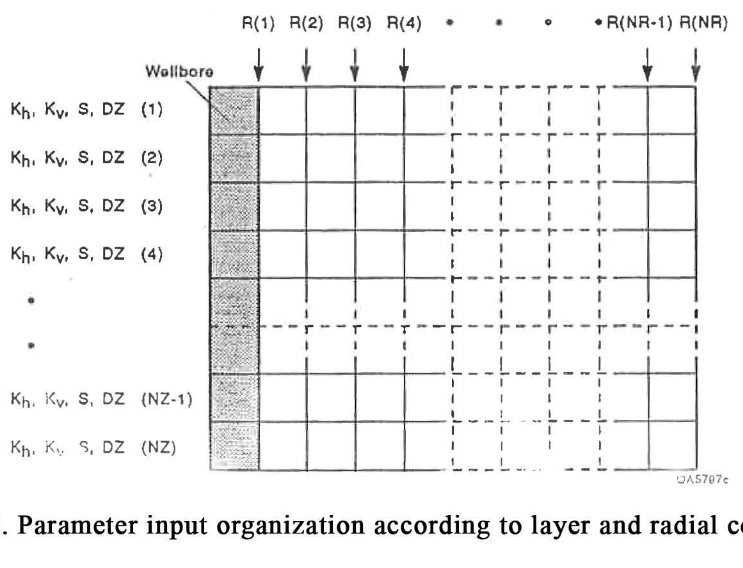

Figure E2. Parameter input organization according to layer and radial column.

As with any modeling care must be taken that boundary effects, cell widths and heights, and time step size do not affect the solution. To establish if the constant head boundary is far enough away from the wellbore, the difference between the head at the boundary and the head in the adjacent cell is reported at the end of the pumping period. If this number is large, then more radial nodes or a reconfiguration of the model should be considered. This boundary effect will lead to an underestimation of the drawdown and recovery and bias results. Experimentation with different cell widths and heights can reveal the sensitivity of the solution to the physical dimensions of the cells. The smaller the cell dimensions, the more accurately the model will predict drawdown and recovery. The magnitude of the time step can also affect the result. Selecting smaller time steps until the differences between solutions are small will ensure the most accurate model.

The model was validated by comparing results from the finite-difference model to results from a numerical solution of Papadopulos and Cooper's (1967) analytical solution (Barker, 1989). For a casing radius of 1.0 ft (0.305 m), uniform well radius of 1.0 ft (0.305 m), pumping rate of 50 ft^3/hr (1.416 m^3/hr), pumping time of 0.5 hr, storage coefficient of 0.003, and a transmissivity of 0.5 ft/hr (0.15 m/hr), the finite-difference model compared favorably to Papadopulos and Cooper's (1967) analytical solution (fig. E3). A grid of 80 radial nodes, 0.5-ft wide by 1.0-ft (.305-m) thick was used in the finite-difference model. A slight difference is observed, which is probably due to cell size in the finite-difference model.

REFERENCES

Barker, J. A., 1989, Programs to simulate and analyze pumping tests in large-diameter wells: Wallingford, England, British Geological Survey Technical Report, Hydrogeology Series WD/89/24, 34 p.

Herbert, R., and Kitching, R., 1981, Determination of aquifer parameters from large-diameter dug well pumping tests: Ground Water, v. 19, p. 593–599.

Papadopulos, I. S., and Cooper, H. H., Jr., 1967, Drawdown in a well of large diameter: Water Resources Research, v. 3, p. 241–244.

Rushton, K. R., and Holt, S. M., 1981, Estimating aquifer parameters for large-diameter wells: Ground Water, v. 19, p. 505–509.

Rushton, K. R., and Redshaw, S. C., 1979, Seepage and groundwater flow: New York, John Wiley and Sons, 339 p.

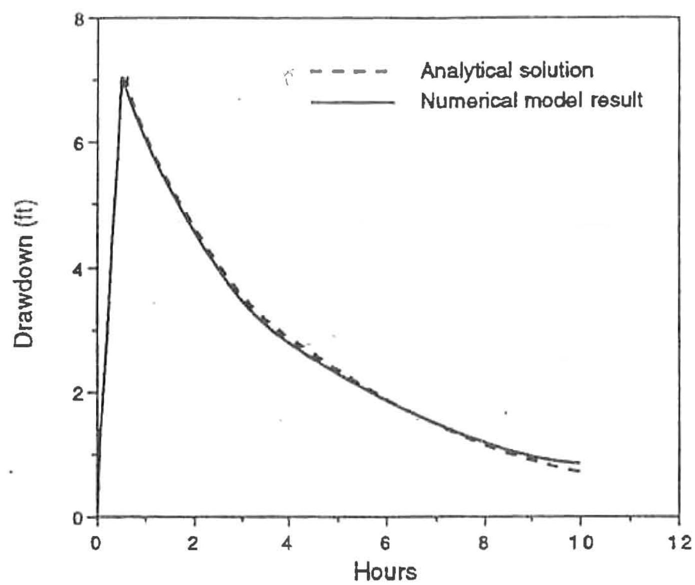

Figure E3. Comparison of the finite-difference model results to output from Barker's simulator.

Addendum E1. Source code for dug well model.

```
c-------------------------------------------------------------
c     FLOW TO A DUG WELL, FINITE-DIFFERENCE SIMULATOR.
c-------------------------------------------------------------

c     finite-difference model
c     can consider variable well geometry and
c     variable pumping rate.

c     Robert E. Mace
c     Bureau of Economic Geology
c     9/16/92

c-------------------------------------------------------------

        REAL inflow,WR
        INTEGER cell(30,30),numq,B
        REAL      Hold(30,30),Hnew(30,30),DZ(30),Kh(30),
     1             Kv(30),S(30),Qrate(100),Qtime(100),interval1,
     1             interval2,multiplier,R(30),DR,DZc,BE
        CHARACTER*50 input1,input2,output1,str,name

c     establish file names
        input1 = 'input.in'
        input2 = 'qrate.in'
        output1= 'output.out'

        OPEN(UNIT=40,FILE=output1,STATUS='UNKNOWN')
        OPEN(UNIT=30,FILE=input1,STATUS='UNKNOWN')
        OPEN(UNIT=20,FILE=input2,STATUS='UNKNOWN')

c     read in simulation name
        WRITE(40,*)'==========================================='
        WRITE(40,*)
        READ(30,'(A)')name
        WRITE(*,'(A)')name
        WRITE(40,'(A)')name
        WRITE(40,*)
        WRITE(40,*)'==========================================='

c     read in well parameter
        READ(30,1000) WR
        WRITE(*,*)'casing radius: ',WR
        WRITE(40,1008)WR
        WRITE(40,*)'-------------------------------------------'

c     read in test parameters
        READ(30,1001)Q,Tpump,Ttest,interval1,interval2
        WRITE(*,*)'         Q      Tpump      Ttest interval1 interval2'
        WRITE(*,1001)Q,Tpump,Ttest,interval1,interval2
        WRITE(40,*)'         Q      Tpump      Ttest interval1 interval2'
```

```
      WRITE(40,*)'--------------------------------------------------'
      WRITE(40,1001)Q,Tpump,Ttest,interval1,interval2
      WRITE(40,*)'--------------------------------------------------'
      multiplier = interval1
      QQ = Q
      Q = Q/(3.1415*WR*WR)

c     read in simulation parameters
      READ(30,1002)DT,Nend,Ho
      WRITE(*,*)'        DT       Nend         Ho'
      WRITE(*,1002)DT,Nend,Ho
      WRITE(40,*)'        DT       Nend         Ho'
      WRITE(40,*)'--------------------------------------------------'
      WRITE(40,1002)DT,Nend,Ho
      WRITE(40,*)'--------------------------------------------------'

c     read in aquifer parameters
      READ(30,1003)NZ,NR
      NZ = NZ + 2
      NR = NR + 2
      WRITE(*,*)'num   DZ(i)      Kh(i)      Kv(i)       S(i)'
      WRITE(40,*)'num   DZ(i)      Kh(i)      Kv(i)       S(i)'
      WRITE(40,*)'--------------------------------------------------'
      DO 5 i = 2,NZ-1
        READ(30,1004)num,DZ(i),Kh(i),Kv(i),S(i)
        WRITE(*,1004)num,DZ(i),Kh(i),Kv(i),S(i)
5       WRITE(40,1004)num,DZ(i),Kh(i),Kv(i),S(i)
      WRITE(40,*)'--------------------------------------------------'
      DZ(1) = DZ(2)
      DZ(NZ)= DZ(NZ-1)

c     read in cell radii
      WRITE(*,*)'cell radii:'
      WRITE(*,*)'--------------------------------------------------'
      WRITE(40,*)'cell radii:'
      WRITE(40,*)'--------------------------------------------------'
      R(1) = 0.0
      R(2) = 0.0
      DO 9 i = 3,NR
        READ(30,1009)num,R(i)
        WRITE(*,1009)num,R(i)
9       WRITE(40,1009)num,R(i)
      R(NR+1) = R(NR)+(R(NR)-R(NR-1))
      WRITE(40,*)'--------------------------------------------------'

c     read in cell parameters
      READ(30,'(A)')str
      WRITE(*,*)'cell assignment:'
      WRITE(40,*)'cell assignment:'
      WRITE(*,*)' format used: ',str
      WRITE(40,*)' format used: ',str
      WRITE(40,*)'--------------------------------------------------'
      DO 6 j = 1,NZ
        READ(30,str) (cell(i,j),i=1,NR)
        WRITE(*,str) (cell(i,j),i=1,NR)
6       WRITE(40,str) (cell(i,j),i=1,NR)
```

```
      WRITE(40,*)'-----------------------------------------------------'

c     read in variable pumping rates

      IF (QQ.eq.9999.) THEN
        READ(30,'(A)')name
        WRITE(*,'(A)')name
        WRITE(40,'(A)')name
        READ(20,1005)numq
        WRITE(40,*)'------------------------'
        WRITE(*,*)'     Qtime      Qrate'
        WRITE(*,*)'------------------------'
        WRITE(40,*)'     Qtime      Qrate'
        WRITE(40,*)'------------------------'
        DO 7 j = 1,numq
          READ(20,1006)Qtime(j),Qrate(j)
          WRITE(*,1006)Qtime(j),Qrate(j)
          WRITE(40,1006)Qtime(j),Qrate(j)
7         Qrate(j) = Qrate(j)/(3.1415*WR*WR)
        m = 2
        Q = Qrate(m-1)
      END IF

      WRITE(*,*)
      WRITE(40,*)
      WRITE(*,*)'       drawdown              time'
      WRITE(*,*)'------------------------------------'
      WRITE(40,*)'-----------------------------------------------------'
      WRITE(40,*)'       drawdown              time'
      WRITE(40,*)'------------------------------------'

c     set initial head values to pre-test values

      DO 10 i=1,NZ
        DO 10 j=1,NR
          Hold(j,i) = Ho
          Hnew(j,i) = Ho
10    CONTINUE

      Hwell = Ho

      Time = DT

cooooooooooooooooooooooooooooooooooooooooooooooooooooooooooooooo
c                      program start
cooooooooooooooooooooooooooooooooooooooooooooooooooooooooooooooo

c     start computing heads throught time
c---------------------------------------------------------------

      tupper = interval1
      p = 1.
      B = 1

      DO 50 n=1,Nend
```

```
c     calculate head in borehole
c-------------------------------------------------------------

          inflow = 0.
          DO 20 j = 2,NZ-1
            DO 25 i = 2,NR-1
              IF (cell(i,j).eq.1) GOTO 25
            IF (cell(i,j).eq.2) GOTO 25
              IF (cell(i+1,j).eq.1) THEN
              DR = (R(i+2)-R(i))/2
                flow = Kh(j)*DZ(j)*R(i+1)*(Hold(i+1,j)-
     1                   Hold(i,j))/DR
              flow = flow/(0.5*WR*WR)
                inflow = inflow + flow
            END IF
              IF (cell(i,j-1).eq.1) THEN
              DZc = (DZ(j-1)+DZ(j))/2
              flow = Kv(j)*(R(i+1)**2.-R(i)**2.)/(2.*DZc)*
     1                   (Hold(i,j-1)-Hold(i,j))
              flow = flow/(0.5*WR*WR)
              inflow = inflow + flow
            END IF
            IF (cell(i,j+1).eq.1) THEN
              DXc = (DZ(j+1)+DZ(j))/2
              flow = -Kv(j)*(R(i+1)**2.-R(i)**2.)/(2.*DZc)*
     1                   (Hold(i,j)-Hold(i,j+1))
              flow = flow/(0.5*WR*WR)
              inflow = inflow + flow
            END IF
25        CONTINUE
20        CONTINUE

c     determine pumping rate status
c-------------------------------------------------------------

          IF (Time.ge.Tpump) Q = 0.0
          IF (Time.ge.Tpump.and.B.eq.1) then
            BE = Hold(2,NR)-Hold(2,NR-1)
            WRITE(*,1010) BE
            B = 2
          END IF
          IF (Time.ge.Tpump) GOTO 8

          IF (QQ.eq.9999.) THEN
            IF (Time.ge.Qtime(m)) THEN
              Q = Qrate(m)
              m = m+1
            END IF
          END IF

8         Hwell = Hwell-Q*DT+inflow*DT

c     print data to output file
c-------------------------------------------------------------

        IF (Time.gt.tupper) THEN
```

```
            write(*,1007)Ho-Hwell,Time
            write(40,1007)Ho-Hwell,Time
          p = p+1
          IF(Time.gt.Tpump) THEN
                multiplier = interval2
            g = 1
            IF (g.eq.1) THEN
              p = tupper/interval2 + 1
              g = 2
            END IF
          END IF
            tupper = (p)*multiplier
      END IF

c     set head in well equal to new value
c--------------------------------------------------------------

        DO 21 j = 2,NZ-1
          DO 21 i = 2,NR-1
21          IF (cell(i,j).eq.0) Hold(i,j) = Hwell

c     calculate new heads
c--------------------------------------------------------------

        DO 55 j = 2,(NZ-1)
          DO 55 i = 2,(NR-1)
          IF (cell(i,j).eq.0) GOTO 55
            A = (R(i+1)**2.-R(i)**2.)/2.
            F1 = DT/(S(j)*DZ(j)*A)

          V1 = (Hold(i,j-1)-Hold(i,j))/((DZ(j)+DZ(j-1))/2)
          V2 = (Hold(i,j+1)-Hold(i,j))/((DZ(j)+DZ(j+1))/2)
          H1 = R(i+1)*(Hold(i+1,j)-Hold(i,j))/((R(i+2)-R(i))/2)
          H2 = R(i)*(Hold(i,j)-Hold(i-1,j))/((R(i+1)-R(i-1))/2)

            D2H = (Kv(j)*A)*(V1+V2)+(Kh(j)*DZ(j))*(H1-H2)
          Hnew(i,j) = Hold(i,j)+(F1*D2H)

55      CONTINUE

        DO 60 i = 2,NR-1
          DO 60 j = 2,NZ-1
          IF (cell(i,j).eq.0) GOTO 60
          Hold(i,j)=Hnew(i,j)
          Hold(i,1)=Hold(i,2)
            Hold(i,NZ)=Hold(i,NZ-1)
          Hold(1,j)=Hold(2,j)
60      CONTINUE

c     increment time
c--------------------------------------------------------------

        DT = DT*1.
        Time = Time+DT
        IF(Time.ge.Ttest) GOTO 90
```

```
50      CONTINUE

c     formats
c--------------------------------------------------------------


1000    FORMAT(F10.2)
1001    FORMAT(F10.2,F10.4,F10.2,2F10.4)
1002    FORMAT(F10.4,I10,F10.2)
1003    FORMAT(2I10)
1004    FORMAT(I3,F7.2,3E10.2)
1005    FORMAT(I10)
1006    FORMAT(F10.4,F10.2)
1007    FORMAT(2F15.4)
1008    FORMAT('  casing radius: ',F10.2)
1009    FORMAT(I3,F10.2)
1010    FORMAT(' DRAWDOWN AT BOUNDARY IS: ',F7.2)

c     end of program
c--------------------------------------------------------------

90      STOP
        END
```

Addendum E2. Format and example of main input file.

FORMAT OF MAIN INPUT FILE

1.	Data:	Heading				
	Format:	50A				
2.	Data:	R_c				
	Format:	F10.2				
3.	Data:	Q	T_p	T_t	int1	int2
	Format:	F10.2	F10.4	F10.2	F10.4	F10.4
4.	Data:	DT	Nend	H_o		
	Format:	F10.5	I10	F10.2		
5.	Data:	lays	cols			
	Format:	I10	I10			
6.	Data:	row no	Dz	Kh	Kv	S
	Format:	I3	F7.2	E10.2	E10.2	E10.2
		(For each layer in model)				
7.	Data:	rad no	radius			
	Format:	I3	F10.2			
		(For each radial node)				
8.	Data:	cell input format				
	Format:	A50				
9.	Data:	cell assignment values				
	Format:	(format input at part 8)				

Heading	=	simulation title printed to the output file
R_c	=	well casing radius in which water levels are changing
Q	=	constant pumping rate. If not constant, '9999.' is used to indicate the variable pumping rate file should be used
T_p	=	time of pumping
T_t	=	length of test, including recovery phase
int1	=	time increment by which head values will be printed to the output file during the abstraction phase
int2	=	time increment by which head values will be printed to the output file during the recovery phase
DT	=	time step for the simulation
Nend	=	number of iterations allowed for model execution
H_o	=	initial head in the aquifer
lays	=	number of layers in the model
cols	=	number of radial columns in the model
row no	=	row number
Dz	=	layer thickness

Kh	=	horizontal permeability
Kv	=	vertical permeability
S	=	storage coefficient
rad no	=	radial node number
radius	=	outer radius of the node

EXAMPLE OF MAIN INPUT FILE

```
  test 1                                                      - simulation name
      1.00                                                    - casing radius
     67.00      0.1400      0.50      0.0010      0.0010      - Q,Tp,Tt,int1,int2
   0.00001      500000     10.00                              - DT,Nend,Ho
        10          25                                        - no rows, no columns
  1   1.00        5.00      1.00  3.00E-03                    - row no,DZ,Kh,Kv,S
  2   1.00        5.00      1.00  3.00E-03                    - row no,DZ,Kh,Kv,S
  3   1.00        5.00      1.00  3.00E-03                    - row no,DZ,Kh,Kv,S
  4   1.00        5.00      1.00  3.00E-03                    - row no,DZ,Kh,Kv,S
  5   1.00        5.00      1.00  3.00E-03                    - row no,DZ,Kh,Kv,S
  6   1.00        5.00      1.00  3.00E-03                    - row no,DZ,Kh,Kv,S
  7   1.00        5.00      1.00  3.00E-03                    - row no,DZ,Kh,Kv,S
  8   1.00        5.00      1.00  3.00E-03                    - row no,DZ,Kh,Kv,S
  9   1.00        5.00      1.00  3.00E-03                    - row no,DZ,Kh,Kv,S
 10   1.00        5.00      1.00  3.00E-03                    - row no,DZ,Kh,Kv,S
  1      1.00                                                 - outer radii input
  2      2.00
  3      3.00
  4      4.00
  5      5.00
  6      6.00
  7      7.00
  8      8.00
  9      9.00
 10     10.00
 11     11.00
 12     12.00
 13     14.40
 14     17.28
 15     20.74
 16     24.88
 17     29.86
 18     35.83
 19     42.99
 20     51.59
 21     61.92
 22     74.30
 23     89.16
 24    106.99
 25    128.39
(27I2)                                                        - cell input format
 2 2 2 2 2 2 2 2 2 2 2 2 2 2 2 2 2 2 2 2 2 2 2 2 2 2 3
 2 0 1 1 1 1 1 1 1 1 1 1 1 1 1 1 1 1 1 1 1 1 1 1 1 1 3
 2 0 1 1 1 1 1 1 1 1 1 1 1 1 1 1 1 1 1 1 1 1 1 1 1 1 3
 2 0 1 1 1 1 1 1 1 1 1 1 1 1 1 1 1 1 1 1 1 1 1 1 1 1 3
 2 0 1 1 1 1 1 1 1 1 1 1 1 1 1 1 1 1 1 1 1 1 1 1 1 1 3
 2 0 0 1 1 1 1 1 1 1 1 1 1 1 1 1 1 1 1 1 1 1 1 1 1 1 3
 2 0 0 0 1 1 1 1 1 1 1 1 1 1 1 1 1 1 1 1 1 1 1 1 1 1 3
 2 0 0 0 0 1 1 1 1 1 1 1 1 1 1 1 1 1 1 1 1 1 1 1 1 1 3
```

```
2 0 0 0 0 1 1 1 1 1 1 1 1 1 1 1 1 1 1 1 1 1 1 1 1 1 3
2 0 0 0 0 1 1 1 1 1 1 1 1 1 1 1 1 1 1 1 1 1 1 1 1 1 3
2 0 0 0 0 1 1 1 1 1 1 1 1 1 1 1 1 1 1 1 1 1 1 1 1 1 3
2 2 2 2 2 2 2 2 2 2 2 2 2 2 2 2 2 2 2 2 2 2 2 2 2 2 3
```

Addendum E3. Format and example of variable pumping rate input file.

FORMAT OF VARIABLE PUMPING RATE INPUT FILE

1.	Data:	Heading	
	Format:	50A	
2.	Data:	num	
	Format:	I10	
3.	Data:	time	Q
	Format:	F10.4	F10.2
		(for each pumping episode)	

Heading	=	simulation title
num	=	number of pumping episodes
time	=	time a new pumping episode begins
Q	=	pumping rate for the episode

EXAMPLE OF VARIABLE PUMPING RATE INPUT FILE

```
test 1
        10
    0.0001     10.00
    0.0002     15.00
    0.0003     20.00
    0.0004     25.00
    0.0005     30.00
    0.0006     35.00
    0.0007     40.00
```

Appendix F. Abandonment of Hand-Dug Wells: A Case Study in Ellis County, Texas

Appendix E. Abandonment of Hand-Dug Wells:
A Case Study in Ellis County, Texas

ABSTRACT

Wells dug by hand that supply water to homes and villages can be found all over the world. Although many are still in use, others have been abandoned, especially in developed countries. An extensive well inventory in Ellis County, Texas, showed that of more than 811 hand-dug wells found on farms and at homes or former homesites, only 10 percent are still in use. These are generally in good condition, although most do not meet the published requirements of a safe shallow-water supply. The unused wells range in disrepair, typically having open tops and failing well crowns. Many have been used as receptacles for discarded bricks, wire, household trash, and other debris. Leachate from trash in these wells has likely caused local contamination of surficial ground waters.

INTRODUCTION

Wells that were dug by hand can be found all over the world and are, or have been, used to supply potable water to households or even small villages. According to the National Ground Water Information Center, the United States alone has more than 1.6 million hand-dug wells which can often be located by their brick well crowns (fig. F1). Many developed countries have abandoned hand-dug wells in favor of wells that can tap ground water from deeper aquifers or treated surface water. Many of these abandoned wells have been improperly sealed and have therefore become a safety concern. Open well bores are not only a physical hazard but also a potential pathway of shallow-ground-water contamination.

Figure F1. Brick well crown of a hand-dug well in Ellis County, Texas.

An intensive well inventory was undertaken in North-Central Texas as part of a hydrogeologic characterization of the site of the Superconducting Super Collider, which was designed as a state-of-the-art particle accelerator. Results from this survey showed that most hand-dug wells in the area were abandoned and remain improperly sealed and uncovered. Wellhead conditions have created a public hazard to people and livestock. Because many well owners have filled their wells with debris and household garbage, leachate from these wells may locally contaminate shallow ground water and nearby springs or streams.

HISTORICAL BACKGROUND

Water is necessary to human existence; thus, even during prehistory, human activity centered around streams, springs, and other sources of fresh water. Before long, however, humans discovered that ground water could be obtained by digging at an appropriate location. Perhaps they learned this by observing animals such as the coyote digging in dry stream beds to find water (Meinzer, 1934).

Whereas evidence of the earliest hand-dug wells can be found in Mesopotamia from 6000 B.C. (Miller, 1982), the oldest known well existing today is located in Pakistan and is dated at 3000 B.C. (Bromehead, 1942). Many early wells were shallow, probably extending no more than 9.84 ft (3 m) into unconsolidated material, but some wells were sunk farther into the ground to reach a deeper water source. One impressive excavation is Joseph's well near Cairo, Egypt (Johnson, 1966). Dug into solid rock, the well is nearly 300 ft (91.5 m) 32.14 ft (9.8 m) across and 108.9 ft (33.2 m) deep. Another large well is located in Greensburg, Nebraska. Dug in the 1880's, this well is 32.14 ft (9.8 m) across and 108.9 ft (33.2 m) deep (Zwingle, 1993).

Because many wells were dug in unconsolidated materials such as glacial or alluvial deposits, hand tools were all that were required, although casing needed to be placed carefully to prevent well collapse and personal injury, especially in wells of great depth (Watt and Wood, 1976; DHV, 1979). Well digging in consolidated rock such as granite, basalt, or limestone presented a more laborious challenge in removing material and was likely attempted only after the development of metal tools. Hammers and wedges were traditionally used to sink wells into hard rock. Another method involved building a fire on the rock surface and then dousing the area with cold water, which caused the rock to craze in response to the abrupt temperature change (Watt and Wood, 1976; Hardcastle, 1987). Explosives offered an easier method of breaking up the rock. More recently, compressed-air tools such as jackhammers and specially designed augers have been used to sink large-diameter, shallow wells into consolidated rock.

Dug wells are typically 3.0 to 0 4.25 ft (0.9 to 1.3 m) in diameter, large enough to accommodate one or two people digging. Wells in hard rock commonly have larger diameters for storage. For instance, wells dug in crystalline rock in India have diameters as great as 32.8 ft (10 m). These wells collect and store rain water during the dry season and serve as production wells during the wet season (Watt and Wood, 1976). Large-diameter wells provide useful ground-water storage from low-permeability aquifers.

Dug wells in shallow aquifers are typically sunk during the dry season. During this time, because water levels are at a lowstand, well diggers need not worry about ground-water inflow. If pumps are available, however, they are used to lower water levels to accommodate the well diggers. These wells can be deepened if they go dry at a later date.

Even in early times, people realized wells needed to be maintained properly to ensure a safe water supply. For instance, covered wells are reported in the Bible, and wells constructed in early Arabia, Britain, Finland, and the Orient show evidence of wellhead protection (Hardcastle, 1987). In modern times, many authors and agencies have addressed dug-well placement, construction, servicing, and destruction (for example, Todd, 1959; Texas State Department of Health, 1970; U.S. Environmental Protection Agency, 1975). However, little public education, enforcement, or incentive ensures compliance with safe well design, upkeep, or destruction.

The first wells in North America were hand dug by Native Americans. In the western and southwestern United States, wells and cisterns constructed by Native Americans are located in

Utah, Colorado, Arizona, New Mexico, and Texas (Toulouse, 1945; Evans, 1951; Wheat, 1952; Crown, 1987). Native Americans dug numerous wells at Mustang Springs north of Midland, Texas, during a long drought around 4600 B.C. (Meltzer, 1991).

Most hand-dug wells in the United States were constructed after European settlers came to North America, however. As settlement moved west, wells were dug at new towns and homesteads to supply water to households and livestock. Major settlement began in Ellis County, Texas, around 1839 after the Native American population had been forcibly driven from the area (Jurney, personal communication, 1992). Initial settlement centered about the Red Oak Creek area near present-day Ovilla, Texas, and later spread to the mesquite-covered prairie near the Trinity River and Chambers and Richland Creeks. In the 1850's, settlement spread to springs near the present towns of Bethel, Boz, and Maypearl. Settlement slowed during the Civil War but grew quickly after the war, the landscape becoming dotted by farms. Because neither springs nor surface water could provide a convenient water supply to farmers who settled on upland prairies, wells were dug in limestone and alluvium. Many of the dug wells in the area date from 1850 to 1930 (Jurney, personal communication, 1992).

After the 1930's, deeper wells were more commonly drilled into regional sandstone aquifers at depths of 820 to 1,968 ft (250 to 600 m) below ground surface. Then, as water-supply districts expanded into rural areas, dug wells became less important as sources of potable water. Large-diameter shallow wells, however, have been used in Ellis County since 1930. Many have been recently constructed by means of homemade 3-ft- (0.91-m-) diameter mechanical augers.

Construction of a Hand-Dug Well in Ellis County

David C. Paul (b. 191?) grew up in Ellis County and worked on his father's farm, which currently lies on the west campus of the SSC. His unpublished memoirs include a detailed description of using pick and powder to sink a well in the Austin Chalk during the fall of 1939 or 1940. Pick, shovel, auger, windlass, black blasting powder, and fuse were the main tools used in constructing the well. The initial well location was decided by means of a water witch and a divining rod, but after digging approximately 20 ft (~6 m) and not reaching water, Paul's father arbitrarily decided on the well's present location. Well sinking consisted of five stages: (1) digging through the soil horizon, (2) breaking through the highly weathered zone, (3) blasting through the consolidated rock, (4) constructing the well curb and pump platform, and (5) placing the pump.

A pick and shovel were used to clear the soil from the well site. The ground was loosened in a 5-ft- (1.5-m-) diameter circle and removed until weathered chalk was reached. The chalk could be removed using a pick and shovel, too, although it took more effort. About 3 ft (1 m) into the ground, solid rock was encountered. At this point, the well radius was reduced about 0.3 ft (0.1 m) to provide a ledge on which to rest the well curb.

Paul and his uncle used blasting powder to remove the solid rock:

> To set off an effective charge, I drilled a hole in the solid rock about eighteen inches deep, frequently removing the auger from the hole so as to keep the hole clear of rock debris. This augering required about twenty to thirty minutes of very hard work. When I reached the desired depth, Uncle Roy sent down the powder, some fuse, and some newspaper. I used about one and one half cupfuls of powder. First I poured about half or less of the powder in the hole I had drilled, and then I inserted the end of a two foot section of fuse, poured in the remaining powder and stuffed in a wad of newspaper. Then with an iron bar, I tamped rock dust and debris in around the fuse a little bit at a time until it was full. The wad of newspaper was to keep the powder from being mixed with the rock dust and debris. Tamping in the debris was to confine the blast to the rock mass rather than have it blow out through the hole I had drilled with the auger.

Charges were placed in the floor near the wall. Paul's uncle lifted him from the well bore via rope and bucket and retreated a safe distance. After blasting, rock dust and powder smoke needed to be removed from the well cavity, which was accomplished by means of wagon sheets:

> By common sense we knew better than to go back down into the well while the rock dust and powder smoke were still present. It would linger for a long time unless we forced it out. We had an ingenious way of getting it out. We held a wagon sheet down into the well. This sheet was about fourteen by six feet, and after the well got deeper we fastened two of them together end to end. We held it so that three or four feet of it was above ground. We turned the side of it to the wind, and if there was even as much as a slight zephyr, this technique cleared the well of bad air in no time at all.

Rock debris was cleared and another charge placed and detonated. Paul recalls blasting and digging into the chalk 1.5 to 2 ft (0.5 to 1.0 m) per day. The rope and rock bucket were used as a plumb to ensure that the well shaft sank linearly.

Paul and his uncle stopped digging without reaching water and felt great disappointment after such an exertion:

> This was an emotion producing occasion—as if we had had a chance to get water and missed it through no fault of our own. There was a loss of hope and expectation. Why go on digging? Why not call the whole thing off? We continued to dig for a day or two more. Maybe we would yet find water. Finally, at a depth of twenty-seven or thirty feet, we quit. I never went down to the bottom of that well again.

However, the well had been dug during a dry period. Once winter rains arrived and the water table rose, their effort was rewarded by a well full of water. After they realized the well would produce water, they constructed a brick curb and an engine platform at the well. The well never went dry during the subsequent 12 to 15 years.

SITE GEOLOGY

Shallow ground water in Ellis County is found beneath the weathered outcrops of the Austin Chalk and Taylor Marl and in overlying Quaternary and Pleistocene alluvium (fig. F2). The Austin Chalk consists of alternating fine-grained chalk and marl beds deposited in a marine deep-water platform environment. The lower Taylor Marl is a fine-grained marl, calcareous mudstone, and shale deposited in marine-shelf environments. The Quaternary and Pleistocene alluvium consists primarily of unconsolidated, stratified clay, sand, granules, and pebbles composed primarily of carbonate-rock fragments typically less than 50 ft (15.2 m) thick.

The chalk and marl are weathered and fractured near land surface, many fractures in these weathered strata possibly resulting from unloading processes that caused bedding-plane separation. These fractures commonly have millimeter-scale apertures and are not healed by mineral fillings, although many joint surfaces have been coated by hematite (Collins and others, 1992). Bedding-plane separations connect vertical fractures and lead to higher permeabilities. Thickness of the weathered chalk is generally less than 12 to 35 ft (3.66 to 10.67 m).

CHARACTERISTICS OF ELLIS COUNTY DUG WELLS

Distribution

The distribution of hand-dug wells was determined by means of a field survey of private property near the Superconducting Super Collider (SSC). An exhaustive evaluation of well location and density was conducted over 1,200 contiguous pieces of property in Ellis County of which land or subsurface rights had been purchased for the SSC. A less exhaustive survey was undertaken inside and outside the SSC site. If possible, physical measurements and descriptive

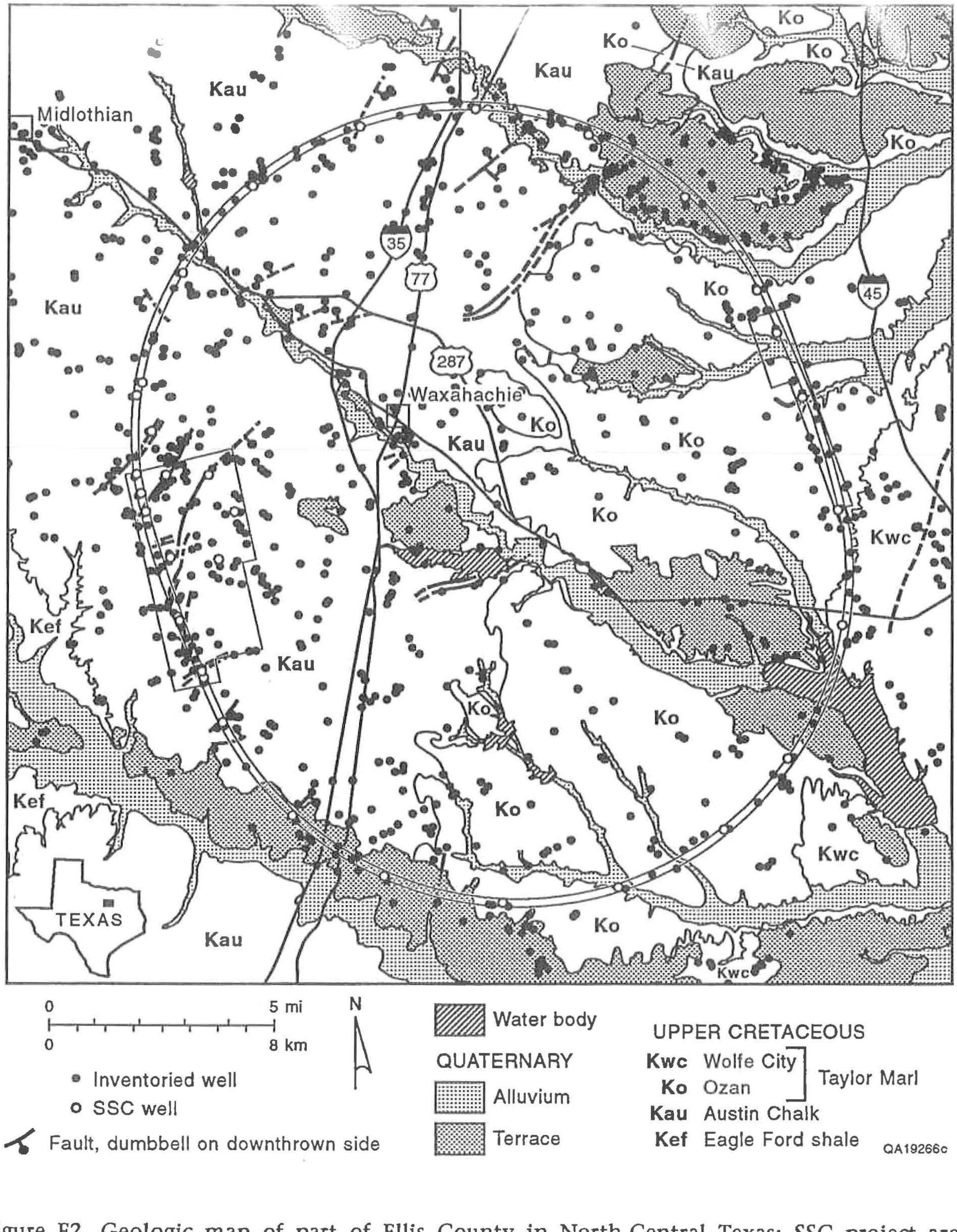

Figure F2. Geologic map of part of Ellis County in North-Central Texas; SSC project area outlined. Black dots show wells inventoried during study.

notes were recorded of well radius, well depth, casing height, geologic formation, casing design and composition, condition of the wellhead, and use of the well. Results from a well survey conducted at an alluvial deposit in the northeast part of the county (Dutton and Wickham, 1992) were included in a data base of the entire county.

A total of 811 hand-dug wells were located in Ellis County (fig. F2), 390 in chalk, 169 in marl, and 171 in alluvium. A thorough well inventory was performed on the SSC's West Campus in the Austin Chalk on the west side of the county (the boxed-in area on the left side of fig. F2). A total of 108 wells were located on this property, corresponding to a density of 9.1 wells/mi^2 (3.5 wells/km^2). If this area can be considered representative of well density in Ellis County, more than 4,300 wells might be located in the 475-mi^2 (1,230-km^2) area in figure F2. A well inventory in the terrace deposit in the northeast part of the SSC site indicated a well density of 7.3 wells/mi^2 (2.82 wells/km^2) (Dutton and Wickham, 1992). These well densities are conservative estimates because many wells reportedly have been filled, their locations now unknown.

Well Design

Thorough measurements of well radius, well depth, casing height, geologic formation, casing design and composition, condition of the wellhead, and use of the well were made at 362 of the shallow wells. The average depth of these wells is approximately 22.4 ft (~6.83 m), ranging from 5 to 50 ft (1.52 to 15.24 m). The average borehole diameter at the surface is 2.9 ft (0.88 m), ranging from 0.6 to 14 ft (0.18 to 4.27 m). All but two wells have circular boreholes. One well in chalk has a square, 4- × 4-ft (1.2- × 1.2-m) borehole and the appearance of a mine shaft. Dimensions of the other well are 14- × 14-ft (4.3- × 4.3-m), and it has a cement crown and railroad-tie well screen. Among the wells having circular cross sections, variation in quality of workmanship was evident from approximately circular, roughly hewn walls to perfectly rounded, smooth walls.

Hand-dug wells characteristically have large diameters owing to construction techniques The well radius has to be large enough for an individual to operate a shovel or pick in excavating the well. Well diameters in many hand-dug wells in the Austin Chalk widen with increasing depth. This widening of the well bore increases the number of fractures intersected, the effective radius, and the storage capacity of the well, thus increasing the usefulness of the well. In local parlance, these wells are referred to as "jug" wells because their shape resembles a narrow-necked jug.

Well radius with depth can be calculated by pumping all the water from a well while measuring water levels over time. If the pumping rate is known, drawdown is measured with time (ground-water inflow from the formation being inconsequential), and if the borehole is circular, then the radius of the well, r_W, at depth z is:

$$r_w = \sqrt{\frac{Q\,\Delta t}{\pi\,\Delta d}} \tag{F1}$$

where r_W is the radius of well at depth d, Q is the pumping rate, Δt is the change in time, and Δd is the change in head in well over Δt. In this manner, well radius with depth can be found and plotted.

A total of 42 hand-dug wells were purged to determine well radius with depth. The 32 wells in chalk can be grouped into four shapes (fig. F3): jug, conical, shaft, and miscellaneous. Jug wells have a narrow, straight neck near land surface that widens at depth to another constant radius (fig. F3a). Conical wells have a narrow neck near ground surface that widens with depth at a constant slope to the flat well bottom (fig. F3b). Shaft wells have the simplest shape, their radius remaining constant with depth (fig. F3c). A variety of shapes are grouped in the fourth category—for example, telescoping shaft wells that were deepened, with a diameter different from that at the top, and wells resembling the profile of a Middle Eastern lamp (fig. F3d). Some of the dug wells were deepened to tap deeper ground water during droughts, such as those redug during 1952 and 1953, which caused the water table to fall below the base of shallow wells.

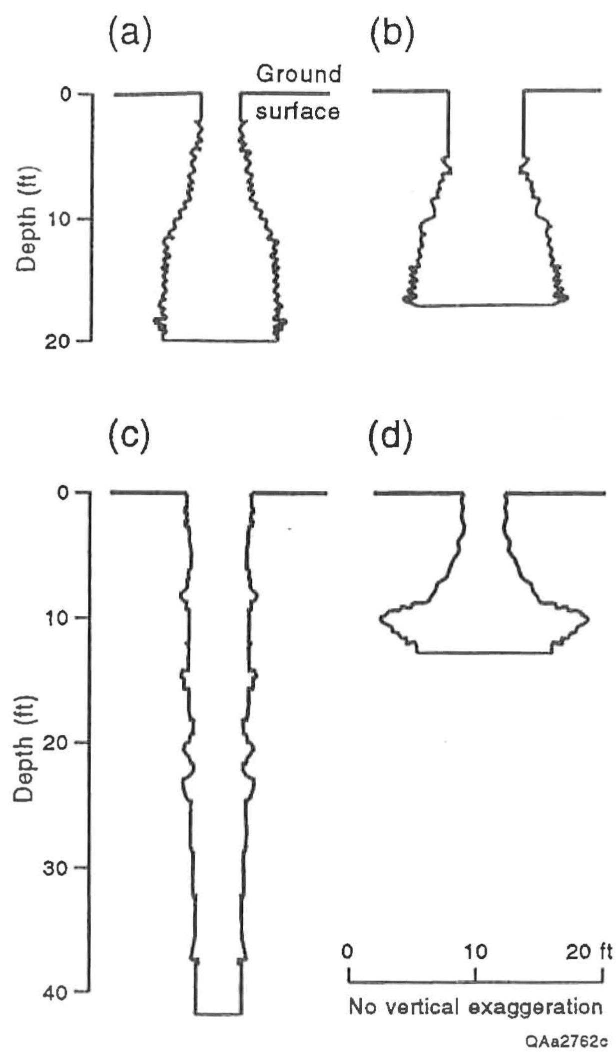

Figure F3. Different well geometries of wells in chalk, which were determined by pumping the well bore.

Typical design of Austin Chalk wells includes a brick collar extending 3 to 6 ft (0.9 to 1.8 m) through the soil horizon to the top of the chalk, the exposed chalk composing the remainder of the well depth. Some wells have collars constructed of cement or mortared pieces of chalk, whereas a few others are collarless.

Wells in the alluvium generally have a uniform radius and are cased in unmortared brick at depth. Smaller-diameter wells are cased in plastic or steel pipe, having been dug more recently. Wells in the marl are typically of constant radius. The walls and floors of many well bores in the marl were completely sealed by cement in an attempt to prevent poor-tasting "gyp" (that is, gypsum- or sulfate-rich) ground water from seeping into the borehole. These cisterns stored rainwater collected from the nearby roof of a home or barn. Several wells in chalk also were used as cisterns during droughts, water being carried from nearby streams and springs. Some wells in chalk had water directed to them from rooftops to complement ground-water seepage to the well.

Past and Present Uses

Most wells were dug to meet domestic and livestock water needs and were probably not used for irrigation because of low yields. Water consumption in homes without indoor plumbing probably was about 10 gal/day (37.9 L/day) per person (Texas State Department of Health, 1970), which most dug wells could easily supply. In comparison, average present-day water consumption at households in municipal areas is between 458 and 692 gal/day (1,733 and 2,619 L/day) (Driscoll, 1986). These usage rates include as much (or more) water for lawn watering as for household consumption. A well dug in Lone Elm in the west part of Ellis County was reportedly a municipal supply well for the small town. This well had an unusually high specific capacity (50 gal min^{-1} ft^{-1} [10.35 L sec^{-1} m^{-1}]).

In times of drought, water was carried from nearby streams, springs, or viable wells and deposited into the borehole (R. E. Davis, 1991, and D. C. Paul, 1992, personal communications).

In this manner many wells dug in chalk were used as cisterns. A particularly severe drought that caused the drying of many dug wells occurred from 1952 through 1953.

Currently, most hand-dug wells are unused or abandoned. Only 82 wells (10 percent of total inventoried) are being used—45 in drinking, cooking, or washing. These wells are generally in good condition, although most do not meet all the requirements of a safe shallow-water supply as determined by the Texas State Department of Health (1970, p. 17), such as:

- well should be protected by a watertight, insect-proof seal,
- surface water should be drained away from the wellhead,
- surface casing should be used to prevent polluted water from seeping into the well, and
- good well construction should prevent the growth of aquatic vegetation that might impart objectionable odors and tastes to well water.

Many hand-dug wells have inadequate well covers that do not prevent surface water from running into well bores. Shallow wells in chalk are particularly susceptible to contamination because they tap into shallow, unconfined, fractured aquifers, which are noted for rapid recharge and accelerated contaminant transport.

Abandoned wells range in condition. Many wells near homes have been sealed to prevent children or pets from falling into well bores, although many others remain unsealed. Numerous other wells vary in disrepair, having collapsed or partially collapsed well crowns and open tops. Landowners spoke of livestock and wild animals falling into wells and tractors getting stuck in old well bores. During early winter months, rats have been observed floating in many unprotected dug wells, apparently attracted to the warmth emanating from the borehole. Other wells have been or are being used in the disposal of household trash, bricks, wire, automobile tires, and roofing shingles. One well had a small automobile in its mouth, and another contained a kitchen sink.

Because of rapid recharge and high ground-water-flow rates, alluvial and weathered bedrock aquifers are susceptible to contamination through these wells. Ground-water contamination has probably been caused by these wells, but no clear cases have been recorded.